UNIVERSITY OF NAIROBI

PHYTOCHEMICAL ANALYSES OF *MUNDULEA SERICEA, TEPHROSIA UNIFLORA* (LEGUMINOSAE) AND, *STREBULUS USAMBARENSIS* (MORACEA) FOR ANTI-INFECTIVE AND CYCTOTOXIC PRINCIPLES

BY

CAROLYNE CHEPKIRUI KENDUIYWO

I80/52251/2017

A Thesis Submitted for Examination in Fulfilment of the Requirements for Award of the Degree of Doctor of Philosophy in Chemistry of the University of Nairobi

2022

DECLARATION

I declare that this thesis is my original work and has not been submitted elsewhere for examination, award of a degree or publication. Where other people's work, or my own work has been used, this has properly been acknowledged and referenced in accordance with the University of Nairobi's requirements.

Signature ..... Date....20/06/22

Chepkirui Carolyne

Department of Chemistry

Faculty of Science and Technology

University of Nairobi

This thesis is submitted for examination with our approval as research supervisors:

Date Signature

Prof. Abiy Yenesew 21/06/22

Department of Chemistry

University of Nairobi

P.O. Box 30197-00100

Nairobi Kenya Email ayenesew@uonbi.ac.ke

Dr. Solomon Derese 21/06/22

Department of Chemistry

University of Nairobi

P.O. Box 30197-00100

Nairobi Kenya Email sderese@uonbi.ac.ke

Dr. Albert Ndakala 20/6/22

Department of Chemistry

University of Nairobi

P.O. Box 30197-00100

Nairobi Kenya Email andakala@uonbi.ac.ke

DEDICATION

I dedicated this thesis to my beloved family for their love and support during my studies.

ACKNOWLEDGEMENTS

I am thankful to the German Academic Exchange Service (DAAD) for the PhD scholarship. I am also thankful for funding assistance from Swedish Research Council (nr, 2016-05857), and the International Science Program (KEN 02).

I am very grateful to my supervisors Prof. Abiy Yenesew, Dr. Albert Ndakala, and Dr. Solomon Derese for their unending support and guidance during my studies. My sincere gratitude goes to Prof. Mate Erdelyi of the Department of Chemistry, Uppsala University, Sweden, for hosting me for five months in his laboratory to conduct part of the study. I appreciate, Mr. Patrick Mutiso of the Herbarium, Department of Biology, University of Nairobi, for collecting and authenticating plant samples.

My heartfelt appreciations go to my family for their unfailing support during my studies. My gratitude goes to all members of faculty and students at the Department of Chemistry, University of Nairobi', Dr. Martha Induli, and the halogen-bonding group of Uppsala University for their support.

ABSTRACT

Phytochemical analysis of the dichloromethane/methanol (1:1) extracts of *Mundulea sericea* and *Tephrosia uniflora* (both Leguminosae) and *Strebulus usambarensis* (Moraceae) yielded thirty-one compounds. Phytochemical analysis of *S. usambarensis* stems and roots resulted in the identification of three novel naphtho-benzofuran derivatives, named usambarin A (**110**), B (**111**), and C (**112**). Eight new naphthalene derivatives named usambarin D (**113**), E (**114**), F(**115**), G (**116**), H (**117**), I (**118**), and L (**125**), phenyl-1-benzoxepin derivative (**120**), two flavans (**119** and **126**), and four known compounds. Similarly, the analysis of the leaves and roots of *M. sericea* yielded ten known compounds; three flavanonols, two flavanols, an isoflavone, one rotenoid, two pterocarpans, and the sterol stigmasterol. Phytochemical investigation of the stems of *T. uniflora* also yielded one new β-hydroxydihydrochalcone (**134**) and three known compounds (an isoflavone, β-hydroxydihydrochalcone and a rotenoid). NMR, X-ray crystallography, UV spectroscopy, electronic circular dichroism and mass spectrometry were used to determine their structures.

The crude extract of *M. sericea* roots exhibited antiplasmodial effect against chloroquine-resistant (W2) (IC_{50} of 0.6 µg/mL) and chloroquine-sensitive (3D7) (IC_{50} 1.8 µg/mL) strains of *Plasmodium falciparum*. Among the major compounds from this plant, lupinifolinol (**129**) (IC_{50} values of 2.0 M for the W2 strain and 6.6 M for the 3D7 strain), and mundulinol (**64**) (IC_{50} of 5.9 µM against the W2 strain and 2.4 µM against the 3D7 strain) were active. The antileishmanial activity of selected compounds was tested against *L. donovani* strains, both antimony-sensitive (MHOM/IN/83/AG83) and antimony-resistant (MHOM/IN/89/GE1), of which sericetin **(130**) was active against antimony-sensitive (IC_{50} 5.0 µM) and antimony-resistant (IC_{50} 38.0 µM) strains. Dehydrolupinifolinol (**128**) was also active against the antimony-sensitive strain (IC_{50} 9.0 µM). The isolated compounds from *S. usambarensis* were tested against *E. coli* and *B. subtilis*. Usambarin D (**113**) had moderate antibacterial activity against *B. subtilis* (MIC = 9.0 µM), however, the other compounds examined were inactive (MIC >100 µM). All the tested compounds were inactive against *E. coli*.

Some of the identified compounds from *S. usambarensis and M. sericea* were investigated for their cytotoxicity against; lung (A549), breast (MCF-7), immortal human hepatocytes non- cancerous (LO2), liver (HepG2), and human bronchial non-cancerous (BEAS-2B) cell lines. Usambarins A

(EC_{50} of 65 μM) and B (EC_{50} of 92 μM) were weakly cytotoxic against the breast cancer cell line, while compounds **114, 115, 119, 120**, and **122** were not cytotoxic to MCF-7 with EC_{50} > 200 μM. The current study has revealed that *M. sericea*, *S. usambarensis*, and *T. uniflora* possess a spectrum of metabolites with unique structural features with potential in the development of antimalarial, anticancer, antibacterial and antileishmanial agents.

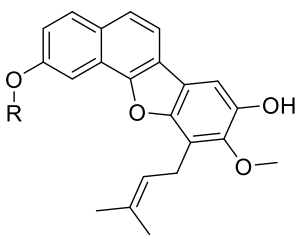

110 R= CH_3
111 R= H

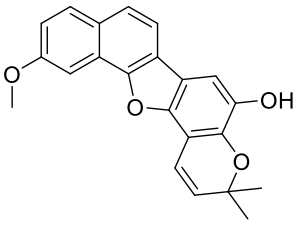

112

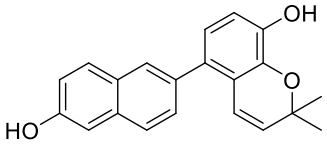

113

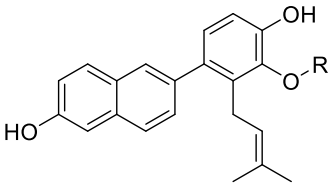

114 R= H
115 R=CH_3

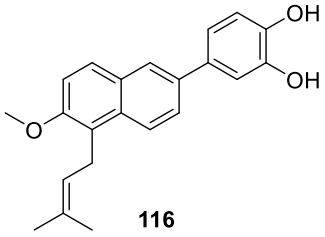

116

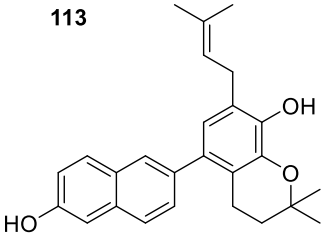

117

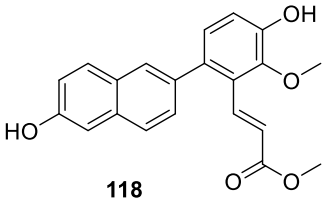

118

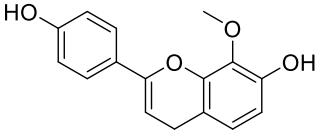

119

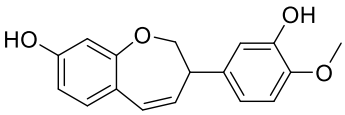

120

TABLE OF CONTENTS

LIST OF TABLES

LIST OF FIGURES

LISTS OF ABBREVIATIONS/ACRONYMS AND SYMBOLS

CH_2Cl_2	Dichloromethane
COSY	Corelation Spesctroscopy
d	Doublet
dd	Doublet of doublet
DMSO	Dimethylsulfoxide
ECD	Electronic Circular Dichroism
ED_{50}	Effective Dose at 50%
EtOAc	Ethyl acetate
HMBC	Heteronuclear Multiple Bond Correlation
HPLC	High Performance Liquid Chromatography
HREIMS	High Resolution Electrospray Ionization Mass Spectrometry
HSQC	Heteronuclear Single Quantum Coherence
IC_{50}	The half-maximal Inhibitory concentration
LC_{50}	Lethal concentration at 50%
m/z	Mass to charge ratio
MeOH	Methanol
MIC	Minimum inhibitory concentration
MTT	(3-(4, 5-dimethylthiazolyl-2)-2, 5-diphenyltetrazolium bromide)
NMR	Nuclear magnetic resonance
PTLC	Preparative Thin Layer Chromatography
s	Singlet
SDS	Sodium Dodecyl Sulfate
t	Triplet
UV	Ultraviolet–visible
WHO	World Health Organization
δ	Chemical shift

CHAPTER ONE

INTRODUCTION

1.1 Background Information

Infectious diseases remain one of the prominent groups of severe human ailments (Fauci, 2001; Li & Yang, 2021; WHO, 2021d). Infectious diseases are disorders caused by parasites, fungi, bacteria, and viruses (Li & Yang, 2021; WHO, 2021d). Acute lower respiratory tract infections, amebiasis, malaria, leishmaniasis, helicobacter pylori, hepatitis and toxoplasmosis are among these infectious illnesses (Fauci, 2001; Mathers *et al*., 2008; Morse, 1995). It is estimated that these infectious diseases kill over a million people each year (Andrews *et al*., 2014). In addition, these infectious diseases have been associated with a variety of human non-infectious diseases (Chen et al., 2017; Cobo & Chadee, 2013). This is due to very complex interactions due to environmental factors (Medvedev, 2013; Porta et al., 2011) Non-infectious diseases (non-communicable) are caused by genetic, environmental, physiological and behavioural factors (Azadnajafabad *et al*., 2021; Lane *et al*., 2021). The four major non-infectious diseases are cardiovascular disease, cancer, chronic respiratory disease and diabetes (Azadnajafabad *et al*., 2021; WHO, 2021c). These non-infectious diseases are responsible for over 41 million fatalities annually (Hunter & Reddy, 2013; WHO, 2021c).

Malaria is the most prevalent among infectious disease, and is caused by protozoan parasites belonging to *Plasmodium* species, *P. knowlesi*, *P. malariae*, *P. falciparum*, *P. ovale*, and *P. vivax.* In 2018, there were 228 million malaria cases globally, with 405,000 fatalities (Zekar & Sharman, 2020). In Kenya, 80 % of the inhabitants reside in malaria-prone regions, with pregnant women

and children being the most vulnerable (KMIS, 2015; WHO, 2017a). It is predicted that 5 million new clinical cases are diagnosed each year resulting in 10,000 fatalities (Prevention, 2019).

Visceral, cutaneous and mucocutaneous leishmaniasis are the three types of leishmaniasis (Rama et al., 2015a). It is projected that a million new cases will be diagnosed each year (Rama et al., 2015a). Above ninety-five percent of visceral leishmaniasis infections were documented in parts of Asia, East and Central Africa in 2018, with about eighty-five percent of cutaneous leishmaniasis infections being reported in parts of Asia, South America, and Africa (Almeida *et al*., 2020).

Cancer is an illness that is identified by abnormal growth of cells (Rakoff-Nahoum, 2006). It is caused by genetic alterations that arise within cancer cells, as well as life-style, environmental factors, infections and exposure to carcinogens (Sung *et al*., 2021; WHO, 2021a). It is the world's top cause of death. In 2020, 19.3 million cases were reported, with approximately 10 million fatalities (WHO, 2021a). Developing countries bear 80 % of the disease burden (Wambalaba *et al*., 2019). In Kenya, among the new cases recorded by 2019, 78.5 % resulted in fatality (Wambalaba *et al*., 2019).

Incidences of cancer and bacterial infections have been reported in malaria and leishmaniasis patients (Ataide *et al*., 2014; Carrillo-Larco *et al*., 2019; Maltha *et al*., 2014; Nordor *et al*., 2018). Malaria and leishmaniasis are associated with inflammations (Pacheco & Kamboh, 2020; Rodrigues *et al*., 2015), which contribute to an increase in uptake of oxygen and the generation of free radicals in the cells. This is a major contributor in the growth of cancer (Hussain *et al*., 2003). There has also been evidence of a link between cancer and malaria (Lehrer, 2010; Suresh *et al*.,

2005). Overall, malaria, leishmaniasis, bacterial infections, and cancer remain the major health challenges for sub-Saharan countries, including Kenya (Alvar *et al*., 2012; Mangeni *et al*., 2017; Mishra *et al*., 2009). Because of the emergence of drug-resistance (Mishra *et al*., 2009; Morita *et al*., 2019; WHO, 2017b), there is a vital need to find alternative agents to fight malaria, cancer, bacterial infections, and leishmaniasis.

Natural products are sources of novel alternative therapies for drug development (Cragg & Newman, 2013; Cragg & Pezzuto, 2016; Lahlou, 2013). To contribute to the search for alternatives, the current study explored some species of the genera *Mundulea*, *Tephrosia*, and *Strebulus* for antimalarial, antibacterial, antileishmanial and anticancer principles.

Plants of the genus *Mundulea* (family Leguminosae) have a wide usage in herbal medicine (Luyengi *et al*., 1994; Pentsil *et al*., 2017; Stark *et al*., 2013). The Leguminosae family contains flavonoids and isoflavonoids that showed anticancer (Cao *et al*., 2004; Tang *et al*., 2014; Tringali, 2001) antimicrobial and antifungal (Mazimba et al., 2012a), antioxidant and antiplasmodial (Khyade & Waman, 2017; Ngbolua, 2016) activities. The genus *Tephrosia* (family Leguminosae) also possesses bioactive flavonoids (Touqeer *et al*., 2013a) with cytotoxic (Chen et al., 2014a), anticancer (Lodhi *et al*., 2006), anti-inflammatory (Shenoy *et al*., 2010) antibacterial, and antiplasmodial properties. Studies involving the isolation of the secondary metabolites of some plants belonging to these genera was predicated to produce bioactive principles.

Other than the family Leguminosae, the Moraceae is one of the few families, which elaborates isoflavonoids. One of the genera of this family, *Strebulus* has approximately 25 species (Kinghorn *et al*., 2016), found within tropics (Ren *et al*., 2016). *Strebulus asper* is used to treat leprosy, dysentery (Chawla *et al*., 1990), filariasis, toothache and cancer (Singh *et al*., 2015). Previous

phytochemical investigation of *S. asper* reveals it contains cardiac glycosides, coumarins, flavonoids and lignans (Adem, 2019; Deng *et al*., 2007; Ren *et al*., 2016; Singh *et al*., 2015). Some of these phytochemicals showed anticancer (Adem, 2019; Fiebig *et al*., 2004), anti-parasitic (Mathai & Devi, 1992; Singh *et al*., 2015) and anti-bacterial (He et al., 2017a; Rao et al., 2014; Singh et al., 2015) activities.

1.2 Statement of the Problem

Infectious diseases pose a serious health risk worldwide. Globally, over five-hundred million individuals are affected (Monzote & Siddiq, 2011). These diseases are responsible for over a million fatalities per year (Andrews *et al*., 2014; Hunter & Reddy, 2013). Due to a lack of or restricted access to chemotherapeutic drugs, developing nations experience high mortality (Gigley et al., 2012; Schmidt et al., 2012). In 2019, WHO reported an estimated 229 million malaria infections, and 409,000 fatalities worldwide. Ninety-four percent of these malaria cases and deaths occurred in Africa (WHO, 2020). Annually, thirty-thousand infections of visceral leishmaniasis and over one million new infections of cutaneous leishmaniasis are recorded (WHO, 2021b), with over 20,000 fatalities (Nafari *et al*., 2020). Cancer, which in some cases is associated with infectious diseases, accounted for approximately ten million fatalities and 19.3 million new infections globally (WHO, 2021a). Chemotherapy and vector control have been helpful in reducing these infections. These modes of treatment and prevention have major shortcomings, which are exacerbated by drug and pesticide resistance (Andrews et al., 2014; Gottesman, 2002; O'Connor, 2007; Zofou et al., 2014). Furthermore, the costs of monitoring and maintaining these medicines are too high for developing nations on the continent to bear (Andrews *et al*., 2014; Kingham *et al*., 2013; Morhason-Bello *et al*., 2013; Volpedo *et al*., 2019). Similarly, these therapies are associated with severe toxicities (Andrews *et al*., 2014; Curigliano *et al*., 2010;

Sereno *et al*., 2008; Volpedo *et al*., 2019). As a result, more research is required to discover safe, low cost and effective options for eliminating malaria, cancer, leishmaniasis and bacterial infections.

1.3 Objectives

1.3.1 General Objective

The general objective of this study is to identify anti-infective principles from *Mundulea sericea*, *Tephrosia uniflora* and *Strebulus usambarensis* species.

1.3.2 Specific Objectives

The specific objectives of this study are:

i. To isolate and characterize secondary metabolites from *Mundulea sericea*, *Tephrosia uniflora* and *Strebulus usambarensis*;
ii. To determine the antiplasmodial activity of the crude extracts and isolated compounds;
iii. To determine the antileishmanial activity of the crude extracts and isolated compounds;
iv. To determine the antibacterial activity of the isolated compounds ;
v. To determine the cytotoxicity of isolated compounds.

1.4 Justification of the Study

Natural products and their modifications have aided in the development of drugs (Kumar *et al*., 2009). The most significant antimalarial medicines produced from plants are quinine and artemisinin (Batista *et al*., 2009; Mojab, 2012). Plumericin (**1**) and isoplumericin (**2**) obtained from the stem of *Himatanthus sucuuba* have potent activity against *Leishmania amazonensis* axenic amastigotes with an IC_{50} of 5 µg/mL (Adebayo & Suleman, 2013). *In vitro* studies of plumericin

have reported a reduction in macrophage infection similar to amphotericin B (the conventional medication) with an IC_{50} of 0.9 µM (Adebayo & Suleman, 2013). Actinomycin D (**3**), doxorubicin (**4**), vinblastine (**5**), camptothecin (**6**), and vincristine (**7)** are some of the anticancer agents derived from natural products. Hence, natural products remain a potential source of diverse structural features that can be explored as lead compounds for the mitigation of infections (Lahlou, 2013). It's worth noting that the Leguminosae (including the genera *Mundulea* and *Tephrosia)* and Moraceae (including the genus *Strebulus*) families generate a wide spectrum of flavonoids, isoflavonoids and alkaloids with diverse biological activities. As a result, isolating and identifying bioactive components from selected members of the Leguminosae and Moraceae families will aid in the quest for novel ways to combat, malaria, leishmaniasis, bacterial infections, and cancer.

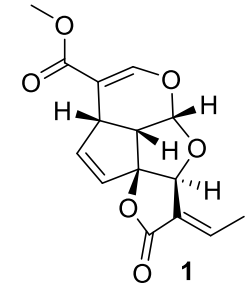

1

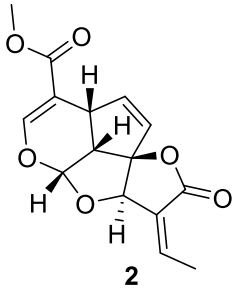

2

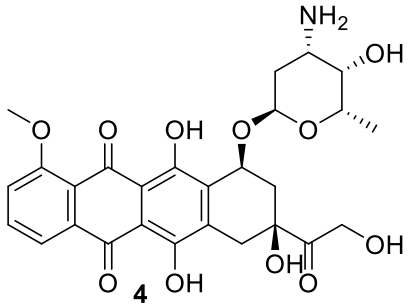

4

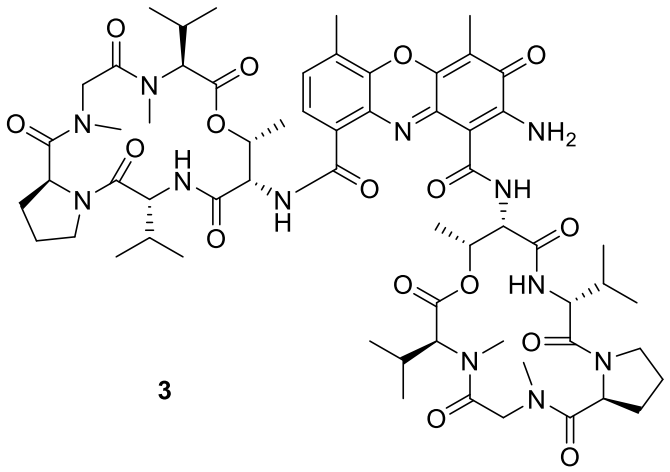

3

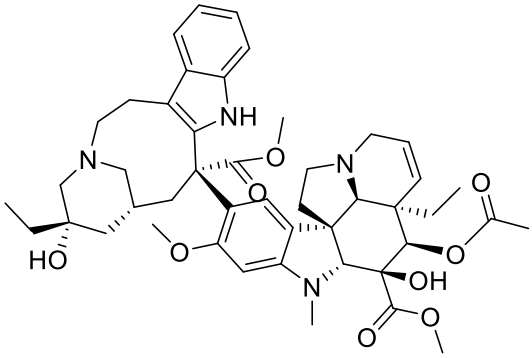

5

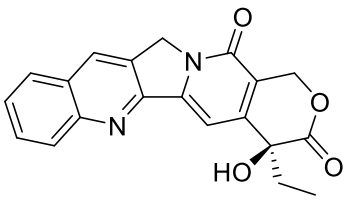

6

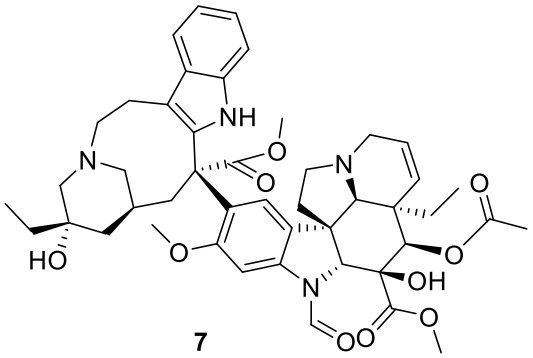

7

CHAPTER TWO

LITERATURE REVIEW

2.1 Infectious and non-infectious Diseases

Infectious diseases have detrimental health and economic consequences (Fauci, 2001; Filardy *et al*., 2018; Li & Yang, 2021). It is estimated that infectious diseases kill over a million people each year (Andrews *et al*., 2014). These diseases are caused by parasites, viruses, fungi and bacteria (Li & Yang, 2021). High death rates by infectious diseases are contributed by acute lower respiratory tract infections, malaria, leishmaniasis, diarrhoea, tuberculosis, and viral infections such as HIV and covid -19 (Fries *et al*., 2021; Kirtane *et al*., 2021). Malaria and leishmaniasis are prevalent in tropical and subtropical locations, with a higher prevalence in developing nations (Rocha *et al*., 2005). In these regions, half a billion people are at risk, resulting in approximately 40 million disability-adjusted life years (Monzote & Siddiq, 2011). Over six-hundred thousand deaths occur yearly due to both malaria and leishmaniasis (Nweze *et al*., 2021; Stuart *et al*., 2008).

On the other hand, non-infectious diseases (non-communicable) are caused by genetic, environmental, physiological, and behavioural factors (Azadnajafabad *et al*., 2021; Lane *et al*., 2021; WHO, 2021c). Cancer, cardiovascular disease, and diabetes are the highest sources of the non-infectious mortality (Azadnajafabad *et al*., 2021; Duan *et al*., 2021). The impacts and incidence of these diseases are high in developing nations, causing over 80 % of deaths in these countries (Ezzati & Riboli, 2013; Hunter & Reddy, 2013; Narayan *et al*., 2010). Malaria, leishmaniasis, bacterial infections (infectious diseases), and cancer (non-infectious disease) are explored in this study.

2.1.1 Leishmaniasis

Leishmaniasis is a disease that manifests itself in three forms: visceral, cutaneous, and mucocutaneous form (Desjeux, 2004; Rama et al., 2015a). It is caused by a protozoan parasite illness that is endemic to tropical and subtropical nations. Promastigotes and amastigotes are the two parasitic types of leishmaniasis in the developmental stage (Rama et al., 2015a). The life cycle begins with a blood meal of an infected sand fly. During the blood meal, a sand fly transmits promastigotes to a human. Promastigotes convert into amastigotes in phagocytic cells. The amastigotes multiply via cell division while infecting other phagocytic cells. This infection results in clinical manifestation of leishmaniasis. The life cycle continues when a sand fly bites an infected individual, the ingested amastigotes will change into promastigotes in the digestive tract of the sand fly (refer to Figure 2. 1) (Gillespie *et al*., 2016; Tempone *et al*., 2011). There are more than one million new cases projected to be diagnosed each year, with around 65,000 fatalities (Cortes et al., 2020).

Leishmaniasis is treated using pentavalent antimonials, which are used as therapeutics for both visceral and cutaneous leishmaniasis (Adebayo & Suleman, 2013). Visceral leishmaniasis is also treated with miltefosine, liposomal amphotericin B, and paromomycin (Et-Touys *et al*., 2017). These drugs, however, present several risks; they are cytotoxic and have negative side effects such as fever, chills, nephrotoxicity and hypokalemia (Et-Touys et al., 2017; Rama et al., 2015a). These medications are extremely costly and must be used for a long time. Exacerbating these problems, is the development of parasite resistance to the pentavalent antimonials (Sujitha *et al*., 2015; Yousuf *et al*., 2016). To address these issues, an urgent need for the development of new drugs.

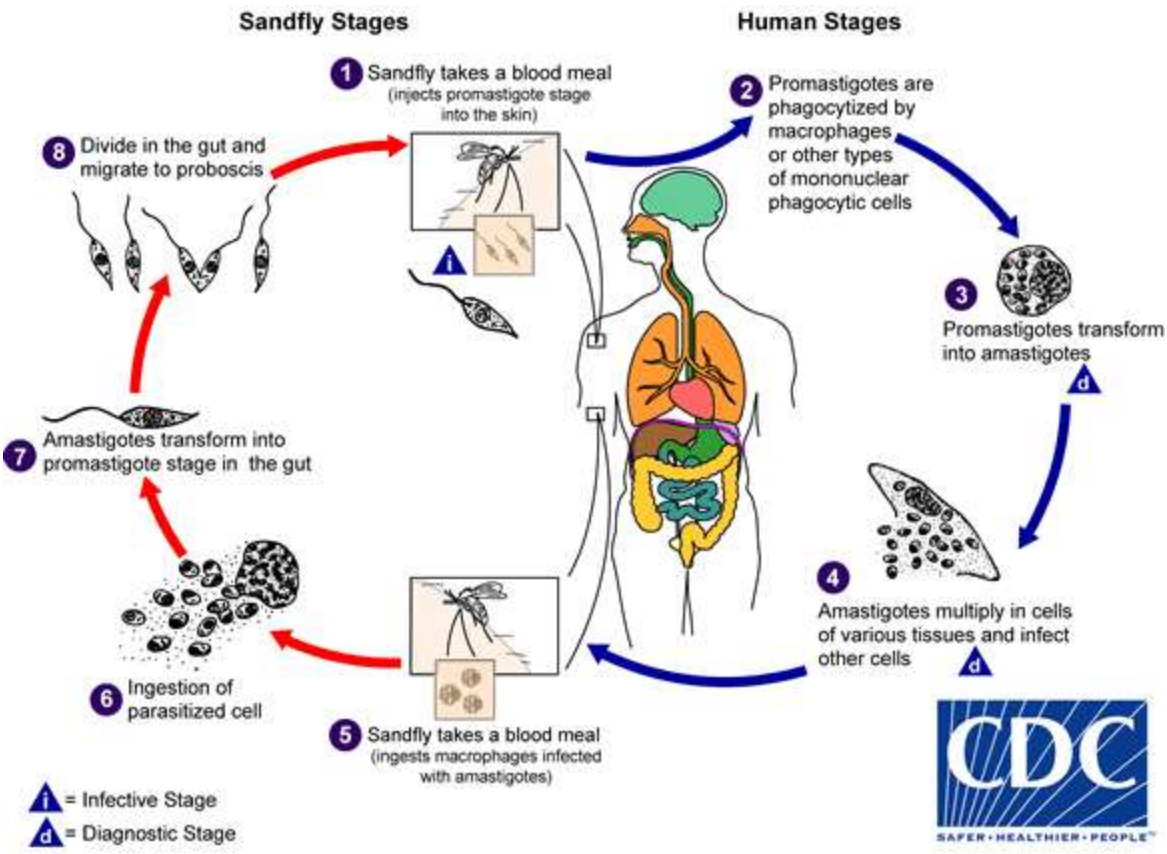

Figure 2. 1: Life cycle of leishmaniasis (Prevention, 2020)

2.1.2 Malaria

Malaria is a deadly parasitic disease spread by the female anopheles mosquitoes and is caused by *Plasmodium* parasites (Tuteja, 2007). In 2019, over two hundred million cases of malaria were recorded globally, with over four hundred thousand fatalities (WHO, 2020). Children under the age of five, account for sixty-seven percent of malaria fatalities globally (WHO, 2020).

Malaria transmission can be prevented by using chemotherapies, indoor spraying of long lasting insecticides, personal protection methods and, use of long-lasting pyrethroids-treated mosquito netting (Raghavendra *et al*., 2011). Malaria control remains a difficult task because of *Plasmodium* resistance to existing antimalarials, and also vector resistance to pesticides (Sougoufara *et al*.,

2014). Thus, in order to reduce malaria burden, continuous research is required to identify bioactive principles that can serve as proto-types for discovery of drugs that are safe, efficacious and long lasting.

2.1.3 Cancer

Cancer is an illness that is identified by abnormal development of cells (Rakoff-Nahoum, 2006). It is caused by chronic inflammations which alters cellular homeostasis (Hussain *et al*., 2003), unhealthy diet (Sung *et al*., 2021), exposure to carcinogens (Clapp *et al*., 2008), occupational stress (Wang *et al*., 2018), unhealthy lifestyle, and hereditary factors (Czene *et al*., 2002). According to (van Elsland & Neefjes, 2018), there are correlations between bacterial infections and cancer. They also identified a link between *Salmonella typhi* and gallbladder cancer, *Salmonella enteritidis* and colon cancer, *Chlamydia trachomatis* and ovarian cancer (van Elsland & Neefjes, 2018) .

According to Wyss *et al* (2020), *Plasmodium falciparum* has been classified as a carcinogenic agent in humans (Wyss *et al*., 2020). Chronic malaria infections lead to excessive generation of reactive oxygen, which is a potential major for cancer (Eze *et al*., 1990). Burkitt lymphoma, a paediatric cancer, is associated with *Plasmodium falciparum* exposure (Mulama *et al*., 2014; Quintana *et al*., 2020). Malaria gene mutation has been linked to prostate cancer in African men (Thomas, 2005). Leishmaniasis infections have also been linked to cancer (Al-Kamel, 2017); for example, cutaneous leishmaniasis is associated with skin cancer (Morsy, 2013). This again is due to inflammatory response, which increases the production of reactive oxygen and nitrogen species, both of which are predisposing factors for cancer (Kocyigit *et al*., 2005).

Cancer therapies are classified into different types (Urruticoechea et al., 2010). Chemotherapy is a treatment, which entails the usage of anticancer drugs to eliminate the cancerous cells. For

example, cisplatin (against ovarian cancer) (Trimmer & Essigmann, 1999), paclitaxel (Spencer & Faulds, 1994), a combination of cyclophosphamide methotrexate and fluorouracil (CMF) (against breast cancer), imatinib mesylate (against leukemia), and avastin (against colon cancer) (Chabner & Roberts, 2005). Surgery is removal of cancerous tumors from the body (Wang *et al*., 2018). Radiation therapy entails using high doses of ionizing radiation, to eradicate malignancies. Targeted therapies are combinations of several treatment options that inhibit the growth of tumours by interfering with specific proteins (Gerber, 2008; Seebacher *et al*., 2019). Hormonal therapy eradicates breast or prostate cancerous cells by altering the amount of hormones, which enhances cancer progression in the body (Wang *et al*., 2018). These treatment options are used depending on the type and stage of cancer (Wang *et al*., 2018).

The challenges facing these cancer therapies are severe toxicity (Holohan *et al*., 2013; Sereno *et al*., 2008), resistance (Gottesman, 2002; Housman *et al*., 2014), and the high cost of treatment (Ehni, 2014; Faden *et al*., 2009). Hence, there is a need for continuous research on development of new drugs.

2.1.4 Co-infections of Malaria and Leishmania

Malaria and leishmaniasis affect approximately half of the global population. They are associated with mortality, morbidity, and long term consequences (Quintana *et al*., 2020). To worsen the situation, co-infection of malaria and leishmania in patients exacerbates the severity by resulting in substantial and compounding complications (McArdle *et al*., 2018).

Bacterial diseases are leading causes of death in patients with leishmaniasis; according to Kadivar (2000), pneumonia, septicaemia, urinary tract infections are deadly bacterial infections, that

complicate the treatment of leishmaniasis (Andrade et al., 1990; Kadivar et al., 2000). Alsamaria and alodaidi (2009), detected the presence of *Staphylococcus epidermidis, E. coli, Proteus* species, *Klebsiella* and *Staphylococcus aureus* in infected lesions in cutaneous leishmaniasis (AlSamarai & AlObaidi, 2009; Ziaei *et al*., 2008). Barati *et al* (2008), showed that immunosuppression and a reduction in white blood cells was linked with severe bacterial co-infection in children with visceral leishmaniasis (Barati *et al*., 2008). Bacterial sepsis also contributed to over 35% deaths in visceral leishmaniasis patients (Endris *et al*., 2014).

Bacterial infections have also been observed among malaria patients, and they are major causes of death among African children (Bassat *et al*., 2009; Sandlund *et al*., 2013). In children, malaria has been linked to increased bloodstream bacterial infections (Gomez-Perez et al., 2014). The most frequent bacteria being *Salmonella enterica* and *Streptococcus pneumoniae* infections (Mooney *et al*., 2019). According to Thiemer *et al* (2012) *Salmonella typhi* and *Streptococcus pneumonia* were the leading causes of blood infection in adult malaria patients (Hogan *et al*., 2018; Thriemer *et al*., 2012).

2.2 Compounds Isolated from Plants with Antileishmanial Activity

Plants contain a vast spectrum of biological properties. Polar extracts, essential oils, alkaloids, terpenoids, lignans, quinones and flavonoids have been reported to show antileishmanial properties (Cortes et al., 2020). For example, Musayeib *et al* (2013) isolated, 3β,11α-dihydroxyurs-12-ene (**8**) (IC_{50} of 3.20 µM) and ursolic acid (**9)** (IC_{50} of 7.40 µM) from *Kleinia odora* (Asteraceae) that showed antileishmanial activity against *L. infantum* (Al Musayeib *et al*., 2013). Cynaropicrin (**10**)

isolated from *Vernonia mespilifolia* (Asteraceae) showed antileishmanial activity against *L. donovani* with half – maximal inhibitory concentration of 1.56 µM (Mokoka *et al*., 2013).

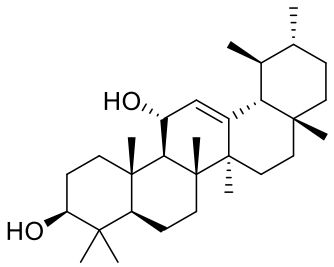

8

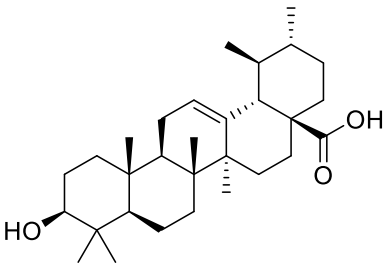

9

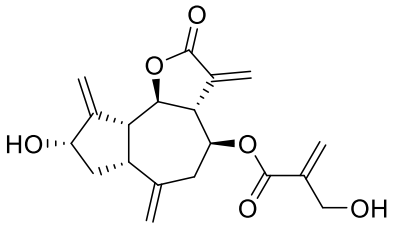

10

Compounds isolated from *Abrus precatorius* (Leguminosae) exhibited antileishmanial activity against *L. major*; abruquinone A (**11**) (IC_{50} of 6.35 µg/mL), abruquinone B (**12**) (IC_{50} of 6.32 µg/mL) and (3S)-7,8,3′,5′-tetramethoxyisoflavan-1′,4′-quinone (**13**) (IC_{50} of 5.00 µM) (Okoro et al., 2019). From *Piliostigma thonningii* (Leguminosae), methyl-ent-3β-hydroxylabd-8(17)-en-15-oate (**14**) (IC_{50} of 7.82 µM) showed antileishmanial activity against *L. donovani* (Afolayan et al., 2018; Cortes et al., 2020).

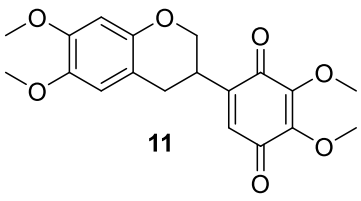

11

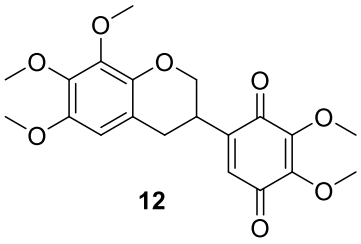

12

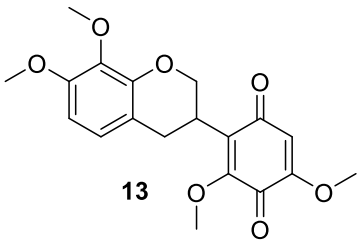

13

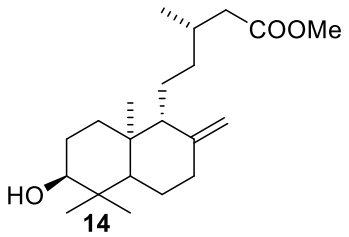

14

Compounds isolated from *Withania coagulans* (Solanaceae) exhibited antileishmanial effect against *L*. *major*; withanolide J (**15**) (IC_{50}, 5.74 µM), withanolide G (**16**) (IC_{50}, 10.34 µM) and, withathanolide C (**17**) (IC_{50}, 10.85 µM) (Cortes et al., 2020). These findings suggest that secondary metabolites and their derivatives have potential as lead molecules for antileishmanial chemotherapy development.

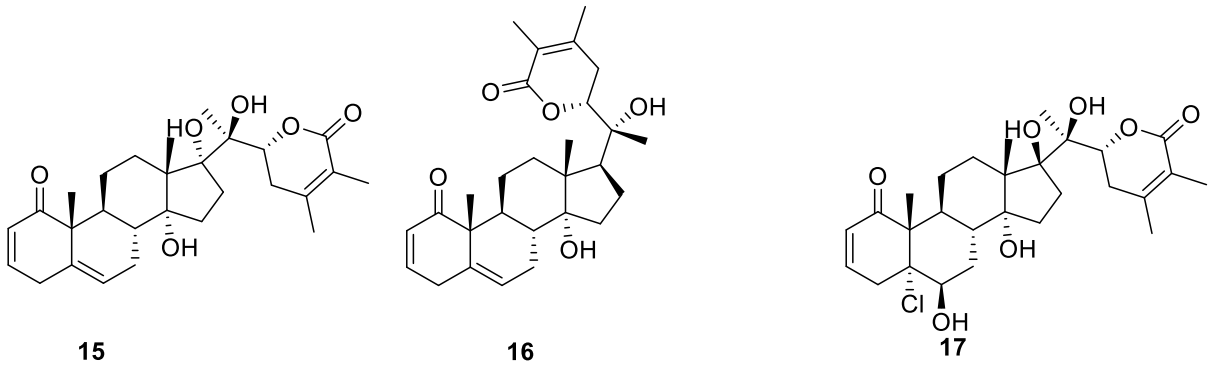

15 **16** **17**

2.3 Compounds isolated from Plants with Potential in Malaria Control

Historically, plants have been very important sources of agents for controlling malaria (Pohlit *et al*., 2011). For example, polysyphorin (**18**) and rhaphidecurperoxin (**19)** isolated from *Rhaphidophora decursiva* (Araceae) showed antiplasmodial properties against *P*. *falciparum* with IC_{50} of 1.5 µM (Pan *et al*., 2018). In addition its compounds, both isolated from the leaves of *Friesodielsia discolor* (Asteraceae), showed antiplasmodial effect against K1 strain of *P*. *falciparu*m, 8-Formyl-7-hydroxy-5-methoxyflavanone (**20**) (IC_{50} 9.3 µM) and tectochrysin (**21**) (IC_{50} 7.8 µM) (Pan *et al*., 2018).

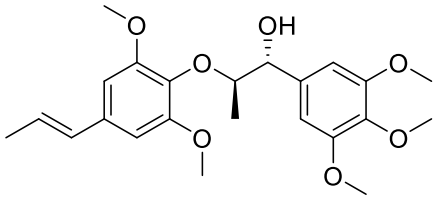

18

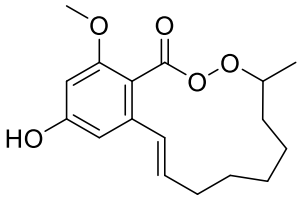

19

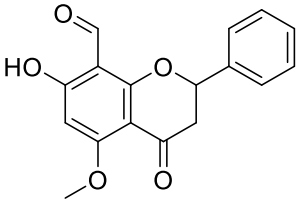

20

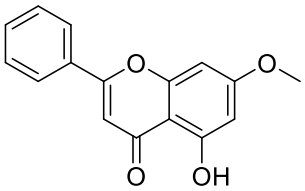

21

Pleiomutinine (**23**) isolated from the roots of *Pleiorcarpa mutica*, had an half-maximal inhibitory concentration of 5 µM against *P. falciparum* (strain K1) (Addae-Kyereme *et al*., 2001). Cajachalcone (**24**) was isolated from *Cajanus cajan* L. (Leguminosae), which has traditionally been used to treat malaria. Cajachalcone (**24**) also exhibited efficacy of (IC_{50} of 7.4 µM) against *P. falciparum* (strain K1) (Pan *et al*., 2018). Secondary metabolites and their derivatives, according to these studies offer a better potential as lead molecules for antimalarial drug development.

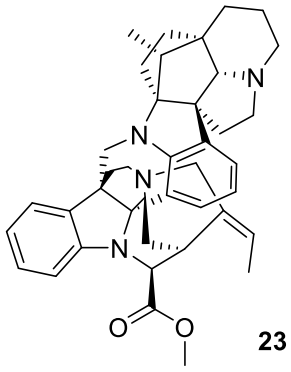

23

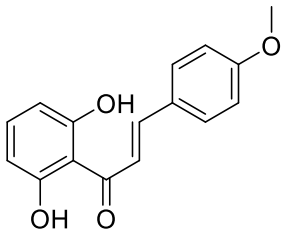

24

2.4 Compounds isolated from Plants with Antibacterial Activities

Flavonoids, tannins, terpenoids, and essential oil components have been documented with significant antibacterial activities (Chassagne et al., 2020; Prasad et al., 2019). Prenylated

flavonoids and phenols isolated from the Leguminosae family have been reported to inhibit the cell wall of bacteria (Chanda *et al*., 2010; Prasad *et al*., 2019).

For example, pseudarflavone A (**25**) and 6-prenylpinocembrin (**26**) isolated from *Pseudarthria hookeri* (Leguminosae), both showed antibacterial effect against *S. aureus* (MIC, 8 µg/mL), and *E. coli* (MIC, 4 µg/mL) (Dzoyem *et al*., 2018).

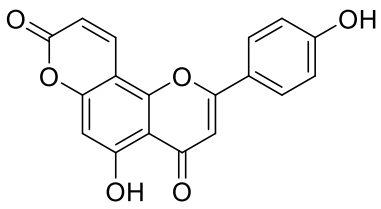

25

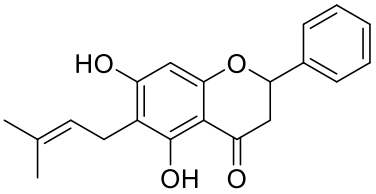

26

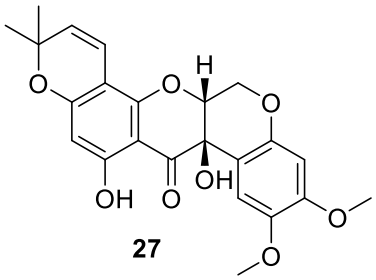

27

12a-Hydroxy-α-toxicarol (**27**) isolated from *Tephrosia toxicaria* Pers (Leguminosae), showed weak antibacterial effect against *S. aureus* (MIC, 256 µg/mL) (Arriaga *et al*., 2017). Alcoholic extract from *T. maxima* (Leguminosae), was reported to be effective against *Helicobacter pylori* infected ulcers (Sandhya, 2018). Glucopyranosyl flavone (**28**) (MIC, 0.34 µg/mL) from alcoholic extract of *T. purpurea* (Leguminosae), inhibited *S. aureus* (Singh *et al*., 2008). Tephrokaempferoside (**29**) (MIC, 150 µg/mL) extracted from the twigs and leaves of *T. preussii* Taub (Leguminosae), showed antibacterial effect against *K. pneumoniae* (Mba Nguekeu *et al*., 2017).

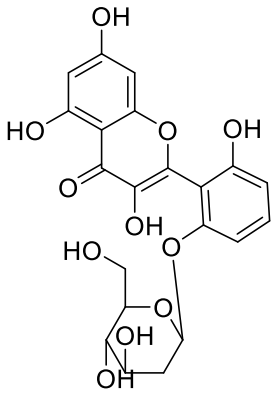

28

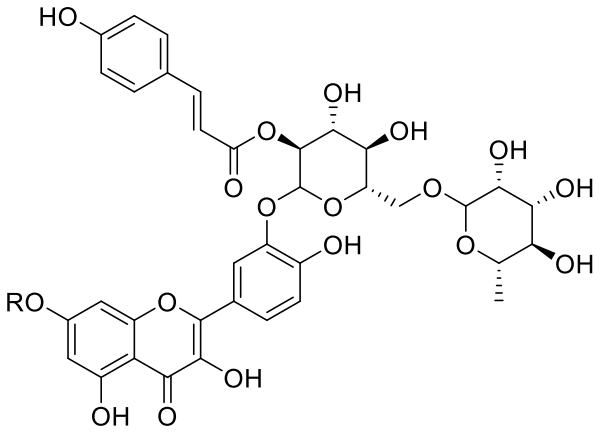

29R= -α-L-rhamnopyranoside

2,4-Dihydroxy-3-(3,7-dimethyl-2,6-octadienyl)benzaldehyde (**30**), isolated from the wood of *Streblus ilicifolius* (Moraceae) exhibited strong antibacterial action (MIC) against methicillin-resistant *S. aureus* (8 µg/mL),, *S. aureus* (8 µg/mL), and *S. epidermidis* (4 µg/mL (Dej-adisai *et al*., 2016). From the leaves of *Canarium patentinervium* (Burseraceae), scopoletin (**31**) (MIC, 25 µg/mL), and scoparone (**32**) (MIC, 50 µg/mL), were effective against *S. aureus* (Mogana *et al*., 2020).

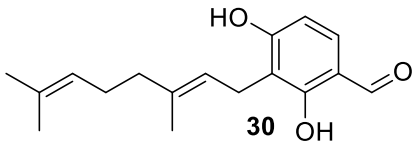

30

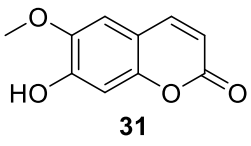

31

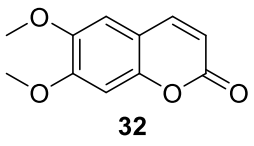

32

2.5 Compounds isolated from Plants with Cytotoxic Activities

Natural products are a rich cradle of bioactive compounds with anticancer activities (Watanabe *et al*., 2011). For example, prenylated flavonoids from Leguminosae and Moracea family have been identified with potential cytotoxicity against cancerous cells (Chen et al., 2014b; Taleghani & Tayarani-Najaran, 2018).

Pseudarflavone A (**25**) and 6-prenylpinocembrin (**26**) isolated from *Pseudarthria hookeri* (Leguminosae), were reported to be cytotoxic against Jurkat (leukemia cells) with IC_{50} of 3.59 and

5.59 µg/mL respectively (Dzoyem *et al*., 2018). Tephrorin A (**33**), tephrorin B (**34**), and tephrosone (**35**) extracted from EtOAc-soluble fraction of *T. purpurea* (Leguminosae), induced quinone reductase in mouse hepatoma cells (Chang *et al*., 2000).

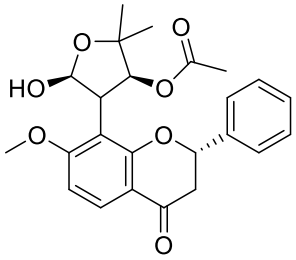

33

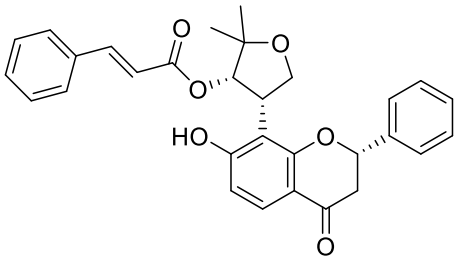

34

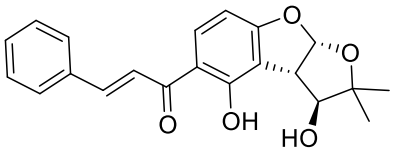

35

Methanolic extract of *T. persica* (Leguminosae), were cytotoxic against brine shrimp with half-maximal inhibitory-concentration of 2.43 µg/mL. The cytotoxicity of chloroform extract was higher, with half-maximal inhibitory-concentration of 1.23 µg/mL (Khalighi-Sigaroodi *et al*., 2012). In an *in silico* experiments of isoquinoline alkaloids; 10,11-dihydroxyerysodine (**36**), 6,7-dihydro-11-methoxyerysotrine (**38**) and, 6,7-dihydro-17-hydroxyerysotrine (**37**) isolated from *Erythrina poeppigiana* (Leguminosae), displayed cytotoxicity against human breast cancer cell lines (Herlina *et al*., 2017).

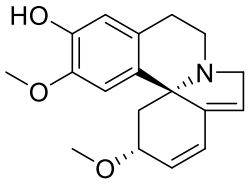

36

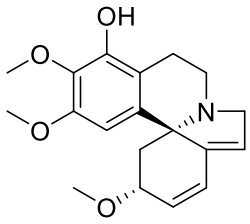

37

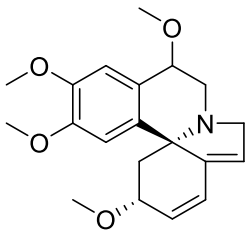

38

Mundulea lactone (**39**), seputheisoflavone (**40**), and seputhecarpan A (**41**), extracted from the root bark of *Ptycholobium contortum* (Leguminosae), exhibited cytotoxicity against lung cancer cell lines with IC_{50} values ranging from 0.59 to 46.70 µM (Ngnintedo *et al*., 2016).

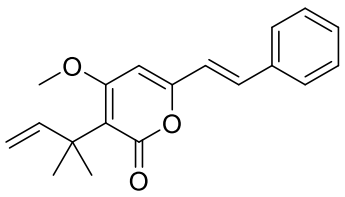

39

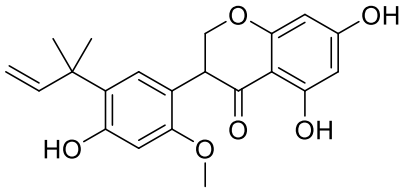

40

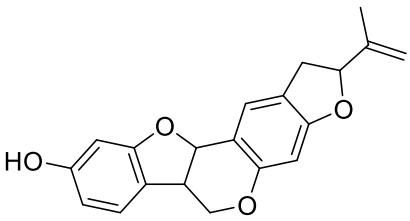

41

2′-De-*O*-methylstrebloside (**42**), 5-de-*O*-hydroxylstrebloside (**43**), and 21-hydroxylstrebloside (**44**) from the roots of *Strebulus asper* (Moraceae), were cytotoxic to A549 lung cancer cells, with half-maximal inhibitory concentration ranging from 0.01 to 0.33 µM (Zhang *et al*., 2021).

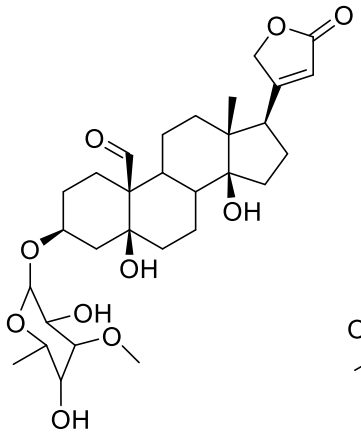

42

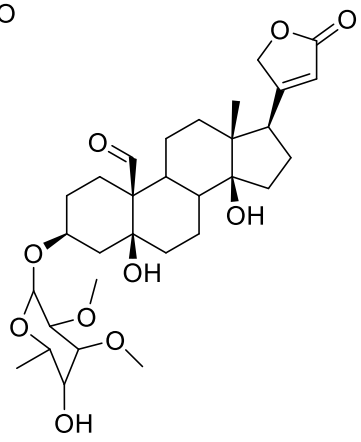

43

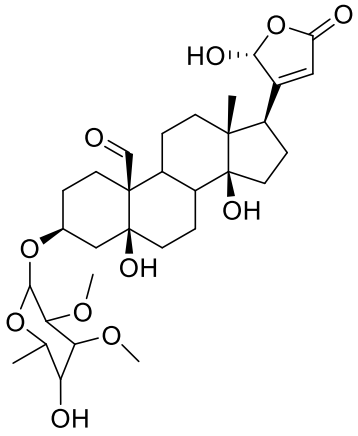

44

Ursolic acid (**9**) extracted from *Ficus exasperata* Vahl (Moraceae), demonstrated cytotoxic efficacy against human colon cancer cell line (HT-29) (IC_{50} of 50.9 µM) and human cervix carcinoma cell line (KB-3−1) (IC_{50} of 34.4 µM) (Popwo Tameye *et al*., 2021).

2.6 Natural Products and the Development of Antiprotozoal Drugs

Plants and their preparationss are still utilized as traditional medicines in developing nations to treat a variety of illnesses (Cortes *et al.*, 2020; Kumar *et al*., 2009). Furthermore, plants have been a source of lead compounds, which led to the development of various pharmaceuticals (Cragg & Newman, 2013; Pan *et al*., 2018). There are various plant metabolites that have inspired the development of antiprotozoal medicines and those that have pharmacological promise.

Quinine (**45**) is an alkaloid extracted from the cinchona tree that has been used to treat malaria (Wright & Phillipson, 1990). In addition, quinine was used as a model in the development of less toxic and more active antiplasmodial drugs such as chloroquine (**46**), primaquine (**47**), and mefloquine (**48**). *In vitro* antiplasmodial activities of berberine (**49**), palmatine (**50**), and jatrorrhizine (**51**) alkaloids contained in several medicinal plants were equivalent to quinine (Bhadra & Kumar, 2011). Artemisinin (**52**) from the *Artemisia annua* plant and its analogs are currently used to treat malaria (Cragg & Newman, 2013).

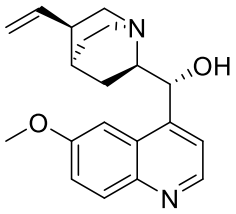

45

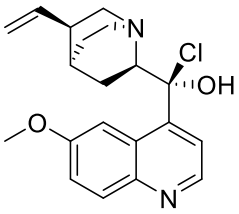

46

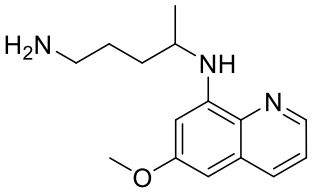

47

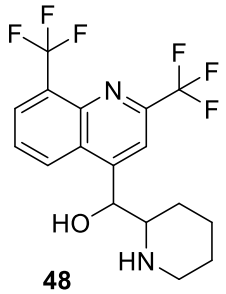

48

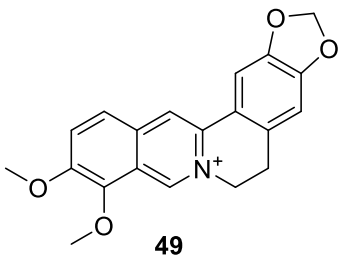

49

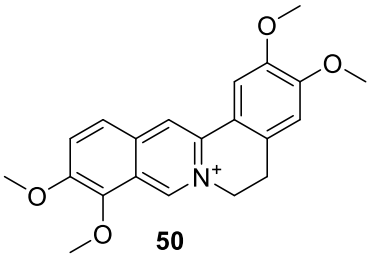

50

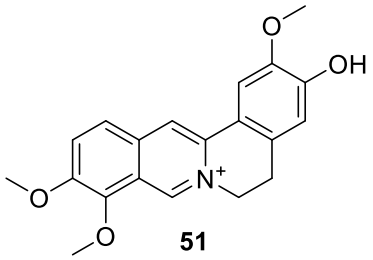

51

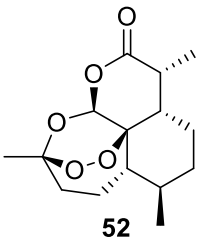

52

For instance, Zhai *et al*. (1995), in their *in vitro* experiments, revealed that licochalcone A (**53**) isolated from the leguminosae family inhibited *L. major* and *L. donovani* promastigotes. Additionally, in their *in vivo* investigations, they revealed that licochalcone A has strong antimalarial activity (Zhai *et al*., 1995). 6-Hydroxy-2-[phenylmethylene]-3(2H)-benzofuranone (**54**) was cytotoxic against promastigotes of *L. infantum*, *L. enriettii*, *L.* donovani, and *L. major* (EC_{50} of 0.45 μg/mL) and amastigote forms of *L. donovani* (EC_{50} of 1.40 μg/mL) (Kayser *et al*., 1999). Argentilactone (**55**) was shown to have the same antileishmanial activity *in vitro* as the reference drug N-methylglucamine antimonite (Rocha *et al*., 2005). Antileishmanial activity was exhibited by chimanine B (**56**), 2-benzoxazolinone (**57**), dictyolamide A (**58**) and, B (**59)**. When compared to pentavalent antimonial medicines, they were less cytotoxic (Rocha *et al*., 2005). Oxylipin (**60**) extracted from *Tridax procumbens* demonstrated potent antileishmanial activity against *L. mexicana* (IC_{50} of 0.478 μg/mL) (Adebayo & Suleman, 2013). The antileishmanial activity (i*n vitro)* of 8-acetyl-13-*O*-ethylpiptocarphol (**61**) was greater than that of amphotericin B, an antifungal antibiotic, against *L. amazonensis* axenic (Adebayo & Suleman, 2013).

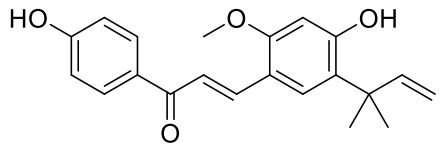

53

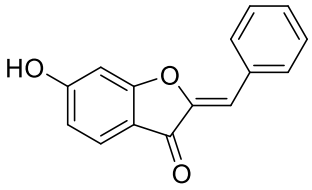

54

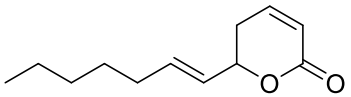

55

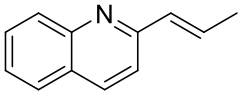

56

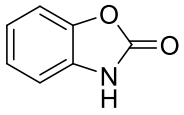

57

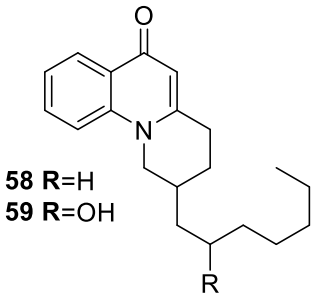

58 R=H
59 R=OH

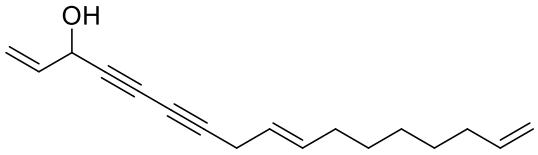

60

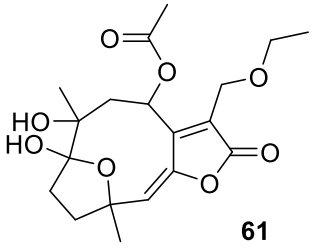

61

2.7 Botanical Information of the Leguminosae and Moraceae Families

2.7.1 The Family Leguminosae

There are approximately 730 genera in the legume family, with over 19,400 species (Wojciechowski *et al*., 2004). It is the third-largest family with diversity in its medical applications (Hira, 2016). Papilionidae, Caesalpinioideae, Dialioideae, Detarioideae, Cercidoideae, and Duparquetioideae are the six subfamilies (Benjamim *et al*., 2020). Alkaloids, flavonoids, coumarins, lignans, anthraquinones and terpenoids are only a handful of bioactive metabolites produced by these families (Benjamim *et al*., 2020; Wink, 2013). The bioactive metabolites have antidiabetic, antileishmanial, antioxidant, anti-inflammatory, anti-wrinkles, antirheumatic,

antimicrobial, antibacterial and cytotoxic activities (Benjamim *et al*., 2020; Hira, 2016; Wu *et al*, 2003).

2.7.1.1 The Genus *Mundulea*

Mundulea belongs to the family Leguminosae and it is widely distributed worldwide (Gangadevi *et al*., 2020). It is found in tropical parts of the world with over 15 species (Langat *et al*., 2012). *Mundulea sericea* is a tiny, slender flowering tree of light bush forests with corky smooth, greenish yellow bark. Leaves are alternate, with uneven number of leaflets (Greenway, 1936). It is found in Angola, Kenya, Madagascar, Namibia, Sudan, Tanzania, Uganda and South Africa (Greenway, 1936).

Figure 2. 2a: leaves and flowers of *Mundulea*

Figure 2. 2b: stems of *Mundulea*

Figure 2. 2c: seed pods of *Mundulea*

Figure 2. 2d: seeds of *Mundulea*

(Bester & Grobler, 2008)

2.7.1.2 The Genus *Tephrosia*

Tephrosia plants are members of the Leguminosae family and are extensively spread in tropical and subtropical regions (Touqeer *et al*., 2013a). In tropical and subtropical regions, the *Tephrosia* genus has more than 350 species, including 30 species found in Kenya (Hegazy *et al*., 2009). *T. uniflora* is found in the Amboseli ecosystem (Ng'ang'a, 2019). *T. uniflora* is a perennial herb, growing from a taproot, it has axillary flowers and small seeds protected by a hard seed coat (Zarina *et al*., 2005).

Figure 2. 3: *T. uniflora* plant parts (Hyde *et al.*, 2021)

2.7.2 The Family Moraceae

There are roughly 60 genera in the Moraceae family, with about 1,400 species found in tropical and subtropical regions (Clement & Weiblen, 2009; Rahman & Khanom, 2013). Artocarpeae R. Br, Castilleae Berg, Dorstenieae Gaudich, Ficeae Gaudich, and Moreau Gaudich are the five tribes (Zerega *et al*., 2005). *Ficus*, *Morus*, and *Artocarpus* are the most phytochemically researched genera, which are widely exploited for their economic and traditional medicinal value (Abdullah

et al., 2017). Phytochemical investigations in diverse plant sections of members of this family have revealed the presence of flavonoids and 2-arylbenzofuran derivatives (Abdullah *et al*., 2017; Kurniadewi *et al*., 2021; Seong *et al*., 2018). Pharmacological studies on the family's plant extracts have proven their value as antioxidants, tyrosine kinase inhibitors, antibacterial, anti-viral, antifungal and anticancer agents (Daud *et al*., 2017; Sun *et al*., 2017).

2.7.2.1 The Genus *Strebulus*

Strebulus is a genus of small deciduous shrub of the Moraceae family with around 25 species found in tropical regions, such as India, Malaysia, South Africa, Thailand, and Philippines (Kinghorn *et al*., 2016; Ren *et al*., 2016). *Strebulus usambarensis* is an evergreen shrub, its bark is smooth and brown. It is found in Guinea, coastal region of Kenya, south of Nigeria, Mozambique and Tanzania, (Adem, 2019; Byng, 2004). *Strebulus usambarensis* has been renamed *Sloetiopsis usambarensis*, because the two different names refered to the same plant according to Mm (2020).

Figure 2. 4: *S. usambarensis* plant parts (Burrows & Burrows)

2.8 Ethnomedical Information of Plants of Leguminosae and Moraceae Family

2.8.1 The Genus *Mundulea*

Mundulea is used in traditional medical practices all over the world. *Mundulea sericea* bark, leaf, root, and seed extracts are utilized as a fish toxin and to suppress budworm in tobacco (Kiania et al., 2014; Mazimba et al., 2012b) Insecticides and pesticides are made from the dust of *M. sericea's* stem bark (Luyengi *et al.*, 1994). The roots of *M. sericea* are used to treat stomach aches (Stark *et al*., 2013). *M. sericea* has been proven to have potential insecticidal properties against a variety of insects and pests found in storage products (Pentsil *et al*., 2017). Branches are used as toothbrushes in Namibia to prevent dental decay (Bester & Grobler, 2008).

2.8.2 The Genus *Tephrosia*

Tephrosia species are widely dispersed and utilized in herbal therapy for a variety of ailments, including stomach aches, diarrhoea, asthma, inflammation and respiratory problems (Atilaw et al., 2017a; Touqeer et al., 2013b). The following are some of the ethno-medical applications that have been documented. Ulcers are treated using the aerial portions of *T. calophylla* and *T. maxima* (Sandhya, 2018). The roots of *T. calophylla* are used to cure diarrhoea, bronchitis, boils and acne (Sindhu & Usha, 2017). *T. purpurea* is used as a laxative to cure coughs and chest infections, and to cure liver, spleen, and kidney blockages (Ahmad *et al*., 1999; Hegazy *et al*., 2009). The dried plant parts of *T. purpurea* is used as a laxative and purgative. The seeds and roots are used to cure, leprous wounds, boils and pimples (Hegazy *et al*., 2009). *T. toxicaria* is used as fish poison (Touqeer *et al*., 2013a). *T. uniflora* is used to treat snake bites (Abreu & Luis, 1996).

2.8.3 The Genus *Strebulus*

The stem bark formulations of *S*trebulus *asper* are used to treat filariasis, relieve fever and toothache (Li et al., 2012b; Singh et al., 2015). The leaves of *S. asper* are used to treat inflammations (Sripanidkulchai *et al*., 2009). The roots of *Strebulus asper* are used to treat ulcers, sinus infections, obesity, and as a snake bite antidote (Singh *et al*., 2015). *Streblus ilicifolius* bark is used in the treatment of pimples (Nguyen *et al*., 2021). In India, several parts of the *S. asper* have been utilized in Ayurveda therapy for eye complications, inflammatory swelling, elephantiasis, dysentery, leprosy, cancer, and epilepsy (Rawat *et al*., 2018; Zhang *et al*., 2021). The bark of *Strebulus indicus* is used to treat inflammation, drowsiness, homeostasis, analgesic and rheumatic diseases (He et al., 2017a; He et al., 2017b). *S. zeylanicus* is used to treat fever, toothache, oedema, inflammation, and dysentery (Zhou *et al*., 2020). The roots of *S. usambarensis* are used to treat eye infections and the seeds as a genital stimulant (Byng, 2004).

2.9 Phytochemical Information and Biological Activities of Plants of Leguminosae and Moraceae Families

2.9.1 Phytochemical Information and Biological Activities of *Mundulea* Species

Chalcones, flavanones, flavanonols, rotenoids and terpenoids are the most prevalent secondary metabolites found among *Mundulea* species. The biological activities of metabolites isolated from this genus have also been investigated. The extracts of the bark of *M. chapelieri* were shown to be toxic against cell lines from ovarian cancer (IC_{50} of 11 μg/ml). The most active compounds were tephrosin (**62**) and rotenone (**63**) with IC_{50} ranging from 0.5 to 0.7 μg/mL. Mundulinol (**64**), MS-II (**65**), rotenolone (**66**), isomundulinol (**67**), 3-deoxy-MS-II (**68**), mundulone (**69**) and munetone

(**70**) were cytotoxic with half-maximal inhibitory concentration range from 9- 33 μg/mL (Cao *et al*., 2004).

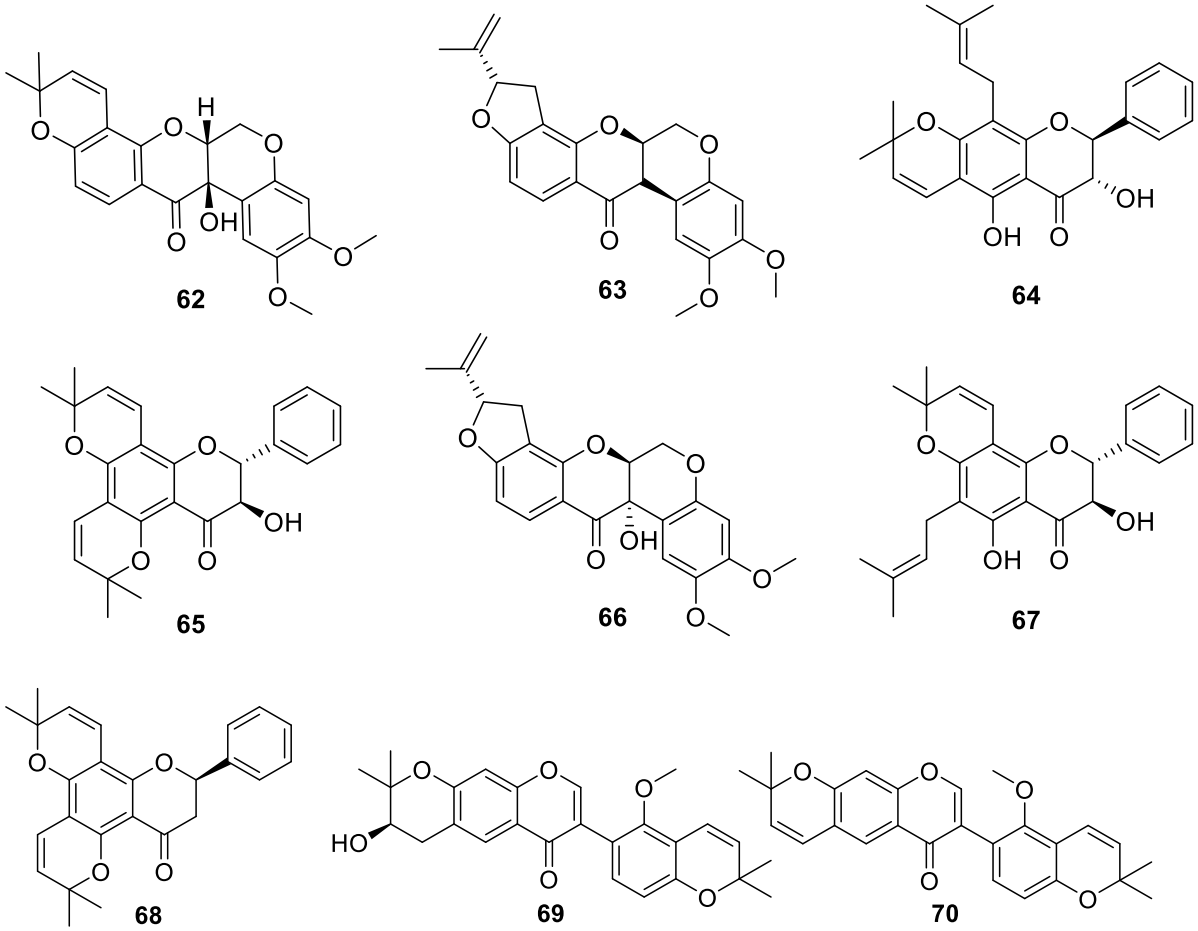

Deguelin (**71**) and rotenone (**66**) extracted from the roots of *M. sericea* inhibited tumours with EC_{50} <1 µg/mL (Baba et al., 2017; Chen et al., 2019; Tringali, 2001). Mundulea lactone (**39**) was cytotoxic against leukaemia cells (IC_{50} 8.84 µM) and breast adenocarcinoma cells (IC_{50} 48.99 µM) (Mbaveng *et al*., 2018).

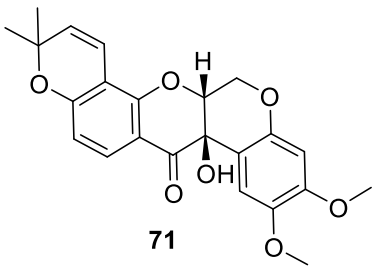

The non-polar leaf extract of *M. sericea* had low efficacy against *B. subtilis*, *E. coli*, and limited antifungal efficacy against *C. albicans* (Mazimba et al., 2012b). Methanol extract of the leaf of *M. sericea* displayed potent antioxidant effect, because of the existence of flavonoids (Khyade & Waman, 2017). The extracts of the bark of *M. sericea* exhibited larvicidal action against *Ae.* Aegypti larvae (4th instar); hexane (LC_{50} of 130 ppm) while methanol had (LC_{50} of 180 ppm) (Langat *et al*., 2012). The seed extracts of *M. antanossarum* had an *in vitro* antiplasmodial action against *Plasmodium falciparum*; the ethanol (IC_{50} of 1.080 μg/mL) and dichloromethane (IC_{50} of 0.215 μg/mL) extracts were also active (Ngbolua, 2016).

13α-Hydroxydeguelin (**72**), 13α-hydroxytephrosin (**73**), munsericin (**74**), and 4-hydroxylonchocarpin (**75**) isolated from the bark of *M. sericea* inhibited tumor formation in cell culture with an IC_{50} value of 0.004, 0.02, 1.0, and 0.7 µg/mL, respectively (Luyengi et al., 1994).

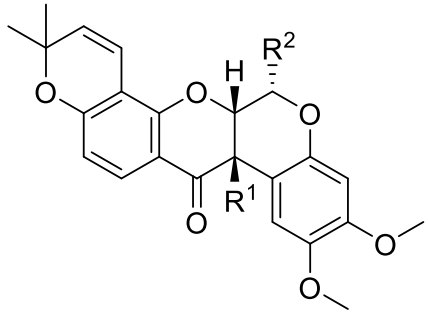

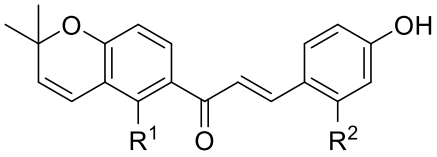

	R^1	R^2
72	H	OH
73	OH	OH

	R^1	**R^2**
74	OH	H
75	H	OH

2.9.2 Phytochemical Information and Biological Activities of *Tephrosia* Species

Tephrosia elaborates a wide variety of rotenoids, flavanones, chalcones and isoflavones with good bioactivities (Chen et al., 2014b; Sindhu & Usha, 2017). The aqueous extracts of the roots of *T. purpurea* had significant anti-ulcer activity (Deshpande *et al*., 2003), whilst the ethanolic extracts

of the aerial parts demonstrated wound healing capabilities (Lodhi *et al*., 2006) and substantial anti-inflammatory effects in rats with sub-acute inflammation (Shenoy *et al*., 2010). In induced diabetes rats, the butanol fraction of *T. purpurea* demonstrated anti-diabetic and pancreatic regeneration effects (Arora *et al*., 2021). *T. maxima* methanol extracts showed significant antibacterial efficacy against *Helicobacter pylori* in, *in vitro* experiments (Sandhya, 2018). Betulinic acid (**76**) isolated from *T. calophylla* proved effective against cancerous and HIV-infected cells, and the methanolic extracts had anti-diabetic properties (Sindhu & Usha, 2017).

The methanol/dichloromethane seed pod extract of *T. elata* inhibited *Plasmodium falciparum*; D6 (IC_{50} 8.4 µg/mL) and W2 (IC_{50} 8.6 µg/mL) strains. It also demonstrated larvicidal efficacy against *Ae. aegypti* (LC_{50} of 68.9 µg/mL) after twenty-four hours (Mutisya, 2014). Aequichalcone A (**77**), aequichalcone B (**78**), aequichalcone C (**79**), obovatachalcone (**80**), praecansone B (**81**) and praecansone A (**82**) were extracted from the roots of *T. aequilata.* They displayed antiplasmodial activities with IC_{50} values ranging from 4.14 µM to 9.75 µM against 3D7 strain (Atilaw et al., 2017a). In an *in vivo* experiment, the EtOAc extract of *T. sinapou* decreased oxidative stress and suppressed cytokine production (Martinez *et al*., 2012).

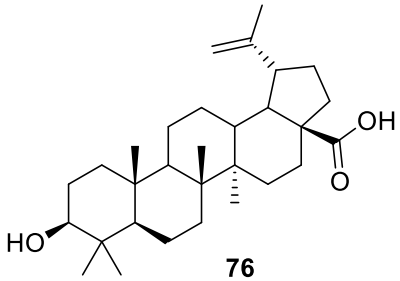

76

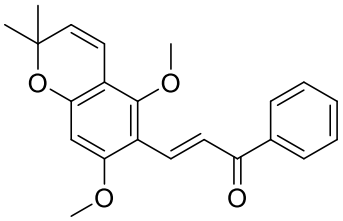

77

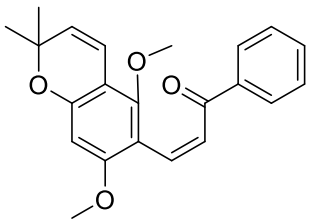

78

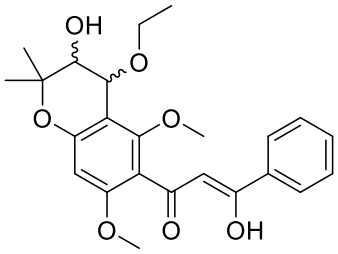

79

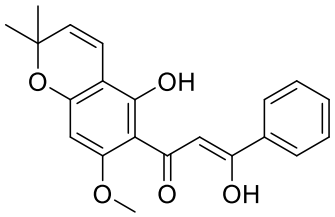

80

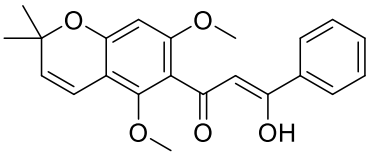

81

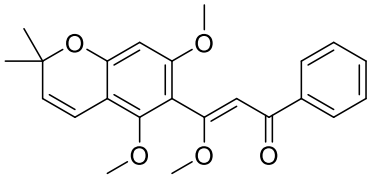

82

Obovatin (**83**) extracted from the *T. toxicaria* displayed a potent antioxidant activity (IC_{50} of 3.370 µg/mL). β-Sitosterol (**84**) reported from *T. purpurea* demonstrated antioxidant activity and lowered high blood cholesterol levels; it also demonstrated cancer-protective properties against prostate, breast and colon cancer (Touqeer *et al*., 2013a). Elatadihydrochalcone (**85**) and obovatin methyl ether (**86**) isolated from the seed pods of *Tephrosia elata* displayed antiplasmodial activity against W2 (IC_{50} of 5.5 µg/mL, 4.4 µg/mL) and D6 (IC_{50} of 2.8 µg/mL, 3.8 µg/mL) strains of *Plasmodium falciparum*, respectively (Mutisya, 2014).

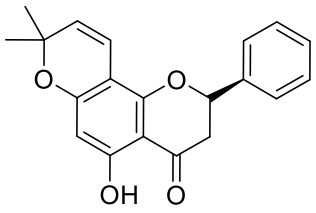

83

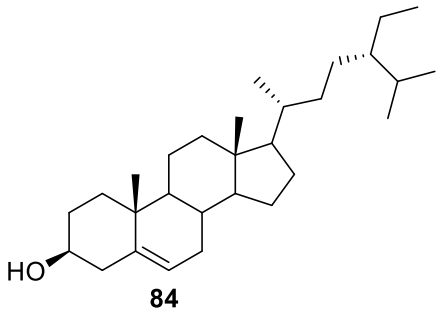

84

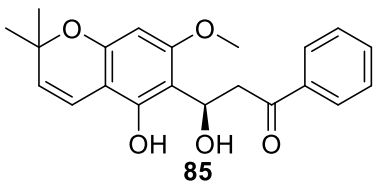

85

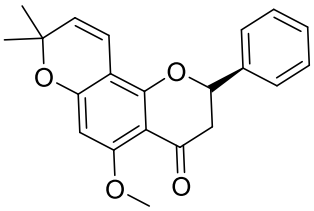

86

β-Sitosterol (**84**), elongatin (**87**), stigmasterol (**88**) and 12a-hydroxyrotenone (**89**) were identified from the roots of *T. uniflora* (Abreu & Luis, 1996). 12a-Hydroxyrotenone (**89**) showed significant toxicity against oral epidermoid carcinoma, breast cancer line, and lung cancer cell, with ED_{50} of 1.6, 0.1, 0.05 µM, respectively (Cheenpracha et al., 2007).

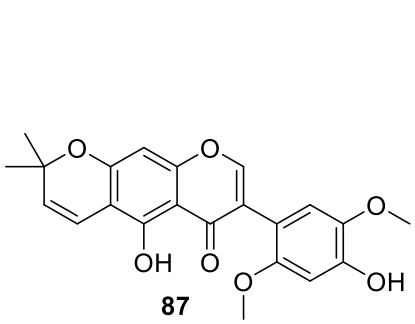

87

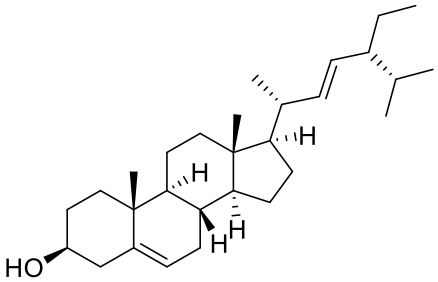

88

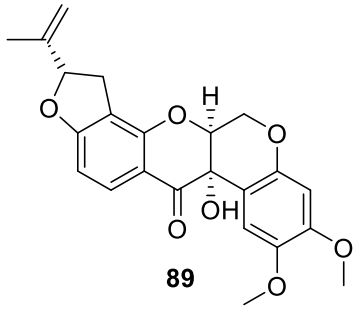

89

2.9.3 Phytochemical Information and Biological Activities of *Strebulus* Species

The genus *Strebulus* elaborates cardiac glycosides, terpenoids, saponins, fatty acids, phytosterol, and lignans (Fiebig *et al*., 2004; Rawat *et al*., 2018; Ren *et al*., 2016). *Strebulus asper* is the only *strebulus* species that has been extensively phytochemically explored.

The cytotoxic components extracted from methanol/dichloromethane stem bark extract of *S. asper* were identified as strebloside (**90**) and mansonine (**91**), with half-maximal inhibitory concentration 0.035 and 0.042 µg/mL in keratin forming tumor cell culture, respectively (Ren *et al*., 2017; Singh *et al*., 2015). *S. asper* methanol extracts exhibited anti-parasitic activity against *Setaria digitata*

(Mathai & Devi, 1995). The essential oils extracted from the leaves of *S. asper*, α-farnesene (**92**), phytol (**93**) and trans-farnesyl acetate (**94**) had considerable cytotoxicity with an ED_{50} of less than 30 µg/mL against lymphocyte leukemia cells (Phutdhawong *et al*., 2004).

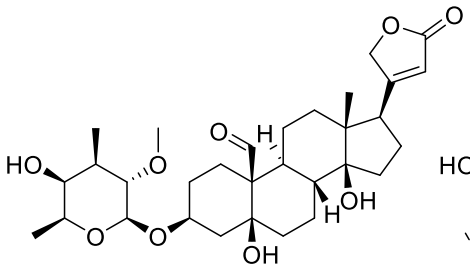

90

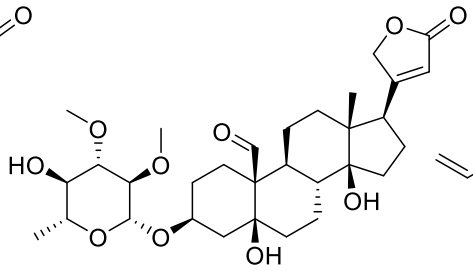

91

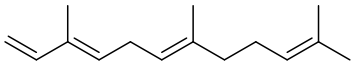

92

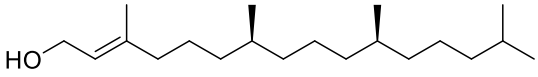

93

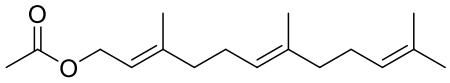

94

6-Hydroxy-7-methoxycoumarin (**95**), ursolic acid (**9**), magnolol (**96**) and 9β-xylopyranosyl-isolariciresinol (**97**) extracted from the heartwood and leaves of *S. asper* inhibited the hepatitis B virus with IC_{50} values of 29.60, 97.61, 2.03, and 6.58 µM, respectively (Li et al., 2012a; Tang et al., 2018). Because of the high phenolic content, the ethanol and aqueous extracts of *S. asper* leaves demonstrated anti-inflammatory and antioxidant properties (Ibrahim *et al*., 2013; Sripanidkulchai *et al*., 2009).

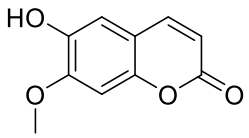

95

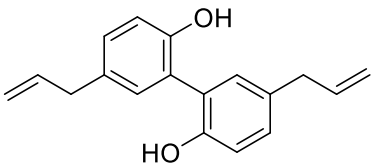

96

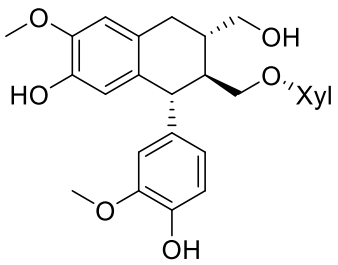

97

Glucopyranosylisoflavone (**28**) extracted from of *S. asper* heartwood showed antibacterial action against *Candida albicans, B. subtilis, S. aureus* and *E. coli* MIC ranging from 0.016 to 0.064 µg/mL (Ji-Guo *et al*., 2012). Asperoside (**98**) and strebloside (**90**) obtained from *S. asper* stem bark displayed antifilarial action towards *L. carinii* (Rastogi *et al*., 2006).

The heartwood of *S. asper* has been shown to contain lignans, magnolignan A-2-*O*-β-D-glucopyranoside (**99**), magnaldehyde D (**100**), magnolignan A (**101**), streblusligna nol (**102**) and magnolol (**96**) are a few examples. Magnolignan A-2-O-β-D-glucopyranoside (**99**) and streblusligna nol (**102**) induced apoptosis in human liver and laryngeal cancer cell lines with IC_{50} values ranging from of 10.1 to 46.4 µM. (Li *et al*., 2008).

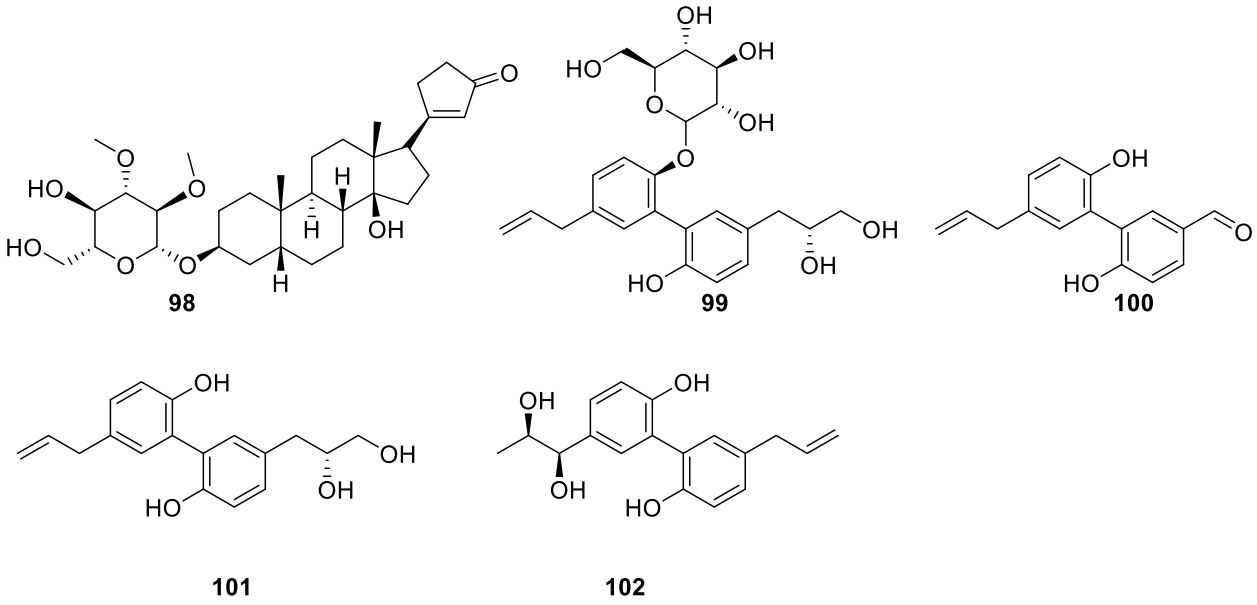

The extracts of *S. asper* stem yielded lignans and allylbenzene derivatives, including streblusol D (**103**), streblusol A (**104**), streblusol E (**105**), streblusquinone (**106**), erythrostreblusol B (**107**), threostreblusol B (**108**), streblusol C (**109**), magnolol (**96**) and, 9β-xylopyranosylisolariciresinol (**97**). Magnolol (**96**) demonstrated anti-HBV effect against both HBsAg (IC_{50}, 2.03 µM) and HBeAg (IC_{50}, 3.76 µM) against the hepatitis B virus (Li et al., 2012a).

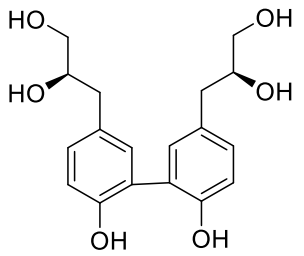

103

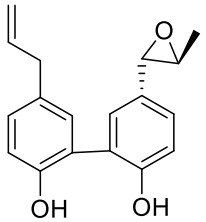

104

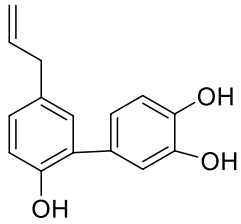

105

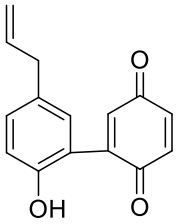

106

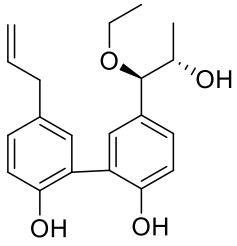

107

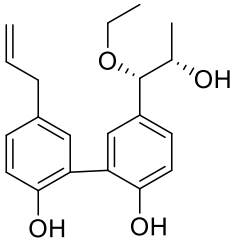

108

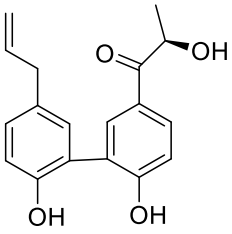

109

Literature survey has revealed that the metabolites from the plants *Mundulea*, *Tephrosia* and *Strebulus* have a diversity of biological activities. The most prevalent activities being cytotoxicity against ovarian, leukemia, breast, prostate, colon, keratin, lung, liver, and laryngeal cancer cell lines. Antibacterial action against a variety of bacteria is also documented. Flavonoids have shown strong antibacterial and cytotoxic properties due to their numerous interactions with a variety of cellular targets (Dzoyem *et al*., 2018). Their antibacterial effect is because of their capability to hinder bacteria's DNA synthesis, metabolism and membrane development (Prasad *et al*., 2019). Antiplasmodial and antileishmanial activities of flavonoids against different strains of the parasites is also predominant. As a result, the antibacterial, antileishmanial, antiplasmodial, and cytotoxicity properties of isolated metabolites from the *Mundulea*, *Tephrosia* and *Strebulus* species, have been evaluated in this study.

CHAPTER THREE

MATERIALS AND METHODS

3.1 Plant Materials

The plant materials were collected as detailed in (Table 3.1). The plant materials were identified by Mr. Pactrick C. Mutiso of the University of Nairobi Herbarium, Department of Biology, where a voucher specimen was stored (Table 3.1)

Table 3.1: Plant collection details

Plant species	Plant part	Place collected	Date	Voucher number
Mundulea sericea	Leaves and roots	Coastal area	July 2017	PCM-2017/23
Strebulus usambarensis	Stem and roots	Gondoni forest	July 2016	PCM-2016/008
Tephrosia uniflora	Stems	Emali-Loitokitok road, Makueni County	July 2016	PCM-2016/010

3.2 General Experimental Procedure

Q-TOF-LC/MS spectrometer at AB Lab, Gothenburg, Sweden was used to obtain HRESI-MS. A SHIMADZU UV-Vis spectrophotometer was used to obtain UV spectra. A Bruker-Avance-NEO 500 MHz spectrometer was used to obtain NMR spectra. MestreNova (v14.0.0) software was used to process the spectra. Residual solvent signals were used as reference. TLC analyses were carried on Merck pre-coated silica gel 60 F_{254} aluminum plates. Preparative reversed-phase High Performance Liquid Chromatography experiments were performed on a Waters 600E system with Chromulan v. 0.88 (Pikron Ltd) software. Column chromatography was done on Sephadex LH-20 (GE Healthcare) and silica gel 60 (230–400) mesh.

3.3 Extraction and Isolation of Secondary Metabolites

3.3.1 Isolation of Secondary Metabolites from the Roots of *Strebulus usambarensis*

Ground roots of *Strebulus usambarensis* (900 g) were extracted (4 x 1L) with CH_2Cl_2/MeOH (1:1) at room temperature to yield a crude extract (98.8 g) after concentration. The crude extract was adsorbed on silica gel, loaded onto a 500 g column, followed by elution with *iso*-hexane containing increasing amounts of EtOAc (1% to 80% v/v). According to their TLC profiles, the eluents were pooled into 21 fractions. Three fractions that were eluted with 3% EtOAc were washed separately with *iso*-hexane, giving compound **112** (14 mg) as white amorphous solid, compound **110** (25 mg) as white crystals, and compound **122** (19 mg) as colourless solids, respectively. Fraction that was eluted with 5% EtOAc was subjected to Prep-HPLC (methanol-water, gradient elution 5%-95% H_2O) giving compound **117** (6 mg) as white solid. Fraction that was eluted with 8% EtOAc was further purified using preparative HPLC (methanol-water, gradient elution 5%-95% H_2O) yielding compound **111** (8 mg) as a white paste and compound **115** (7 mg) as white amorphous solid. Fraction that was eluted with 15% EtOAc was purified using preparative HPLC (methanol-water, gradient elution 5%-95% H_2O) to give compound **124** (10 mg) as white solid.

3.3.2 Isolation of Secondary Metabolites from the Stems of *Strebulus usambarensis*

Ground stems of *Strebulus usambarensis* (965 g) were extracted with CH_2Cl_2/MeOH (1:1) at room temperature. The crude extract (91.2 g) was partitioned between H_2O and EtOAc. The EtOAc layer was concentrated on a rotary evaporator to give crude extract (45.0 g). The EtOAc extract was adsorbed on a silica gel, loaded onto a 500 g column, followed by elution with *iso*-hexane containing increasing amounts of EtOAc (1 to 99% v/v). The eluents were then pooled into 24

fractions. Fraction that was eluted with 5% ethyl acetate was subjected to CC over Sephadex (eluting with CH_2Cl_2/MeOH , 1:1) to yield compound **121** (17 mg) as colorless needles. Fractions that were eluted with 8% EtOAc were subjected to CC over Sephadex (CH_2Cl_2/MeOH, 1:1), followed by purification on Prep-HPLC (methanol-water, gradient elution 5%-90% H_2O) giving compound **114** (21 mg) as white crystals and compound **116** (9 mg) as white solid. Fraction that was eluted with 8% EtOAc was subjected to Sephadex (CH_2Cl_2/MeOH, 1:1) and further purification on Prep-HPLC (methanol-water, gradient elution 5%-90% H_2O) to provide compounds **120** (6 mg) as a white solid and **125** (9 mg) as a white solid. Fraction that was eluted with 10% EtOAc was subjected to CC over Sephadex (CH_2Cl_2/MeOH, 1:1) and further purification on Prep-HPLC (methanol-water, gradient elution 5%-90% H_2O) to give compounds **119** (6 mg) as a white paste and **123** (8 mg) as a white paste. Fraction that was eluted with 15% EtOAc was purified by preparative HPLC (methanol-water, gradient elution 5%-90% H_2O) to give compound **113** (10 mg), and compound **118** (9 mg).

3.3.3 Isolation of Secondary Metabolites from the Leaves of *M. sericea*

Ground leaves of *Mundulea sericea* (835 g) were extracted with CH_2Cl_2/MeOH (1:1) at room temperature to yield a crude extract (113.8 g). The crude extract was adsorbed on silica gel, loaded onto a 500 g column. The column was eluted with *n*-hexane containing increasing amounts of EtOAc (1% to 80% v/v). The eluent was divided into 20 fractions. The fraction obtained from two-percent ethyl acetate in *n*-C_6H_{14} gave compound **127** (20 mg) as a white amorphous solid after further purification on a 50g column, and eluted with *n*-hexane containing increasing amounts of EtOAc (1% to 99% v/v). The fraction obtained from 3% EtOAc in *n*-hexane gave compound **70** (16 mg) as a yellow paste after washing with *n*-hexane. The obtained from four-percent EtOAc in

n-hexane gave compound **63** (17 mg) as yellow crystals that were recrystallized from CH_2Cl_2/*n*-hexane. The fraction eluted with 10% EtOAc in *n*-hexane gave compound **129** (22 mg) as a white amorphous solid after further purification on a silica gel (50 g) column, and eluted with *n*-hexane containing increasing amounts of EtOAc (1% to 99% v/v). The fraction eluted with 75% EtOAc in *n*-hexane provided compound **128** (10 mg) as yellow amorphous solid after further purification on a Sephadex (Methanol/ dichloromethane, 1:1) column.

3.3.4 Isolation of Secondary Metabolites from the Roots of *Mundulea sericea*

Ground roots of *Mundulea sericea* (965 g) were extracted (4 x 1 liters) with dichloromethane/ methanol (1:1) at room temperature to yield a crude extract (91.2 g) after concentration on a rotary evaporator. The crude extract was adsorbed on silica gel, loaded onto a 500 g column, followed by elution with *n*-hexane containing increasing amounts of EtOAc (1% to 99% v/v) and the eluents were pooled into 24 fractions. The fraction obtained from six % ethyl acetate in *n*-hexane gave compound **64** (30 mg) as colorless crystals after further purification on a 50 g column, and eluted with *n*-C_6H_{14} containing increasing amounts of CH_2Cl_2 (1% to 99% v/v). The fraction obtained from six-percent ethyl acetate in *n*-hexane gave compound **130** (17 mg) as white solid after further purification on Preparative TLC eluting with *n*-hexane/EtOAc (7:3). The fraction from 8% ethyl acetate in *n*-hexane gave compound **131** (10 mg) as a white solid after further purification on PTLC with *n*-hexane/EtOAc (7:3). The fraction eluted with fifteen-percent ethyl acetate in *n*-hexane gave compound **132** (10 mg) as a white solid and compound **88** (10 mg) after further purification on PTLC with *n*-hexane/EtOAc (7:3).

3.3.5 Isolation of Compounds from the Stems of *Tephrosia uniflora*

Ground stems of *T. uniflora* (500 g) were extracted with CH_2Cl_2/MeOH (1:1) at room temperature. The crude extract (60 g) was partitioned between water and ethyl acetate. The ethyl acetate layer was concentrated to yield a crude extract (30 g). The crude extract was adsorbed on silica gel, loaded onto a silica gel (300 g) column, and eluted with *iso*-hexane containing increasing amounts of EtOAc (1% to 99% v/v). According to their TLC profiles, the eluents were then pooled into 15 fractions. Fraction obtained from 3% ethyl acetate was subjected to Prep-HPLC (methanol-water, gradient elution 5%-95% H_2O) to yield compound **133** (20 mg) as a white amorphous solid. Fraction that was eluted with 3% EtOAc was subjected to Sephadex (methanol/dichloromethane, 1:1), and further purification on Preparative TLC (*iso*-hexane/EtOAc (7:3) to yield compound **87** (8 mg). Fraction obtained from five percent ethyl acetate was further purified on preparative HPLC (methanol-water, gradient elution 5%-95% H_2O) to give compound **85** (10 mg) and compound **123** (12 mg) as white solids.

3.4 In vitro Antiplasmodial Assay

The antimalarial reference drugs alongside pure compounds and crude extracts were tested for antiplasmodial activity against chloroquine resistant (W2) and chloroquine sensitive (3D7) clones using established protocol (Rama et al., 2015b; Smilkstein et al., 2004a) to raise fluorescence of stained nucleic acids and enhance assay sensitivity. Briefly, the components of the lysis buffer were adjusted and the amount of the SYBR Green stain increased as described by Cheruiyot *et al*. (2016) .

3.5 Antibacterial Assays

The crude extracts and major compounds **87**, **110**, **111**, **113**, **114**, **119**,**120** and **122** were assessed for antibacterial assay against *E. coli* and *B. subtilis* bacterial strains based on procedures described by Kalenga *et al*. (2021). Initially, each sample was dissolved in DMSO to constitute 10 mg/mL and subsequently kept at -20 °C.

The culturing of bacterial strains followed the standard protocols described by Muller *et al*. (2004), with minor modifications. Briefly, bacterial cultures were allowed to grow in Mueller-Hinton broth for 24 hours to an optical density (O.D) = 0.5 (λ=540nm). A 10-fold dilution of the broth bacterial suspension was then performed. The samples were incorporated into the medium to constitute a concentration of 35 μg /mL. A100 μL portion of pre-warmed medium with the samples were introduced into a ninety-six micro plate well, incubated at 37 °C without shaking, for twenty –four hours.

The resazurin assay for assessing viability was then performed as described by Sarker *et al.* (2007). Consequently, 10 μL of Alamar Blue staining solution was introduced per well continuously for 1 h at a constant temperature of 37 °C. The fluorescence emitted by the viable cells was determined using POLARstar Omega (BMG Labtech, Cape Town, S.A) set at excitation λ=540 nm and emission filter λ=590 nm. As a positive control, a standard antibiotic, ampicillin, was used while DMSO was both utilized as a negative control solvent and in dissolving the test substances. The bleed-through between the wells was controlled by leaving an empty well in-between (thus 384-well plates were considered for this purpose). These assays were performed in triplicates. Minimum Inhibitory Concentrations (MIC) and Effective Concentrations (EC) were determined using EC_{90} calculator webtool (AAT Bioquest, Inc) and the Quest Graph EC_{50}.

3.6 Antileishmanial Assay

Antileishmanial activity and anti-proliferative effect of compounds **88**, **128** and **130** was evaluated against antimony-sensitive *L. donovani* (MHOM/IN/83/AG83) and antimony-resistant *L. donovani* (MHOM/IN/89/GE1**)** using established protocols (Dey *et al*., 2015).

For AG83, promastigotes were generated from infected BALB/c mice's splenic intracellular amastigotes in a complete M199 medium (Invitrogen) supplemented with 1% penicillin-streptomycin (Invitrogen) and 10% FCS (GIBCO) at 22^{o}C. The MTT assay micro technique was used to calculate the percentage of inhibition (Dey *et al*., 2015; Dutta *et al*., 2005; Yousuf *et al*., 2016). Briefly, the promastigotes cultures were cultured for forty-eight hours in a ninety-six well plate (200 µL per well, BD Falcon) in a complete M199 medium with or without (control) the selected compounds in increasing concentrations. An equal volume of DMSO was added in control experiments. After 48 hours of incubation, MTT (5 mg/mL, 20 µL per well) was applied to each well, and the plate was incubated for another 4 hours at 37^{o}C. After stopping the reaction with acidified isopropanol (C_3H_8O) (0.4 mL of 10 N hydrochloric acid in 100 mL C_3H_8O, 100 L each well), the absorbance at 595 nm was measured. The plots of percent inhibition versus increasing concentrations were used to calculate the 50% inhibitory concentrations of the test samples.

The cytotoxic effects of compounds **64**, **88**, **127**, **128**, **129** and **130** were also evaluated on RAW 264.7 cells in comparison to the reference drug (Miltefosine). Nitric Oxide generation was assayed by using Griess reagent as described by Dutta *et al*. (2005) with minor modifications. Briefly, for the estimation of nitric oxide (NO) in RAW 264.7 cells, cells supernatants were collected and distributed (100 µL per well) in 96-well plates, and an equal volume of Griess reagent was added per well, incubated at 37^{o}C for 15 minutes, and the absorbance at 540 nm was determined using

microplate reader (Green *et al*., 1990). For each compound, three or more independent trials were carried out in triplicate. All experiments were statistically analysed using one-way ANOVA, and a post hoc Holm-Sidak analysis using Sigma Plot software (version 11.0) (Yousuf *et al*., 2016).

3.7 Cytotoxicity Assay

3.7.1 *Mundulea sericea*

The cell-lines A549, HepG2, and non-tumor cells (BEAS-2B and LO2) were all purchased from ATCC. Cells were cultured in Roswell Park Memorial Institute as described by Atilaw et al. (2017b) .

The cytotoxicity of compounds **64**, **88**, **127**, **128**, **129** and **130** was evaluated against immortal human hepatocytes (LO2), human lung adenocarcinoma cell line (A549), lung/bronchus cell line (epithelial virus-transformed) (BEAS-2B), and human liver cancer cell line (HepG2). Before usage, all the samples were dissolved in dimethyl sulfoxide (50 mmol/L) and kept at -20°C. The MTT (5.0 mg/mL) assay was used to determine cytotoxicity, as previously described by Coghi *et al*. (2018). Briefly, 4, 000 cells were seeded in ninety-six-well plates per well and cultured overnight. For the next 72 hours, varied concentrations of selected compounds were added to the cells with dosage ranging from 0.039–100 µM/L. Subsequently, 10 µL of diphenyltetrazolium bromide solution was introduced per well and incubated at 37ºC for four hours before addition of 100 µL of SDS (10%)–HCl (0.01M) buffer and incubating overnight. Cells without selected compounds were used as controls. The absorbance of each well was then determined the next day using a wavelength of 570 nm. The following formula was used to compute the percentage of cell viability:

$$Cell\ viability\ (\%) = Absorbance_{treated} / Absorbance_{control} \times 100$$

The standard error was calculated from the data obtained from three replicate experiments.

3.7.2 *Strebulus usambarensis* and *Tephrosia uniflora*

The MCF-7 cells were used to evaluate the cytotoxic effect of compounds **87**, **110**, **111**, **113**, **114**, **119**,**120**, **122** and crude extracts, following the protocol by Koudokpon *et al*. (2018). Briefly, the cells were cultured and kept in exponential growth in a modified medium, as described by Umereweneza *et al*. (2021).

PrestoBlue was used to determine the cell viability (ThermoFisher) for a twenty-four-hour incubation period as per the manufacturer's recommendations. The fluorescence from resorufin was determined and measured using POLARstar Omega (BMG Labtech, Cape Town, S.A) set at excitation λ=540 nm and emission filter λ=590 nm. Cell viability, EC_{90} and EC_{50} values for each compound were determined as described by Umereweneza *et al*. (2021).

CHAPTER FOUR

RESULTS AND DISCUSSION

Strebulus usambarensis (Moraceae), and *Mundulea sericea* (Leguminosae) and *Tephrosia uniflora* (Leguminosae) were investigated for their phytochemicals. Some of the metabolites isolated from these plants were tested for their antiplasmodial, antileishmanial, antibacterial and cytotoxicity activities. In this chapter, the structural elucidation and biological activity of these compounds are discussed.

A total of thirty-one compounds, including 13 new compounds, were isolated and characterized. These includes, three novel naphtho-benzofuran derivatives, [usambarins A (**110**), B (**111**), C (**112**)]. Seven novel naphthalene derivatives, [usambarins D (**113**), E (**114**), F (**115**), G (**116**), H (**117**), I (**118**) and M (**126**)], a novel phenyl-1-benzoxepin derivative (**120**), two novel flavans [**119** and **126**], two coumarins [**121** and **122**], a rotenoid (**123**), and cinammic acid derivative (**125**) from *Strebulus usambarensis.* Three flavanonols [**127- 129**], two flavanols [**64** and **130**], an isoflavone (**70**), a rotenoid (**63**), two pterocarpans[**131** and **132**], and a sterol, stigmasterol (**88**) from *Mundulea sericea.* Two β-hydroxydihydrochalcones [**87** and **133**], an isoflavone (**81**), and a rotenoid (**89**) from *Tephrosia uniflora*.

4.1 Compounds isolated from the Roots and Stem of *Streblus usambarensis*

Extraction and chromatographic separation of *Streblus usambarensis* roots resulted in the isolation of usambarin A (**110**), B (**111**), C (**112**), G (**116**), I (**118**), bergaptol (**122**), and ferulic acid (**124**). Similar investigation of the stem of this plant yielded, usambarin D (**113**), E (**114**), F(**115**), H

(**117**), J (**119**), L (1**25**), and two flavans [**119** and **126**], phenyl-1-benzoxepin derivative (**120**), bergapten (**121**), and 12a-hydroxydeguelin (**123**).

4.1.1 Usambarin A (110)

Compound **110** was obtained as white crystals. It was given a molecular formula $C_{23}H_{22}O_4$ from HREIMS $[M+1]^+$ peak *m/z* 363.1596 and NMR (Table 4.1). The UV (λ_{max} 270, 310 nm), NMR data (Table 4.1), (Appendix 1A-1K) and X-ray diffraction data (Figure 4. 1) showed a presence of a naphtho[1,2-b]benzofuran skeleton (Adem, 2019). The NMR data further indicated the existence of two methoxy, a hydroxy, and a dimethylallyl substituents (Table 4.1).

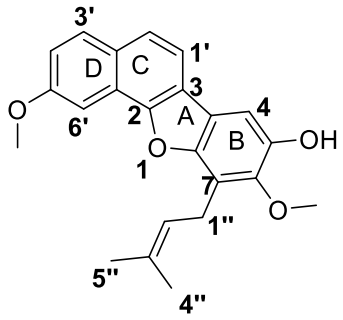

110

In the ^{1}HNMR spectrum, ring D exhibits an AMX spin designation at δ_H 8.02 (*d, J* = 8.9 Hz, H-3'), 7.60 (*d*, *J* = 2.6 Hz, H-6') and, 7.25 (*dd*, *J* = 8.9, 2.6 Hz, H-4'), with their carbons resonating at δ_C 130.3 (C-3'), 98.7 (C-6') and 117.9 (C-4'), requiring a substituent (methoxy) at C-5'. The location of the methoxy at C-5' (δ_C 157.3) of ring D was established by HMBC and NOESY experiments (Table 4.1). Ring C, contained *ortho* correlated protons appearing at δ_H 7.91 and δ_H 7.78 (*d, J* = 8.4 Hz, H-1'/H-2') with corresponding carbon appearing at δ_C 116.1 (C-1') and 122.8 (C-2').

Ring B is trisubstituted with a hydroxy, a methoxy, and γ,γ-dimethylallyl groups, with the only aromatic proton appearing at δ_H 7.40 (*s* H-4, δ_C 103.9). Using HMBC correlation (Table 4.1); the

hydroxy (δ_H 9.37) group was placed at C-5 (δ_C 147.3) due to its correlation with C-4 and C-5; the γ,γ-dimethylallyl group was placed at C-7 (δ_C 118.9) due to the correlation of the signal at δ_H 3.71 (H-1") with C-6 and C-7; and the methoxy group was then placed at C-6 (δ_C 145.5). X-Ray crystallography was used to confirm the structure of this compound (Figure 4. 1). Therefore, compound **110** was characterized as 6,6'-dimethoxy-7-prenylnaphtho[1,2-b]benzofuran-5-ol, which is a new compound, and named usambarin A.

Table 4.1: NMR data for usambarin A (**110**) in DMSO-d6

No	**^{1}H NMR (δ_H)** (J in Hz)	**^{13}C NMR (δ_C)**	**HMBC (H→C)**	**NOESY**	**TOCSY**
2	-	150.7	-	-	-
3	-	119.8	-	-	-
3a	-	119.3	-	-	-
4	7.40 *s*	103.9	C-3a,C-5, C-6	5-OH	-
5	-	147.3	-	-	-
6	-	145.5	-	-	-
7a	-	147.8	-	-	-
7	-	118.9	-	-	-
1'	7.91 *d* (8.4)	116.1	C-2, C-3a, C-2', C-2'a,	-	-
2'	7.78 *m*	122.8	C-2 C-3, C-1',, C-2'a, C-3', C-6'a	-	-
2'a	-	127.3	-	-	-
3'	8.02 *d* (8.9)	130.3	C-2', C-2'a,C-5', C-6'a	-	H-4'
4'	7.25 *dd* (8.9, 2.6)	117.9	C-2'a,C-5', C-6'	5'-OMe	H-3'
5'	-	157.3	-	-	-
6'	7.60 *d* (2.6)	98.7	C-2, C-2'a, C-4', C-5'	H-4", 5'-OMe	-
6'a	-	121.6	-	-	-
1"	3.71*d* (7.5)	22.8	C-6, C-7, C-7a, C-2", C-3"	H-4", H-2"	-
2"	5.37 *m*	122.1	C-1", C-4", C-5"	5", 1"	-
3"	-	131.5	-	-	-
4"	1.97 *m*	17.1	C-2", C-5"	H-1", H-6'	-
5"	1.71 *d* (1.6)	24.9	C-2", C-4"	H-2''	-
5-OH	9.37 *s*	-	C-4,C-5, C-6	6-Ome, H-4	-
5'OMe	3.99 *s*	54.7	C-5'	H-4', H-6'	-
6-OMe	3.85 *s*	59.9	C-6	5-OH	-

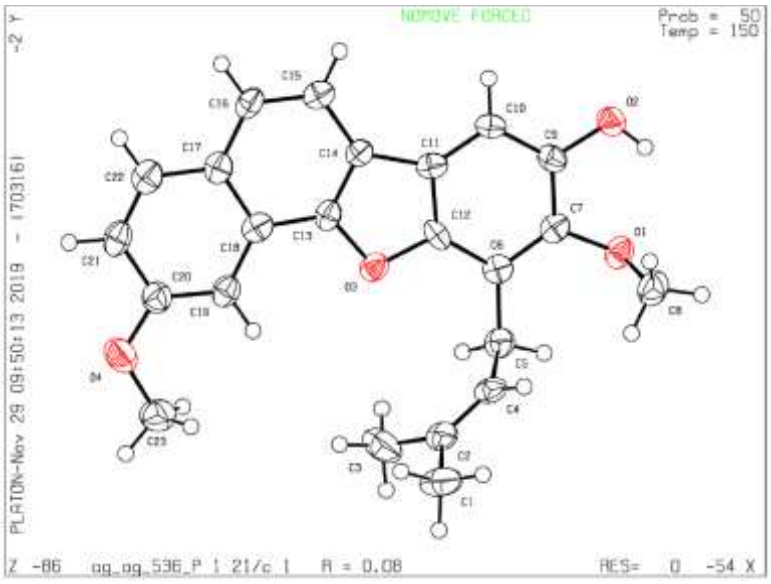

Figure 4. 1: X-ray single crystal structure of compound **110**

4.1.2 Usambarin B (111)

Compound **111** was obtained as a white solid. It was given a molecular formula $C_{23}H_{22}O_4$ from HREIMS ($[M+1]^+$ peak *m/z* 349.1440), NMR (Table 4.2) and (Appendix 2A-2H). The NMR spectra data (Table 4.2), as in compound 110 showed a presence of a naphtho[1,2-b]benzofuran skeleton (Adem, 2019).

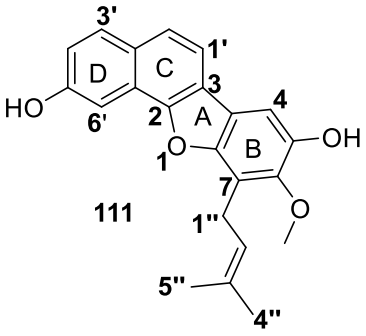

Ring D in compound **111** is identical to that of compound **110**, with an AMX spin system at δ_H 7.84 (*d*, J = 8.8 Hz, H-3'), 7.59 (*d*, J = 2.4 Hz, H-6') and, 7.10 (*dd*, J = 8.8, 2.5 Hz, H-4'), with the

corresponding carbons resonating at δ_C 131.3 (C-3'), 118.8 (C-4') and 103.2 (C-6'). A comparison of compound **111** spectroscopic data with compound **110**, showed that, the only difference between the two compounds is that the methoxy group in ring D of **110** is replaced with a hydroxy substituent at C-5' (δ_C 157.2) in this compound. Ring C is also identical to that of compound **110**. The NMR spectra revealed *ortho* (J = 8.5 Hz) protons at δ_H 7.63 (H-2') and δ_H 7.68 (H-1') with their carbons resonating at δ_C 123.9 (C-2') and δ_C 116.0(C-1').

Ring B in compound **111** is identical to that of compound **110**. It is also trisubstituted with a γ,γ-dimethylallyl moiety at C-7 (δ_C 120.6), methoxy at C-6 (δ_C 146.7), hydroxy at C-5 (δ_C 148.3) and, aromatic siglet at δ_H 7.29 (H-4, δ_C 104.4). The placement of the substituents was confirmed through HMBC experiments (Table 4.2). The prenyl substituent was located to C-7 (δ_C 120.6), [δ_H 3.75 (H-1") associated with C-6 and C-7] and methoxy substituent was assigned to C-6 (δ_C 145.5) from its down-field chemical shift value (δ_C 61.6), being typical of di-ortho substituted. Therefore, compound **111** was characterized as 6-methoxy-7-prenylnaphtho[1,2-b]benzofuran-5,6'-diol, a new compound and named usambarin B.

Table 4.2: NMR data for Usambarin B (**111**) in CD_3OD

No	**^{1}H NMR (δ_H)** (J in Hz)	**^{13}C NMR (δ_C)**	**HMBC (H→C)**	**COSY**	**NOESY**	**TOCSY**
2	-	152.7	-	-	-	-
3	-	124.0	-	-	-	-
3a	-	121.1	-	-	-	-
4	7.29 *s*	104.4	C-5, C-3a, C-6,	-	-	-
5	-	148.3	-	-	-	-
6	-	146.7	-	-	-	-
7a	-	150.0	-	-	-	-
7	-	120.6	-	-	-	-
1'	7.68 *d* (8.4)	116.0	C-2, C-2'a, C-6'a	-	-	-

2'	7.63 *d* (8.5)	123.9	C-3,C-2'a, C-3a C-3',	-	-	-
2'a	-	128.8	-	-	-	-
3'	7.84 *d* (8.8)	131.3	C-2', C-5'	H-4'	H-4'	H-4',H-6'
4'	7.10 *dd* (8.8, 2.5)	118.8	C-2'a, C-6'	H-3'	H-3'	H-3', H-6'
5'	-	157.2	-	-	-	-
6'	7.59 *d* (2.4)	103.2	C-4'	-	-	H-3', H-4'
6'a	-	121.6	-	-	-	-
1"	3.75 *d* (7.4)	24.6	C-6, C-7, C-7a, C-2", C-3"	H-2"	-	H-2", H-4", H-5"
2"	5.44 *ddp* (7.4,5.9,1.4)	123.4	-	H-1", H-5"	-	H-1"
3"	-	133.1	-	-	-	-
4"	1.77	25.9	C-3', C-2", C-5"	-	-	H-1"
5"	1.99 *d* (1.4)	18.2	C-2", C-3", C-4"	H-2"	-	H-1"
6-OMe	3.89 *s*	61.6	C-6	-	-	-

4.1.3 Usambarin C (112)

Compound **112** was isolated as a white amorphous solid. Its molecular formula $C_{23}H_{22}O_4$, was determined based on HREIMS that showed $[M+1]^+$ peak at *m/z* 347.1283, NMR data (Table 4.3) and (Appendix 3A-3H). The UV (λ_{max} 270, 310 nm), and NMR spectra data (Table 4.3) showed a presence of a naphtho[1,2-b]benzofuran skeleton (Adem, 2019).

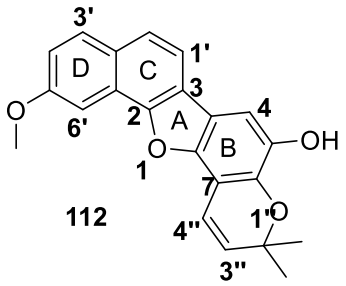

Ring D in compound **112** is identical to that of compound **110**, with an AMX spin designation at δ_H 7.85 (*d*, J = 8.9 Hz, H-3'), 7.67 (br *s*, H-6') and 7.16 (*dd*, J = 9.0 Hz, 2.6 Hz, H-4') and their

corresponding carbon resonated at δ_C 118.2 (C-4'), 130.2 (C-3') and 99.1 (C-6'). The only substituent in this ring is a methoxy group and was placed at C-5' (δ_C 158.3), established based on HMBC and NOESYdata (Table 4.3). Ring C is also identical to that of compound **110**, with a pair of *ortho* correlated (J = 8.3 Hz) protons at δ_H 7.73 (H-1') and δ_H 7.64 (H-2') with corresponding carbon appearing at δ_C 115.8 (C-1') and 123.0 (C-2').

The only difference between compounds **110** and **112** is in the nature of ring B, where in compound **112** it is substituted with a hydroxy group and a 2,2-dimethylpyrano ring. The singlet proton at δ_H 7.36 was assigned to H-4 (δ_C 104.6 for C-4). HMBC correlation verified the hydroxy group's placement at C-5 (C 138.7), where the signal at δ_H 5.45 (5-OH) corresponded to C-4 and C-5. Also, HMBC experiments of δ_H 7.06 (H-4") to C-7 (δ_C 106.8) and C-6 (δ_C 141.7) established the location of the pyran ring to C6/C-7. Hence, compound (**112)** was identified as 5'-methoxy-2',2'-dimethyl-3H-naphtho[2',1':4,5]furo[2,3-f]chromen-5-ol, and named usambarin C.

Table 4.3: NMR data for usambarin C (**112**) in $CDCl_3$

No	**^{1}H NMR (δ_H)** (J in Hz)	**^{13}C NMR (δ_C)**	**HMBC (H→C)**	**COSY**
2	-	151.6	-	-
3	-	127.8	-	-
3a	-	120.5	-	-
4	7.36 *s*	104.6	C-3a, C-5, C-6, C-7, C-7a	-
5	-	138.7	-	-
6	-	141.7	-	-
7	-	106.8	-	-
7a	-	146.1	-	-
1'	7.73 *d* (8.3)	115.8	C-2, C-3, C-3a, C-6a,	-
2'	7.64 *d* (8.3)	123.0	C-3, C-3a, C-3'	-
2'a	-	117.8	-	-
3'	7.85 *d* (8.9)	130.2	C-2, C-3, C-2', C-5', C-6'	H-4'
4'	7.16 *dd* (9.0, 2.6)	118.2	C-5', C-6'	H-3'
5'	-	158.3	-	-
6'	7.67 *s*	99.1	C-2, C-6a, C-3', C-5'	-
6'a	-	122.4	-	-
2"	-	78.0	-	-

3"	5.81 *d* (9.9)	130.8	C-5, C-7, C-2", C-2"-Me, C-4"	-
4"	7.06 *d* (9.8)	116.7	C-5, C-6, C-7, C-7a, C-2", C-2"-Me	-
2'-'Me_2	1.56 *d* (2.0)	27.9	C-3", C-4"	-
5-OMe	4.03 *s*	55.7	-	-
5-OH	5.45 *s*	-	C-4, C-5, C-6	-

4.1.4 Usambarin D (113)

Compound **113** was isolated as white crystals. It was given a molecular formula of $C_{23}H_{22}O_4$ from HREIMS which showed ($[M+1]^+$ peak at *m/z* 319.1334. The UV (λ_{max} 230, 255 nm), NMR data (Table 4.4) and (Appendix 4A-4I) suggested the presence of a naphthol-phenol C-C-linked biaryl skeleton, which was confirmed by X-ray diffraction data (Figure 4. 2).

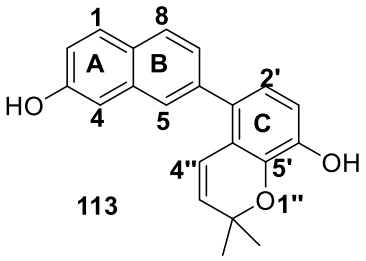

113

In the naphthol moiety, the NMR data, showed an AMX spin pattern for protons of ring A at δ_H 7.78 (*dd*, J = 8.5, 3.4 Hz, H-1; δ_C 129.7 for C-1), 7.16 (*d*, J = 2.5 Hz, H-4; δ_C 109.7 for C-4) and 7.10 (*dd*, J = 8.5, 1.8 Hz, H-2; δ_C 117.9 for C-2) and a hydroxy substituent at C-3 (δ_C 153.9). Ring B also showed an AXY spin system at δ_H 7.78 (*dd*, J =8.5, 3.4 Hz, H-8), 7.59 (br *s*, H-5) and 7.31 (*dd*, J = 8.5, 1.8 Hz, H-7),) with corresponding carbon resonating at δ_C 127.6 (C-8), 126.2 (C-7) and 126.8 (C-5), with C-6 being linked to the phenol moiety (ring C).

Ring C, contained *ortho* correlated (J = 8.3 Hz) protons appearing δ_H 6.87 (H-2') and δ_H 6.89 (H-3'), which otherwise is substituted with a hydroxy substituent and a 2,2-dimethylpyrano ring. The

hydroxy group (δ_H 5.50) was located to C-4' (δ_C 144.2) [established through HMBC correlation (Table 4.4) of 4'-OH (δ_H 5.50) to C-2', C-3', C-4' and C-5'], and the pyran ring at C5'/C-6' [due to the HMBC cross peak of H-4" (δ_H 6.40) to C-5' (δ_C 139.6) and C-6' (δ_C 119.2)]. Single crystal X-ray crystallographic analysis validated the structure (Figure 4. 2). Therefore, the new compound **4** was identified as 3'-(3-hydroxynaphthalen-7-yl)-2",2"-dimethyl-2"H-chromen-8-ol and named usambarin D.

Table 4.4: NMR data for usambarinD (**113**) in $CDCl_3$

No	**^{1}H NMR (δ_H) (J in Hz)**	**^{13}C NMR (δ_C)**	**HMBC**	**COSY**	**NOESY**	**TOCSY**
1	7.78 *dd* (8.5, 3.4)	129.7	C-3, C-4, C-8a, C-8	H-2	-	H-2, H-4
2	7.11 *dd* (8.5, 1.8)	117.9	C-1, C-4	H-1	-	H-1
3	-	153.9	-	-	-	-
4	7.16 *d* (2.5)	109.7	C-1, C-2, C-3, C-5	-	-	H-1
4a	-	134.6	-	-	-	-
5	7.59 (s)	126.8	C-4, C-7, C-4a, C-1'	H-8	H-7	H-7, H-8
6	-	138.1	-	-	-	-
7	7.30 *dd* (8.5, 1.8)	126.2	C-5, C-1'	H-8	H-5	H-5, H-8
8	7.78 *d* (8.5, 3.4)	127.6	C-1, C-6, C-8a	H-7, H-5	-	H-7, H-5
8a	-	127.9	-	-	-	-
1'	-	131.5	-	-	-	-
2'	6.87 *d* (8.3)	114.6	C-6, C-4', C-6'	-	-	-
3'	6.90 *d* (8.3)	122.4	C-1', C-4', C-5'	-	-	-
4'	-	144.2	-	-	-	-
5'	-	139.6	-	-	-	-
6'	-	119.2	-	-	-	-
2"	-	76.5	-	-	-	-
3"	5.61 *d* (10.1)	130.5	C-6', C-2", C-2"Me,	H-4"	2"Me, H-4"	H-4"
4"	6.40 *d* (10.1)	121.1	C-1', C-5', C-6', C-2", C-3"	H-3"	H-3"	H-3"
2"Me	1.52 s	27.9	C-2"Me, C-2",C -3"	-	H-3"	-
2"Me2	1.52 s	27.9	-	-	-	-
3-OH	5.13	-	C-2, C-3, C-4	-	-	-
4'-OH	5.55 s	-	C-2',C-4', C-5'	-	-	-

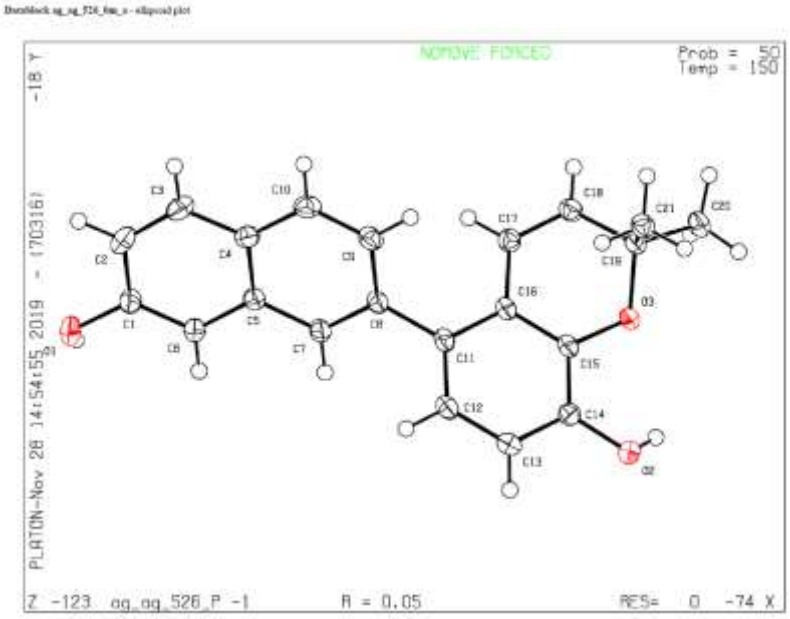

Figure 4. 2: X-ray single crystal structure of compound **113**

4.1.5 Usambarin E (114)

Compound **114** was isolated as a white solid. It was assigned a molecular formula of $C_{23}H_{22}O_4$ based on HREIMS data which showed an $[M+1]^+$ peak at *m/z* 321.1491 and (Table 4.4). The UV (λ_{max} 234, 262sh, 290 sh nm), NMR data (Table 4.4) and (Appendix 5A-5I) suggested a naphthol-phenol C-C-linked biaryl skeleton for compound **114**.

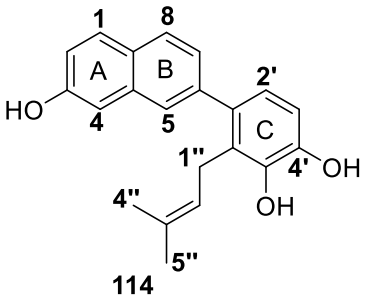

Ring A in compound **114** is identical to that of compound **113**, with an ABX spin designation appearing at δ_H 7.14 (*d*, *J* = 2.6 Hz, H-4; δ_C 109.7 for C-4), 7.76 (*d*, *J* = 8.2 Hz, H-1; δ_C 129.8 for C-1), and 7.10 (*dd*, *J* = 8.2, 2.6 Hz, H-2; δ_C 117.8 for C-2), and a hydroxy substituent which was placed at C-3 (δ_C 153.8). Ring B is also identical to that of compound **113**, with an AXY spin system at δ_H 7.55 (*s*, H-5), 7.76 (*dd*, *J* = 8.6, 3.0 Hz, H-8) and 7.24 (*d*, *J* = 1.8 Hz, H-7), with their carbons resonating at δ_C 126.8 (C-5), 126.2 (C-6) and 127.5 (C-8).

In Ring C, the NMR data revealed the presence of *ortho* correlated (*J* = 8.2 Hz) signals appearing at δ_H 6.83 and δ_H 686 for H-2' and H of-3', having identical substitution pattern as in compound **113**. The only difference between compounds **114** and **113** is in ring C, whereby the 2,2-dimethylpyrano ring in compound **113** is now replaced with a γ,γ-dimethylallyl moiety. This substitution also accounts for the existence of two hydroxy substituents in ring C of compound **114**. The position of prenyl substituent at position C-6' (δ_C 125.4) was supported by HMBC experiments [δ_H 3.36 (H-1") to C-5' and C-6']. The chemical shift values of the oxygenated carbon atoms in this ring fit with the placements of the two hydroxy groups at C-5' (δ_C 144.4) and C-4' (δ_C 142.0). Therefore, compound **114** was identified as 3'-(3-hydroxynaphthalen-7-yl)-6'-prenylbenzene-1,2-diol, named usambarin E, which is a new compound.

Table 4.4: NMR data for usambarin E (**114**) in $CDCl_3$

No	**^{1}H NMR (δ_H)** (J in Hz)	**^{13}C NMR (δ_C)**	**HMBC**	**COSY**	**NOESY**	**TOCSY**
1	7.76 *dd* (8.6, 3.0)	129.8	C-3, C-8a, C-8	H-2	-	H-2
2	7.10 *dd* (8.8, 2.6)	117.8	C-4	H-1	-	H-1
3	-	153.8	-	-	-	-
4	7.14 *d* (2.6)	109.7	C-2, C-3, C-4a, C-5	-	-	-
4a	-	127.8	-	-	-	-

5	7.55 *s*	126.8	C-4, C-4a, C-6, C-7	-	H-1", H-7	H-7, H-8
6	-	134.6	-	-	-	-
7	7.24 *d* (1.8)	126.2	C-8, C-1'	H-8	H-1", H-5, H-8	H-5, H-8
8a	-	139.9	-	-	-	-
8	7.76 *dd* (8.6, 3.0)	127.5	C-1, C-8a, C-6	H-7	H-7	H-5, H-7
1'	-	134.9	-	-	-	-
2'	6.86 *d* (8.2)	112.9	C-4', C-6'	-	-	-
3'	6.83 *d* (8.2)	122.8	C-1', C-5'	-	-	-
4'	-	144.0	-	-	-	-
5'	-	142.4	-	-	-	-
6'	-	125.4	-	-	-	-
1"	3.36 *d* (6.8)	27.7	C-5', C-6', C-2", C-3"	H-2"	H-7, H-5, H-2", H-5", 5'-OH	H-2", H-5"
2"	5.29 *m*	122.2	C-4", C-5"	H-1"	H-1", H-5"	H-1", H-4", H-5"
3"	-	135.7	-	-	-	-
4"	1.68 *s*	25.9	C-2", C-3"	-	-	H-2"
5"	1.76 *s*	18.1	C-2", C-3"	-	H-1", H-2"	H-1", H-2"
3-OH	5.00 *s*	-	C-2, C-3, C-4	-	-	-
4'-OH	5.43 *s*	-	C-2', C-5', C-4'	-	-	-
5'-OH	5.55 *s*	-	C-4', C-5', C-6'	-	H-1"	-

4.1.6 Usambarin F (115)

Compound **115** was isolated as a white solid. It was assigned a molecular formula $C_{23}H_{22}O_4$ from HREIMS $[M+1]^+$ peak at *m/z* 335.1647. The UV (λ_{max} 234 nm), NMR data (Table 4.5), and (Appendix 6A-6I) showed the presence of a naphthol-phenol C-C-linked biaryl skeleton as in compounds **113** and **114**.

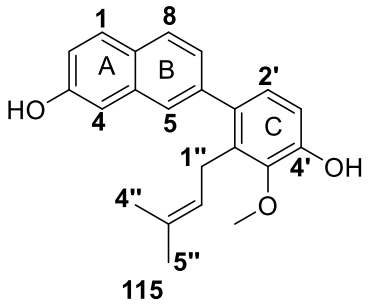

Ring A in compound **115**, is identical to that of compound **114**, with an AXY spin system at δ_H 7.12 (*d*, J = 2.5 Hz, H-4; δ_C 129.7 for C-4), 7.10 (*dd*, J = 8.7 Hz, 2.5, H-2; δ_C 117.7 for C-2) and 7.78 (*d*, J =3.5 Hz, H-1; δ_C 109.7 for C-1) and a hydroxy substituent which was placed to C-3 (δ_C 153.7). Ring B is also similar to that of compound **114**, the NMR data showed an AXY spin system at δ_H 7.77 (*d*, J=8.5, H-8), 7.25 (*m*, H-7) and 7.55 (*s*, H-5) with corresponding carbon resonating at δ_C 126.9 (C-5), 126.2 (C-6) and 127.2 (C-8).

In Ring C, the NMR data revealed *ortho* correlated (J = 8.3 Hz) signals appearing δ_H 6.97 and 6.90 for H-2' and 3'. The only difference between compounds **115** and **114** is in Ring C, the hydroxy substituent at C-5' in compound **114** is now replaced with a methoxy substituent. The ^{13}C NMR chemical shift value of the methoxy (δ_C 61.4) is deshielded, typical of di-ortho substituted and is consistent with it being at C-5' rather than C-3 or C-4'. Similar to compound **114**, the HMBC spectrum, which showed correlation of H_2-1" (δ_H 3.33) to C-6' (δ_C 133.3) and C-5' (δ_C 145.6), supported the location of the prenyl substituent at C-6'. Hence, the new compound (**115)** was identified as 7-(4'-hydroxy-5'-methoxy-6'-prenylphenyl)naphthalen-3-ol, and named usambarin F.

Table 4.5: NMR data for usambarin F (**115**) in $CDCl_3$

No	**^{1}H NMR (δ_H)** (J in Hz)	**^{13}C NMR (δ_C)**	**HMBC**	**COSY**	**NOESY**	**TOCSY**
1	7.78 *dd* (8.5, 7.4)	129.7	C-3, C-8, C-8a	H-2	H-2	H-2, H-4

2	7.10 *dd* (8.7, 2.6	117.7	C-3, C-4	H-1	H-1	H-1
3	-	153.8	-	-	-	-
4	7.12 *d* (2.5)	109.7	C-2, C-3, C-4a	-	-	H-1
4a	-	127.8	-	-	-	-
5	7.55 *m*	126.9	C-4, C-4a, C-7, C-1'	H-7	-	H-8
6	-	139.9	-	-	-	-
7	7.25 *m*	126.2	C-8, C-1'	H-5, H-8	-	H-8
8	7.78 *d* (8.5, 7.4)	127.4a	C-1, C-7	H-7	-	H-5, H-7
8a	-	134.6	-	-	-	-
1'	-	135.7	-	-	-	-
2'	6.97 *d* (8.3)	126.9aa	C-6, C-4', C-6',	-	-	H-2'
3'	6.90 *d* (8.2)	113.3	C-1', C-4', C-5',	-	-	H-5'
4'	-	148.5	-	-	-	-
5'	-	145.6	-	-	-	-
6'	-	133.3	-	-	-	-
1"	3.33 *dt* (6.6,1.3)	26.9	C-1', C-5', C-6', C-2", C-3"	H-2", H-4", H-5"	H-2", H-5, H-5"	H-2"
2"	5.08 *m*	123.5	C-4", C-5"	H-1", H-4", H-5"	H-4"	H-1"
3"	-	131.5	-	-	-	-
4"	1.58 *d* (1.4)	25.8	C-2", C-3", C-5"	H-1", H-2"	H-2"	
5"	1.35 *d* (1.4)	17.8	C-2", C-3", C-4"	H-1", H-2"	-	f
3-OH	5.58 *s*	-	-	-	-	-
4'-OH	5.30 *s*	-	-	-	-	-
5'-OMe	3.86 *s*	61.4	C-5'		-	-

4.1.7 Usambarin G (116)

Compound **116** was obtained as a white solid. It was given a molecular formula $C_{22}H_{22}O_3$ from HREIMS analysis which showed $[M+1]^+$ ion at *m/z* 335.1647, NMR data (Table 4. 6), and (Appendix 7A-7H). The NMR data (Table 4. 6) suggested the evidence of a naphthol-phenol C-C-linked biaryl skeleton as in compound **116**.

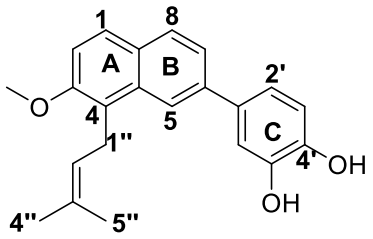

116

In Ring A, the NMR data revealed *ortho* correlated (J = 8.9 Hz) protons appearing δ_H 7.73 and 7.26 for H-1 and H-2, respectively, with the corresponding carbons resonating at δ_C 127.1 (C-1) and 113.8 (C-2). Ring A is otherwise disubstituted with a methoxy and prenyl groups (Table 4. 6). The methoxy substituent was positioned at C-3 (δ_C 154.6) using HMBC correlation of its protons to C-3. The HMBC experiments also supported the placement of the prenyl substituent at C-4 (δ_C 128.5) where CH_2-1" (δ_H 3.83) correlated to C-3 (δ_C 154.6), C-4 (δ_C 133.7), and C-4a (δ_C 133.4).

Ring B in compound **116** is similar to that of compound **114**, where the NMR data displayed an AMX spin pattern at δ_H 7.81 (*d*, J = 8.9 Hz, H-5), 8.04 (*d*, J = 2.0, H-8) and 7.52 (*dd*, J = 8.5, 1.8 Hz, H-6) with corresponding carbon atoms resonating at δ_C 121.4 (C-5), 123.0 (C-6) and 129.1 (C-8). In ring C, the aromatic protons displayed an ABX spin pattern at δ_H 7.25 (*m*, H-2'), and 7.17 (*dd*, J = 8.2, 2.1, Hz, H-6') 6.98 (*d*, J = 8.2 Hz, H-3'). Their corresponding carbons resonated at δ_C 114.8 (C-2'), 115.9 (C-3') and 120.5 (C-6'), allowing two hydroxy substituents to be positioned at C-5' (δ_C 143.2) and C-4' (δ_C 143.9), as in the other related compounds of this plant. Therefore, this new compound (**116)** was characterized as 4-(6-methoxy-5-prenylnaphthalen-2-yl)benzene-1,2-diol, and was named as usambarin G.

Table 4. 6: NMR data for Usambarin G (**116**) in CDCl3

No	**δ_H (Multiplicity, *J*)**	**δ_C**	**HMBC**	**COSY**	**TOCSY**

1	7.72 *d* (8.9)	127.4	C-3, C-8a, C-8	H-2	H-2
2	7.25 *m*	113.8	C-3, C-4, C-2"	H-1	H-1
3	-	154.7	-	-	-
4	-	128.5	-	-	-
4a	-	133.4	-	-	-
5	8.04 *s*	121.4	C-4, C-6, C-7	H-6	H-8
6	-	135.5	-	-	-
7	7.52 *dd* (8.5, 1.8)	123.0	C-5, C-7, C-8	H-5, H-8	H-8
8	7.81 *d* (8.5)	129.1	C-1, C-8a, C-1'	-	H-5, H-6
8a	-	133.4	-	-	-
1'	-	138.3	-	-	-
2'	6.98 *d* (8.2)	115.9	C-6, C-4'	-	H-6'
3'	7.17 *dd*, (8.2, 2.1)	120.4	C-1', C-5', C-6'	-	H-3'
4'	-	143.9	-	-	-
5'	-	143.2	-	-	-
6'	7.25 *m*	114.8	C-1', C-3', C-5'	-	-
1"	3.83 *d* (6.8)	24.3	C-3, C-2", C-3"	-	-
2"	5.23 *m*	123.5	C-4", C-5"	-	-
3"	-	131.6	-	-	-
4"	1.91 *d* (1.3)	18.3	C-2", C-3"	-	-
5"	1.69 *d* (1.3)	25.9	C-2", C-3"	-	-
3-OMe	3.95 *s*	57.0	-	-	-
4'-OH	5.25 *m*	-	C-2', C-4'	-	-
5'-OH	5.21 *m*	-	C-5,' C-6'	-	-

4.1.8 Usambarin H (117)

Compound **117** was obtained as a white solid. Its molecular formula $C_{23}H_{22}O_4$ was determined using HREIMS ($[M+1]^+$ at *m/z* 389.2117), NMR data (Table 4.7), and (Appendix 8A-8H) The NMR data (Table 4.7) suggested the evidence of a naphthol-phenol C-C-linked biaryl skeleton.

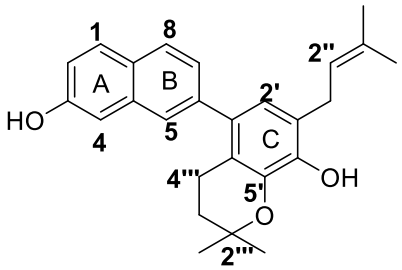

117

Ring A in compound **117**, is identical to that of compound **114** that was evident from the AXY spin system appearing at δ_H 7.79 (*d*, J = 8.5 Hz, H-1; δ_C 129.8 for C-1), 7.10 (*d*, J = 2.0 Hz, H-4; δc126.5 for C-4), and7.13 (*d*, J = 9.5, Hz, H-2; δ_C 117.7 for C-2), with a hydroxy substituent placed at C-3 (δ_C 153.6). Ring B also showed an AMX spin pattern at δ_H 7.77 (*d*, J = 2.3 Hz, H-8; δ_C 127.7 for C-8) 7.45 (*d*, J = 1.6 Hz, H-5; δ_C 127.2 for C-5), and 7.11 (*d*, J = 5.8 Hz, 1H, H-6; δ_C 109.6 for C-6).

In Ring C, the NMR data revealed a singlet at δ_H 6.75 (H-2'), having a 2,2-dimethyldihydropyrano moiety, a γ,γ-dimethylallyl moiety and a hydroxy substituent at C-4' (δ_C 144.5). The prenyl substituent was placed at C-3' (δ_C 131.3) using the HMBC association of H-1" (δ_H 2.96 to C-2' (δ_C 112.4), C-4'(δ_C 144.5) and C-3' (δ_C 131.3). This leaves the dihydropyran ring to be placed at C5'/C-6' which was established through HMBC association of H-4'" (δ_H 1.33) to C-5' and C-6'. Therefore, compound **117** was characterized as 5-(6-hydroxynaphthalen-2-yl)-2,2-dimethyl-7-prenylchroman-8-ol, which again is a new compound and named as usambarin H.

Table 4.7: NMR data for Usambarin H (**117**) in $CDCl_3$

No	**δ_H (Multiplicity, *J*)**	**δ_C**	**HMBC**	**COSY**	**NOESY**	**TOCSY**
1	7.78 *dd* (8.5, 2.3)	129.8	C-3, C-8, C-8a,	H-2, H-4	H-2	H-2, H-4
2	7.13 *d* (9.5)	117.7	C-3	H-1	H-1	H-1
3	-	153.7	-	-	-	-
4	7.10 *d* (2.0)	109.6	C-2, C-3	H-1	-	H-1
4a	-	127.9	-	-	-	-
5	7.45 *d* (1.6)	127.2	C-4, C-4a, C-7, C-1'	H-6	H-6	H-6, H-8
6	-	138.5	-	-	-	-
7	7.11 *d* (5.8)	126.5	C-8, C-1'	H-5	H-5	H-5, H-8
8	7.78 *dd* (8.5, 2.3)	127.7	C-1, C-7, C-8a	-	-	H-5, H-8
8a	-	134.8	-	-	-	-
1'	-	132.6	-	-	-	-
2'	6.75 *s*	112.4	C-1', C-4', C-5', C-1"	-	-	-
3'	-	131.3	-	-	-	-
4'	-	144.5	-	-	-	-
5'	-	139.0	-	-	-	-

6'	-	119.7	-	-	-	-
1"	2.96 *d* (7.4)	32.0	C-2', C-3', C-2", C-3"	H-2"	-	H-2", H-5"
2"	5.12 *m*	123.9	-	H-1", H-5"	-	H-1"
3"	-	131.6	-	-	-	-
4"	1.33 *s*	17.7	C-3", C-5"	-	-	-
5"	1.62 *d* (1.6)	25.9	C-2", C-3", C-4"	H-2"	-	H-1"
2'"	-	74.8	-	-	-	-
3'"	1.68 *t* (6.8)	33.2	C-6', C-2'", C-4'", C-2'"Me,	H-4'"	-	-
4'"	2.32 *m*	21.9	C-1', C-5', C-6', C-2'", C-3'"	H-3'"	-	-
2'"Me2	1.34 *s*	27.0	C-2'", C-3'"	-	-	-
2'"Me	1.34 *s*	27.0	C-2'"	-	-	-
3-OH	4.94 *s*	-	-	-	-	-
4'-OH	5.60 *s*	-	C-2', C-4', C-5'	-	-	-

4.1.9 Usambarin I (118)

Compound **118** was obtained as a white solid. It was given a molecular formula of $C_{21}H_{18}O_3$ from EIMS, $[M+1]^+$ at *m/z* 334.37, and NMR (Table 4.8), and (Appendix 9A-9E). The NMR data further provided the evidence of a naphthol-phenol C-C-linked biaryl skeleton.

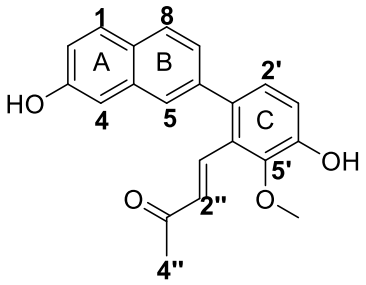

118

Ring A in compound **118** is identical to that of compound **115**. It had an AMX spin pattern appearing at δ_H 7.78 (*d*, J = 8.7 Hz, H-1; δ_C 129.8 for C-1), 7.23 (*dd*, J = 8.3 Hz, 1.8, H-2; δ_C 117.7 for C-2), 7.13 (*d*, J = 1.8, H-4; δ_C 127.5 for C-4) with the hydroxy group at C-3 (δ_C 154.1) as in the

other related compounds of this plant. Ring B is also identical to that of compound **115**, as shown by the NMR data (Table 4.8) that revealed an ABX spin designation at δ_H 7.56 (*s*, H-5; δ_C 127.2 for C-5), 7.55 (*d*, J = 8.7 Hz, H-8; δ_C 127.7 for C-8), and 7.14 (*d*, J = 8.7 Hz, H-7; δ_C 118.3 for C-7).

In Ring C, NMR data revealed *ortho* correlated protons (J = 8.2 Hz) signals appearing at δ_H 7.15 and 7.08, for H-2' and H-3'), which requires substituents at C-5', C-4' and C-6'. The NMR spectra (Table 4.8) showed the substituents to be a hydroxy, a methoxy and a modified prenyl group, a but-3-en-2-one. In fact, the only difference between compounds **115** and **118** is in ring C, where the prenyl substituents at C-6' in compound **115** is now replaced with a but-3-en-2-one group. Similarly with compound **118**, HMBC correlation supported the placement of this moiety at C-6' (δ_C 128.0) [δ_H 7.42 (H-1") correlated to C-1', C-5' and C-6']. Therefore, compound **118** was characterized as 4-(3-hydroxy-6-(6-hydroxynaphthalen-2-yl)-2-methoxyphenyl) but-3-en-2-one, which again is a new compound, and named Usambarin I.

Table 4.8: NMR data for C usambarin I (**118**) in $CDCl_3$

No	**δ_H (Multiplicity, *J*)**	**δ_C**	**HMBC**
1	7.78 *d* (8.7)	129.8	C-3, C-8, C-8a
2	7.23 *dd* (8.3, 1.8)	117.7	C-4
3	-	154.1	-
4	7.13 *m*	127.5	C-2, C-3
4a	-	129.8	-
5	7.56 *d* (1.6)	127.2	C-6, C-8,
6	-	138.4	-
7	7.14 *m*	118.3	C-6, C-8
8	7.77 *d* (1.6)	127.7	C-1, C-6, C-8a
8a	-	134.6	-
1'	-	136.5	-
2'	7.15 *m*	109.7	C-4'
3'	7.08 *d* (8.3)	117.0	-
4'	-	148.9	-
5'	-	146.2	-
6'	-	128.0	-

1"	7.42 *d* (16.6)	139.0	C-1', C-5', C-2", C-3"
2"	6.86 *d* (16.6)	132.4	C-3"
3"	-	199.4	-
4"	2.14 *s*	27.2	C-2",C-3"
3-OH	5.06 *s*	-	C-2, C-3, C-6
4'-OH	5.82 *s*	-	C-3', C-4', C-5'
5'-OMe	3.76 *s*	60.8	C-5'

4.1.10 Usambarin J (119)

Compound **119** was obtained as a white solid. It was given a molecular formula of $C_{16}H_{14}O_4$ from HREIMS, $[M+1]^+$ at *m/z* 271.0970, NMR (Table 4.9), and (Appendix 10A-10H). The UV (λ_{max} 234 nm), and NMR (Table 4.9) data suggested the evidence of a flavan-2-ene skeleton. Thus, the ring C protons appearing at δ_H 6.35 (*d*, J = 1.0 Hz, 1H, H-3) and 3.95 (*s*, 2H, CH_2-4) with their corresponding carbon atoms appearing at δ_C 157.1 (C-2), 102.6 (C-3) and 33.1 (C-4).

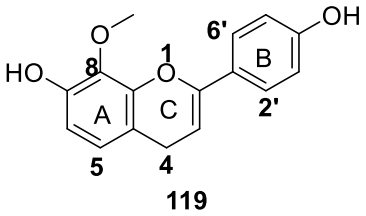

119

Ring A showed ortho correlated (J = 8.3 Hz) protons resonating at δ_H 6.97 and δ_H 6.72 for H-5 and H-6) with their carbons at δ_C 114.0 (C-5) and 113.0 (C-6). This ring is substituted at C-8 (δ_C 132.2) and C-7 (δ_C 145.9) with methoxy (δ_H 3.89; δ_C 60.1) and hydroxy groups. The down-field shifted chemical shift value of the methoxy carbon (δ_C 60.1) is typical of it being di-ortho-substituted and hence consistent at C-8, rather than C-4' or C-7. Ring B showed the presence of AA'XX' spin system, appearing at δ_H 7.10 (H-2'/6') and 6.71 (H-3'/5') with their carbon atoms resonating at δ_C 129.6 (C-2'/6'), 115.2 (C-3'/5') with hydroxy at C-4' (δ_C 155.9). Therefore, compound **119** was characterized as 2-(4-hydroxyphenyl)-8-methoxy-4H-chromen-7-ol, a new flav-2-ene, and named usambarin J.

Table 4.9: NMR data for usambarin J (**119**) in DMSO-d_6

No	^{1}H NMR (δ_H) (J in Hz)	^{13}C NMR(δ_C)	HMBC	NOESY
2	-	157.1	-	-
3	6.35 *d* (1.0)	102.6	C-2, C-4a,C-8a	H-4
4	3.95 *s*	33.1	C-2, C-3, C-8, C-1'	H-3,H-2', H-6'
4a	-	122.1	-	-
5	6.97 *d* (8.3)	114.0	C-3, C-4a, C-8, C-8a	-
6	6.72 *d* (8.3)	113.0	C-4a, C-7, C-8	7-OH
7	-	145.9	-	-
8a	-	147.0	-	-
8	-	132.2	-	-
1'	-	127.6	-	-
2'/6'	7.10 AA'	129.6	C-3', C-4', C-5', C-6'	H-4
3'/5'	6.71 XX'	115.2	C-1', C-5'	4'-OH
4'	-	155.9	-	-
7-OH	9.06 *s*	-	C-5, C-6, C-7, C-8,	H-6
4-'OH	9.26 *s*	-	C-3', C-4', C-5'	H-3', H-5'
8-OMe	3.89 *s*	60.1	C-8	-

4.1.11 Phenyl-1-benzoxepin derivative (120)

Compound **120** was obtained as a white paste. It was given a molecular formula $C_{23}H_{22}O_4$ from HREIMS $[M+1]^+$ *m/z* 285.1127. The NMR data (Table 4. 10), (Appendix 11A-11H) is identical to that of phenyl-1-benzoxepin derivative skeleton (Barbic et al., 2012). Thus, for ring C, the ^{13}C NMR data showed the existence of two sp^3 hybridized carbons [C-2 (δ_C 75.5), and C-3 (δ_C 49.9)] and two sp^2 hybridized carbon atoms [C-4 (δ_C 130.3), and C-5 (δ_C 127.7)], the corresponding ^{1}H NMR signals appeared at δ_H 4.29 (*ddd*, 11.7, 3.2, 1.0 Hz, H-2a), 4.15 (*m*, H-2b) and 3.90 (*dd*, 5.5, 3.2 Hz, H-3, 5.87 (*dd*, 11.8, 4.0 Hz, H-4) and 6.39 (*dd*, 11.8, 2.0 Hz, H-5).

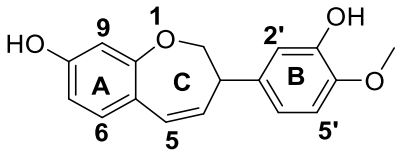

120

Ring B is disubstituted with hydroxy and methoxy groups, the ^{1}H NMR spectrum revealed AXY spin system at δ_H 6.87 (*d*, J = 8.0 Hz, H-5'), 6.75 (*dd*, 8.0, 2.0 Hz, H-6'), and 6.72 (*d*, J = 2.0 Hz, H-2') with their carbons appearing at δ_C 121.3 (C-6'), 114.3 (C-5') and 110.8 (C-2'). HMBC correlations supported the positioning of hydroxy substituent at C-3' (δ_C 144.8) [δ_H 5.52 (3'-OH) to C-4', C-2 and C-3'] and methoxy group at C-4' (δ_C 146.6). HMBC correlations of the signals at δ_H 6.72 (H-2') and 6.40 (H-5) with C-3 (δ_C 49.9) indicated the connection of ring B to ring C.

In ring-A, the ^{1}H NMR data revealed an AMX spin pattern at δ_H 7.11 (*d*, J = 8.3 Hz, H-6), 6.52 (*dd*, 8.4, 2.6 Hz, H-7), and 6.47 (*d*, J =2.6 Hz, H-9) with corresponding carbon resonating at δ_C 133.8 (C-6), 110.1 (C-7) and 107.0 (C-9) and a hydroxy substituent which was placed to C-8 (δ_C 155.7). Therefore, compound **120** was characterized as 3-(3-hydroxy-4-methoxyphenyl)-2,3-dihydrobenzo[b]oxepin-8-ol, a new compound named usambarin K. The absolute configuration at C-3 has not been determined.

Table 4. 10: NMR data for usambarin K (**120**) in $CDCl_3$

No	**δ_H (Multiplicity, *J*, Hz)**	**δ_C**	**HMBC**	**COSY**	**NOESY**	**TOCSY**
2	4.29 *ddd*, (11.7, 3.2, 1.0), 4.14 dd (11.8, 6.7)	75.4	C-3, C-4, C-9a, C-1'	-	H-6'	H-3
3	3.90 *dd* (5.5, 3.2)	49.9	-	H-4	H-4, H-6'	H-2', H-2'
4	5.87 *dd* (11.8, 4.0)	130.7	C-2, C-3, C-5a, C-1'	H-5, H-3	H-3, H-5, H-6'	-
5a	-	120.0	-	-	-	-
5	6.40 *dd* (11.8, 2.0)	128.1	C-3, C-6, C-9a,	H-4	H-4, H-6	-
6	7.11 *d* (8.3)	134.1	C-5, C-8, C-9a,	H-7	H-5, H-7	H-7
7	6.52 *dd* (8.4, 2.6)	110.1	C-5a, C-8, C-9	H-6	H-6, 8-OH	H-6
8	-	155.7	-	-	-	-
9a	-	160.5	-	-	-	-
9	6.47 *d* (2.6)	107.0	C-5a,C-7, C-8, C-9a	-	8-OH	-

1'	-	133.1	-	-	-	-
2'	6.72 *d* (2.0)	110.9	C-3, C-1', C-3', C-4', C-6',	-	-	-
3'	-	144.8	-	-	-	-
4'	-	146.6	-	-	-	-
5'	6.87 *d* (8.0)	114.5	C-1', C-3', C-4',	-	-	H-6'
6'	6.75 *dd* (8.0, 2.0)	121.3	C-2', C-3, C-4',	-	H-2', H-2", H-3, H-4,	H-5'
3'OH	5.52 *s*	-	C-2', C-3', C-4',	-	-	-
8OH	4.75 *s*	-	C-7, C-8, C-9	-	H-7, H-9	-
4'OMe	3.84 *s*	56.1	C-4'	-	-	-

4.1.12 Bergapten (121)

Bergapten was isolated as white crystals. It was given a molecular formula of $C_{23}H_{22}O_4$ based on EIMS $[M+1]^+$ *m/z* 216.04, NMR data (Table 4.11), and (Appendix 12A-12H). The UV (λ_{max} 312 nm), and NMR data (Table 4.11) is typical of coumarins (Prachyawarakorn *et al*., 2000).

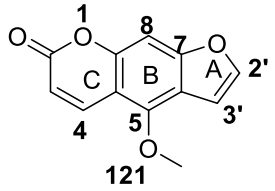

The ^{1}H NMR spectra revealed an aromatic singlet proton at δ_H 7.14 (*s*, H-8) and two mutually coupled olefinic protons at δ_H 8.16 (*d*, *J* = 9.8 Hz, H-4) and 6.28 (*d*, *J* = 9.7 Hz, H-3) indicating a 5,7,8-trisubstituted (with methoxy and with furan at C-7/8) coumarin skeleton. This was established by HMBC experiments of a signal at δ_H 7.14 with δ_C 158.8 (C-7) and 113.6 (C-6). The furan ring (ring A), displayed signals at δ_H 7.02 (*d*, *J* = 2.0 Hz, H-2') and 7.59 (*d*, *J* = 2.4 Hz, H-3') with the corresponding carbons peaks at δ_C 145.2 (C-2') and 105.4 (C-3'). A singlet proton at δ_H 4.28 was assigned to a methoxy substituent (δ_H 4.27; δ_C 60.5) at C-5 (δ_C 149.5) group. The placement was established through HMBC correlation of H-4 (δ_H 8.15) with C-5. Therefore,

compound **121** was identified as bergapten previously reported from members of the Moraceae family (Caceres et al., 2001; Muller et al., 2004).

Table 4.11: NMR data for bergapten (**121**) in $CDCl_3$

No	^{1}H NMR (δ_H) (J in Hz)	^{13}C NMR (δ_C)	HMBC	COSY	NOESY	TOCSY
2	-	161.6	-	-	-	-
3	6.28 *d* (9.7)	113.0	C-4a, C-2	H-4	H-4	H-4
4	8.16 (9.8)	139.7	C-2, C-5, C-8a	H-3	H-3	H-3
4a	-	106.8	-	-	-	-
5	-	150.0	-	-	-	-
6	-	113.1	-	-	-	-
7	-	158.8	-	-	-	-
8	7.14 *s*	94.3	C-4a, C-6, C-7, C-8a	-	-	-
8a	-	153.1	-	-	-	-
9	4.27 *s*	60.5	C-5	-	2'	-
2'	7.59 *d* (2.4)	145.2	C-6, C-7, C-2',	H-2'	-	H-2'
3'	7.02 *d* (2.0)	105.4	C-6, C-7,C-3'	H-3'	H-9	H-3'

4.1.13 Bergaptol (122)

Compound **122** was isolated as white crystals. It was given a molecular formula $C_{23}H_{22}O_4$ from EIMS $[M+1]^+$ *m/z* 186.04. The UV (λ_{max} 312 nm), (Appendix 13A-13E) and, NMR data (Table 4.12) is typical of a coumarins (Prachyawarakorn *et al*., 2000).

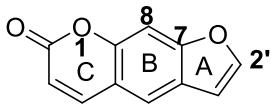

122

Compound **122** similar to **121,** the only difference is absence of the methoxy substituent at C-5 in compound **121.** NMR data (Table 4.12) revealed aromatic signals at δ_H 7.48 (*s*, H-8) and 7.70 (*s*, H-5). Olefinic protons at δ_H 7.80 (*d*, *J* = 9.5 Hz, H-4) and 6.38 (*d*, *J* = 9.6 Hz, H-3) indicating a 6,7,5-trisubstituted coumarin skeleton. In Ring A, signals at δ_H 7.68 (*d*, *J* = 2.0 Hz, H-2') and 6.33

(*dd*, *J* = 2.2, 1.1 Hz, H-3') with their carbon atoms peaks at δ_C 147.0 (C-2') and 106.5 (C-3') was assigned to the furan ring. Therefore, compound **122** was identified as bergaptol, previously reported from members of the Moraceae family (Caceres *et al*., 2001).

Table 4.12: NMR data for Bergaptol (**123**) in $CDCl_3$

No	δ_H Multiplicity(*J* in Hz)	δ_C	HMBC	COSY
2	-	161.2	-	-
3	6.38 *d* (9.6)	114.8	C-2, C-4a	H-4
4	7.80 *d* (9.5)	144.2	C-4a, C-5, C-8	H-3
4a	-	115.6	-	-
5	7.70 *d* (2.3)	120.0	C-6, C-3'	H-3'
6	-	125.0	-	-
7	-	156.6	-	-
8	7.48 *s*	100.0	C-4a, C-6	H-3'
8a	-	152.2	-	-
2'	7.68 *s*	147.0	C-3'	H-3'
3'	6.83 *dd* (2.2,1.0)	106.5	C-6, C-7, C-2'	H-5, H-8, H-2',

4.1.14 12a-Hydroxydeguelin (123)

Compound **123** was isolated as yellow oil. (Appendix 14A-14G) and NMR (Table 4.13) signals at δ_H 4.48 (*dd*, *J* = 12.4, 1.1 Hz, 1H, H-6; δ_C 64.0), 4.62 (*dd*, *J* = 12.1, 2.5 Hz, 1H, H-6; δ_C 64.0), and 4.57 (*dd*, *J* = 2.5, 1.0 Hz, 1H, H-6a; δ_C 76.1) and δ_C 67.6 (C-12a) are consistent with a 12a-hydroxyrotenoid skeleton. The NMR data (Table 4.13) in ring D revealed a pair of ortho-correlated protons at δ_H 6.47 (*d*, *J* = 8.7 Hz) and 7.73 (*d*, *J* = 8.7 Hz) that were ascribed to H-10 and H-11 respectively. Further, NMR data revealed that ring D is substituted with 2,2-dimethylpyrano group at C-8/C-9. The placement of 2,2-dimethylpyrano was confirmed by HMBC association of H-4' to C-7a and C-9.

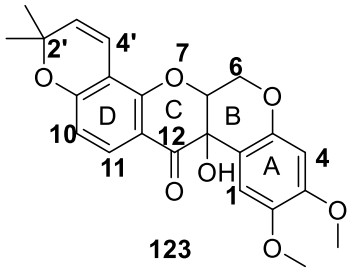

Ring A is disubstituted with a pair of methoxy groups at C-2 and C-3, and aromatic signals at δ_H 6.56 and 6.45 were assigned to H-1 and H-4, respectively. The placement of the methoxy groups was established through HMBC cross peaks of methoxy substituents at δ_H 3.73 with C-2 (δ_C 144.1), and δ_H 3.82 with C-3 (δ_C 151.2); and also correlation of δ_H 6.56 (H-1) and δ_H 6.46 (H-4) to C-2 and C-3. Hence, compound **123** was characterized as 12a-hydroxydeguelin (Tephrosin). The relative configuration was determined as cis (6β, 12aβ) based on the chemical shift value of H-1 (δ_H 6.56); in trans compounds this proton is substantially deshielded (Lawson et al., 2010).

Table 4.13: NMR data for 12a-hydroxydeguelin (**123**) in $CDCl_3$

No	**^{1}H NMR (δ_H)** (J in Hz)	**^{13}C NMR(δ_C)**	**HMBC**	**COSY**	**NOESY**	**TOCSY**
1	6.56 *s*	109.5	C-2, C-3, C-4a, C-12a	-	2-OMe	-
1a	-	108.8	-	-	-	-
2	-	144.1	-	-	-	-
3	-	151.2	-	-	-	-
4	6.48 *s*	101.2	C-2, C-3, C-1a, C-4a	-	-	-
4a	-	148.5	-	-	-	-
6'	4.62 dd (12.1, 2.5) 4.48 (12.2, 1.1)	64.0	C-1a, C-4a, C-6a, C-12a	-	-	-
6a	4.57 *dd* (2.5,1.0)	76.1	C-12a	-	-	-
7a	-	160.9	-	-	-	-
8	-	109.3	-	-	-	-
9	-	156.8	-	-	-	-
10	6.46 *d*, (8.7)	112.0	-	H-11	H-11, 3-OMe	H-11
11	7.73 *d*, (8.7)	129.0	C-7a, C-9, C-12,	H-10	H-10	H-10

11a	-	111.2	-	-	-	-
12	-	191.5	-	-	-	-
12a	-	67.6	-	-	-	-
2'	-	78.2	-	-	-	-
3'	5.55 *d*, (10.1)	128.7	C-8, C-2', C-2'Me	H-4'	H-4'	H-4'
4'	6.60 *d*, (10.1)	115.6	C-7a, C-2'	H-3'	H-3'	H-3'
12a-OH	4.40 *s*	-	C-6a, C-12a, C-12	-	-	-
2'-Me	1.45 *s*	28.7	C-2', C-3', C-2'Me_2	-	-	-
2'-Me_2	1.39 *s*	28.7	C-2', C-3', C-2'Me	-	-	-
2-OMe	3.73 *s*	56.0	C-2	-	H-1	-
3-OMe	3.82 *s*	56.5	C-3	-	H-10	-

4.1.15 Ferulaldehyde (124)

Compound **124** was isolated as colourless solid. The (Appendix 15A-15E) and NMR data (Table 4. 14) revealed a tri-substituted benzene ring with ABX protons at δ_H 7.07 (*d*, J = 1.9, H-2, δ_C 109.6), 7.13 (*dd*, J = 8.2, 2.0, H-6, δ_C 124.2), 6.96 (*d*, J = 8.2, H-5, δ_C 115.1), a methoxy (δ_H 3.95) and a hydroxy (δ_H 5.95) substituents. NMR data, further revealed olefinic protons at δ_H 7.40 (*d*, J = 15.9 Hz, 1H, H-7, δ_C 153.2), δ_H 6.60 (*dd*, J = 15.8, 7.7 Hz, 1H, H-8, δ_C 126.6). An aldehyde proton at δ_H 9.66 (*d*, J = 7.7 Hz, H-10), with the corresponding carbons at δ_C 193.8 was also evident. From HMBC correlation [δ_H 7.40 (H-7) to C-8, C-2, C-9 and C-6 and δ_H 9.66 (H-10) to C-8)] supported the placement of the aldehyde adjacent to the olefinic protons. Compound **124** was thus characterized as 3-(4-hydroxy-3-methoxy-phenyl)-propenal (Sajjadi *et al*., 2012).

Table 4. 14: NMR data for ferulaldehyde (**124**) in $CDCl_3$

No	**^{1}H NMR (δ_H)** (J in Hz)	**^{13}C NMR(δ_C)**	**HMBC**	**COSY**
1	-	126.8	-	
2	7.07 *d* (1.9)	109.6	C-3, C-4, C-6, C-7	

3	-	149.1	-	
4OH	5.95 s	-	C-4, C-5	
4	-	147.1	-	
5	6.96 *d* (8.2)	115.1	C-6, C-4, C-1	
6	7.13 *dd* (8.2,2.0)	124.2	C-2, C-5, C,3, C-7	
7	7.40 *d* (15.9)	153.2	C-9, C-2, C-6, C-8, C-1	H-8
8	6.60 *dd* (15.8,7.7)	126.6	C-1	H-10, H-7
9	9.66 *d* (7.7)	193.8	C-8	H-8
3OMe	3.95 *s*	56.2	C-3	

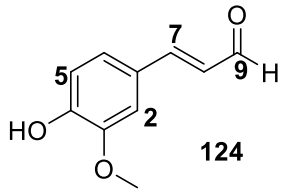

124

4.1.16 Usambarin L (125)

Compound **125** was obtained as white solids. The (Appendix 16A-16G) and NMR data (Table 4.15) suggested the presence of a naphthalene skeleton as in compound **114**. Ring A in compound **125** is identical to that of compound **114**, with an AXY spin system at δ_H 7.76 (*d*, *J* = 7.9 Hz, H-1, δ_C 129.7), 7.11 (*d*, *J* = 2.6 Hz, H-4; δ_C 117.7 for C-4) 7.12 (*dd*, *J* = 8.8, 2.6 Hz, H-2; δ_C109.7 for C-2), and a hydroxy group which was placed at C-3 (δ_C 153.7). Ring B is also identical to that of compound **114**, with its protons appearing at δ_H 7.55 (Br *s*, H-5), 7.76 (*d*, *J* = 7.9 Hz, H-8) and 7.24 (*m*, H-7) with the corresponding carbons resonating at δ_C 126.8 (C-5), 126.2 (C-7) and 127.3 (C-8).

In ring C, aromatic protons displayed an ABX spin pattern at δ_H 6.98 (*d*, J = 8.2 Hz, H-2'), and 6.38 (*d*, J = 8.2 Hz, H-6') 6.38 (*d*, J = 8.2 Hz, H-3'). Their corresponding carbons resonated at δ_C 127.3 (C-2'), 103.7 (C-3') and 107.9 (C-6'), allowing two hydroxy substituents to be positioned at C-5' (δ_C 156.2) and C-4' (δ_C 154.9), as in the other related compounds of this plant. as in compound. The only difference between compound **125** and **114** is in ring C; in compound **125** C-6' is

unsubtituted. Therefore, compound **125** was characterized as 4-(6-hydroxynaphthalen-2-yl)benzene-1,2-diol, a new compound named usambarin L.

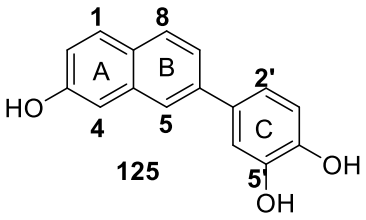

Table 4.15: NMR data for usambarin L (**125**) in $CDCl_3$

No	**^{1}H NMR (δ_H)** (J in Hz)	**^{13}C NMR (δ_C)**	**HMBC**
1	7.76 *d* (7.9)	129.7	C-3, C-4a, C-8
2	7.12 *dd* (8.8, 2.6)	109.7	C-1, C-3, C-4
3-OH	5.02	153.7	C-2, C-3, C-4
4	7.11 *d* (2.6)	117.7	C-1, C-2, C-3
4a	-	134.5	-
5	7.55 *s*	126.8	C-4, C-6, C-6, C-8a
6	-	133.3	-
7	7.24 *d* (1.8)	126.2	C-8, C-1'
8	7.76 *d* (7.9)	127.3	C-1, C-4a, C-6
8a	-	139.9	-
1'	-	114.4	-
2'	6.98 *d* (8.2)	127.3	C-7,
3'	6.38 *d* (8.2)	103.7	C-1', C-2' C-4'
4'-OH	4.65	154.9	C-2', C-3', C-4'
5'	-	156.2	-
6'	6.38 *d* (8.2)	107.9	C-1', C-3', C-4'

4.1.17 Usambarin M (126)

Compound **126** was obtained as white solid. The (Appendix 16A-16G) and ^{1}H NMR data (Table 4. 16) displayed signals for ring C protons typical of a flavan skeleton [δ_H 4.93 (*dd*, J=10.3, 2.4 Hz, 1H, H-2), 2.09 (*m*, 2H, H-3), 2.90 (*dd*, J= 11.4, 6.0 Hz, 1H, H-4α) and 2.73 (*dd*, J= 11.4, 6.0 Hz, 1H, H-4β)]. In agreement with this, the ^{13}C NMR data (Table 4. 16) revealed signals resonating at δ_C 24.8 (C-4), 30.1 (C-3) and 78.0 (C-2).

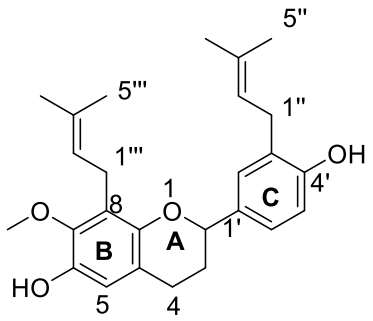

126

Ring B is trisubstituted with a hydroxy (δ_H 5.57), at C-6 (δ_C 148.5) a methoxy (δ_H 3.86; δ_C 61.4) at C-7, and a γ,γ-dimethylallyl moiety at C-8 (Table 4. 16). The only unsubstituted carbon is C-5, with a proton at δ_H 6.90 (δ_C 113.3). The placement of methoxy substituent at C-7 and the γ,γ-dimethylallyl moiety at C-8 was supported by HMBC experiments; δ_H 5.57 (6-OH) association with C-6 (δ_C 148.5), C-7 (δ_C 45.6), and C-5 (δ_C 113.3) allowing the location of methoxy group at C-7. H_2-1''' (δ_H 3.33) associated with C-2''' and C-8 allowing the placement of the γ,γ-dimethylallyl moiety at C-8.

Ring C revealed aromatic signals resonating at δ_H 7.15 (*d*, J = 7.1, 1H, H-6'), 6.81 (*d*, J = 8.8, 1H, H-5') and 7.15 (*m*, 1H, H-2') with corresponding carbon resonating at δ_C 117.72 (C-6'), 115.9 (C-5') and 109.7 (C-2'). Ring C is also disubstituted with a γ,γ-dimethylallyl moiety and hydroxy substituent C-4' (δ_C 154.3). The placement of the γ,γ-dimethylallyl moiety at C-3' was supported by HMBC correlation, whereby 4'-OH (δ_H 5.13) correlated with C-3' (δ_C126.9), and C-5' (δ_C115.9); H-1" (δ_H 3.37) associated with C-2' (δ_C 109.7) and C-3' (δ_C 126.9). Therefore, compound **126** was characterized as 2-(4-hydroxy-3-prenylphenyl)-7-methoxy-8-prenylchroman-6-ol, a new compound named usambarin M. the absolute configuration at C-2 has not been established, but the large coupling constant (J= 10.3 Hz) between H-2 and H-3ax, is consistent with H-2 being axial and hence ring C is in the more stable equatorial orientation.

Table 4. 16: NMR data for usambarin M (**126**) in $CDCl_3$

Position	**^{1}H NMR (δ_H)**	**^{13}C NMR(δ_C)**	**COSY**	**HMBC**
2	4.93 *dd* (10.3, 2.4)	78.0	H-3	C-4, C-2', C-6',
3	2.09 *m*	30.1	H-3, H-4	C-2, C-5
4	2.90 *dd*, (11.4,6.0) 2.73 *dd*, (11.4, 5.3 3.1)	24.8	H-2	C-2, C-3, C-5
4a		-		
5	6.90 *d* (8.0)	113.3		C-4, C-6, C-7, C-8
6-OH	5.57 s	148.5		C-5, C-6, C-7
7		145.6		
8		135.6		
8a		-		
1'		127.8		
2'	7.15 *m*	109.7		C-2, C-3, C-6', C-4'
3'		126.9		
4'-OH	5.13	154.3		C-3', C-5'
5'	6.81 *d* (8.8)	115.9	H-6'	C-3', C-4'
6'	7.15 *d* (7.1)	117.7	H-5'	C-2, C-3, C-4', C-6',
1"	3.37 *d* (7.3)	30.1	H-2"	C-4', C-3', C-2"
2"	5.33 *m*	121.8	H-1"	C-4", C-5"
3"		135.2		
4"- **CH_3**	1.78	18.1		C-1", C-2",
5" **-CH_3**	1.78	25.8		
1'"	3.33 *d* (6.7)	27.0		C-8, C-2'", C-4'", C-5'"
2'"	5.08	123.5		C-4'", C-5'"
3'"		131.5		
4'"-**CH_3**	1.56	26.0		C-2'", C-3'", C-5'"
5'"-**CH_3**	1.35	17.8		C-2'", C-3'", C-4'"
7-**OMe**	3.86	61.4		C-7

4.2 Compounds isolated from the roots and leaves of *Mundulea sericea*

The extraction of *Mundulea sericea* stems followed by chromatographic separation resulted in the isolation of five compounds identified as lupinifolinol (**127**), dehydrolupinifolinol (**128**), lupinifolin (**129**), mundulinol (**64**) and sericetin (**130**). Similar phytochemical investigation of the

roots led to the identification of mutenone (**70**), rotenone (**63**), striatine (**131**), stigmasterol (**88)**, and 7-hydxoxy-9-methoxy-2'-isopropenyldihydrofuranpterocarpan (**132**).

4.2.1 Lupinifolinol (127)

Compound **127** was isolated as a white amorphous solid. It was given a molecular formula, $C_{25}H_{26}O_6$, from HREI-MS, which showed a molecular peak ion at *m/z* 423.1807. The UV (λ_{max} 260, 320 nm), NMR data (Table 4.17), and (Appendix 17A-17I) are consistent with the presence of a flavanonol skeleton (Muiva-Mutisya *et al*., 2018). The NMR data showed typical signals for ring C protons of a flavanonol at δ_H 4.98 (H-2), 4.51 (H-3) and 3.60 (3-OH) (Muiva-Mutisya *et al*., 2018). In agreement with this, the ^{13}C NMR data (Table 4.17) revealed carbon resonances at δ_C 83.0 (C-2), 72.6 (C-3) and 196.2 (C-4). The nature of ring C was confirmed by the HMBC cross peaks of H-2 with C-3, C-4 and C-1', as well as by those of H-3 with C-1', C-2 and C-4'.

In ring B, the proton NMR spectrum showed an AA'XX' spin designation appearing at δ_H 7.40 (H-2'/6', δ_C 129.1) and δ_H 6.84 (H-3'/5', δ_C 115.6) and with oxygenation at C-4' (δ_C 156.4). Ring A is fully substituted with a 2,2-dimethylpyrano ring, a hydroxy substituent at C-5 (δ_H 11.37), and γ,γ-dimethylallyl moiety. Considering that the C-5 and C-7 positions of flavononols are expected to be oxygenated on the basis of biosynthesis, there are two possible structures (**127** and **127a**) differing in the placement of the pyrano ring and the prenyl unit. One of the olefinic protons of the pyran ring, H-4" (δ_H 6.64), showed HMBC association with C-6 (δ_C 103.3), allowing the placement of this substituent at C-7/C-6, and hence the location of the prenyl substituent is at C-8. Moreover, H-1'" of the prenyl group showed HMBC correlation with C-8a (δ_C 159.5) and C-7 (δ_C 160.9). Based on the above spectroscopic evidence, compound **127** was identified as lupinifolinol (Ingham *et al*., 1988).

Its relative configuration at C-3/C-2 was determined as *trans* from the large vicinal coupling constant (J = 11.9 Hz) between H-2 (δ_H 4.98) and H-3 (δ_H 4.51), suggesting a 1,2-diaxial relationship of these protons. Hence, two absolute configurations, (2*R*,3*R*) and (2*S*,3*S*) were possible (Muiva-Mutisya *et al*., 2018). The electronic circular dichroism (ECD) spectrum (Appendix 17I) showed a negative Cotton effect within the range of the $\pi \rightarrow \pi^*$ transitions (*ca*. 300–340 nm), consistent with the (2*R*,3*R*) absolute configuration of **127** (Muiva-Mutisya *et al*., 2018).

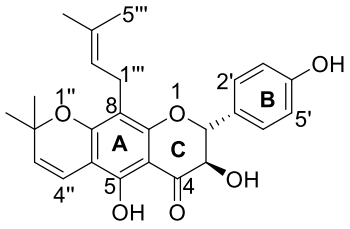

127

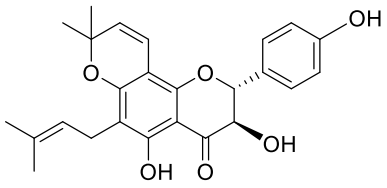

127 a

Table 4.17: NMR data for lupinifolinol (**127**) in $CDCl_3$

No	**^{1}H NMR (δ_H)** (J in Hz)	**^{13}C NMR(δ_C)**	**HMBC**
2	4.98 *d* (11.9)	83.0	C-3, C-4, C-1'
3	4.52 *dd* (11.9, 1.6)	72.6	C-2, C-4, C-1'
4		196.2	
4a		100.4	
5		156.4	
6		103.4	
7		160.9	
8		109.4	
8a		159.5	
1'		128.8	
2'/6'	7.40 AA'	129.1	C-2, C-1', C-3'/5', C-4'
3'/5'	6.84 XX'	115.6	C-1', C-2'/6', C-4'
4'		156.4	
2''		78.6	
3''	5.53 *d* (10.1)	126.5	C-6, C-2''
4''	6.64 *d* (10.0)	115.5	C-7, C-6, C-2''
2''-$(CH_3)_2$	1.45	28.5	C-2'', C-3'', C-4''
1'''	3.19 *m*	21.4	C-8, C-2''', C-3''',
2'''	5.12 *m*	122.2	C-1''', C-4''', C-5'''

3'''		131.5	
4'''-CH_3	1.64 br s	26.0	C-2''', C-3''', C-5'''
5'''-CH_3	1.60 br s	17.9	C-2''', C-3''', C-4'''
5-OH	11.37 *s*		C-4a, C-5, C-6

4.2.2 Dehydrolupinifolinol (128)

Compound **128** was obtained as a yellow solid. It was given a molecular formula of $C_{25}H_{24}O_6$ from HREI-MS (at *m/z* 420.1560 $[M]^+$). (Appendix 18A-18G) and NMR data (Table 4. 18) particularly the ring C carbon atoms resonating at δ_C 147.3 (C-2), 136.7 (C-3) and 177.0 (C-4) suggested that it is a 3-hydroxyflavone derivative. In the ^1H NMR spectrum (Table 4. 18) displayed an AA'XX' spin designation appearing at δ_H 7.05 (H-3′/5') and at δ_H 8.19 (H-2′/6')] with the corresponding carbon at δ_C 116.5 (C-3′/5') and δ_C 130.6 (C-6′/2') is consistent with a 4′-oxygenated ring B.

As in compound **127** and the other flavonoids of this plant, ring A is fully substituted with a 2,2-dimethylpyrano ring, a hydroxy substituent and, a γ,γ-dimethylallyl moiety. The placement of the pyrano ring and the prenyl unit, was fixed based on HMBC correlations. One of the olefinic protons of the pyran ring, H-4" (δ_H 6.64), showed HMBC association with C-6 (δ_C 103.3), placing this substituent at C-6/C-7 junction, and hence locating the prenyl moiety at C-8. Moreover, H_2-1''' of the prenyl group showed HMBC correlation with C-7 (δ_C 160.9) and C-8a (δ_C 159.5). Further evidence on the prenyl group's location was obtained *via* NOESY spectrum, which showed an interaction between H_2-1''' and H-2' of ring B. This compound, was therefore, characterized as dehydrolupinifolinol (**128**), previously reported from the roots of *Sophora tonkinensis* (Deng *et al*., 2007).

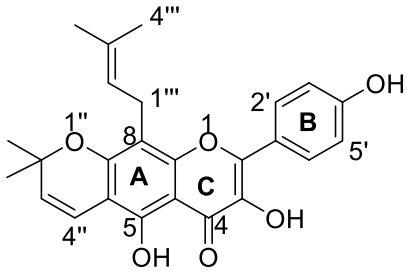

128

Table 4. 18: NMR data for dehydrolupinifolinol (**128**) in $CDCl_3$

Position	**^{1}H NMR (δ_H) (J in Hz)**	**^{13}C NMR (δ_C)**	**HMBC**	**NOESY**
2		147.4		
3		157.4		
4		177.0		
4a		105.4		
5		154.3		
6		104.4		
7		153.7		
8		108.9		
8a		154.2		
1'		123.6		
2'/6'	8.19 *d* AA'	130.6	C-2, C-2', C-4'	H-1'''
3'/5'	7.05 *d* XX'	116.5	C-2, C-3'/ C-5', C-1'	
4'		160.4		
2"		78.8		
3"	5.80 *d* (10.0)	129.4	C-6, C-2", C-4",	H-4"
4"	6.71 *d* (10.0)	116.2	C-5, C-7, C-2", C-3"	H-3"
2"-$(CH_3)_2$	1.68	27.5		
1'''	3.55 *d* (7.1)	21.4	C-7, C-8, C-8a, C-2''', C-3'''	H-2', H-2''', H-5'''
2'''	5.26 *m*	123.3	C-4''', C-5'''	H-1''', H-4'''
3'''		132.6		
4'''-CH_3	1.65 *s*	25.4	C-4''', C-5'''	H-2'''
5'''-CH_3	1.85 *s*	17.0		H-1'''
OH	12.49 br s			

4.2.3 Lupinifolin (129)

Compound **129** was isolated as colourless crystals. The (Appendix 19A-19G), NMR data (Table 4. 19), displayed three typical flavanone skeleton signals at δ_H 5.34 (H-2), 2.80 (H-3) and 3.04 (H-3). In support of this, the ^{13}C NMR spectrum showed carbon resonances at δ_C 78.7 (C-2), δ_C 196.7 (C-4) and δ_C 43.24 (C-3).

Ring B of compound **129** is identical to that of compound **127**, where the proton NMR spectrum showed an AA'XX' spin system at δ_H 6.88 (H-3'/5'), and 7.32 (H-2'/6') with their carbon resonating at δ_C 115.7 (C-3'/5') and 127.9 (C-6'/2'). Ring A is also identical to that of compound **127,** it is fully substituted with hydroxy group at C-5 (δ_H 12.2), 2,2-dimethylpyrano ring and γ,γ-dimethylallyl group. As in compound **127**, H_2-1" of the prenyl group associated with C-7 (160.1) and C-8a (156.0) hence the prenyl substituent was placed at C-6, while the olefinic protons in the pyran ring, H-1'" (δ_H 6.63) showed correlation with C-8 (δ_C 108.8) placing the 2,2-dimethylpyrano ring at C-7/C-6 junction. This compound was therefore characterized as the known flavanone lupinifolin (**129**) (Khaomek *et al*., 2008).

Table 4. 19: NMR data for lupinifolin (**129**) in $CDCl_3$

Position	**^{1}H NMR (δ_H)**	**^{13}C NMR(δ_C)**	**HMBC**
2	5.34 *dd* (12.1, 3.0)	78.6	
3	3.04 *dd*, (17.0, 12.0) 2.80 *dd*, (17.1, 3.1)	43.4	C-4a, C-4/C-2, C-1', C-4
4		196.7	
4a		103.0	
5-OH	12.2 *s*	159.5	
6		102.8	
7		160.1	
8		108.8	
8a		156.0	
1'		131.3	
2'/6'	7.32 *m*	127.9	
3'/5'	6.88 *m*	115.7	

4'		156.7	
2"		78.3	
3"	5.50 *d* (10.0)	126.1	C-8, C-2"
4"	6.63 *d* (10.0)	115.8	C-8, C-8a , C-2"
2"-(CH_3)$_2$	1.44 *s*	28.5	
1'"	3.23 m	21.6	C-5, C-6, C-7, C-1'", C-2'", C-4'", C-5'"
2'"	5.14 *tt* (7.6, 7.6, 1.5, 1.5)	122.6	
3'"		131.2	
4'"-CH_3	1.65 *m*	18.0	
5'"-CH_3		26.0	

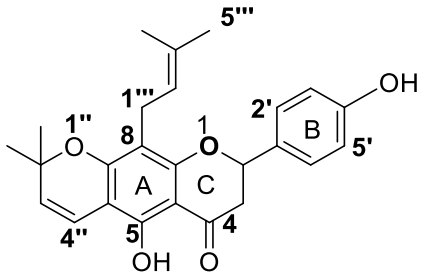

129

4.2.4 Mundulinol (64)

Compound **64** was isolated as a white paste. The (Appendix 20A-20G) and NMR data (Table 4. 20), displayed three typical proton signals of a flavanonol skeleton [δ_H 4.53 (H-3), 5.05 (H-2) and 3.55 (3-OH)]. The ^{13}C NMR showed a carbonyl signal (δ_C 196.7, C-4), an oxymethine peak (δ_C 83.1, C-2) and a methine signal (δ_C 72.5, C-3).

Ring B was unsubstituted, as shown from the NMR data which displayed protons at δ_H 7.59 (*dd*, H-3'/5'), 7.45 (H-2'/6'), 7.45 (H-4') with their carbons resonating at δ_C 127.4 (C-3'/5'), 129.1 (C-4') and 128.5 (C-6'/2'). Ring A is identical to that of compound **127**. It is fully substituted with a hydroxy group at C-5 (δ_H 11.43), 2,2-dimethylpyrano ring and γ,γ-dimethylallyl moiety. As in compound **127**, H-1'" of the pyran ring at δ_H 6.67 correlated with C-6 (δ_C 103.2) placing the 2,2-

dimethylpyrano ring at C-7/C-6 junction. H_2-1" of the γ,γ-dimethylallyl correlated with C-7 and C-8a, hence placing the prenyl substituent at C-8. This compound was therefore characterized as mundulinol (**64**) (Cao *et al*., 2004). Its relative configuration at C-3/C-2 was determined as *trans* from the large vicinal coupling constant (J = 11.9 Hz) between H-2 (δ_H 5.08) and H-3 (δ_H 4.53), suggesting a 1,2-diaxial relationship of these protons. Hence, two absolute configurations, (2*R*,3*R*) and (2*S*,3*S*) were possible (Muiva-Mutisya *et al*., 2018).

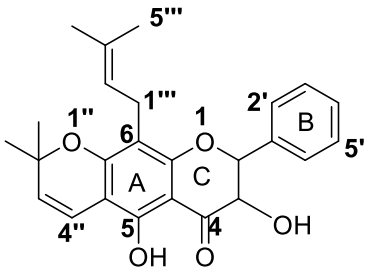

64

Table 4. 20: NMR data for mundulinol (**64**) in $CDCl_3$

Position	**^{1}HNMR (δ_H)**	**^{13}CNMR(δ_C)**	**HMBC**
2	5.08 *d* (11.9)	83.1	C-3, C-2'/6'
3	4.53 *d* (11.9)	72.5	C-2, C-4a
4		196.7	
4a		136.6	
5-**OH**	11.43 *s*	160.7	
6		103.2	
7		159.3	
8		109.3	
8a		156.0	
1'		131.4	
2'/6'	7.45 *t* (7.41, 7.4)	128.5	
3'/5'	7.57 *d* (7.5)	127.4	
4'	7.45 *t* (7.2, 7.2)	129.1	
2"		78.6	
3"	5.56 *d* (10.0)	126.3	
4"	6.67 *d* (10.0)	115.5	C-8, C-8a, C-2"
2"-**(CH_3)$_2$**	1.49 *s*	28.4	
1'''	3.22 *qd* (14.0, 14.0, 14.0, 7.3)	22.7	C-6, C-7, C-2''', C-3''', C-5'''
2'''	5.17 *m*	122.2	C-1''', C-4''', C-5'''

3'''		131.4
4'''-**CH_3**	1.68 *s*	17.8
5'''-**CH_3**	1.68 *s*	26.9

4.2.5 Sericetin (130)

Compound **130** was obtained as a yellow amorphous solid. Similar to compound **129**, The (Appendix 21A-21G), ^{13}C NMR spectral data (Table 4. 21), particularly the ring C carbon atoms resonating at δ_C 144.9 (C-2), 175.4 (C-4) and 136.4 (C-3) suggested that the compound is a 3-hydroxyflavone (Burns et al., 2007).

Ring B was unsubstituted, the NMR data showed protons at δ_H 8.23 (H-5'/3', δ_C 127.6), 7.55 (*dd*, H-2'/6', δ_C 128.7), 7.49 (H-4', δ_C 130.1)]. Ring A is identical to compound **127**, it is fully substituted with a hydroxy group at C-5 (δ_H 11.23), a 2,2-dimethylpyrano ring, and prenyl moiety. The placement of these groups was confirmed by HMBC correlation. As in compound **127**, H-1''' of the pyran protons at δ_H 6.77 showed correlation with C-6 (δ_C 104.9) placing the 2,2-dimethylpyrano ring at C-7/C-6 junction. The prenyl substituent was located at C-8, since H-1'' of γ,γ-dimethylallyl associated with C-8a (δ_C 156.0) and C-8 (δ_C 109.3). Therefore this compound is characterized as sericetin (**130**) (Jain & Zutshi, 1973).

Table 4. 21: NMR data for Sericetin (**130**) in $CDCl_3$

Position	**^{1}H NMR (δH) (J in Hz)**	**^{13}C NMR (δC)**	**HMBC)**
2		144.9	
3		136.4	
4		175.7	
4a		103.6	
5-**OH**	11.23 *s*	157.2	
6		104.9	
7		153.7	
8		107.8	
8a		153.1	

1'		131.2	
2'/6'	7.55 *dd* (8.5, 7.0)	128.7	
3'/5'	8.23 *m*	127.6	C-2'/6', C-4'
4'	7.49 *m*	130.1	
2"		78.8	
3"	5.68 *d* (10.0)	128.3	C-8, C-2"
4"	6.77 *d* (9.9)	115.7	C-8, C-8a, C-2"
2"-**(CH_3)$_2$**	1.5 *s*	28.3	
1'"	3.56 *d* (7.1)	21.6	C-5, C-6, C-7, C-2'", C-3'"
2'"	5.26 *tt* (7.3,7.3, 1.4 1.4)	122.5	
3'"		131.1	
4'"-**CH_3**	1.72 (1.4)	25.8	
5'"-**CH_3**	1.86 (1.6)	18.2	

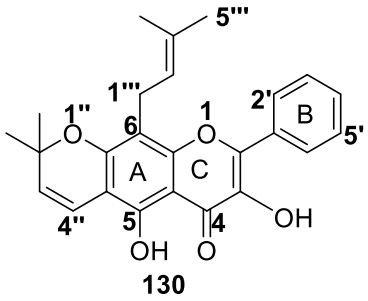

130

4.2.6 Munetone (70)

Compound **70** was isolated as a yellow amorphous solid. The UV (λ_{max} 280 nm), (Appendix 22A-22E) and NMR data (Table 4. 22), showing an up-field singlet at δ_H 7.93 (δ_C 156.8), corresponding to H-2 of ring C, is characteristic of isoflavones. Furthermore the ^{1}H NMR data (Table 4. 22) showed the existence of a methoxyl and a pair of 2,2-dimethylpyrano groups.

Ring A had two singlet protons at δ_H 6.81 (H-5, δ_C 104.2) and δ_H 7.89 (H-8, δ_C 123.6). Then the 2,2-dimethyl pyran group was placed at C-7/ C-6, a placement that was established through HMBC relationships between H-8 (δ_H 6.81), with C-8a (δ_C 154.3) and C-7 (157.6), together with the association of H-4'" (δ_H 6.47) with C-7 (157.6) and C-6 (δ_C 119.6).

Ring B had a pair of doublets at δ_H 6.66 and 7.14 that were ascribed to H-5' (δ_C 112.4) and H-6' (δ_C 131.7) respectively. In addition, the ring is disubstituted with a methoxy group and the second 2,2-dimethylpyrano moiety, the methoxy substituent was placed at C-4' (δ_C 154.1). The placement of the 2,2-dimethylpyrano residue was confirmed using HMBC correlation whereby H-4" correlated with C-6' (δ_C 131.7). Therefore compound **70** was identified as munetone, previously isolated from *Mundulea suberosa* (Rao *et al*., 1999).

Table 4. 22: NMR data for munetone (**70**) in $CDCl_3$

Position	**^{1}H NMR (δH) (J in Hz)**	**^{13}C NMR (δC)**	**HMBC)**
2	7.93 *s*	158.8	C-3, C-4, C-8a, C-1'
3		121.5	
4		176.0	
4a		118.6	
5	7.89 *s*	123.6	C-4, C-4a, C-6
6		119.6	
7		157.6	
8	6.81*s*	104.2	C-7, C-8a
8a		154.3	
1'		117.1	
2'		154.3	
3'		114.9	
4'		154.1	
5'	6.66 *d* (8.4)	112.4	C-1', C-4'
6'	7.14 *d* (8.4)	131.7	C-4, C-3', C-4'
2"		76.0	
3"	5.67*d* (9.0)	130.4	C-2", C-3"
4"	6.64 *d* (9.0)	117.2	C-6', C-2"
2"-**(CH_3)$_2$**	1.47	26.3	
2"'		77.9	
3"'	5.76 *d* (10.0)	131.7	C-6
4"'	6.47 *d* (10.0)	121.3	C-6, C-7
2"-**(CH_3)$_2$**	1.5	28.4	
2'-**OCH_3**	3.61	61.9	

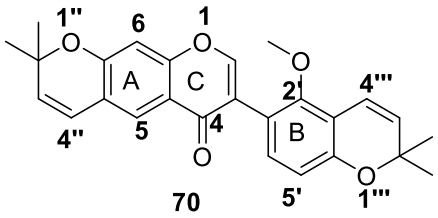

4.2.7 Rotenone (63)

Compound **63** was isolated as a white paste.The (Appendix 23A-23E), NMR data (Table 4. 23) [δ_H 4.19 (*dd, J* = 12.2, 1.0 Hz, 1H, H-6, δ_C 66.3), 4.62 (*dd, J* = 12.1, 3.1 Hz, 1H, H-6, δ_C 66.3), 4.94 (*ddd, J* = 3.1, 1.5, 1.2 Hz, 1H, H-6a, δ_C 72.2) and 3.84 (*d,* 1H, H-12a, δ_C 44.6)] are typical of a rotenoid skeleton (Luyengi *et al*., 1994).

In Ring D, NMR data (Table 4. 23), displayed *ortho*-correlated protons at δ_H 7.85 and 6.52 (*d, J* = 8.7 Hz, H-11/H-10). The substituent on ring D was identified to be 2'-isopropenyldihydrofuran moiety from the proton signals at δ_H 2.96 (*dd J* = 15.8, 8.1, 1H, H-3'β), 3.33 (*dd J* = 15.8, 9.8, 1H, H-3'α), 5.09 (*dt J* = 1.7, 0.9, 1H, H-5'), 5.25 (*dd J*=9.7, 8.2, 1H, H-2') and methyl signal at 1.76 (*s,* 3H). The location of the isopropenyldihydrofuran residue between C-8 (δ_C 113.0) and C-9 (δC 167.4) of ring D was confirmed by HMBC association of H-3', H-11 and H-10 with C-9 and C-8.

In ring A, signals at δ_H 6.77 (s) and δ_H 6.46 (s) were ascribed to H-1 and H-4, respectively. It is also disubstituted with two methoxy groups (δ_H 3.73 and 3.77). The placement of the methoxy substituents was established by HMBC correlation of methoxy signals at δ_H 3.73 to C-3 (δ_C 147.3) and δ_H 3.77 to C-2 (δC 143.8) and also correlation of δ_H 6.77 (H-1) and δ_H 6.47 (H-4) correlation with C-3 and C-2. This compound **63** was identified as rotenone (Gupta, 2012).

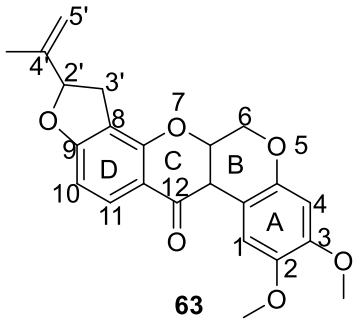

63

Table 4. 23: NMR data for Rotenone (**63**) in $CDCl_3$

Position	**^{1}H NMR (δH) (J in Hz)**	**^{13}C NMR (δC)**	**HMBC)**
1	6.77*s*	112.6	C-3, C-4, C-4a, C-12a, C-12b,
2		143.8	
3		147.3	
4	6.46 *s*	100.9	C-2, C-12a, C-12b,
4a		149.4	
5			
6	4.19 *dt* (12.2, 1.0, 1.0) 4.62 *dd* (12.1, 3.1)	66.3	C-4a, C-6a, C-12, C-12a
6a	4.94 *ddd* (3.1, 1.5, 1.5, 1.2)	72.2	C-6, C-12b, C-12
7a		158	
8		113.0	
9		167.4	
10	6.52 *d* (8.6)	104.9	C-8, C-9, C-11
11	7.85 *d* (8.7)	130.0	C-8, C-9, C-12
11a		113.3	
12		189.1	
12a	3.84 *d*	44.6	C-4a, C-12, C-12b
12b		104.7	
2'	5.25 *dd* (9.7, 8.2),	87.8	C-4', C-8'
3'	3.33 *dd* (15.8, 9.8), 2.96 *dd* (15.8, 8.1)	31.3	C-9, C-2', C-4', C-5'
4'		143.0	
5'	5.09 *dt* (1.7, 0.9)	113.3	C-2', C-4'
4'- **CH_3**	1.75 *s*	18.4	
2- **OCH_3**	3.77 *s*	56.3	C-2
3- **OCH_3**	3.73 *s*	58.4	C-3

4.2.8 Striatine (131)

Compound **131** was obtained as a white amorphous solid. The (Appendix 24A-24G), ^{1}H [δ_H 3.52 (*m*, 1H, H-6a), 4.25 (*m*, 1H, H-6α), 3.62 (*m*, 1H, H-6β), and 3.84 (*m*, H-12a)] and ^{13}C [at δ_C 66.5 (C-6) and 40.1 (C-6a)] NMR data (Table 4.24) are typical of a pterocarpan skeleton. The existence of two hydroxy and two dimethylallyl substituents were also evident from the NMR data (Table 4.24), and the placement of the hydroxy groups at C-3 and C-9 was based on the expected oxygenation from biogenetic consideration of pterocarpans of *Mundulea* (Manjary *et al*., 1993).

In ring A, there was, two singlet proton signals at δ_H 7.43 (H-1) and 6.47 (H-4), allowing the placement of one of the of dimethylallyl substituents at C-2 (δ_C 126.6). The placement was established by HMBC association [CH_3 and H-1 both correlated with C-2]. In ring D, the two *ortho* correlated (*J*= 8.0 Hz) signals at δ_H 6.42 and δ_H 6.99 were ascribed to H-7 and H-8, respectively, with their carbons appearing at δ_C 122.4 (C-7) and 108.2 (C-8). The second dimethylallyl substituent can then be placed at C-10 (δ_C 110.3) of ring D. The placement was confirmed by HMBC association [H_2-1' and H-8 both associated with C-10]. Therefore, compound **131** was identified as striatine (Manjary *et al*., 1993).

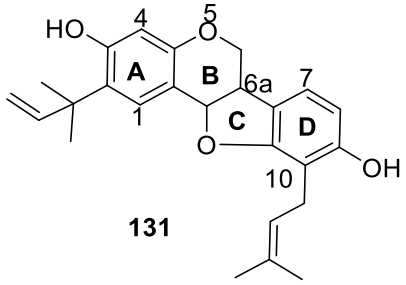

131

Table 4.24: NMR data for striatine (**131**) in $CDCl_3$

Position	^{1}HNMR (δ_H)	^{13}CNMR(δ_C)	HMBC
1	7.43 *s*	128.9	C-1a, C-2, C-3, C-4, C-11a, C-1'''
1a		112.1	

2		126.6	
3		155.9	
4	6.48 *s*	105.6	C-1a, C-2, C-3, C-11a, C-1'''
4a		155.6	
6	4.25 *m* , 3.62 *m*	66.5	C-4a, C-6a, C-6b, C-11a
6a	3.52 *m*	40.1	C-6, C-6b, C-7, C-11a
6b		118.8	
7	6.99 *d* (*J*= 8.0)	122.4	C-6, C-6a, C-9, C-10, C-10a
8	6.42 *d* (*J*= 8.0)	108.2	C-6a, C-6b, C-9, C-10, C-10a, C-1'
9		156.3	
10		110.3	
10a		158.4	
11a	5.48 *m*	78.4	C-1a, C-2, C-6, C-6a, C-6b, C-10a
1'	3.42	23.3	C-9, C-10, C-10a, C-2', C-3'
2'	5.34 *m*	121.5	
3'		135.2	
4'	1.78 *s*	25.9	C-10, C-2', C-3', C-5'
5'	1.84 *s*	17.9	C-10, C-1', C-2', C-3',
1"		39.9	
2"	1.50 *s*	27.1	C-2, C-1", C-4"
3"	1.50 *s*	27.1	C-2, C-1", C-4"
4"	6.23 *dd* (*J*= 17.7, 10.5)	147.9	C-2, C-1", C-2"
5"	5.41 *m*	113.8	C-2, C-1", C- 4"

4.2.9 7-Hydxoxy-9-methoxy-2,3-(prop-1-en-2-yl)-dihydrofuranpterocarpan (132)

Compound **132** was obtained as a white amorphous solid. (Appendix 25A-25D) and ^{1}H (Table 4. 25) NMR [δ_H 3.56 (*m*, 1H, H-6a), 4.26 (*m*, 1H, H-6α), 3.66 (*m*, 1H, H-6β) and 5.49 (*m*, H-12a)] and the ^{13}C NMR δ_C 66.7 (C-6) 40.3 (C-6a), and C-12a] data are typical of a pterocarpan skeleton. The evidence for the presence of 2'-isopropenyldihydrofuran, methoxy, hydroxy substituents was also obtained from the NMR data (Table 4. 25). The compound is oxygenation at C-3 and C-9 as expected for pterocarpans on biogenetic ground (Manjary *et al*., 1993).

In ring A, signals at δ_H 7.28 (*s*) and δ_H 6.46 (*s*) were ascribed to H-1 and H-4, respectively, with their carbons appearing at δ_C 126.7 (C-1) and δ_C 97.7 (C-4). This requires the presence of

substituent at C-2 and C-3 in ring A. This substituent was established to be 2'-isopropenyldihydrofuran from the long range proton-carbon correlation [H-3' and H-1 associated with C-2; H-4 correlated with C-3]. The methoxy and hydroxy groups should then be placed in ring D.

In ring D, two broad singlets appearing at δ_H 6.87 and δ_H 6.37 were ascribed to H-10 and H-8, respectively, with their carbons at δ_C 97.5 (C-8) and δ_C 107.0 (C-10) respectively. This requires the placement of methoxy and hydroxy groups at C-7 and C-9 of ring D. HMBC correlation of the methoxy protons (δ_H 3.89) with C-9] supported its placement at C-9, and hence the hydroxy at C-7. Therefore, compound **132** was identified as 7-hydxoxy-9-methoxy-2'-isopropenyldihydrofuranpterocarpan.

Table 4. 25: NMR data for compound **132** in $CDCl_3$

Position	**^{1}H NMR (δ_H)**	**^{13}C NMR(δ_C)**	**HMBC**
1	7.28 *s*	126.7	C-2, C-3, C-3'
1a		119.7	
2		126.6	
3		160.4	
4	6.46 *s*	102.9	C- 2, C-3, C-4a
4a		154.0	
6	4.26, *dd*, (*J*=10.9, 4.8), 3.66, *d*, (*J*=10.7)	66.7	C-4a, C-6a, C-6b, C-11a
6a	3.56 *d*, (*J*=7.1)	40.3	C-6, C-6b, C-7, C-11a
6b		111.5	
7	6.37 *s*	97.5	
8		140.9	C-6a, C-6b, C-9, C-10
9		153.8	
10	6.87*s*	107.0	
10a		147.5	
11a	5.49 *m*	78.6	
2'	5.22 *m*	86.7	C-4'
3'	3.36 *ddd*, (*J*=15.4, 9.5, 1.2), 3.02 *m*	33.9	C-2, C-2', C-4', C-5'
4'		144.2	
5'	5.09 *m*	111.7	C-2', C-4'
4'- **CH_3**	1.79 *t*, (*J*=1.2, 1.2)	16.9	

2-OH	5.77 *s*		
3- **OCH$_3$**	3.89 *s*	56.9	C-9

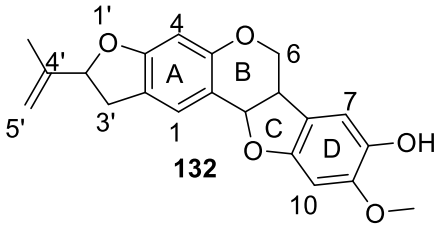

132

4.2.10 Stigmasterol (88)

Compound **88** was obtained as white crystals. The (Appendix 26A-26E) and NMR data revealed the existence of 29 carbon peaks, including four olefinic carbons [δ_C 140.9 (C-5), δ_C 121.9 (C-6), 138.5 (C-22), and 129.4 (C-23)] and an oxygenated carbon (δ_C 72.0, C-3). The proton NMR spectrum revealed signals at δ_H 5.02 *dd* (*J* = 151, 8.7 Hz, H-22), 5.15 *dd* (*J* = 15.2, 8.6 Hz, H-23), δ_H 3.52 m (H-3) and δ_H 5.35 m (H-6). Therefore, compound **88** was identified as stigmasterol (Pierre & Moses, 2015).

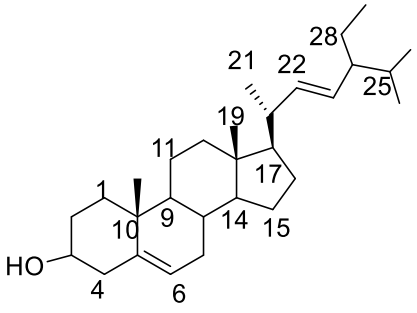

88

4.3 Compounds isolated from the stems of *Tephrosia uniflora*

Chromatographic separation of the stems of *T. uniflora*, yielded a new chalcone, (*S*)-elatadihydrochalcone-2'-methyl ether (**133**), elongatin (**87**), elatadihydrochalcone (**85**), and 12a-hydroxydeguelin (**123)**.

4.3.1 (*S*)-elatadihydrochalcone-2'-methyl ether (133)

Compound **1** was isolated as a colourless solid, and was assigned a molecular formula $C_{22}H_{24}O_5$ based on HREIMS $[M+1]^+$ *m/z* 369.1702, (Appendix 27A-27K), and NMR data (Table 4. 26). The UV (λ_{max} 214, 263, 310 nm), ^{1}H NMR [δ_H 3.25 (*dd*, J = 17.4, 3.8 Hz) and 3.15 (*dd*, J = 17.3 9.5 Hz) for CH_2-α; 5.28 (*dd*, J = 9.5, 2.8 Hz, for H-β] and ^{13}C NMR (δ_C 204.4 (C=O), 53.6 (C-α), and 70.6 (C-β) showed the compound has a β-hydroxydihydrochalcone skeleton (Muiva et al., 2009).

Ring A is unsubstituted, as revealed by the ^{1}H NMR spectrum which displayed signals at δ_H 7.40 (H-2/6), 7.34 (H-3/5), and 7.26 (H-4) with the corresponding carbon resonances appearing at δ_C 126.0 (C-2/6), 128.5 (C-3/5), 127.8 (C-4). Ring B, on the other hand, is tetra-substituted with two methoxy and a 2,2-dimethylpyran groups (Table 4. 26), with C-2′, C-4′ and C-6′ oxygenated as expected from biogenetic considerations of chalcones. This was supported by ESI-MS fragment ion at *m/z* 247 (**1a**). The HMBC correlation of H-5' (δ_H 6.19) to C-3' (δ_C 108.3), C-4" (δ_C 116.4), and C-4' (δ_C 156.6); H-4" (δ_H 6.47 to C-4' (δ_C 156.6) allowed the placement of the 2,2-dimethylpyran group between C-3′ and C-4′ with the oxygen at C-4′. The two methoxy groups were therefore placed at C-2′ (δ_C 154.6) and C-6′ (δ_C 157.9). Hence, the gross structure of the new compound (**1**) was characterized as 2',6'-dimethoxy-3'/4'(2",2"-dimethyl-2H-chromen-6-yl)-β-hydroxydihydrochalcone, trivial name elatadihydrochalcone-2' methyl ether. The ECD spectrum showed a negative Cotton effect at 275 nm suggesting *S*-configuration at the β carbon as

elatadihydrochalcone (**3**), a co-metabolite, which has earlier been reported from *T. elata* (Muiva et al., 2009), and synthetic β-hydroxydihydrochalcone (Nel et al., 1999).

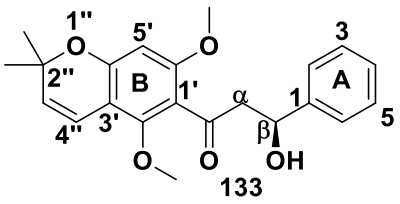

Table 4. 26: NMR data for (*S*)-elatadihydrochalcone-2'-methyl ether (**133**) in $CDCl_3$

No	**δ_H** (J in Hz)	**(δ_C)**	**HMBC**	**COSY**	**NOESY**	**TOCSY**
CH_2-α	3.25 *dd* (17.4, 3.8)	53.6	C-7, C-β	H-β	-	H-β
	3.15 *dd* (17.3 9.5)		C-7, C-β	-	-	-
β	5.28 *dd* (9.5, 2.8)	70.6	C-1, C-3, C-5	H-α	H-α	H-α
1	-	143.2	-	-	-	-
2/6	7.40 *m*	126.0	C-4, C-β	-	-	-
3/5	7.34 *m*	128.5	C-1, C-3, C-5	-	-	-
4	7.26 *m*	127.8	C-2, C-6	-	-	-
7	-	204.4	-	-	-	-
1'	-	117.6	-	-	-	-
2'	-	157.9	-	-	-	-
3'	-	108.3		-	-	-
4'	-	156.6	-	-	-	-
5'	6.19 *s*	96.3	C-3', C-4', C-4"	-	6-OMe	-
6'	-	154.6	-	-	-	-
2"	-	77.4	-	-	-	-
3"	5.55 *d* (9.9)	127.6	C-3', C-2"	H-4"	2"-Me, C-4"	H-4"
4"	6.47 *d* (9.9)	116.4	C-4', C-2"	H-3"	2-OMe, H-3"	H-3"
2"-Me_2	1.43 *s*	28.1	C-2"-Me, C-2"	-	H-3"	-
2-OMe	3.76 *s*	63.9	C-2'	-	H-4"	-
6-OMe	3.75 *s*	56.0	C-6'	-	H-5'	-

4.3.2 Elongatin (87)

Compound **87** was isolated as a white solid. The UV (λ_{max} 280 nm), (Appendix 28A-20I) and the NMR data (Table 4. 27), which showed an up-field singlet at δ_H 8.02 (δ_C 156.8), corresponding to H-2 of ring C, is characteristic of isoflavones (Nazir et al., 2008). Further, the NMR data revealed the existence of two methoxy and a 2,2-dimethylpyrano groups.

In Ring A, a singlet proton at δ_H 6.38 (δ_C 98.0) was assigned to H-8, a ring which otherwise is substituted with the 2,2-dimethyl pyran moiety at C-7/C-6 and hydroxy at C-5. The placement of the 2,2-dimethyl pyran moiety at C-7/C-6 was established by HMBC correlation of H-8 (δ_H 6.38) with C-8a (δ_C 159.8) and C-7 (163.0); H-4" (δ_H 6.71) correlated with C-5 and C-7. In Ring B, a pair of singlets at δ_H 6.61 (H-3'; δ_C 101.7 for C-3') and 6.89 (H-6'; δ_C 117.1 for C-6') requires substitution at C-2', C-4' and C-5. The placement of the methoxy groups was confirmed using HMBC experiments. The methoxy group at δ_H 3.75 was placed at C-2' (δ_C 151.5) due to its correlation to C-2', while the methoxy group at δ_H 3.85 was placed at C-5' (δ_C 144.9) due to its correlation to C-5'. Therefore, compound **87** was identified as elongatin previously isolated from *T. uniflora* (Abreu & Luis, 2006).

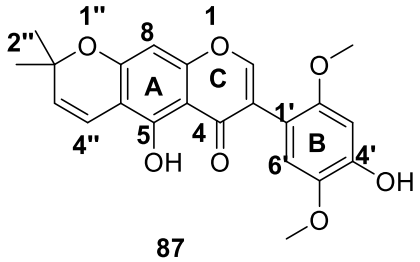

87

Table 4. 27: NMR data for elongatin (**87**) in CD_3OD

No	^{1}H NMR (δ_H) (J in Hz)	^{13}C NMR(δ_C)	HMBC	COSY	NOESY	TOCSY
2	8.02 *s*	156.8	C-3, C-4, C-8a, C-1'	-	-	-
3	-	122.3	-	-	-	-
4	-	182.5	-	-	-	-
4a	-	106.9	-	-	-	-
5	-	158.9	-	-	-	-
6	-	106.5	-	-	-	-
7	-	163.0	-	-	-	-
8	6.38 *s*	98.0	C-4a, C-7, C-8a	-	-	-
8a	-	159.8	-	-	-	-
1'	-	111.0	-	-	-	-
2'	-	151.5	-	-	-	-
3'	6.61 *s*	101.7	C-1', C-2', C-4', C-5'	-	2'-OMe	-
4'	-	153.9	-	-	-	-
5'	-	144.9	-	-	-	-
6'	6.89 *s*	117.1	C-3, C-1', C-2', C-4', C-5'	-	2'-OMe	-
2"	-	81.4	-	-	-	-
3"	5.74 *d* (10.1)	131.8	C-6, C-2"	H-4"	H-4", 2"-Me,	H-4"
4"	6.71 *d* (10.1)	116.1	C-5, C-7, C-2"	H-3"	H-3"	H-3"
2'-'Me	1.50	30.7	C-2"Me	-	-	-
2"-Me	1.50	30.7	C-2"Me	-	H-3"	-
2'-OMe	3.75	56.7	C-2'	-	H-3', H-6'	-
5'-OMe	3.85	57.4	C-5'	-	-	-

4.3.3 Elatadihydrochalcone (85)

Compound **85** was isolated as a yellow oil. The (Appendix 29A-29I) and NMR data (Table 4. 28) (δ_H 3.37 (*dd J* = 18.2, 9.4 Hz) and 3.45 (*dd J* = 12.8, 10.2 Hz) for $CH_2\alpha$; 5.28 (*d J* = 9.2 Hz) for H-β) and ^{13}C (δ_C = 204.4 for carbonyl, 52.9 for α–carbon, 70.4 for β-carbon) was evident of a β-hydroxydihydrochalcone derivative (Muiva *et al*., 2009).

Ring B is unsubstituted, as shown from the proton NMR spectrum [(δ_H 7.37 (H-3/5), 7.29 (H-4), 7.43 (H-2/6), with the corresponding carbons at δ_C 125.9 (C-2/6), 127.6 (C-4, 128.6 (C-3/5]. Ring A is trisubstituted with a hydroxy, a methoxy and a 2,2-dimethylpyran groups. The existence of a hydroxy group which is highly deshielded (δ_H 13.97) suggested that there was strong intramolecular hydrogen bonding between the hydroxy at C-6' (δ_C 162.9) and carbonyl at C-7 (δ_C 204.4). The location of the 2,2-dimethylpyran group between C-4' and C-5' was established from HMBC spectrum [δ_H 13.97 (6'-OH) to C-6' (C 162.9) and C-5' (C 103.0); δ_H 6.66 (H-4'') to C-5' and C-4']. The methoxy substituent was therefore placed at C-2' (δ_C 163.2). Hence, compound **85** was characterized as elatadihydrochalcone, previously isolated from the seedpods of *Tephrosia elata* (Muiva *et al*., 2009),.

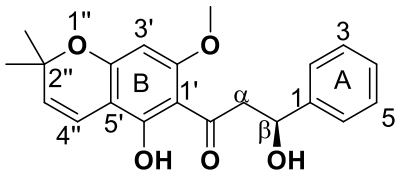

85

Table 4. 28: NMR data for elatadihydrochalcone (**85**) in $CDCl_3$

No	**^{1}H NMR (δ_H)** (J in Hz)	**δ_C**	**HMBC**	**COSY**	**NOESY**	**TOCSY**
α'	3.45 *dd* (12.8, 10.2)	52.9	C-β, C-7	H-β	-	H-β
α''	3.37 *dd* (18.2, 9.4)	52.9	C-β, C-7	-	-	-
β	5.28 *d* (9.2)	70.4	C-2, C-6	H-α'	H-6	H-α'
1'	-	105.8	-	-	-	-
2'	-	163.2	-	-	-	-
3'	5.87 *s*	91.5	C-1', C-2', C-4', C-5'	-	2'-OMe	-
4'	-	160.8	-	-	-	-
5'	-	103.0	-	-	-	-
6'	-	162.1	-	-	-	-
7	-	204.4	-	-	-	-
1	-	143.5	-	-	-	-

2	7.43 *d* (6.9)	125.9	C-β, C-4, C-6	-	-	-
3	7.37 *t* (7.5)	128.6	C-1, C-5	-	-	-
4	7.29 *m*	127.6	C-2, C-6	-	-	-
5	7.37 *t* (7.5)	128.6	C-1, C-3	-	-	-
6	7.43 *d* (6.9)	125.9	C-β, C-2, C-4	-	H-β	-
2"	-	78.5	-	-	-	-
3"	5.46	125.7	C-5, C-2", C-2"Me	H-4"	H-4", H-2"Me, H-2"Me2	H-4"
4"	6.66 *d* (10.0)	115.8	C-4, C-5, C-2"	H-3"	H-3"	H-3"
2"Me/2"Me2	1.44 *s*	28.5	C-2", C-4", C-2"Me	-	H-3"	-
6'-OH	13.97 *s*	-	C-1', C-6'	-	-	-
β-OH	3.43 *d*, (2.7)	-	-	-	-	-
2'-OMe	3.79 *s*	55.8	C-2'	-	H-3'	-

4.3.4 Tephrosin (123)

Compound **124** was isolated as a yellow oil. The (Appendix 30A-30G) and NMR data (Table 4. 29) [δ_H 4.49 (*dd*, *J* = 12.4, 1.1 Hz, H-6, δ_C 64.0), 4.63 (*dd*, *J* = 12.1, 2.5 HzH-6, δ_C 64.0), and 4.57 (*dd*, *J* = 2.4, 1.1 Hz, H-6a, δ_C 77.3)] and δ_C 67.6 (C-12a)] are consistent with a 12a-dydroxyrotenoid skeleton. The ^{1}H NMR data of ring D revealed a pair of *ortho*-correlated (*J* = 8.8 Hz) protons at δ_H 7.73 and 6.47 assigned to H-11 and H10, respectively, with substituents at C-8 (δ_C 111.3) and C-9 (δ_C 160.9). The placement of the substituent which is a 2,2-dimethylpyrano group (Table 4. 29) was established by HMBC association of H-4' to C-9 and C-7a.

Ring A is disubstituted with two methoxy groups, which otherwise displayed two aromatic singlets at δ_H 6.56 (H-1) and 6.46 (H-4). The location of the methoxy groups was established by HMBC association of methoxy signals at δ_H 3.73 to C-2 (δ_C 144.1); and δ_H 3.81 to C-3 (δ_C 151.3) and also correlation of H-4 (δ_H 6.46) and H-1 (δ_H 6.56) to C-2 and C-3. Hence, compound **124** was characterized as tephrosin, previously reported from *M. sericea* (Luyengi *et al*., 1994).

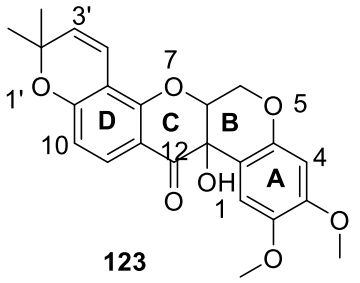

123

Table 4. 29: NMR data for tephrosin (**123**) in $CDCl_3$

No	**^{1}H NMR (δ_H)** (J in Hz)	**^{13}C NMR(δ_C)**	**HMBC**
1	6.56 *s*	109.5	C-2, C-3
1a	-	111.3	-
2	-	144.1	-
3	-	151.3	-
4	6.46 *s*	101.2	-
4a	-	148.5	-
5	-	-	-
6a	4.57 *dd* (2.4, 1.1)	77.3	-
6	4.49 *dd* (12.1, 1.1), *4.63 dd* (12.1, 2.5)	64.0	-
7a	-	156.8	-
8	-	111.3	-
9	-	160.9	-
10	6.47 *d* (11.1)	112.0	-
11	7.73 *d*, (8.8)	129.0	-
11a	-	109.3	-
12	-	191.5	-
12a	-	67.6	-
2'Me2	1.45 *s*	28.7	-
2'Me	1.45 *s*	28.7	-
2'	-	78.2	-
3'	5.55 *d* (10.1)	128.7	C-2'
4'	6.60 *d* (10.1)	115.6	C-7a, C-9, C-2'
2-OMe	3.73 *s*	56.5	C-2
3-OMe	3.81 *s*	56.0, 56.5	C-3
12a-OH	4.40	-	-

4.4 Bioactivity

The anti-plasmodial activity of the crude extract and some selected metabolites of *M. sericea* were evaluated against chloroquine-resistant (W2) and chloroquine-sensitive (3D7) strains of

Plasmodium falciparum. The antileishmanial action of selected metabolites was also investigated against *L. donovani* strains, both antimony-sensitive (MHOM/IN/83/AG83) and antimony-resistant (MHOM/IN/89/GE1). The isolated compounds were also evaluated for their cytotoxicity against human lung adenocarcinoma (A549), human liver cancer (HepG2), human lung/bronchus cells (epithelial virus-transformed, BEAS-2B), immortal human hepatocytes (LO2), and human breast cancer cell line (MCF-7).

4.4.1 *In vitro* antiplasmodial activity

Flavonoids have previously been reported to be effective antimalarial and antileishmanial agents both *in vitro* and *in vivo* (Kaur, Jain, Kaur, & Jain, 2009; Tasdemir *et al*., 2006) prompting for the evaluation of the bioactivities of the isolated metabolites. Using the established protocols, antiplasmodial activity of crude extracts of the roots of *M. sericea* was tested against chloroquine-sensitive (3D7) and chloroquine-resistant (W2) strains of *Plasmodium falciparum* (Smilkstein et al., 2004b). The root extract exhibited antiplasmodial activity against the W2, and 3D7 strains, with IC_{50} values of 0.62 and 1.86 µg/mL, respectively. Some of the isolated compounds from this plant were also evaluated for antiplasmodial activity (Table 4. 30). Lupinifolinol (**127)** showed half-maximal inhibitory concentration of 2.0 µM and 6.68 µM against the W2, and 3D7 respectively. Lupinifolin **(130)** showed IC_{50} of 12.1 µM against the W2, and 3.7 µM against the 3D7, while mundulinol (**64**) showed IC_{50} of 5.9 µM against W2, and IC_{50} of 2.4 µM against 3D7.

Table 4. 30: Anti-plasmodial activities of the root extract and selected compounds from *M. sericea*

Sample	**IC_{50}**	
	W2	**3D7**
Lupinifolinol (**127)**	2.02 µM	6.68 µM
Lupinifolin **(129)**	12.10 µM	3.69 µM
Mundulinol **(64)**	5.93 µM	2.46 µM
Roots	0.62 µg/mL	1.86 µg/mL

Chloroquine	0.08 µM	0.08 µM

4.4.2 Antibacterial Activity

The crude extract of the roots and the major isolated metabolites were tested for antibacterial activities against *E. coli* and *B. subtilis*. Usambarin D (**113**) isolated from *S. usambarensis* showed modest antibacterial efficacy (MIC = 9.0 µM) against *B. subtilis*, whilst the other evaluated compounds exhibited no significant activity (MIC >100 µM) against *B. subtilis*. Elongatin (**87**) isolated from *T. uniflora* showed moderate antibacterial activity (EC_{50} of 25.0 µM and EC_{90} of 33.0 µM) against *Bactilus subtilis*. All of the compounds investigated were ineffective against *E. coli* (**Error! Reference source not found.**).

Table 4.32: Antibacterial activities (µM) of root and stem extracts and isolated compounds from *S. usambarensis* and *T. uniflora*.

	E. coli					***B. subtilis***						
S/N	**EC_{50}**	**SE range**		**EC_{90}**	**MIC**	**EC 50**	**SE range**		**EC 90**	**SE range**		**MIC**
87	-	-	-	-		25	23	29	33	28	40	>1200
110	>6600	-	-	-	>6600	-	-	-	-	-	-	-
111	>3400	-	-	-	>3400	-	-	-	-	-	-	-
113	-	-	-	-	-	18	16	20	22	18	26	9.0
114	>2500			>2500	>2500	189	187	190	230	220	240	106.3
119	-	-	-	-	-	400	325	475	540	420	660	>798
120	-	-	-	-	-	6200	6100	6300	8200	8100	8300	>2400
122	5100	5000	5200	-	>5700	-	-	-	-	-	-	-

Roots	-	-	-	-	-	-	-	-	-	-		>798
Ampicillin	13.7	19.927	10.568	20.8	-	7.5	6.382	8.933	62.2	49.065	73.343	-

4.4.3 Antileishmanial Activity

Selected compounds were also evaluated for antileishmanial activity against *L. donovani* using an antimony-sensitive (MHOM/IN/83/AG83) and antimony-resistant strains (MHOM/IN/89/GE1) (Table 4.31). Sericetin (**130**) showed IC_{50} of 5.0 µM and 38.0 µM against the antimony-sensitive, strains. Dehydrolupinifolinol (**128**) showed IC_{50} of 9.0 µM against the antimony-sensitive strain.

Nitric oxide (NO) is considered to be a crucial host anti-leishmanial defense substance. Hence selected compounds were evaluated for nitric oxide generation. Dehydrolupinifolinol (**128**) and sericetin (**130**) showed visible increases in NO production in a cell culture with respect to a control in an amastigote assay. Dehydrolupinifolinol **(128)** induced the highest NO production (3.3-fold) in the test cells, conferring a stronger NO-mediated protection.

Table 4.31: Anti-leishmanial activities of selected compounds from *M. sericea* against *L. donovani*

S/NO	**IC_{50} (µM)**			
	antimony-sensitive *L. donovani* (MHOM/IN/83/AG83)	**antimony-resistant *L. donovani* (MHOM/IN/89/GE1)**	**For RAW 264.7 cells**	**Nitric oxide generation**
128	9	Activity not observed	40.9	3.31
130	5	38	31.4	1.05
88	6.75	Activity not observed	21.01	0.87
Miltefosine	5.5	6.7	19.8	NT

4.4.5 Cytotoxicity

4.4.5.1 Cytotoxicity of compounds from *Mundulea sericea*

The selected metabolites of *M. sericea* were investigated for their cytotoxicity against human cancer cell lines; liver cancer (HepG2), lung adenocarcinoma (A549). Normal cell; immortal hepatocytes (LO2), lung/bronchus and (epithelial virus transformed, BEAS-2B) (Table 4.32). Dehydrolupinifolinol **(128)**, mundulinol (**64**) and sericetin (**130**) did not show significant toxicity against any of the cell lines (IC_{50} >100 µM). Cell viability was above 50% at all concentrations (Figure 4.3).

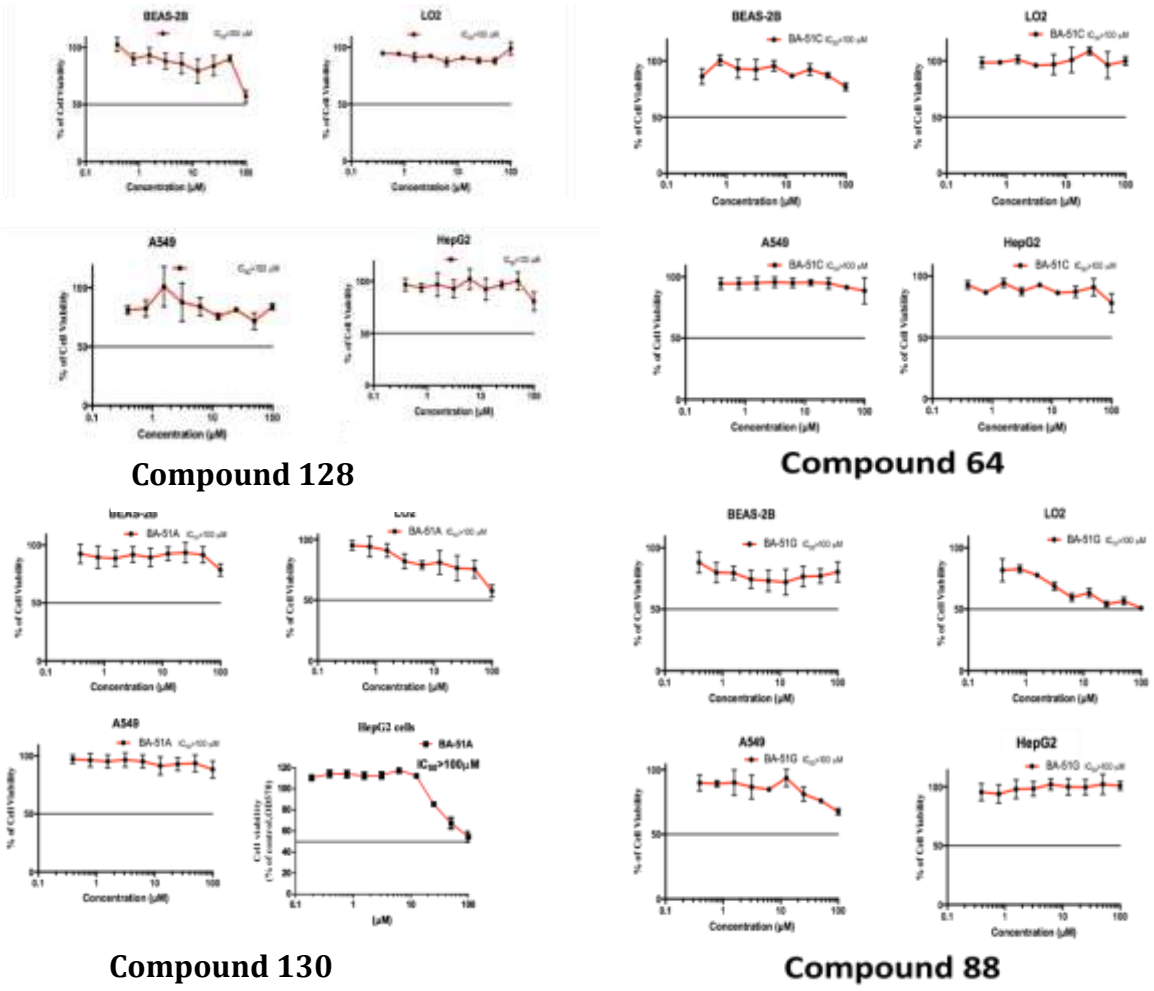

Figure 4.3: Cell viability curve for dehydrolupinifolinol **(128)**, sericetin **(130),** stigmasterol **(88)** and mundulinol **(64)**

Lupinifolinol (**127**) was moderately cytotoxic to LO2 (IC_{50} of 39.7 µM) and, BEAS-2B (IC_{50} of 36.6 µM), while lupinifolin (**129**) was moderately cytotoxic to LO2 (IC_{50} of 36.6 µM) and strongly cytotoxicity to BEAS-2B (IC_{50} 4.9 µM) (Table 4.32). The cell viability decreased with increase in concentrations (Figure 4. 4).

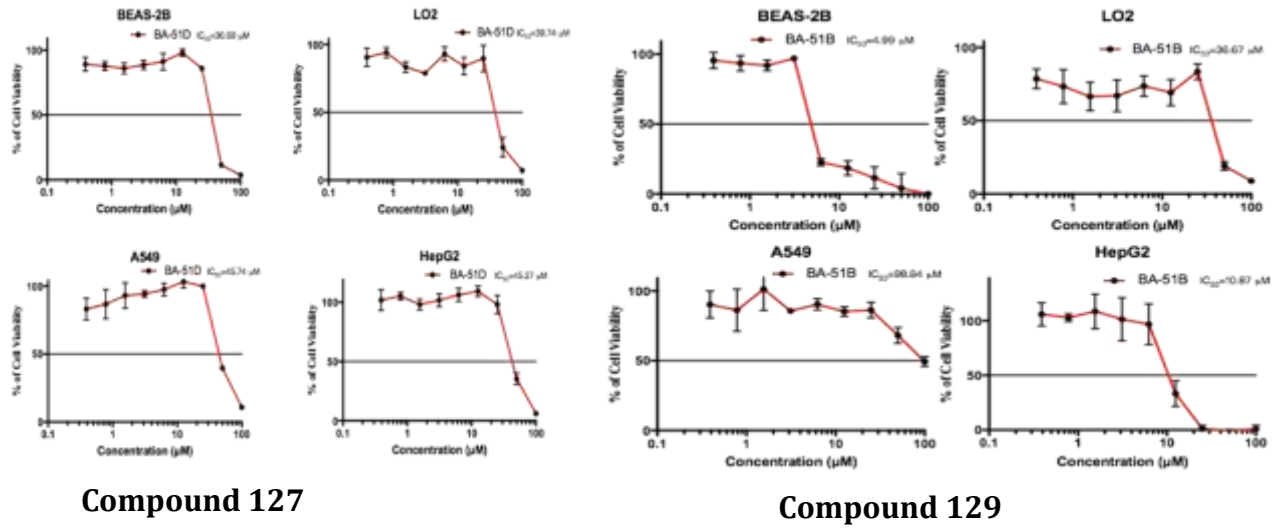

Figure 4. 4: Cell viability curve for lupinifolin (**129**) and lupinifolinol (**127**)

Table 4.32: Cytotoxicity of selected compounds from *M. sericea*

S/N	IC_{50}			
	A549 (C)	**BEAS-2B (N)**	**LO2 (N)**	**HePG2 (C)**
127	45.74 µM	36.69 µM	39.74 µM	45.27 µM
128	>100 µM	>100 µM	>100 µM	>100 µM
129	98.84 µM	4.99 µM	36.67 µM	10.87 µM
64	>100 µM	>100 µM	>100 µM	>100 µM
130	>100 µM	>100 µM	>100 µM	>100 µM
88	>100 µM	>100 µM	>100 µM	>100 µM
Paclitaxel	0.0033 µM	<0.1 µM	<0.1 µM	0.19 µM

4.4.5.2 Cytotoxicity from *Strebulus usambarensis*

The Crude extract and the isolated metabolites from *S. usambarensis* were tested for cytotoxicity against the MCF-7 human breast cancer cell line. Usambarin A (**110)** and usambarin B (**111**) were cytotoxic against the MCF-7 human breast cancer cell line with EC_{50} of 65 and 92 μM respectively while compounds **113**, **114**, **120**, **121** and **122** were not cytotoxic with EC_{50} > 200 μM (Table 4. 33).

Table 4. 33: cytotoxic activities of isolated compounds from *S. usambarensis*

	Cytotoxicity MCF-7		
S/N	**EC50 (μM)**	**SE range (μM)**	
Usambarin A (**110)**	65	50	83
Usambarin B (**111**)	92	86	100
Usambarin D **(113)**	247	90	380
Usambarin E (**114)**	570	560	580
Usambarin K **(120)**	>740	-	-
Bergapten **(121)**	>700	-	-
Bergaptol **(122)**	>1100	-	-

4.4.5.3 Cytotoxicity from *Tephrosia uniflora*

Elongatin **(87)** was tested for cytotoxicity against the MCF-7 human breast cancer cell line. It was also cytotoxic against the MCF-7 human breast cancer cell line with EC50 of 41 μM (Figure 4. 5).

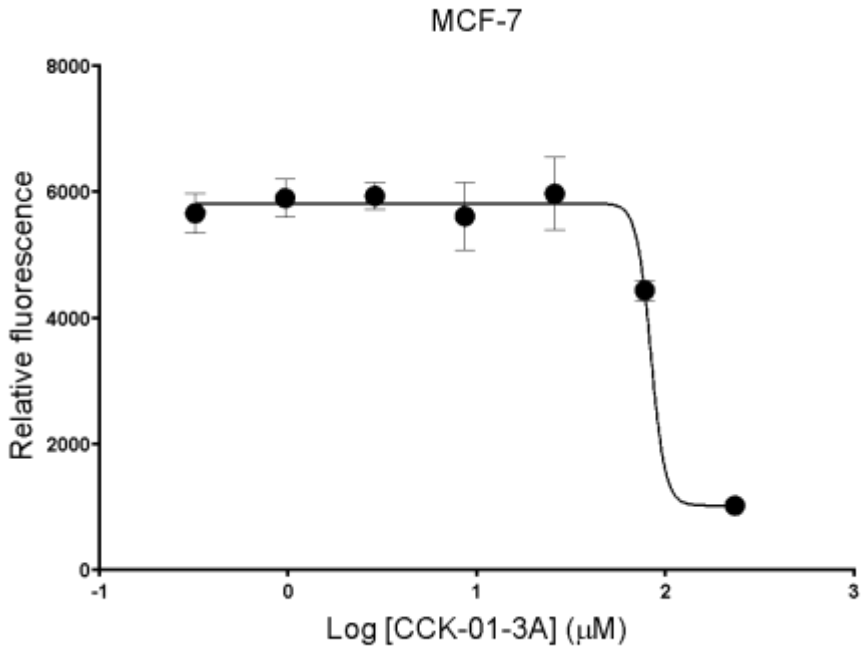

Figure 4. 5. Cytotoxicity dose-response curves (SD = 2.8; SE range of 39.6 to 42.6).

CHAPTER FIVE

CONCLUSIONS AND RECOMMENDATIONS

5.1 Conclusions

Strebulus usambarensis (Moraceae), and *Mundulea sericea* (Leguminosae) and *Tephrosia uniflora* (Leguminosae) were investigated for their phytochemicals. The structures of isolated metabolites were characterized using NMR, X-ray crystallography, UV spectroscopy, electronic circular dichroism and mass spectrometry. Some of the metabolites isolated from these plants were tested for their antiplasmodial, antileishmanial, antibacterial and cytotoxicity activities.

The anti-plasmodial activity of the crude extract of the roots and selected compounds of *M. sericea,* against the chloroquine-resistant (W2) and chloroquine-sensitive (3D7) strains of *Plasmodium falciparum* was determined using established protocols. Antileishmanial activity and anti-proliferative effect of selected compounds of *M. sericea* against *L. donovani* using antimony-sensitive (MHOM/IN/83/AG83) and an antimony-resistant strains (MHOM/IN/89/GE1) were evaluated using MTT assay. Antibacterial activity of the isolated compounds and the crude extracts was determined against *B. subtilis* and *E. coli*. The cytotoxicity of some of the isolated metabolites from *S. usambarensis* were evaluated against human breast cancer cell line (MCF-7), using MTT assay. The cytotoxicity of some of the isolated compounds from *M. sericea* were evaluated against against human cancer cell lines; liver cancer (HepG2), lung adenocarcinoma (A549), normal immortal hepatocytes (LO2), lung/bronchus and (epithelial virus transformed, BEAS-2B) using MTT assay.

The conclusions drawn from these studies are:

1. Phytochemical analysis of the plants *Mundulea sericea*, *Tephrosia uniflora* and *Strebulus usambarensis* resulted in the identification of thirty one compounds of which the new compounds reported were, usambarin A (**110**), B (**111**), C (**112**), D (**113**), E (**114**), F(**115**), G (**116**), H (**117**), I (**118**), J (**119**), K (**120**), L (**125**) and M (**126**), and elatadihydrochalcone-2' methyl ether (**133**). Compounds from the roots of *Strebulus usambarensis* usambarin A (**110**), B (**111**), C (**112**), and D (**113**), have a novel skeleton, while compounds from the stems of *Strebulus usambarensis* usambarin D (**113**), E (**114**), F(**115**), G (**116**), H (**117**), I (**118**), and L (**125**) have a novel skeleton.
2. The crude extract of *M. sericea* roots showed antiplasmodial effect against the chloroquine-resistant (W2) and chloroquine-sensitive (3D7) strains with half-maximal inhibitory concentration values of 0.6 µg/mL and 1.8 µg/mL, respectively. Lupinifolinol (**127**) had an IC_{50} of 2.0 µM and 6.6 µM against the W2, and 3D7 strain respectively, mundulinol (**64**) had an IC_{50} of 5.9 µM against the W2 strain and 2.4 µM against the 3D7 strain, and lupinifolin **(129)** showed IC_{50} of 12.1 µM against the W2, and 3.7 µM against the 3D7.
3. Sericetin (**130**) and dehydrolupinifolinol (**128**) showed efficacy against the antimony-sensitive strain with IC_{50} value below 10.0 µM. Sericetin (**130**) was also effective against antimony-resistant strain with IC_{50} valueof 38.0 µM.
4. Usambarin D (**113**) and elongatin (**87**) had modest antibacterial activity against *B. subtilis* with EC_{50} of 18.0 µM and EC_{90} of 26.0 µM, EC_{50} of 25.0 µM and EC_{90} of 33.0 µM, respectively. However, the other compounds examined were not active (MIC >100 µM).
5. Usambarin A (**110)** and usambarin B (**111**) were cytotoxic with EC_{50} values of 65 and 92 µM, respectively, while compounds **113**, **114**, **120**, **121** and **122** were not cytotoxic with EC_{50} > 200

μM). Lupinifolinol (**127**) was moderately cytotoxic to the epithelial virus transformed (IC_{50} 36.6 μM) and immortal hepatocytes (IC_{50} of 39.7 μM), while lupinifolin (**129**) was moderately cytotoxic to LO2 (IC_{50} 36.6 μM) and strongly cytotoxicity to BEAS-2B (IC_{50} of 4.9 μM). Dehydrolupinifolinol **(128)**, mundulinol (**64**) and sericetin (**130**) did not show significant cytotoxicity against any of the cell lines (IC_{50} >100 μM)

5.2 Recommendations

This study recommends:

1. This study resulted in the identification of new compounds with novel skeletons from *Strebulus usambarensis* hence further phytochemical investigation is needed,
2. Some of the compounds isolated from *M. sericea* showed potent antiplasmodial activity however they were cytototoxic against both cancer and normal cell lines, therefore flavonoids from *Mundulea* should be derivatized with aim of retaining the anti-plasmodial activity and reducing their cytotoxicity.

REFERENCES

Abdullah, S. A., Jamil, S., Basar, N., Abdul Lathiff, S. M., & Mohd Arriffin, N. (2017). Flavonoids from the leaves and heartwoods of Artocarpus lowii King and their bioactivities. *Nat Prod Res*, *31*(10), 1113-1120. https://doi.org/10.1080/14786419.2016.1222387

Abreu, P. M., & Luis, M. H. (1996). Constituents ofTephrosia Uniflora. *Natural Product Letters*, *9*(2), 81-86. https://doi.org/10.1080/10575639608044930

Addae-Kyereme, J., Croft, S. L., Kendrick, H., & Wright, C. W. (2001). Antiplasmodial activities of some Ghanaian plants traditionally used for fever/malaria treatment and of some alkaloids isolated from Pleiocarpa mutica; in vivo antimalarial activity of pleiocarpine. *Journal of Ethnopharmacology*, *76*(1), 99-103. https://doi.org/10.1016/s0378-8741(01)00212-4

Adebayo, O. L., & Suleman, D. (2013). NATURAL PRODUCTS IN ANTILEISHMANIAL DRUG DISCOVERY: A REVIEW. *Journal of Asian Scientific Research*, 17.

Adem, F. A. (2019). *Phytochemical Analysis of Selected Plants in the Leguminosae and Moraceae Families for Anticancer Principles* University of Nairobi]. Zotero.

Afolayan, M., Srivedavyasasri, R., Asekun, O. T., Familoni, O. B., Orishadipe, A., Zulfiqar, F., . . . Ross, S. A. (2018). Phytochemical study of Piliostigma thonningii, a medicinal plant grown in Nigeria. *Med Chem Res*, *27*(10), 2325-2330. https://doi.org/10.1007/s00044-018-2238-1

Ahmad, V. U., Ali, Z., Hussaini, S. R., Iqbal, F., Zahid, M., Abbas, M., & Saba, N. (1999). Flavonoids of Tephrosia purpurea. *Fitoterapia*, *70*(4), 443-445. https://doi.org/10.1016/s0367-326x(99)00046-5

Al-Kamel, M. A. N. (2017). Leishmaniasis and Malignancy: A Review and Perspective. *Clinical Skin Cancer*, *2*(1-2), 54-58. https://doi.org/10.1016/j.clsc.2017.10.003

Al Musayeib, N. M., Mothana, R. A., Gamal, A. A., Al-Massarani, S. M., & Maes, L. (2013). In vitro antiprotozoal activity of triterpenoid constituents of Kleinia odora growing in Saudi Arabia. *Molecules*, *18*(8), 9207-9218. https://doi.org/10.3390/molecules18089207

Almeida, C. P., Cavalcante, F. R. A., Moreno, J. O., Florencio, C., Cavalcante, K. K. S., & Alencar, C. H. (2020). Visceral Leishmaniasis: temporal and spatial distribution in Fortaleza, Ceara State, Brazil, 2007-2017. *Epidemiol Serv Saude*, *29*(5), e2019422. https://doi.org/10.1590/S1679-49742020000500002 (Leishmaniose visceral: distribuicao temporal e espacial em Fortaleza, Ceara, 2007-2017.)

AlSamarai, A. M., & AlObaidi, H. S. (2009). Cutaneous leishmaniasis in Iraq. *J Infect Dev Ctries*, *3*(2), 123-129. https://doi.org/10.3855/jidc.59

Alvar, J., Velez, I. D., Bern, C., Herrero, M., Desjeux, P., Cano, J., . . . Team, W. H. O. L. C. (2012). Leishmaniasis worldwide and global estimates of its incidence. *PLoS ONE*, *7*(5), e35671. https://doi.org/10.1371/journal.pone.0035671

Andrade, T. M., Carvalho, E. M., & Rocha, H. (1990). Bacterial infections in patients with visceral leishmaniasis. *J Infect Dis*, *162*(6), 1354-1359. https://doi.org/10.1093/infdis/162.6.1354

Andrews, K. T., Fisher, G., & Skinner-Adams, T. S. (2014). Drug repurposing and human parasitic protozoan diseases. *Int J Parasitol Drugs Drug Resist*, *4*(2), 95-111. https://doi.org/10.1016/j.ijpddr.2014.02.002

Arora, S. K., Verma, P. R., Itankar, P. R., Prasad, S. K., & Nakhate, K. T. (2021). Evaluation of pancreatic regeneration activity of Tephrosia purpurea leaves in rats with streptozotocin-

induced diabetes. *J Tradit Complement Med*, *11*(5), 435-445. https://doi.org/10.1016/j.jtcme.2021.03.001

Arriaga, A. M. C., Silva, F. R. L. D., Texeira, M. V. S., Pereira, I. G., Da Silva, M. R., Mafezoli, J., . . . Rodrigues, F. F. G. (2017). Chemical Compounds and Antibacterial Activity of Tephrosia Toxicaria Pers. *Oriental Journal of Chemistry*, *33*(5), 2173-2178. https://doi.org/10.13005/ojc/330504

Ataide, M. A., Andrade, W. A., Zamboni, D. S., Wang, D., Souza Mdo, C., Franklin, B. S., . . . Gazzinelli, R. T. (2014). Malaria-induced NLRP12/NLRP3-dependent caspase-1 activation mediates inflammation and hypersensitivity to bacterial superinfection. *PLoS Pathog*, *10*(1), e1003885. https://doi.org/10.1371/journal.ppat.1003885

Atilaw, Y., Duffy, S., Heydenreich, M., Muiva-Mutisya, L., Avery, V. M., Erdelyi, M., & Yenesew, A. (2017a). Three Chalconoids and a Pterocarpene from the Roots of Tephrosia aequilata. *Molecules*, *22*(2), 318. https://doi.org/10.3390/molecules22020318

Atilaw, Y., Muiva-Mutisya, L., Ndakala, A., Akala, H. M., Yeda, R., Wu, Y. J., . . . Yenesew, A. (2017b). Four Prenylflavone Derivatives with Antiplasmodial Activities from the Stem of Tephrosia purpurea subsp. leptostachya. *Molecules*, *22*(9), 1514. https://doi.org/10.3390/molecules22091514

Azadnajafabad, S., Mohammadi, E., Aminorroaya, A., Fattahi, N., Rezaei, S., Haghshenas, R., . . . Farzadfar, F. (2021). Non-communicable diseases' risk factors in Iran; a review of the present status and action plans. *J Diabetes Metab Disord*, 1-9. https://doi.org/10.1007/s40200-020-00709-8

Baba, Y., Maeda, T., Suzuki, A., Takada, S., Fujii, M., & Kato, Y. (2017). Deguelin Potentiates Apoptotic Activity of an EGFR Tyrosine Kinase Inhibitor (AG1478) in PIK3CA-Mutated Head and Neck Squamous Cell Carcinoma. *Int J Mol Sci*, *18*(2), 262. https://doi.org/10.3390/ijms18020262

Barati, M., Sharifi, I., Daie Parizi, M., & Fasihi Harandi, M. (2008). Bacterial infections in children with visceral leishmaniasis: observations made in Kerman province, southern Iran, between 1997 and 2007. *Ann Trop Med Parasitol*, *102*(7), 635-641. https://doi.org/10.1179/136485908X311858

Barbic, M., Schmidt, T. J., & Jurgenliemk, G. (2012). Novel phenyl-1-benzoxepinols from butcher's broom (Rusci rhizoma). *Chem Biodivers*, *9*(6), 1077-1083. https://doi.org/10.1002/cbdv.201100158

Bassat, Q., Guinovart, C., Sigauque, B., Mandomando, I., Aide, P., Sacarlal, J., . . . Alonso, P. L. (2009). Severe malaria and concomitant bacteraemia in children admitted to a rural Mozambican hospital. *Trop Med Int Health*, *14*(9), 1011-1019. https://doi.org/10.1111/j.1365-3156.2009.02326.x

Batista, R., Silva Ade, J., Jr., & de Oliveira, A. B. (2009). Plant-derived antimalarial agents: new leads and efficient phytomedicines. Part II. Non-alkaloidal natural products. *Molecules*, *14*(8), 3037-3072. https://doi.org/10.3390/molecules14083037

Benjamim, J. K. F., Dias da Costa, K. A., & Silva Santos, A. (2020). Chemical, Botanical and Pharmacological Aspects of the Leguminosae. *Pharmacognosy Reviews*, *14*(28), 106-120. https://doi.org/10.5530/phrev.2020.14.15

Bester, S. B., & Grobler, A. (2008). Mundulea sericea | Plantz Africa.

Bhadra, K., & Kumar, G. S. (2011). Therapeutic potential of nucleic acid-binding isoquinoline alkaloids: binding aspects and implications for drug design. *Med Res Rev*, *31*(6), 821-862. https://doi.org/10.1002/med.20202

Burns, D. C., Ellis, D. A., & March, R. E. (2007). A predictive tool for assessing 13C NMR chemical shifts of flavonoids. *Magnetic Resonance in Chemistry*, *45*(10), 835-845.

Burrows, J. E., & Burrows, S. *Trees and shrubs Mozambique*.

Byng, J. W. (2004). *The Flowering Plants Handbook: A practical guide to families and genera of the world* (1 ed.). Plant Gateway Ltd.

Caceres, A., Rastrelli, L., De Simone, F., De Martino, G., Saturnino, C., Saturnino, P., & Aquino, R. (2001). Furanocoumarins from the aerial parts of Dorstenia contrajerva. *Fitoterapia*, *72*(4), 376-381. https://doi.org/10.1016/s0367-326x(00)00328-2

Cao, S., Schilling, J. K., Miller, J. S., Andriantsiferana, R., Rasamison, V. E., & Kingston, D. G. (2004). Cytotoxic compounds from Mundulea chapelieri from the Madagascar Rainforest. *J Nat Prod*, *67*(3), 454-456. https://doi.org/10.1021/np0303815

Carrillo-Larco, R. M., Acevedo-Rodriguez, J. G., Altez-Fernandez, C., Ortiz-Acha, K., & Ugarte-Gil, C. (2019). Is there an association between cutaneous leishmaniasis and skin cancer? A systematic review. *Wellcome Open Res*, *4*, 110. https://doi.org/10.12688/wellcomeopenres.15367.1

Chabner, B. A., & Roberts, T. G., Jr. (2005). Timeline: Chemotherapy and the war on cancer. *Nat Rev Cancer*, *5*(1), 65-72. https://doi.org/10.1038/nrc1529

Chanda, S., Dudhatra, S., & Kaneria, M. (2010). Antioxidative and antibacterial effects of seeds and fruit rind of nutraceutical plants belonging to the Fabaceae family. *Food Funct*, *1*(3), 308-315. https://doi.org/10.1039/c0fo00028k

Chang, L. C., Chavez, D., Song, l. L., Pezzuto, J. M., & Kinghorn, A. D. (2000). Absolute Configuration of Novel Bioactive Flavonoids from Tephrosia purpurea | Organic Letters. *organic letters*, *2*(4), 515-518.

Chassagne, F., Samarakoon, T., Porras, G., Lyles, J. T., Dettweiler, M., Marquez, L., . . . Quave, C. L. (2020). A Systematic Review of Plants With Antibacterial Activities: A Taxonomic and Phylogenetic Perspective. *Front Pharmacol*, *11*, 586548. https://doi.org/10.3389/fphar.2020.586548

Chawla, A. S., Kapoor, V. K., Mukhopadhyay, R., & Singh, M. (1990). Constituents of Streblus asper. *Fitoterapia*, *61*(2).

Cheenpracha, S., Karalai, C., Ponglimanont, C., & Chantrapromma, K. (2007). Cytotoxic rotenoloids from the stems of Derris trifoliata. *Canadian Journal of Chemistry*, *85*(12), 1019-1022. https://doi.org/10.1139/v07-120

Chen, L., Jiang, K., Chen, H., Tang, Y., Zhou, X., Tan, Y., . . . Ding, K. (2019). Deguelin induces apoptosis in colorectal cancer cells by activating the p38 MAPK pathway. *Cancer Manag Res*, *11*, 95-105. https://doi.org/10.2147/CMAR.S169476

Chen, X., Huang, Y.-A., You, Z.-H., Yan, G.-Y., & Wang, X.-S. (2017). A novel approach based on KATZ measure to predict associations of human microbiota with non-infectious diseases. *Bioinformatics*, *33*(5), 733-739.

Chen, X., Mukwaya, E., Wong, M. S., & Zhang, Y. (2014a). A systematic review on biological activities of prenylated flavonoids. *Pharm Biol*, *52*(5), 655-660. https://doi.org/10.3109/13880209.2013.853809

Chen, Y., Yan, T., Gao, C., Cao, W., & Huang, R. (2014b). Natural products from the genus tephrosia. *Molecules*, *19*(2), 1432-1458. https://doi.org/10.3390/molecules19021432

Cheruiyot, A. C., Auschwitz, J. M., Lee, P. J., Yeda, R. A., Okello, C. O., Leed, S. E., . . . Hickman, M. R. (2016). Assessment of the Worldwide antimalarial resistance network standardized procedure for in vitro malaria drug sensitivity testing using SYBR green assay for field

samples with various initial parasitemia levels. *Antimicrobial Agents and Chemotherapy*, *60*(4), 2417-2424.
Clapp, R. W., Jacobs, M. M., & Loechler, E. L. (2008). Environmental and occupational causes of cancer: new evidence 2005-2007. *Rev Environ Health*, *23*(1), 1-37. https://doi.org/10.1515/reveh.2008.23.1.1
Clement, W. L., & Weiblen, G. D. (2009). Morphological Evolution in the Mulberry Family (Moraceae). *Systematic Botany*, *34*(3), 530-552. https://doi.org/10.1600/036364409789271155
Cobo, E. R., & Chadee, K. (2013). Antimicrobial human β-defensins in the colon and their role in infectious and non-infectious diseases. *Pathogens*, *2*(1), 177-192.
Cortes, S., Bruno de Sousa, C., Morais, T., Lago, J., & Campino, L. (2020). Potential of the natural products against leishmaniasis in Old World - a review of in-vitro studies. *Pathog Glob Health*, *114*(4), 170-182. https://doi.org/10.1080/20477724.2020.1754655
Cragg, G. M., & Newman, D. J. (2013). Natural products: a continuing source of novel drug leads. *Biochim Biophys Acta*, *1830*(6), 3670-3695. https://doi.org/10.1016/j.bbagen.2013.02.008
Cragg, G. M., & Pezzuto, J. M. (2016). Natural Products as a Vital Source for the Discovery of Cancer Chemotherapeutic and Chemopreventive Agents. *Medical Principles and Practice*, *25*(2), 41-59. https://doi.org/10.1159/000443404
Curigliano, G., Mayer, E. L., Burstein, H. J., Winer, E. P., & Goldhirsch, A. (2010). Cardiac toxicity from systemic cancer therapy: a comprehensive review. *Prog Cardiovasc Dis*, *53*(2), 94-104. https://doi.org/10.1016/j.pcad.2010.05.006
Czene, K., Lichtenstein, P., & Hemminki, K. (2002). Environmental and heritable causes of cancer among 9.6 million individuals in the Swedish Family-Cancer Database. *Int J Cancer*, *99*(2), 260-266. https://doi.org/10.1002/ijc.10332
Daud, M. N. H., Fatanah, D. N., Abdullah, N., & Ahmad, R. (2017). Evaluation of antioxidant potential of Artocarpus heterophyllus L. J33 variety fruit waste from different extraction methods and identification of phenolic constituents by LCMS. *Food Chem*, *232*, 621-632. https://doi.org/10.1016/j.foodchem.2017.04.018
Dej-adisai, S., Parndaeng, K., & Wattanapiromsakul, C. (2016). Determination of Phytochemical Compounds, and Tyrosinase Inhibitory and Antimicrobial Activities of Bioactive Compounds from Streblus ilicifolius (S Vidal) Corner. *Tropical Journal of Pharmaceutical Research*, *15*(3), 497-506. https://doi.org/10.4314/tjpr.v15i3.10
Deng, Y. H., Xu, K. P., Zhou, Y. J., Li, F. S., Zeng, G. Y., & Tan, G. S. (2007). A new flavonol from *Sophora tonkinensis*. *J Asian Nat Prod Res*, *9*(1), 45-48. https://doi.org/10.1080/10286020500289634
Deshpande, S. S., Shah, G. B., & Parmar, N. S. (2003). ANTIULCER ACTIVITY OF TEPHROSIA PURPUREA IN RATS. 5.
Desjeux, P. (2004). Leishmaniasis: current situation and new perspectives. *Comp Immunol Microbiol Infect Dis*, *27*(5), 305-318. https://doi.org/10.1016/j.cimid.2004.03.004
Dey, S., Mukherjee, D., Chakraborty, S., Mallick, S., Dutta, A., Ghosh, J., . . . Pal, C. (2015). Protective effect of Croton caudatus Geisel leaf extract against experimental visceral leishmaniasis induces proinflammatory cytokines in vitro and in vivo. *Exp Parasitol*, *151-152*, 84-95. https://doi.org/10.1016/j.exppara.2015.01.012
Duan, Y., Shang, B., Liang, W., Du, G., Yang, M., & Rhodes, R. E. (2021). Effects of eHealth-Based Multiple Health Behavior Change Interventions on Physical Activity, Healthy Diet,

and Weight in People With Noncommunicable Diseases: Systematic Review and Meta-analysis. *J Med Internet Res*, *23*(2), e23786. https://doi.org/10.2196/23786

Dutta, A., Bandyopadhyay, S., Mandal, C., & Chatterjee, M. (2005). Development of a modified MTT assay for screening antimonial resistant field isolates of Indian visceral leishmaniasis. *Parasitol Int*, *54*(2), 119-122. https://doi.org/10.1016/j.parint.2005.01.001

Dzoyem, J. P., Tchamgoue, J., Tchouankeu, J. C., Kouam, S. F., Choudhary, M. I., & Bakowsky, U. (2018). Antibacterial activity and cytotoxicity of flavonoids compounds isolated from Pseudarthria hookeri Wight & Arn. (Fabaceae). *South African Journal of Botany*, *114*, 100-103. https://doi.org/10.1016/j.sajb.2017.11.001

Ehni, H. J. (2014). Expensive cancer drugs and just health care. *Best Pract Res Clin Gastroenterol*, *28*(2), 327-337. https://doi.org/10.1016/j.bpg.2014.02.008

Endris, M., Takele, Y., Woldeyohannes, D., Tiruneh, M., Mohammed, R., Moges, F., . . . Diro, E. (2014). Bacterial sepsis in patients with visceral leishmaniasis in Northwest Ethiopia. *Biomed Res Int*, *2014*, 361058. https://doi.org/10.1155/2014/361058

Et-Touys, A., Bouyahya, A., Fellah, H., Mniouil, M., El Boury, H., Dakka, N., . . . Bakri, Y. (2017). Antileishmanial activity of medicinal plants from Africa: A review. *Asian Pacific Journal of Tropical Disease*, *7*(12), 826-840. https://doi.org/10.12980/apjtd.7.2017D7-215

Eze, M. O., Hunting, D. J., & Ogan, A. U. (1990). Reactive oxygen production against malaria — A potential cancer risk factor. *Medical Hypotheses*, *32*(2), 121-123. https://doi.org/10.1016/0306-9877(90)90034-c

Ezzati, M., & Riboli, E. (2013). Behavioral and dietary risk factors for noncommunicable diseases. *N Engl J Med*, *369*(10), 954-964. https://doi.org/10.1056/NEJMra1203528

Faden, R. R., Chalkidou, K., Appleby, J., Waters, H. R., & Leider, J. P. (2009). Expensive cancer drugs: a comparison between the United States and the United Kingdom. *Milbank Q*, *87*(4), 789-819. https://doi.org/10.1111/j.1468-0009.2009.00579.x

Fauci, A. S. (2001). Infectious diseases: considerations for the 21st century. *Clin Infect Dis*, *32*(5), 675-685. https://doi.org/10.1086/319235

Fiebig, M., Duh, C.-Y., Pezzuto, J. M., Kinghorn, A. D., & Farnsworth, N. R. (2004, July 1, 2004). *Plant Anticancer Agents, XLI. Cardiac Glycosides from Streblus asper*.

Filardy, A. A., Guimaraes-Pinto, K., Nunes, M. P., Zukeram, K., Fliess, L., Pereira, L., . . . Morrot, A. (2018). Human Kinetoplastid Protozoan Infections: Where Are We Going Next? *Front Immunol*, *9*, 1493. https://doi.org/10.3389/fimmu.2018.01493

Fries, C. N., Curvino, E. J., Chen, J. L., Permar, S. R., Fouda, G. G., & Collier, J. H. (2021). Advances in nanomaterial vaccine strategies to address infectious diseases impacting global health. *Nat Nanotechnol*, *16*(4), 1-14. https://doi.org/10.1038/s41565-020-0739-9

Gangadevi, S., Kalimuthu, K., & Viswanathan, P. (2020). Anti-diabetic and Cytotoxicity Studies of Ethanol Extract of Mundulea sericea: A Threatened Medicinal Plant. In *Phytomedicine* (pp. 139-144). CRC Press.

Gerber, D. E. (2008). Targeted therapies: a new generation of cancer treatments. *Am Fam Physician*, *77*(3), 311-319. https://www.ncbi.nlm.nih.gov/pubmed/18297955

Gigley, J. P., Bhadra, R., Moretto, M. M., & Khan, I. A. (2012). T cell exhaustion in protozoan disease. *Trends Parasitol*, *28*(9), 377-384. https://doi.org/10.1016/j.pt.2012.07.001

Gillespie, P. M., Beaumier, C. M., Strych, U., Hayward, T., Hotez, P. J., & Bottazzi, M. E. (2016). Status of vaccine research and development of vaccines for leishmaniasis. *Vaccine*, *34*(26), 2992-2995. https://doi.org/10.1016/j.vaccine.2015.12.071

Gomez-Perez, G. P., van Bruggen, R., Grobusch, M. P., & Dobano, C. (2014). Plasmodium falciparum malaria and invasive bacterial co-infection in young African children: the dysfunctional spleen hypothesis. *Malar J*, *13*(1), 335. https://doi.org/10.1186/1475-2875-13-335

Gottesman, M. M. (2002). Mechanisms of cancer drug resistance. *Annu Rev Med*, *53*(1), 615-627. https://doi.org/10.1146/annurev.med.53.082901.103929

Green, S. J., Meltzer, M. S., Hibbs, J. B., Jr., & Nacy, C. A. (1990). Activated macrophages destroy intracellular Leishmania major amastigotes by an L-arginine-dependent killing mechanism. *J Immunol*, *144*(1), 278-283. https://www.ncbi.nlm.nih.gov/pubmed/2104889

Greenway, P. J. (1936). Mundulea Fish Poison. *Bulletin of Miscellaneous Information (Royal Gardens, Kew)*, *1936*(4), 245-250. https://doi.org/10.2307/4111862

Gupta, R. C. (2012). Rotenone. In *Veterinary Toxicology* (pp. 620-623). Elsevier.

He, R., Deng, S., Nie, H., Huang, Y., Liu, B., Yang, R., . . . Zhang, Y. (2017a). Two new coumarins from the bark of Streblus indicus (Bur.) Corner. *Nat Prod Res*, *31*(9), 1052-1058. https://doi.org/10.1080/14786419.2016.1269098

He, R., Zhang, Y., Wu, L., Nie, H., Huang, Y., Liu, B., . . . Chen, H. (2017b). Benzofuran glycosides and coumarins from the bark of Streblus indicus (Bur.) Corner. *Phytochemistry*, *138*, 170-177. https://doi.org/10.1016/j.phytochem.2017.01.011

Hegazy, M. E., Abd el-Razek, M. H., Nagashima, F., Asakawa, Y., & Pare, P. W. (2009). Rare prenylated flavonoids from Tephrosia purpurea. *Phytochemistry*, *70*(11-12), 1474-1477. https://doi.org/10.1016/j.phytochem.2009.08.001

Herlina, T., Mardianingrum, R., Gaffar, S., & Supratman, U. (2017). Isoquinoline Alkaloids fromErythrinapoeppigiana(Leguminosae) and Cytotoxic Activity Against Breast Cancer Cells Line MCF-7 In Silico. *Journal of Physics: Conference Series*, *812*, 012091. https://doi.org/10.1088/1742-6596/812/1/012091

Hira, S., Ahmad, F. (2016). REVIEW ON MEDICINAL IMPORTANCE OF FABACEAE FAMILY. *pharmacologyOnline*, *3*, 151-156.

Hogan, B., Eibach, D., Krumkamp, R., Sarpong, N., Dekker, D., Kreuels, B., . . . Fever Without Source Study, G. (2018). Malaria Coinfections in Febrile Pediatric Inpatients: A Hospital-Based Study From Ghana. *Clin Infect Dis*, *66*(12), 1838-1845. https://doi.org/10.1093/cid/cix1120

Holohan, C., Van Schaeybroeck, S., Longley, D. B., & Johnston, P. G. (2013). Cancer drug resistance: an evolving paradigm. *Nat Rev Cancer*, *13*(10), 714-726. https://doi.org/10.1038/nrc3599

Housman, G., Byler, S., Heerboth, S., Lapinska, K., Longacre, M., Snyder, N., & Sarkar, S. (2014). Drug resistance in cancer: an overview. *Cancers (Basel)*, *6*(3), 1769-1792. https://doi.org/10.3390/cancers6031769

Hunter, D. J., & Reddy, K. S. (2013). Noncommunicable diseases. *N Engl J Med*, *369*(14), 1336-1343. https://doi.org/10.1056/NEJMra1109345

Hussain, S. P., Hofseth, L. J., & Harris, C. C. (2003). Radical causes of cancer. *Nat Rev Cancer*, *3*(4), 276-285. https://doi.org/10.1038/nrc1046

Hyde, M. A., Wursten, B. T., Ballings, P., & Coates Palgrave, M. (2021, 2021). *Flora of Botswana: Species information: Tephrosia uniflora subsp. uniflora*.

Ibrahim, N. M., Mat, I., Lim, V., & Ahmad, R. (2013). Antioxidant Activity and Phenolic Content of Streblus asper Leaves from Various Drying Methods. *Antioxidants (Basel)*, *2*(3), 156-166. https://doi.org/10.3390/antiox2030156

Ingham, J. L., Tahara, S., & Dziedzic, S. (1988). Major Flavanones from Lonchocarpus guatamalensis. *Zeitschrift für Naturforschung C*, *43*(11-12), 818-822. https://doi.org/10.1515/znc-1988-11-1205

Jain, A. C., & Zutshi, M. K. (1973). The synthesis of sericetin and related flavonols. *Tetrahedron*, *29*(21), 3347-3350. https://doi.org/10.1016/s0040-4020(01)93487-8

Ji-Guo, H., Jun, L., Qiang, W., Rui-Yun, Y., Shan, L., Zi-Zhan, C., & Lu-Qing, L. (2012). Constituents from Heartwood of Streblus asper and Their Antibacterial Activity. *Natural Product Research & Development*, *24*(6), 780-827.

Kadivar, M. R., Kajbaf, T. Z., Karimi, A., & Alborzi, A. (2000). Childhood visceral leishmaniasis complicated by bacterial infections. *East Mediterr Health J*, *6*(5-6), 879-883. https://www.ncbi.nlm.nih.gov/pubmed/12197344

Kalenga, T. M., Ndoile, M. M., Atilaw, Y., Gilissen, P. J., Munissi, J. J. E., Rudenko, A., . . . Erdelyi, M. (2021). Biflavanones, Chalconoids, and Flavonoid Analogues from the Stem Bark of Ochna holstii. *J Nat Prod*, *84*(2), 364-372. https://doi.org/10.1021/acs.jnatprod.0c01017

Kayser, O., Kiderlen, A. F., Folkens, U., & Kolodziej, H. (1999). In vitro leishmanicidal activity of aurones. *Planta Med*, *65*(4), 316-319. https://doi.org/10.1055/s-1999-13993

Khalighi-Sigaroodi, F., Ahvazi, M., Hadjiakhoondi, A., Taghizadeh, M., Yazdani, D., Khalighi-Sigaroodi, S., & Bidel, S. (2012). Cytotoxicity and antioxidant activity of 23 plant species of leguminosae family. *Iran J Pharm Res*, *11*(1), 295-302. https://www.ncbi.nlm.nih.gov/pubmed/24250452

Khaomek, P., Ichino, C., Ishiyama, A., Sekiguchi, H., Namatame, M., Ruangrungsi, N., . . . Yamada, H. (2008). In vitro antimalarial activity of prenylated flavonoids from Erythrina fusca. *J Nat Med*, *62*(2), 217-220. https://doi.org/10.1007/s11418-007-0214-z

Khyade, M. S., & Waman, M. B. (2017). Chemical Profile and Antioxidant Properties of Mundulea sericea. *Pharmacognosy Journal*, *9*(2), 213-220. https://doi.org/10.5530/pj.2017.2.36

Kiania, N. M., Mueke, J., & Rukunga, G. (2014). Larvicidal efficacy of Mundulea sericea (Leguminosaea) plant extract against Anopheles gambiae (Giles) and Culex quinqefasciatus (Say) (Diptera: Culicidae). *Open Science Repository Pharmaceutics*(open-access), e23050491. https://doi.org/10.7392/openaccess.23050491

Kingham, T. P., Alatise, O. I., Vanderpuye, V., Casper, C., Abantanga, F. A., Kamara, T. B., . . . Denny, L. (2013). Treatment of cancer in sub-Saharan Africa. *Lancet Oncol*, *14*(4), e158-167. https://doi.org/10.1016/S1470-2045(12)70472-2

Kinghorn, A. D., Ren, Y., Chen, W. L., Lantvit, D. D., Ninh, T. N., Sass, E. J., . . . Burdette, J. E. (2016, 2016/12). Strebloside, a Constituent of Streblus asper with Antineoplastic Activity. Abstracts 9th Joint Meeting of AFERP, ASP, GA, JSP, PSE & SIF,

Kirtane, A. R., Verma, M., Karandikar, P., Furin, J., Langer, R., & Traverso, G. (2021). Nanotechnology approaches for global infectious diseases. *Nat Nanotechnol*, *16*(4), 369-384. https://doi.org/10.1038/s41565-021-00866-8

KMIS. (2015). By the Division of Malaria Control in the Ministry of Public Health and Sanitation in partnership with the Kenya National Bureau of Statistics. In.

Kocyigit, A., Keles, H., Selek, S., Guzel, S., Celik, H., & Erel, O. (2005). Increased DNA damage and oxidative stress in patients with cutaneous leishmaniasis. *Mutat Res*, *585*(1-2), 71-78. https://doi.org/10.1016/j.mrgentox.2005.04.012

Koudokpon, H., Armstrong, N., Dougnon, T. V., Fah, L., Hounsa, E., Bankole, H. S., . . . Rolain, J. M. (2018). Antibacterial Activity of Chalcone and Dihydrochalcone Compounds from *Uvaria chamae* Roots against Multidrug-Resistant Bacteria. *Biomed Res Int*, *2018*, 1453173. https://doi.org/10.1155/2018/1453173

Kumar, V., Mahajan, A., & Chibale, K. (2009). Synthetic medicinal chemistry of selected antimalarial natural products. *Bioorg Med Chem*, *17*(6), 2236-2275. https://doi.org/10.1016/j.bmc.2008.10.072

Kurniadewi, F., Dianhar, H., Mutiah, S., & Al-Liatsi, Z. Z. (2021). Two flavonoid derivatives from the wood of Nangkadak (Moraceae). *AIP Conference Proceedings*, *2331*(1), 040039. https://doi.org/10.1063/5.0041840

Lahlou, M. (2013). The Success of Natural Products in Drug Discovery. *Pharmacology & Pharmacy*, *04*(03), 17-31. https://doi.org/10.4236/pp.2013.43A003

Lane, M. M., Davis, J. A., Beattie, S., Gomez-Donoso, C., Loughman, A., O'Neil, A., . . . Rocks, T. (2021). Ultraprocessed food and chronic noncommunicable diseases: A systematic review and meta-analysis of 43 observational studies. *Obes Rev*, *22*(3), e13146. https://doi.org/10.1111/obr.13146

Langat, B. K., Siele, D. K., Wainaina, C., Mwandawiro, C., Ondicho, J., Tonui, W. K., . . . Mutai, C. K. (2012). Larvicidal effect of Mundulea sericea (Leguminosaea) plant extract against Aedes aegypti (L.)(Diptera: Culicidae). *African Journal of Pharmacology and Therapeutics*, *1*(3).

Lawson, M. A., Kaouadji, M., & Chulia, A. J. (2010). A single chalcone and additional rotenoids from Lonchocarpus nicou. *Tetrahedron Letters*, *51*(47), 6116-6119.

Lehrer, S. (2010). Association Between Malaria Incidence and All Cancer Mortality in Fifty U.S. States and the District of Columbia. *Anticancer Research*, *30*(3), 1371-1374.

Li, J., Huang, Y., Guan, X. L., Li, J., Deng, S. P., Wu, Q., . . . Yang, R. Y. (2012a). Anti-hepatitis B virus constituents from the stem bark of Streblus asper. *Phytochemistry*, *82*, 100-109. https://doi.org/10.1016/j.phytochem.2012.06.023

Li, J., Zhang, Y. J., Jin, B. F., Su, X. J., Tao, Y. W., She, Z. G., & Lin, Y. C. (2008). 1H and 13C NMR assignments for two lignans from the heartwood of Streblus asper. *Magn Reson Chem*, *46*(5), 497-500. https://doi.org/10.1002/mrc.2186

Li, L. Q., Li, J., Huang, Y., Wu, Q., Deng, S. P., Su, X. J., . . . Li, S. (2012b). Lignans from the heartwood of Streblus asper and their inhibiting activities to hepatitis B virus. *Fitoterapia*, *83*(2), 303-309. https://doi.org/10.1016/j.fitote.2011.11.008

Li, X., & Yang, C. (2021). Analytical chemistry for infectious disease detection and prevention. *Anal Bioanal Chem*, *413*(18), 4561-4562. https://doi.org/10.1007/s00216-021-03441-1

Lodhi, S., Pawar, R. S., Jain, A. P., & Singhai, A. K. (2006). Wound healing potential of Tephrosia purpurea (Linn.) Pers. in rats. *J Ethnopharmacol*, *108*(2), 204-210. https://doi.org/10.1016/j.jep.2006.05.011

Luyengi, L., Lee, I.-S., Mar, W., Fong, H. H., Pezzuto, J. M., & Kinghorn, A. D. (1994). Rotenoids and chalcones from Mundulea sericea that inhibit phorbol ester-induced ornithine decarboxylase activity. *Phytochemistry*, *36*(6), 1523–1526.

Maltha, J., Guiraud, I., Kabore, B., Lompo, P., Ley, B., Bottieau, E., . . . Jacobs, J. (2014). Frequency of severe malaria and invasive bacterial infections among children admitted to a rural hospital in Burkina Faso. *PLoS ONE*, *9*(2), e89103. https://doi.org/10.1371/journal.pone.0089103

Mangeni, J. N., Ongore, D., Mwangi, A., Vulule, J., Ocala, A., & O'Meara, W. P. (2017). Malaria "hotspots" within a larger hotspot; what's the role of behavioural factors in fine scale heterogeneity in western Kenya? *East African Medical Journal*, *94*(5), 369-384.

Manjary, F., Petitjean, A., Conan, J.-Y., Thérèse Martin, M., Frappier, F., Rasoanaivo, P., & Ratsimamanga-Urverg, S. (1993). A prenylated pterocarpan from Mundulea striata. *Phytochemistry*, *33*(2), 515-517. https://doi.org/10.1016/0031-9422(93)85554-5

Martinez, R. M., Zarpelon, A. C., Zimermann, V. V. M., Georgetti, S. R., Baracat, M. M., Fonseca, M. J. V., . . . Casagrande, R. (2012). Tephrosia sinapou extract reduces inflammatory leukocyte recruitment in mice: effect on oxidative stress, nitric oxide and cytokine production. *Revista Brasileira de Farmacognosia*, *22*(3), 587-597. https://doi.org/10.1590/s0102-695x2012005000006

Mathai, A., & Devi, K. S. (1992). Anti-parasitic activity of certain indigeous plants. *Anc Sci Life*, *12*(1-2), 271-273. https://www.ncbi.nlm.nih.gov/pubmed/22556601

Mathai, A., & Devi, K. S. (1995). THE CHANGES IN VARIOUS TISSUES COMPONENTS OF SETARIA DIGITATA EXPOSED TO THE METHANOL EXTRACT OF STREBULUS ASPER. *Ancient Science of Life*, *14*(4), 248-252.

Mathers, C., Fat, D. M., & Boerma, J. T. (2008). *The global burden of disease: 2004 update*. World Health Organization.

Mazimba, O., Masesane, I. B., & Majinda, R. R. (2012a). A flavanone and antimicrobial activities of the constituents of extracts from *Mundulea sericea*. *Nat Prod Res*, *26*(19), 1817-1823. https://doi.org/10.1080/14786419.2011.616504

Mazimba, O., Masesane, I. B., Majinda, R. R. T., & Muzila, A. (2012b). GC-MS Analysis and Antimicrobial Activities of the Non-polar Extracts of Mundulea sericea. *S. Afr. J. Chem.*, *65*(1), 50-52.

Mba Nguekeu, Y. M., Awouafack, M. D., Tane, P., Nguedia Lando, M. R., Kodama, T., & Morita, H. (2017). A kaempferol triglycoside from *Tephrosia preussii* Taub. (Fabaceae). *Nat Prod Res*, *31*(21), 2520-2526. https://doi.org/10.1080/14786419.2017.1315720

Mbaveng, A. T., Fotso, G. W., Ngnintedo, D., Kuete, V., Ngadjui, B. T., Keumedjio, F., . . . Efferth, T. (2018). Cytotoxicity of epunctanone and four other phytochemicals isolated from the medicinal plants Garcinia epunctata and Ptycholobium contortum towards multi-factorial drug resistant cancer cells. *Phytomedicine*, *48*, 112-119. https://doi.org/10.1016/j.phymed.2017.12.016

McArdle, A. J., Turkova, A., & Cunnington, A. J. (2018). When do co-infections matter? *Curr Opin Infect Dis*, *31*(3), 209-215. https://doi.org/10.1097/QCO.0000000000000447

Medvedev, A. E. (2013). Toll-like receptor polymorphisms, inflammatory and infectious diseases, allergies, and cancer. *J Interferon Cytokine Res*, *33*(9), 467-484. https://doi.org/10.1089/jir.2012.0140

Mishra, B. B., Singh, R. K., Srivastava, A., Tripathi, V. J., & Tiwari, V. K. (2009). Fighting against Leishmaniasis: search of alkaloids as future true potential anti-Leishmanial agents. *Mini Rev Med Chem*, *9*(1), 107-123. https://doi.org/10.2174/138955709787001758

Mm, K. (2020). *REVIEW OF BOTANICAL NAME CHANGE OF TREES, SHRUBS AND HERBS IN KENYA*.

Mogana, R., Adhikari, A., Tzar, M. N., Ramliza, R., & Wiart, C. (2020). Antibacterial activities of the extracts, fractions and isolated compounds from Canarium patentinervium Miq. against bacterial clinical isolates. *BMC Complement Med Ther*, *20*(1), 55. https://doi.org/10.1186/s12906-020-2837-5

Mojab, F. (2012). Antimalarial natural products: a review. *Avicenna J Phytomed*, *2*(2), 52-62. https://www.ncbi.nlm.nih.gov/pubmed/25050231

Mokoka, T. A., Xolani, P. K., Zimmermann, S., Hata, Y., Adams, M., Kaiser, M., . . . Fouche, G. (2013). Antiprotozoal screening of 60 South African plants, and the identification of the antitrypanosomal germacranolides schkuhrin I and II. *Planta Med*, *79*(14), 1380-1384. https://doi.org/10.1055/s-0033-1350691

Monzote, L., & Siddiq, A. (2011). Drug development to protozoan diseases. *Open Med Chem J*, *5*, 1-3. https://doi.org/10.2174/1874104501105010001

Mooney, J. P., Galloway, L. J., & Riley, E. M. (2019). Malaria, anemia, and invasive bacterial disease: A neutrophil problem? *J Leukoc Biol*, *105*(4), 645-655. https://doi.org/10.1002/JLB.3RI1018-400R

Morhason-Bello, I. O., Odedina, F., Rebbeck, T. R., Harford, J., Dangou, J. M., Denny, L., & Adewole, I. F. (2013). Challenges and opportunities in cancer control in Africa: a perspective from the African Organisation for Research and Training in Cancer. *Lancet Oncol*, *14*(4), e142-151. https://doi.org/10.1016/S1470-2045(12)70482-5

Morita, M., Hayashi, K., Sato, A., Hiramoto, A., Kaneko, O., Isogawa, R., . . . Kim, H. S. (2019). Genomic and biological features of Plasmodium falciparum resistance against antimalarial endoperoxide N-89. *Gene*, *716*, 144016. https://doi.org/10.1016/j.gene.2019.144016

Morse, S. S. (1995). Factors in the emergence of infectious diseases. *Emerg Infect Dis*, *1*(1), 7-15. https://doi.org/10.3201/eid0101.950102

Morsy, T. A. (2013). Cutaneous leishmaniasis predisposing to human skin cancer: forty years local and regional studies. *J Egypt Soc Parasitol*, *43*(3), 629-648. https://doi.org/10.12816/0006420

Muiva-Mutisya, L. M., Atilaw, Y., Heydenreich, M., Koch, A., Akala, H. M., Cheruiyot, A. C., . . . Yenesew, A. (2018). Antiplasmodial prenylated flavanonols from *Tephrosia subtriflora*. *Nat Prod Res*, *32*(12), 1407-1414. https://doi.org/10.1080/14786419.2017.1353510

Muiva, L. M., Yenesew, A., Derese, S., Heydenreich, M., Peter, M. G., Akala, H. M., . . . Walsh, D. (2009). Antiplasmodial β-hydroxydihydrochalcone from seedpods of Tephrosia elata. *Phytochemistry Letters*, *2*(3), 99-102. https://doi.org/10.1016/j.phytol.2009.01.002

Mulama, D. H., Bailey, J. A., Foley, J., Chelimo, K., Ouma, C., Jura, W. G., . . . Moormann, A. M. (2014). Sickle cell trait is not associated with endemic Burkitt lymphoma: an ethnicity and malaria endemicity-matched case-control study suggests factors controlling EBV may serve as a predictive biomarker for this pediatric cancer. *Int J Cancer*, *134*(3), 645-653. https://doi.org/10.1002/ijc.28378

Muller, M., Byres, M., Jaspars, M., Kumarasamy, Y., Middleton, M., Nahar, L., . . . Sarker, S. D. (2004). 2D NMR spectroscopic analyses of archangelicin from the seeds of Angelica archangelica. *Acta Pharm*, *54*(4), 277-285. https://www.ncbi.nlm.nih.gov/pubmed/15634612

Mutisya, L. M. M. (2014). *Antiplasmodial and Larvicidal Flavonoids from the Seedpods of Tephrosia elata and Tephrosia aequilata* [Thesis, ir.jkuat.ac.ke.

Nafari, A., Cheraghipour, K., Sepahvand, M., Shahrokhi, G., Gabal, E., & Mahmoudvand, H. (2020). Nanoparticles: New agents toward treatment of leishmaniasis. *Parasite Epidemiol Control*, *10*, e00156. https://doi.org/10.1016/j.parepi.2020.e00156

Narayan, K. M., Ali, M. K., & Koplan, J. P. (2010). Global noncommunicable diseases--where worlds meet. *N Engl J Med*, *363*(13), 1196-1198. https://doi.org/10.1056/NEJMp1002024

Nazir, N., Koul, S., Qurishi, M. A., Taneja, S. C., Purnima, B., & Qazi, G. N. (2008). New isoflavones from Iris kashmiriana. *J Asian Nat Prod Res*, *10*(11-12), 1137-1141. https://doi.org/10.1080/10286020802413296

Nel, R. J. J., van Rensburg, H., van Heerden, P. S., Coetzee, J., & Ferreira, D. (1999). Stereoselective synthesis of flavonoids. Part 7. Poly-oxygenated β-hydroxydihydrochalcone derivatives. *Tetrahedron*, *55*(32), 9727-9736. https://doi.org/10.1016/s0040-4020(99)00554-2

Ng'ang'a, R. (2019). *Molecular and Morphological Identification of Plants Consumed by Yellow Baboons in Amboseli, Kenya* [Thesis, University of Nairobi]. erepository.uonbi.ac.ke.

Ngbolua, K.-t.-N. (2016). Phytochemical screening and Antiplasmodial activity of Mundulea antanossarum seeds from Madagascar. *Discovery Phytomedicine*, *3*(1), 1. https://doi.org/10.15562/phytomedicine.2016.30

Ngnintedo, D., Fotso, G. W., Kuete, V., Nana, F., Sandjo, L. P., Karaosmanoglu, O., . . . Andrae-Marobela, K. (2016). Two new pterocarpans and a new pyrone derivative with cytotoxic activities from Ptycholobium contortum (N.E.Br.) Brummitt (Leguminosae): revised NMR assignment of mundulea lactone. *Chem Cent J*, *10*(1), 58. https://doi.org/10.1186/s13065-016-0204-x

Nguyen, N. T., Nguyen, H. X., Le, T. H., Nguyen, D. H., Do, T. N. V., Dang, P. H., & Nguyen, M. T. T. (2021). Two new derivatives of 8-prenyl-5,7-dihydroxycoumarin from the stems of Streblus ilicifolius (S.Vidal) Corn. *Nat Prod Res*, *0*(0), 1-6. https://doi.org/10.1080/14786419.2021.1914611

Nordor, A. V., Bellet, D., & Siwo, G. H. (2018). Cancer-malaria: hidden connections. *Open Biol*, *8*(10), 180127. https://doi.org/10.1098/rsob.180127

Nweze, J. A., Mbaoji, F. N., Li, Y. M., Yang, L. Y., Huang, S. S., Chigor, V. N., . . . Yang, D. F. (2021). Potentials of marine natural products against malaria, leishmaniasis, and trypanosomiasis parasites: a review of recent articles. *Infect Dis Poverty*, *10*(1), 9. https://doi.org/10.1186/s40249-021-00796-6

O'Connor, R. (2007). The pharmacology of cancer resistance. *Anticancer Res*, *27*(3A), 1267-1272. https://www.ncbi.nlm.nih.gov/pubmed/17593618

Okoro, E. E., Ahmad, M. S., Osoniyi, O. R., & Onajobi, F. D. (2019). Antifungal and antileishmanial activities of fractions and isolated isoflavanquinones from the roots of Abrus precatorius. *Comparative Clinical Pathology*, *29*(2), 391-396. https://doi.org/10.1007/s00580-019-03073-z

Pacheco, G. A. B., & Kamboh, A. A. (2020). *Parasitology and Microbiology Research*. BoD – Books on Demand.

Pan, W. H., Xu, X. Y., Shi, N., Tsang, S. W., & Zhang, H. J. (2018). Antimalarial Activity of Plant Metabolites. *Int J Mol Sci*, *19*(5), 1382. https://doi.org/10.3390/ijms19051382

Pentsil, S., Cobbinah, J. R., & Bosu, P. P. (2017). *Handbook of Plants with Pesticidal Properties in Ghana*.

Phutdhawong, W., Donchai, A., Korth, J., Pyne, S. G., Picha, P., Ngamkham, J., & Buddhasukh, D. (2004). The components and anticancer activity of the volatile oil fromStreblus asper. *Flavour and Fragrance Journal*, *19*(5), 445-447. https://doi.org/10.1002/ffj.1342

Pierre, L. L., & Moses, M. N. (2015). Isolation and Characterisation of Stigmasterol and B -Sitosterol from Odontonema Strictum (Acanthaceae). *2*, 8.

Pohlit, A. M., Lopes, N. P., Gama, R. A., Tadei, W. P., & Neto, V. F. (2011). Patent literature on mosquito repellent inventions which contain plant essential oils--a review. *Planta Med*, *77*(6), 598-617. https://doi.org/10.1055/s-0030-1270723

Popwo Tameye, S. C., Djamen Mbeunkeu, A. B., Fouokeng, Y., Jouwa Tameye, N. S., Tabekoueng, G. B., Wansi, J. D., . . . Azebaze, A. G. B. (2021). Ficusanolide A and ficusanolide B, two new cinnamic acid derivative stereoisomers and other constituents of the stem barks of Ficus exasperata Vahl. (Moraceae). *Phytochemistry Letters*, *43*, 150-153. https://doi.org/10.1016/j.phytol.2021.03.027

Porta, C., Riboldi, E., Totaro, M. G., Strauss, L., Sica, A., & Mantovani, A. (2011). Macrophages in cancer and infectious diseases: the 'good'and the 'bad'. *Immunotherapy*, *3*(10), 1185-1202.

Prachyawarakorn, V., Mahidol, C., & Ruchirawat, S. (2000). NMR study of seven coumarins from mammea siamensis. *Pharm Biol*, *38 Suppl 1*(sup1), 58-62. https://doi.org/10.1076/phbi.38.6.58.5962

Prasad, M. A., Zolnik, C. P., & Molina, J. (2019). Leveraging phytochemicals: the plant phylogeny predicts sources of novel antibacterial compounds. *Future Sci OA*, *5*(7), FSO407. https://doi.org/10.2144/fsoa-2018-0124

Prevention, C.-C. f. D. C. a. (2019, 2019-01-31T02:10:53Z/). *CDC - Malaria - Malaria Worldwide - CDC's Global Malaria Activities - Kenya*.

Prevention, C.-C. f. D. C. a. (2020, 2020-02-18T06:01:52Z). *CDC - Leishmaniasis - Biology*.

Quintana, M. D. P., Smith-Togobo, C., Moormann, A., & Hviid, L. (2020). Endemic Burkitt lymphoma - an aggressive childhood cancer linked to Plasmodium falciparum exposure, but not to exposure to other malaria parasites. *APMIS*, *128*(2), 129-135. https://doi.org/10.1111/apm.13018

Raghavendra, K., Barik, T. K., Reddy, B. P., Sharma, P., & Dash, A. P. (2011). Malaria vector control: from past to future. *Parasitol Res*, *108*(4), 757-779. https://doi.org/10.1007/s00436-010-2232-0

Rahman, A. H. M., & Khanom, A. (2013). Taxonomic and Ethno-Medicinal Study of Species from Moraceae (Mulberry) Family in Bangladesh Flora. *Research in Plant Sciences*, *1*, 53-57. https://doi.org/10.12691/plant-1-3-1

Rakoff-Nahoum, S. (2006). Why cancer and inflammation? *Yale J Biol Med*, *79*(3-4), 123-130. https://www.ncbi.nlm.nih.gov/pubmed/17940622

Rama, M., Kumar, N. V., & Balaji, S. (2015a). A comprehensive review of patented antileishmanial agents. *Pharm Pat Anal*, *4*(1), 37-56. https://doi.org/10.4155/ppa.14.55

Rama, M., Kumar, N. V. A., & Balaji, S. (2015b). A comprehensive review of patented antileishmanial agents. *Pharmaceutical Patent Analyst*, *4*(1), 37-56.

Rao, D. S., Penmatsa, T., Kumar, A. K., Reddy, M. N., Gautam, N. S., & Gautam, N. R. (2014). Antibacterial activity of aqueous extracts of Indian chewing sticks on dental plaque: An in vitro study. *J Pharm Bioallied Sci*, *6*(Suppl 1), S140-145. https://doi.org/10.4103/0975-7406.137426

Rao, E. V., Sridhar, P., Rao, B. N., & Ellaiah, P. (1999). A prenylated dihydroflavonol from Mundulea suberosa. *Phytochemistry*, *50*(8), 1417–1418.

Rastogi, S., Kulshreshtha, D. K., & Rawat, A. K. (2006). Streblus asper Lour. (Shakhotaka): A Review of its Chemical, Pharmacological and Ethnomedicinal Properties. *Evid Based Complement Alternat Med*, *3*(2), 217-222. https://doi.org/10.1093/ecam/nel018

Rawat, P., Kumar, A., Singh, T. D., & Pal, M. (2018). Chemical Composition and Cytotoxic Activity of Methanol Extract and its Fractions of Streblus asper Leaves on Human Cancer Cell Lines. *Pharmacogn Mag*, *14*(54), 141-144. https://doi.org/10.4103/pm.pm_391_17

Ren, Y., Chen, W.-L., Lantvit, D. D., Sass, E. J., Shriwas, P., Ninh, T. N., . . . Kinghorn, A. D. (2016, December 16, 2016). *Cardiac Glycoside Constituents of Streblus asper with Potential Antineoplastic Activity*.

Ren, Y., Chen, W. L., Lantvit, D. D., Sass, E. J., Shriwas, P., Ninh, T. N., . . . Kinghorn, A. D. (2017). Cardiac Glycoside Constituents of Streblus asper with Potential Antineoplastic Activity. *J Nat Prod*, *80*(3), 648-658. https://doi.org/10.1021/acs.jnatprod.6b00924

Rocha, L. G., Almeida, J. R., Macedo, R. O., & Barbosa-Filho, J. M. (2005). A review of natural products with antileishmanial activity. *Phytomedicine*, *12*(6-7), 514-535. https://doi.org/10.1016/j.phymed.2003.10.006

Rodrigues, I. A., Mazotto, A. M., Cardoso, V., Alves, R. L., Amaral, A. C., Silva, J. R., . . . Vermelho, A. B. (2015). Natural Products: Insights into Leishmaniasis Inflammatory Response. *Mediators Inflamm*, *2015*, 835910. https://doi.org/10.1155/2015/835910

Sajjadi, S. E., Shokoohinia, Y., & Moayedi, N. S. (2012). Isolation and Identification of Ferulic Acid From Aerial Parts of Kelussia odoratissima Mozaff. *Jundishapur J Nat Pharm Prod*, *7*(4), 159-162. https://www.ncbi.nlm.nih.gov/pubmed/24624175

Sandhya, S. (2018). Comparative Assessment of the Antibacterial activity of Three Tephrosia Species against Helicobacter pylori. *Indian Journal of Pharmaceutical Sciences*, *80*(3), 460-469. https://doi.org/10.4172/pharmaceutical-sciences.1000379

Sandlund, J., Naucler, P., Dashti, S., Shokri, A., Eriksson, S., Hjertqvist, M., . . . Farnert, A. (2013). Bacterial coinfections in travelers with malaria: rationale for antibiotic therapy. *J Clin Microbiol*, *51*(1), 15-21. https://doi.org/10.1128/JCM.02149-12

Schmidt, T. J., Khalid, S. A., Romanha, A. J., Alves, T. M., Biavatti, M. W., Brun, R., . . . Ogungbe, I. V. (2012). The Potential of Secondary Metabolites from Plants as Drugs or Leads Against Protozoan Neglected Diseases - Part II. *Current Medicinal Chemistry*, *19*(14), 2176-2228. https://doi.org/10.2174/092986712800229087

Seebacher, N. A., Stacy, A. E., Porter, G. M., & Merlot, A. M. (2019). Clinical development of targeted and immune based anti-cancer therapies. *J Exp Clin Cancer Res*, *38*(1), 156. https://doi.org/10.1186/s13046-019-1094-2

Seong, S. H., Ha, M. T., Min, B. S., Jung, H. A., & Choi, J. S. (2018). Moracin derivatives from Morus Radix as dual BACE1 and cholinesterase inhibitors with antioxidant and anti-glycation capacities. *Life Sci*, *210*, 20-28. https://doi.org/10.1016/j.lfs.2018.08.060

Sereno, M., Brunello, A., Chiappori, A., Barriuso, J., Casado, E., Belda, C., . . . Gonzalez-Baron, M. (2008). Cardiac toxicity: old and new issues in anti-cancer drugs. *Clin Transl Oncol*, *10*(1), 35-46. https://doi.org/10.1007/s12094-008-0150-8

Shenoy, S., Shwetha, K., Prabhu, K., Maradi, R., Bairy, K. L., & Shanbhag, T. (2010). Evaluation of antiinflammatory activity of Tephrosia purpurea in rats. *Asian Pacific Journal of Tropical Medicine*, *3*(3), 193-195. https://doi.org/10.1016/s1995-7645(10)60007-7

Sindhu, & Usha. (2017). A Review On The Pharmacological Profile Of Tephrosia Calophylla. https://doi.org/10.5281/ZENODO.804315

Singh, S. P., Verma, N. K., & Tripathi, A. K. (2015). A brief study on Strebulus asper L. -A Review. *Research Journal of Phytomedicine*.

Singh, V., Saxena, R. C., & Singh, A. K. (2008). A flavonoid out of Tephrosia purpurea extract and its antimicrobial effect. *Biomedical &pharmacology journal*, *1*(2), 465-468.

Smilkstein, M., Sriwilaijaroen, N., Kelly, J. X., Wilairat, P., & Riscoe, M. (2004a). Simple and inexpensive fluorescence-based technique for high-throughput antimalarial drug screening. *Antimicrobial Agents and Chemotherapy*, *48*(5), 1803-1806.

Smilkstein, M., Sriwilaijaroen, N., Kelly, J. X., Wilairat, P., & Riscoe, M. (2004b). Simple and inexpensive fluorescence-based technique for high-throughput antimalarial drug screening. *Antimicrob Agents Chemother*, *48*(5), 1803-1806. https://doi.org/10.1128/AAC.48.5.1803-1806.2004

Sougoufara, S., Diédhiou, S. M., Doucouré, S., Diagne, N., Sembène, P. M., Harry, M., . . . Ndiath, M. O. (2014). Biting by Anopheles funestus in broad daylight after use of long-lasting insecticidal nets: a new challenge to malaria elimination. *Malaria Journal*, *13*(1), 125.

Spencer, C. M., & Faulds, D. (1994). Paclitaxel. A review of its pharmacodynamic and pharmacokinetic properties and therapeutic potential in the treatment of cancer. *Drugs*, *48*(5), 794-847. https://doi.org/10.2165/00003495-199448050-00009

Sripanidkulchai, B., Junlatat, J., Wara-aswapati, N., & Hormdee, D. (2009). Anti-inflammatory effect of Streblus asper leaf extract in rats and its modulation on inflammation-associated genes expression in RAW 264.7 macrophage cells. *J Ethnopharmacol*, *124*(3), 566-570. https://doi.org/10.1016/j.jep.2009.04.061

Stark, T. D., Mtui, D. J., & Balemba, O. B. (2013). Ethnopharmacological Survey of Plants Used in the Traditional Treatment of Gastrointestinal Pain, Inflammation and Diarrhea in Africa: Future Perspectives for Integration into Modern Medicine. *Animals (Basel)*, *3*(1), 158-227. https://doi.org/10.3390/ani3010158

Stuart, K., Brun, R., Croft, S., Fairlamb, A., Gurtler, R. E., McKerrow, J., . . . Tarleton, R. (2008). Kinetoplastids: related protozoan pathogens, different diseases. *J Clin Invest*, *118*(4), 1301-1310. https://doi.org/10.1172/JCI33945

Sujitha, V., Murugan, K., Paulpandi, M., Panneerselvam, C., Suresh, U., Roni, M., . . . Benelli, G. (2015). Green-synthesized silver nanoparticles as a novel control tool against dengue virus (DEN-2) and its primary vector Aedes aegypti. *Parasitol Res*, *114*(9), 3315-3325. https://doi.org/10.1007/s00436-015-4556-2

Sun, G., Zheng, Z., Lee, M. H., Xu, Y., Kang, S., Dong, Z., . . . Chen, W. (2017). Chemoprevention of Colorectal Cancer by Artocarpin, a Dietary Phytochemical from Artocarpus heterophyllus. *J Agric Food Chem*, *65*(17), 3474-3480. https://doi.org/10.1021/acs.jafc.7b00278

Sung, H., Ferlay, J., Siegel, R. L., Laversanne, M., Soerjomataram, I., Jemal, A., & Bray, F. (2021). Global Cancer Statistics 2020: GLOBOCAN Estimates of Incidence and Mortality Worldwide for 36 Cancers in 185 Countries. *CA Cancer J Clin*, *71*(3), 209-249. https://doi.org/10.3322/caac.21660

Suresh, S., Spatz, J., Mills, J. P., Micoulet, A., Dao, M., Lim, C. T., . . . Seufferlein, T. (2005). Connections between single-cell biomechanics and human disease states: gastrointestinal cancer and malaria. *Acta Biomater*, *1*(1), 15-30. https://doi.org/10.1016/j.actbio.2004.09.001

Taleghani, A., & Tayarani-Najaran, Z. (2018). Potent Cytotoxic Natural Flavonoids: The Limits of Perspective. *Curr Pharm Des*, *24*(46), 5555-5579. https://doi.org/10.2174/1381612825666190222142537

Tang, C., Yang, L., Jiang, X., Xu, C., Wang, M., Wang, Q., . . . Cui, H. (2014). Antibiotic drug tigecycline inhibited cell proliferation and induced autophagy in gastric cancer cells.

Biochem Biophys Res Commun, *446*(1), 105-112. https://doi.org/10.1016/j.bbrc.2014.02.043

Tang, H., Zhang, Y., Li, D., Fu, S., Tang, M., Wan, L., . . . Chen, L. (2018). Discovery and synthesis of novel magnolol derivatives with potent anticancer activity in non-small cell lung cancer. *Eur J Med Chem*, *156*, 190-205. https://doi.org/10.1016/j.ejmech.2018.06.048

Tempone, A. G., Martins de Oliveira, C., & Berlinck, R. G. (2011). Current approaches to discover marine antileishmanial natural products. *Planta Med*, *77*(6), 572-585. https://doi.org/10.1055/s-0030-1250663

Thomas, L. (2005). Malaria gene linked to prostate-cancer incidence. *Lancet Oncol*, *6*(5), 266. https://doi.org/10.1016/s1470-2045(05)70156-x

Thriemer, K., Ley, B., Ame, S., von Seidlein, L., Pak, G. D., Chang, N. Y., . . . Deen, J. L. (2012). The burden of invasive bacterial infections in Pemba, Zanzibar. *PLoS ONE*, *7*(2), e30350. https://doi.org/10.1371/journal.pone.0030350

Touqeer, S., Saeed, M., & Ajaib, M. (2013a). A Review on the Phytochemistry and Pharmacology of Genus Tephrosia. In.

Touqeer, S., Saeed, M. A., & Ajaib, M. (2013b). A Review on the Phytochemistry and Pharmacology of Genus. 41.

Trimmer, E. E., & Essigmann, J. M. (1999). Cisplatin. *Essays Biochem*, *34*, 191-211. https://doi.org/10.1042/bse0340191

Tringali, C. (2001). *Bioactive compounds from natural sources: isolation, characterisation, and biological properties*. Taylor & Francis.

Tuteja, R. (2007). Malaria - an overview. *FEBS J*, *274*(18), 4670-4679. https://doi.org/10.1111/j.1742-4658.2007.05997.x

Umereweneza, D., Atilaw, Y., Rudenko, A., Gutlin, Y., Bourgard, C., Gupta, A. K., . . . Gogoll, A. (2021). Antibacterial and cytotoxic prenylated dihydrochalcones from Eriosema montanum. *Fitoterapia*, *149*, 104809. https://doi.org/10.1016/j.fitote.2020.104809

Urruticoechea, A., Alemany, R., Balart, J., Villanueva, A., Vinals, F., & Capella, G. (2010). Recent advances in cancer therapy: an overview. *Curr Pharm Des*, *16*(1), 3-10. https://doi.org/10.2174/138161210789941847

van Elsland, D., & Neefjes, J. (2018). Bacterial infections and cancer. *EMBO Rep*, *19*(11), e46632. https://doi.org/10.15252/embr.201846632

Volpedo, G., Costa, L., Ryan, N., Halsey, G., Satoskar, A., & Oghumu, S. (2019). Nanoparticulate drug delivery systems for the treatment of neglected tropical protozoan diseases. *J Venom Anim Toxins Incl Trop Dis*, *25*, e144118. https://doi.org/10.1590/1678-9199-JVATITD-1441-18

Wambalaba, F. W., Son, B., Wambalaba, A. E., Nyong'o, D., & Nyong'o, A. (2019). Prevalence and Capacity of Cancer Diagnostics and Treatment: A Demand and Supply Survey of Health-Care Facilities in Kenya. *Cancer Control*, *26*(1), 1073274819886930. https://doi.org/10.1177/1073274819886930

Wang, J. J., Lei, K. F., & Han, F. (2018). Tumor microenvironment: recent advances in various cancer treatments. *Tumor microenvironment*, *22*(12), 3855-3864.

Watanabe, M. A., Amarante, M. K., Conti, B. J., & Sforcin, J. M. (2011). Cytotoxic constituents of propolis inducing anticancer effects: a review. *J Pharm Pharmacol*, *63*(11), 1378-1386. https://doi.org/10.1111/j.2042-7158.2011.01331.x

WHO. (2017a). Malaria in pregnant women. In.

WHO. (2017b, 2017). *Status report on artemisinin and ACT resistance*.

WHO. (2021a, 2021). *Cancer*.
WHO. (2021b, 2021). *Leishmaniasis*.
WHO. (2021c, 2021). *Non communicable diseases*.
WHO. (2021d, 2021). *WHO EMRO | Infectious diseases | Health topics*.
WHO, W. (2020). World malaria report 2020: 20 years of global progress and challenges. 299.
Wink, M. (2013). Evolution of secondary metabolites in legumes (Fabaceae). *South African Journal of Botany*, *89*, 164-175. https://doi.org/10.1016/j.sajb.2013.06.006
Wojciechowski, M. F., Lavin, M., & Sanderson, M. J. (2004). A phylogeny of legumes (Leguminosae) based on analysis of the plastid matK gene resolves many well-supported subclades within the family. *Am J Bot*, *91*(11), 1846-1862. https://doi.org/10.3732/ajb.91.11.1846
Wright, C. W., & Phillipson, J. D. (1990). Natural products and the development of selective antiprotozoal drugs. *Phytotherapy Research*, *4*(4), 127-139. https://doi.org/10.1002/ptr.2650040402
Wu et al, m. r., shu-miaw chaw. (2003). Naturalized Fabaceae (Leguminosae) species in Taiwan: the first approximation. *Botanical Bulletin of Academia Sinica*, 44.
Wyss, K., Granath, F., Wangdahl, A., Djarv, T., Fored, M., Naucler, P., & Farnert, A. (2020). Malaria and risk of lymphoid neoplasms and other cancer: a nationwide population-based cohort study. *BMC Med*, *18*(1), 296. https://doi.org/10.1186/s12916-020-01759-8
Yousuf, M., Mukherjee, D., Dey, S., Pal, C., & Adhikari, S. (2016). Antileishmanial ferrocenylquinoline derivatives: Synthesis and biological evaluation against Leishmania donovani. *Eur J Med Chem*, *124*, 468-479. https://doi.org/10.1016/j.ejmech.2016.08.049
Zarina, A., Siddiqui, I. A., Shaukat, S. S., & Shaukat, R. (2005). Seed characteristics, germination and phenotypic plasticity of tephrosia uniflora populations in southern sindh. *International journal of biology and biotechnology*, 7.
Zekar, L., & Sharman, T. (2020). Plasmodium Falciparum Malaria. In *StatPearls*. StatPearls Publishing.
Zerega, N. J., Clement, W. L., Datwyler, S. L., & Weiblen, G. D. (2005). Biogeography and divergence times in the mulberry family (Moraceae). *Mol Phylogenet Evol*, *37*(2), 402-416. https://doi.org/10.1016/j.ympev.2005.07.004
Zhai, L., Blom, J., Chen, M., Christensen, S. B., & Kharazmi, A. (1995). The antileishmanial agent licochalcone A interferes with the function of parasite mitochondria. *Antimicrob Agents Chemother*, *39*(12), 2742-2748. https://doi.org/10.1128/AAC.39.12.2742
Zhang, B. D., Zhu, W. F., Akihisa, T., Kikuchi, T., Ukiya, M., Maya, F., . . . Zhang, J. (2021). Cardiac glycosides from the roots of Streblus asper Lour. and their apoptosis-inducing activities in A549 cells. *Phytochemistry*, *181*, 112544. https://doi.org/10.1016/j.phytochem.2020.112544
Zhou, D., Huang, X., Liu, W., Huang, Y., Yang, R., Deng, S., & Li, J. (2020). Bioactivity-guided isolation of anti-inflammatory constituents from the bark of Streblus zeylanicus. *Fitoterapia*, *147*, 104770. https://doi.org/10.1016/j.fitote.2020.104770
Ziaei, H., Sadeghian, G., & Hejazi, S. H. (2008). Distribution frequency of pathogenic bacteria isolated from cutaneus leishmaniasis lesions. *Korean J Parasitol*, *46*(3), 191-193. https://doi.org/10.3347/kjp.2008.46.3.191
Zofou, D., Nyasa, R. B., Nsagha, D. S., Ntie-Kang, F., Meriki, H. D., Assob, J. C., & Kuete, V. (2014). Control of malaria and other vector-borne protozoan diseases in the tropics:

enduring challenges despite considerable progress and achievements. *Infect Dis Poverty*, *3*(1), 1. https://doi.org/10.1186/2049-9957-3-1

APPENDICES

Physical and Spectroscopic Data of Compounds

Compound **110**, A white crystal, HREIMS $[M+1]^+$ m/z 363.1396, UV λ_{max} 270 nm, 310 nm, ^{1}H NMR (DMSO-d_6, 600 MHz) δ_H 9.35 (s, 5-OH), 8.00 (*d*, *J* = 8.9 Hz, H-3'), 7.89 (*d*, *J* = 8.4 Hz, H-1'), 7.78 (m, H-2'), 7.59 (*d*, *J* = 2.6 Hz, H-6'), 7.38 (s, H-4), 7.23 (*dd*, *J* = 8.9, 2.6 Hz, H-4'), 5.35 (m, *J* = 7.5, 1.3 Hz, H-2''), 3.97 (s, 5'-OMe), 3.83 (s, 6-OMe), 3.71 (*d*, *J* = 7.5 Hz, H-1''), 1.97 (m, H-4''), 1.69 (*d*, *J* = 1.6 Hz, H-5''). ^{13}C NMR (DMSO-d_6, 150 MHz) δ_C 157.9 (C-5'), 150.7 (C-2), 147.8 (C-7a), 147.3 (C-5), 145.5 (C-6), 131.5 (C-3''), 127.3 (C-2'a), 122.8 (C-2'), 122.1 (C-2''), 119.8 (C-3), 119.3 (C-3a), 118.9 (C-7), 103.9 (C-4), 98.7 (C-6')-, 60.5 (6-OMe), 55.3 (5'-OMe), 25.5 (C-5''), 23.3 (C-1''), 17.7 (C-4'').

Compound **111**, A white solid, HREIMS $[M+1]^+$ m/z 349.1440,^{1}H NMR (Methanol-d_4, 500 MHz) δ_H 7.84 (*d*, *J* = 8.8 Hz, H-3'), 7.68 (*d*, *J* = 8.4 Hz, H-1'), 7.63 (*d*, *J* = 8.5 Hz, H-2'), 7.59 (*d*, *J* = 2.5 Hz, H-6'), 7.29 (s, H-4), 7.10 (*dd*, *J* = 8.8, 2.5 Hz, H-4'), 5.44 (*ddp*, *J* = 7.4, 5.9, 1.5 Hz, H-2''), 3.89 (s, 6-OMe), 3.75 (*d*, *J* = 7.4 Hz, H-1''), 1.99 (*d*, *J* = 1.4 Hz, H-5''), 1.73 (*d*, *J* = 1.5 Hz). ^{13}C NMR (Methanol-d_4, 125 MHz) δ 157.3 (C-5'), 152.7 (C-2), 150.0 (C-7a), 146.7 (C-6), 133.1 (C-3''), 131.3 (C-3'), 128.8 (C-2'a), 124.0 (C-3), 123.9 (C-2'), 123.4 (C-4''), 121.63 (C-6'a), 121.1 (C-3a), 120.6 (C-7), 116.0 (C-1'), 104.4 (C-4), 103.2 (C-6'), 61.6 (6-OMe), 26.0 (C-4''), 24.6 (C-1''), 18.2 (C-5'').

Compound **112**, A white amorphous solid. HREIMS $[M+1]^+$ m/z 347.1283, ^{1}H NMR (Chloroform-*d*, 500 MHz) δ_H 7.85 (*d*, *J* = 8.9 Hz, H-3'), 7.73 (*d*, *J* = 8.3 Hz, H-1'), 7.67 (*s*, H-6'), 7.64 (*d*, *J* = 3.1 Hz, H-2'), 7.36 (*s*, H-4), 7.16 (*dd*, *J* = 9.0, 2.6 Hz, H-4'), 7.06 (d, *J* = 9.8 Hz, H-4''), 5.81 (d, *J* = 9.9 Hz, H-3''), 4.03 (s, 5-OMe), 1.56 (d, *J* = 2.0 Hz, H-2''-$(Me)_2$). ^{13}C NMR (Chloroform-*d*, 125 MHz) δ 158.3 (C-5'), 151.6 (C-2), 146.1 (C-7a), 141.8 (C-6), 138.7 (C-5), 130.8 (C-3''), 130.2 (C-3'), 127.8 (C-3), 123.0 (C-2'), 122.4 (C-6'a), 120.5 (C-3a), 118.2 (C-4'), 117.8(C-2'a), 116.7(C-4''), 115.8(C-1'), 106.8 (C-7), 104.6 (C-4), 78.0 (C-2''), 55.7 (5'-OMe), 27.9 (C-2''-$(Me)_2$).

Compound **113,** A white amorphous solid, EIMS $[M+1]^+$ m/z 348.17, ^{1}H NMR (Chloroform-*d*, 500 MHz) δ_H 7.86 (*d*, *J* = 8.9 Hz, H-3'), 7.75 (*d*, *J* = 8.3 Hz, H-1'), 7.67 – 7.64 (*m*, H-2', H-6'), 7.39 (*s*, H-4), 7.19 (*dd*, *J* = 8.9, 2.6 Hz, H-4'), 5.58 (*s*, 5-OH), 5.47 (*tp*, *J* = 7.2, 1.4 Hz, H-2"), 4.03 (*s*,5-OMe), 3.92 (*s*, 5'-OMe), 3.81 (*dt*, *J* = 7.1, 1.2 Hz, H-1'"), 2.00 (*d*, *J* = 1.5 Hz, H-5'"), 1.75 (*q*, *J* = 1.4 Hz, H-4'"). ^{13}C NMR (126 MHz, Chloroform-*d*) δ 158.3 (C-5'), 152.1 (C-2), 149.3 (C-7a), 145.9 (C-6), 144.5 (C-5) 132.7 (C-3"), 130.2 (C-3'), 128.1 (C-2'a), 122.8 (C-2'), 122.5 (C-3), 122.0 (C-2'"), 121.1 (C- 6a), 120.2 (C-3a), 119.2 (C-7), 118.3 (C- 4'), 116.1 (C-1'), 103.0 (C-4), 99.5 (C-6'), 62.3 (C-5OMe), 55.6 (C-5'OMe), 26.0 (C-4"), 24.1 (C-1"), 18.1 (C-5").

Compound **114**, A white crystal, HREIMS $[M+1]^+$ m/z 319.1334, UV λ_{max} 230 nm, 255 nm, ^{1}H NMR (Chloroform-*d*, 500 MHz) δ_H 7.78 (*dd*, *J* = 8.5, 3.4 Hz, H-8), 7.59 (*s*, H-5), 7.30 (*dd*, *J* = 8.4, 1.8 Hz), 7.16 (*d*, *J* = 2.5 Hz, H-4), 7.11 (*dd*, *J* = 8.8, 2.4 Hz, H-2), 6.90 (*d*, *J* = 8.3 Hz, H-3'), 6.87 (*d*, *J* = 8.3 Hz, H-2'), 6.40 (*d*, *J* = 10.0 Hz, H-4"), 5.61 (*d*, *J* = 10.1 Hz, H-3"), 5.55 (*s*, 4'-OH), 5.13 (*s*, 3-OH), 1.52 (s, H-2"-$(Me)_2$). ^{13}C NMR (Chloroform-*d*, 125 MHz) δ_C 153.9 (C-3), 144.2 (C-4'), 139.6 (C-5'), 138.1 (C-7), 134.6 (C-4a), 131.5 (C-1'), 130.5 (C-3"), 129.7 (C-1), 127.9 (C-8a), 127.6 (C-8), 126.9 (C-5), 121.1 (C-4"), 119.2 (C-6'), 114.6 (C-2'), 109.7 (C-4), 76.5 (C-2"), 27.9 (C-2"-$(Me)_2$).

Compound **115**, A white solid, HREIMS $[M+1]^+$ m/z 321.1491, UV λ_{max} 234 nm, ^{1}H NMR (Chloroform-*d*, 500 MHz) δ_H 7.76 (*d*, *J* = 8.2 Hz, H-8), 7.76 (*d*, *J* = 8.2 Hz, H-1), 7.55 (*s*, H-5), 7.24 (d, *J* = 1.8 Hz, H-6), 7.14 (*d*, *J* = 2.5 Hz, H-4), 7.10 (*dd*, *J* = 8.8, 2.6 Hz, H-2), 6.85 (*q*, *J* = 8.2 Hz, H-2', 3'), 5.55 (*s*, 5'-OH), 5.43 (*s*, 4'-OH), 5.29 (*m*, H-2"), 5.00 (*s*,3-OH), 3.36 (*d*, *J* = 6.8 Hz, H-1"), 1.76 (*s*, H-5"), 1.68 (*s*, H-4"). ^{13}C NMR (Chloroform-*d*, 126 MHz) δ_C 153.8 (C-3), 144.0 (C-4'), 142.4 (C-5'), 139.9 (C-4a), 135.7 (C-3"), 134.9 (C-1'), 134.6 (C-7), 129.8 (C-1), 127.8 (C-8), 127.5 (C-8a) 126.8 (C-5), 126.2 (C-6) 125.4 (C-6'), 122.2(C-2'), 117.8 (C-2), 112.9(C-3'), 109.7 (C-4), 27.7 (C-1"), 25.9 (C-4"), 18.1 (C-5").

Compound **116**, A white solid, HREIMS $[M+1]^+$ m/z 335.1647, ^{1}H NMR (Chloroform-*d*, 500 MHz) δ_H 7.78 (*d*, *J* = 7.4 Hz, H-1), 7.77 (*d*, *J* = 8.5 Hz, H-8), 7.55(*m*, H-5), 7.26(*m*, H-6), 7.11(*m*,

H-4), 7.09 (*m*, H-2), 6.97 (*d*, *J* = 8.3 Hz, H-3'), 6.90 (*d*, *J* = 8.2 Hz, H-2'), 5.58 (*s*, 3-OH), 5.30 (*s*, 4'OH), 5.08 (*dq*, *J* = 6.6, 1.5 Hz, H-2''), 3.86 (*s*, 5'-OMe), 3.33 (*dt*, *J* = 6.6, 1.3 Hz, H-1''), 1.58 (*d*, *J* = 1.4 Hz, H-4''), 1.35 (*d*, *J* = 1.4 Hz, H-5''). ^{13}C NMR (Chloroform-*d*, 126 MHz) δ_C 153.8 (C-3), 148.5 (C-4'), 145.6 (C-5'), 139.9 (C-7), 135.7 (C-1'), 134.6 (C-8a), 133.3 (C-6'), 131.5 (C-3''), 129.7(C-1), 127.8 (C-4a), 127.2 (C-8), 126.9 (C-5), 126.9 (C-5'), 123.5 (C-2''), 117.7 (C-2), 113.3 (C-2'), 109.7 (C-4), 61.4 (5'-OMe), 26.9 (C-1''), 25.8 (C-4''), 17.8 (C-5'').

Compound **117**, A white solid, HREIMS $[M+1]^+$ m/z 335.1647, ^{1}H NMR (Chloroform-*d*, 500 MHz) δ_H 8.04(*m*, H-5), 7.81 (*d*, *J* = 8.5 Hz, H-8), 7.72 (*d*, *J* = 8.9 Hz, H-1), 7.52 (*dd*, *J* = 8.5, 1.7 Hz, H-6), 7.27 (*m*, H-2), 7.25 (*m*, H-2'), 7.17 (*dd*, *J* = 8.2, 2.1 Hz, H-6'), 6.98 (*d*, *J* = 8.2 Hz, H-3'), 5.23 (*m*, H-2'', 4'OH, 5'OH), 3.95 (*s*, 3OMe), 3.83 (*d*, *J* = 6.8 Hz, H-1''), 1.91 (*d*, *J* = 1.3 Hz ,H-4''), 1.69 (*d*, *J* = 1.5 Hz, H-5''). ^{13}C NMR (Chloroform-*d*, 125 MHz) δ_C 154.7 (C-3), 143.9 (C-4'), 143.2 (C-5'), 138.3 (C-1'), 135.5 (C-7), 133.4 (C-4a, C-8a), 131.6 (C-3''), 129.1 (C-8), 128.5 (C-4), 127.4 (C-1), 123.5 (C-2''), 123.0 (C-6), 121.4 (C-5), 120.4 (C-6'), 115.9 (C-3'), 114.8 (C-2'), 113.8 (C-2), 57.0 (3-OMe), 25.9 (C-5''), 24.3 (C-1''), 18.3 (C-4'').

Compound **118**, A white solid, HREIMS $[M+1]^+$ m/z 389.2117, ^{1}H NMR (500 MHz, Chloroform-*d*) δ_H 7.78 (*m*, H-1), 7.77 (*m*, H-8), 7.45 (*d*, *J* = 1.6 Hz, H-5), 7.13-7.09 (*ddd*, *J* = 9.5, 5.8, 2.0 Hz, H-2, H-4, H-6), 6.75 (*s*, H-2'), 5.60 (*s*, 3-OH), 5.12 (*m*, H- 2''), 4.94 (*s*, 4-'OH), 2.96 (*d*, *J* = 7.4 Hz, H-1''), 2.32 (*dt*, *J* = 9.0, 6.7 Hz, H-4'''), 1.68 (*t*, *J* = 6.8 Hz, H-3'''), 1.62 (*d*, *J* = 1.6 Hz, H-5''), 1.34 (*s*, H-2'''-$(Me)_2$), 1.33 (s, H-4''). ^{13}C NMR (Chloroform-*d*, 125 MHz) δ_C 153.7 (C-3), 144.5 (C-4'), 139.0 (C-5'), 138.5 (C-7), 134.8 (C-8a), 132.6 (C-1'), 131.3 (C-3'), 129.8 (C-1), 127.9 (C-4a), 127.7 (C-8), 127.2 (C-5), 126.5 (C-4), 123.9 (C-2''), 119.7 (C-6'), 117.7 (C-5'), 112.4 (C-2'), 109.6 (C-6), 74.8 (C-2'''), 33.2 (C-3'''), 32.0 (C-1''), 27.0 (C-2'''-$(Me)_2$), 25.9 (C-5''), 21.9 (C-4'''), 17.7 (C-4'').

Compound **119**, A white solid, EIMS $[M+1]^+$ m/z 334.37, ^{1}H NMR (Chloroform-d, 500 MHz) δ_H 7.78 (*dd*, J = 8.7, 1.4 Hz, H-1, H-8), 7.56 (*d*, J = 1.7 Hz, H-5), 7.42 (*d*, J = 16.6 Hz, 1''), 7.23 (*dd*, J = 8.4, 1.8 Hz, H-2), 7.16 – 7.10 (*m*, H-2', H-4, H-6), 7.08 (*d*, J = 8.3 Hz, H-3'), 6.86 (*d*, J = 16.6 Hz, H-2''), 5.82 (*s*, 4'-OH), 5.09 (*s*, 3-OH), 3.76 (*s*, 5'OMe), 2.14 (*s*, H-4'')^{13}C NMR (Chloroform-

d, 126 MHz) δ 199.4 (C-3"), 154.1 (C-3), 148.9 (C-4'), 146.2 (C-5'), 138.9(C-1"), 138.4 (C-7), 136.5 (C-1'), 134.6 (C-8a), 132.4 (C-2"), 129.9 (C-1), 129.8 (C-4a), 128.1 (C-6'), 127.7 (C-8), 127.5 (C-4), 127.4 (C-5), 126.2 (C-2'), 118.3 (C-6), 117.0 (C-3'), 109.7 (C-2), 60.8 (5'OMe), 27.3 (C-4")

Compound **120,** A white solid, HREIMS $[M+1]^+$ m/z 271.0970, UV λ_{max} 234 nm, ^{1}H NMR (DMSO-d_6, 600 MHz) δ_H 9.26 (*s*, 4'-OH), 9.06 (*s*, 7-OH), 7.10 (*d*, *J* = 2.0 Hz, H-2'), 7.10 (*d*, *J* = 2.1 Hz, H-2'), 6.97 (*d*, *J* = 8.3 Hz, H-5), 6.72 (*d*, *J* = 3.2 Hz, H-6), 6.71 (*dd*, *J* = 3.9, 2.5 Hz, H-3'/5'), 6.35 (*d*, *J* = 1.0 Hz, H-3), 3.95 (*s*, H-4), 3.89 (*s*, 8-OMe). ^{13}C NMR (DMSO-d_6, 150 MHz) δ 157.1 (C-2), 155.9 (C-4'), 147.0 (C-8a), 145.9 (C-7), 132.2 (C-8), 129.6 (C-2', 6'), 127.6 (C-1'), 122.3 (C-4a), 114.1 (C-5), 113.0 (C-6), 102.9 (C-3), 60.1 (8-OMe), 33.1 (C-4).

Compound **121**, A white solid, HREIMS $[M+1]^+$ m/z 285.1127,^{1}H NMR (Chloroform-*d*, 500 MHz) δ_H 7.11 (*d*, *J* = 8.3 Hz, H-6), 6.87 (*d*, *J* = 8.0 Hz, H-5'), 6.75 (*dd*, *J* = 8.0, 2.0 Hz,H-6'), 6.72 (d, *J* = 2.0 Hz, H-2'), 6.52 (*dd*, *J* = 8.4, 2.6 Hz, H-7), 6.47 (*d*, *J* = 2.6 Hz, H-9), 6.40 (*dd*, *J* = 11.8, 2.0 Hz, H-5), 5.87 (*dd*, *J* = 11.8, 4.0 Hz, H-4), 4.29 (*ddd*, *J* = 11.7, 3.2, 1.0 Hz, 2^{α}), 4.15(*m*, 2^{β}), 3.90 (*dd*, *J* = 5.5, 3.2 Hz, H-3), 3.85 (*s*, 4'-OMe). ^{13}C NMR (Chloroform-*d*, 125 MHz) δ 160.5 (C-9a), 155.7 (C-8), 146.6 (C-4'), 144.8 (C-3'), 134.1(C-6), 133.1 (C-1'), 128.1 (C-5), 121.3 (C-6'), 114.5 (C-5'), 110.9 (C-2'), 110.1 (C-7), 107.0 (C-9), 75.3 (C-2), 56.1 (4'-OMe), 49.9 (C-3).

Compound **122**, A white crystal, EIMS $[M+1]^+$ m/z 216.04, UV λ_{max} 234 nm, ^{1}H NMR (Chloroform-*d*, 500 MHz) δ_H 8.16 (*d*, *J* = 9.8 Hz, H-4), 7.59 (*d*, *J* = 2.4 Hz, H-2'), 7.14 (*z*, H-8), 7.02 (m, H-3'), 6.28 (*d*, *J* = 9.7 Hz, H-3), 4.27 (*s*, 5-OMe). ^{13}C NMR (Chloroform-*d*, 126 MHz) δ_C 161.7 (C-2), 158.9 (C-7), 153.1 (C-8a), 150.0 (C-5) 145.2 (C-2'), 139.7 (C-4), 113.0 (C-3), 113.0 (C-6), 106.8 (C-4a), 105.4 (C-3'), 94.3 (C-8), 60.5 (C-5-OMe).

Compound **123**, A white crystal, EIMS $[M+1]^+$ m/z 216.04, UV λ_{max} 234 nm, ^{1}H NMR (Chloroform-*d*, 500 MHz) δ_H 7.80 (*d*, *J* = 9.6 Hz, H-4), 7.70 (*d*, *J* = 2.3 Hz, H-2'), 7.68 (*s*, H-5), 7.48 (*s*, H-8), 6.83 (*dd*, *J* = 2.3, 1.0 Hz, H-3'), 6.38 (*d*, *J* = 9.6 Hz, H-3). ^{13}C NMR (Chloroform-*d*, 125 MHz) δ_C 161.2 (C-2), 156.6 (C-7), 152.2 (C-8a), 147.1 (C-2'), 144.2 (C-4), 125.0 (C-6), 120.0 (C-5), 115.6 (C-4a), 106.5 (C-3'), 100.0 (C-8).

Compound **124**, A yellow oil, ^{1}H NMR (Chloroform-*d*, 500 MHz) δ_H 7.73 (*d*, *J* = 8.7 Hz, H-11), 6.60 (*dd*, *J* = 10.1, 0.7 Hz, H- 4'), 6.56 (*s*, H-1), 6.48 (*s*, H-4), 6.46 (*d*, *J* = 0.7 Hz, H-10), 5.56 (*d*, *J* = 10.1 Hz, H-3'), 4.63 (*dd*, *J* = 12.1, 2.5 Hz, H-6), 4.57 (*dd*, *J* = 2.5, 1.0 Hz, H-6a), 4.49 (*dd*, *J* = 12.2, 1.1 Hz, H-6), 4.40 (*s*, 12a-OH), 3.82 (*s*, 3-OMe), 3.73 (*s*, 2-OMe), 1.45 (*s*, 2'Me), 1.39 (*s*, 2'Me$_2$). ^{13}C NMR (Chloroform-*d*, 126 MHz) δ 191.5 (C-12), 160.9 (C-7a), 156.8 (C-9), 151.2 (C-3), 148.5 (C-4a), 144.1 (C-2), 129.0 (C-11), 128.7 (C-3'), 115.6 (C-4'), 112.0 (C-10), 111.2 (C-11a), 109.5 (C-1), 109.3 (C-8), 108.8 (C-1a), 101.2 (C-4), 78.2 (C-2'), 76.4 (C-6a), 67.6 (C-12a), 64.0 (C-6), 56.5 (3-OMe), 56.0 (2-OMe), 28.7 (2'Me2, 2'Me).

Compound **125**, A colorless solid, ^{1}H NMR (Chloroform-*d*, 500 MHz) δ_H 9.66 (*d*, *J* = 7.7 Hz, H-10), 7.40 (*d*, *J* = 15.9 Hz, H-7), 7.13 (*dd*, *J* = 8.2, 2.0 Hz, H-6), 7.07 (*d*, *J* = 1.9 Hz, H-2), 6.96 (*d*, *J* = 8.2 Hz, H-5), 6.60 (*dd*, *J* = 15.8, 7.7 Hz, H-8), 5.95 (*s*, 4OH), 3.95 (*s*, 3OMe), 2.17 (*d*, *J* = 0.9 Hz). ^{13}C NMR (Chloroform-*d*, 126 MHz) δ 193.8 (C-9), 153.2 (C-7), 149.1 (C-3), 147.1 (C-4), 126.8 (C-1), 126.6 (C-8), 124.2 (C-6), 115.1 (C-5), 109.6 (C-2), 56.2 (3OMe, C-14)

Compound 128 A white amorphous solid; UV λ_{max}: 260, 320 nm. ^{1}H NMR (800 MHz, CD_2Cl_2): δ_H 4.98 (*d*, *J*=11.9 Hz , H-2), 4.52 (*d*, *J*= 11.9 Hz, H-3), 7.40(*m*, H-2'/6'), 6.84(*m*, H-3'/5'), 5.53 (*d*, *J*=10.0Hz, H-3"), 6.64 (*d*, *J*=10.0 Hz , H-4"), 1.45(*s*, H-2"-(Me)$_2$), 3.19 (*m*, H-1'"), 5.12 (*m*, H-2'"), 1.64*****(*s*, H-4'"), 1.60*****(*s*, H-5'"), 11.37 (*s*, 5-OH); ^{13}C NMR (125 MHz, CD_2Cl_2): δ_C 83.0(C-2), 72.6(C-3), 196.2(C-4), 100.4(C-4a), 159.5(C-5), 109.4(C-6), 160.9(C-7), 103.3(C-8), 156.4(C-8a), 128.8(C-1'), 129.1(C-2'/6'), 115.6(C-3'/5'), 156.4(C-4'), 126.5(C-3"), 115.5(C-4"), 78.6(C-2"), 28.5 (C-2"-(Me)$_2$), 21.4(C-1'"), 122.2(C-2'"), 131.5(C-3'"), 26.0*****(C-4'"), 17.9*****(C-5'"). EIMS, *m*/*z* (rel. int.): 420 (63, [M]$^+$, 4.5 (100, [M-Me]$^+$, 377 (12), 365 (6). HRMS found 423.1807 for [M+1]$^+$ $C_{25}H_{27}O_6$ calculated for 423.1808.

Compound 129, A yellow solid, HREIMS [M+1]$^+$ m/z 420.1560, UV λ_{max} 266 nm, 366 nm, ^{1}H NMR (DMSO-d_6, 500 MHz) δ_H 8.04 (*d*, *J* = 8.9, H-2'/6'), 6.94 (*d*, *J* = 8.9, H-3'/5'), 6.62 (*d*, *J* = 10.0 Hz, H-4"), 5.80 (*d*, *J* = 10.0 Hz, H-3"), 5.15 (*t*, *J* = 7.1, H-2'"), 3.43 (*d*, *J* = 6.9, 1.2 H-1'"), 1.76***** (*s*, H-4'"), 1.63***** (*s*, H-5'"), 1.42 (s, H-2"-(Me)$_2$), 9.51 (s, 3-OH), 12.82 (s, 5-OH), 10.15 (s, 4'-OH). ^{13}C NMR (DMSO-d_6, 126 MHz) δc 176.3 (C-4), 159.3 (C-4'), 155.6 (C-7), 152.6 (C-5),

132.7 (C-8a), 147.1 (C-2), 135.8 (C-3), 131.2 (C-3'''), 129.4 (C-2'/6'), 128.7 (C-3''), 121.8 (C-1'), 115.5 (C-3'/5'), 114.9 (C-4''), 106.7 (C-8), 103.7 (C-6), 103.9 (C-4a) 77.7 (C-2''), 27.7 (C-2''-$(Me)_2$), 25.5***** (C-4'''), 21.1 (C-1'''), 17.8***** (C-5''').

Compound 130 A yellow solid; ^{1}H NMR (800 MHz, CD_2Cl_2): δ_H 5.34 (*dd*, *J* = 12.9, 3.0, H-2), 3.04 (*dd*, *J* = 17.0, 12.9, H-3), 2.80 (*dd*, *J* = 17.0, 3.1, H-3), 7.32 (*m*, H-2'/6'), 6.88 (*m*, H-3'/5'), 5.50 (*d*, *J* = 10.0, H-3''), 6.63 (*d*, *J* =10.1 , H-4''), 1.44 (*d*, H-2''-$(Me)_2$), 3.20 (*m*, H-1'''), 5.14 (*tt*, *J* = 7.6, 7.6, 1.6, H-2'''), 1.65***** (*s*, H-4'''/5'''), 5.21 (*d*, *J* = 1.8, 4'-OH), 12.24 (s, 5-OH); ^{13}C NMR (200 MHz, CD_2Cl_2): δ_C 78.7 (C-2), 43.4 (C-3), 196.7 (C-4), 102.8 (C-4a), 159.5 (C-5), 108.8 (C-6), 160.1 (C-7), 103.0 (C-8), 156.7 (C-8a), 131.2 (C-1'), 127.9 (C-2'/6'), 115.7 (C-3'/5'), 156.0 (C-4'), 78.3 (C-2''), 126.1 (C-3''), 115.4 (C-4''), 28.5 (C-2''-$(Me)_2$), 21.6 (C-1'''), 122.6 (C-2'''), 131.3 (C-3'''), 26.0***** (4'''), 18.0***** (5''').

Compound 64 A yellow paste; ^{1}H NMR (800 MHz, CD_2Cl_2): δ_H 5.08 (*d*, *J* = 11.9, H-2), 4.51 (*d*, *J* = 11.9, H-3), 7.46 (*t*, *J* = 7.4, H-2'/6'), 7.57 (*d*, *J* = 7.5, H-3'/5'), 7.42 (*t*, *J* =7.4, 4'), 5.54 (*d*, *J* = 10.0, H-3''), 6.65 (*d*, *J* =10.0 , H-4''), 1.47 (*s*, H-2''-$(Me)_2$), 3.20 (*qd*, *J* = 14.0, 7.3, H-1'''), 5.14 (*m*, H-2'''), 1.66***** (*s*, H-5'''), 1.62***** (*s*, H-4'''), 11.41 (*s*, 5-OH); ^{13}C NMR (125 MHz, CD_2Cl_2): δ_C 83.1 (C-2), 72.6 (C-3), 196.2 (C-4), 136.7 (C-4a), 159.3 (C-5), 109.4 (C-6), 160.7 (C-7), 103.3 (C-8), 156.1 (C-8a), 136.7 (C-1'), 128.7 (C-2'/6'), 127.5 (C-3'/5'), 129.2 (C-4'), 78.6 (C-2''), 126.4 (C-3''), 115. 5 (C-4''), 28.5 (C-2''-$(Me)_2$), 21.4 (C-1'''), 122.3 (C-2'''), 131.5 (C-3'''), 25.9***** (4'''), 17.9***** (5''').

Compound 131, A yellow amorphous solid; ^{1}H NMR (800 MHz, CD_2Cl_2): δ_H 7.52 (*m*, H-3'/5'), 8.21 (*m*, H-2'/6'), 7.47 (*m*, H-4'), 5.65 (*d*, *J* = 10.0, H-3''), 6.75 (*d*, *J* =9.9 , H-4''), 1.48 (*s*, H-2''-$(Me)_2$), 3.53 (*d*, *J*= 7.1, H-1'''), 5.23 (*tt*, *J* = 7.3, 1.4, H-2'''), 1.69***** (*d*, *J* =1.6, H-4'''), 1.84***** (*d*, *J* = 1.6, H-5'''), 6.69 (*s*, 3-OH), 11.87 (*s*, 5-OH); ^{13}C NMR (200 MHz, CD_2Cl_2): δ_C 145.0 (C-2), 136.5 (C-3), 175.9 (C-4), 103.8 (C-4a), 153.2 (C-5), 107.9 (C-6), 153.2 (C-7), 105.1 (C-8), 157.4 (C-8a), 131.3 (C-1'), 128.8 (C-3'/5'), 127.7 (C-2'/6'), 130.2 (C-4'), 78.1 (C-2''), 128.4 (C-3''), 115.8 (C-4''), 28.5 (C-2''-$(Me)_2$), 21.7 (C-1'''), 122.3 (C-2'''), 132.0 (C-3'''), 25.9***** (4'''), 18.2***** (5''').

Compound 70 A colourless solid; ^{1}H NMR (500 MHz, CD_2Cl_2): δ_H 7.91 (*s*, H-2), 7.87 (*s*, H-5), 6.79 (*d*, *J* = 0.7, H-8), 7.12 (*d*, *J* = 8.4 , H-2'), 6.63 (*dd*, *J* = 8.4, 0.8 Hz, H-3'), 5.64 (*d*, *J* = 9.0, H-

3''), 6.60 (*d*, *J* =8.4 , H-4''), 1.46 (*s*, H-2''-$(Me)_2$), 5.74 (*d*, *J* = 9.9, H-3'''), 6.45 (*d*, *J* = 10.0, H-4'''), 1.5 (*s*, H-2-Me_2), 3.59 (*s*, 6'-OMe); ^{13}C NMR (125 MHz, CD_2Cl_2): δ_C 153.9 (C-2), 121.7 (C-3), 176.1 (C-4), 118.7 (C-4a), 123.7 (C-5), 119.6 (C-6), 158.1 (C-7), 104.1 (C-8), 157.7 (C-8a), 117.2 (C-1'), 131.8 (C-2'), 112.5 (C-3'), 154.5 (C-4'), 115.0 (C-5'), 154.3 (C-6'), 76.1 (C-2''), 130.4 (C-3''), 117.3 (C-4''), 28.6 (C-2''-$(Me)_2$), 78.0 (C-2'''), 131.8 (C-3'''), 121.5 (4'''), 28.0 (C-2'''-$(Me)_2$), 62.0 (6'-OMe).

Compound 63 A white solids; ^{1}H NMR (500 MHz, CD_2Cl_2): δ_H 6.75 (*d*, *J* = 1.0, H-1), 6.44 (*s*, H-4), 4.17 (*dt*, *J* = 12.2, 1.0, H-6), 4.60 (*dd*, *J* = 12.1, 3.1, H-6), 4.94 (*dq*, *J* = 3.1, 1.5, H-6a), 6.49 (*d*, *J*= 8.6, H-10), 7.82 (*d*, *J* = 8.6, H-11), 3.84 (*m*, H-12a), 5.23 (*dd*, *J* = 9.7, 8.2, H-2'), 3.31 (*dd*, *J* = 15.8, 9.8, H-3'), 2.94 (*dd*, *J* = 15.8, 8.1, H-3'), 1.75 (t, *J* = 1.2, 4'-Me).5.06 (*dt*, *J* = 1.7, 1.0, H-5'), 3.79 (*s*, 2-OMe), 3.75 (*s*, 3- OMe); ^{13}C NMR (125 MHz, CD_2Cl_2): δ_C 110.3 (C-1), 143.9 (C-2), 149.5 (C-3), 100.9 (C-4), 147.4 (C-4a), 66.4 (C-6), 72.3 (C-6a), 158.1 (C-7a), 113.1 (C-8), 167.5 (C-9), 105.0 (C-10), 130.1 (C-11), 113.4 (C-11a), 189.2 (C-12), 44.7 (C-12a), 104.9 (C-12b), 88.0 (C-2'), 31.3 (C-3'), 56.4 (3-OMe), 55.9 (2-OMe), 17.2 (4-'Me).

Compound 132 A yellow oil; ^{1}H NMR (500 MHz, CD_2Cl_2): δ_H 7.41 (*s*, H-1), 6.45 (*s*, H-4), 4.22 (*ddd*, *J* = 10.9, 5.1, 0.8, H-6), 3.59 (*m*, H-6), 3.50 (*m*, H-6a), 6.97 (*d*, *J* = 8.0, H-7), 6.38 (*d*, *J* = 8.0, H-8), 5.46 (*m*, H-11a), 3.40 (*m*, H-1'), 5.30 (*m*, H-2'), 1.75 (*t*, *J* = 1.4 Hz, H-4'), 1.82 (*d*, *J* = 1.3, H-5'), 1.48 (*s*, H-3''), 6.21 (*dd*, *J*=17.7, 10.5, 4'') , 5.36 (*m*, H-5''), 6.00 (s, 3-OH), 5.42 (*s*, 9-OH); ^{13}C NMR (125 MHz, CD_2Cl_2): δ_C 129.0 (C-1), 112.2 (C-11b), 126.7 (C-2), 156.3 (C-3), 105.7 (C-4), 155.6 (C-4a), 66.6 (C-6), 40.1 (C-6a), 118.9 (C-6b), 122.5 (C-7), 108.3 (C-8), 156.0 (C-9), 110.4 (C-10), 158.5 (C-10a), 78.6 (C-11a), 23.4, (C-1'), 121.6 (C-2'), 135.3 (C-3'), 18.0 (C-4'), 26.0 (C-5'), 40.2 (C-1''), 27.2 (C-2''), 27.2 (C-3''), 148.0 (C-4''), 113.9 (C-5'').

Compound 133, A white amorphous solid,^{1}H NMR (Methylene Chloride-d_2, 500 MHz) δ_H 7.28 (*s*, H-1), 6.87 (*s*, H-10), 6.46 (*s*, H-4), 6.37 (*s*, H-8), 5.77 (*s*, 7-OH), 5.49 (*d*, J = 7.1 Hz, H-11a), 5.22 (*s*, H-2'), 5.17 – 5.05 (*m*, H-5'), 4.93 (*t*, J = 1.7 Hz, H-6), 4.26 (*dd*, J = 10.9, 4.8 Hz, H-6), 3.56 (*ddd*, J = 10.8, 7.1, 4.9 Hz, H-6a), 3.36 (ddd, J = 15.4, 9.5, 1.2 Hz, H-3'), 3.02 (*ddd*, J = 15.3, 7.7, 1.3 Hz, H-3'), 1.79 (t, J = 1.2 Hz, 4'-Me). ^{13}C NMR (Methylene Chloride-d2, 126 MHz) δ 160.6 (C-3), 154.0 (C-4a), 146.5 (C-7), 144.2 (C-4'), 126.9 (C-1), 120.8 (C-2), 119.7 (C-1a), 111.5

(C- 6b), 102.9 (C-4), 97.4 (C-8, C-10), 86.6 (C-2'), 78.6 (C-11a), 68.3 (C-6), 40.3 (C-6a), 33.9 (C-3'), 16.9 (C-4'Me).

Compound 85, A yellow oil, HREIMS $[M+1]^+$ *m/z* 369.1702, UV λ_{max} 210, 254, 310 nm, ^{1}H NMR (Chloroform-*d*, 500 MHz) δ_H 7.43 – 7.38 (*m*, H-3, 4, 5), 7.38 – 7.30 (*m*, H-2, 6), 6.46 (*d*, *J* = 9.9 Hz, H-4), 6.19 (*s*, H-5'), 5.54 (*dd*, *J* = 10.0, 2.2 Hz, H-3"), 5.30 – 5.24 (*dd*, J = 9.5, 2,8, β), 3.76 (*d*, *J* = 2.0 Hz, 6'-OMe), 3.75 (*s*, 2'-OMe), 3.25 (*dd*, *J* = 17.4, 2.8 Hz, α'), 3.15 (*dd*, 17.3,9.5,α"), 1.43 (*s*, 2"Me_2, 2"Me). ^{13}C NMR (Chloroform-*d*, 126 MHz) δ 204.4 (C-7), 157.9 (C-2'), 156.6 (C-6'), 154.6 (C-4'), 143.2 (C-1), 128.5 (C-2, 6), 128.2 (C-4), 127.2 (C-3"), 126.0 (C-3, 5), 116.4 (C-4"), 108.3 (C-3'), 96.3 (C-5'), 70.6 (C-β), 63.9 (2'-OMe), 56.0 (6'-OMe), 53.7 (C-α), 28.1 (2"Me_2, 2"Me).

Compound 87 , A white solid, Uv λ_{max} 280 nm, ^{1}H NMR (Methanol-d_4, 500 MHz) δ_H 8.00 (*s*, H-2), 6.89 (*s*, H-6'), 6.70 (d, *J* = 10.0 Hz, H-4"), 6.61 (*s*, H-8), 6.38 (*d*, *J* = 0.7 Hz, H-3'), 5.73 (*d*, *J* = 10.1 Hz, H-3"), 3.83 (*s*, 5'OMe), 3.73 (*s*, 2'OMe), 1.47 (*s*, 2"Me_2). ^{13}C NMR (Methanol-d_4, 126 MHz) δ_C 182.5 (C-4), 160.9 (C-7), 157.6 (C-8a), 153.9 (C-5), 149.3 (2'), 142.8 (5'), 129.7 (3"), 122.3 (C-3), 117.1 (C-6'), 116.1(C-4"), 111.0 (C-1), 106.5 (C-4a), 101.7 (C-3'), 95.9 (C-8), 79.2 (C-2"), 57.4 (2'OMe), 56.7 (5'OMe), 28.5 (2 2"Me_2).

Compound 124, A yellow oil, ^{1}H NMR (Chloroform-*d*, 500 MHz) δ_H 7.73 (*d*, *J* = 8.7 Hz, H-11), 6.60 (*dd*, *J* = 10.1, 0.7 Hz, H- 4'), 6.56 (*s*, H-1), 6.48 (*s*, H-4), 6.46 (*d*, *J* = 0.7 Hz, H-10), 5.56 (*d*, *J* = 10.1 Hz, H-3'), 4.63 (*dd*, *J* = 12.1, 2.5 Hz, H-6), 4.57 (*dd*, *J* = 2.5, 1.0 Hz, H-6a), 4.49 (*dd*, *J* = 12.2, 1.1 Hz, H-6), 4.40 (*s*, 12a-OH), 3.82 (*s*, 3-OMe), 3.73 (*s*, 2-OMe), 1.45 (*s*, 2'Me), 1.39 (*s*, 2'Me_2). ^{13}C NMR (Chloroform-*d*, 126 MHz) δ 191.5 (C-12), 160.9 (C-7a), 156.8 (C-9), 151.2 (C-3), 148.5 (C-4a), 144.1 (C-2), 129.0 (C-11), 128.7 (C-3'), 115.6 (C-4'), 112.0 (C-10), 111.2 (C-11a), 109.5 (C-1), 109.3 (C-8), 108.8 (C-1a), 101.2 (C-4), 78.2 (C-2'), 76.4 (C-6a), 67.6 (C-12a), 64.0 (C-6), 56.5 (3-OMe), 56.0 (2-OMe), 28.7 (2'Me2, 2'Me).

Appendix 1A: ^{1}H NMR (600 MHz, DMSO, 25°C) spectrum of usambarin A (110).

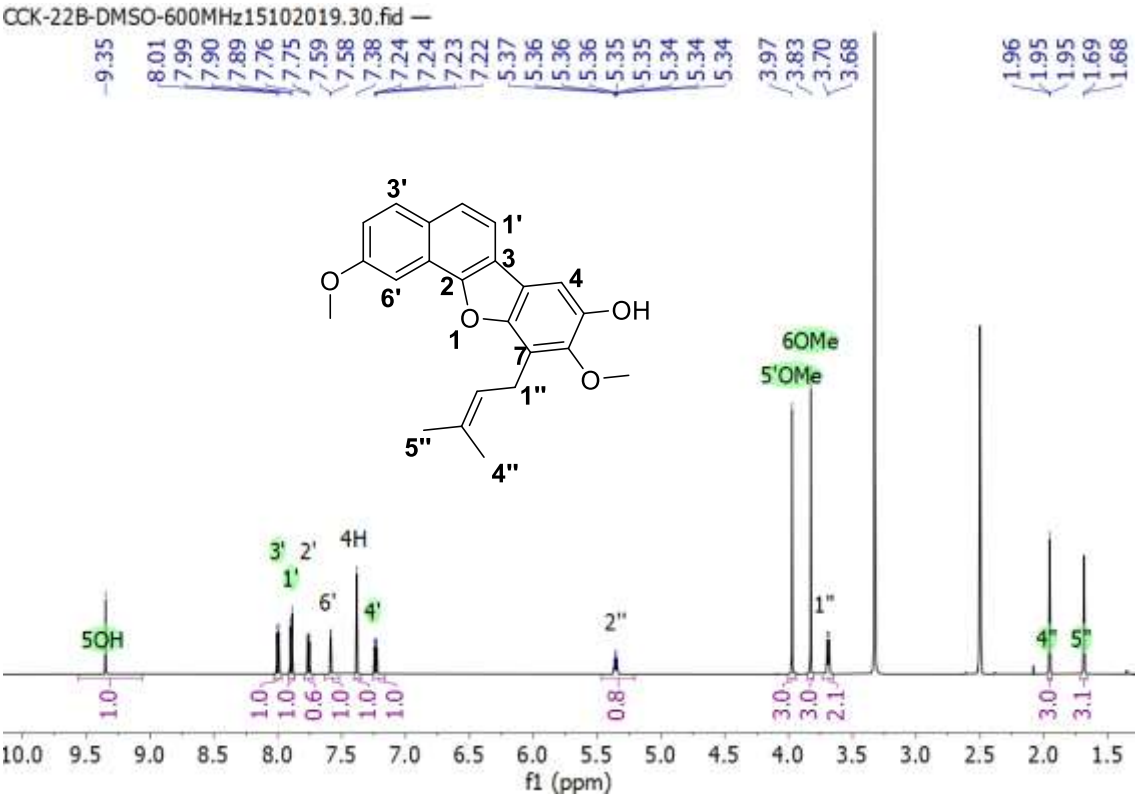

Appendix 1B:. ^{13}C NMR (150 MHz, DMSO, 25°C) spectrum of usambarin A (**110**).

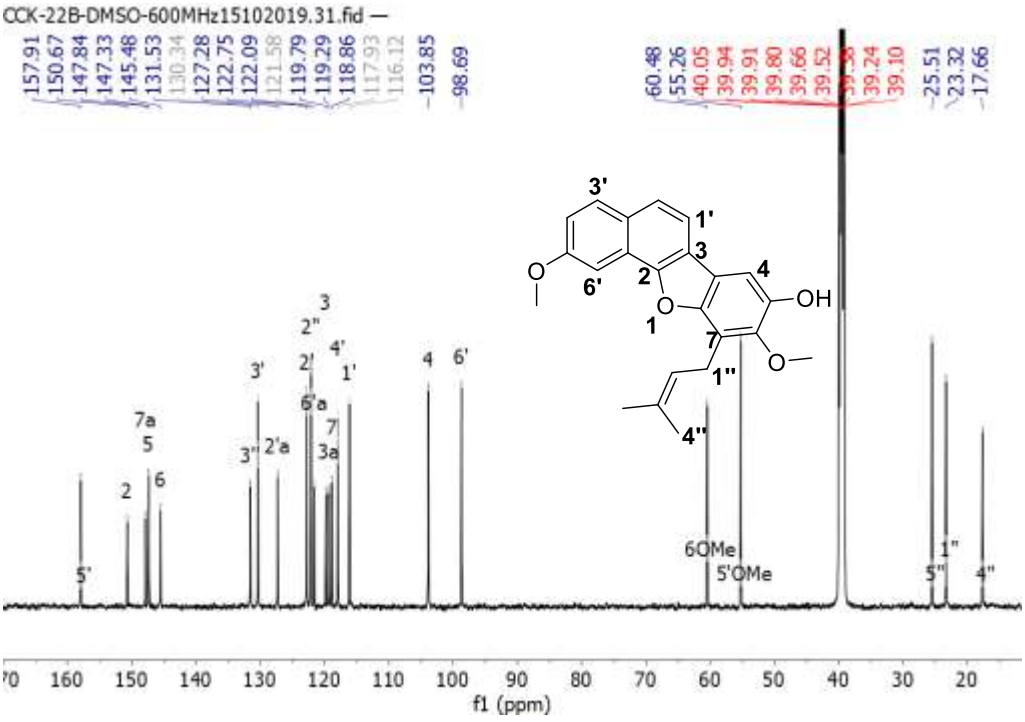

Appendix 1C: COSY (600 MHz, DMSO, 25°C) spectrum of usambarin A (**110**).

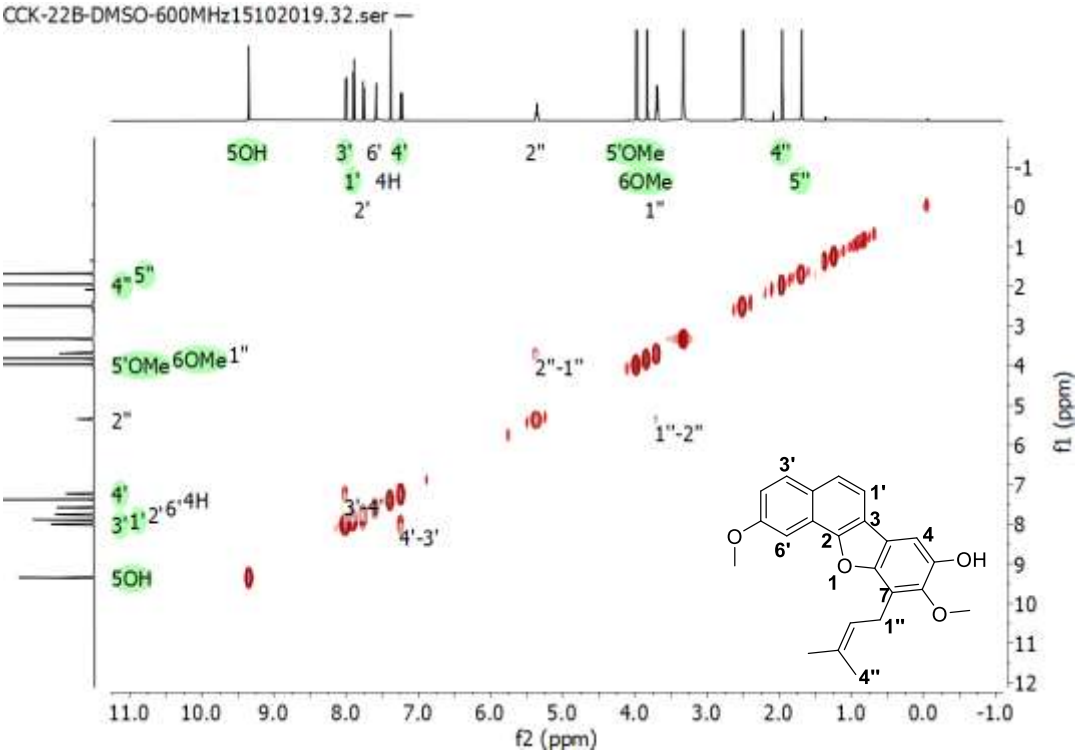

Appendix 1D: HSQC (600 MHz, DMSO, 25°C) spectrum of usambarin A (**110**).

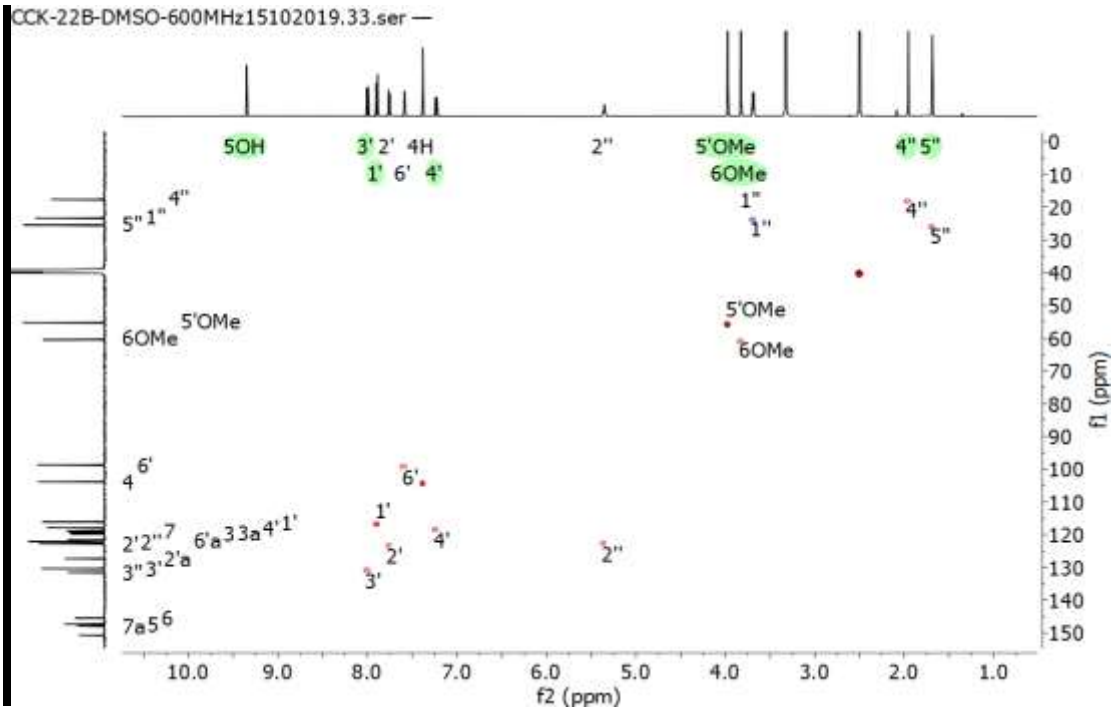

Appendix 1E: HMBC (600 MHz, DMSO, 25°C) spectrum of usambarin A (**110**).

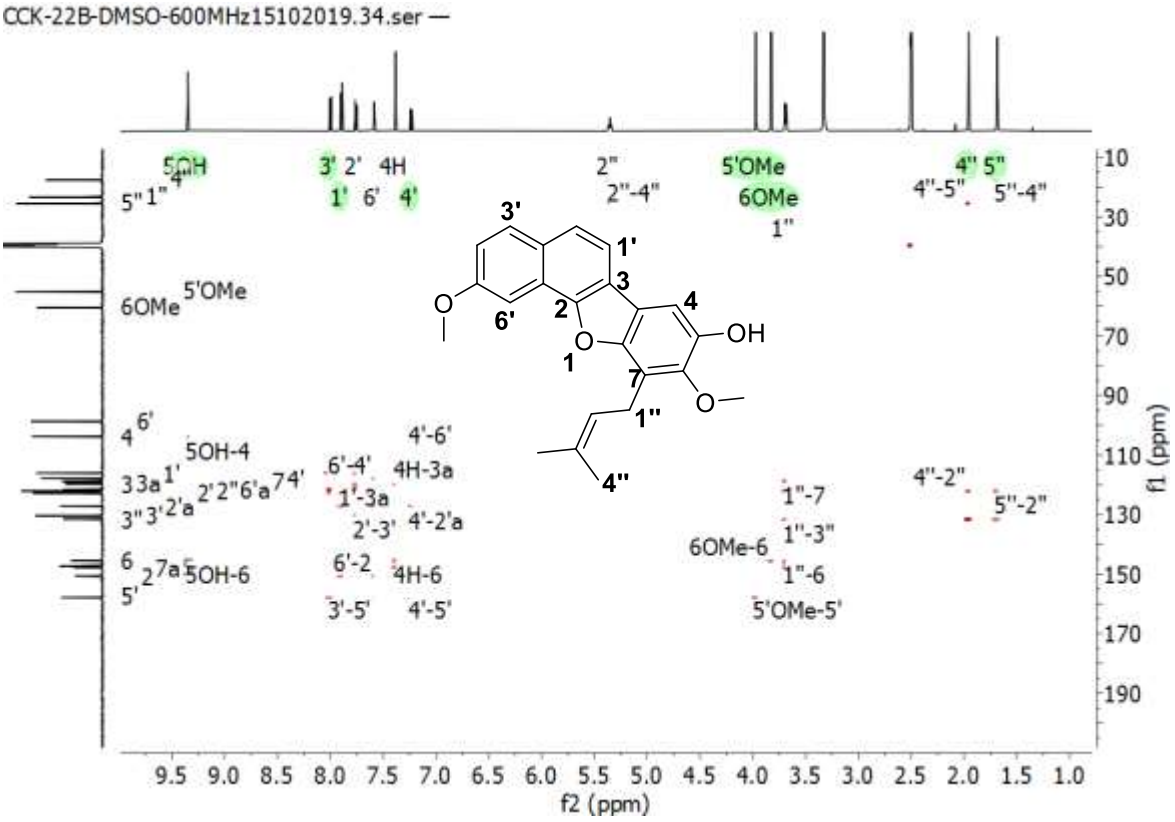

Appendix 1F:. NOESY (600 MHz, DMSO, 25°C) spectrum of usambarin A (**110**).

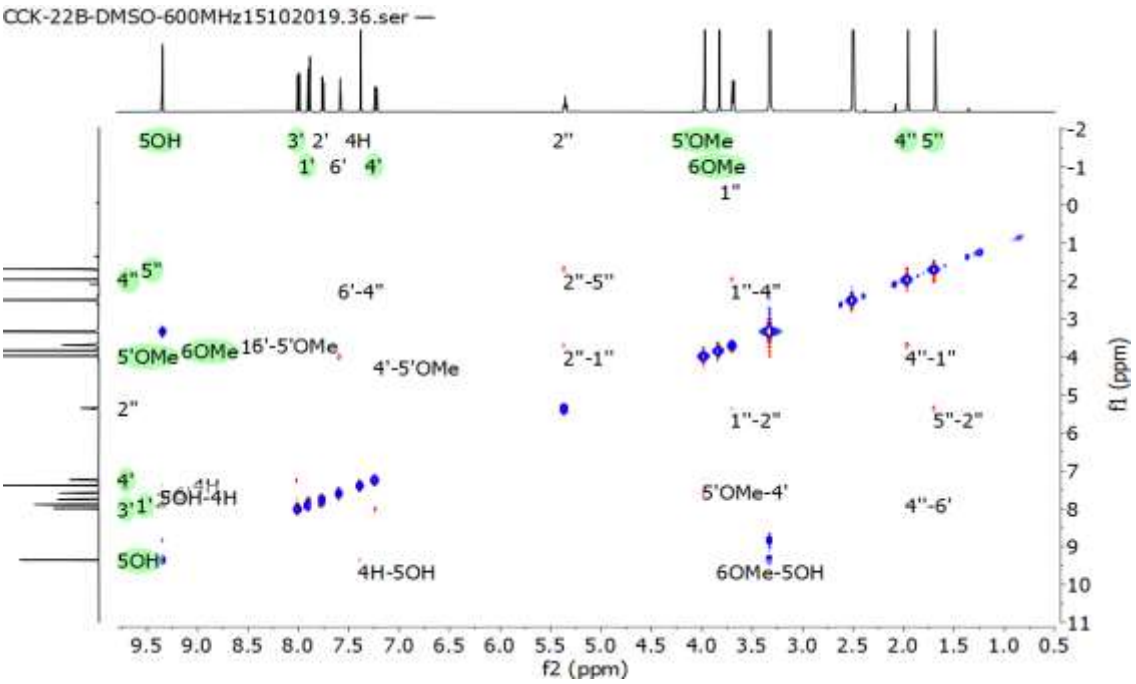

Appendix 1G:.TOCSY (600 MHz, DMSO, 25°C) spectrum of usambarin A (**110**).

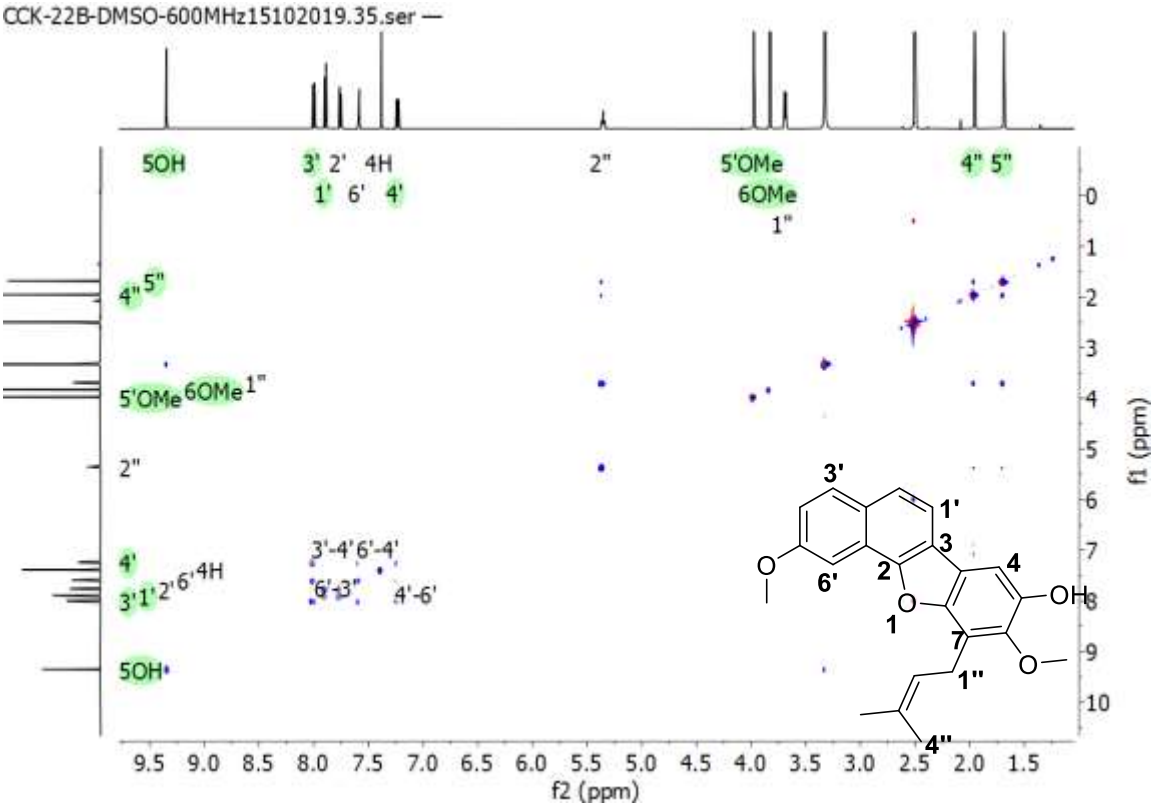

Appendix 1H: HRMS spectrum of usambarin A (**110**).

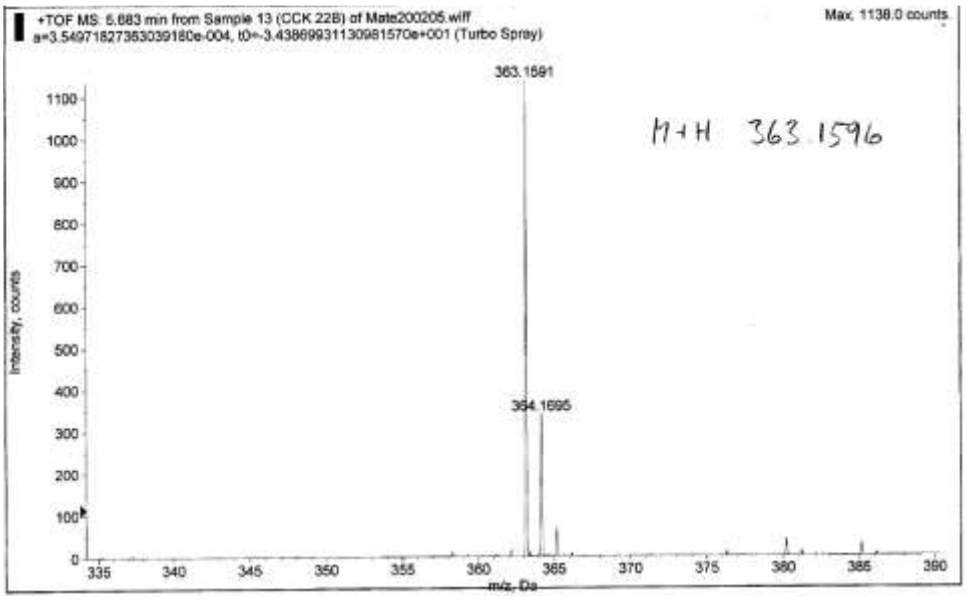

Appendix 1J:. UV spectrum of usambarin A (**110**).

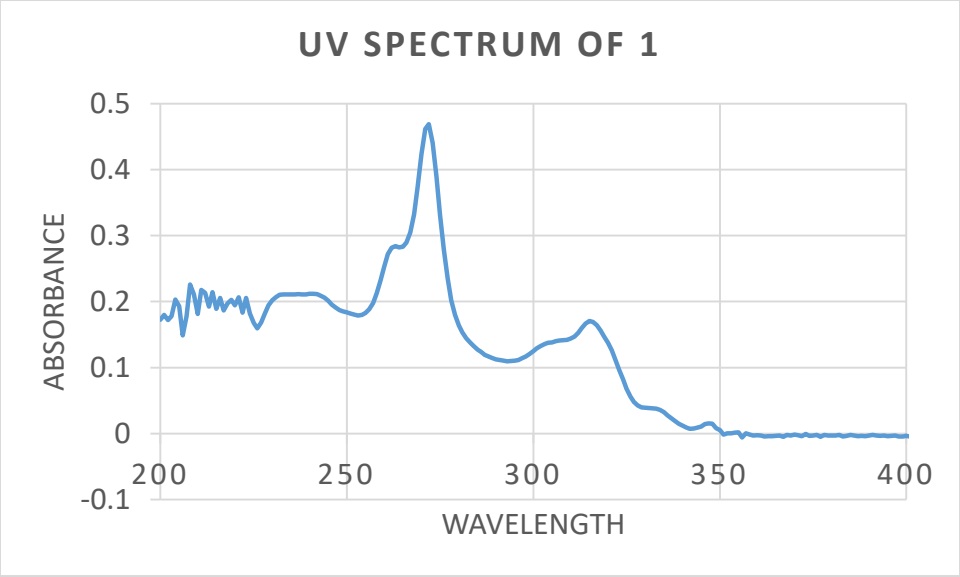

Appendix 1K:. X-ray structure of usambarin A (**110**).

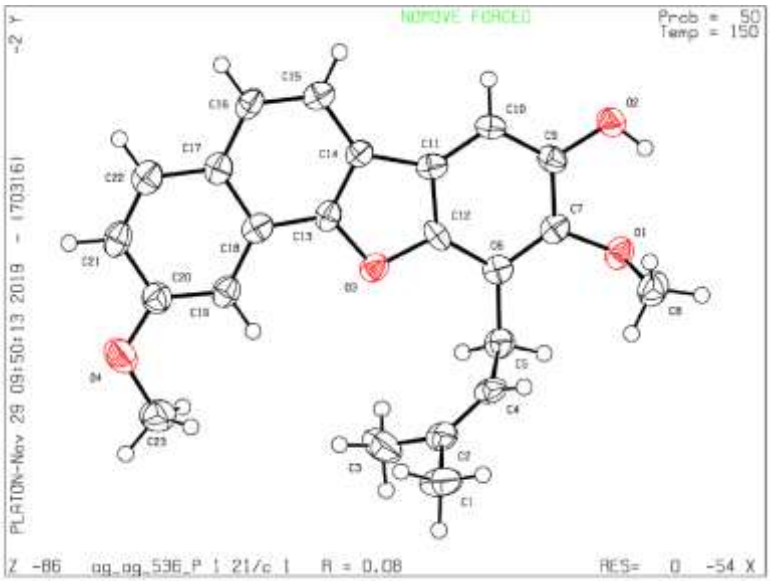

Appendix 2A: ^{1}H NMR (500 MHz, CD_3OD, 25°C) spectrum of usambarin B (111).

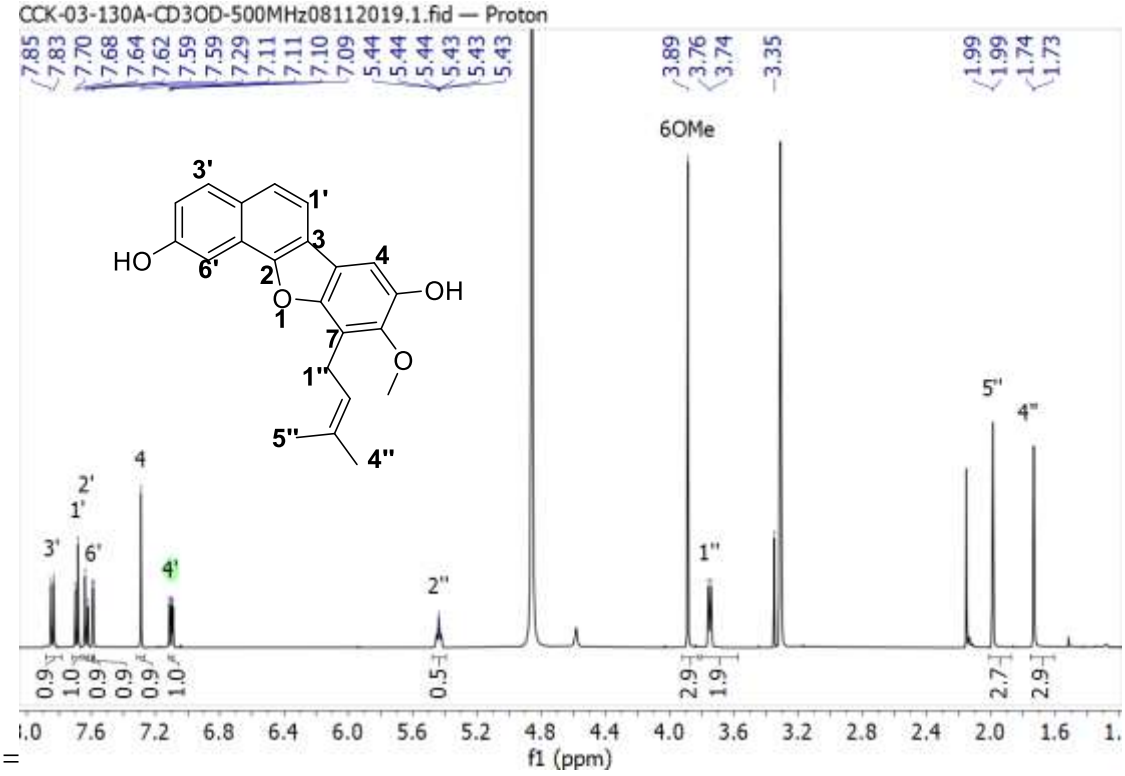

Appendix 2B:. ^{13}C NMR (125 MHz, CD_3OD, 25°C) spectrum of usambarin B (**111**).

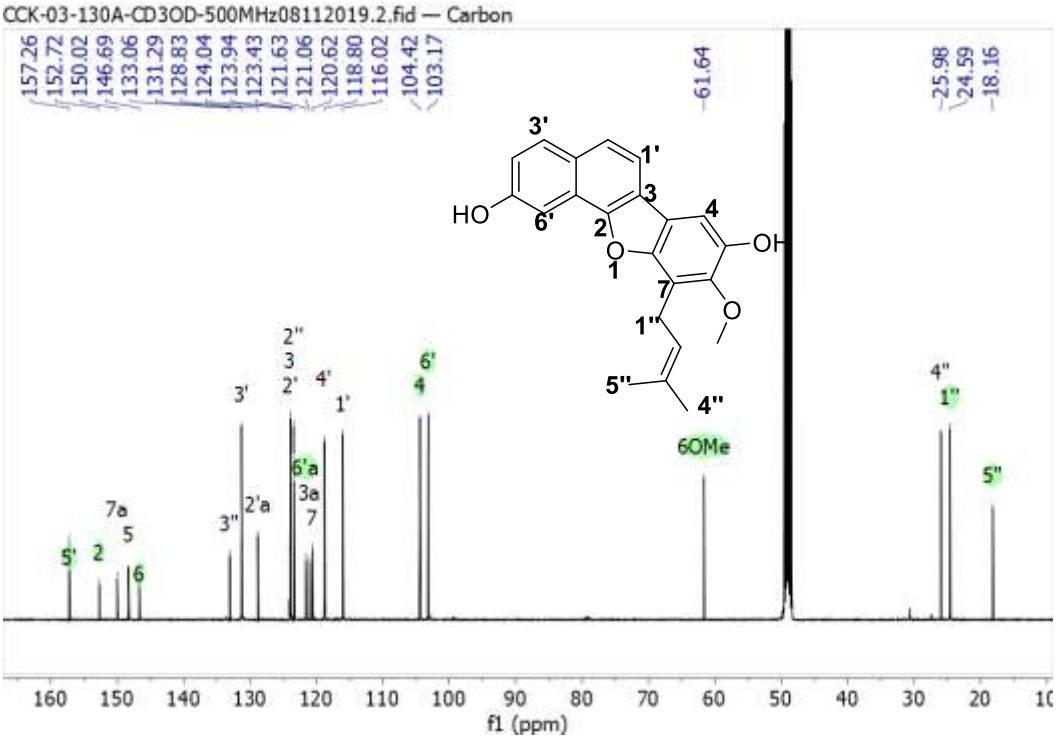

Appendix 2C: COSY (500 MHz, CD_3OD, 25°C) spectrum of usambarin B (**111**).

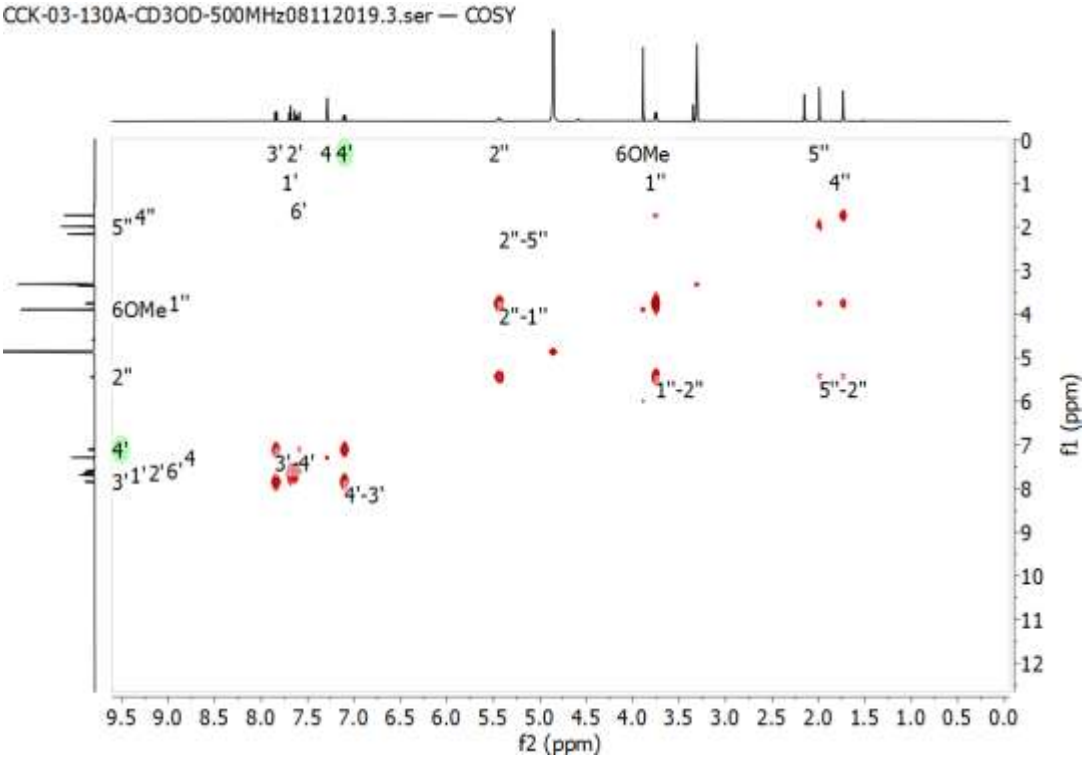

Appendix 2D:. HSQC (500 MHz, CD_3OD, 25°C) spectrum of usambarin B (**111**).

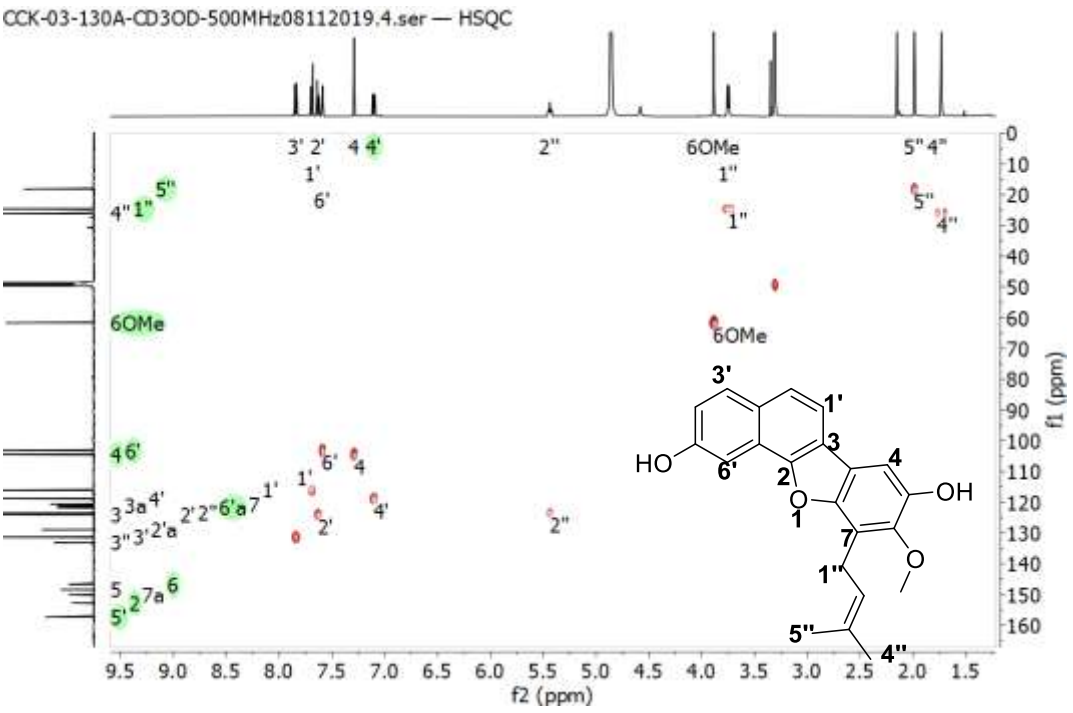

Appendix 2F:. HMBC (500 MHz, CD_3OD, 25°C) spectrum of usambarin B (**111**).

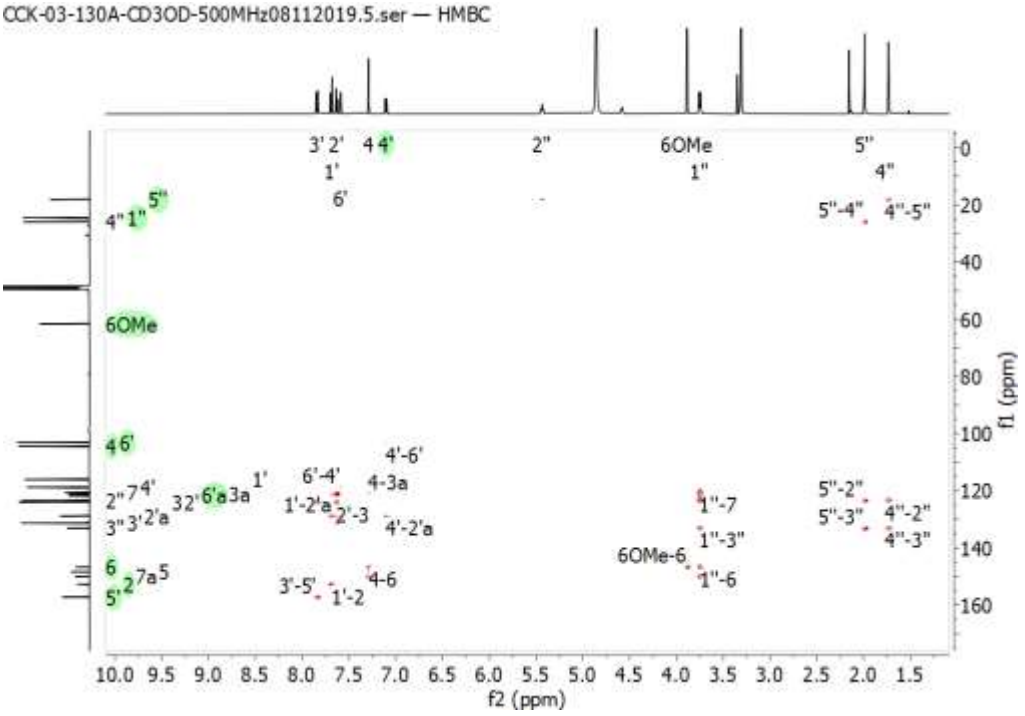

Appendix 2G:. NOESY (500 MHz, CD_3OD, 25°C) spectrum of usambarin B (**111**).

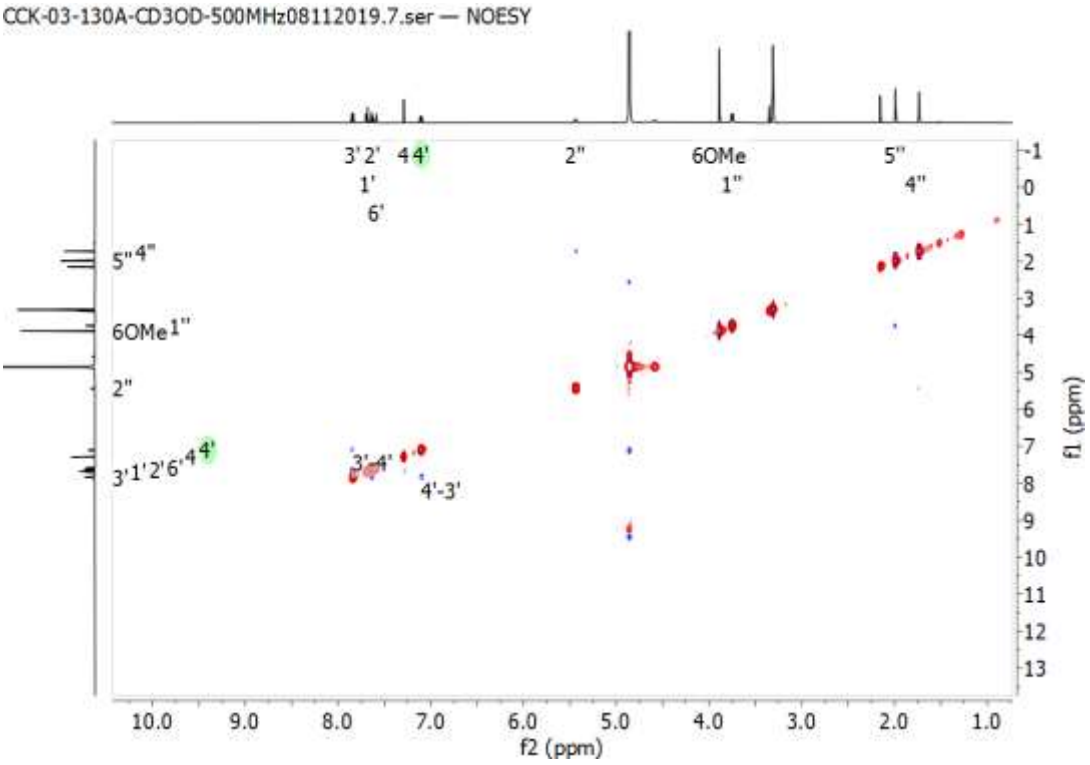

Appendix 2H:.TOCSY (500 MHz, CD_3OD, 25°C) spectrum of usambarin B (**111**).

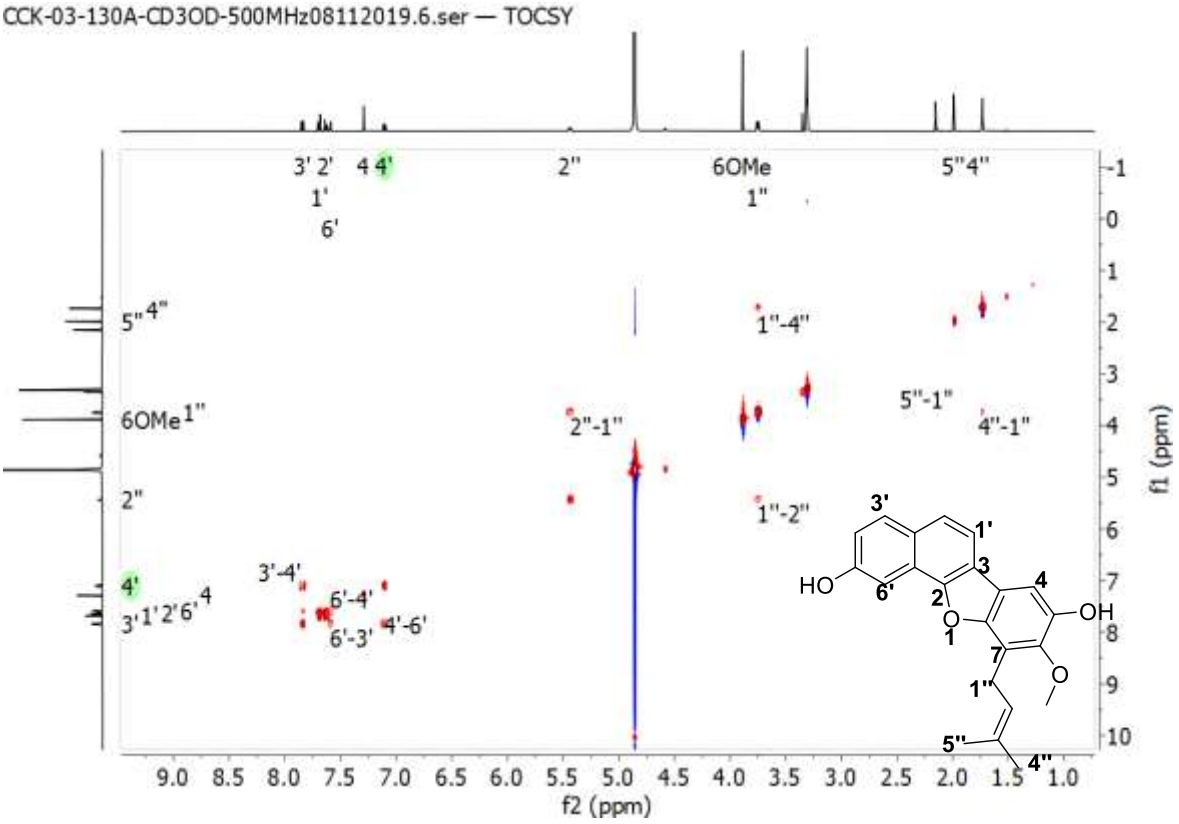

Appendix 2I:.HRMS spectrum of usambarin B (**111**).

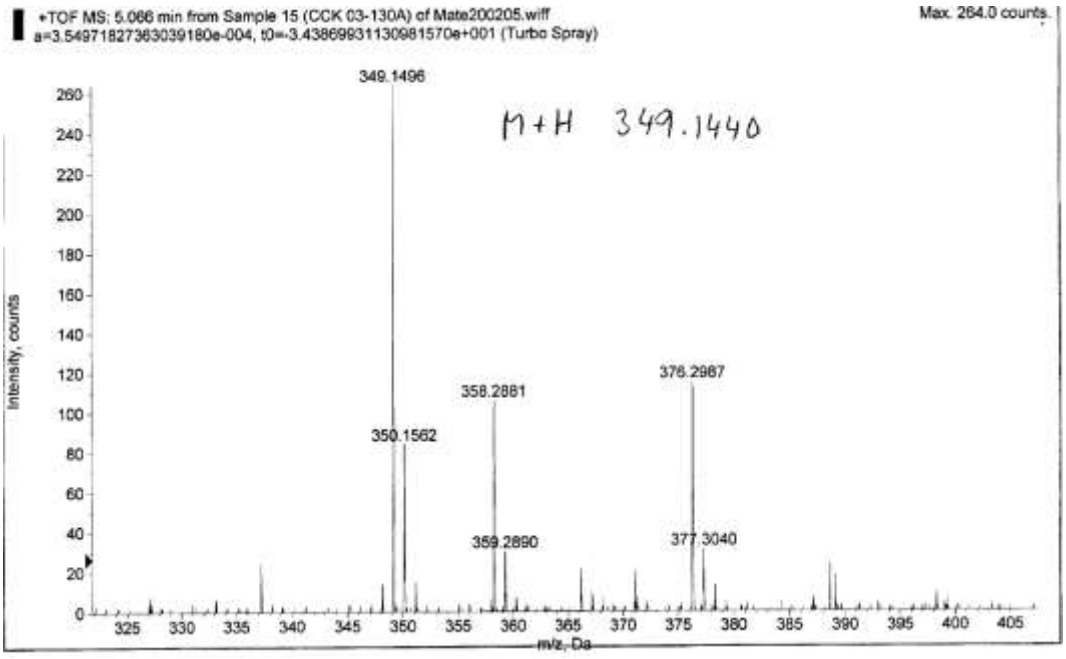

Appendix 3A: 1H NMR (500 MHz, $CDCl_3$, 25°C) spectrum of usambarin C (112)

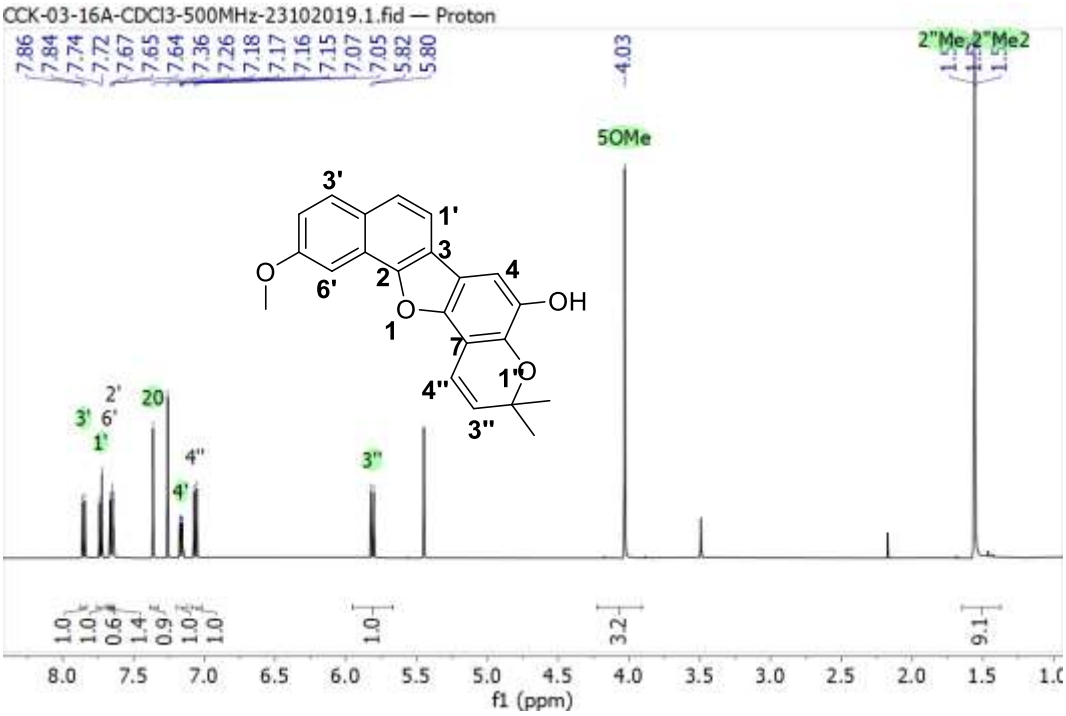

Appendix 3B: ^{13}C NMR (125 MHz, $CDCl_3$, 25°C) spectrum of usambarin C (**112)**

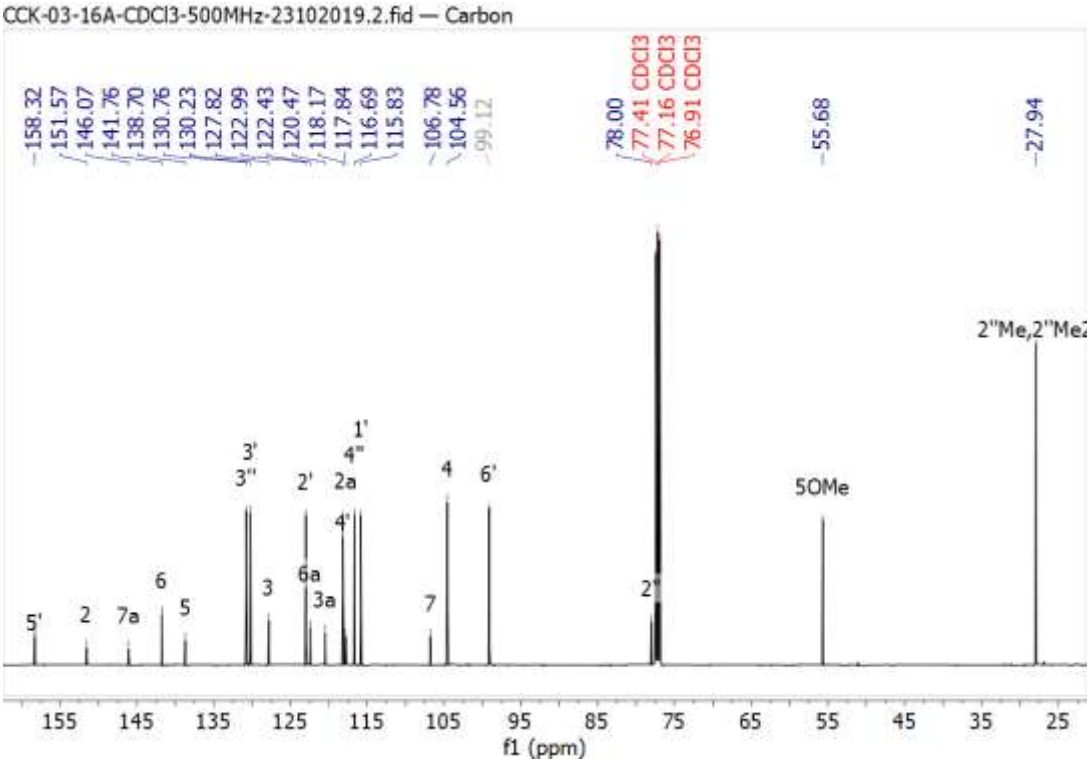

Appendix 3C:.COSY (500 MHz, $CDCl_3$, 25°C) spectrum of usambarin C (**112)**

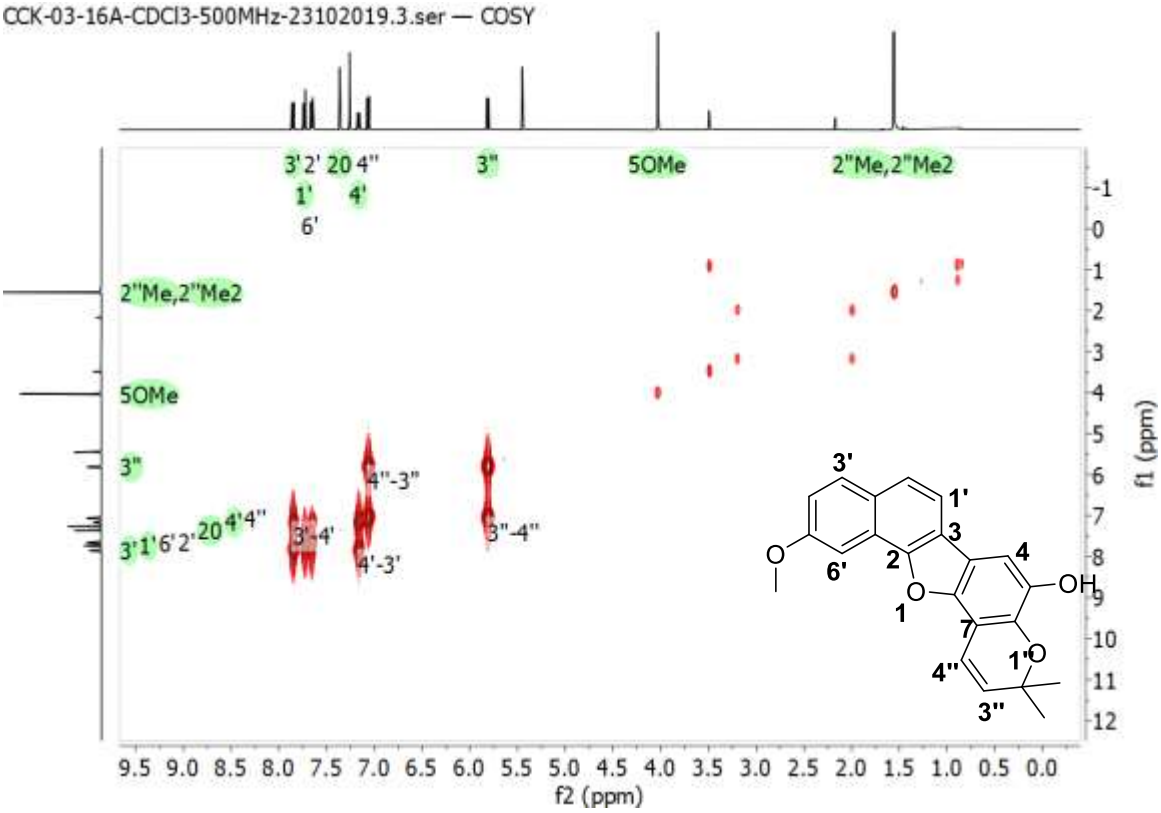

Appendix 3D:.HSQC (500 MHz, $CDCl_3$, 25°C) spectrum of usambarin C (**112)**

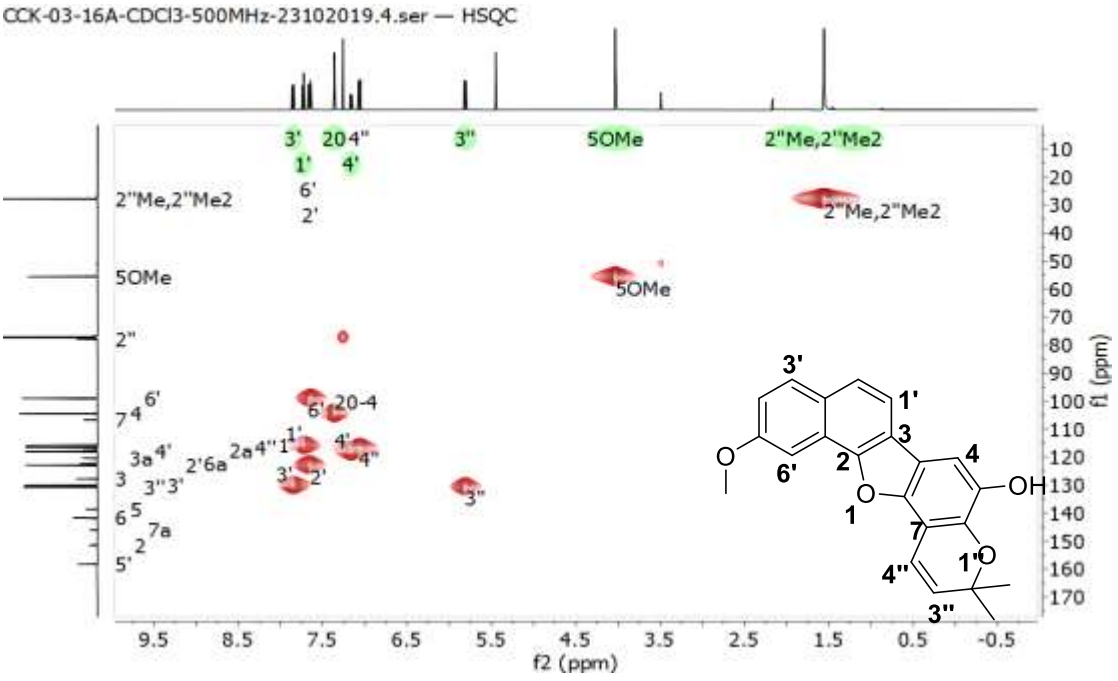

Appendix 3E:. HMBC (500 MHz, $CDCl_3$, 25°C) spectrum of usambarin C (**112)**

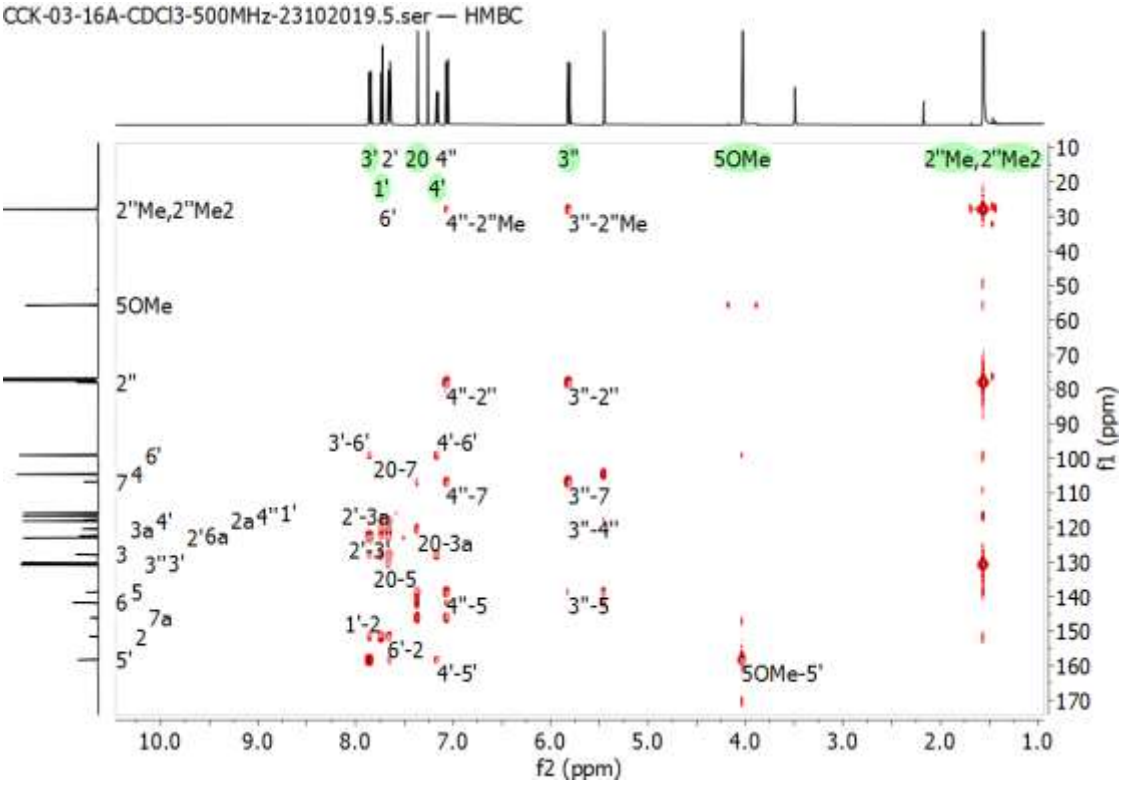

Appendix 3F: TOCSY (500 MHz, $CDCl_3$, 25°C) spectrum of usambarin C (**112)**

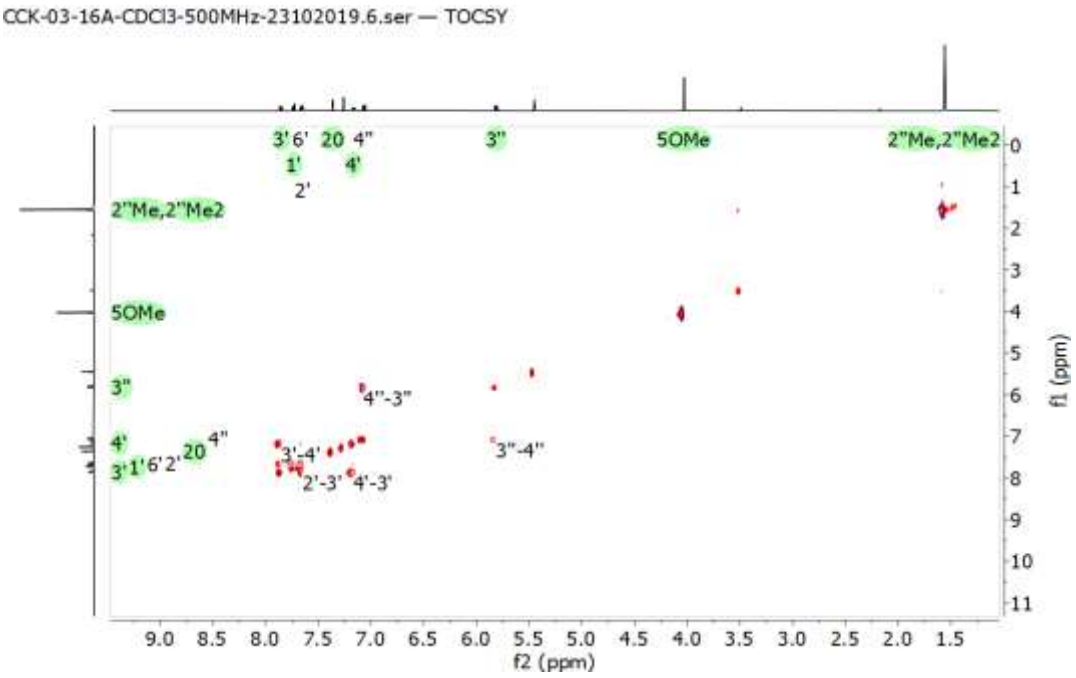

Appendix 3G: NOESY (500 MHz, $CDCl_3$, 25°C) spectrum of usambarin C (**112)**

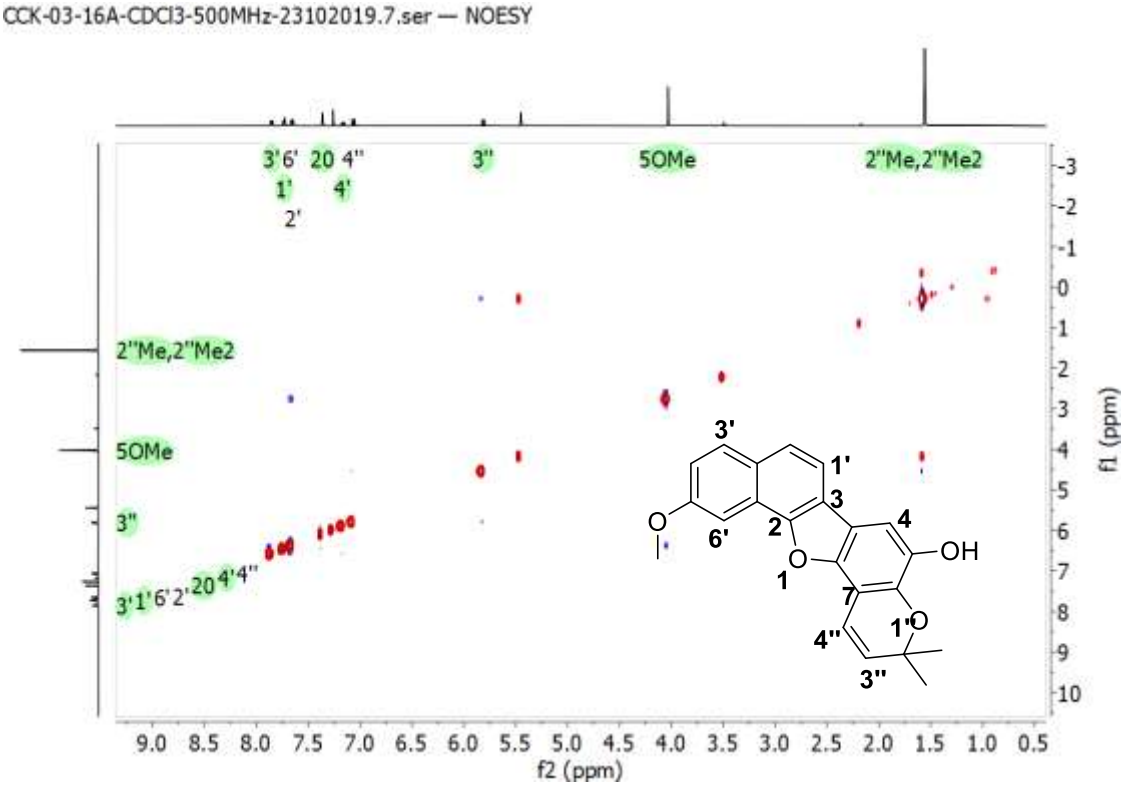

Appendix 3H: HRMS spectrum of usambarin C (**112)**

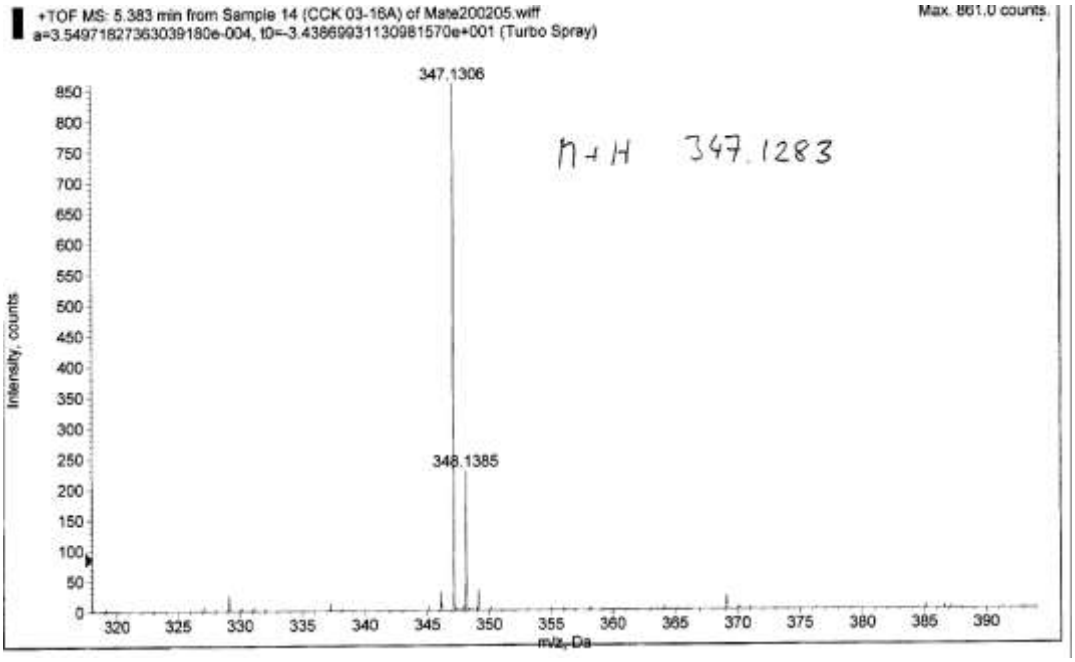

Appendix 4A: ^{1}H NMR (500 MHz, $CDCl_3$, 25°C) spectrum of usambarin D (113)

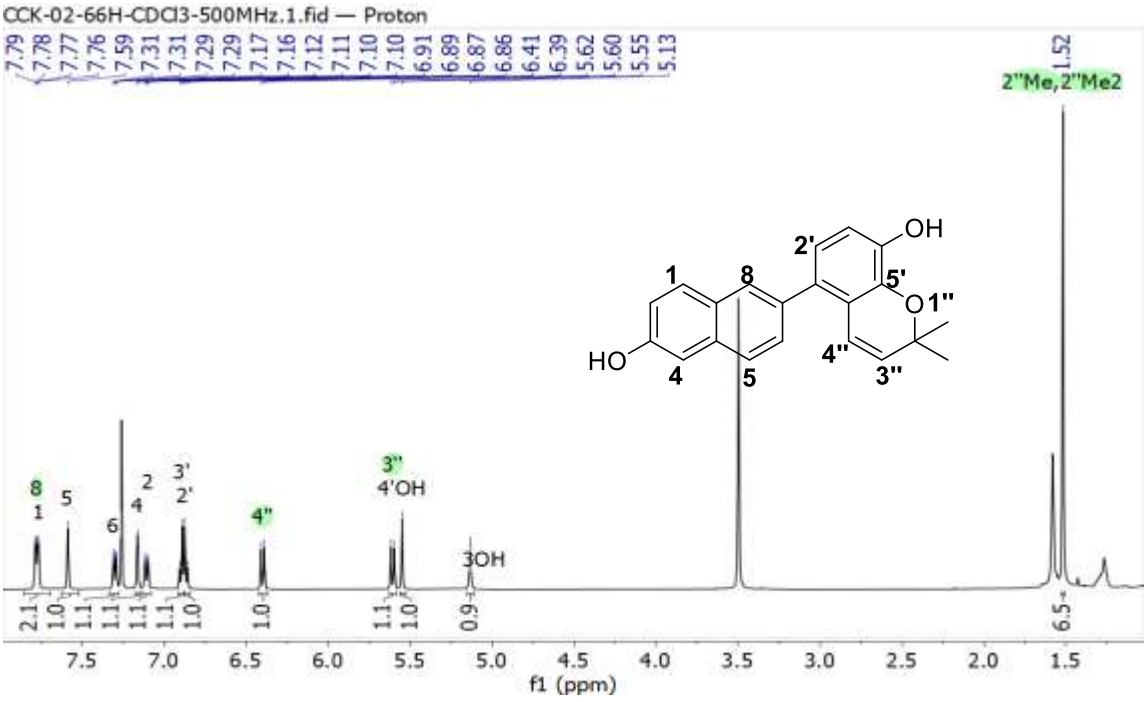

Appendix 4B: ^{13}C NMR (500 MHz, $CDCl_3$, 25°C) spectrum of usambarin D (**113)**

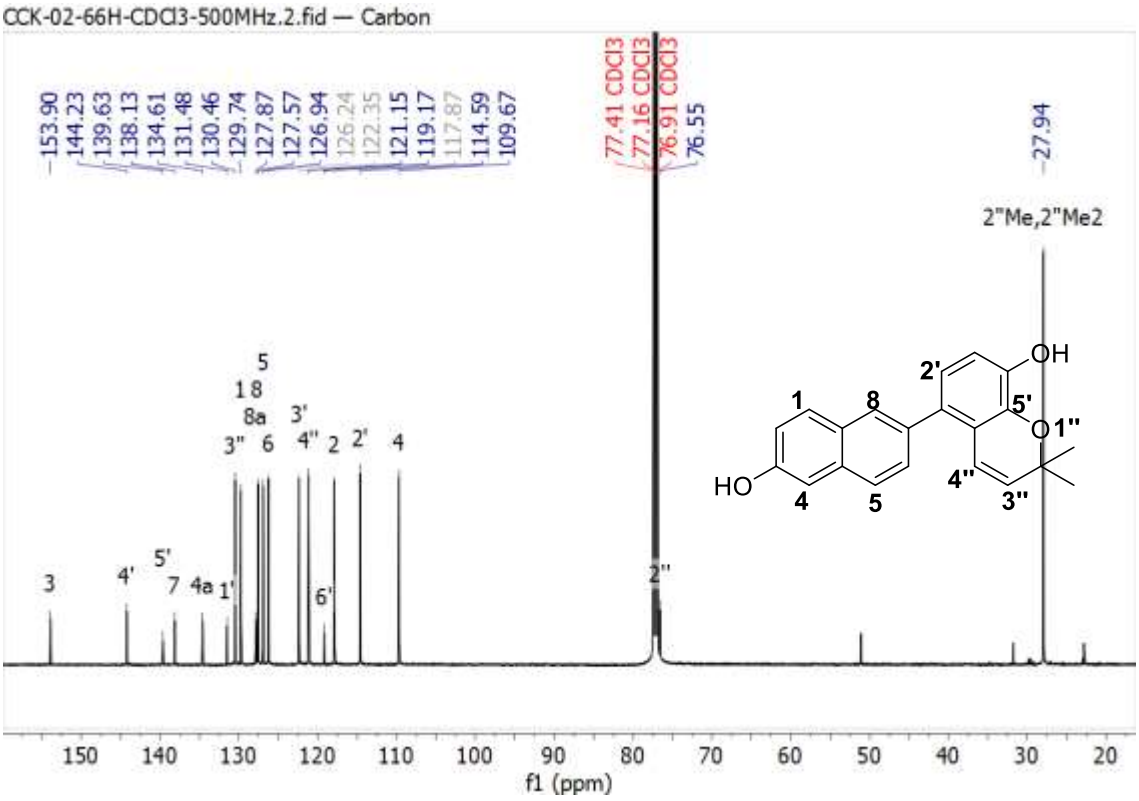

Appendix 4C: COSY (500 MHz, $CDCl_3$, 25°C) spectrum of usambarin D (**113)**

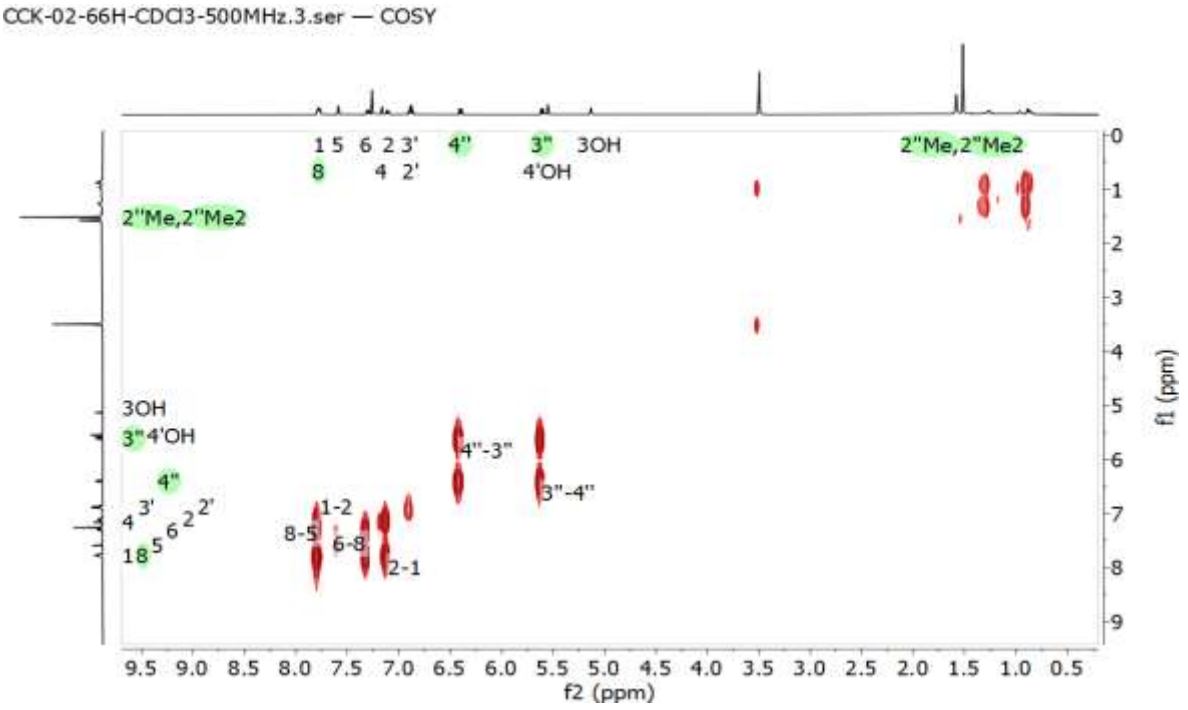

Appendix 4D:. HSQC (500 MHz, $CDCl_3$, 25°C) spectrum of usambarin D (**113)**

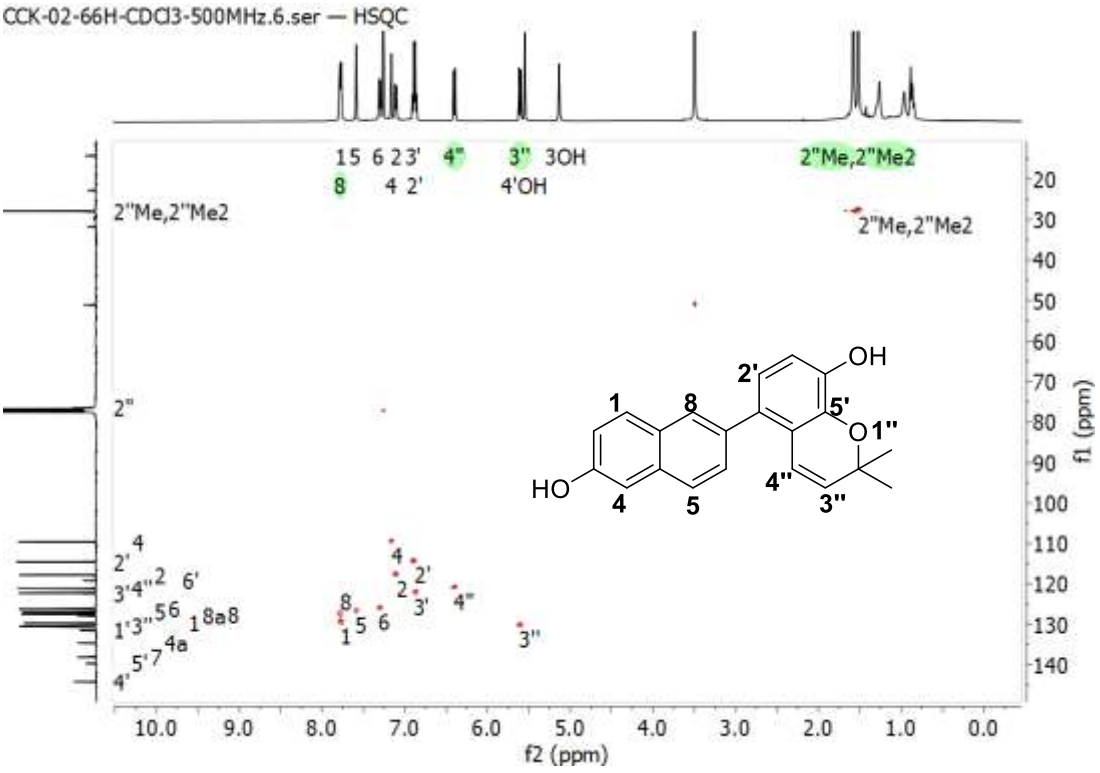

Appendix 4E:.HMBC (500 MHz, $CDCl_3$, 25°C) spectrum of usambarin D (**113)**

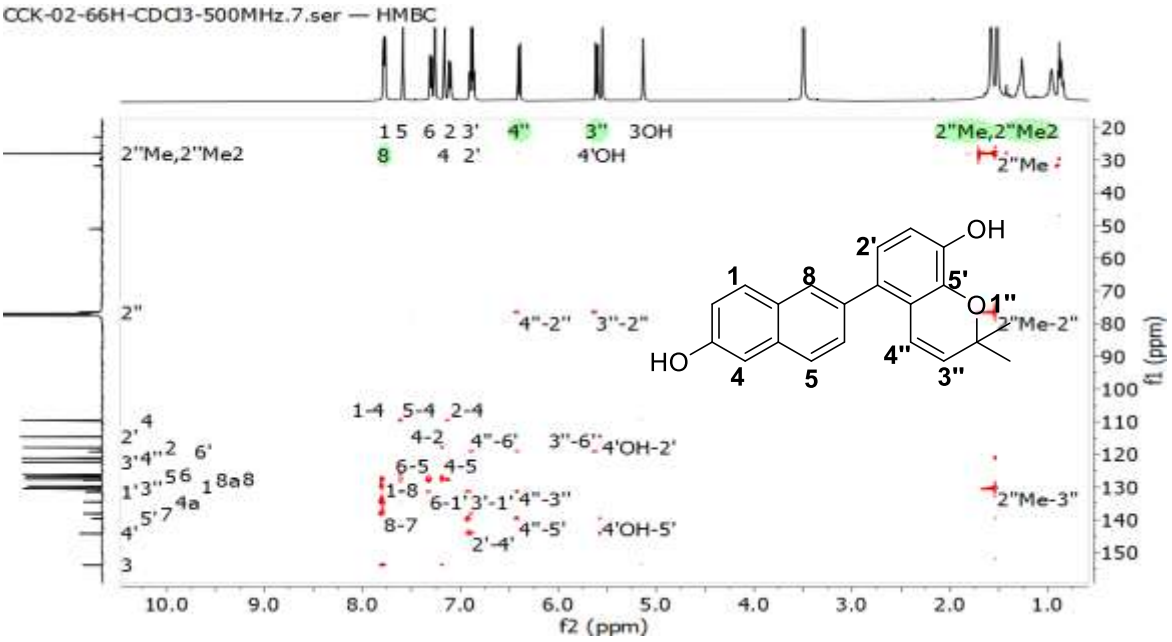

Appendix 4F:. TOCSY (500 MHz, $CDCl_3$, 25°C) spectrum of usambarin D (**113)**

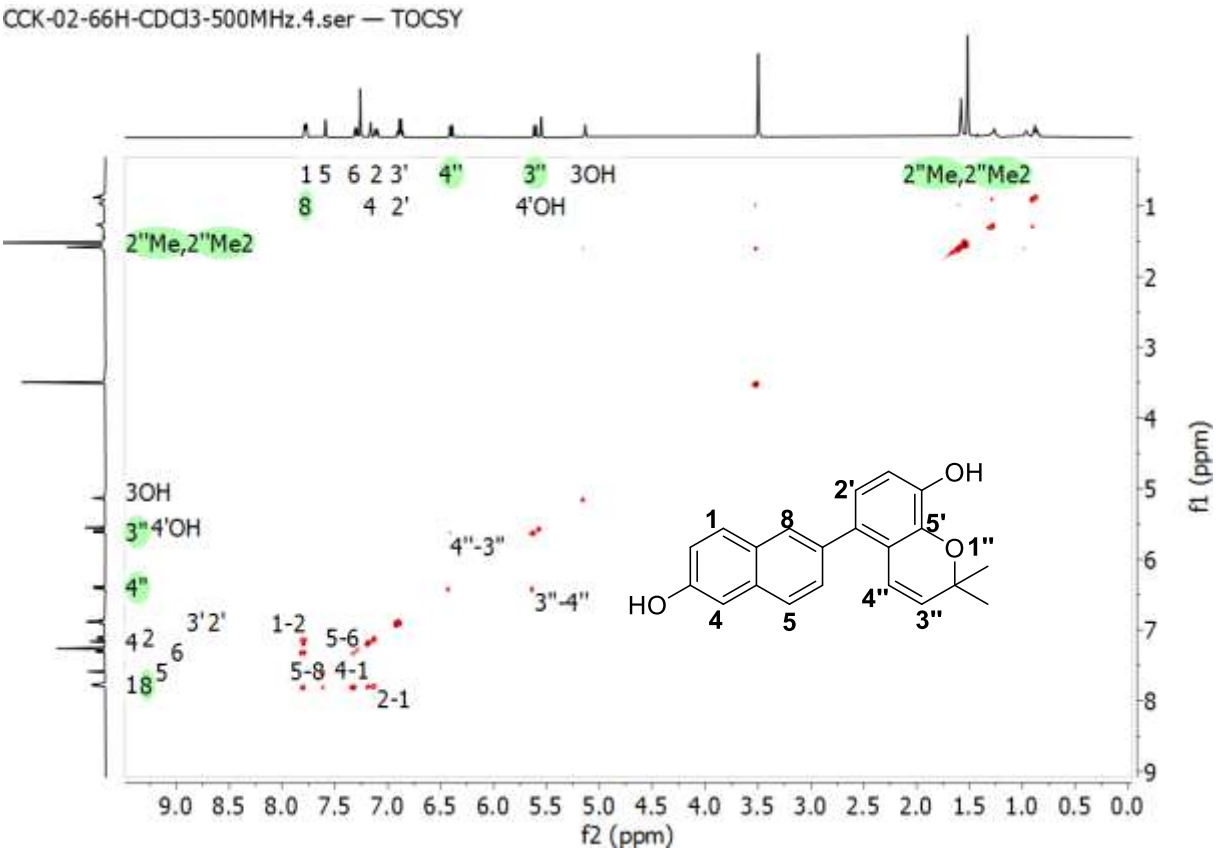

Appendix 4G. NOESY (500 MHz, $CDCl_3$, 25°C) spectrum of usambarin D (**113)**

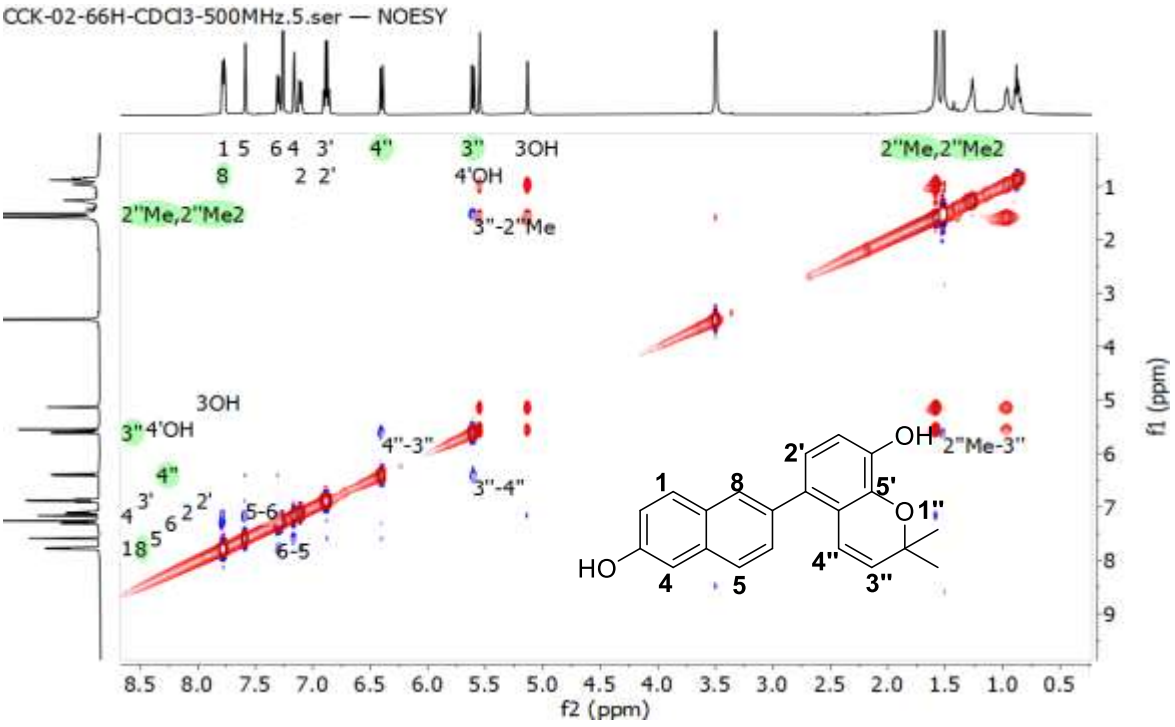

Appendix 4H. HRMS spectrum of usambarin D (**113)**

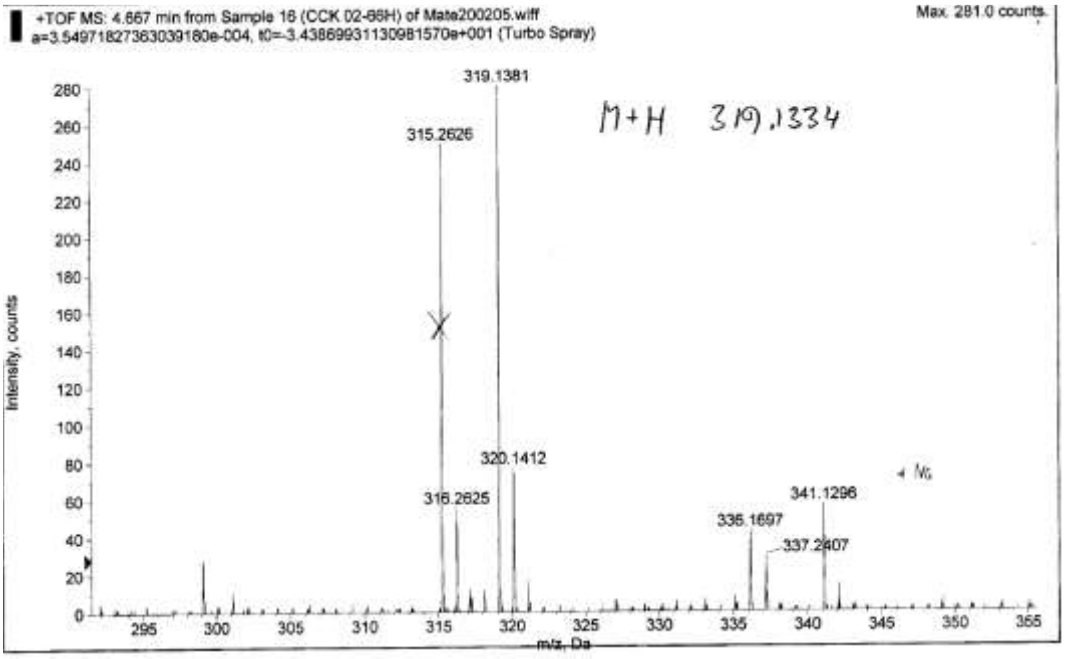

Appendix 4I: X-ray structure of usambarin D (**113)**

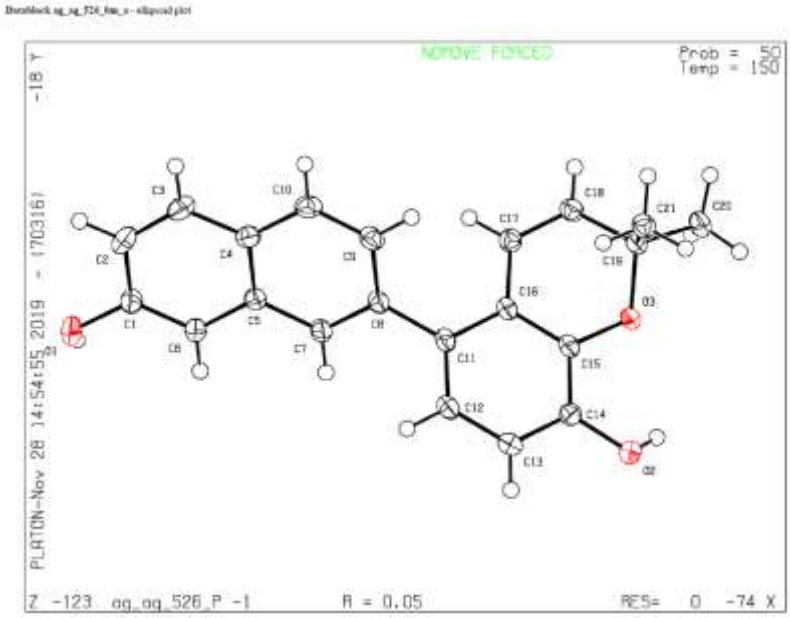

Appendix 4J:. Uv spectrum of usambarin D (**113)**

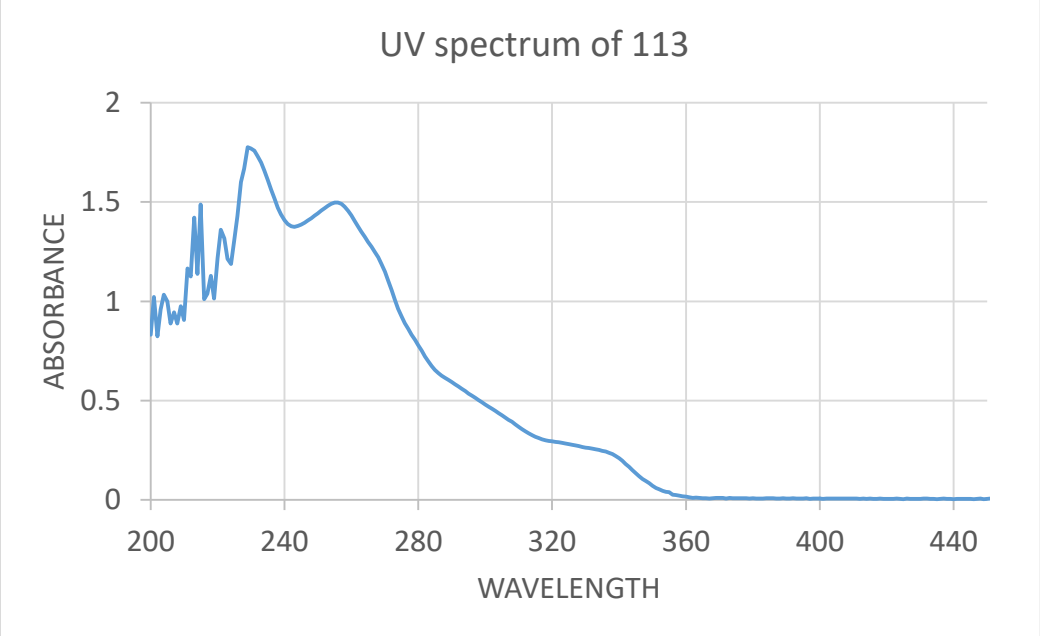

Appendix 5A:. ^{1}H NMR (500 MHz, $CDCl_3$, 25°C) spectrum of usambarin E (114)

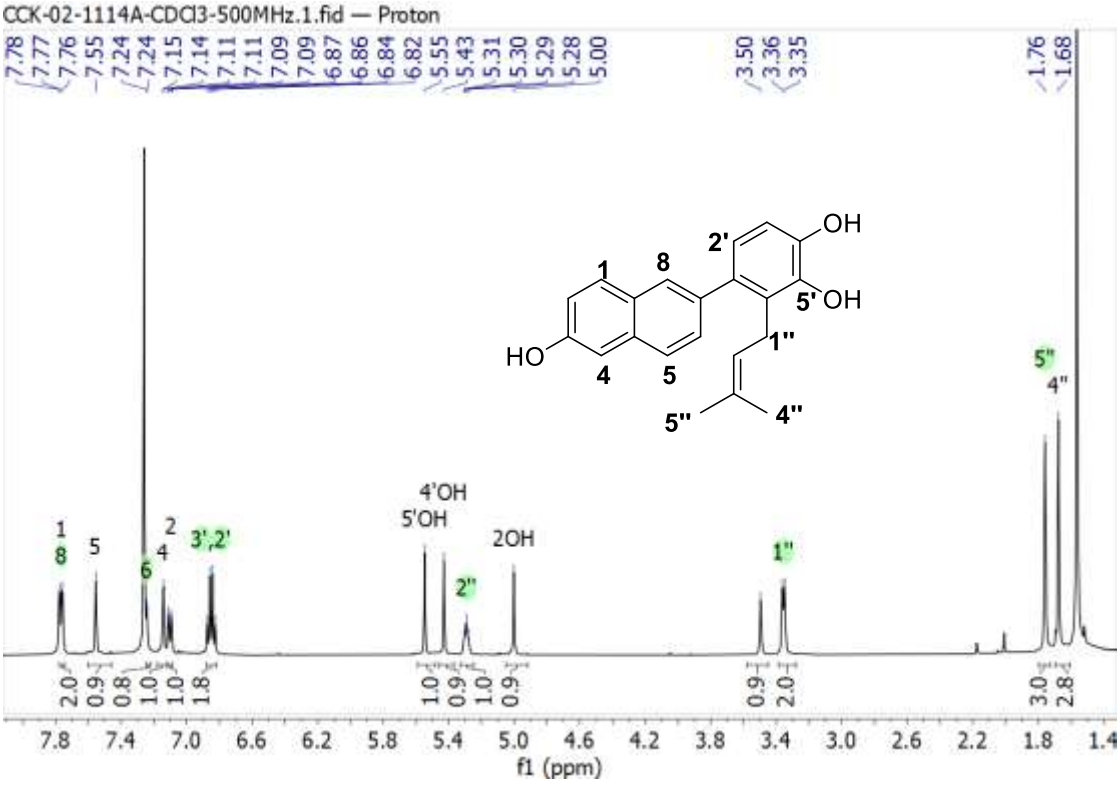

Appendix 5B:. ^{13}C NMR (500 MHz, $CDCl_3$, 25°C) spectrum of usambarin E (**114)**

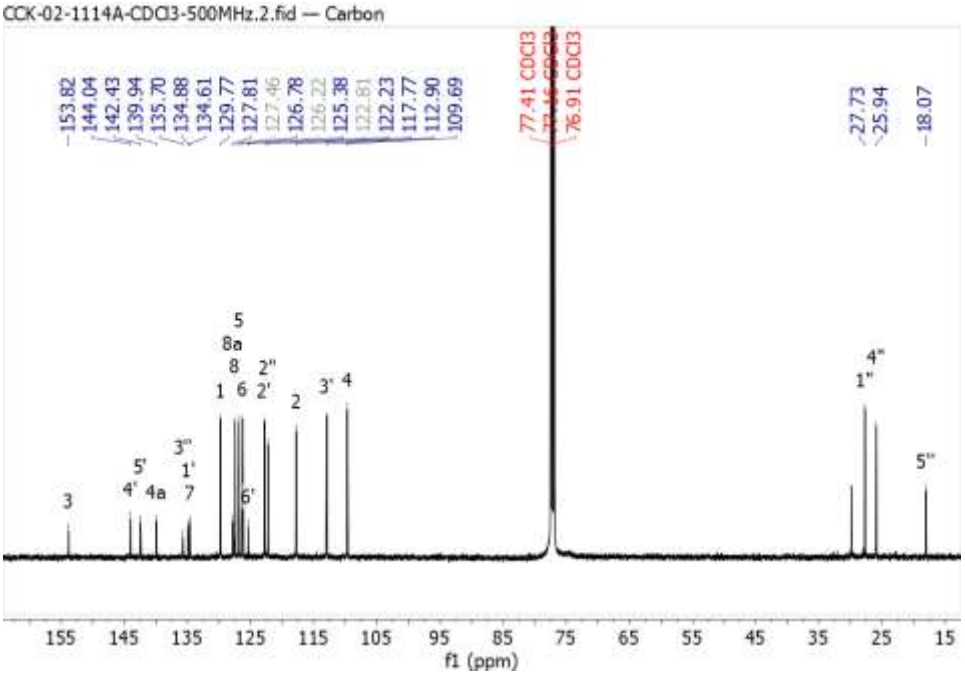

Appendix 5C:. COSY (500 MHz, $CDCl_3$, 25°C) spectrum of usambarin E (**114)**

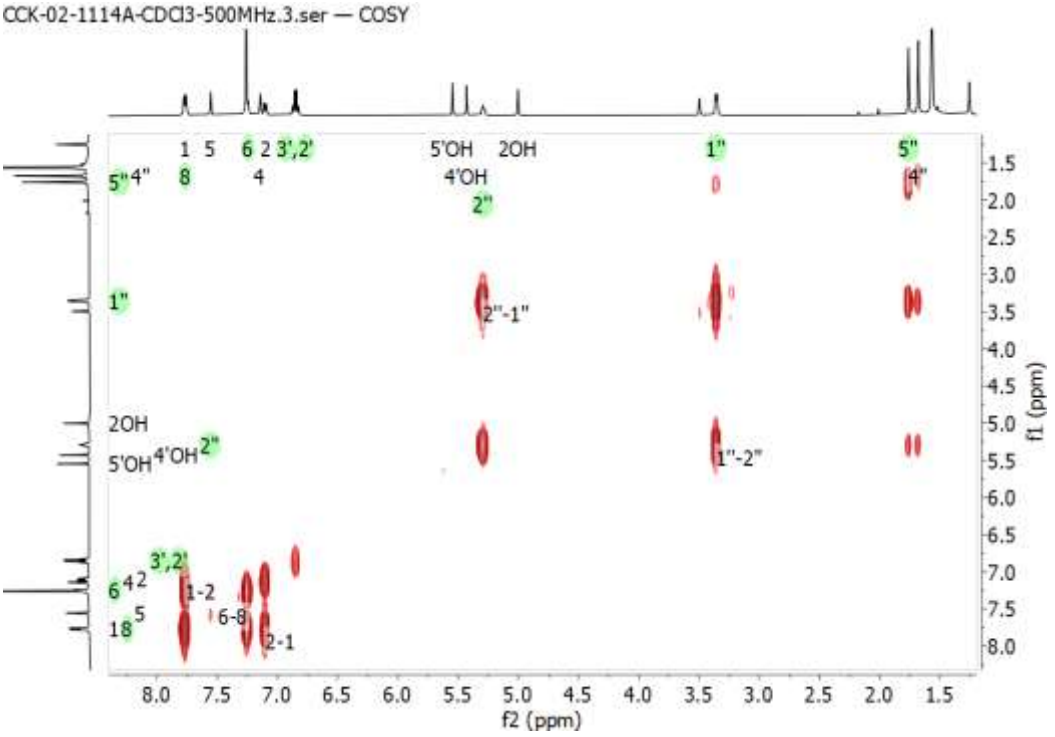

Appendix 5D:. HSQC (500 MHz, $CDCl_3$, 25°C) spectrum of usambarin E (**114)**

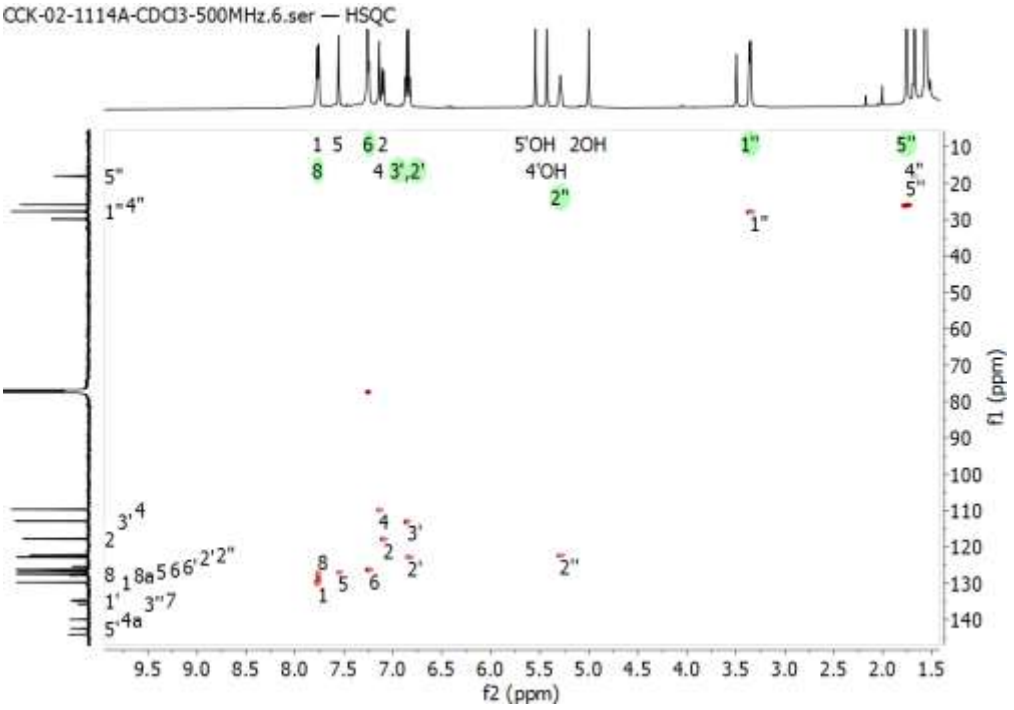

Appendix 5E:. HMBC (500 MHz, $CDCl_3$, 25°C) spectrum of usambarin E (**114)**

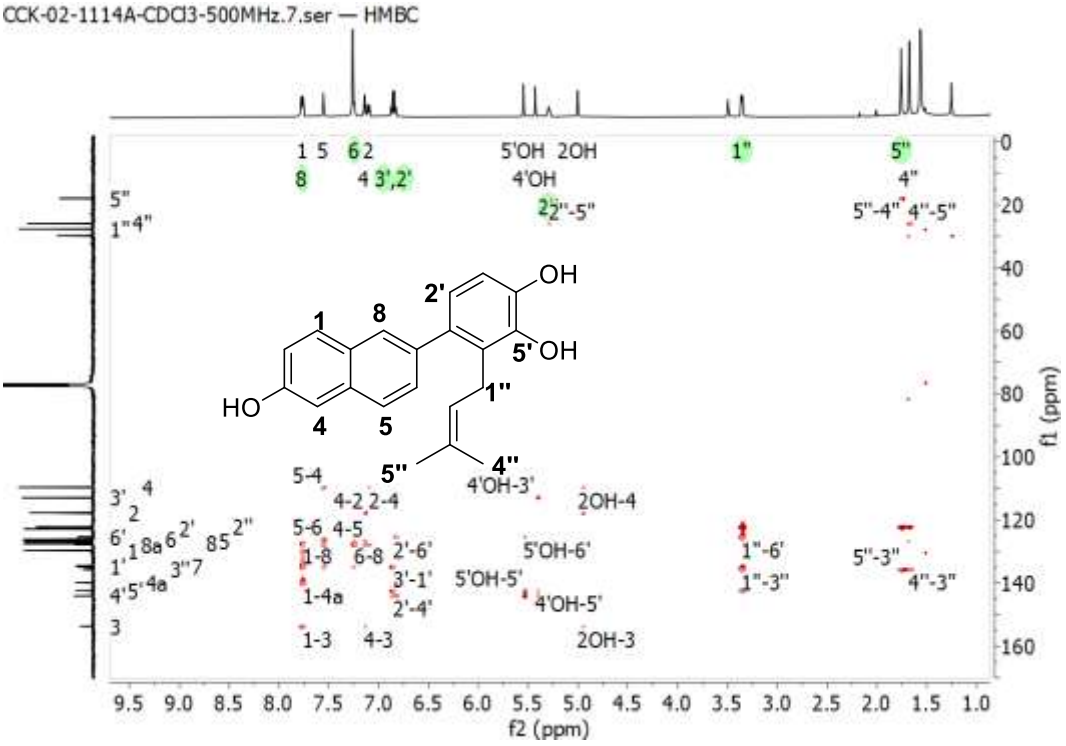

Appendix 5F:.NOESY (500 MHz, $CDCl_3$, 25°C) spectrum of usambarin E (**114)**

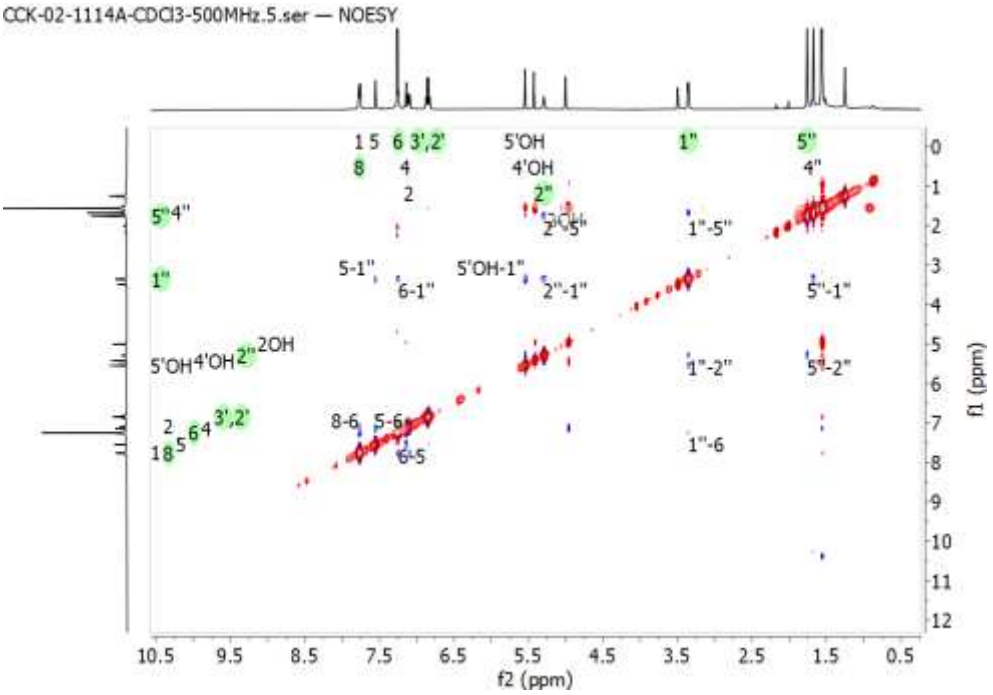

Appendix 5G: TOCSY (500 MHz, $CDCl_3$, 25°C) spectrum of usambarin E (**114)**

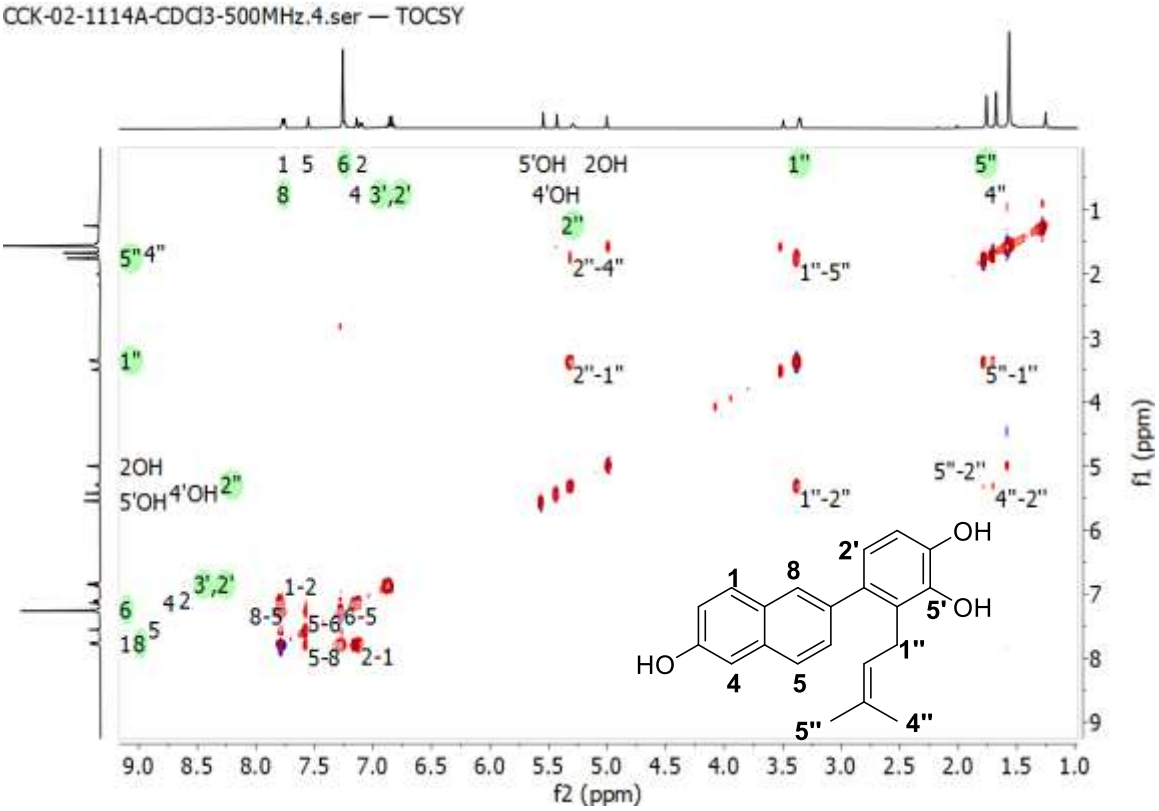

Appendix 5H: HRMS spectrum of usambarin E (**114)**

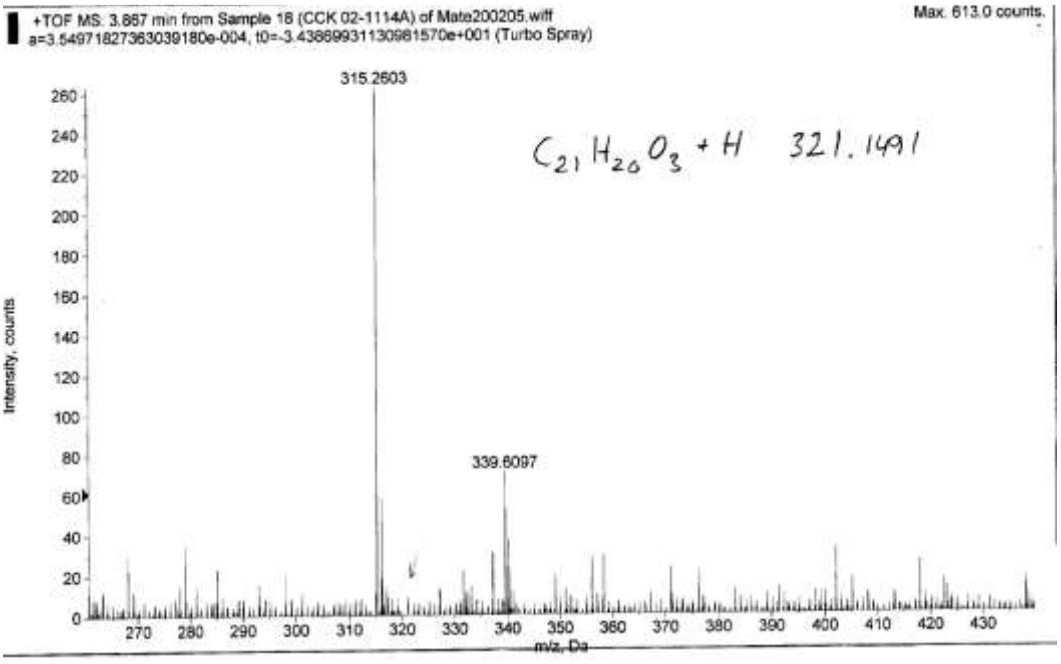

Appendix 51: Uv spectrum of usambarin E (114)

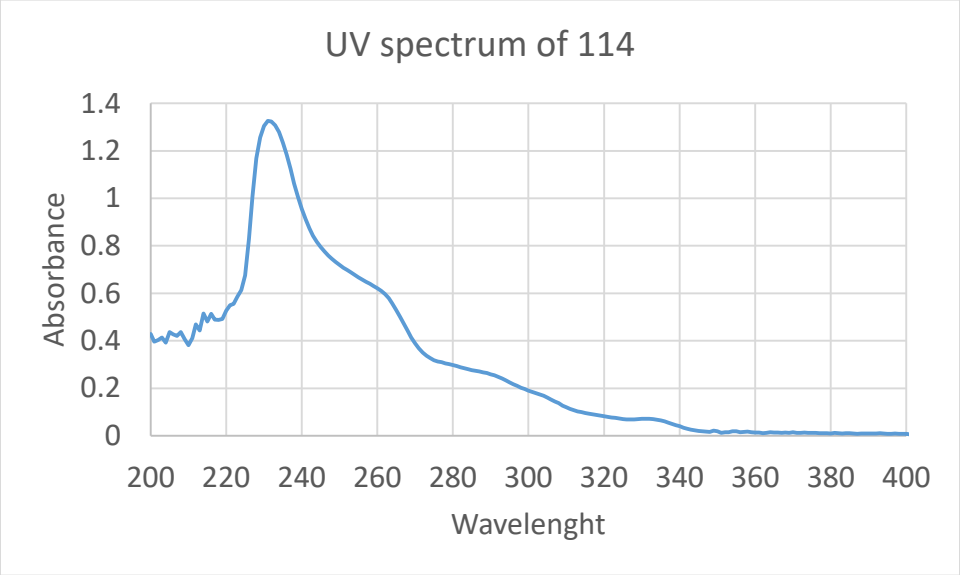

Appendix 6A: ^{1}H NMR (500 MHz, $CDCl_3$, 25°C) spectrum of usambarin F(115)

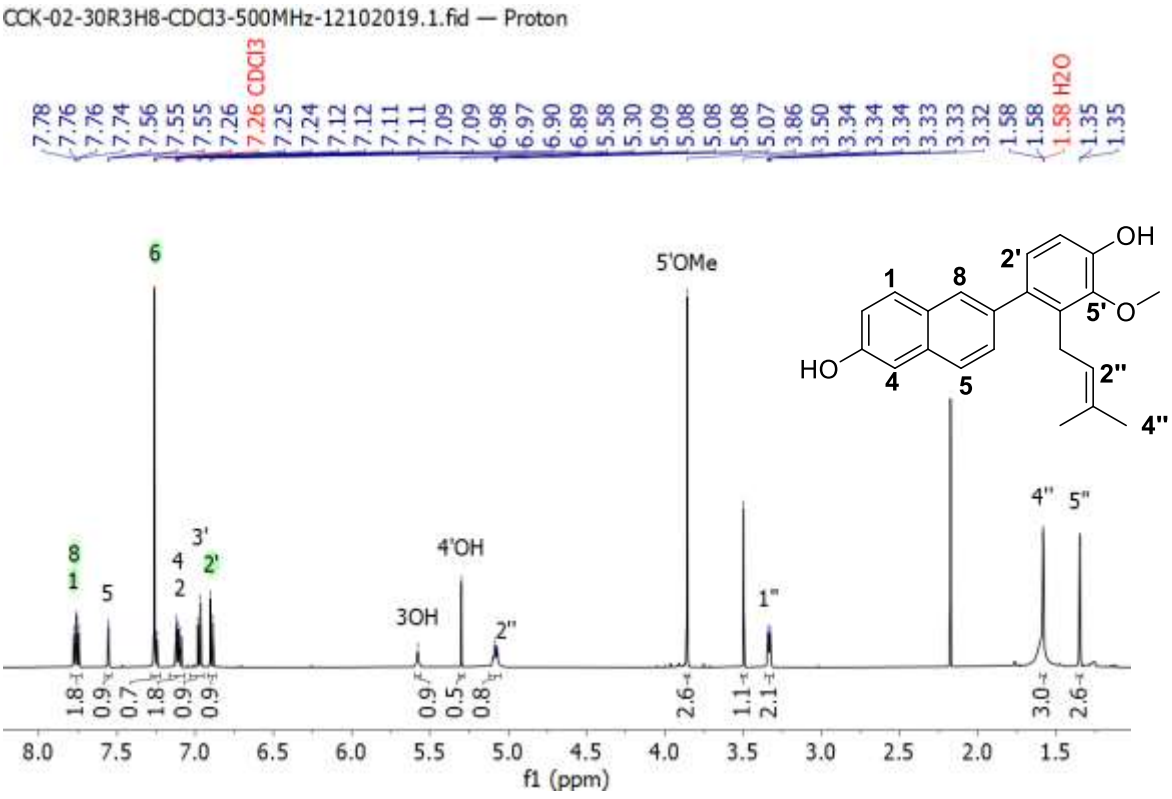

Appendix 6B**:** ^{13}C NMR (500 MHz, $CDCl_3$, 25°C) spectrum of usambarin F (**115)**

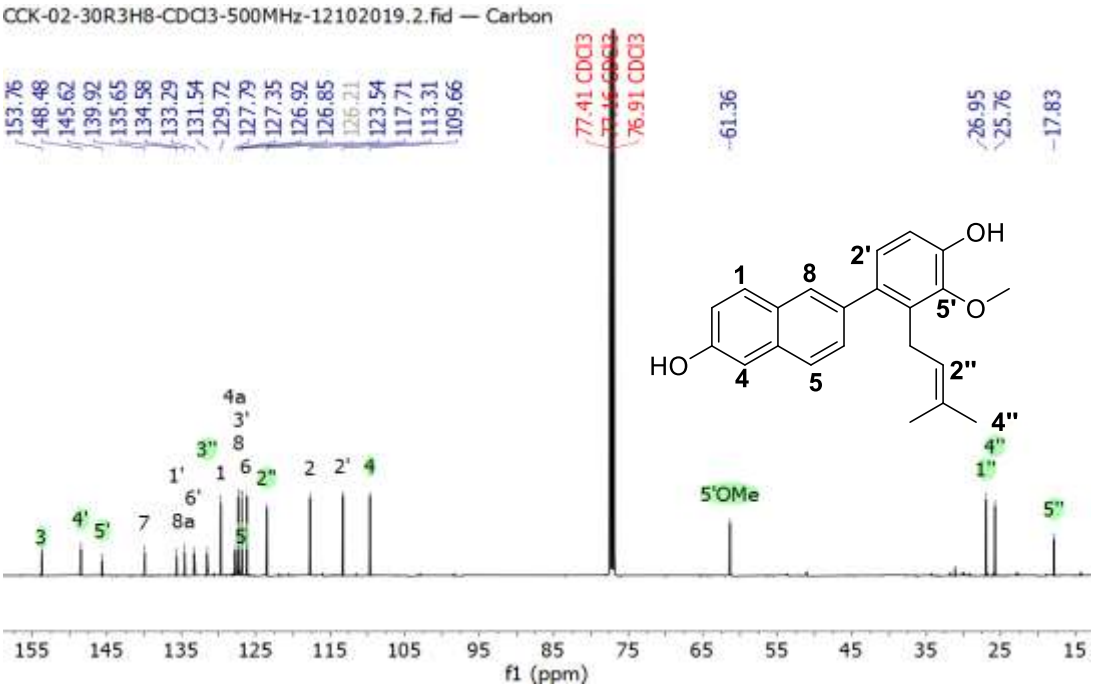

Appendix 6C: COSY (500 MHz, $CDCl_3$, 25°C) spectrum of usambarin F (**115)**

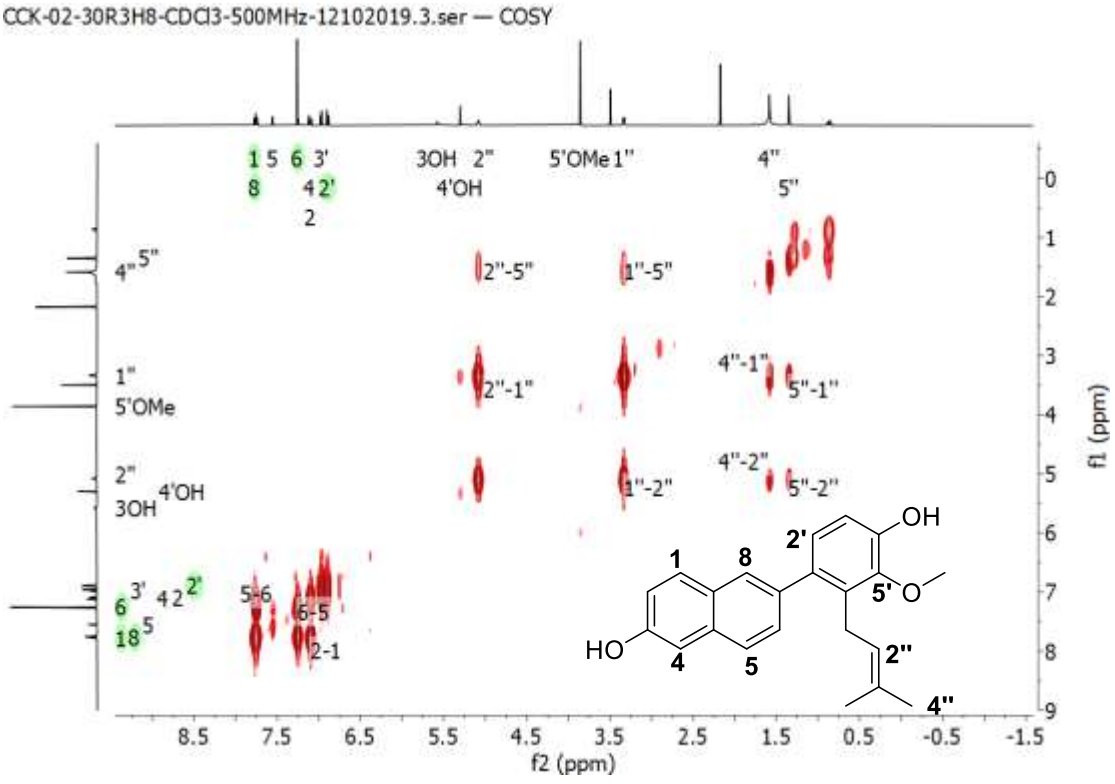

Appendix 6D: HSQC (500 MHz, $CDCl_3$, 25°C) spectrum of usambarin F (**115)**

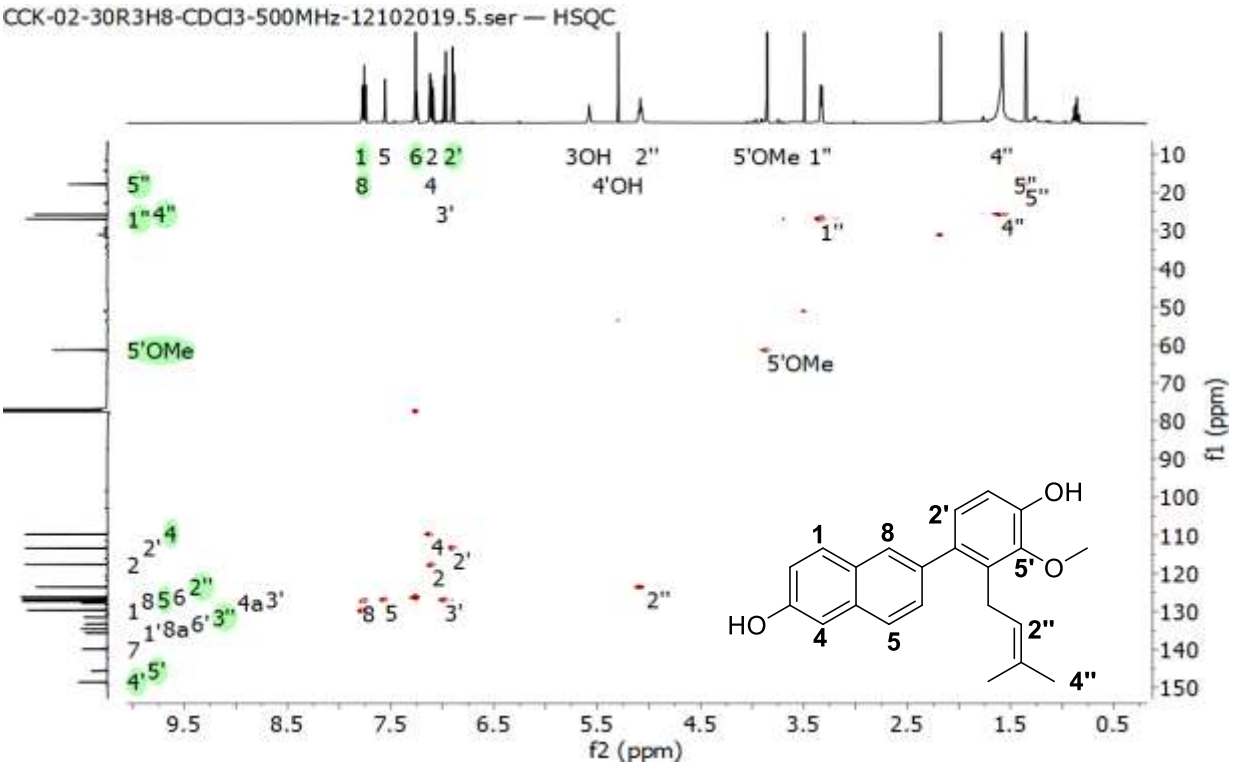

Appendix 6E: HMBC (500 MHz, $CDCl_3$, 25°C) spectrum of usambarin F (**115)**

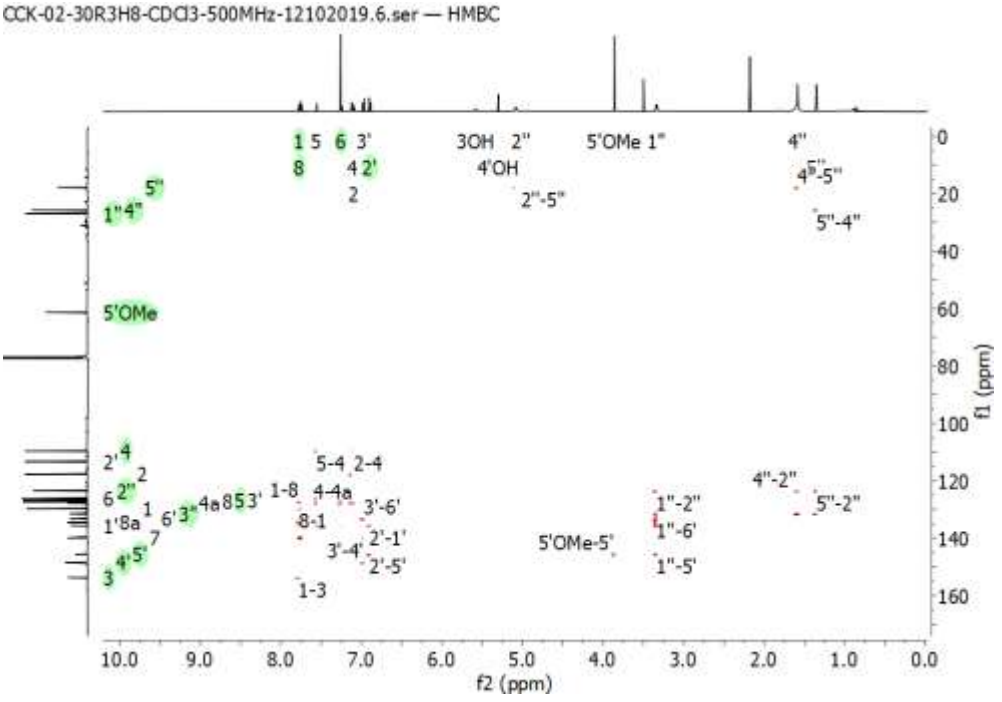

Appendix 6F: NOESY (500 MHz, $CDCl_3$, 25°C) spectrum of usambarin F (**115)**

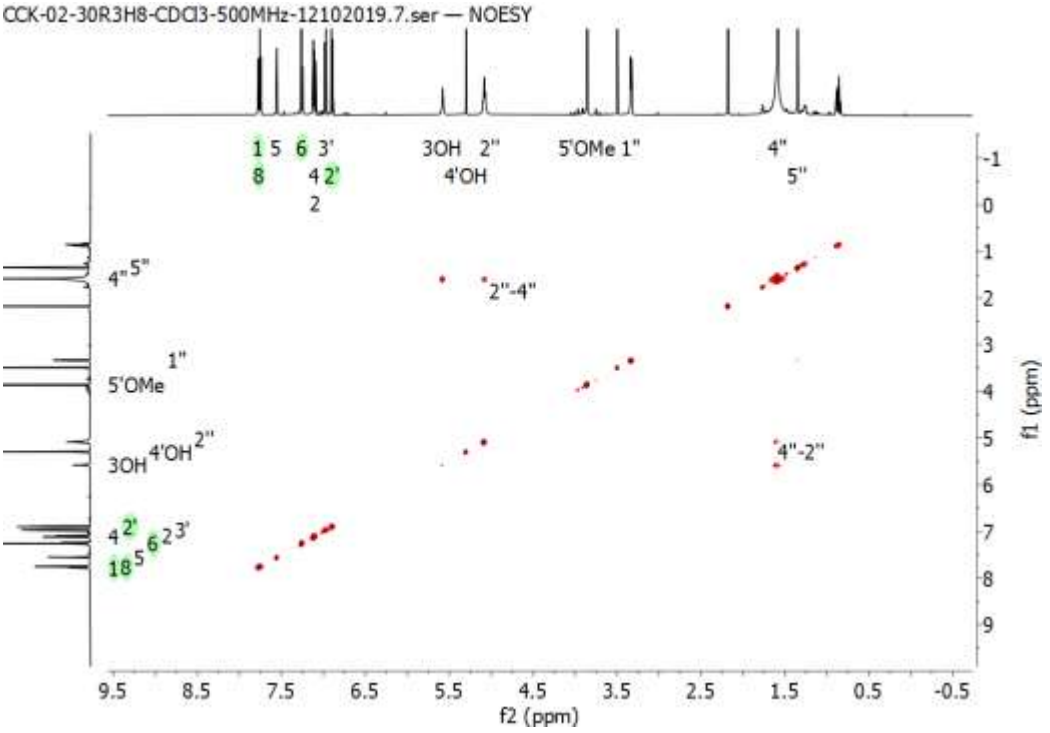

Appendix 6G:.TOCSY (500 MHz, $CDCl_3$, 25°C) spectrum of usambarin F (**115)**

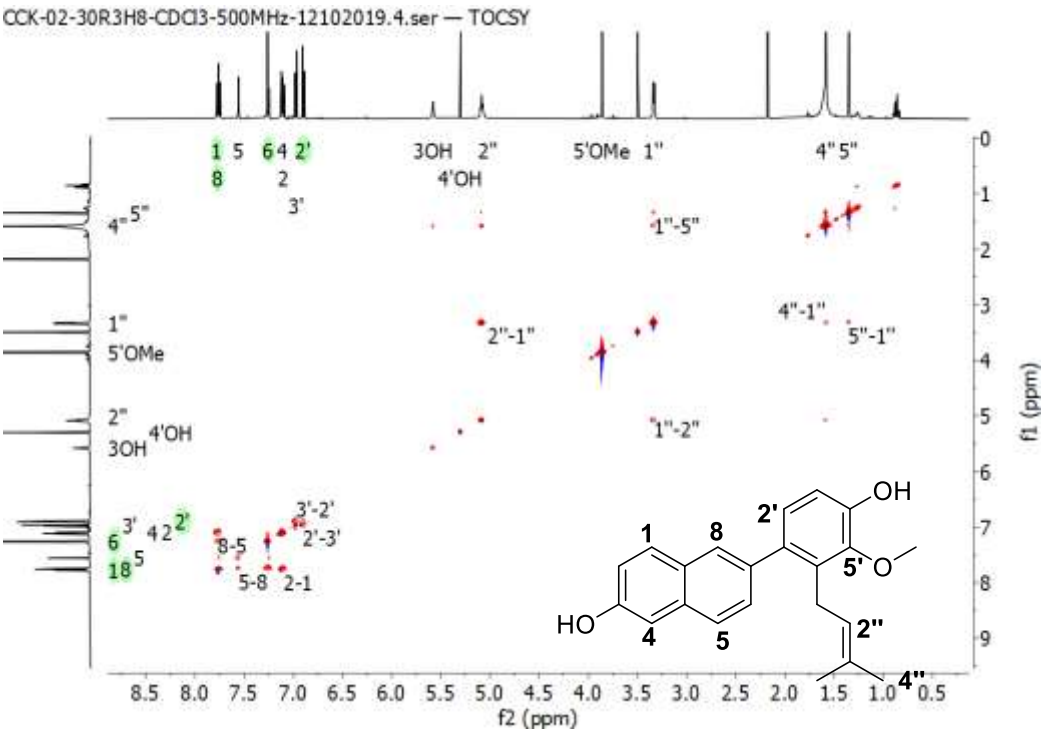

Appendix 6H:.HRMS spectrum of usambarin F (**115)**

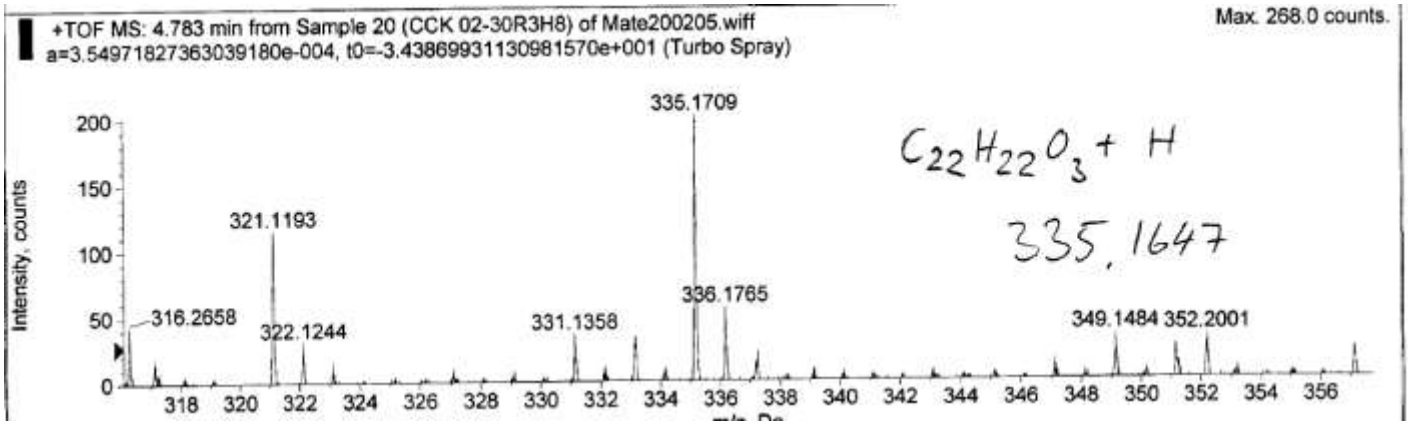

Appendix 61: Uv spectrum of usambarin F (**115)**

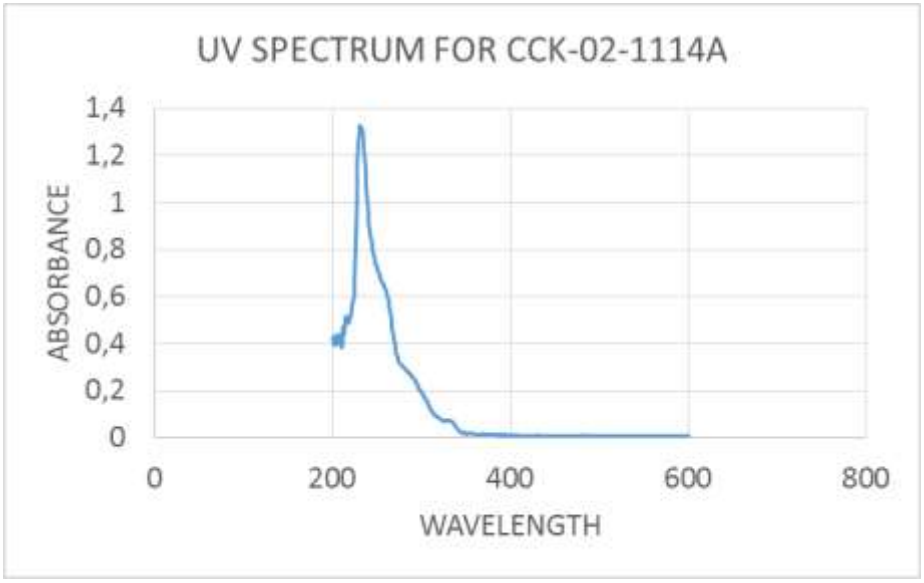

Appendix 7A: ^{1}H NMR (500 MHz, $CDCl_3$, 25°C) spectrum of usambarin G (116)

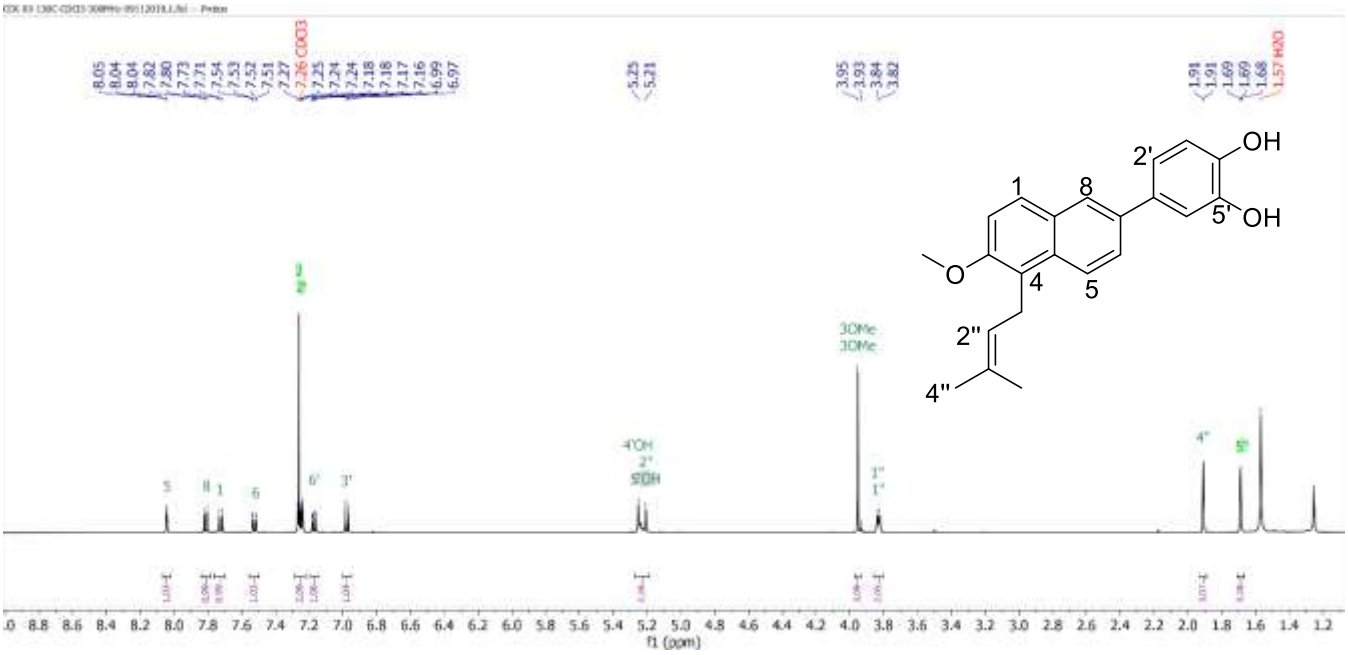

Appendix 7B: ^{13}C NMR (500 MHz, $CDCl_3$, 25°C) spectrum of usambarin G (**116)**

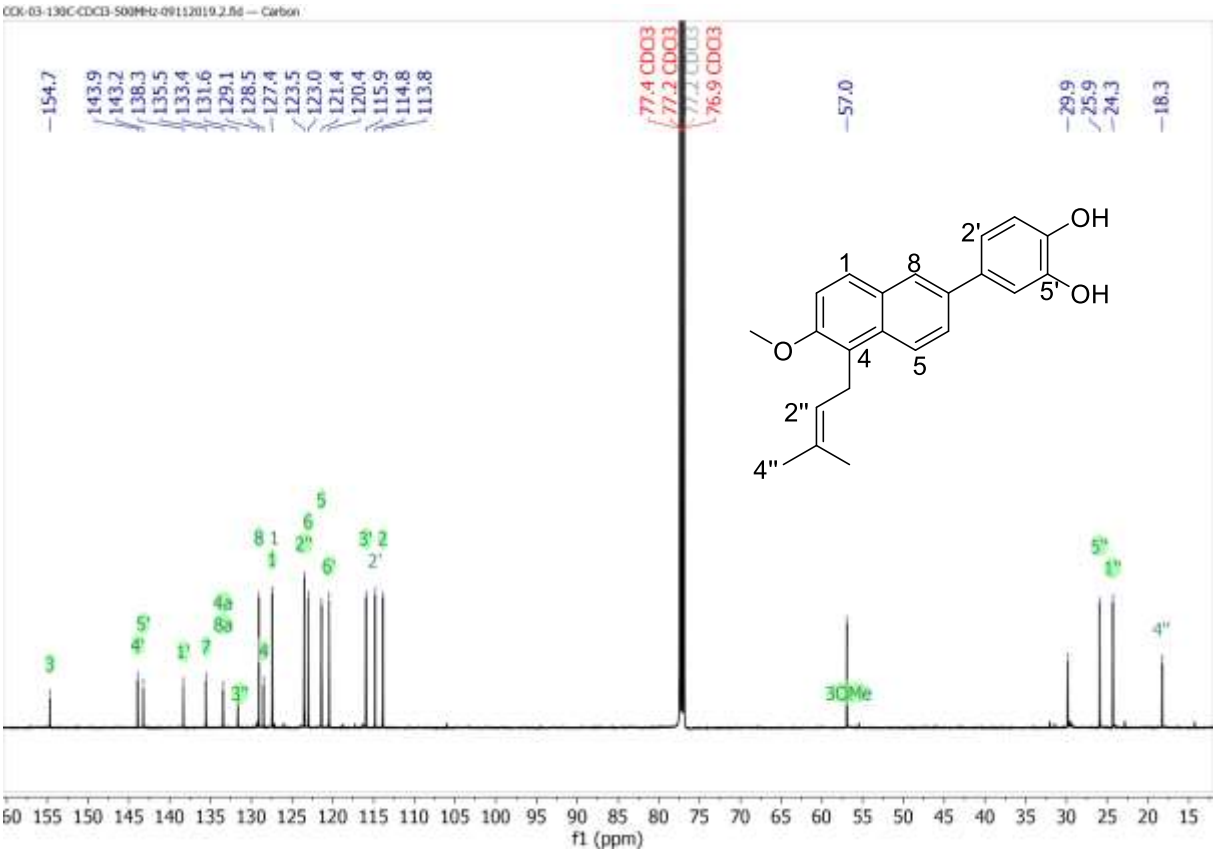

Appendix 7C: COSY (500 MHz, $CDCl_3$, 25°C) spectrum of usambarin G (**116)**

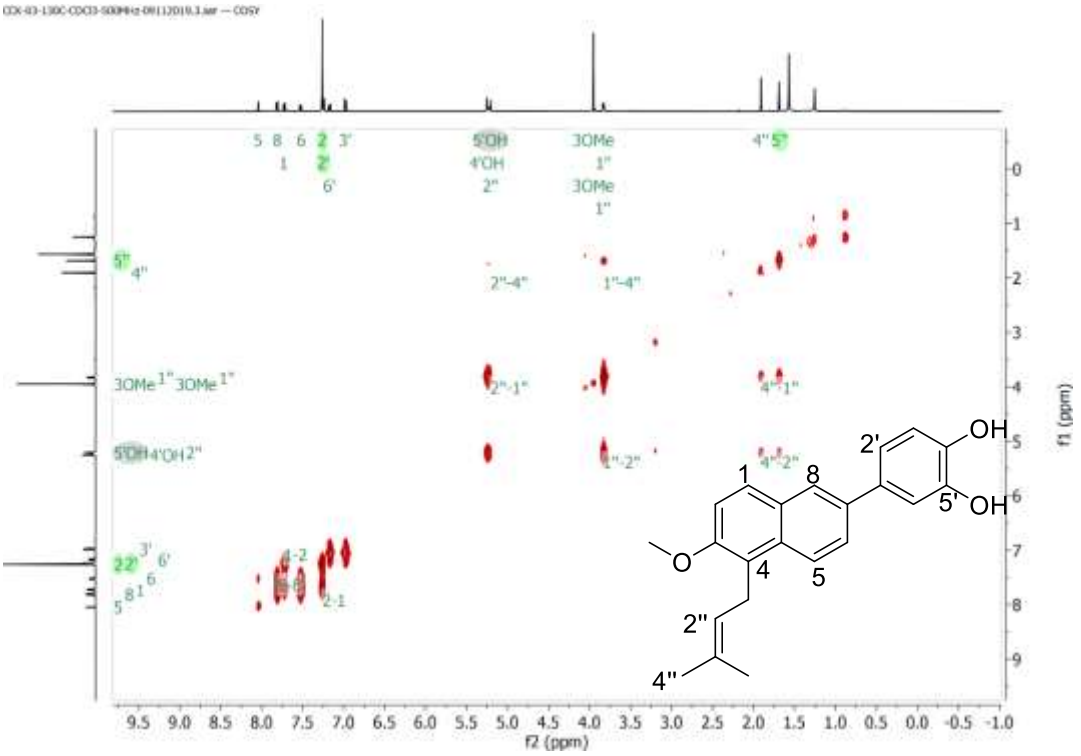

Appendix 7D: HSQC (500 MHz, $CDCl_3$, 25°C) spectrum of usambarin G (**116)**

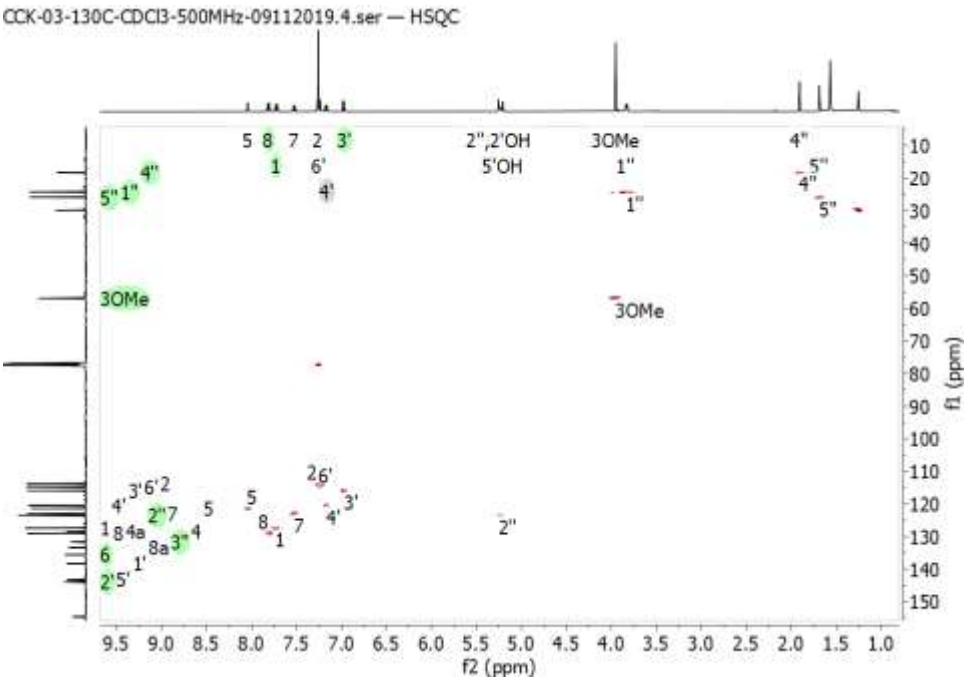

Appendix 7E: HMBC (500 MHz, $CDCl_3$, 25°C) spectrum of usambarin G (**116)**

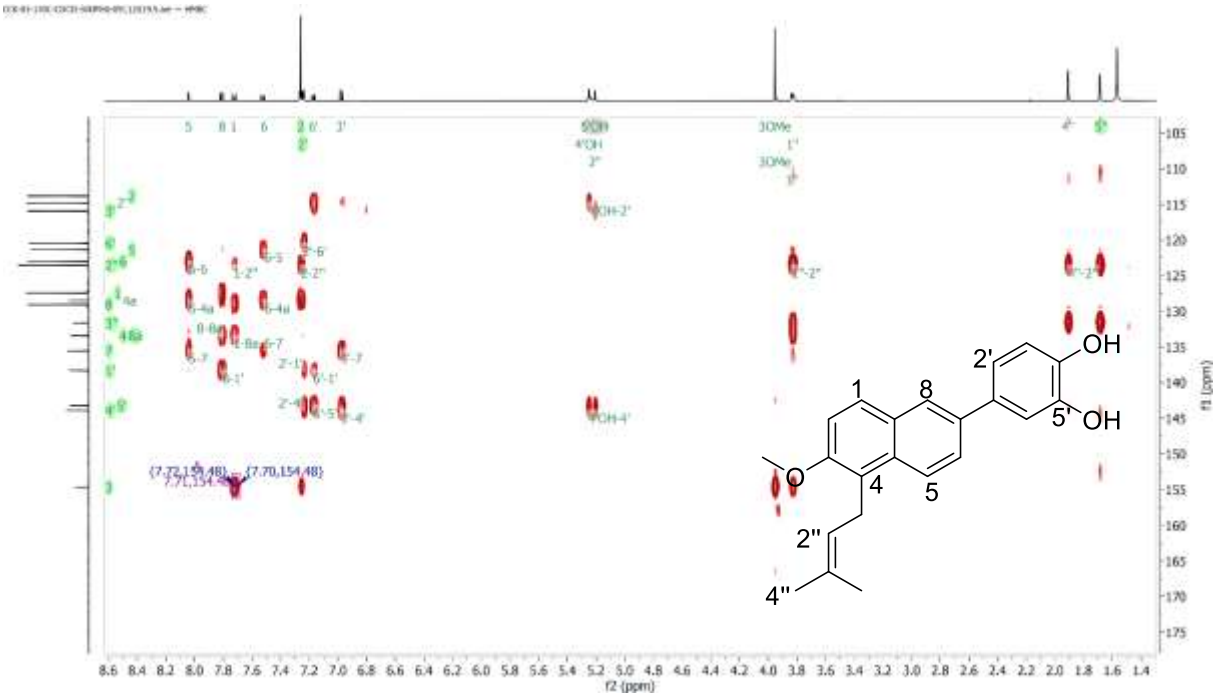

Appendix 7F: TOCSY (500 MHz, $CDCl_3$, 25°C) spectrum of usambarin G (**116)**

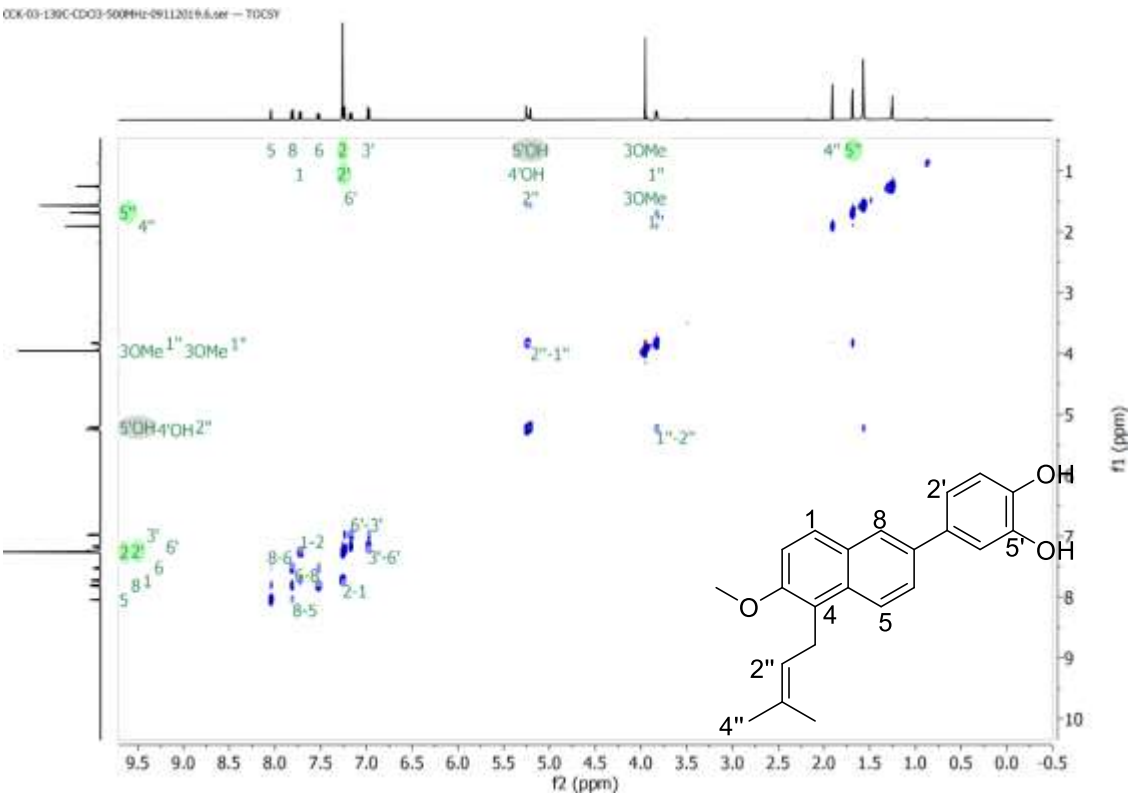

Appendix 7G: NOESY (500 MHz, $CDCl_3$, 25°C) spectrum of usambarin G (**116)**

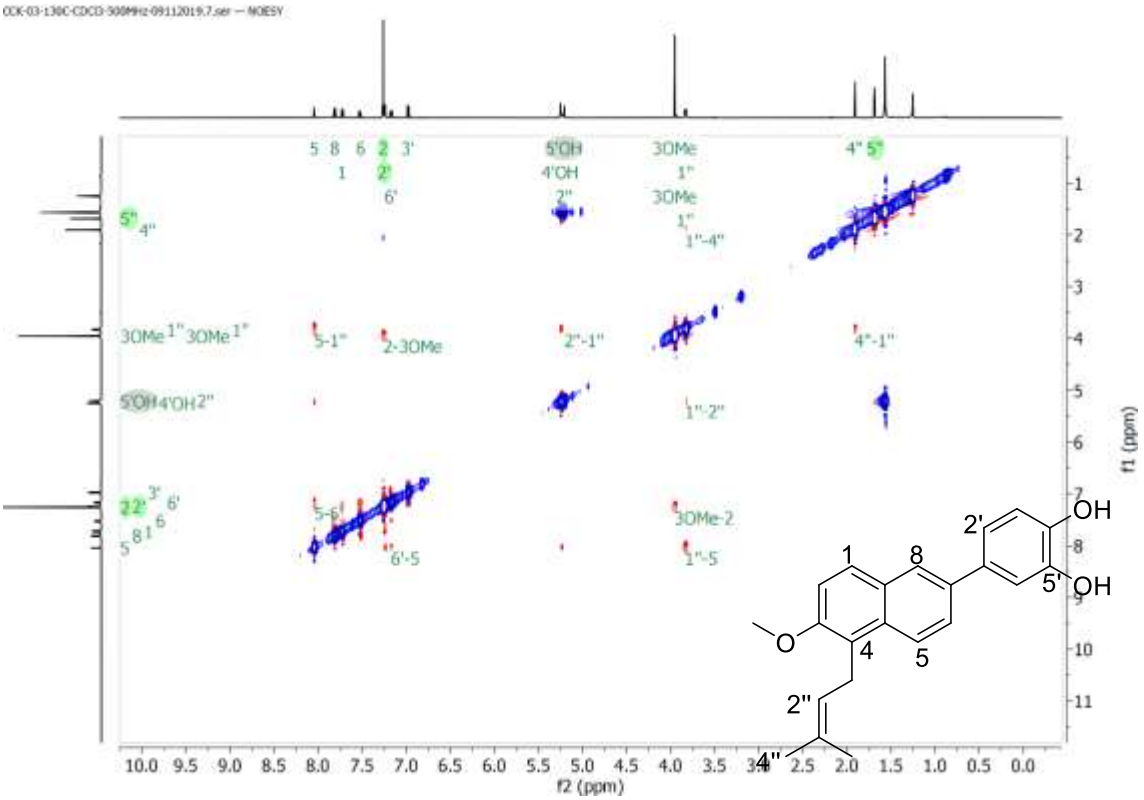

Appendix 7H: HRMS spectrum of usambarin G (**116)**

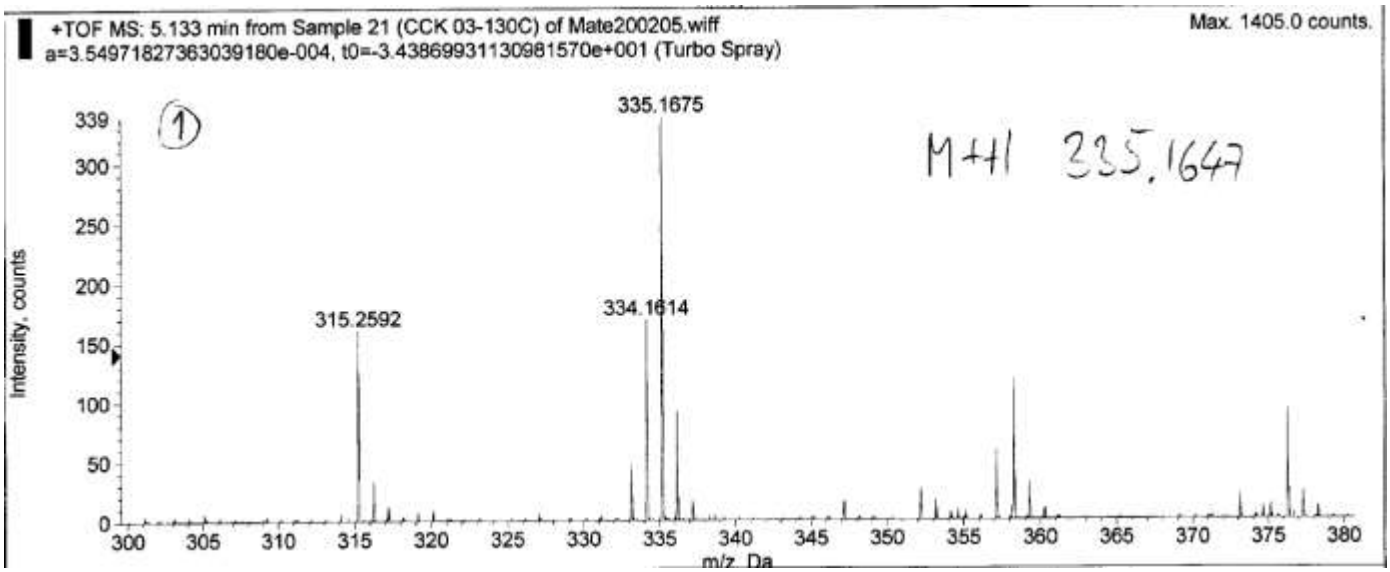

Appendix 8A: ^{1}H NMR (500 MHz, $CDCl_3$, 25°C) spectrum of usambarin H (117)

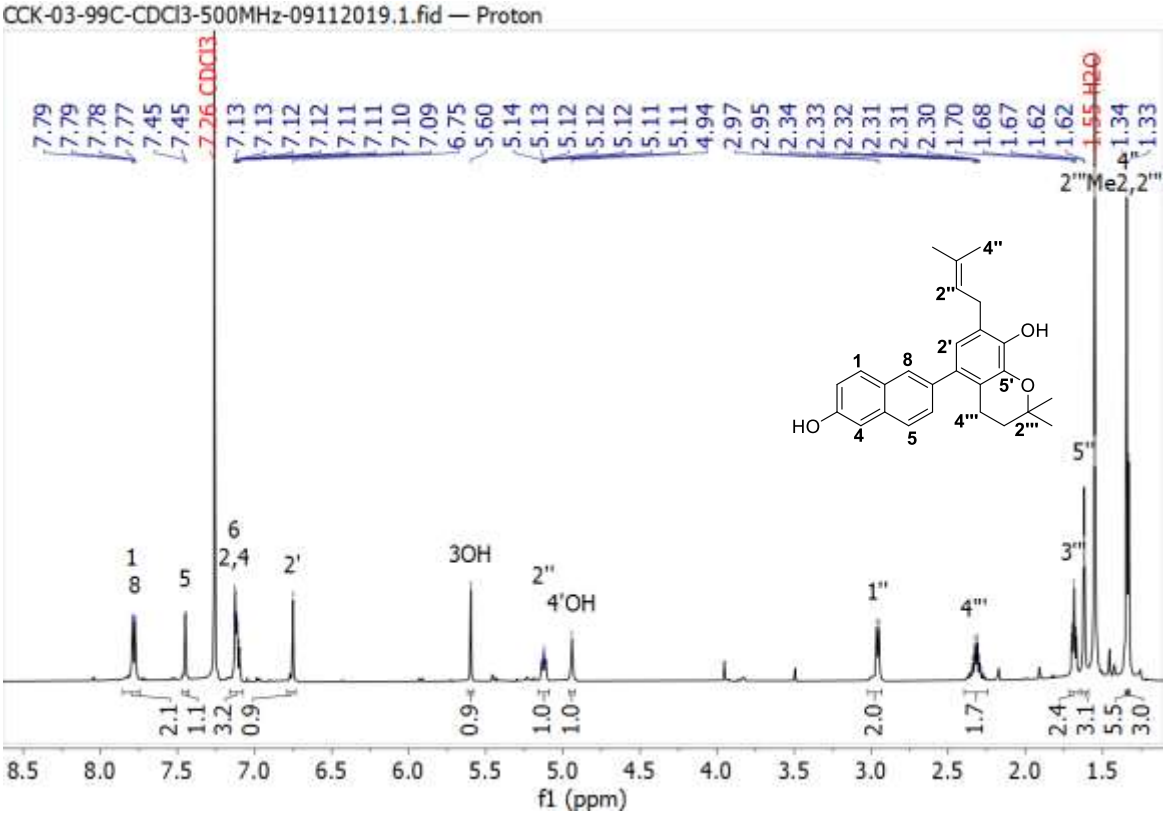

Appendix 8B. ^{13}C NMR (500 MHz, $CDCl_3$, 25°C) spectrum of usambarin H (**117)**

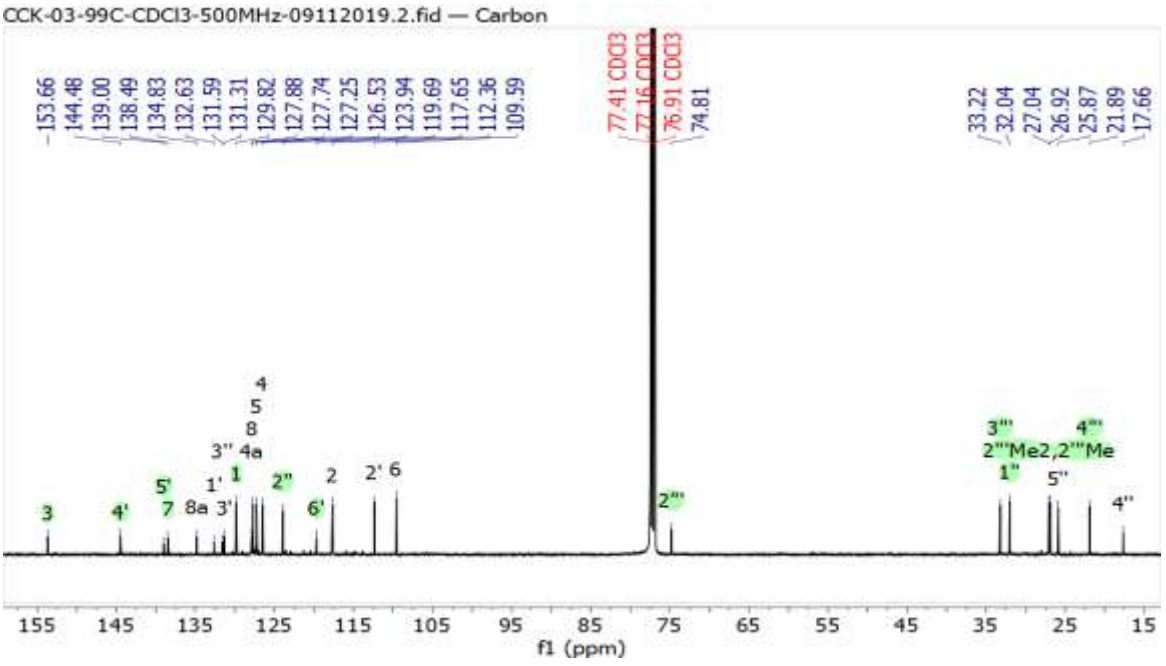

Appendix 8C.. COSY (500 MHz, $CDCl_3$, 25°C) spectrum of usambarin H (**117)**

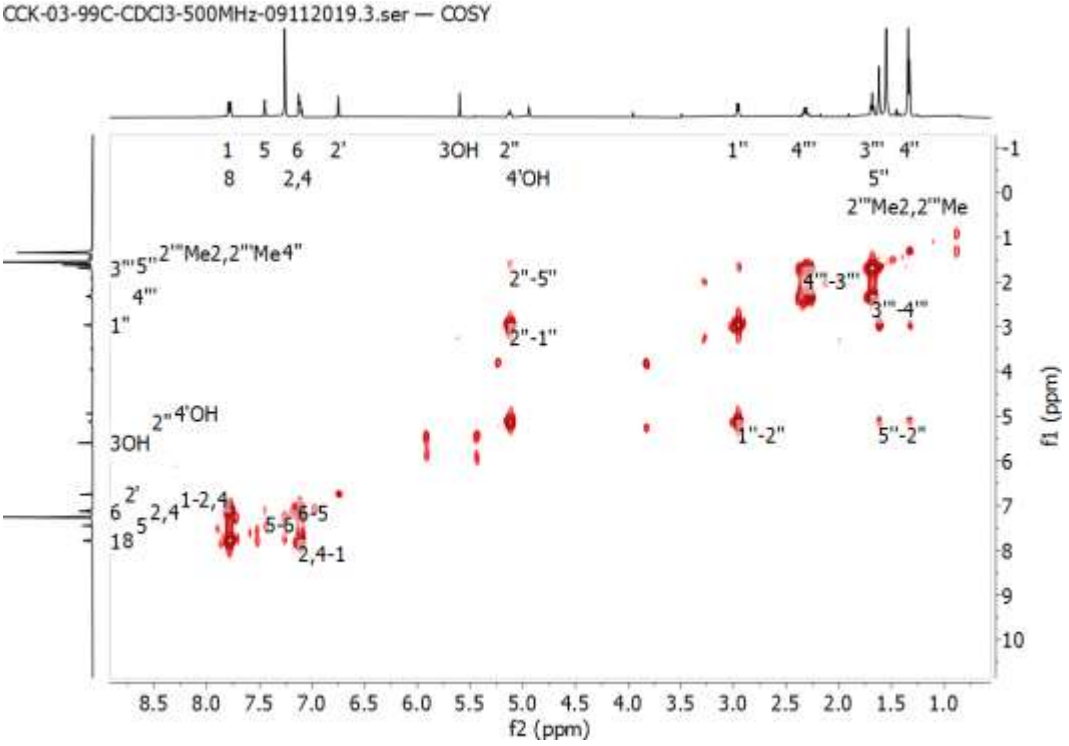

Appendix 8D: HSQC (500 MHz, $CDCl_3$, 25°C) spectrum of usambarin H (**117)**

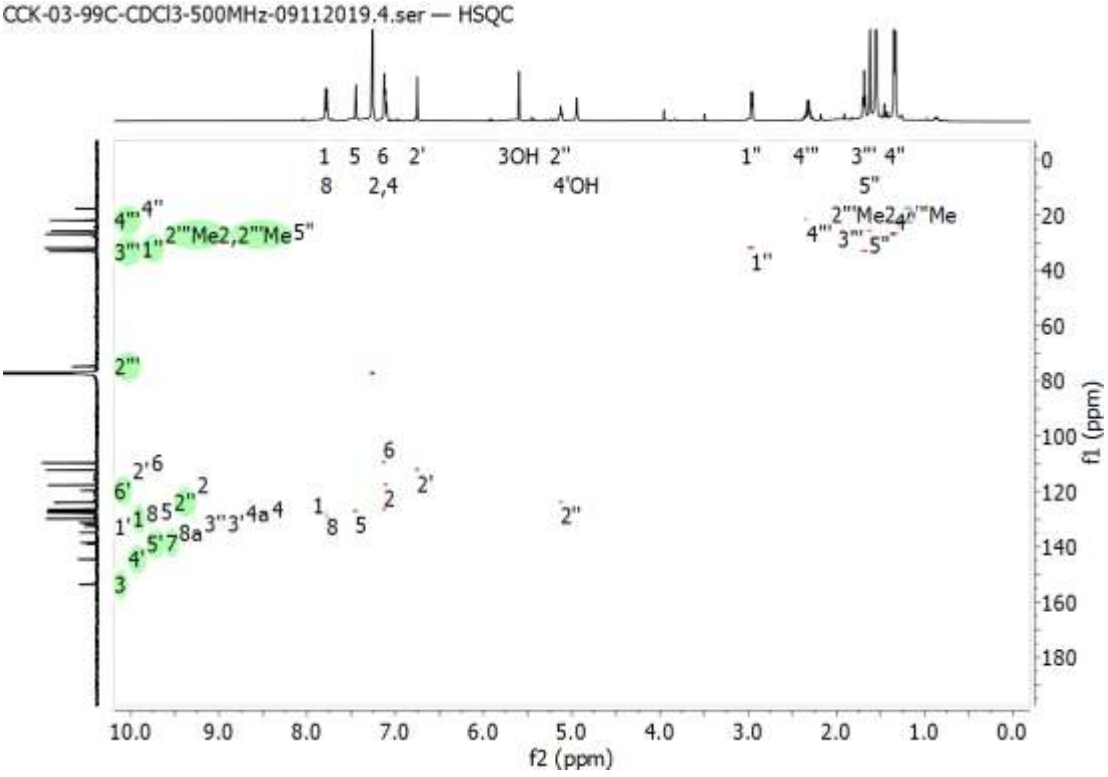

Appendix 8E: HMBC (500 MHz, $CDCl_3$, 25°C) spectrum of usambarin H (**117**)

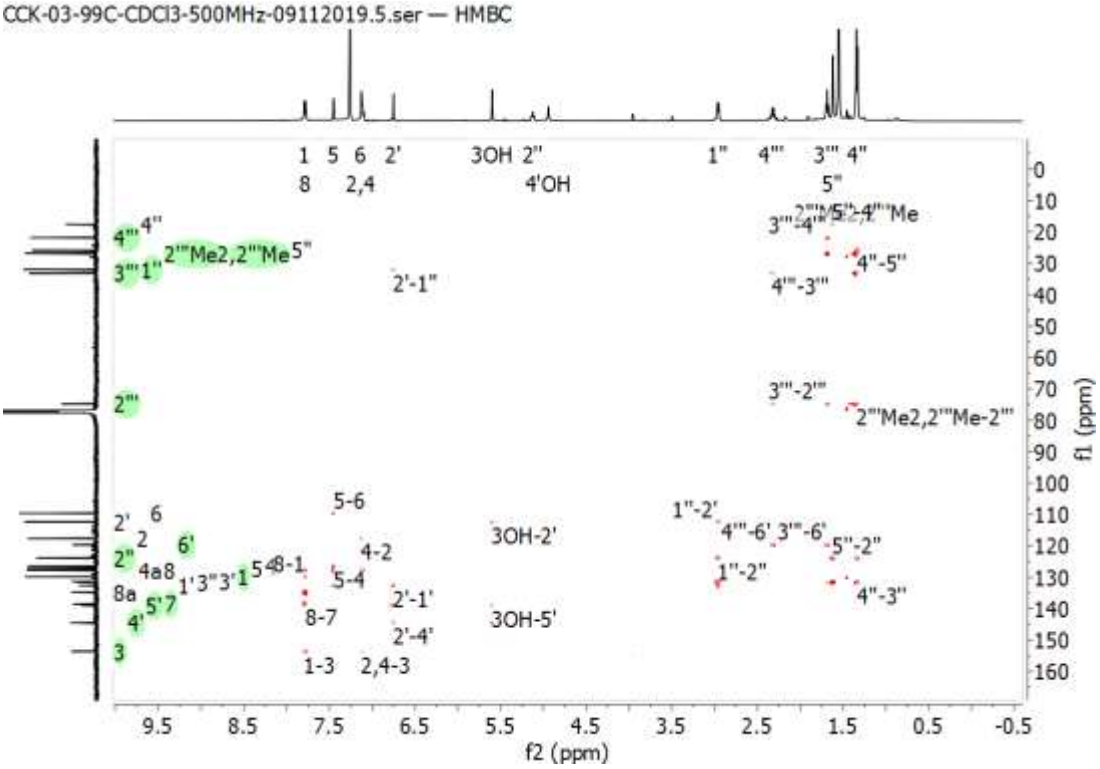

Appendix 8F: NOESY (500 MHz, $CDCl_3$, 25°C) spectrum of usambarin H (**117**)

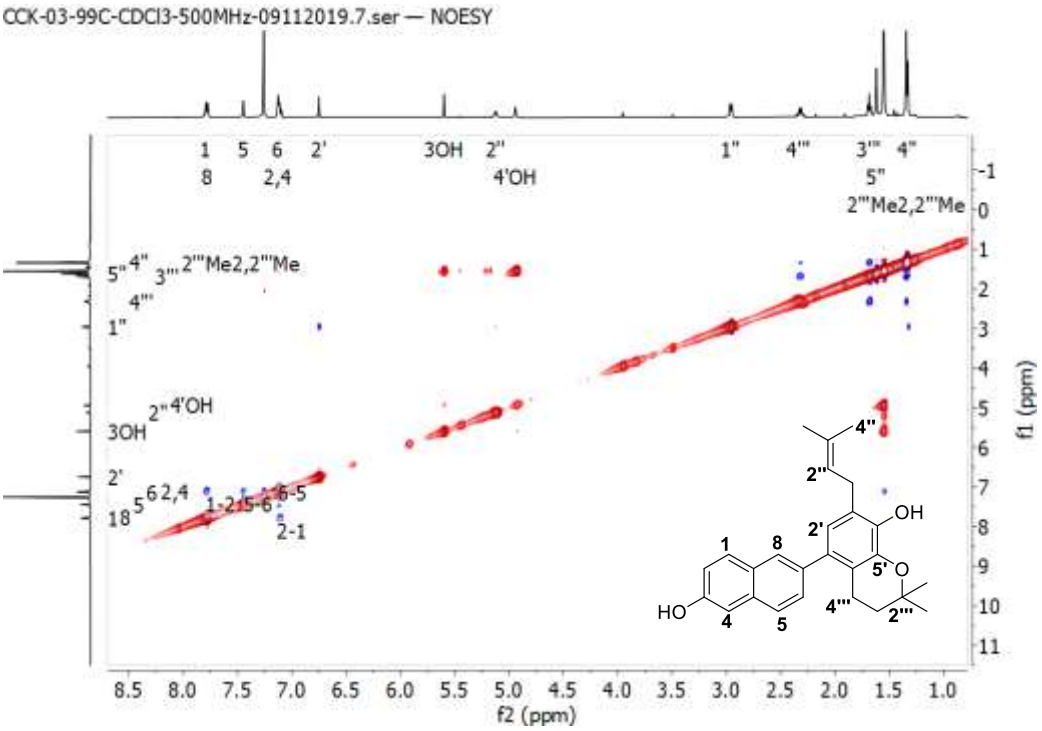

Appendix 8G. TOCSY (500 MHz, $CDCl_3$, 25°C) spectrum of usambarin H (**117**)

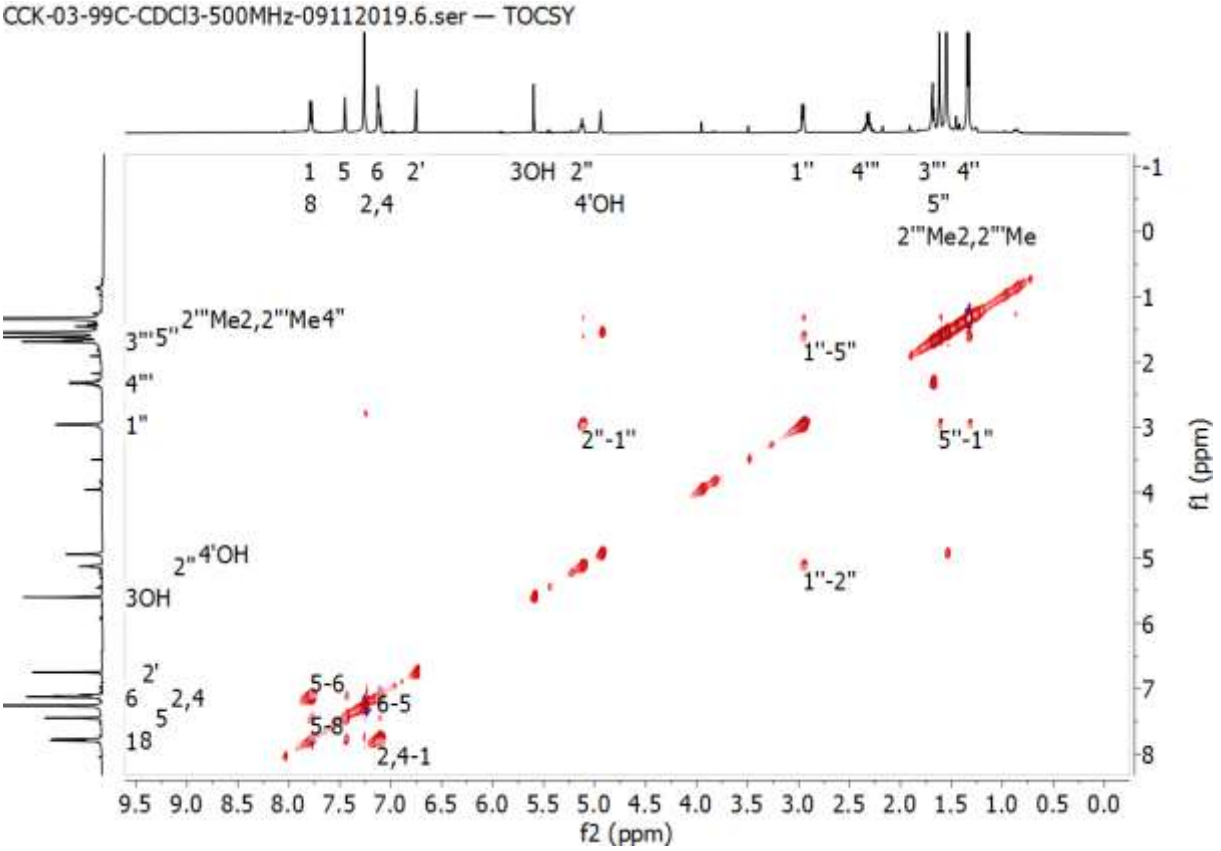

Appendix 8H. HRMS spectrum of usambarin H (**117**)

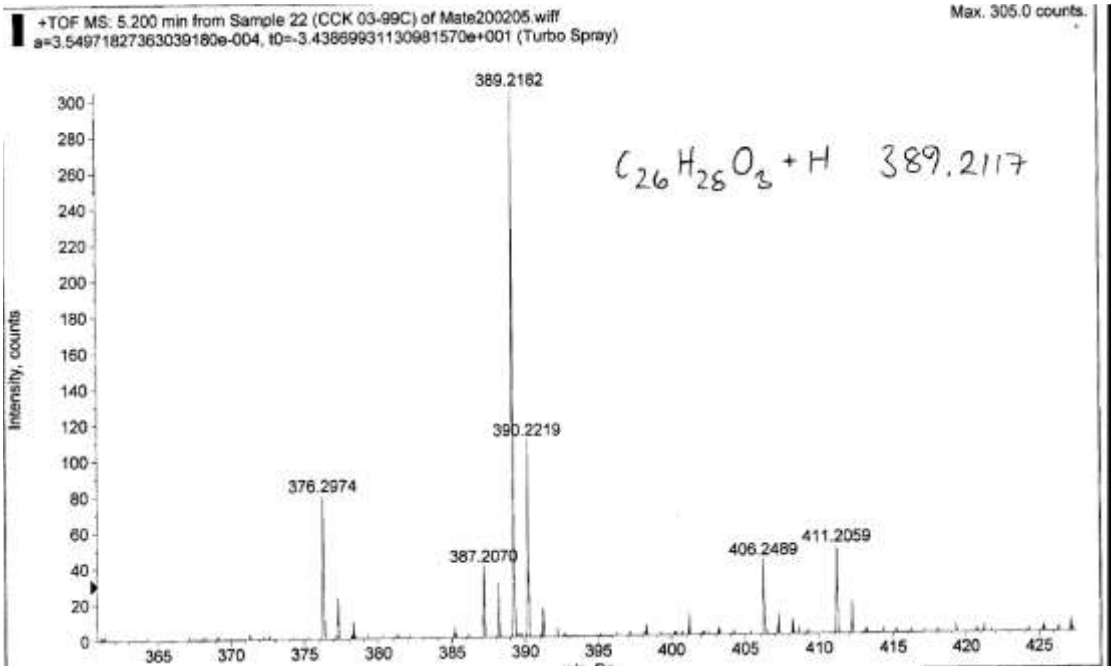

Appendix 9A: ^{1}H NMR (500 MHz, $CDCl_3$, 25°C) spectrum of usambarin I (118)

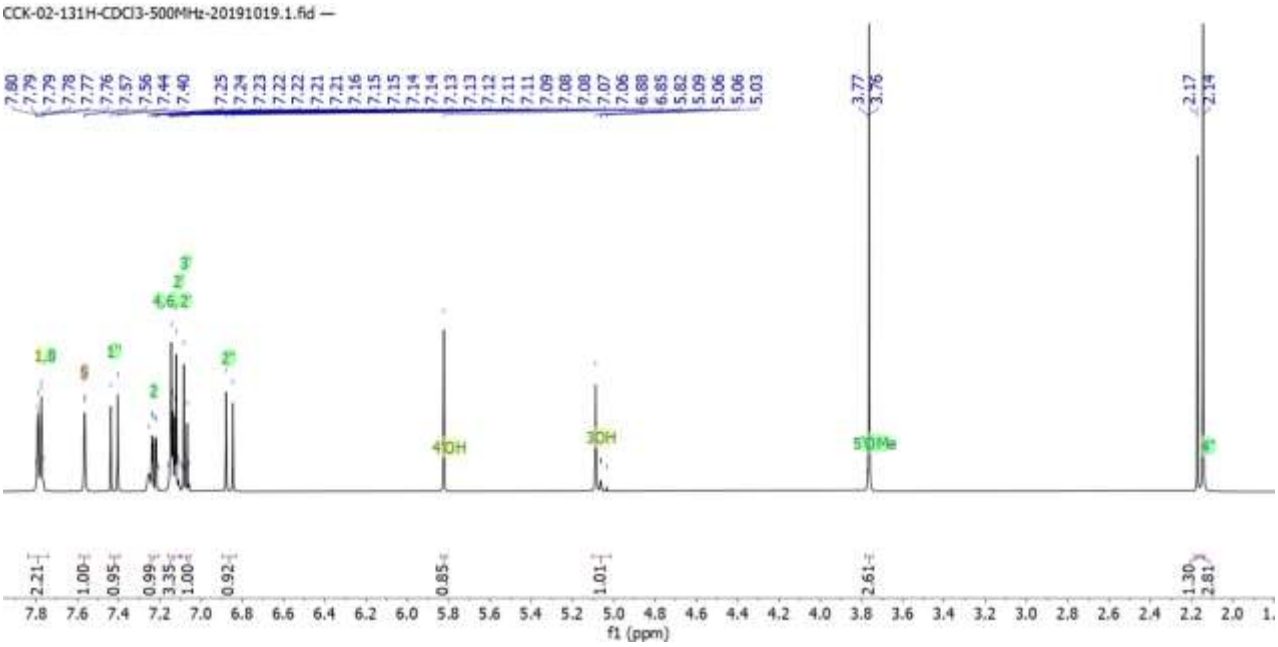

Appendix 9B. ^{13}C NMR (500 MHz, $CDCl_3$, 25°C) spectrum of usambarin I (**118)**

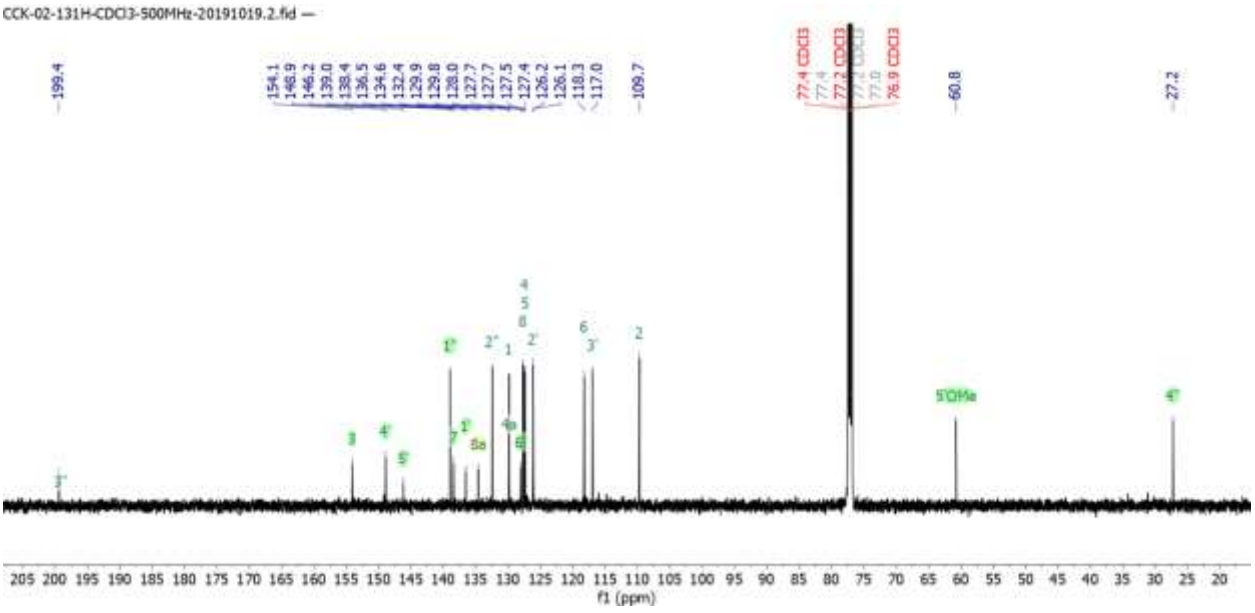

Appendix 9C. COSY (500 MHz, $CDCl_3$, 25°C) spectrum of usambarin I (**118)**

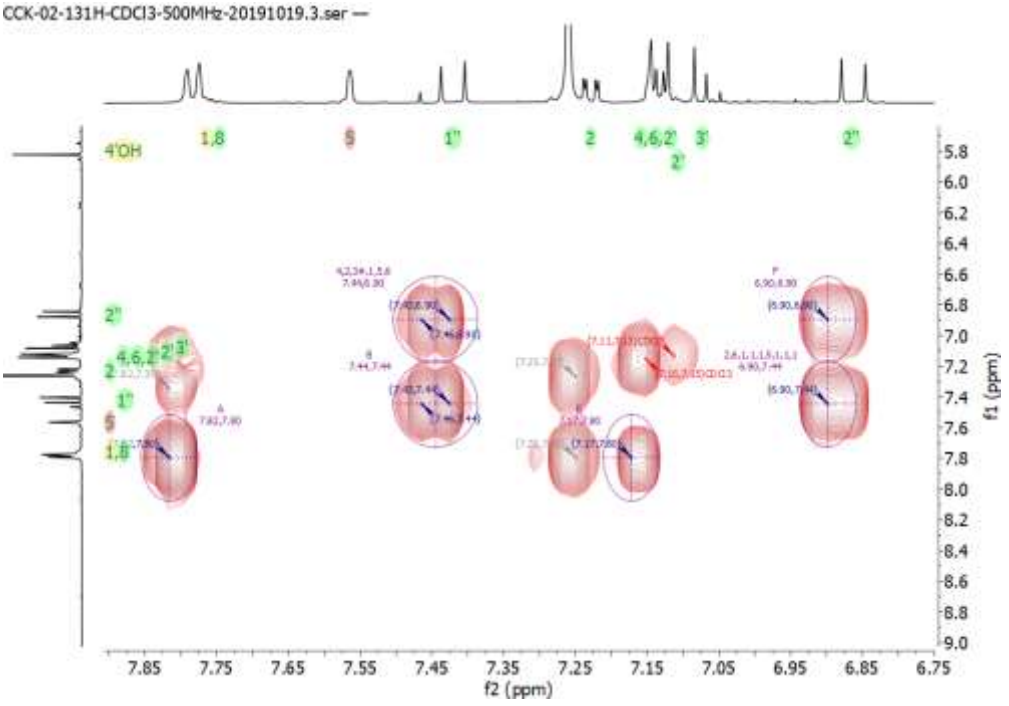

Appendix 9D: HSQC (500 MHz, $CDCl_3$, 25°C) spectrum of usambarin I (**118)**

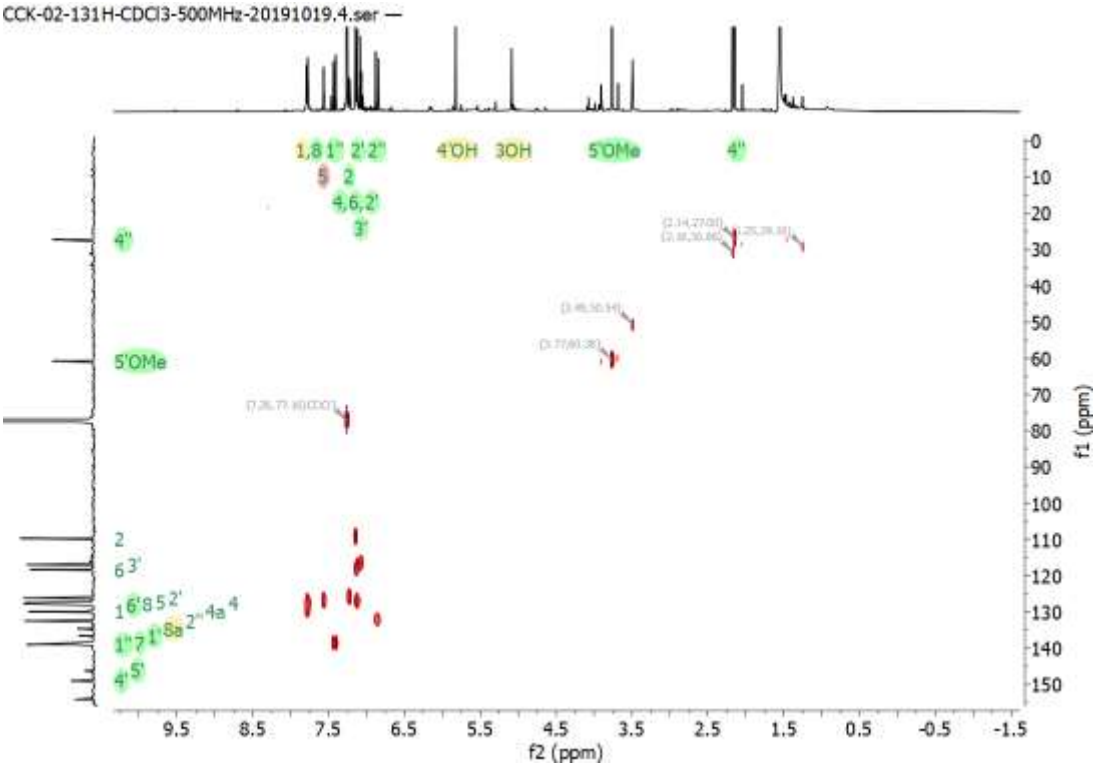

Appendix 9E: HMBC (500 MHz, $CDCl_3$, 25°C) spectrum of usambarin I (**118)**

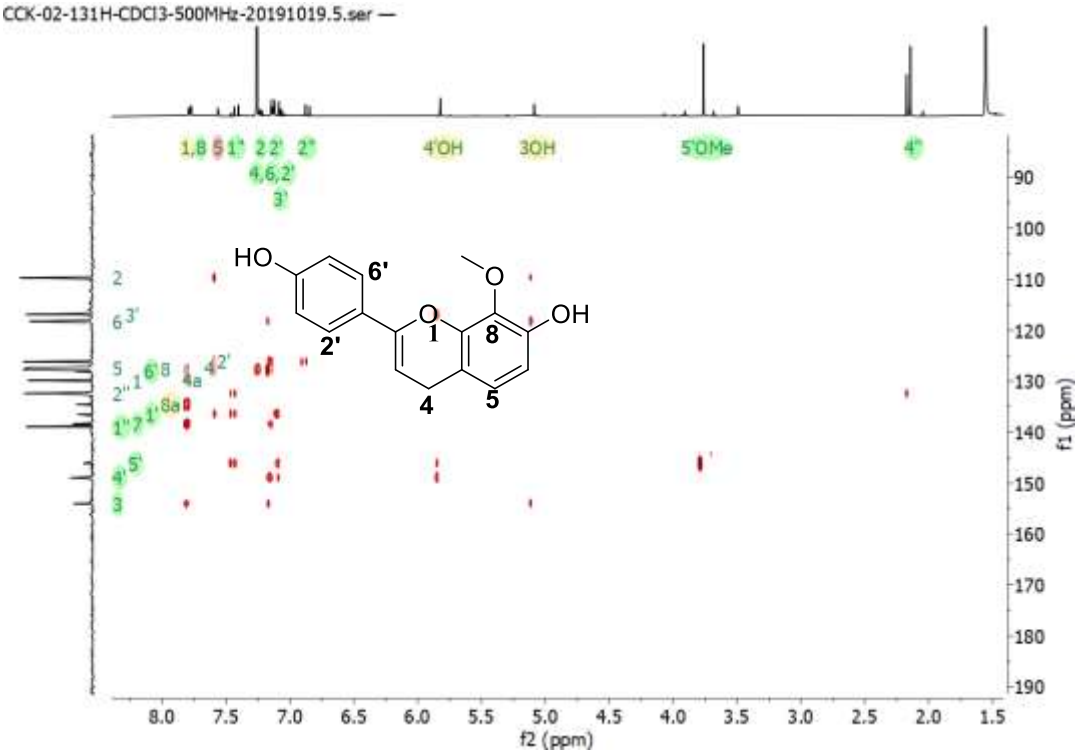

Appendix 10A: ^{1}H NMR (600 MHz, DMSO, 25°C) spectrum of usambarin J (119)

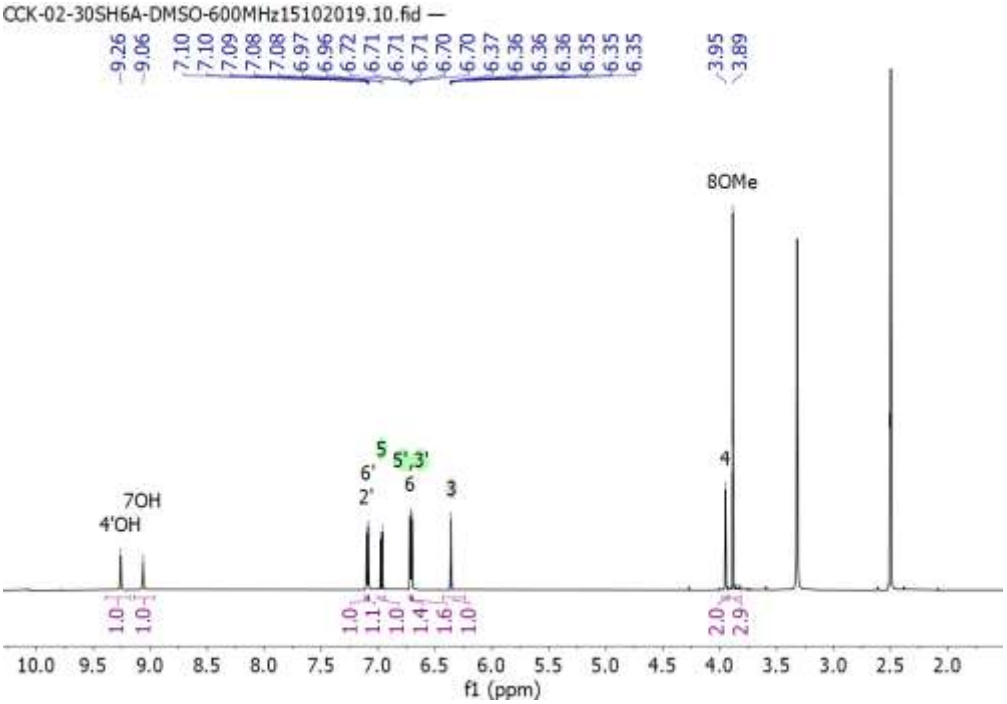

Appendix 10B: ^{13}C NMR (600 MHz, DMSO, 25°C) spectrum of **usambarin J (119)**

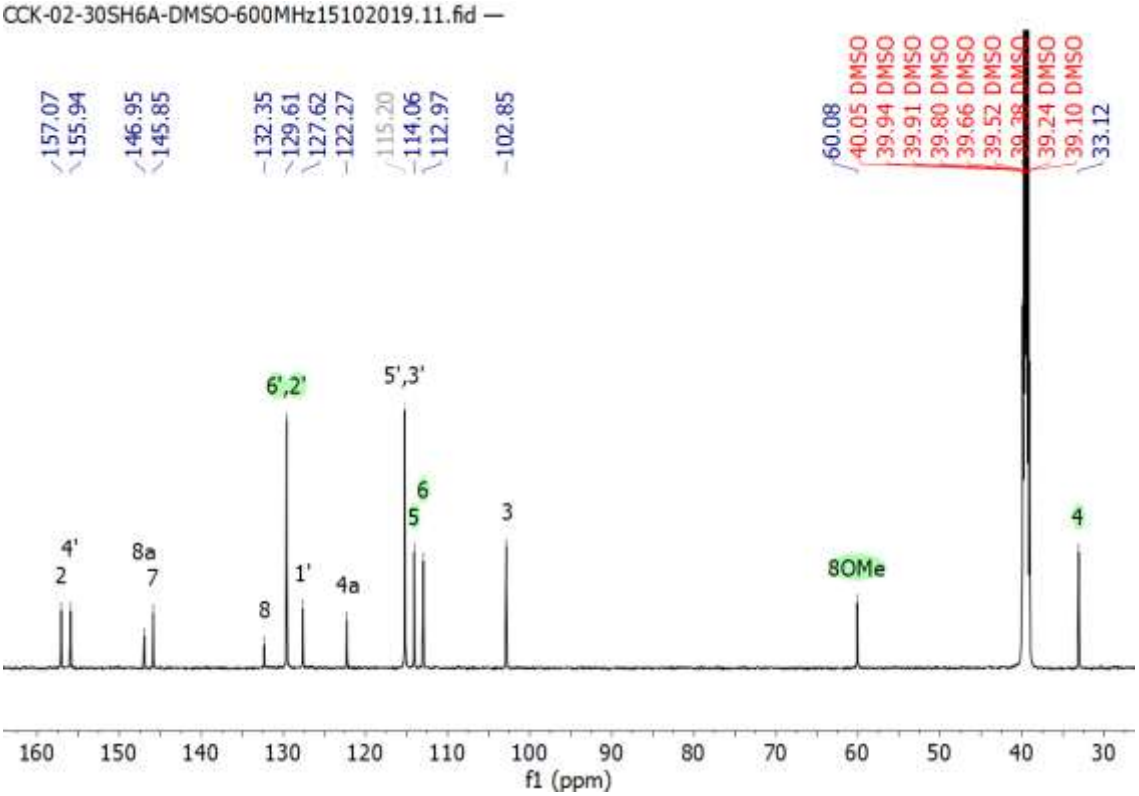

Appendix 10C: COSY (600 MHz, DMSO, 25°C) spectrum of **usambarin J (119)**

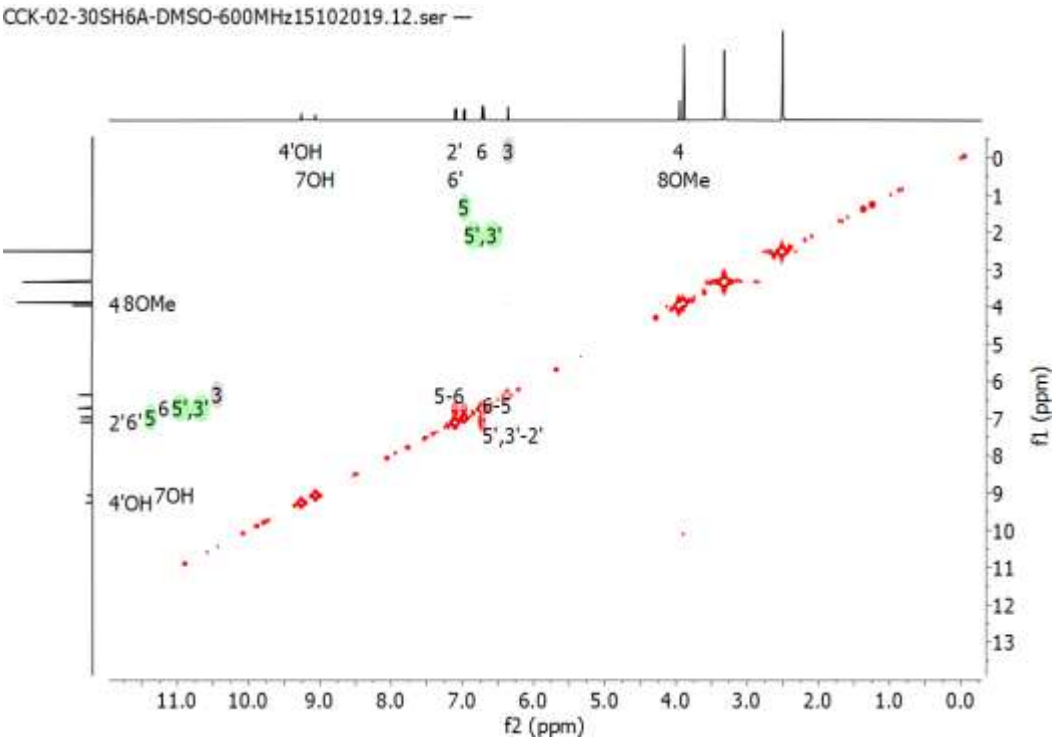

Appendix 10D: HSQC (600 MHz, DMSO, 25°C) spectrum of **usambarin J (119)**

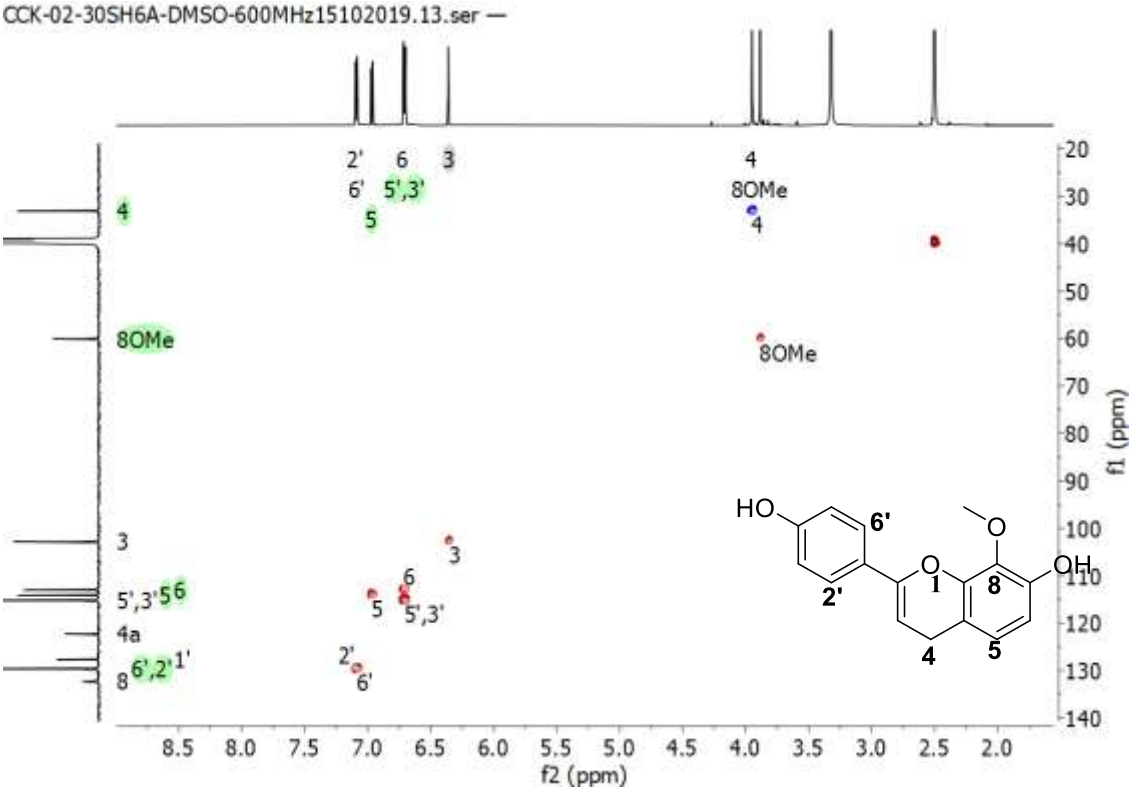

Appendix 10E: HMBC (600 MHz, DMSO, 25°C) spectrum of **usambarin J (119)**

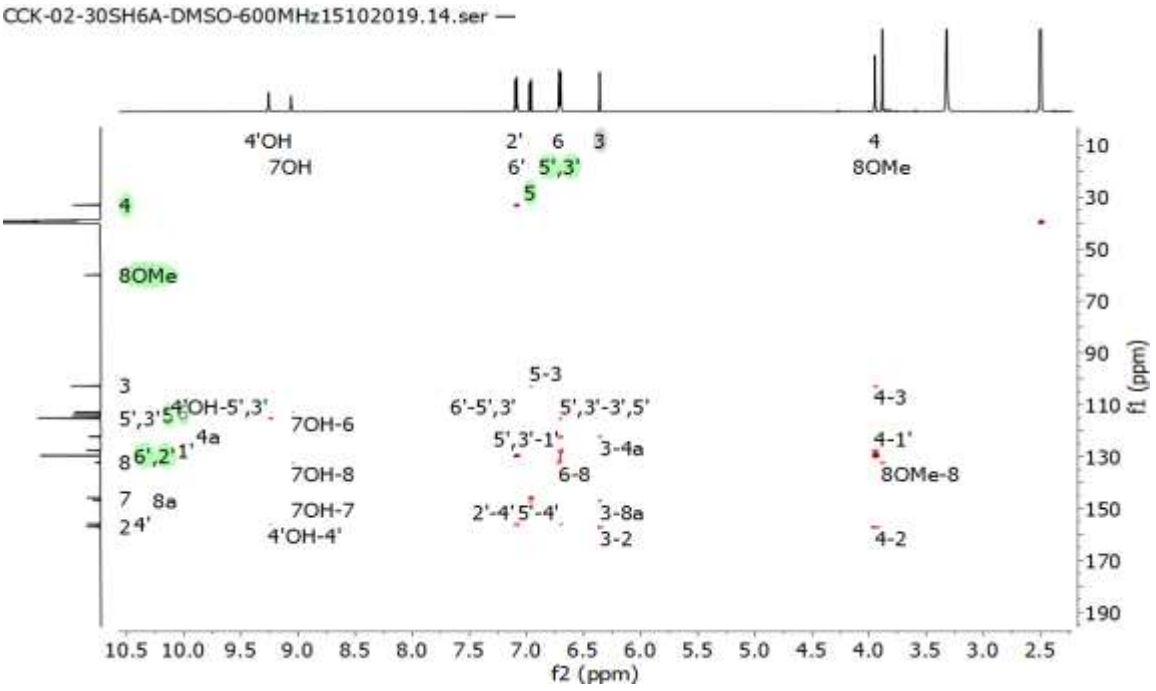

Appendix 10F: NOESY (600 MHz, DMSO, 25°C) spectrum of **usambarin J (119)**

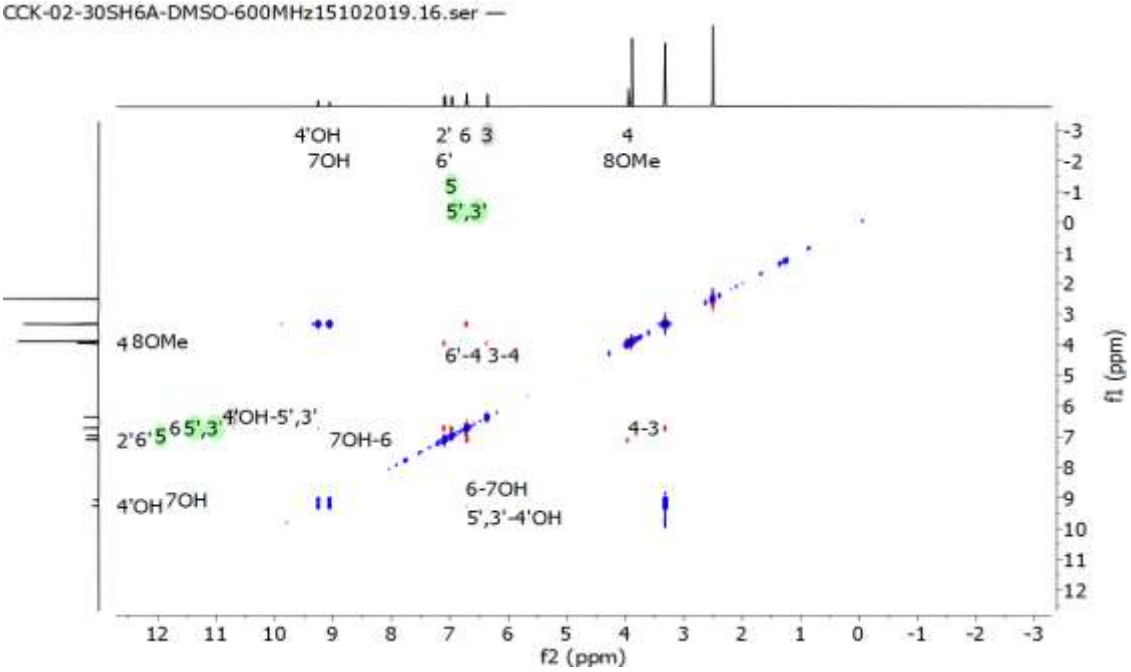

Appendix 10 G: TOCSY (600 MHz, DMSO, 25°C) spectrum of **usambarin J (119)**

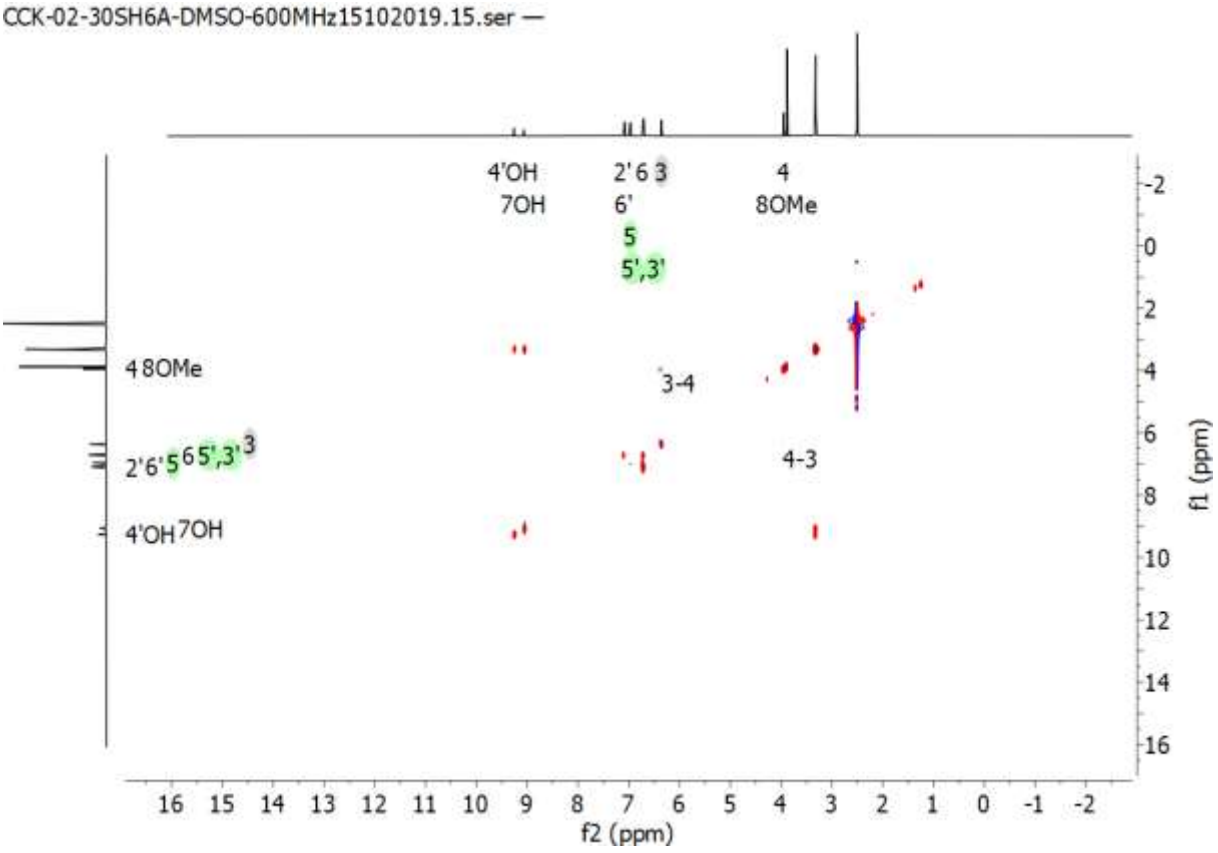

Appendix 10H: HRMS spectrum of **usambarin J (119)**

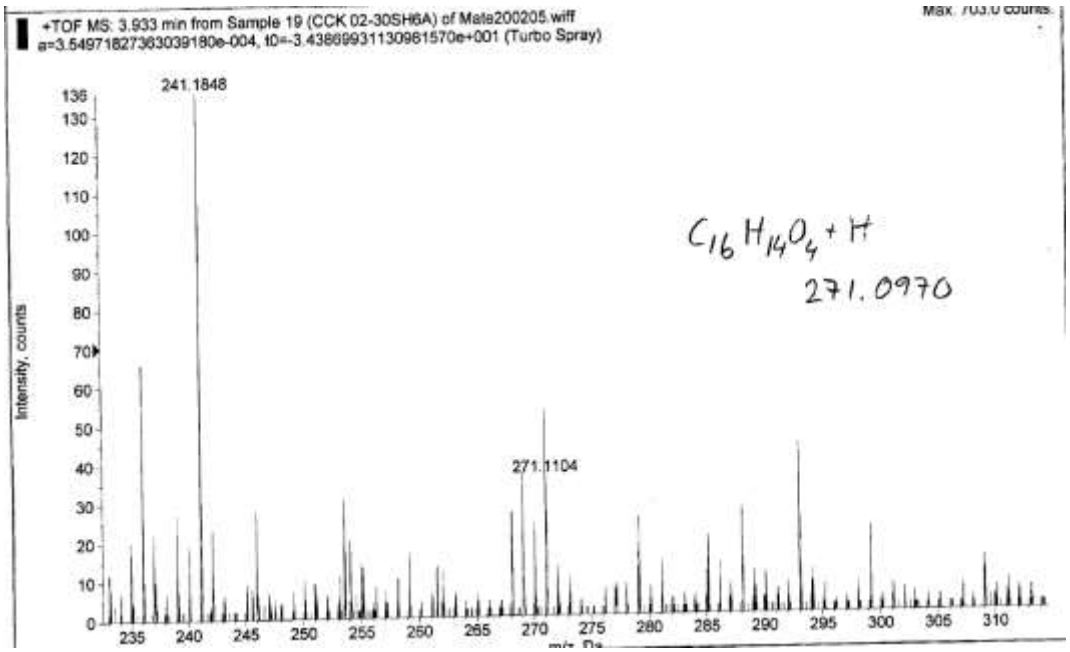

Appendix 11A: ^{1}H NMR (500 MHz, CDCl3, 25°C) spectrum of usambarin K (120)

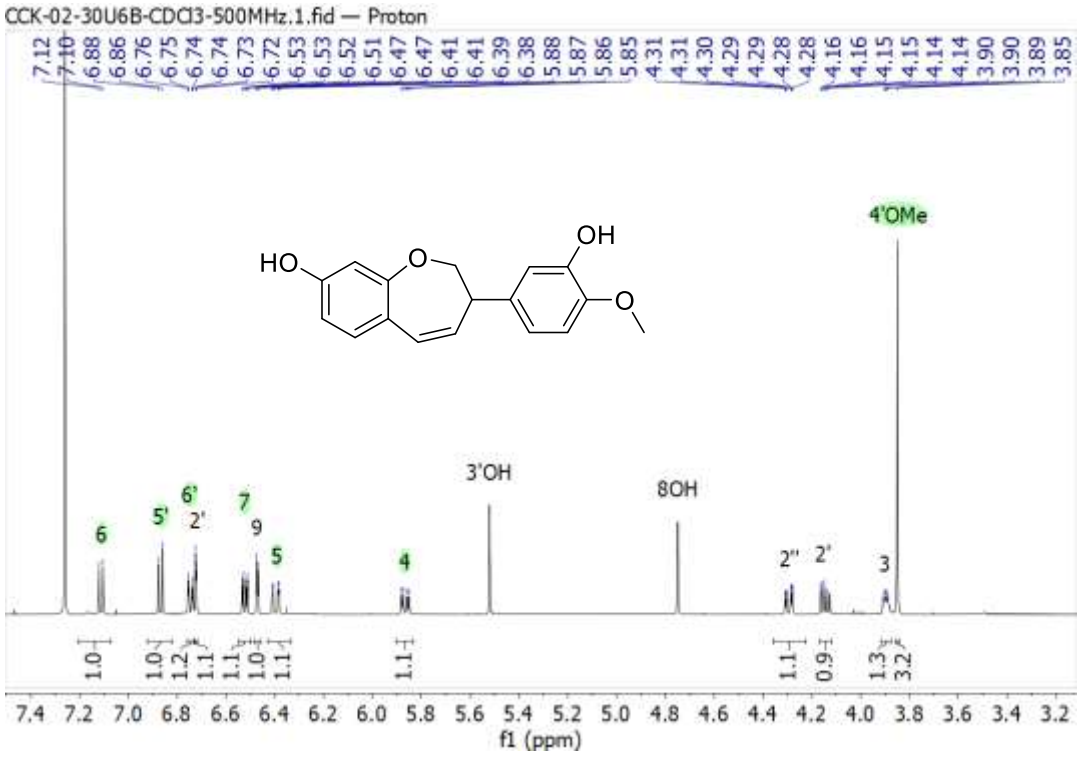

Appendix 11B: ^{13}C NMR (500 MHz, $CDCl_3$, 25°C) spectrum of **usambarin K (120)**

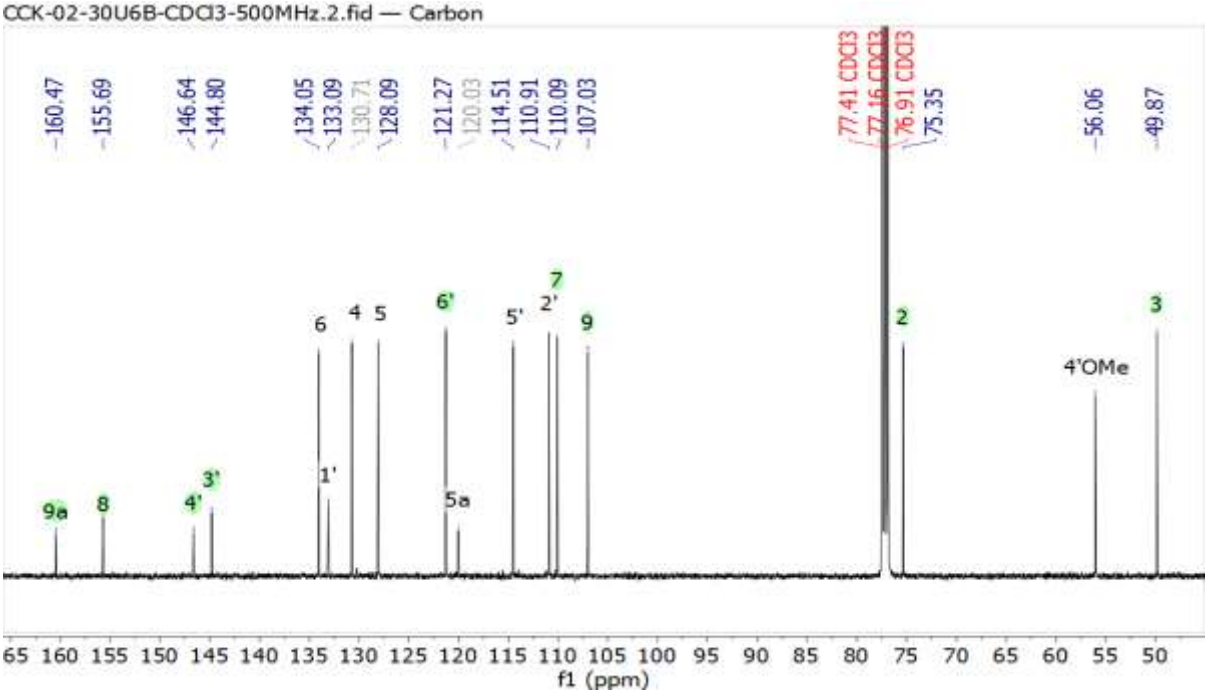

Appendix 11C: COSY (500 MHz, $CDCl_3$, 25°C) spectrum of **usambarin K (120)**

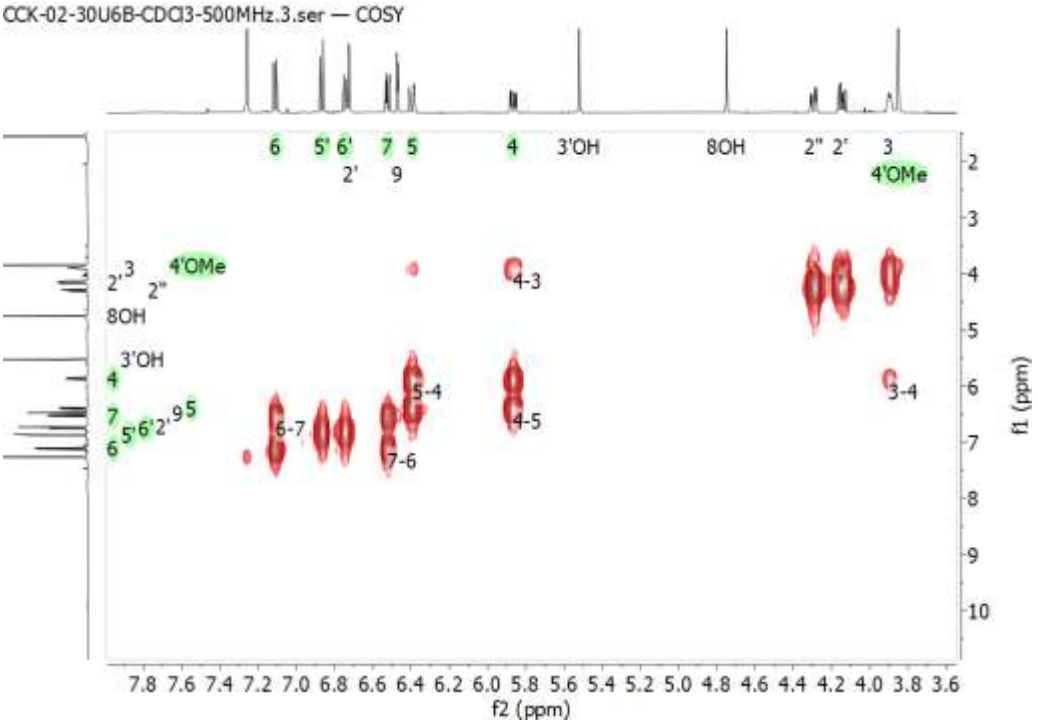

Appendix 11D. HSQC (500 MHz, $CDCl_3$, 25°C) spectrum of **usambarin K (120)**

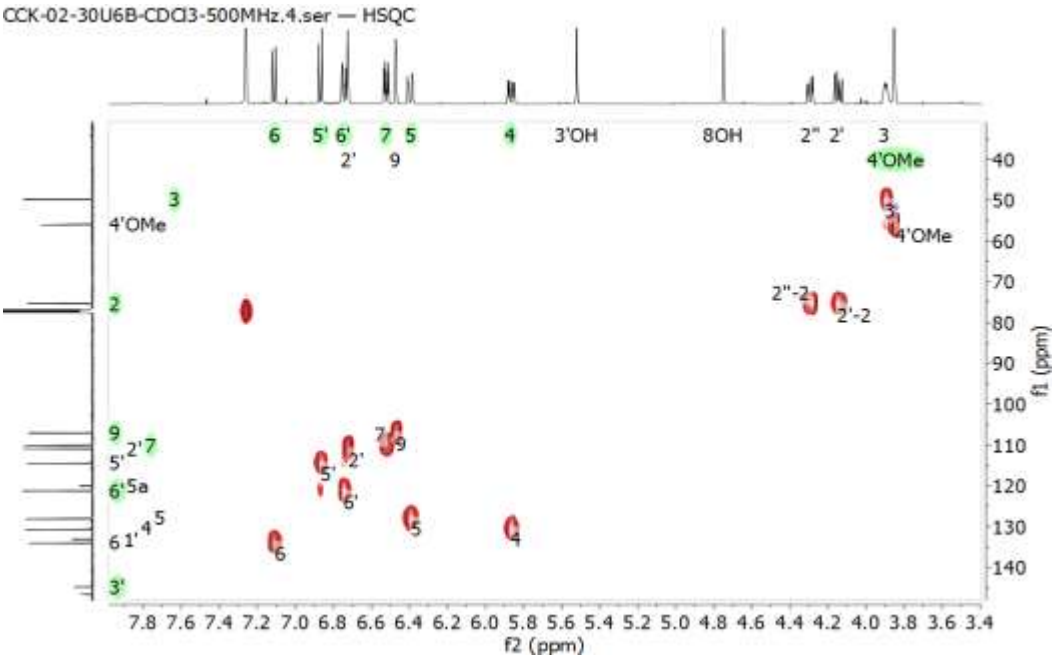

Appendix 11E: HMBC (500 MHz, $CDCl_3$, 25°C) spectrum of **usambarin K (120)**

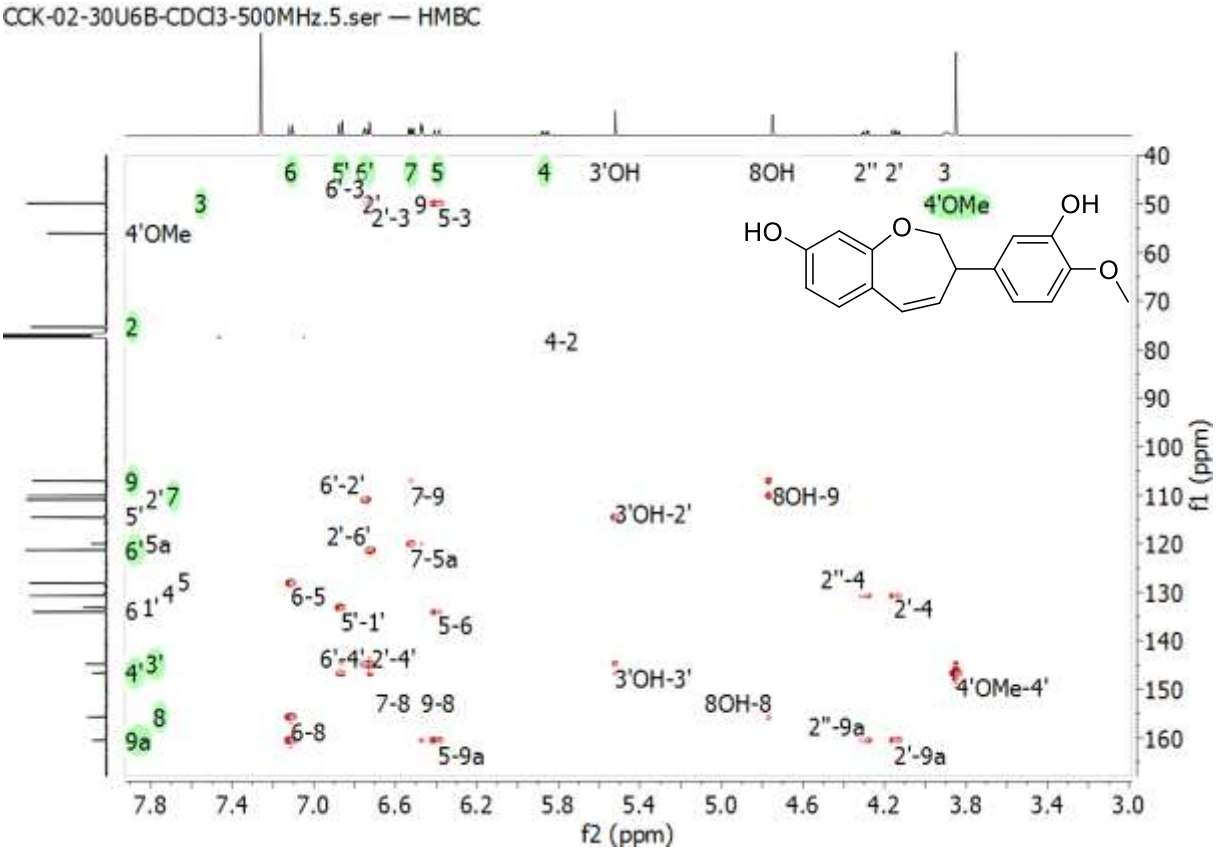

Appendix 11F. NOESY (500 MHz, $CDCl_3$, 25°C) spectrum of **usambarin K (120)**

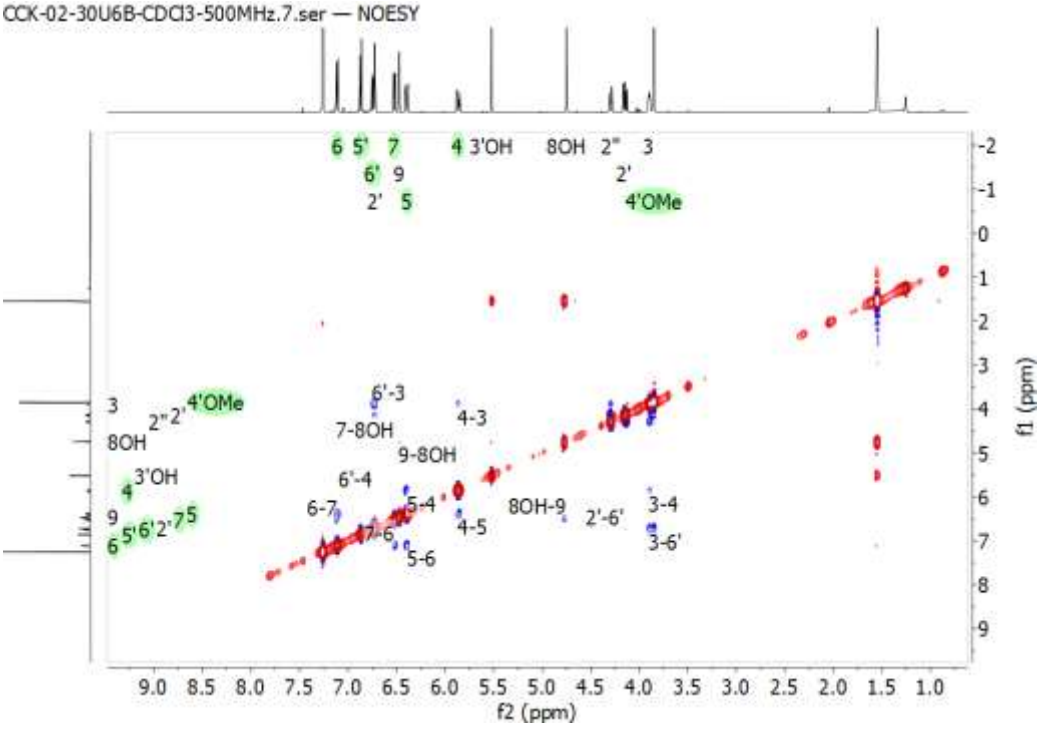

Appendix 11G. TOCSY (500 MHz, $CDCl_3$, 25°C) spectrum of **usambarin K (120)**

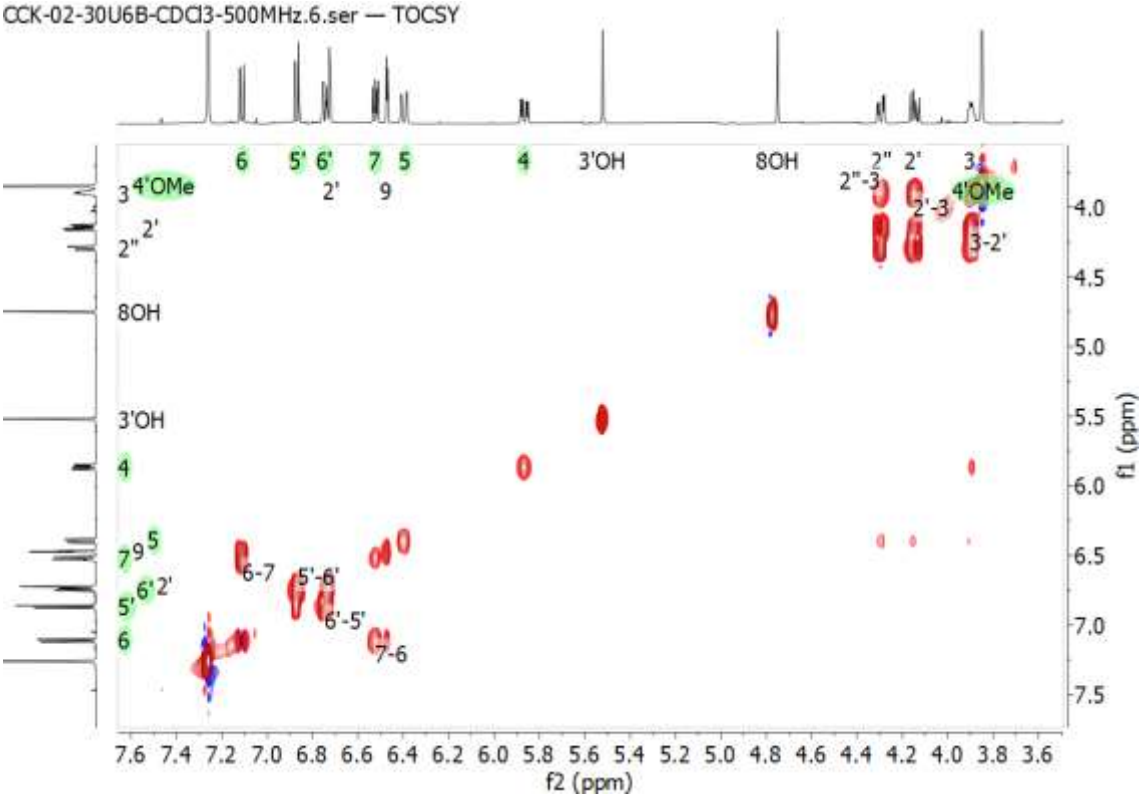

Appendix 11H. HRMS spectrum of **usambarin K (120)**

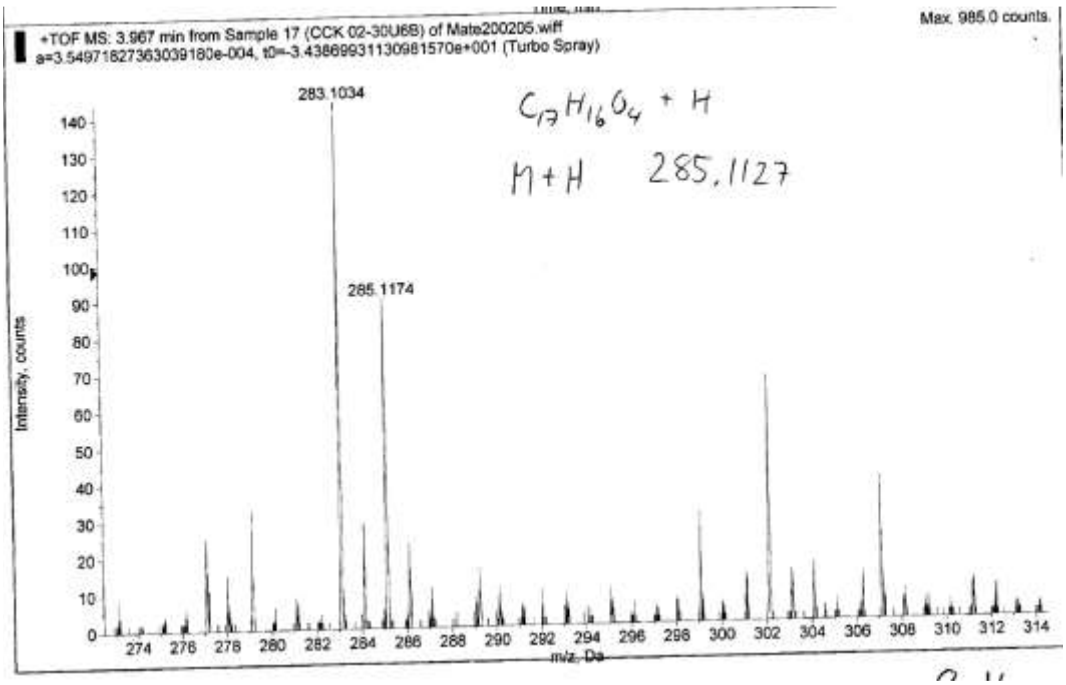

Appendix 12A: ^{1}H NMR (500 MHz, $CDCl_3$, 25°C) spectrum of Bergapten (121)

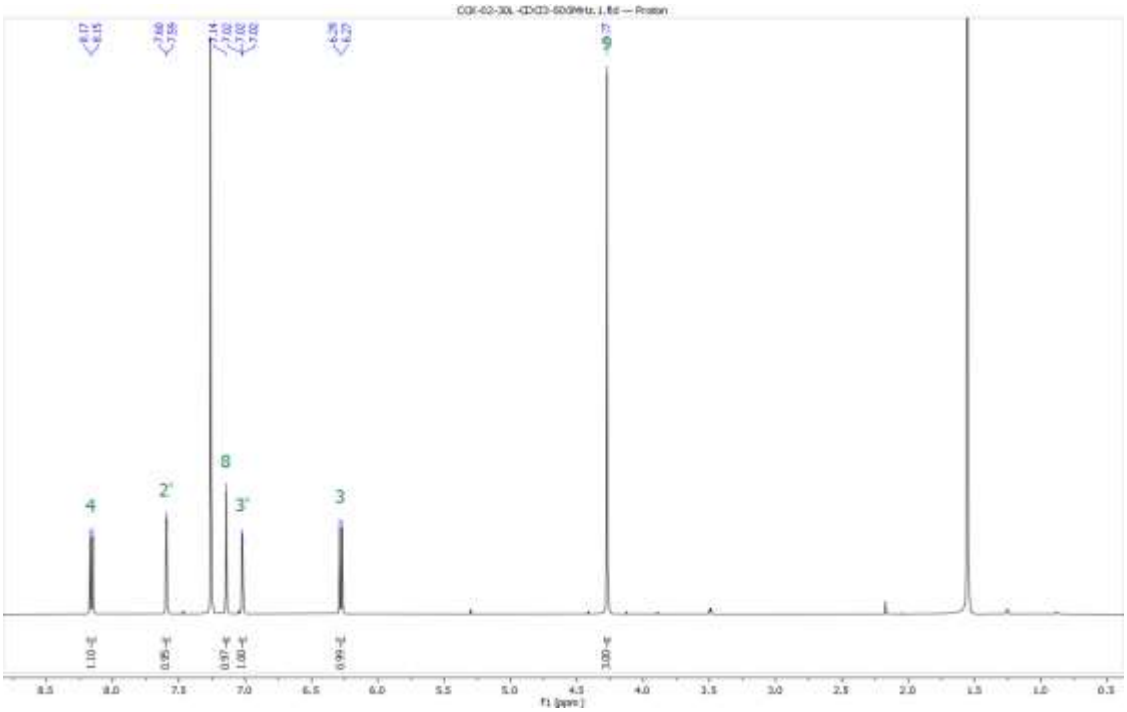

Appendix 12B. ^{13}C NMR (500 MHz, $CDCl_3$, 25°C) spectrum of bergapten (**121)**

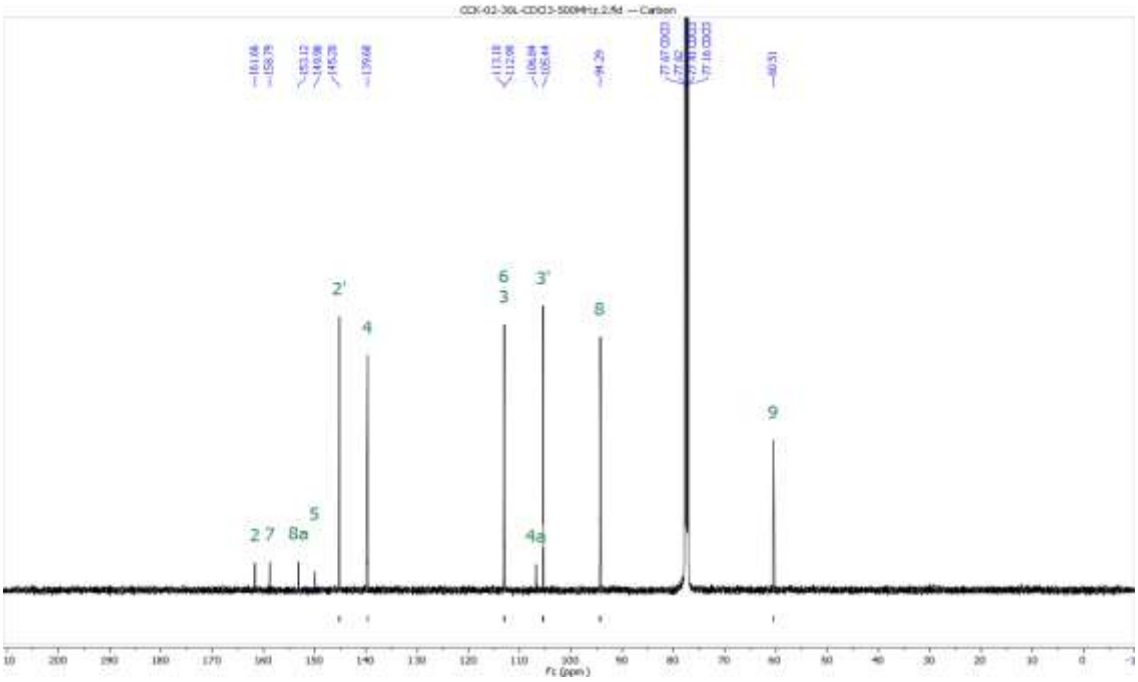

Appendix 12C. COSY (500 MHz, $CDCl_3$, 25°C) spectrum of bergapten (**121)**

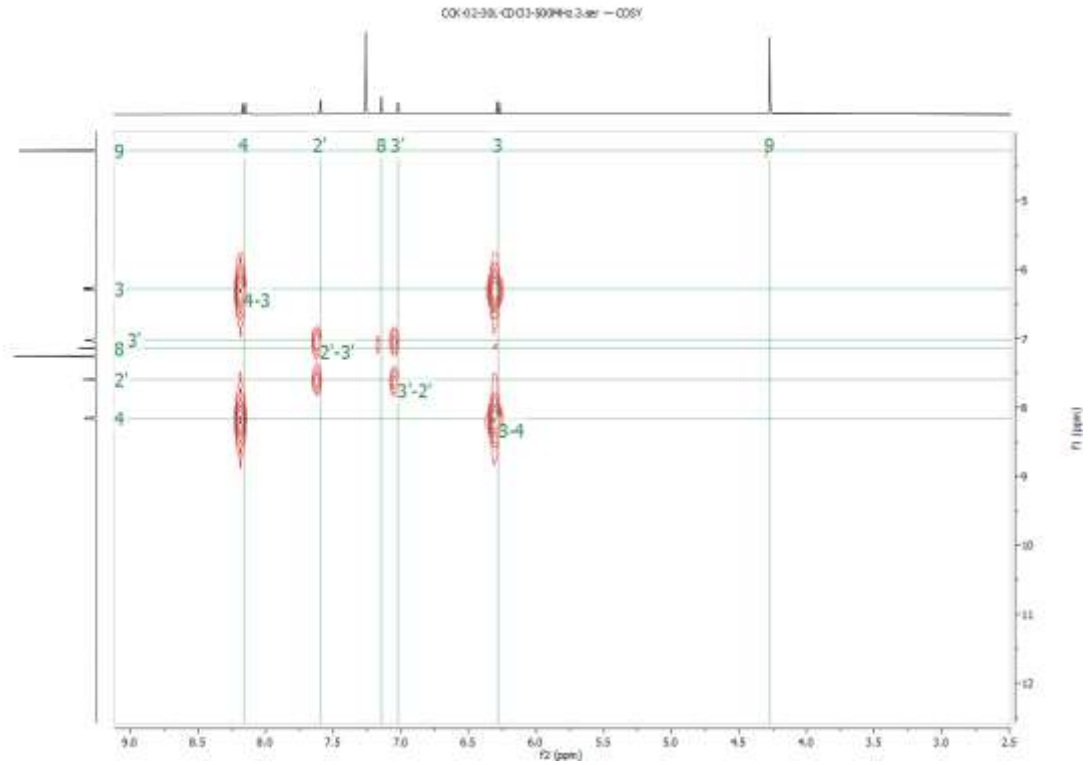

Appendix 12D: HSQC (500 MHz, $CDCl_3$, 25°C) spectrum of bergapten (**121)**

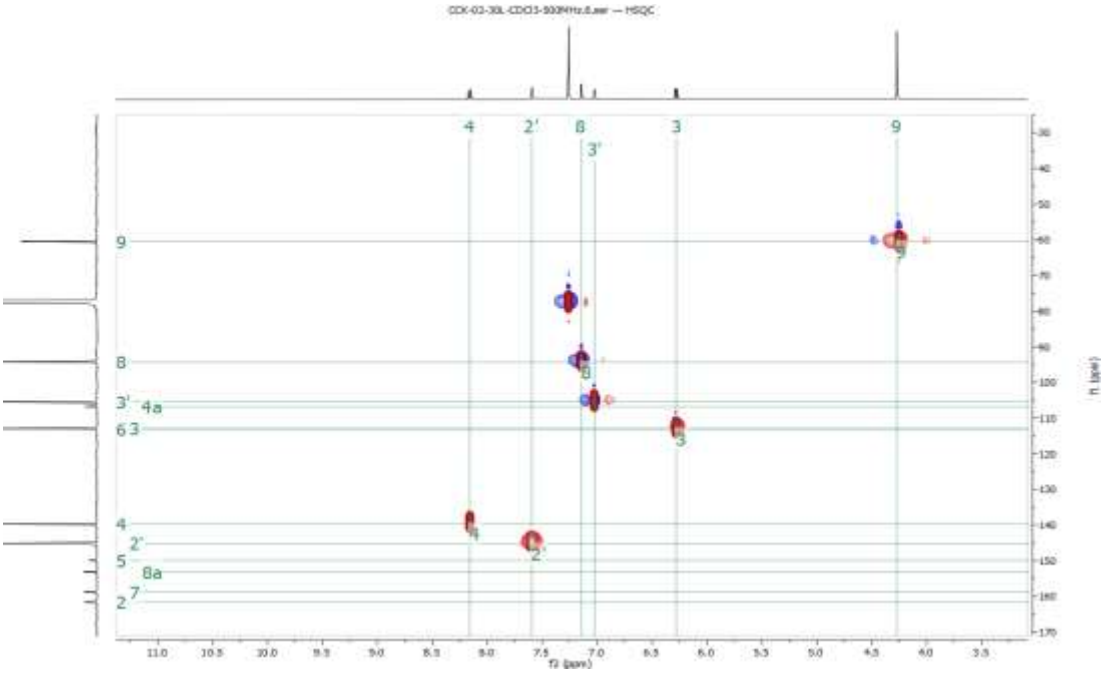

Appendix 12E: HMBC (500 MHz, $CDCl_3$, 25°C) spectrum of bergapten (**121)**

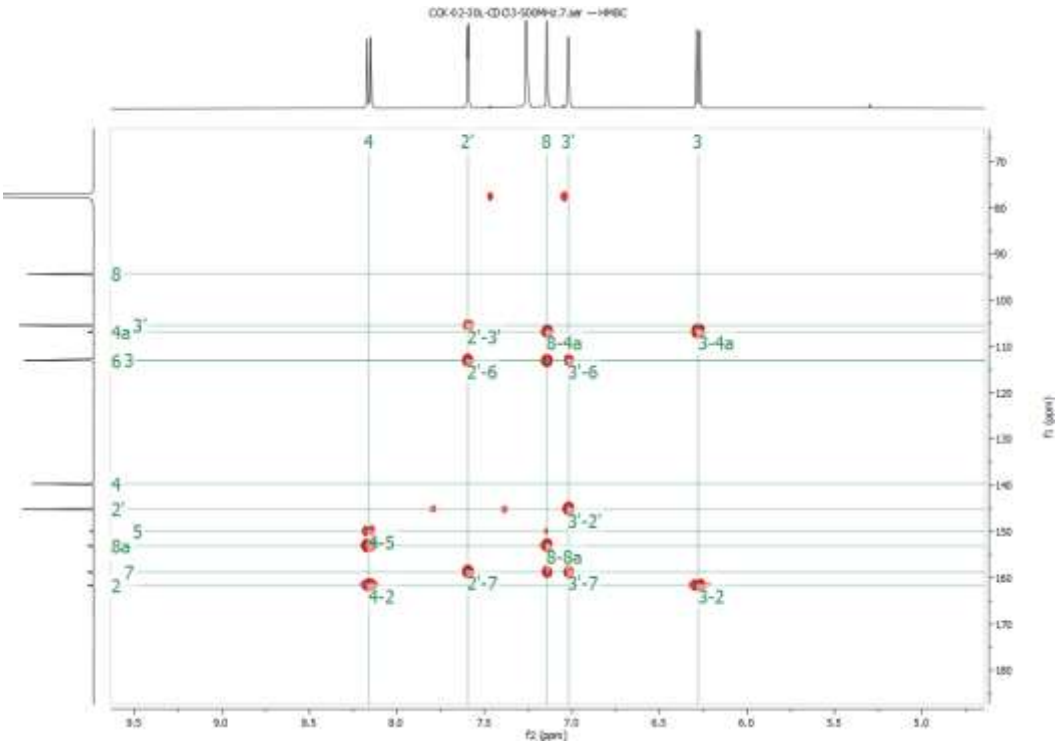

Appendix 12F: NOESY (500 MHz, $CDCl_3$, 25°C) spectrum of bergapten (**121)**

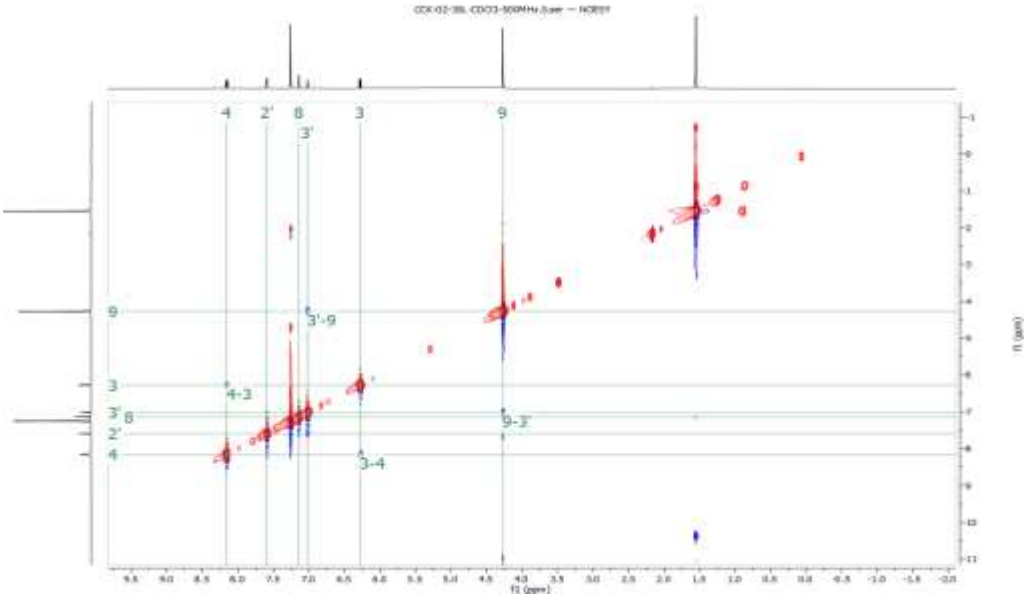

Appendix 12G. TOCSY (500 MHz, $CDCl_3$, 25°C) spectrum of bergapten (**121)**

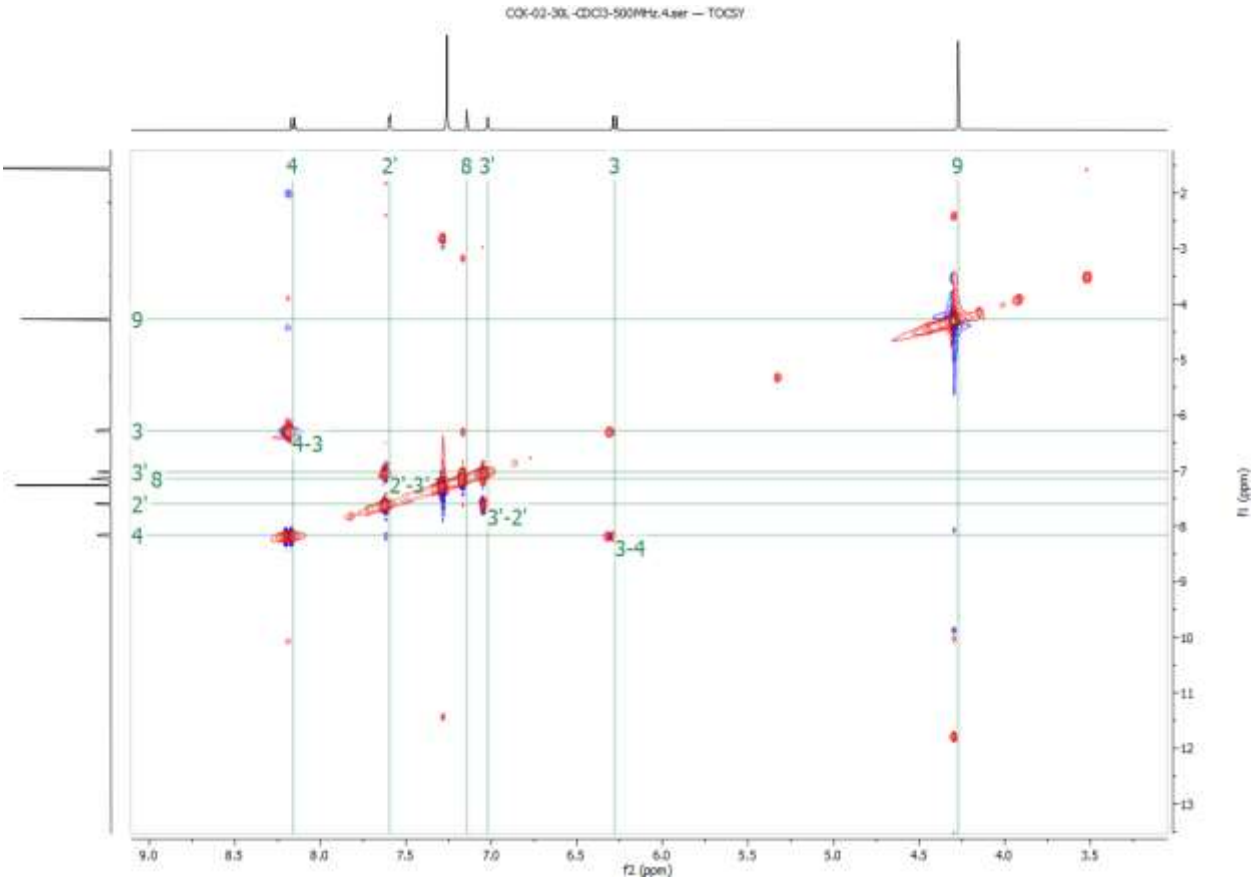

Appendix 12H: Uv spectrum of bergapten (**121)**

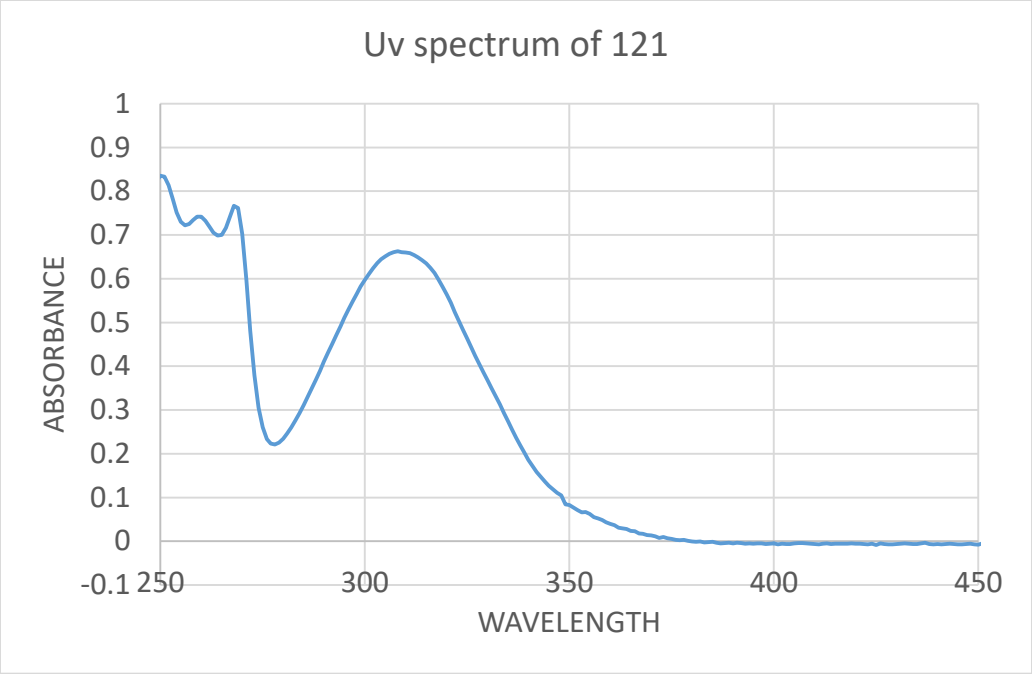

Appendix 13A: ^{1}H NMR (500 MHz, $CDCl_3$, 25°C) spectrum of Bergatol (122)

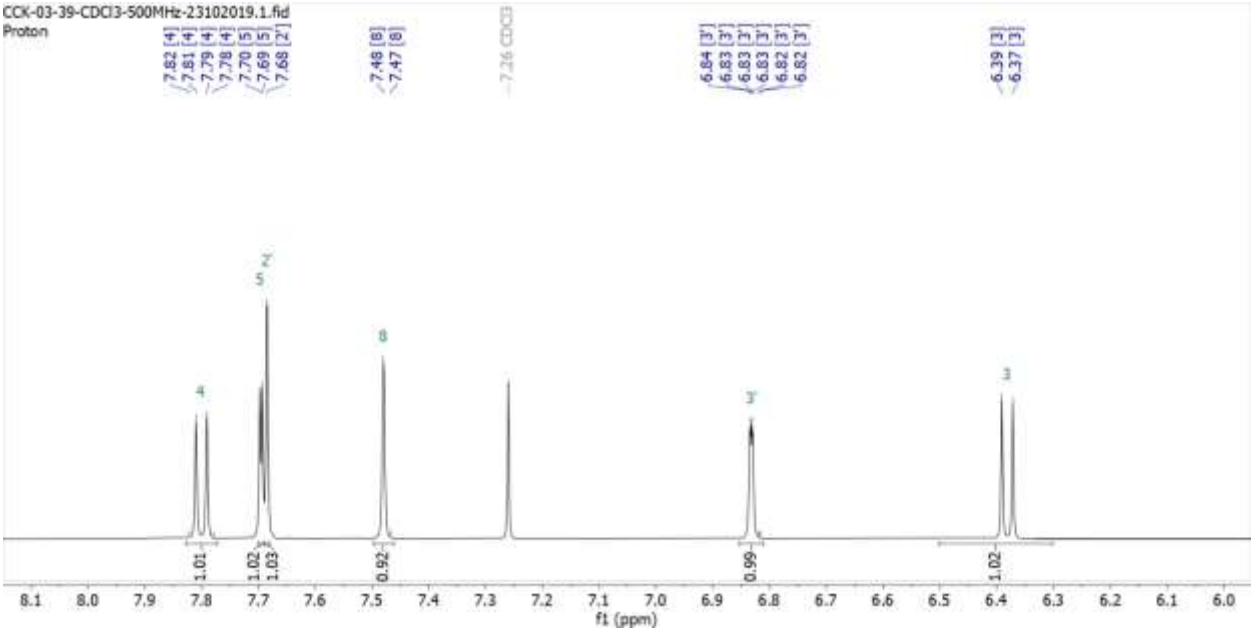

Appendix 13B. ^{13}C NMR (500 MHz, $CDCl_3$, 25°C) spectrum of Bergatol (**123**)

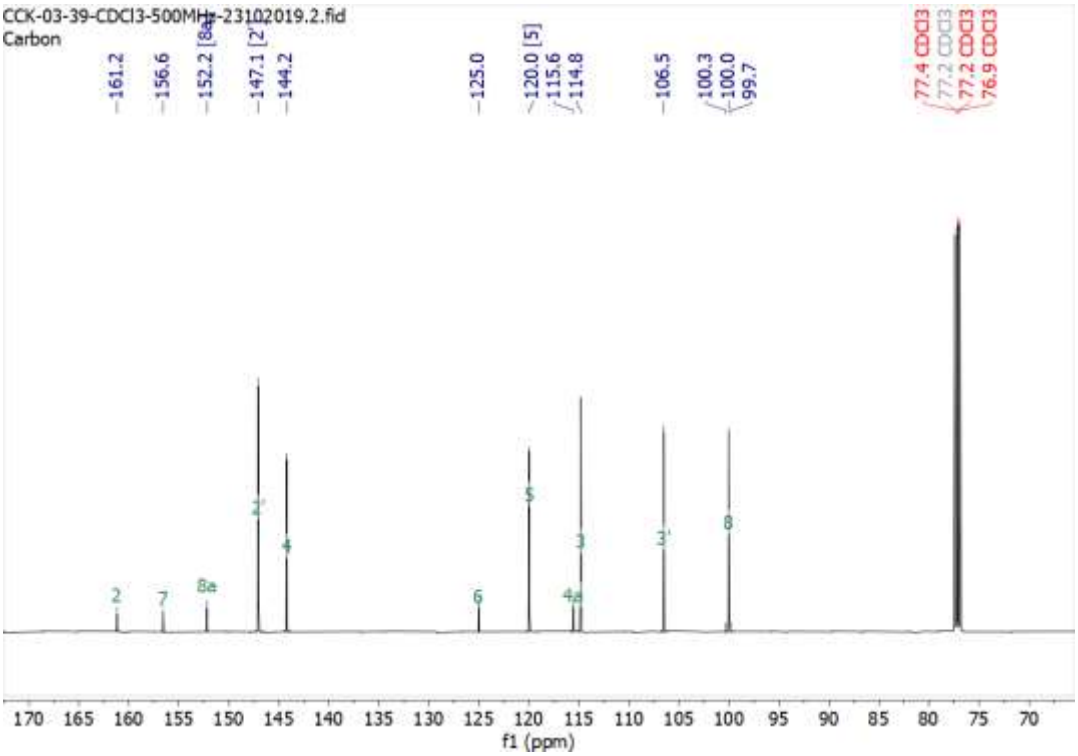

Appendix 13C. COSY (500 MHz, $CDCl_3$, 25°C) spectrum of Bergatol (**122**)

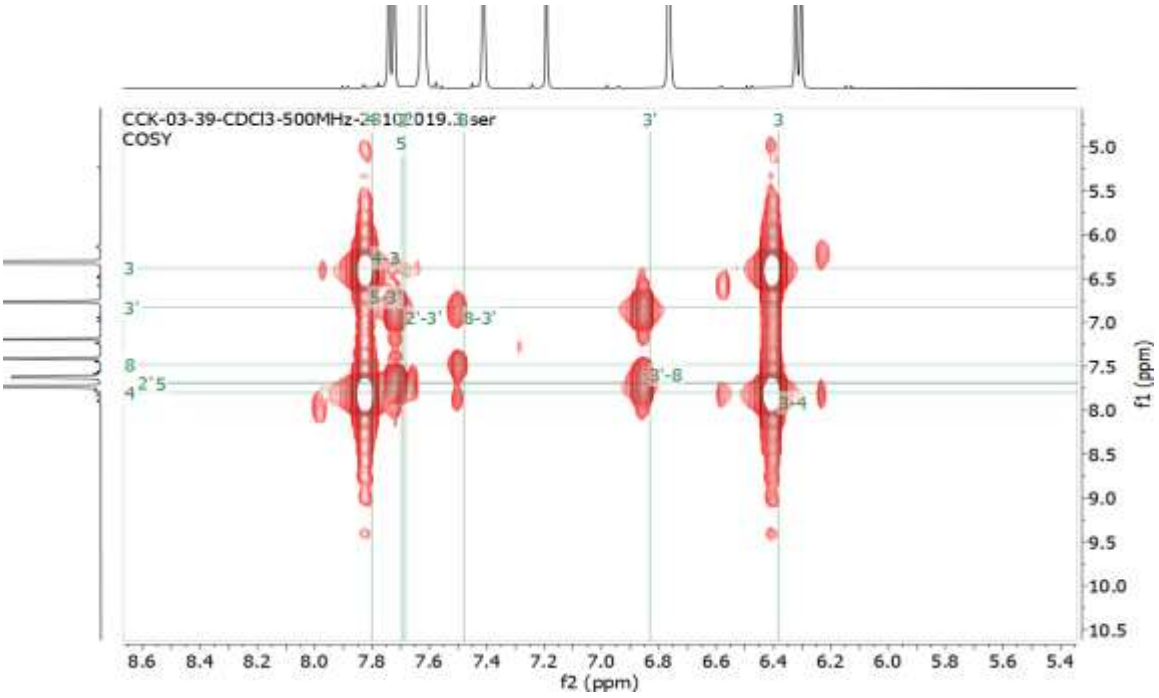

Appendix 13D: HSQC (500 MHz, $CDCl_3$, 25°C) spectrum of Bergatol (**122**)

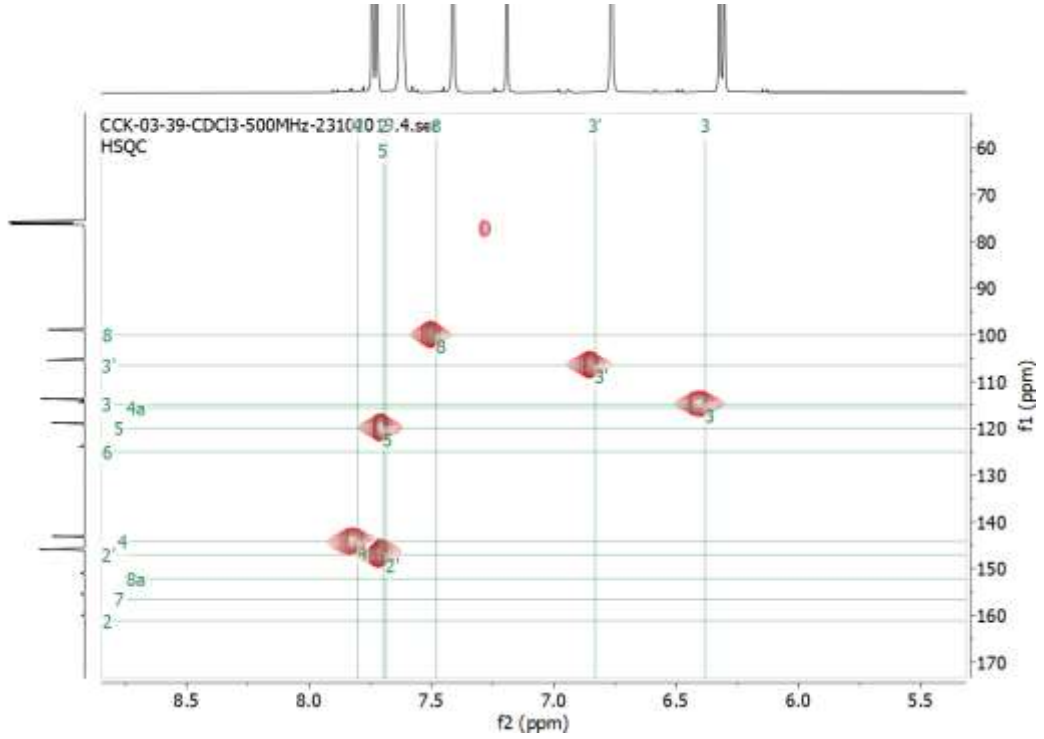

Appendix 13E: HMBC (500 MHz, $CDCl_3$, 25°C) spectrum of Bergatol (**122**)

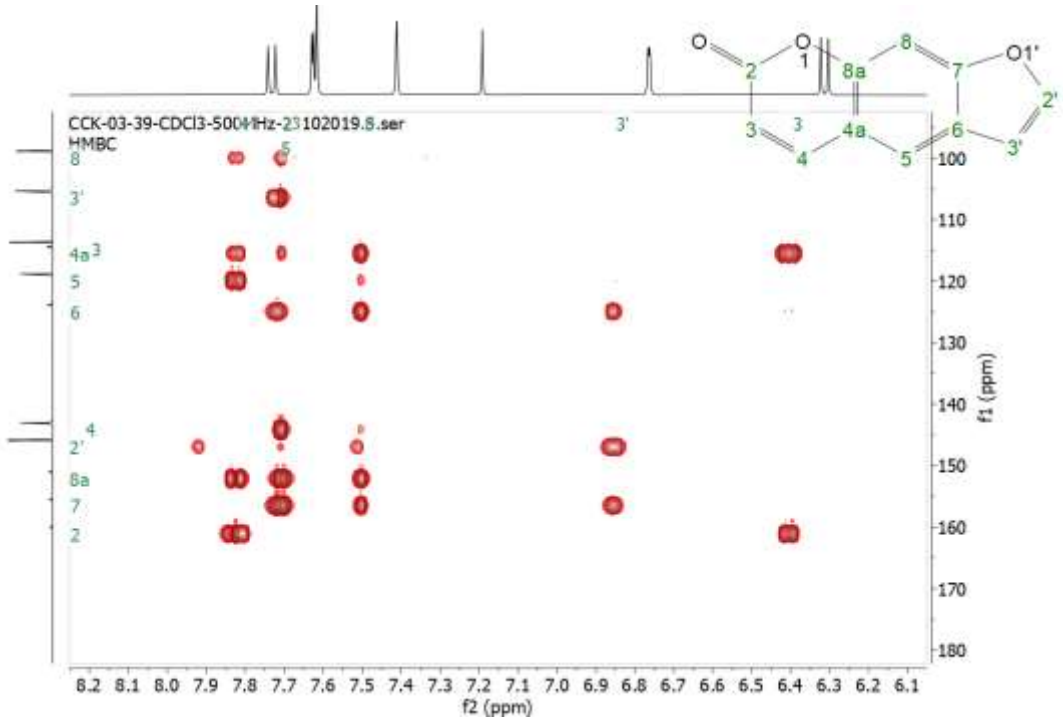

Appendix 14A: ^{1}H NMR (500 MHz, $CDCl_3$, 25°C) spectrum of 12a-hydroxydeguelin (123)

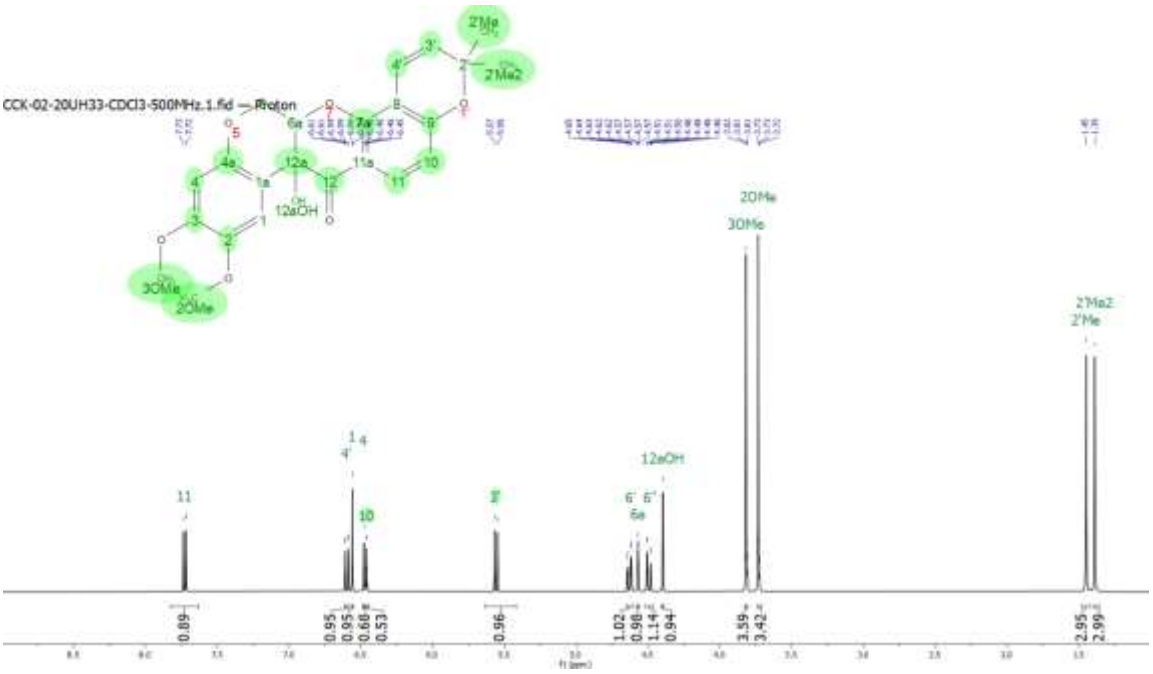

Appendix 14B. ^{13}C NMR (500 MHz, $CDCl_3$, 25°C) spectrum of 12a-hydroxydeguelin **(123)**

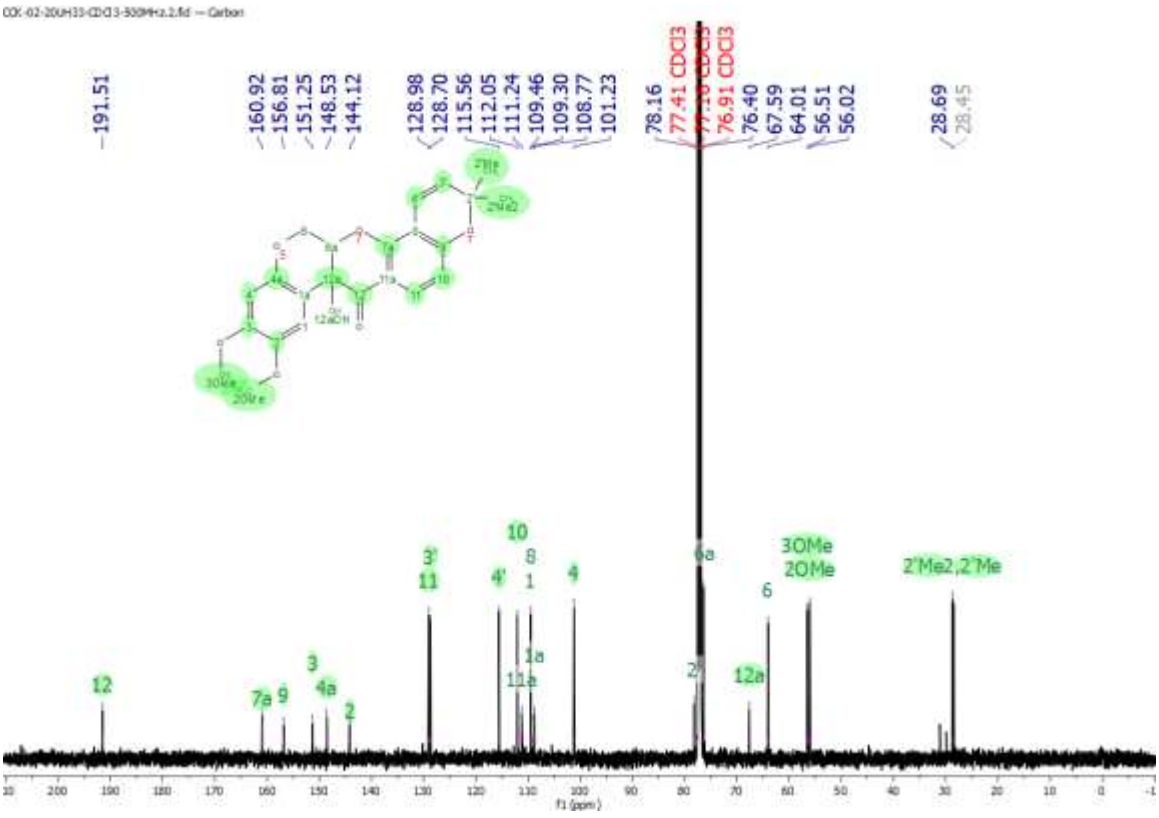

Appendix 14C. COSY (500 MHz, $CDCl_3$, 25°C) spectrum of 12a-hydroxydeguelin **(123)**

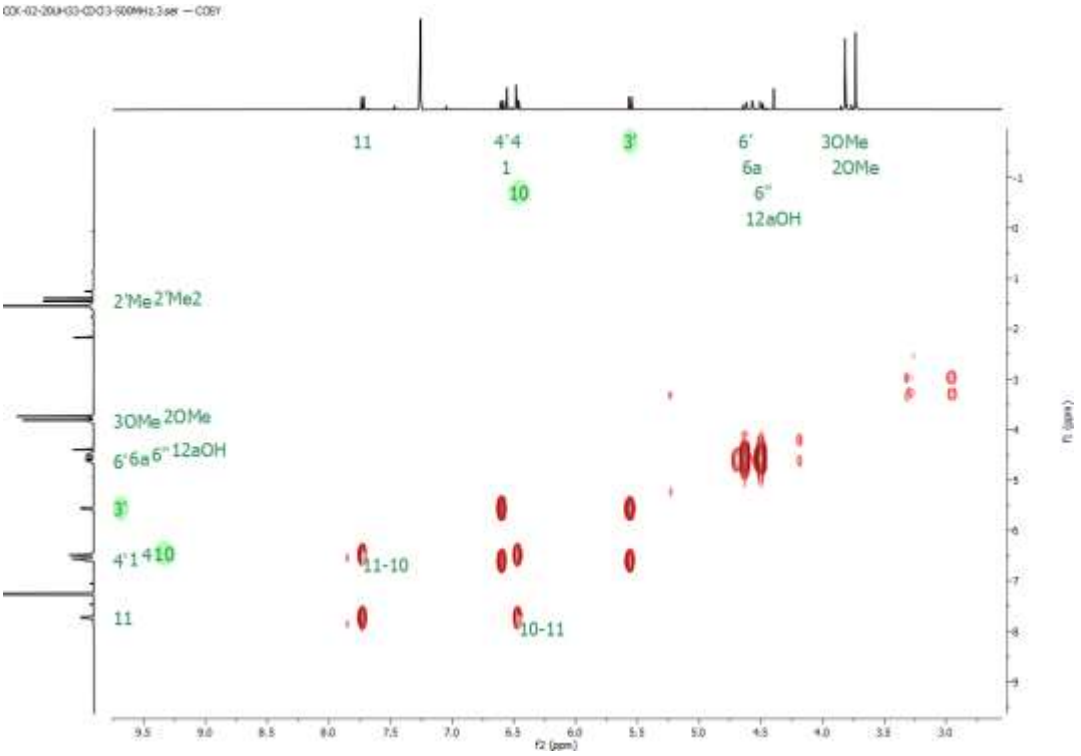

Appendix 14D: HSQC (500 MHz, $CDCl_3$, 25°C) spectrum of 12a-hydroxydeguelin **(123)**

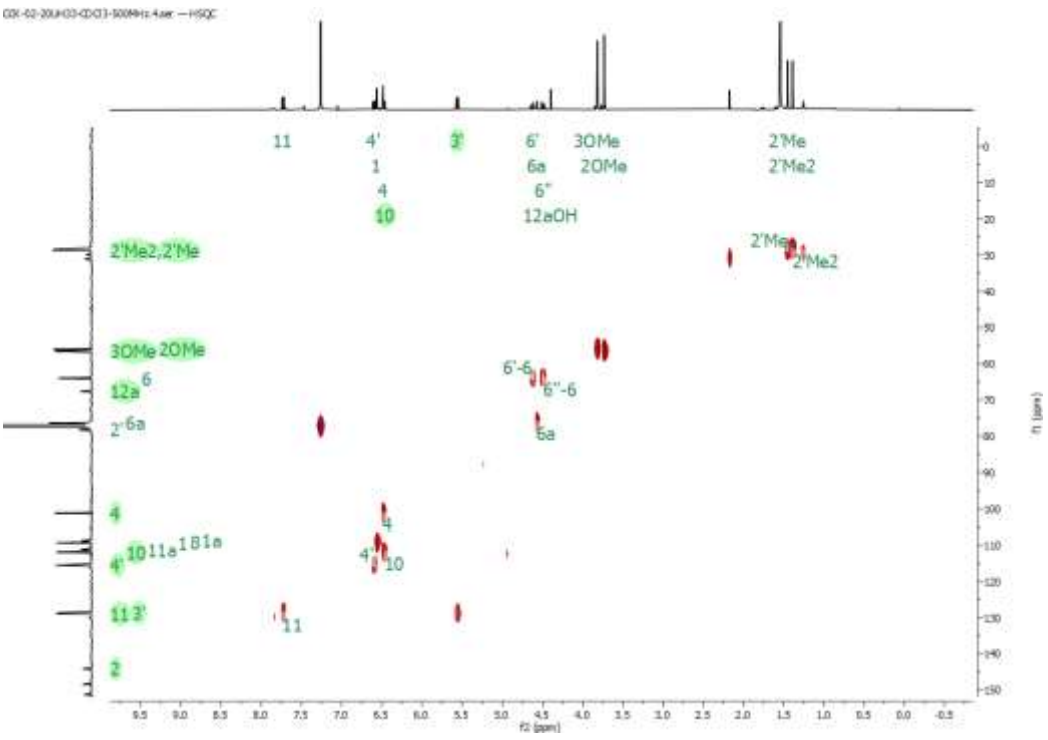

Appendix 14E: HMBC (500 MHz, $CDCl_3$, 25°C) spectrum of 12a-hydroxydeguelin **(123)**

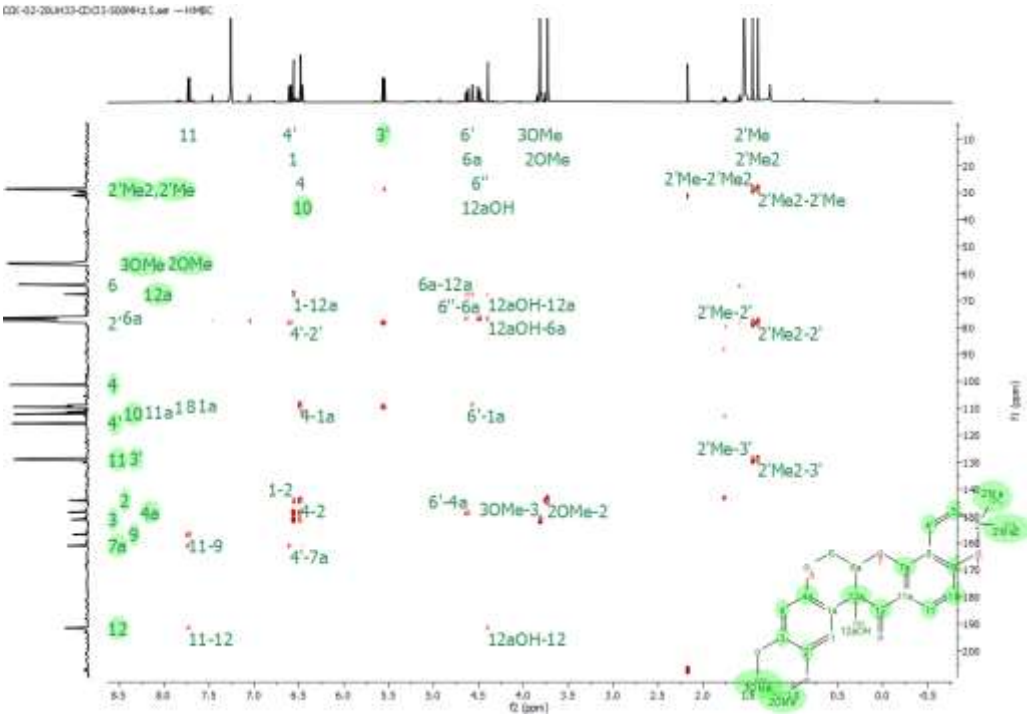

Appendix 14F: NOESY (500 MHz, $CDCl_3$, 25°C) spectrum of 12a-hydroxydeguelin **(123)**

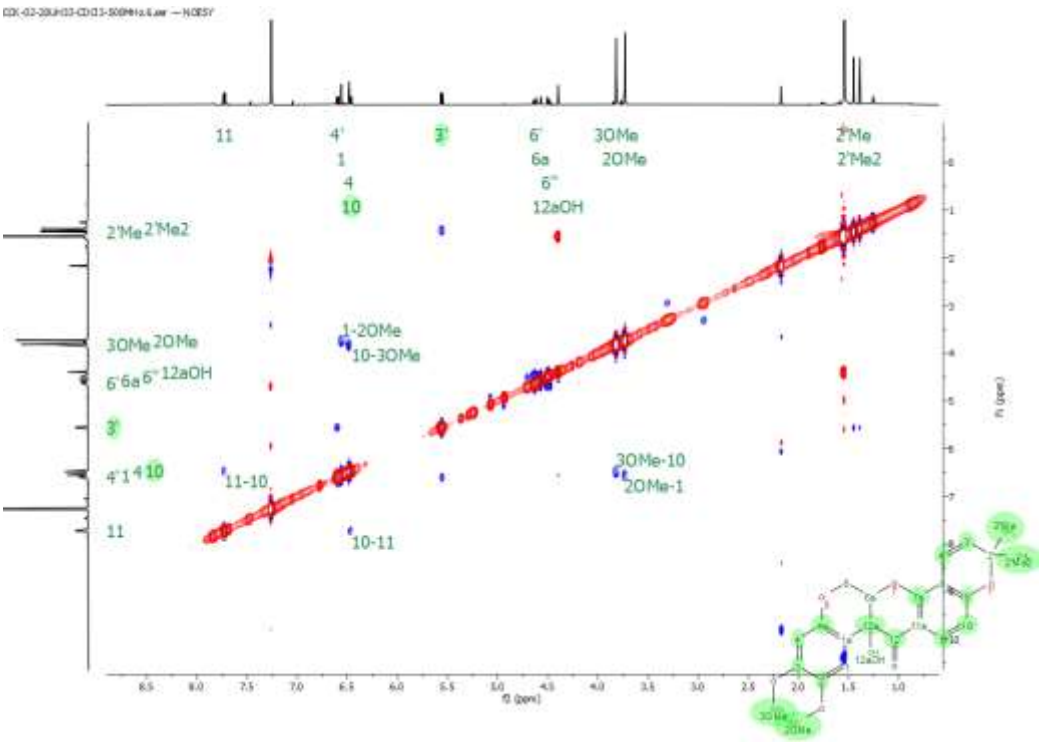

Appendix 14G. TOCSY (500 MHz, $CDCl_3$, 25°C) spectrum of 12a-hydroxydeguelin **(123)**

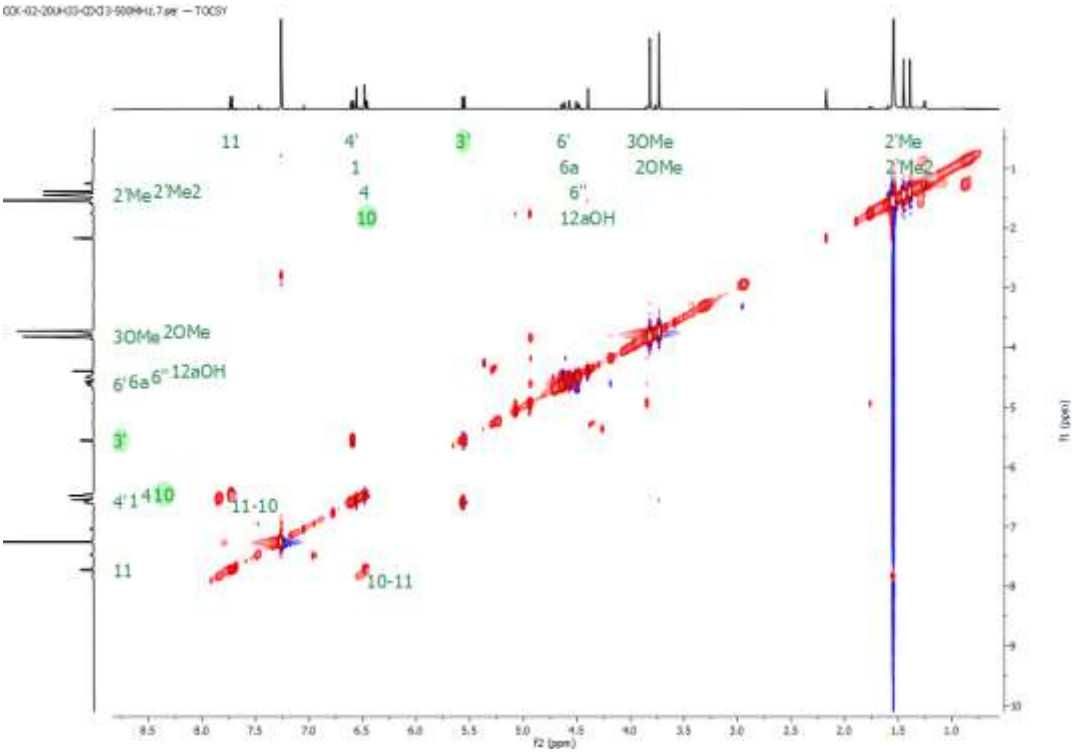

Appendix 15A: ^{1}H NMR (500 MHz, $CDCl_3$, 25°C) spectrum of Furaladehyde (124)

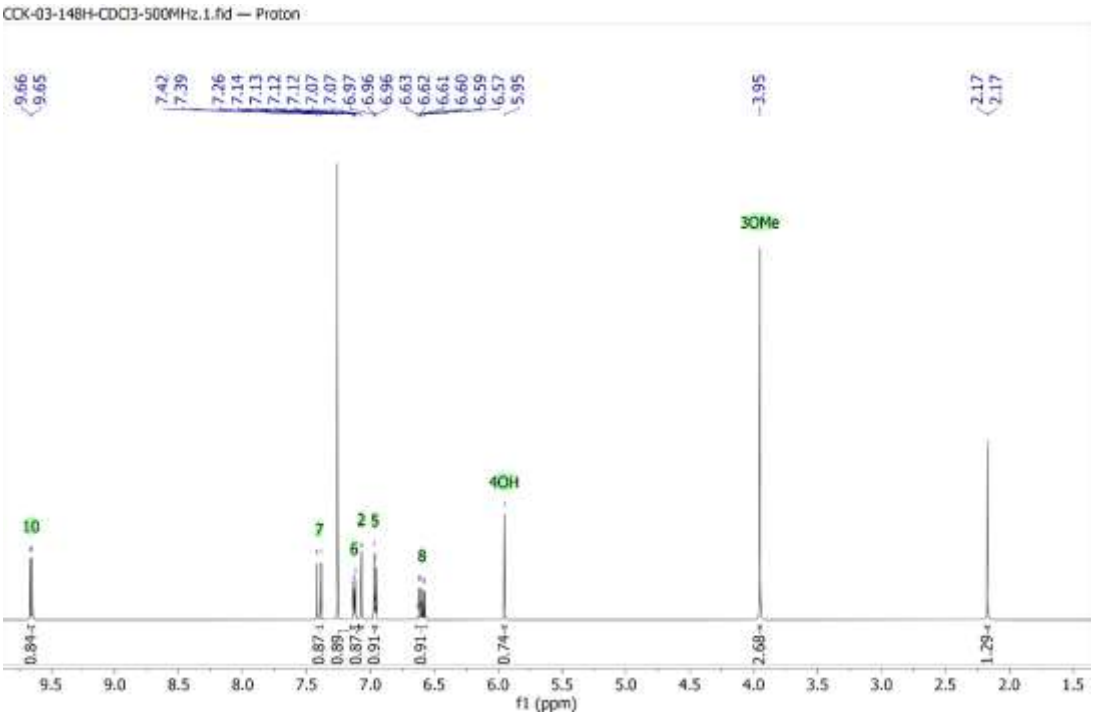

Appendix 15B. ^{13}C NMR (500 MHz, $CDCl_3$, 25°C) spectrum of Furaladehyde **(124)**

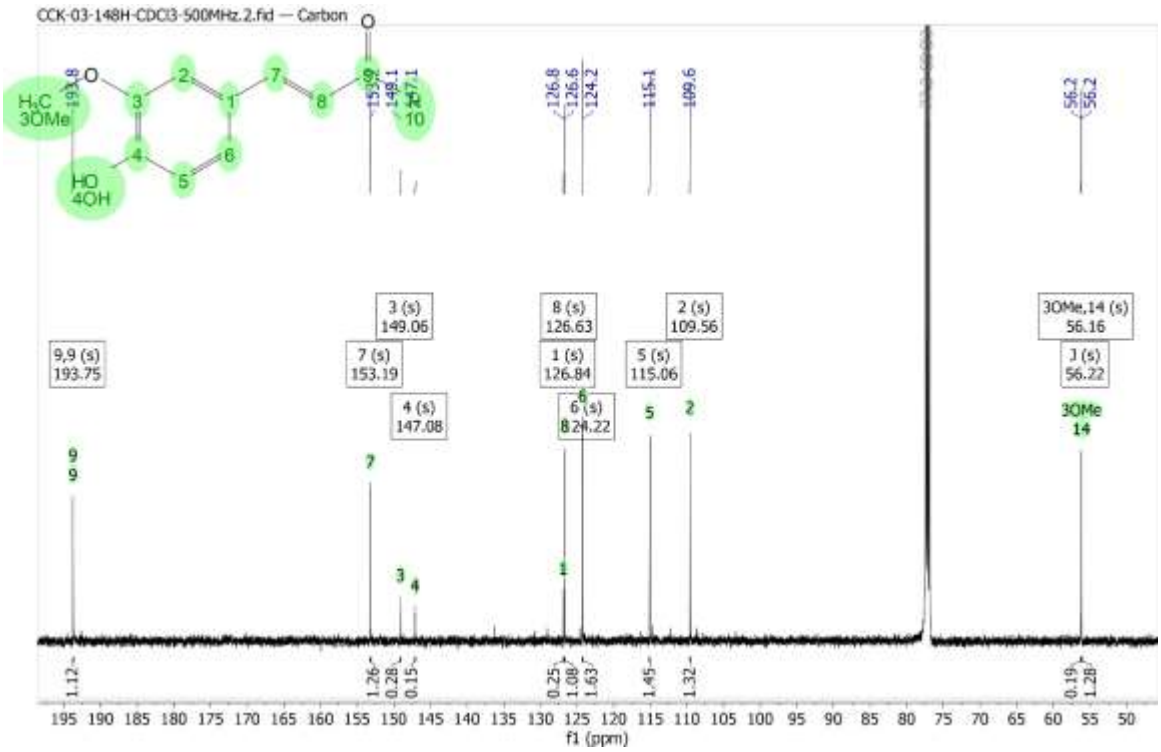

Appendix 15C. COSY (500 MHz, $CDCl_3$, 25°C) spectrum of Furaladehyde **(124)**

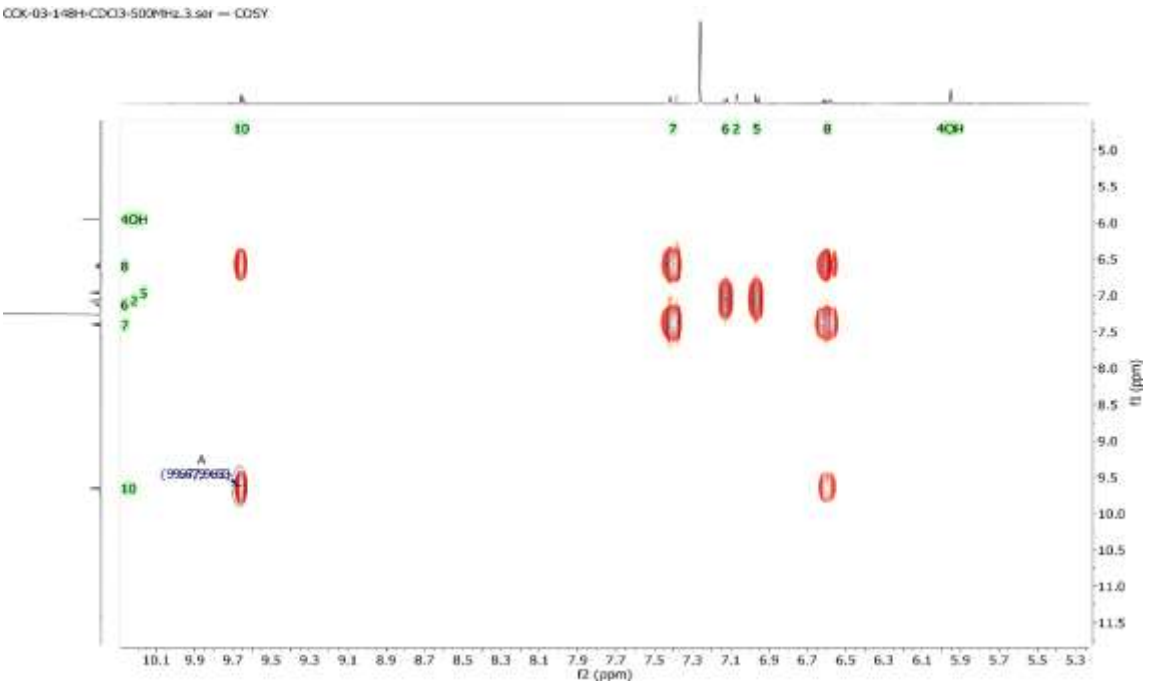

Appendix 15D: HSQC (500 MHz, $CDCl_3$, 25°C) spectrum of Furaladehyde **(124)**

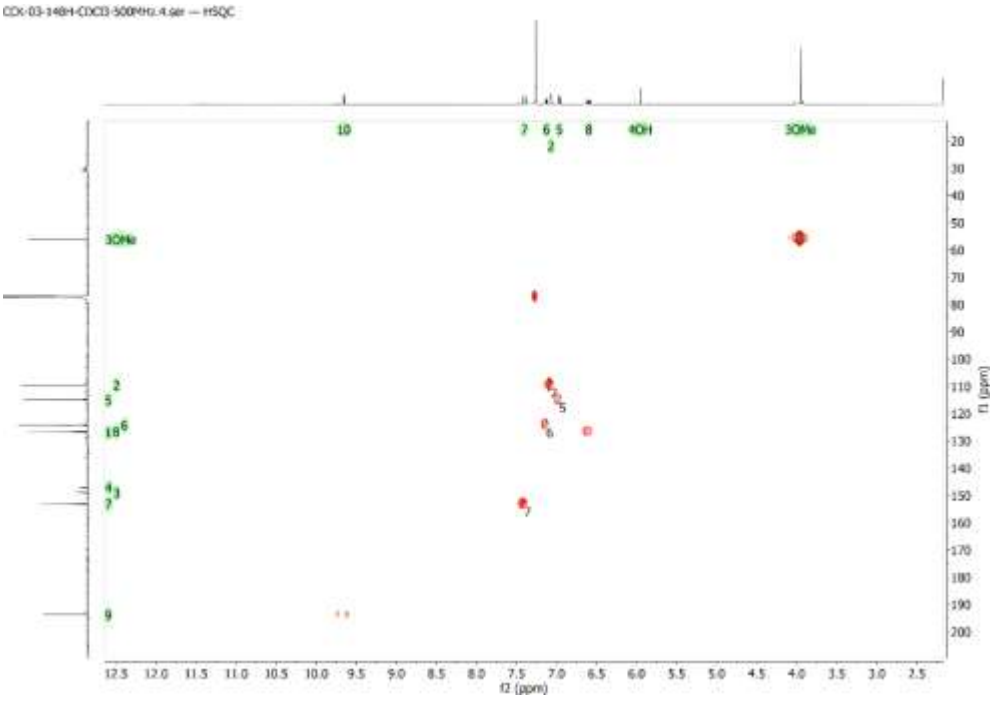

Appendix 15E: HMBC (500 MHz, $CDCl_3$, 25°C) spectrum of Furaladehyde **(124)**

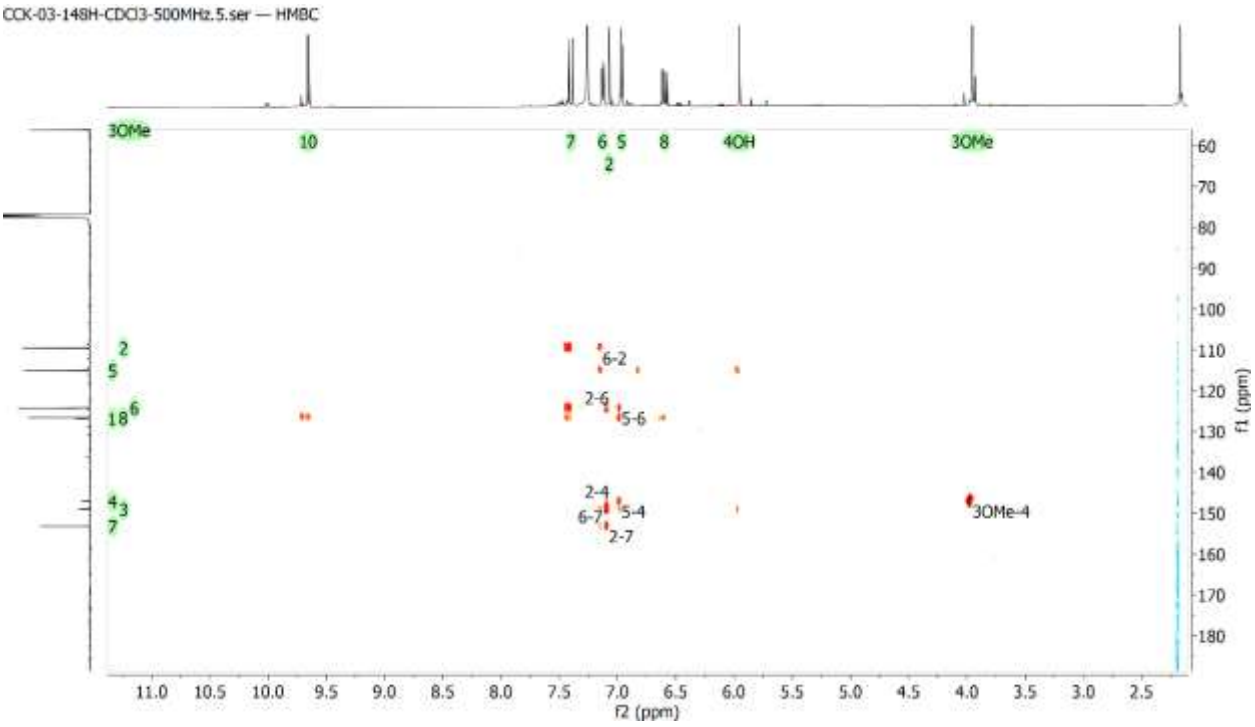

Appendix 16A: 1H NMR (500 MHz, CDCl3, 25°C) spectrum of usambarin L and M (125 & 126)

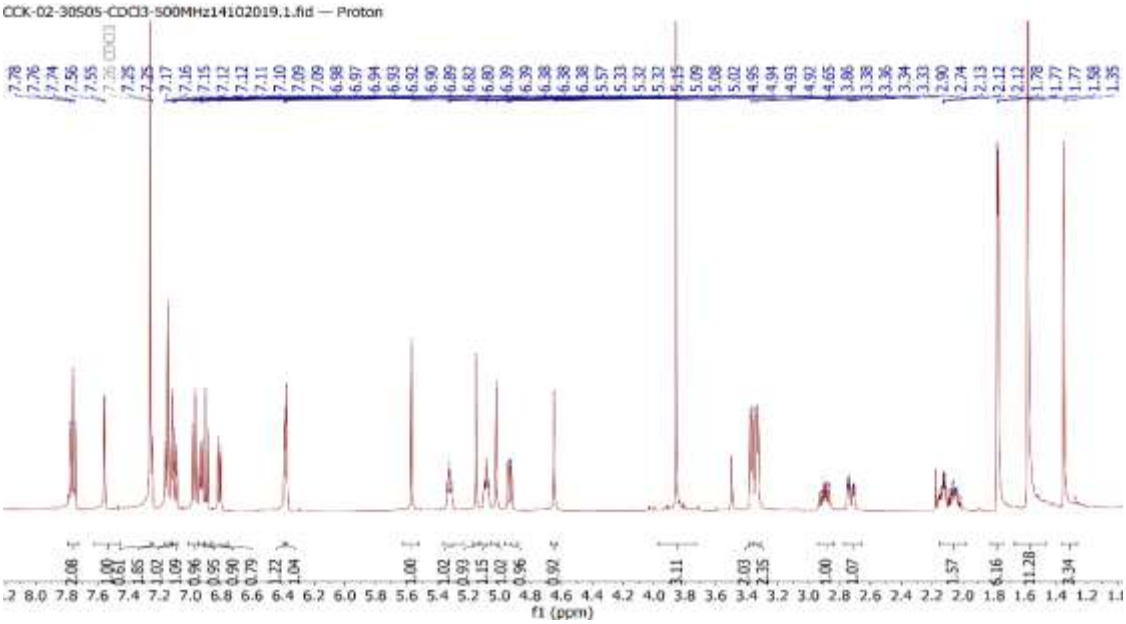

Appendix 16B. ^{13}C NMR (500 MHz, $CDCl_3$, 25°C) spectrum of **usambarin Land M (125 & 126)**

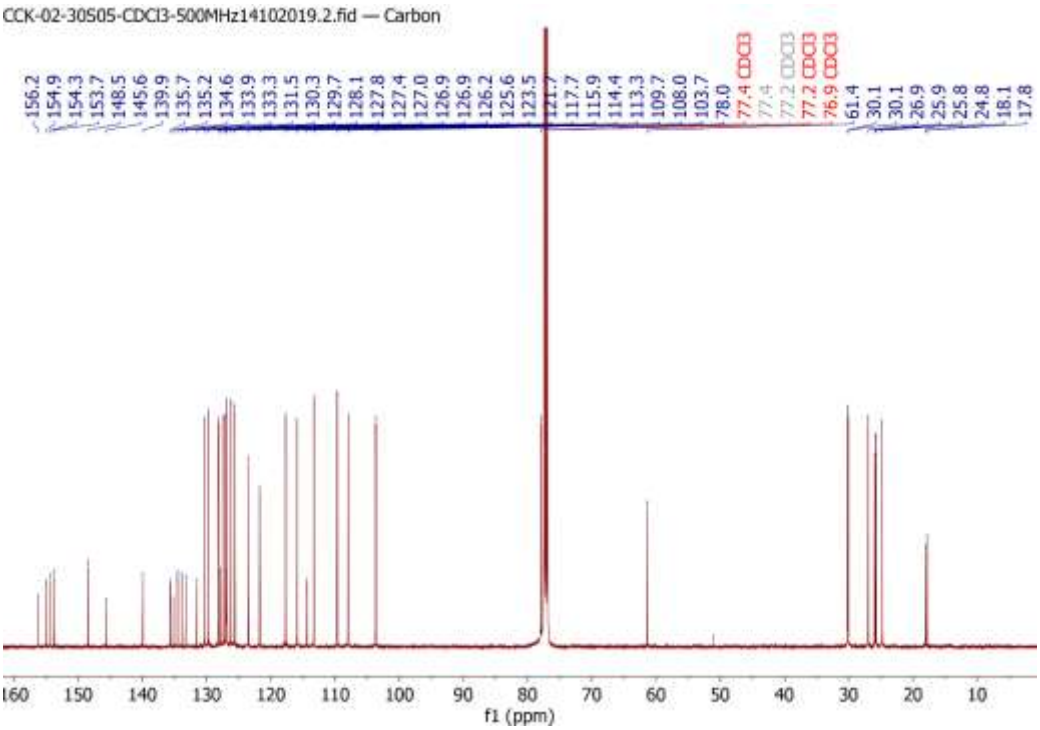

Appendix 16C. COSY (500 MHz, $CDCl_3$, 25°C) spectrum of usambarin L and M (125 & 126)

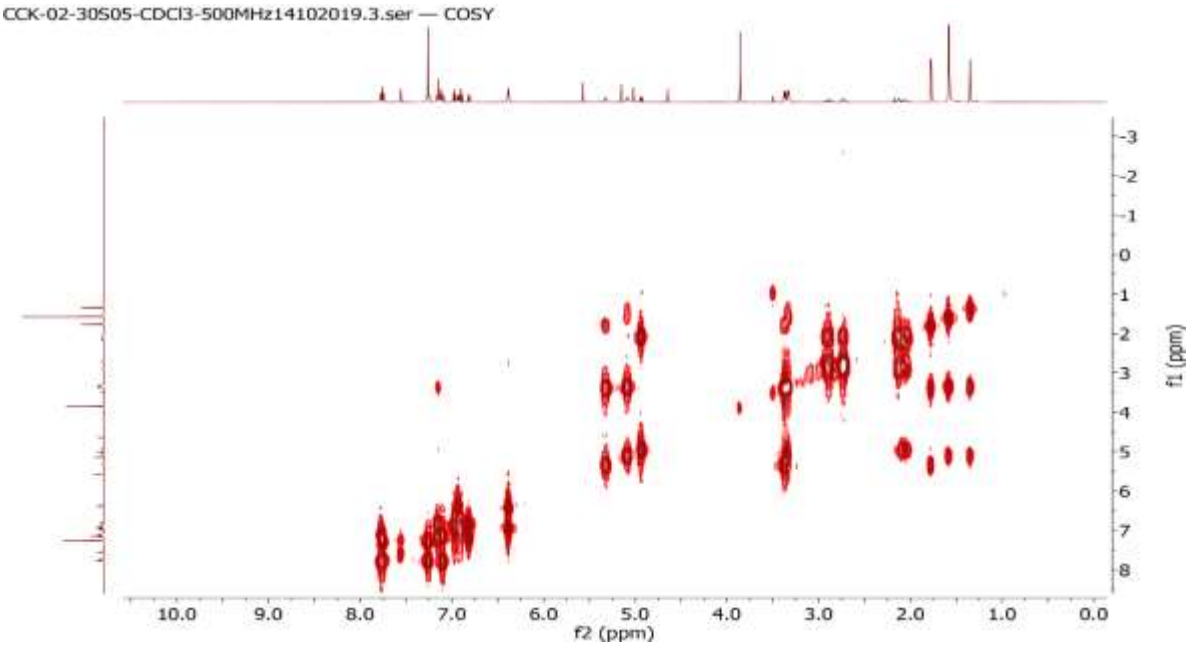

Appendix 16D: HSQC (500 MHz, $CDCl_3$, 25°C) spectrum of usambarin Land M (125 & 126)

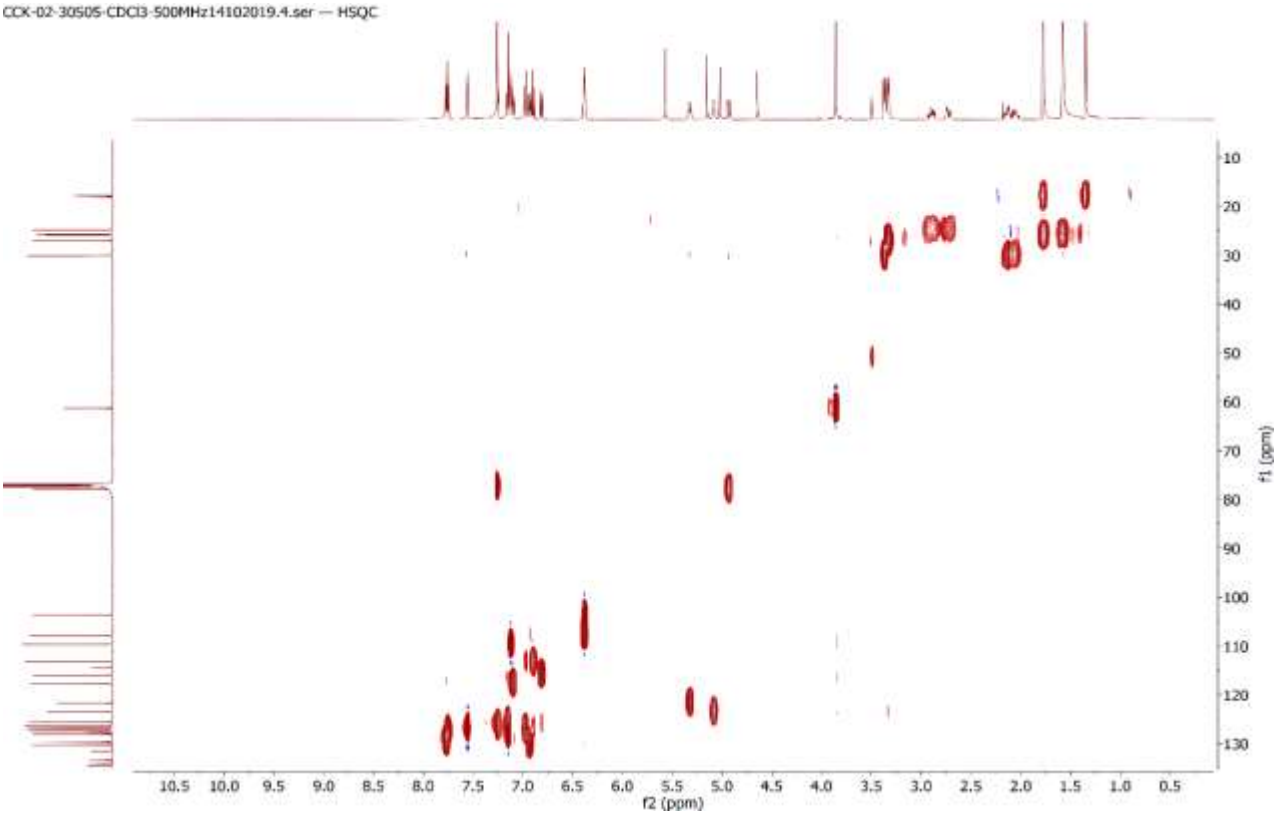

Appendix 16E: HMBC (500 MHz, $CDCl_3$, 25°C) spectrum of usambarin L and M (125 & 126)

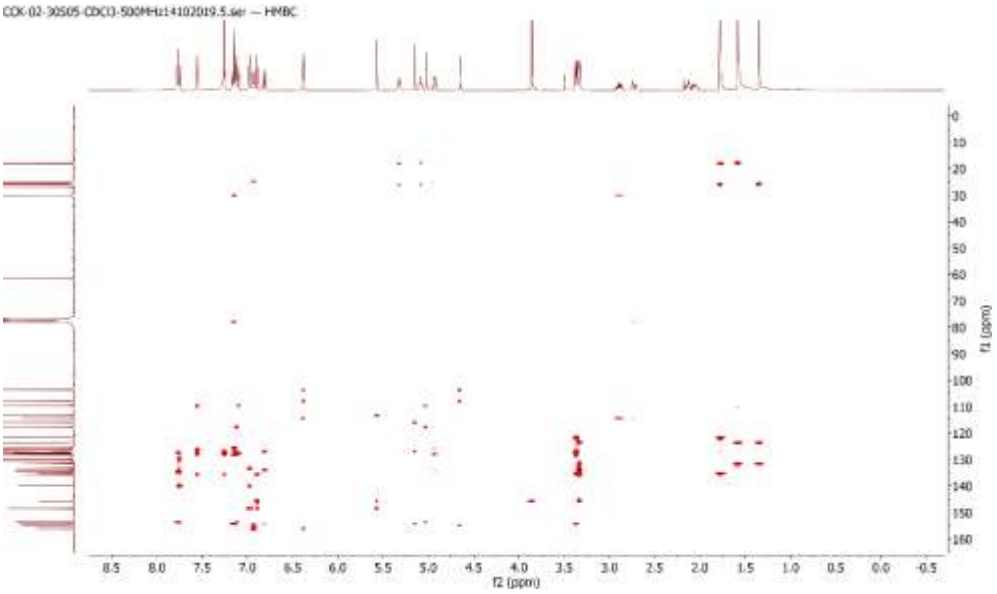

Appendix 16F: NOESY (500 MHz, $CDCl_3$, 25°C) spectrum of usambarin L and M (125 & 126)

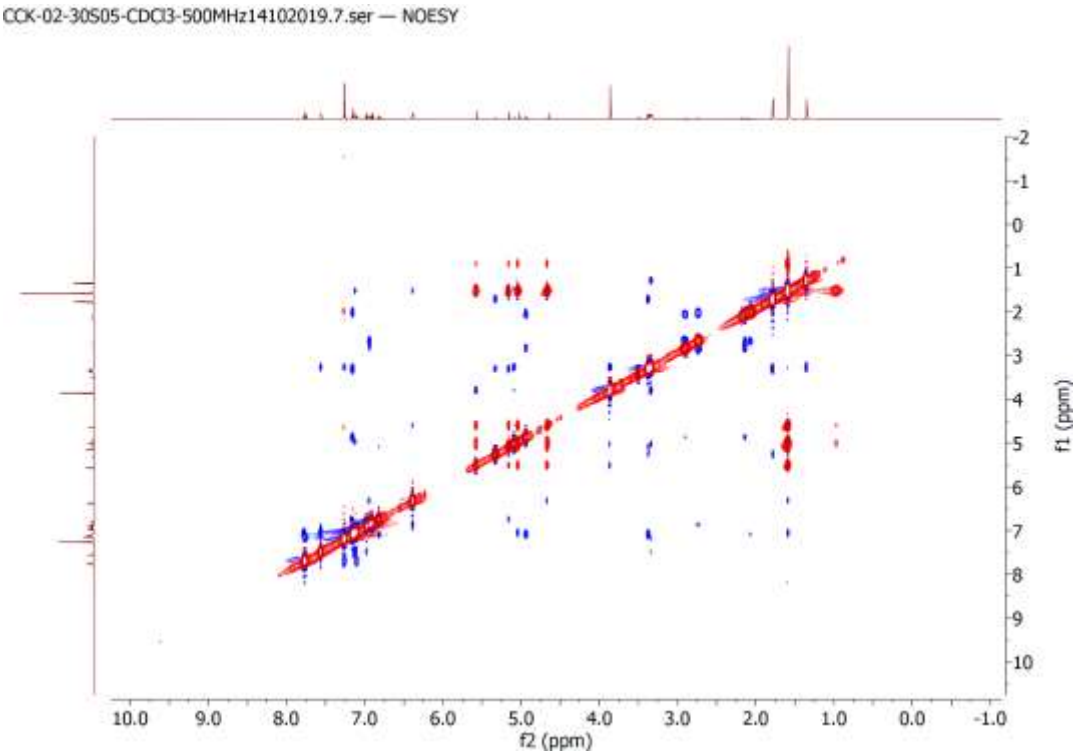

Appendix 16G. TOCSY (500 MHz, $CDCl_3$, 25°C) spectrum of usambarin L and M (125 & 126)

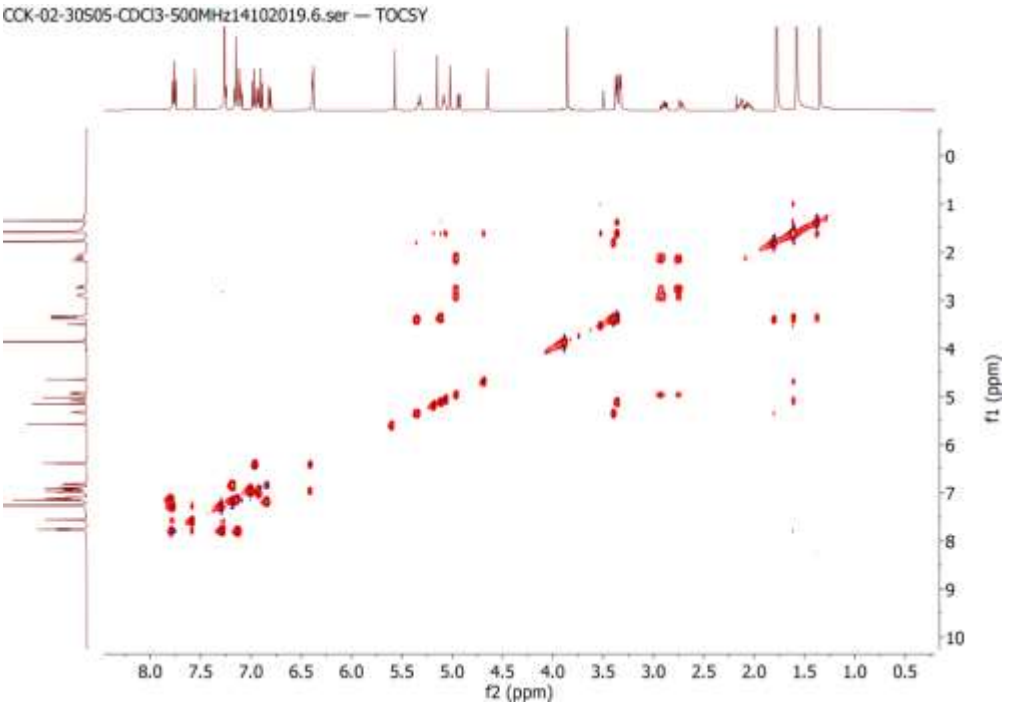

Appendix 17A. 1H NMR (800 MHz, CDCl3, 25°C) spectrum of Lupinifolinol (127)

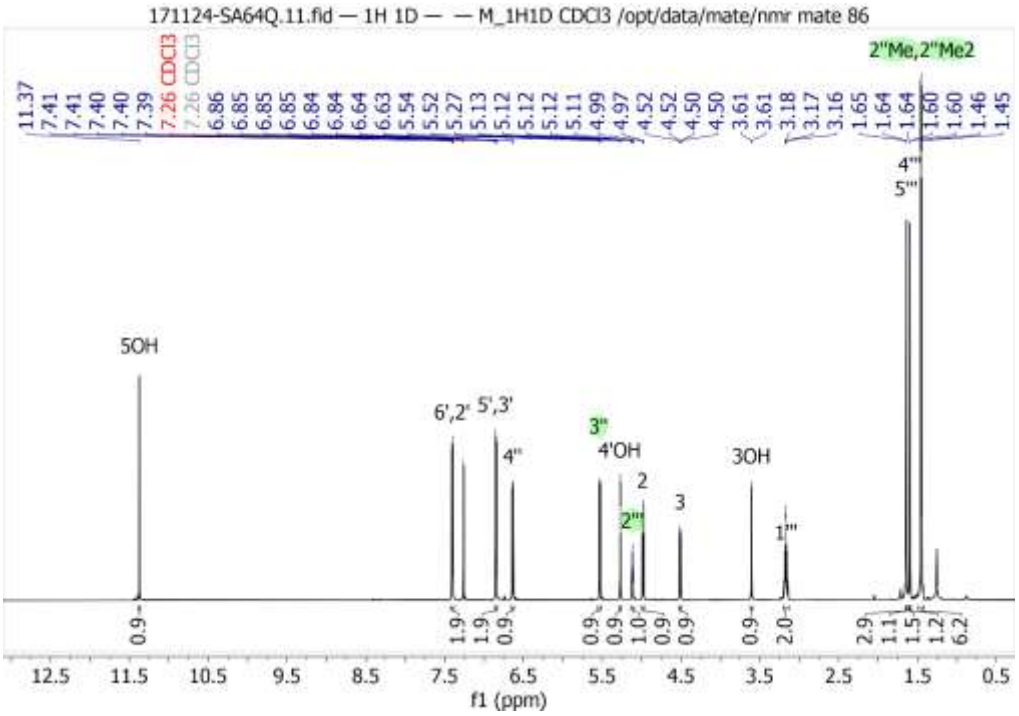

Appendix 17B. ^{13}C NMR (200 MHz, $CDCl_3$, 25°C) spectrum of Lupinifolinol (**127**)

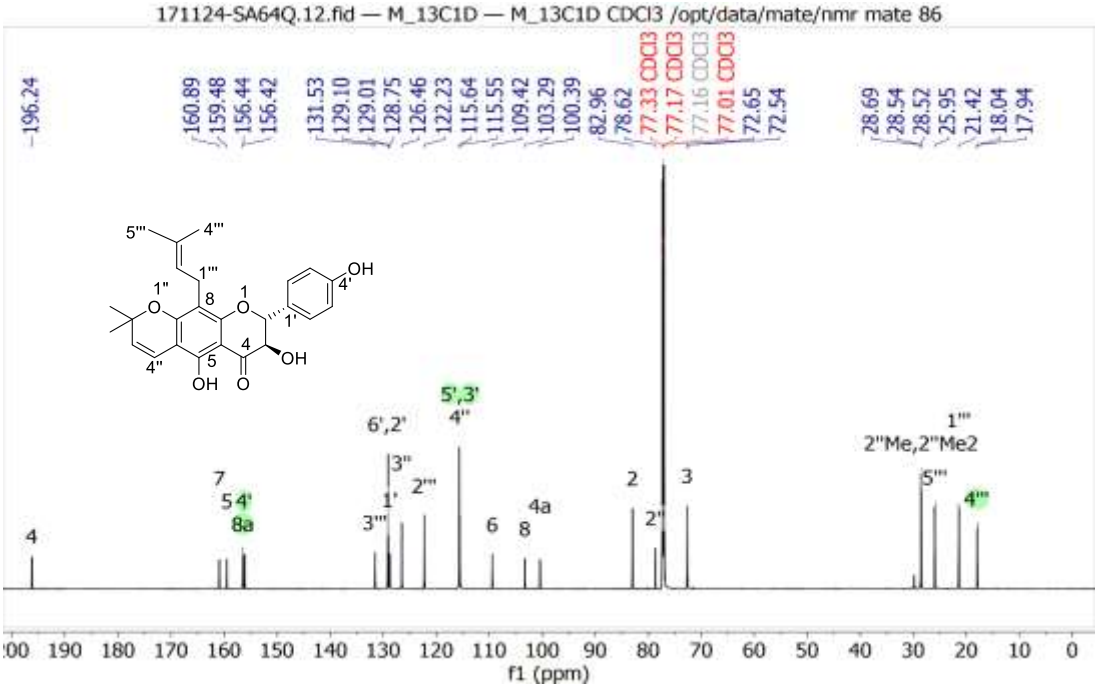

Appendix 17C. COSY (800 MHz, $CDCl_3$, 25°C) spectrum of Lupinifolinol (**127**)

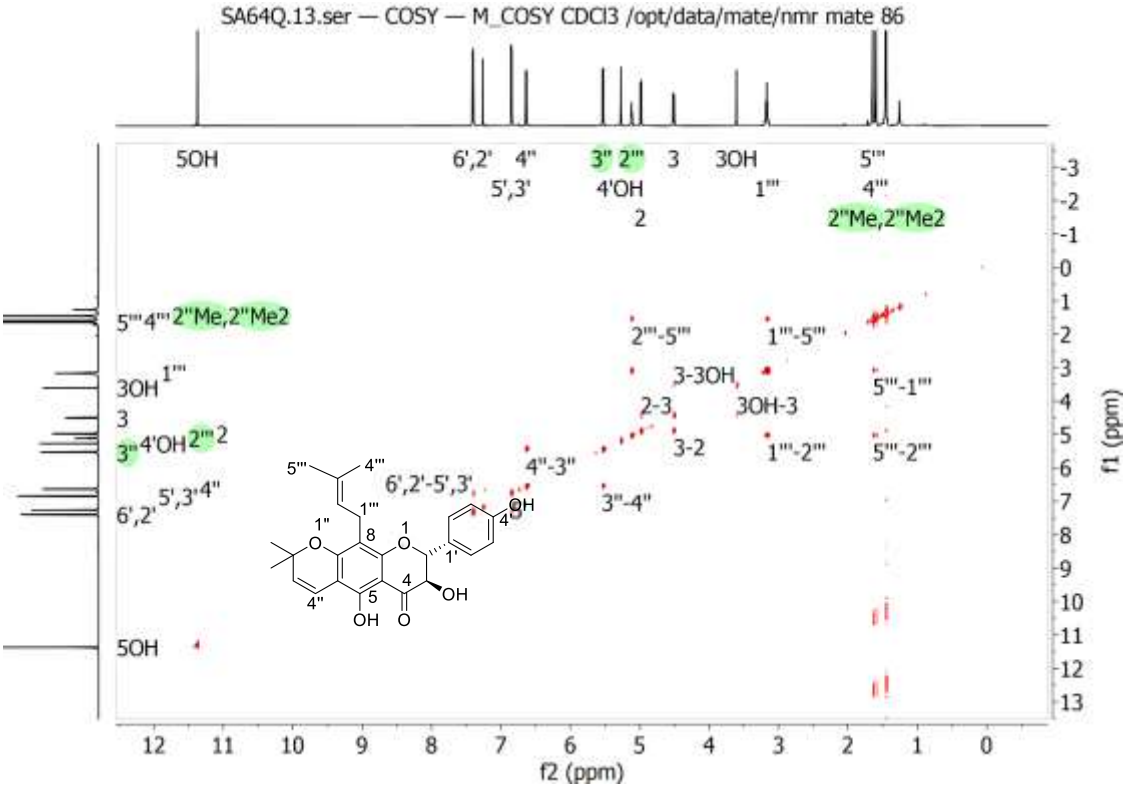

Appendix 17D. HSQC (800 MHz, CDCl3, 25°C) spectrum of Lupinifolinol (**127**)

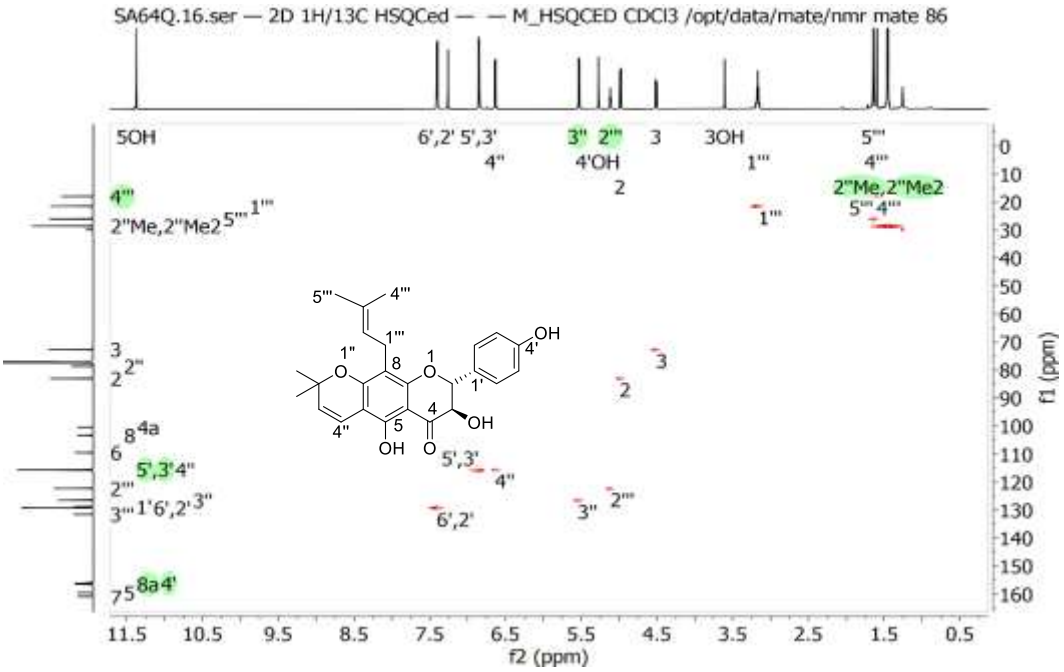

Appendix 17E. HMBC (800 MHz, $CDCl_3$, 25°C) spectrum of Lupinifolinol (**127**)

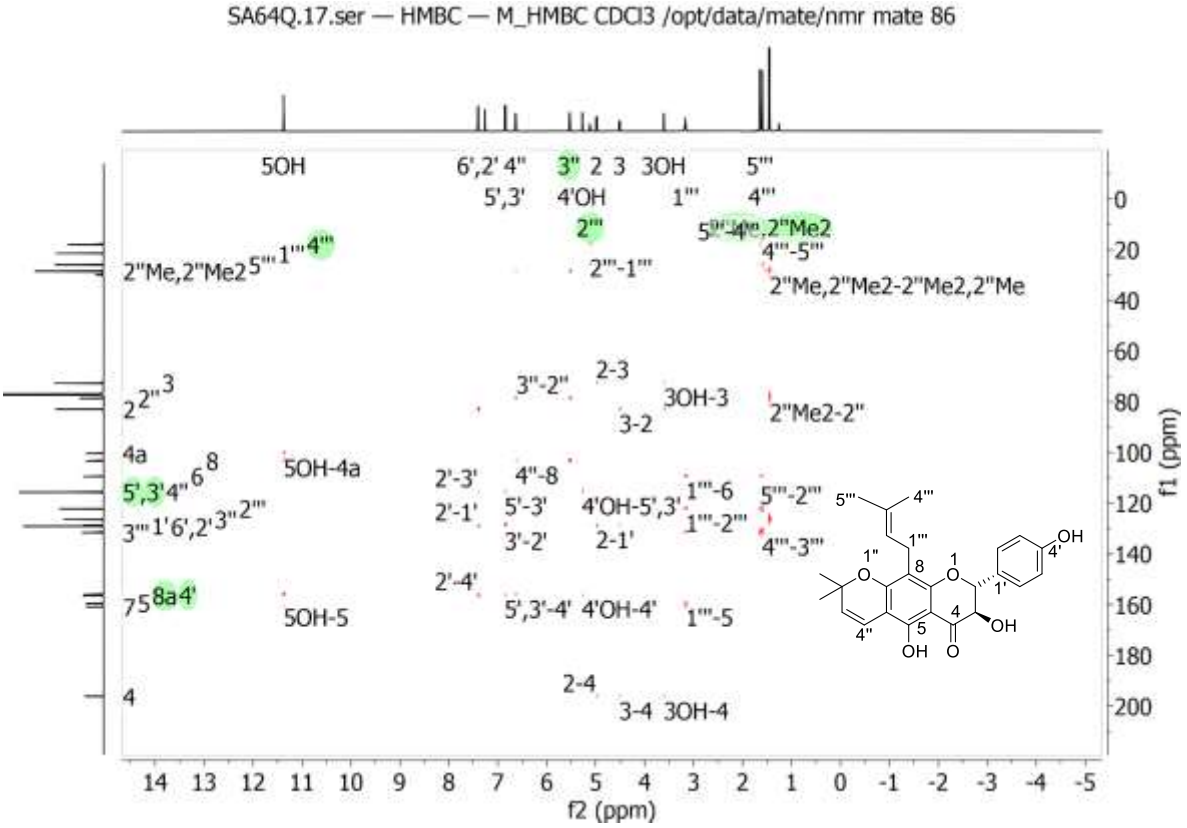

Appendix 17 F. TOCSY (800 MHz, $CDCl_3$, 25°C) spectrum of Lupinifolinol (**127**)

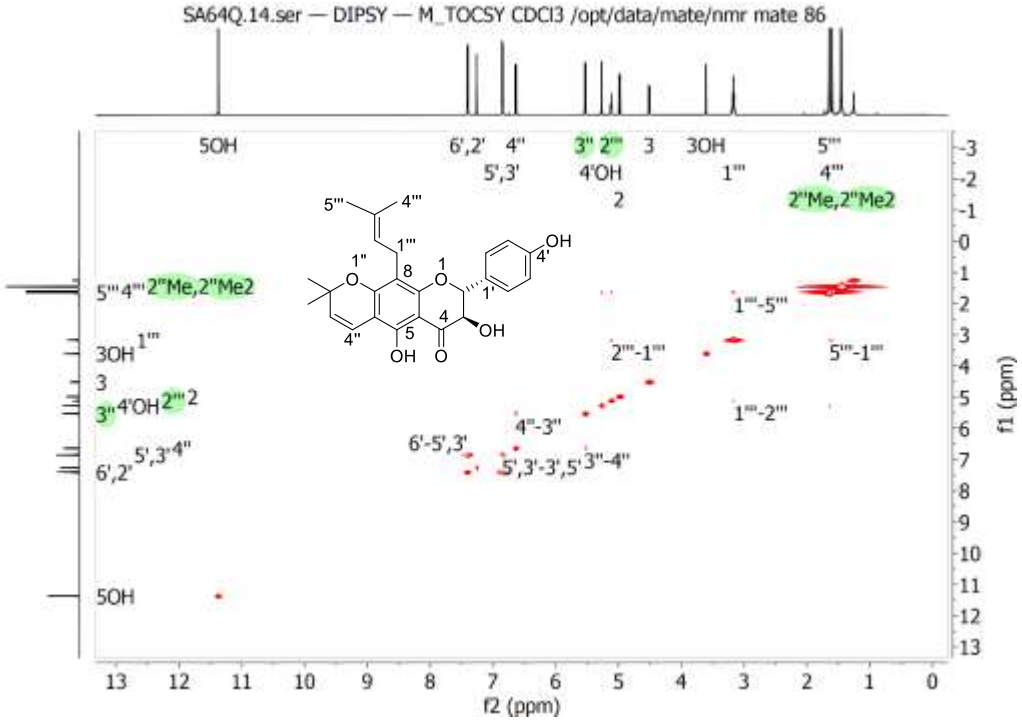

Appendix 17 G. NOESY (800 MHz, $CDCl_3$, 25°C) spectrum of Lupinifolinol (**127**)

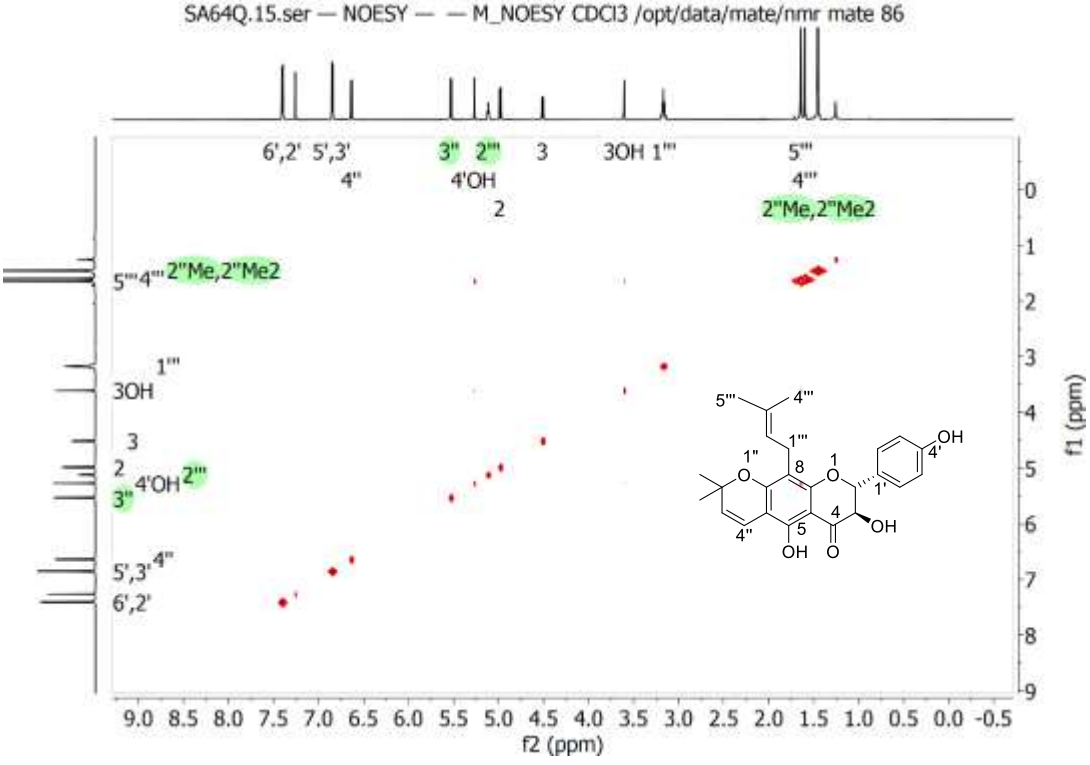

Appendix 17 H. HREI-MS of Lupinifolinol (**127**)

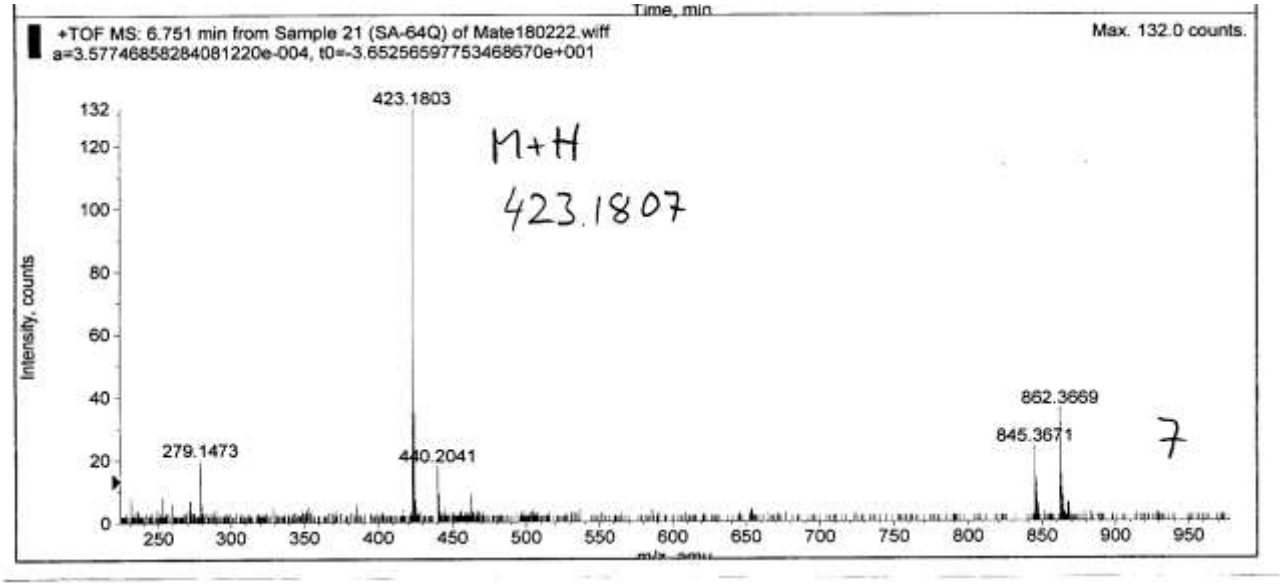

Appendix 17 I: UV spectrum of **128**

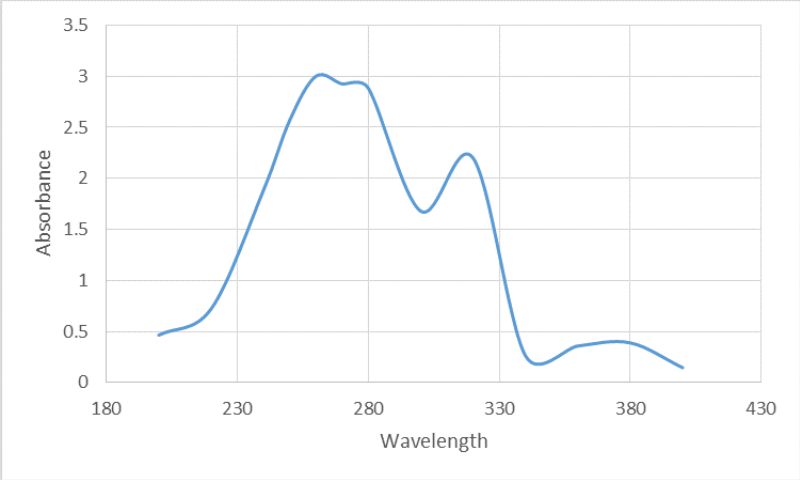

Appendix 17J: ECD spectrum of **128** (in methanol) (0.01M)

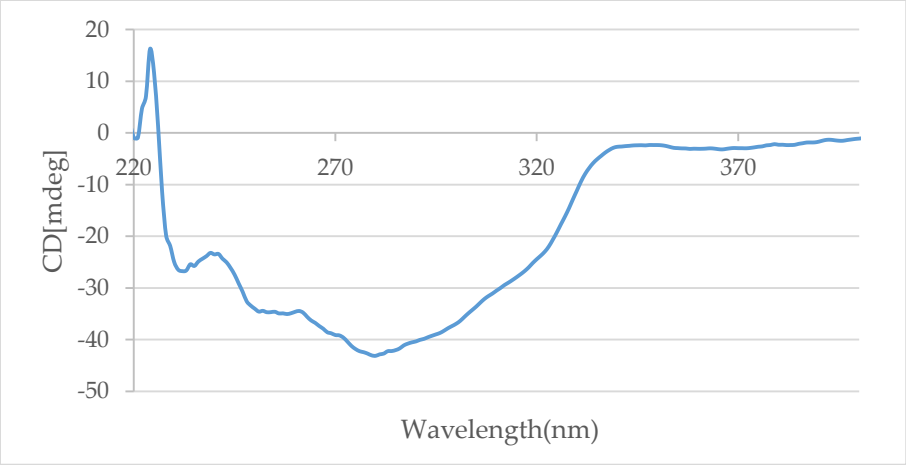

Appendix 18A: ^{1}H NMR (500 MHz, $CDCl_3$, 25°C) spectrum of dehydrolupinifolinol (128)

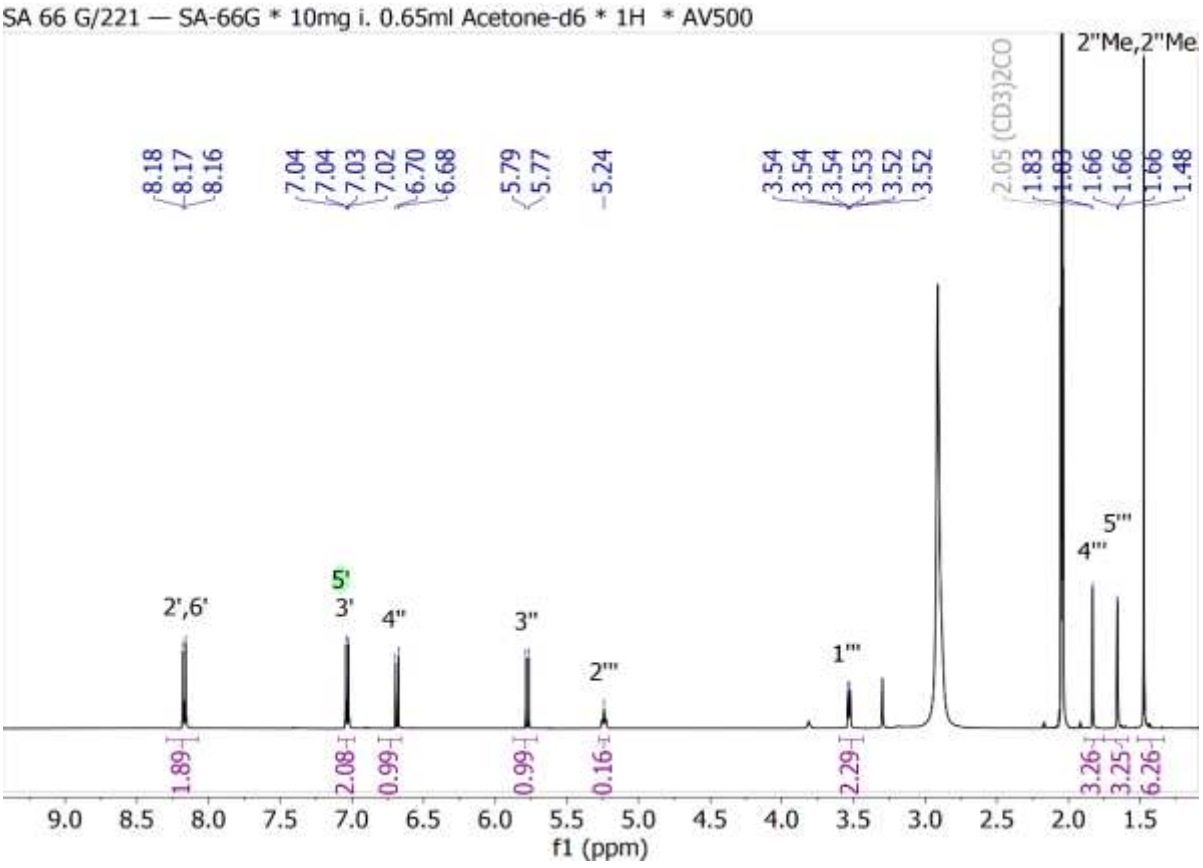

Appendix 18B. ^{13}C NMR (500 MHz, $CDCl_3$, 25°C) spectrum of dehydrolupinifolinol (**128**)

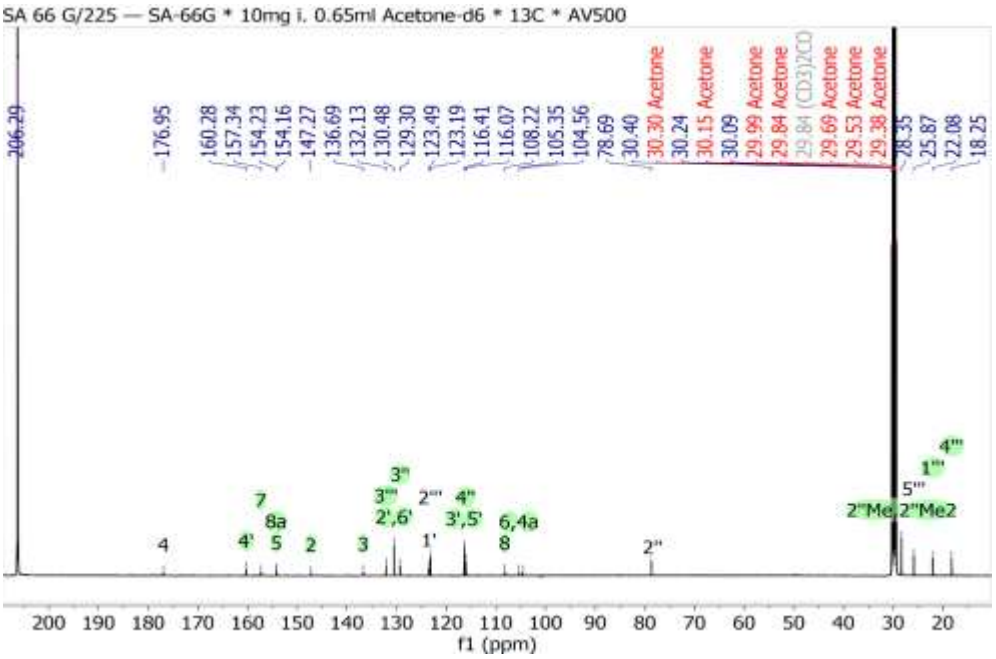

Appendix 18C. COSY (500 MHz, $CDCl_3$, 25°C) spectrum of dehydrolupinifolinol (**128**)

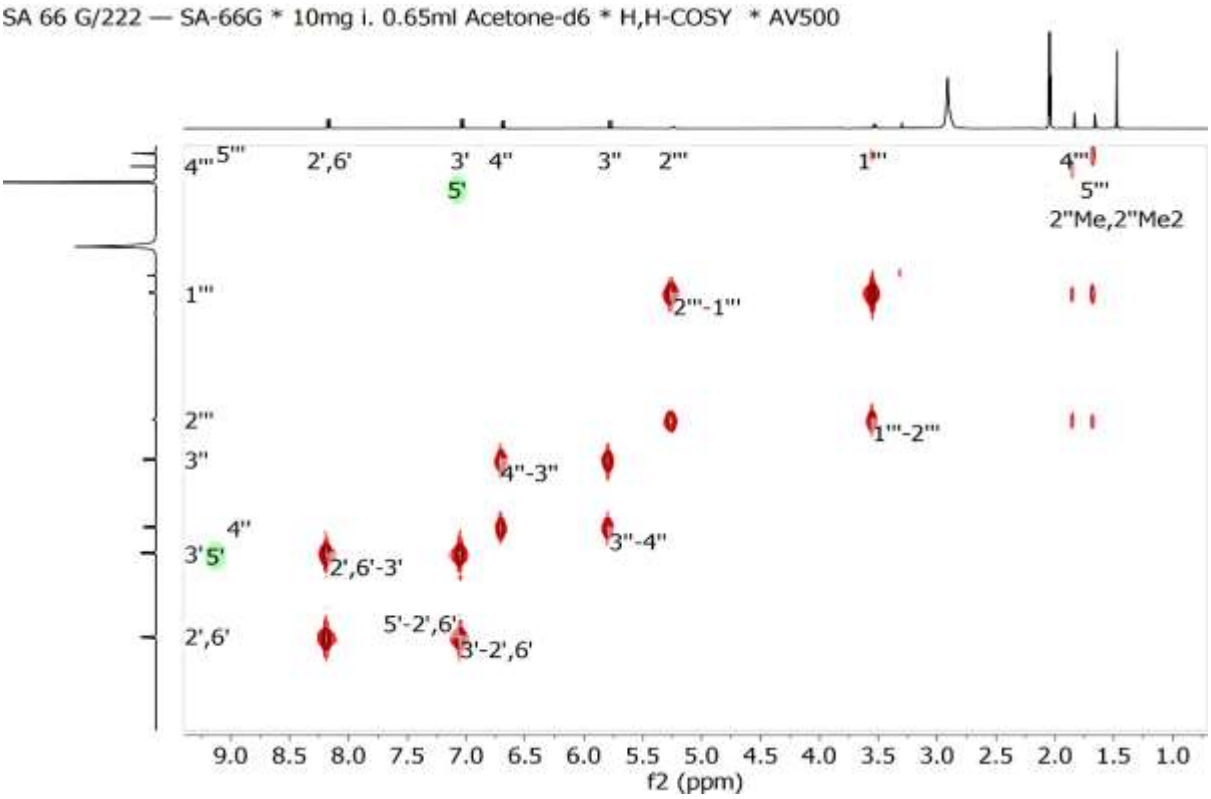

Appendix 18D: HSQC (500 MHz, $CDCl_3$, 25°C) spectrum of dehydrolupinifolinol (**128**)

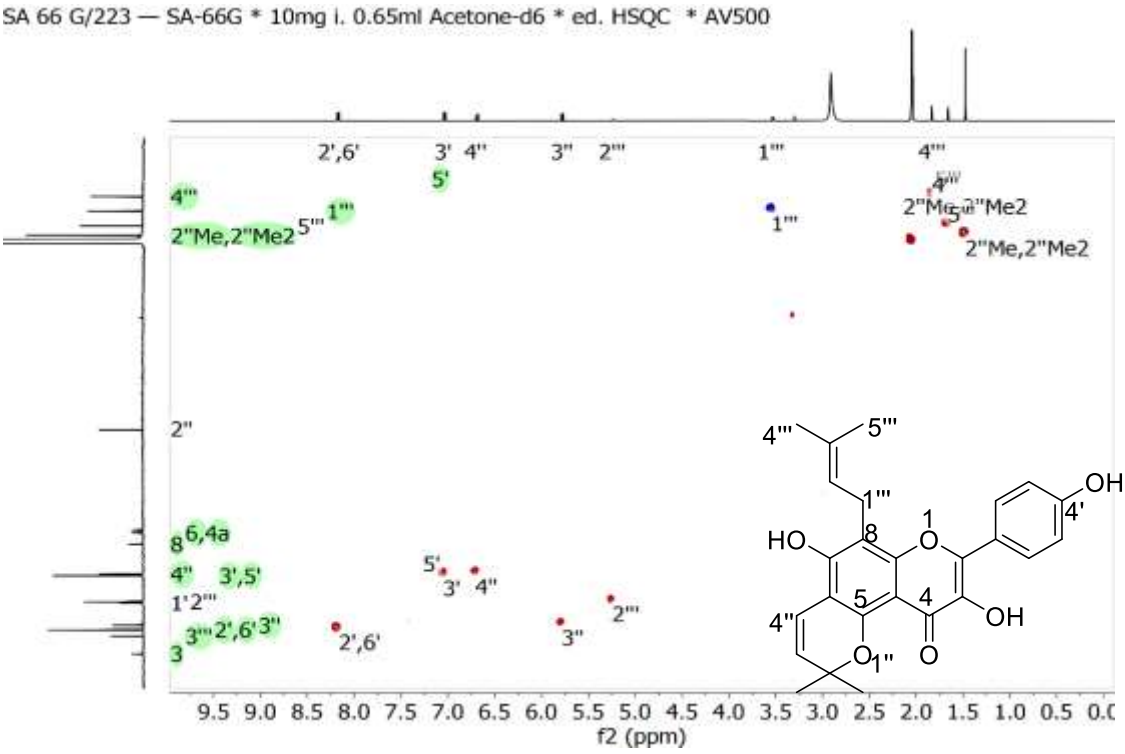

Appendix 18E: HMBC (500 MHz, $CDCl_3$, 25°C) spectrum of dehydrolupinifolinol (**129**)

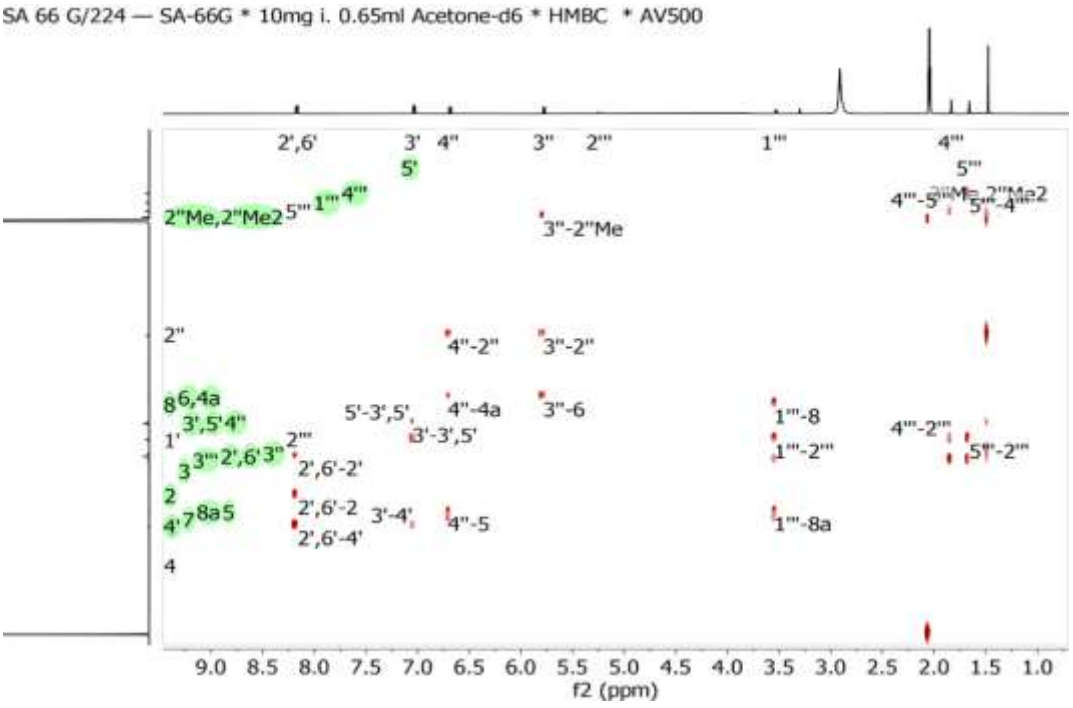

Appendix 18F: NOESY (500 MHz, $CDCl_3$, 25°C) spectrum of dehydrolupinifolinol (**128**)

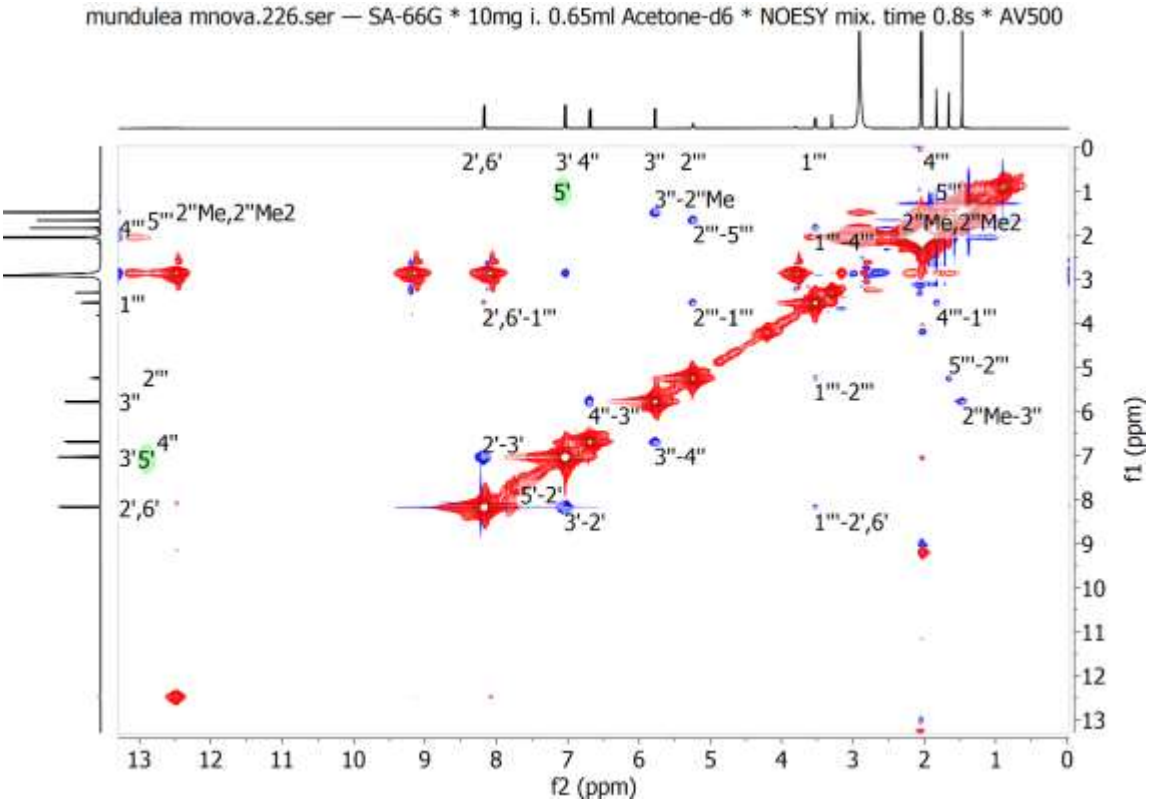

Appendix 18 G. HREI-MS of dehydrolupinifolinol (**128**)

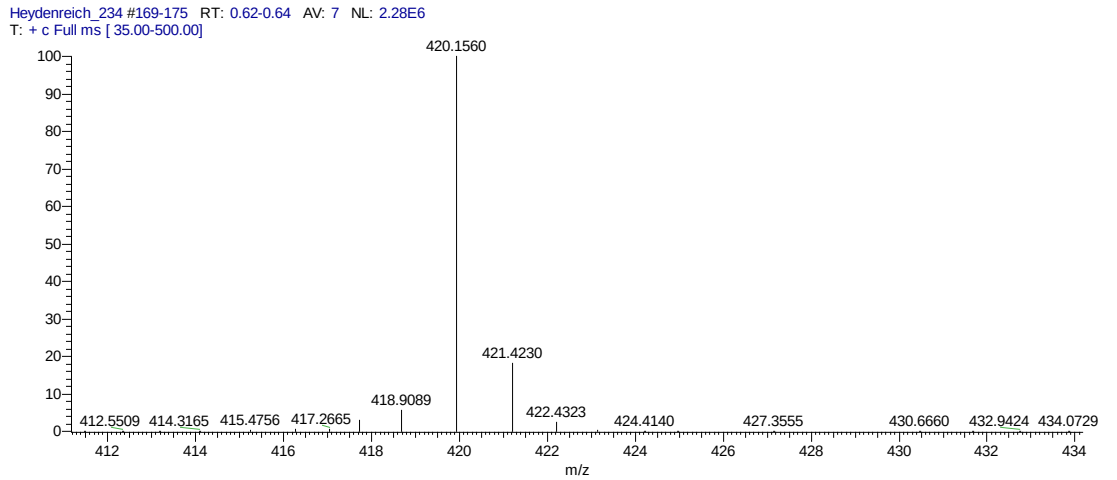

Appendix 19A: 1H NMR (500 MHz, CDCl3, 25°C) spectrum of Lupinifolin (129)

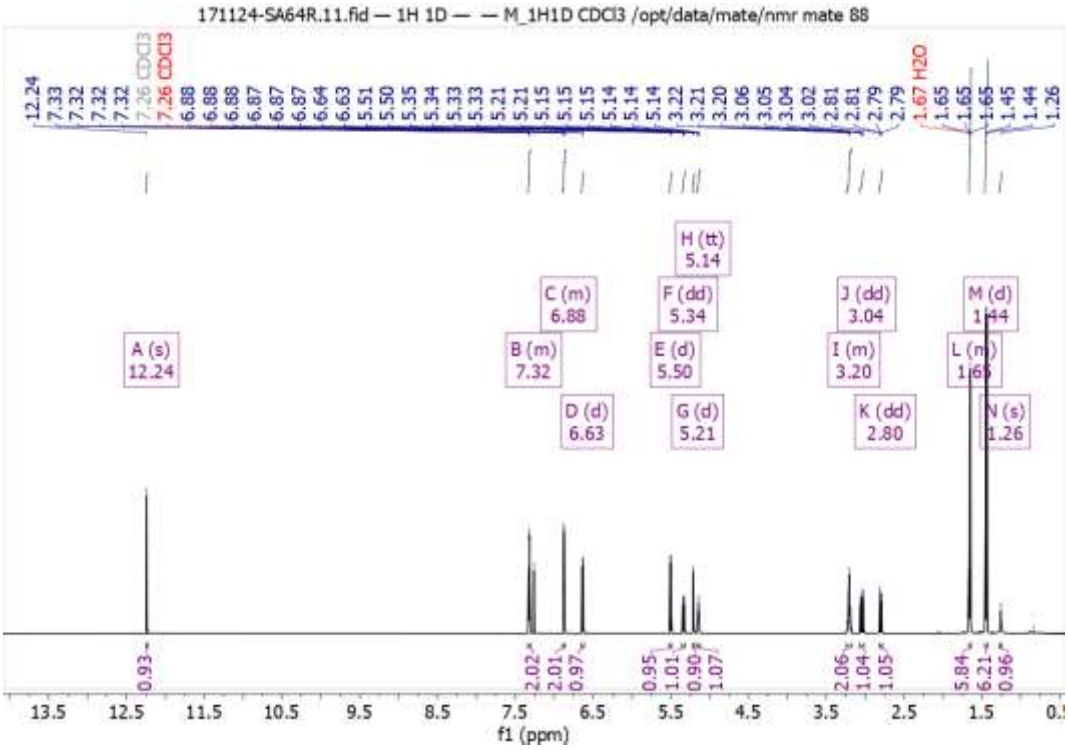

Appendix 19B. 13C NMR (500 MHz, CDCl3, 25°C) spectrum of Lupinifolin (129)

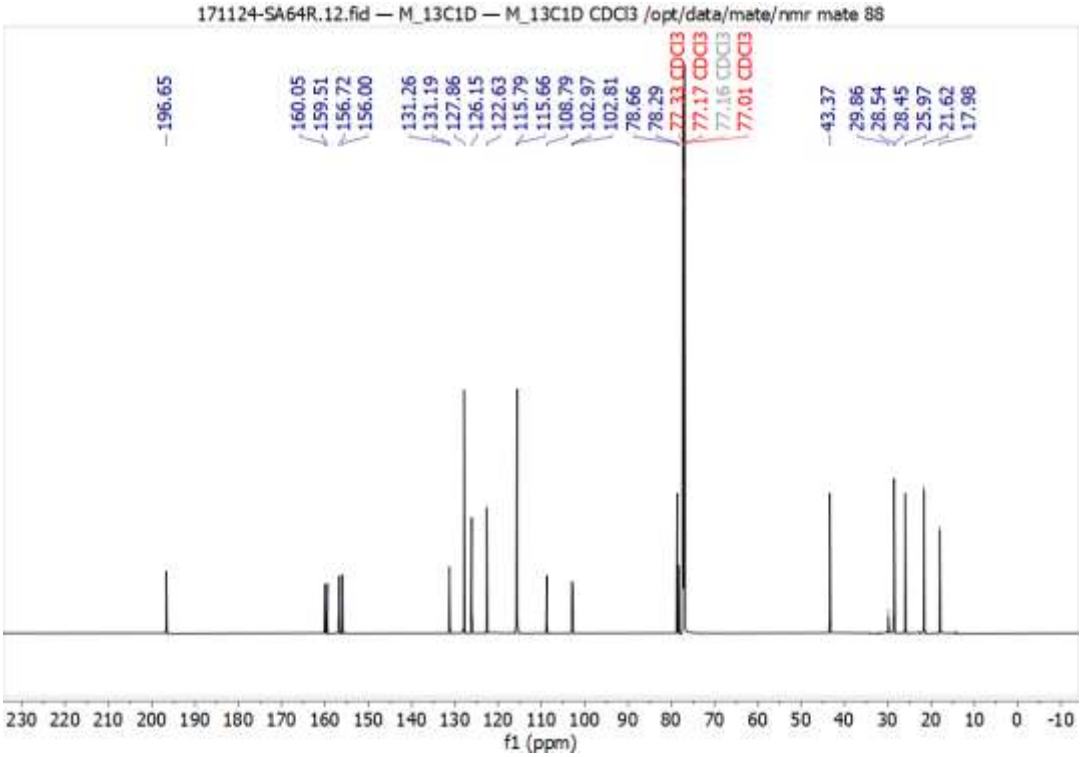

Appendix 19C. COSY (500 MHz, CDCl3, 25°C) spectrum of Lupinifolin (129)

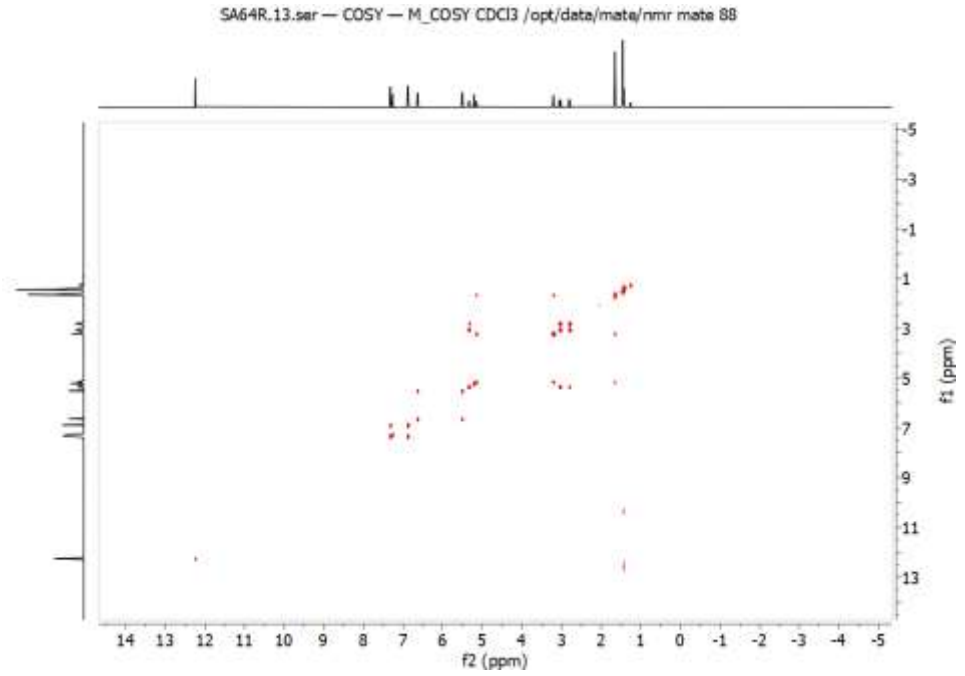

Appendix 19D: HSQC (500 MHz, CDCl3, 25°C) spectrum of Lupinifolin (129)

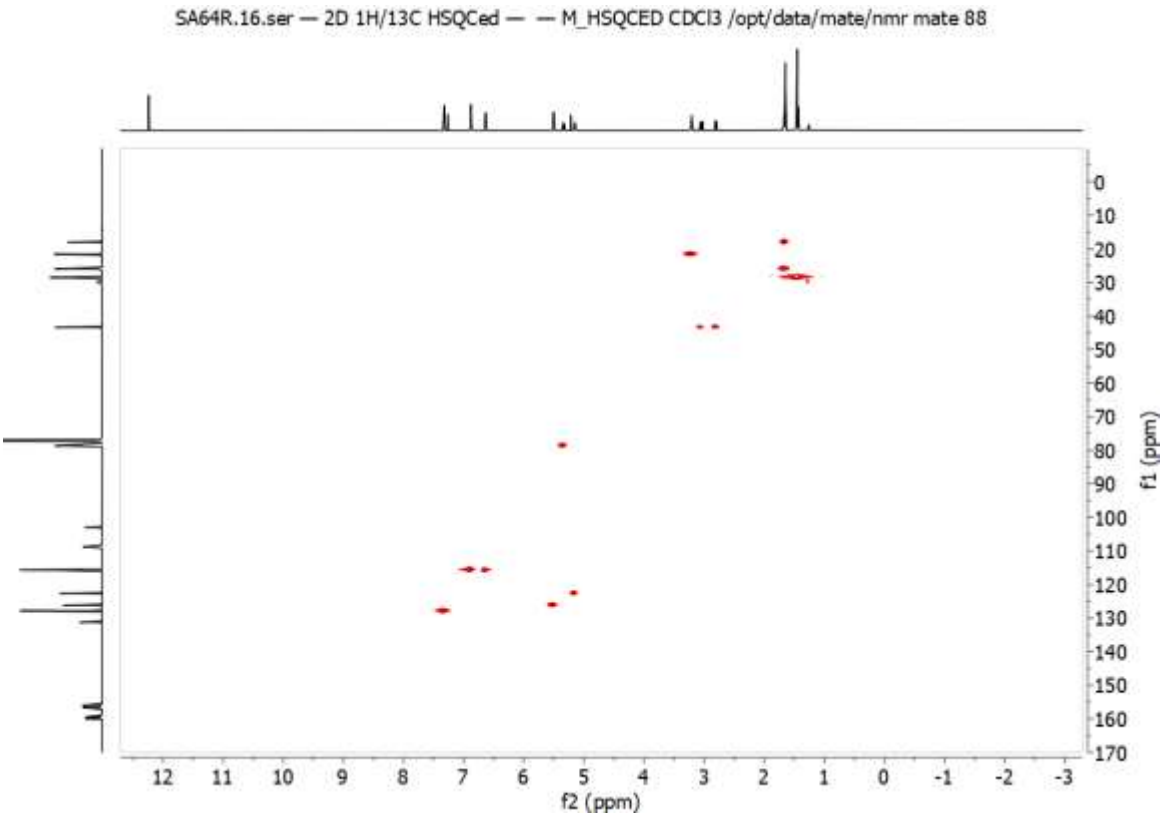

Appendix 19E: HMBC (500 MHz, CDCl3, 25°C) spectrum of Lupinifolin (129)

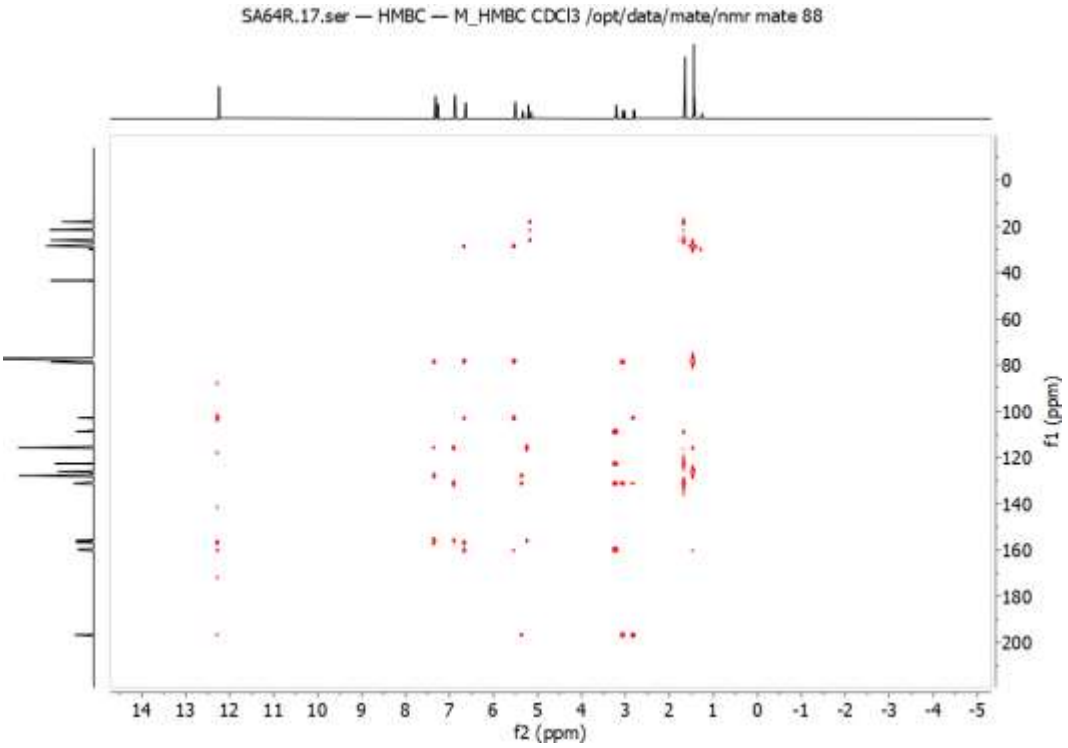

Appendix 19F: NOESY (500 MHz, CDCl3, 25°C) spectrum of Lupinifolin (129)

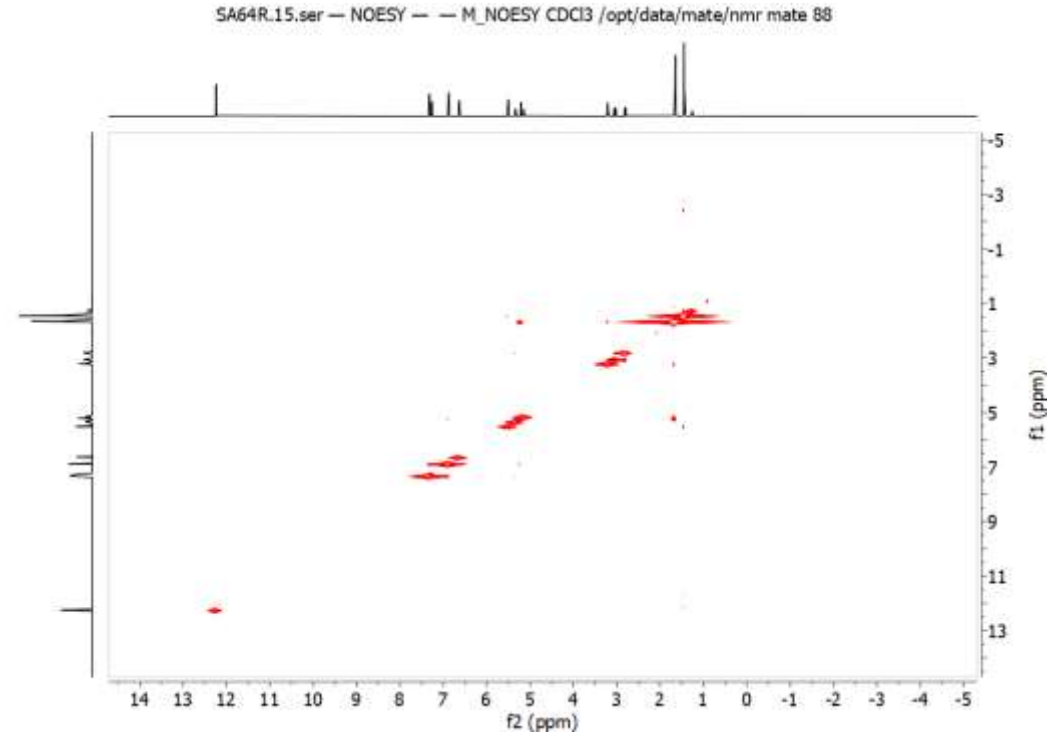

Appendix 19G. TOCSY (500 MHz, CDCl3, 25°C) spectrum of Lupinifolin (129)

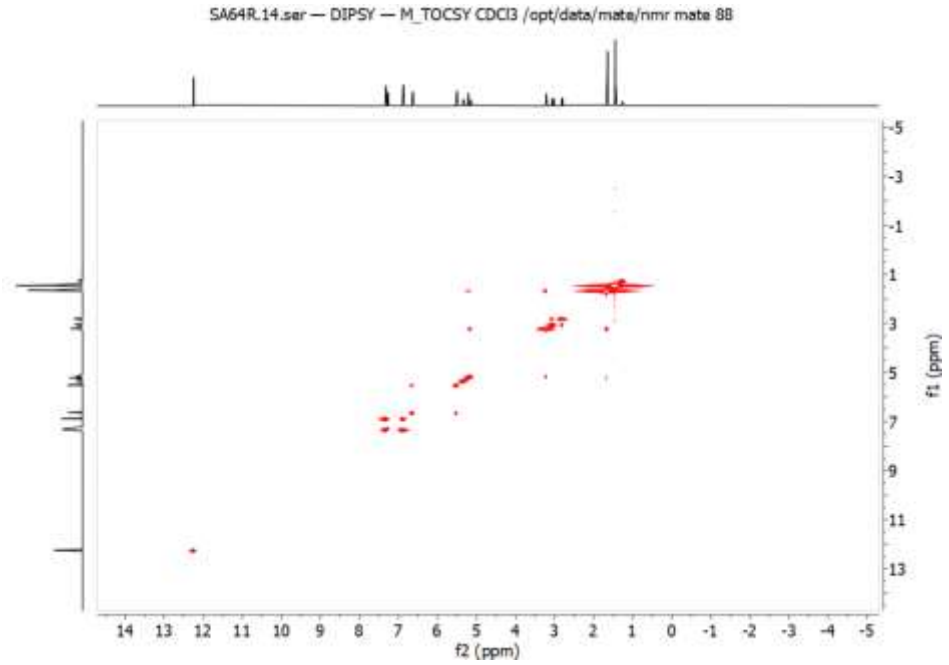

Appendix 20A: ^{1}H NMR (500 MHz, $CDCl_3$, 25°C) spectrum of Mundulinol (64)

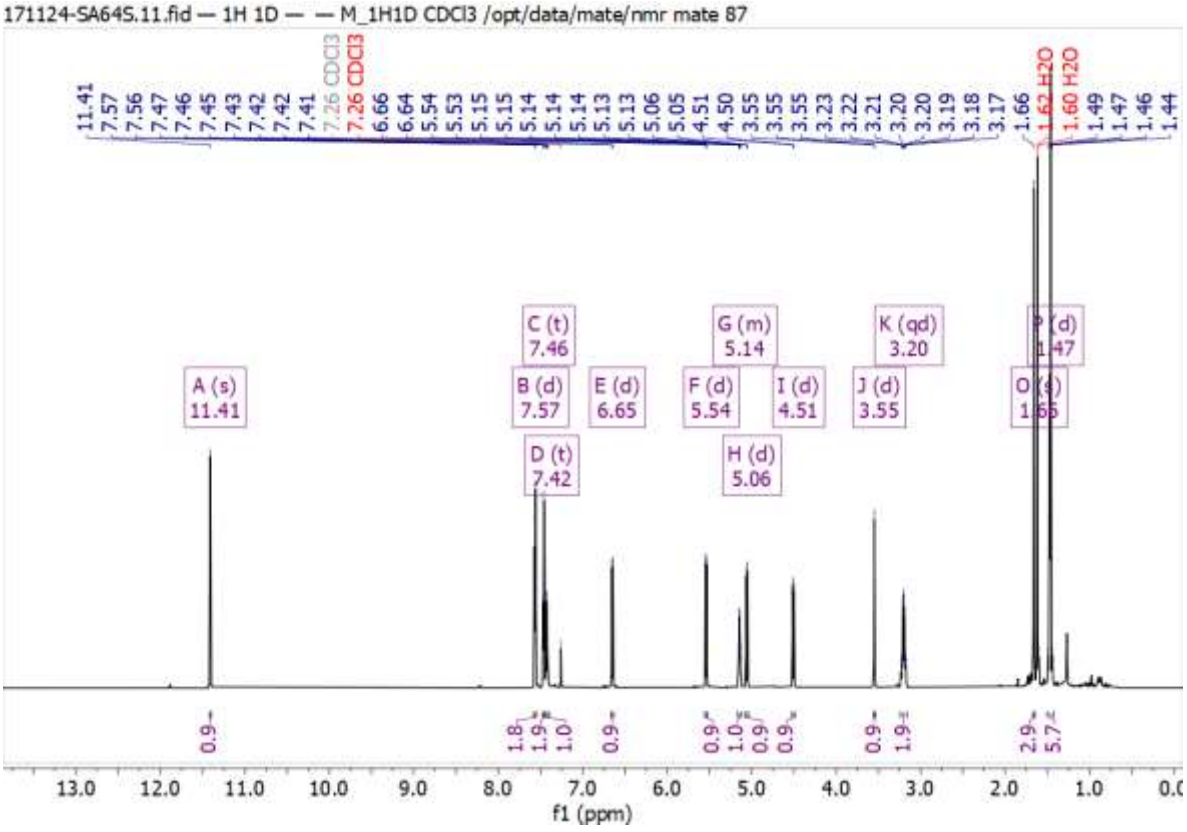

Appendix 20B. ^{13}C NMR (500 MHz, $CDCl_3$, 25°C) spectrum of Mundulinol (64)

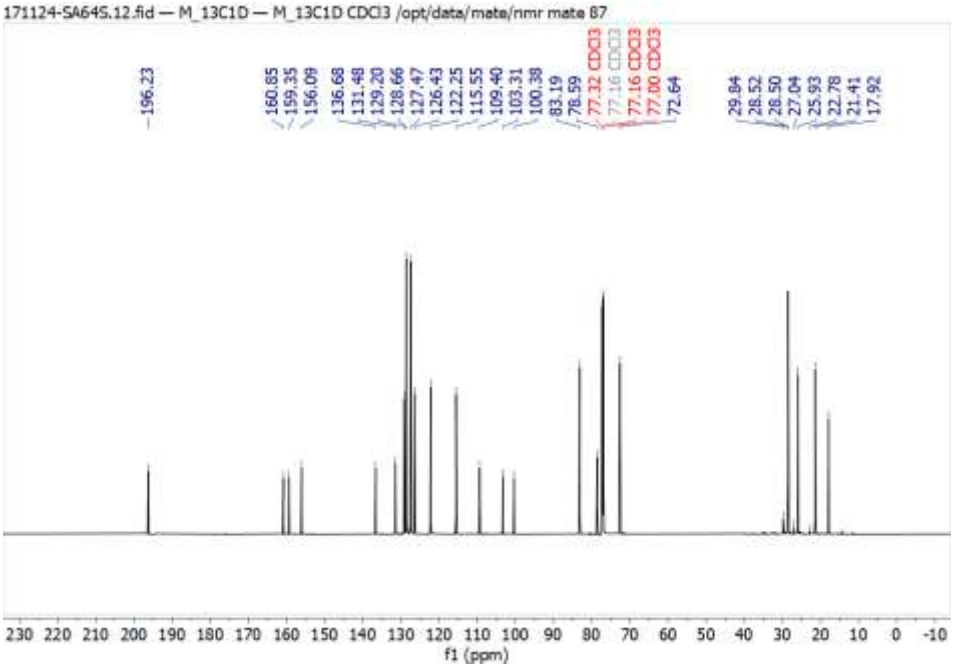

Appendix 20C. COSY (500 MHz, $CDCl_3$, 25°C) spectrum of Mundulinol (64)

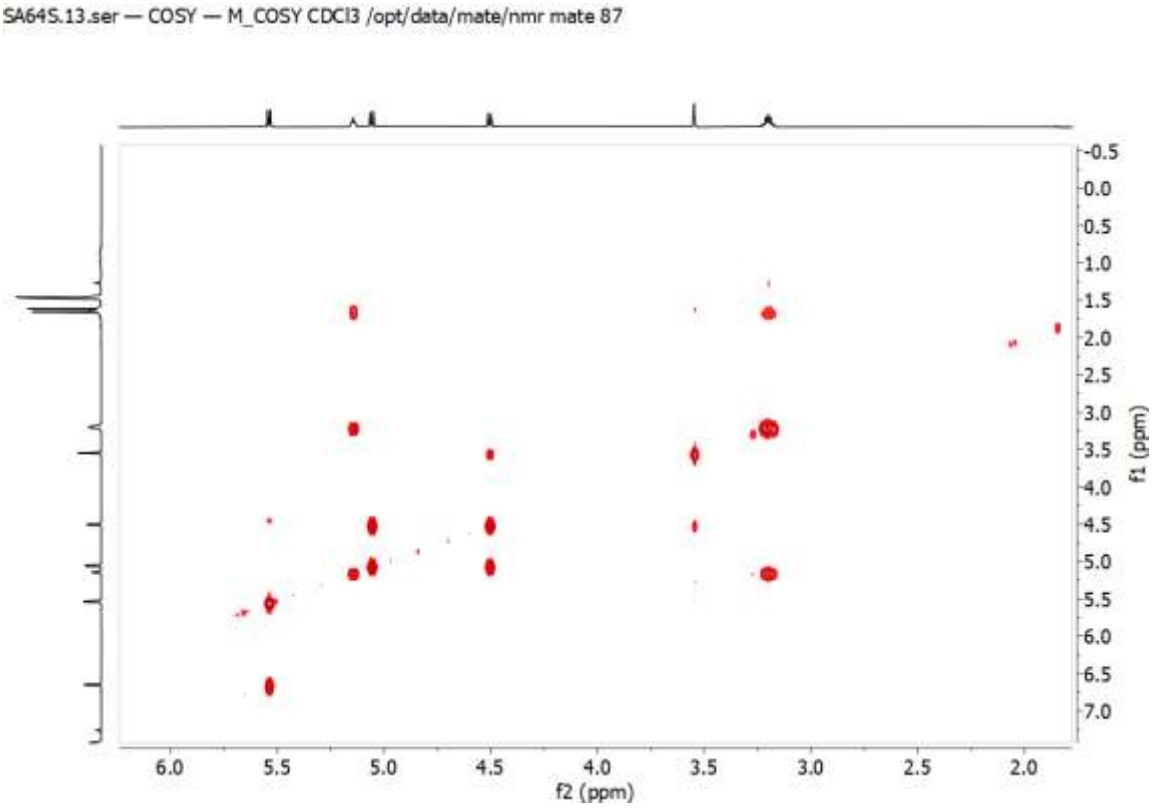

Appendix 20D: HSQC (500 MHz, $CDCl_3$, 25°C) spectrum of Mundulinol (64)

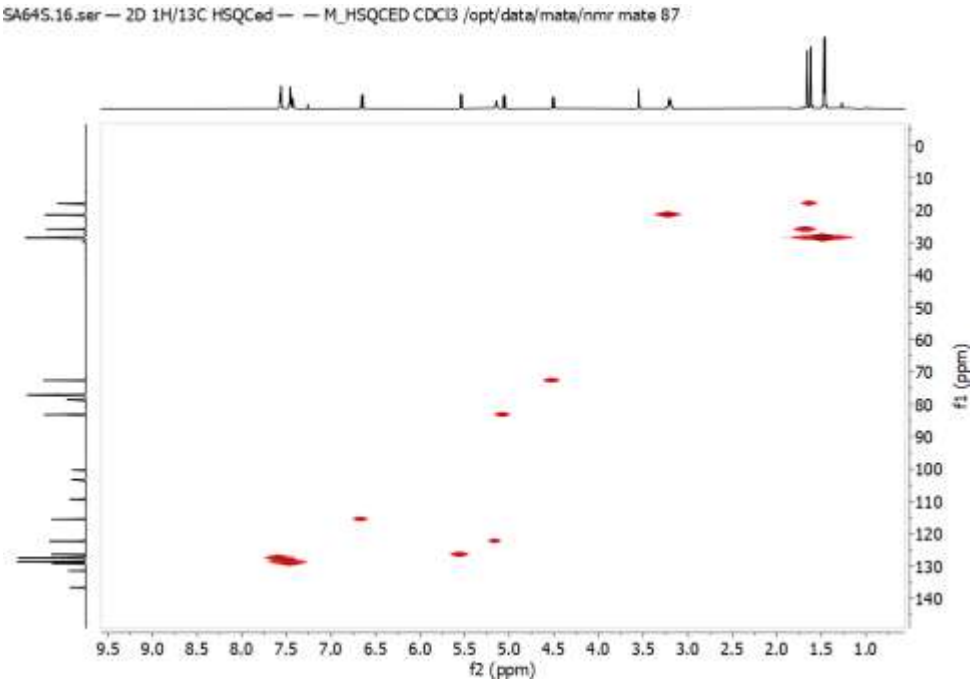

Appendix 20E: HMBC (500 MHz, $CDCl_3$, 25°C) spectrum of Mundulinol (64)

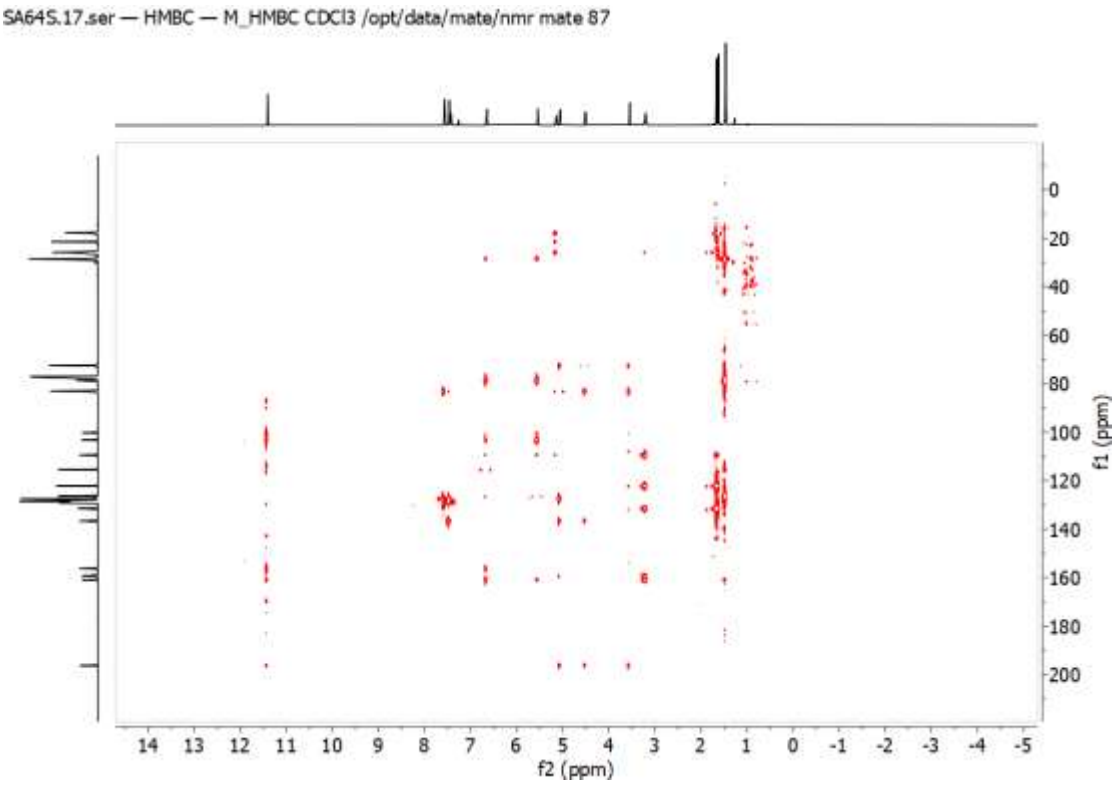

Appendix 20F: NOESY (500 MHz, $CDCl_3$, 25°C) spectrum of Mundulinol (64)

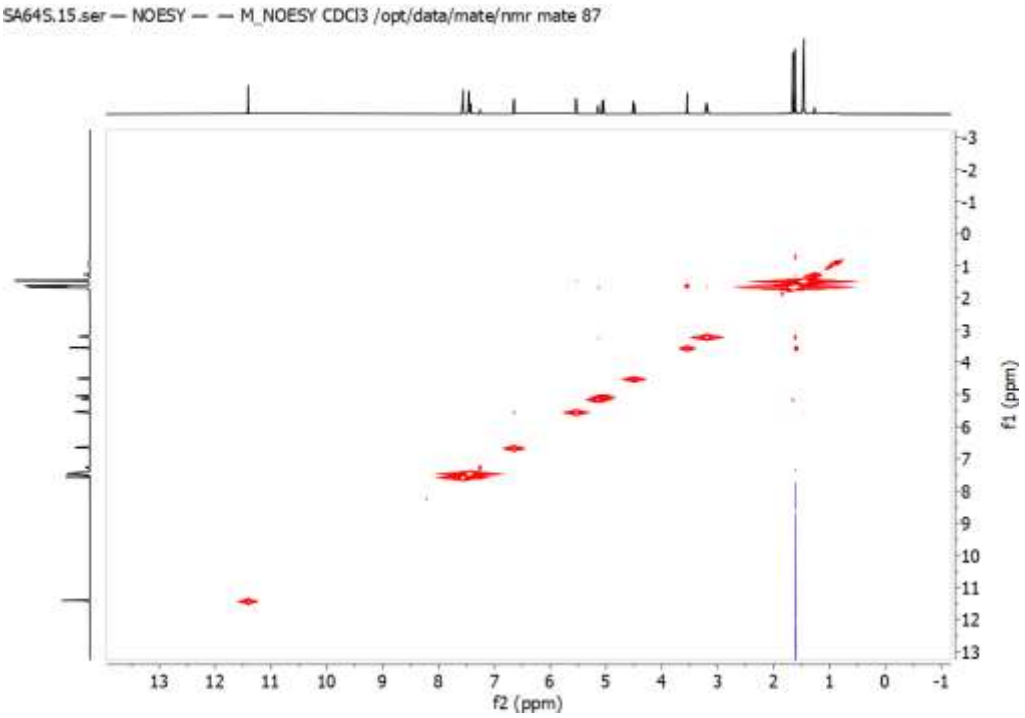

Appendix 20G. TOCSY (500 MHz, $CDCl_3$, 25°C) spectrum of Mundulinol (64)

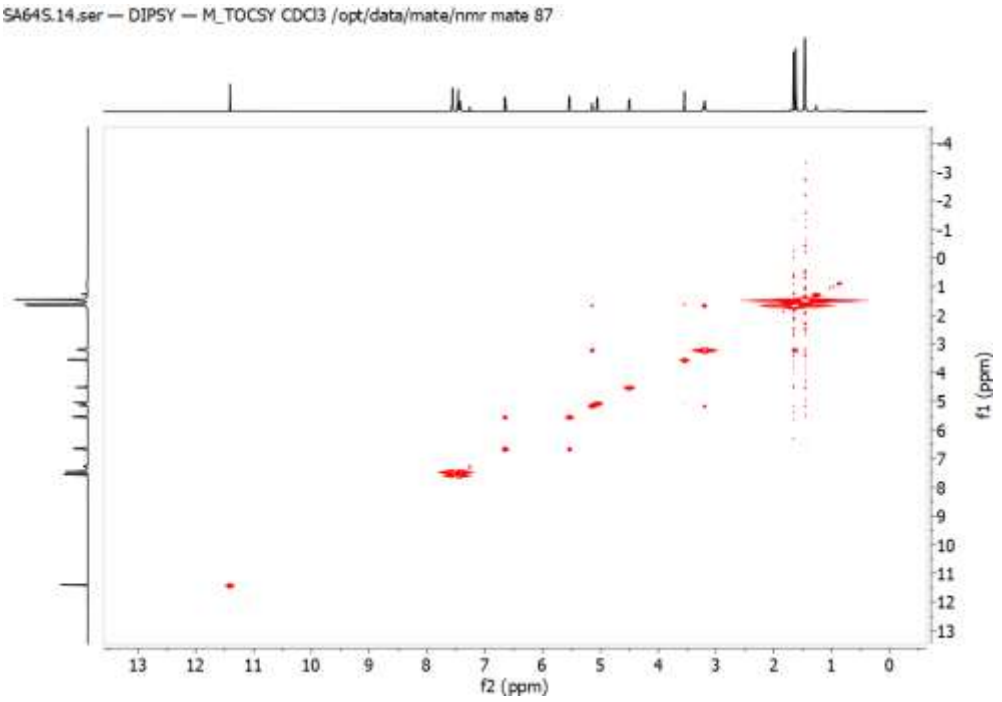

Appendix 21A: ^{1}H NMR (500 MHz, $CDCl_3$, 25°C) spectrum of Sericetin (130)

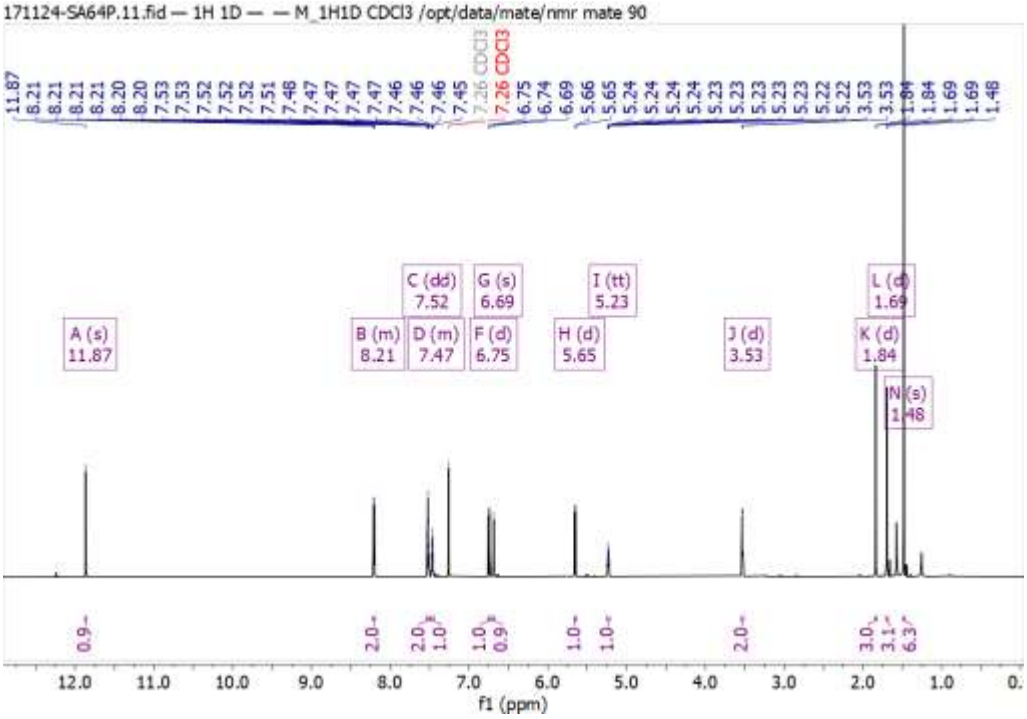

Appendix 21B. ^{13}C NMR (500 MHz, $CDCl_3$, 25°C) spectrum of Sericetin (130)

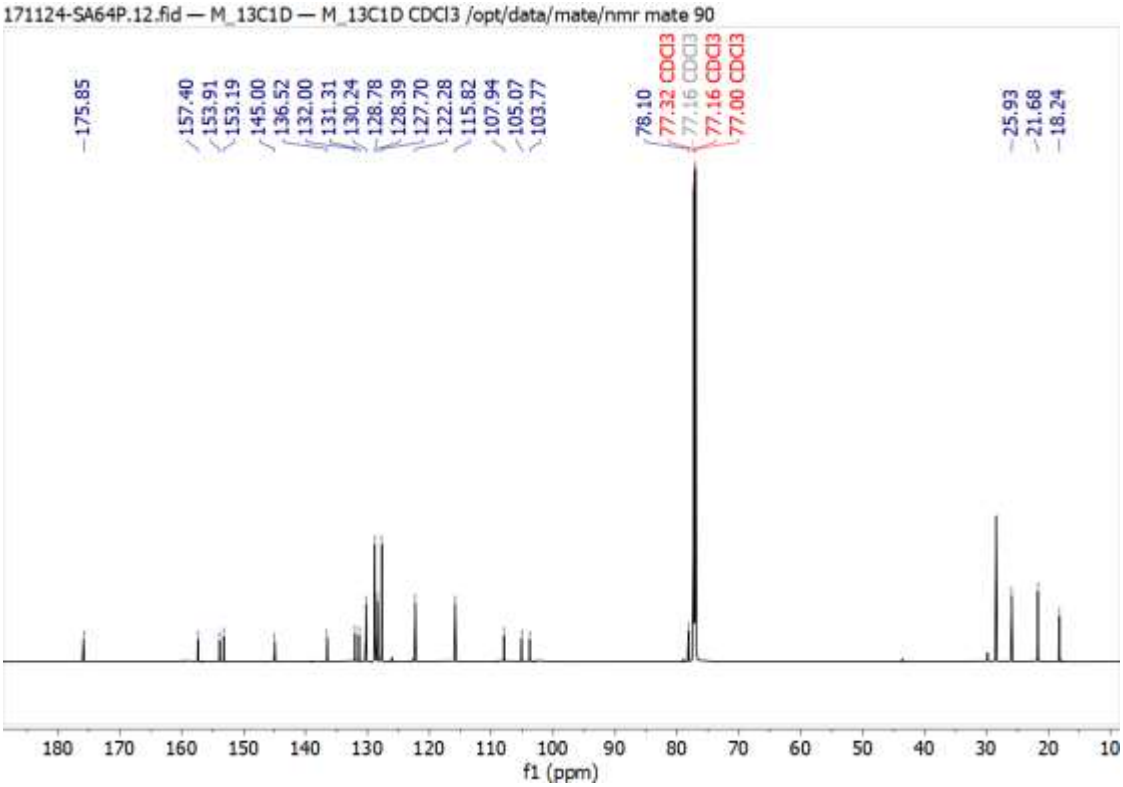

Appendix 21C. COSY (500 MHz, $CDCl_3$, 25°C) spectrum of Sericetin (130)

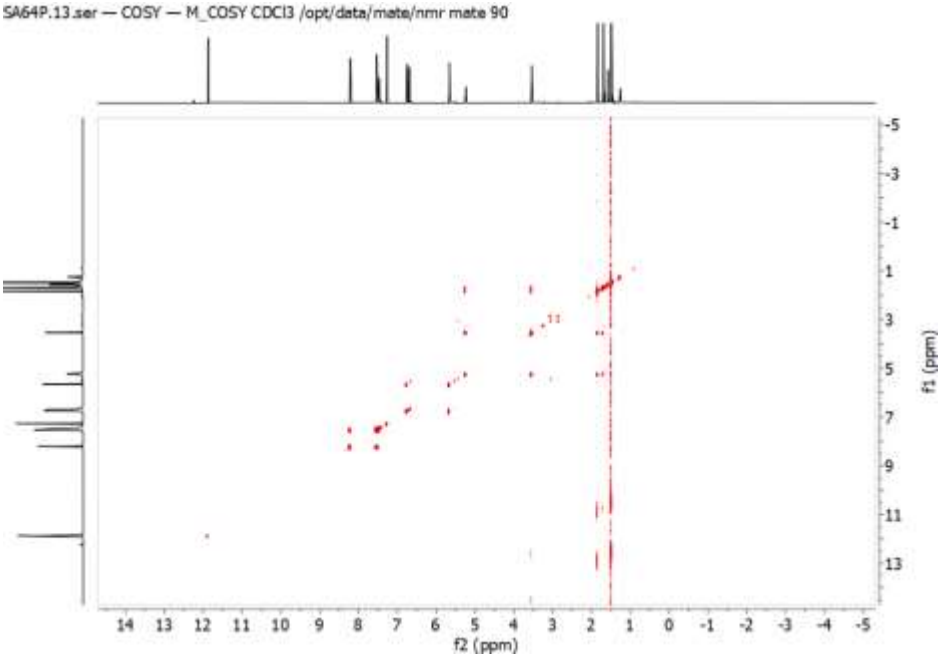

Appendix 21D: HSQC (500 MHz, $CDCl_3$, 25°C) spectrum of Sericetin (130)

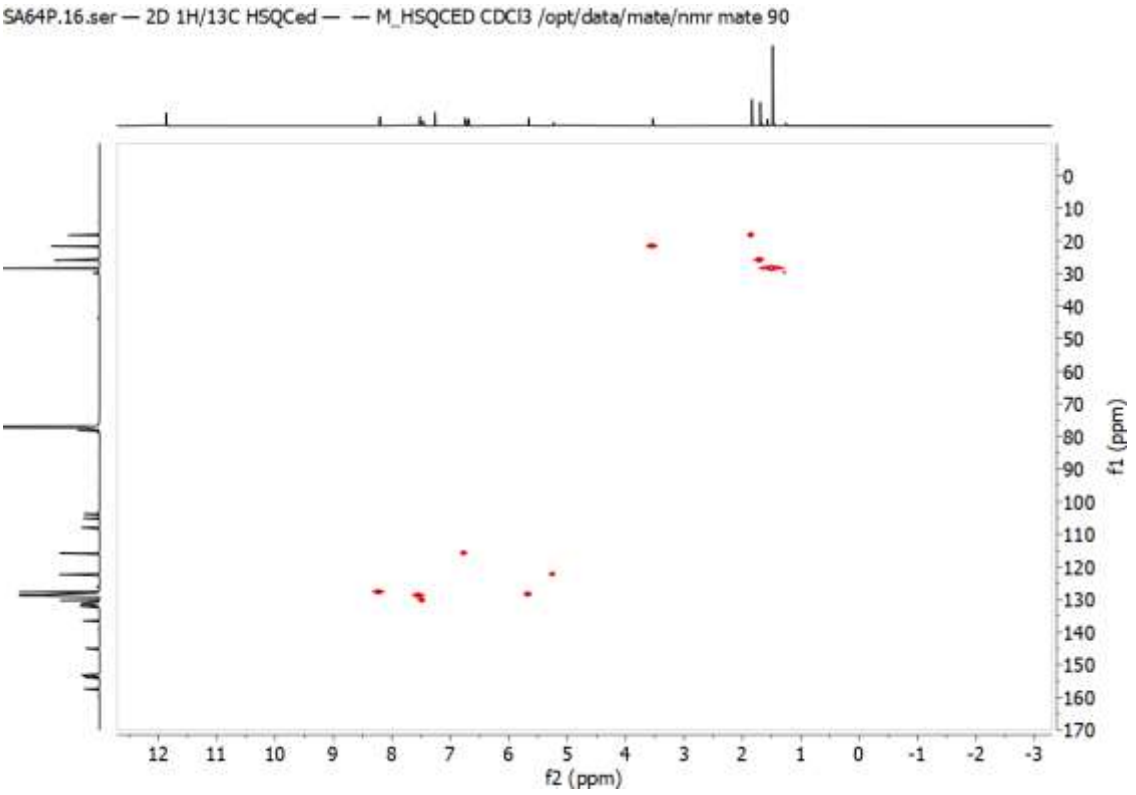

Appendix 21E: HMBC (500 MHz, $CDCl_3$, 25°C) spectrum of Sericetin (130)

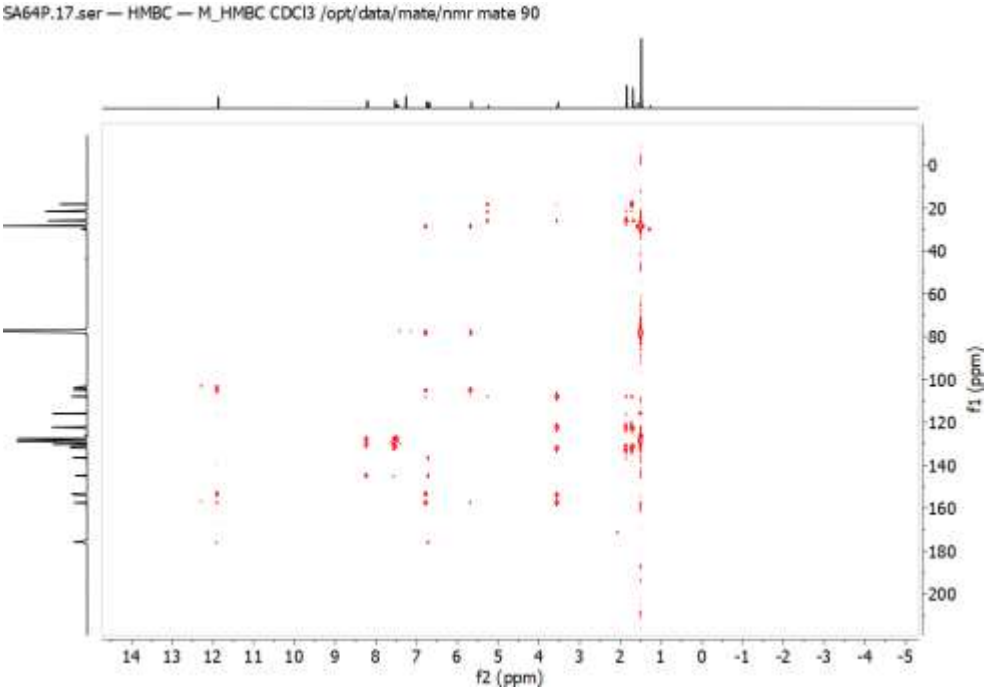

Appendix 21F: NOESY (500 MHz, $CDCl_3$, 25°C) spectrum of Sericetin (130)

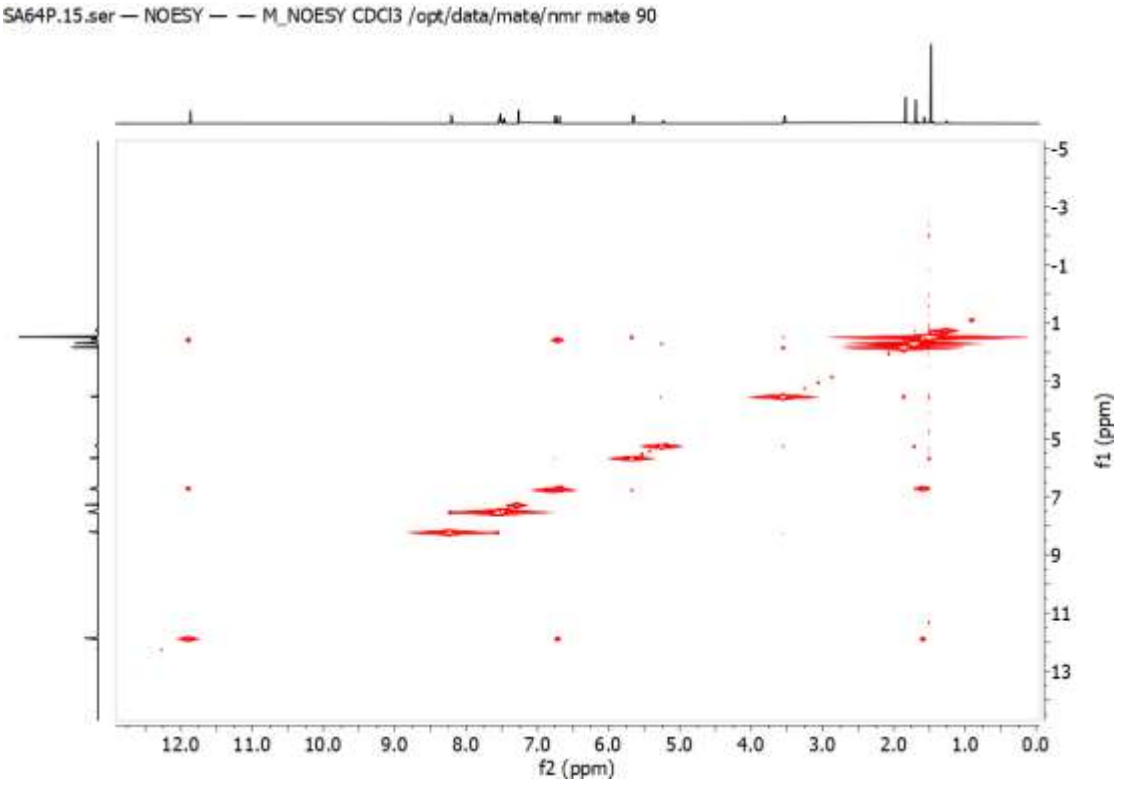

Appendix 21G. TOCSY (500 MHz, $CDCl_3$, 25°C) spectrum of Sericetin (130)

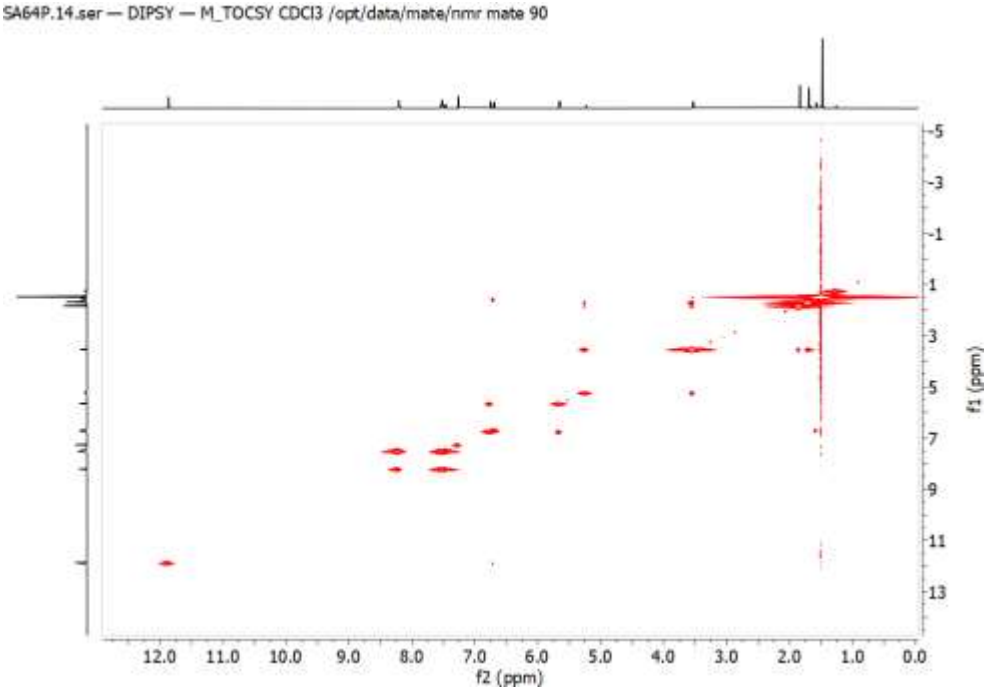

Appendix 22A: ^1H NMR (500 MHz, $CDCl_3$, 25°C) spectrum of munetone (70)

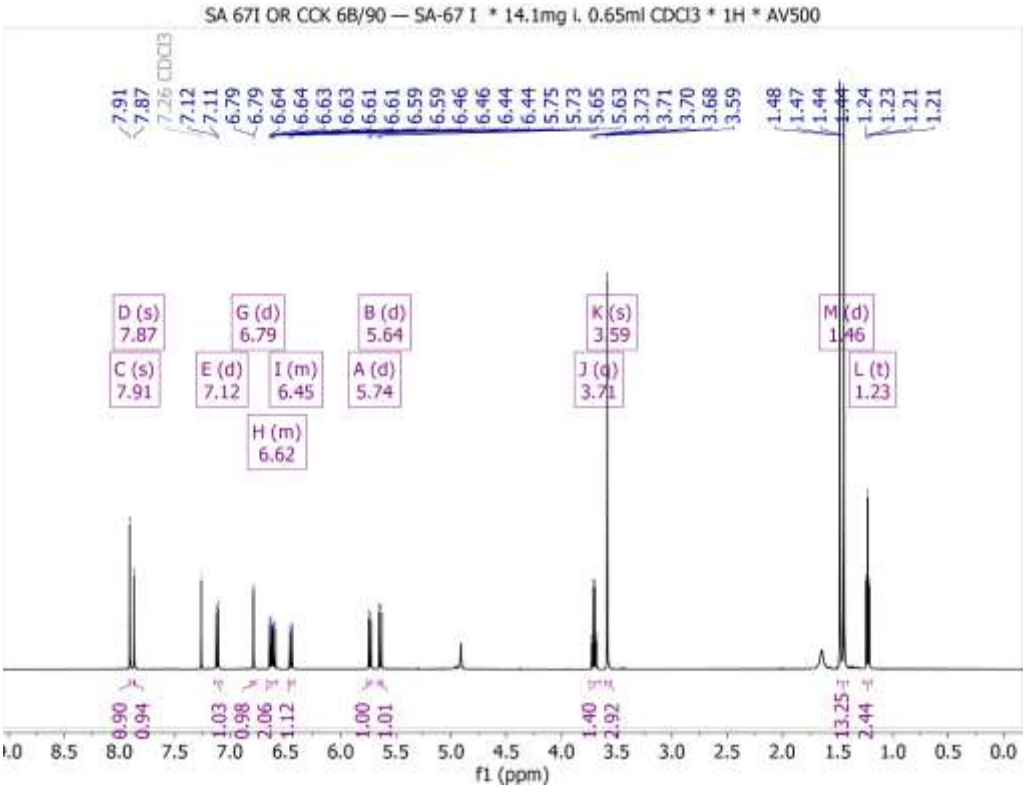

Appendix 22B. ^{13}C NMR (500 MHz, $CDCl_3$, 25°C) spectrum of **munetone (70)**

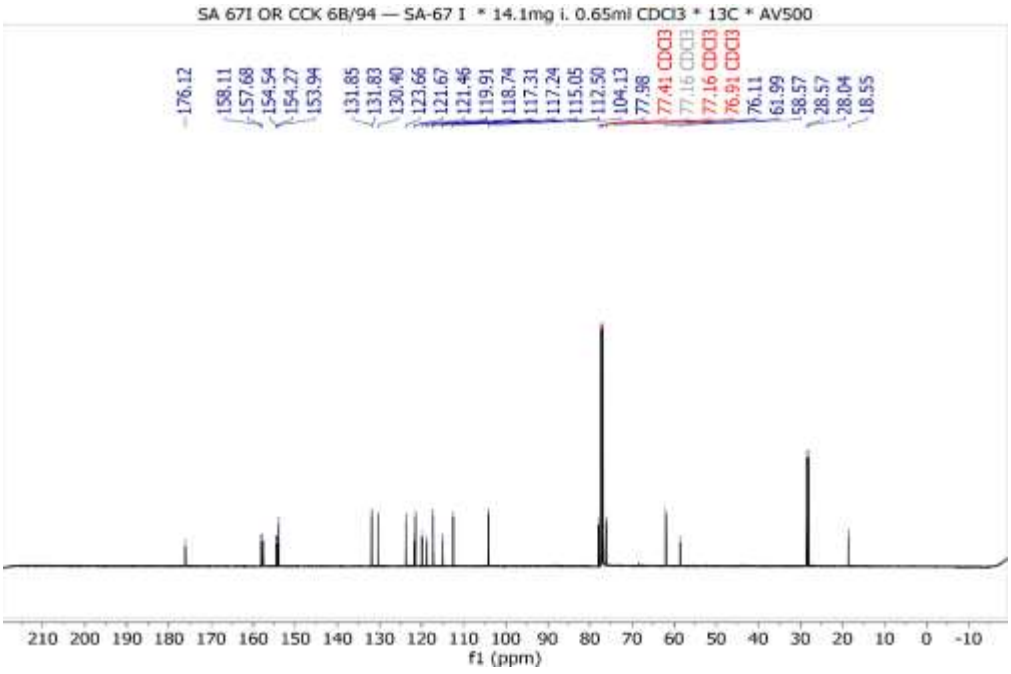

Appendix 22C. COSY (500 MHz, $CDCl_3$, 25°C) spectrum of **munetone (70)**

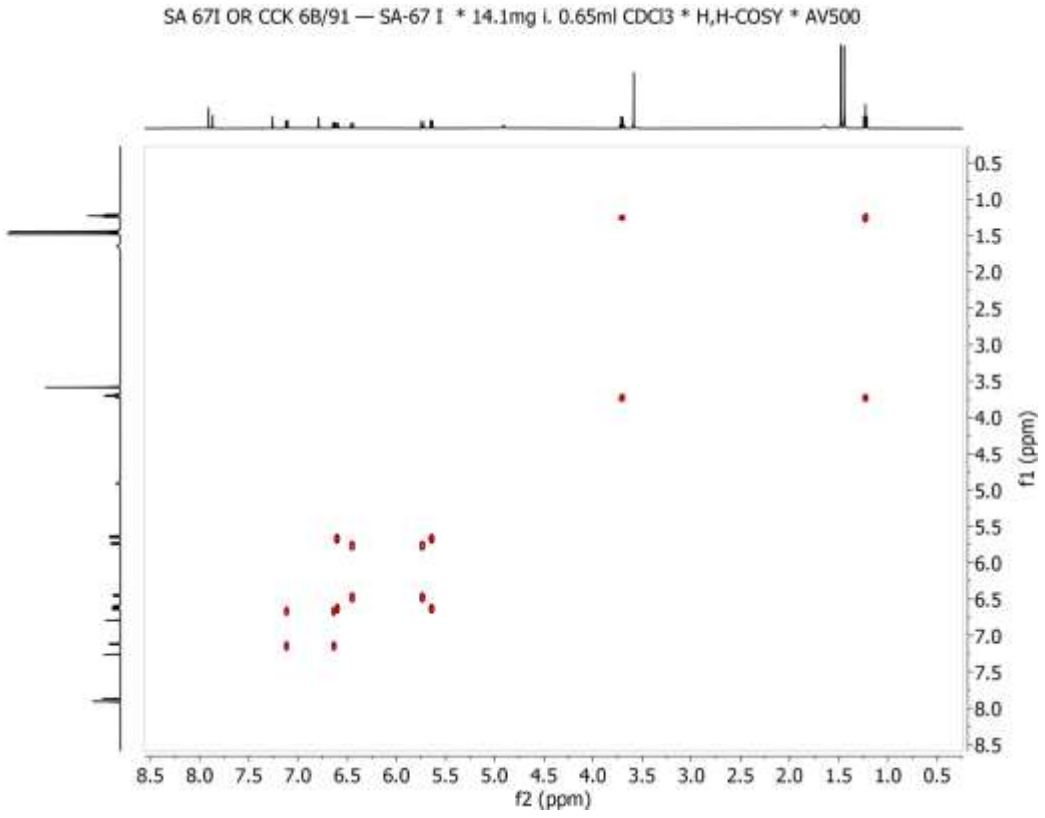

Appendix 22D: HSQC (500 MHz, $CDCl_3$, 25°C) spectrum of **munetone (70)**

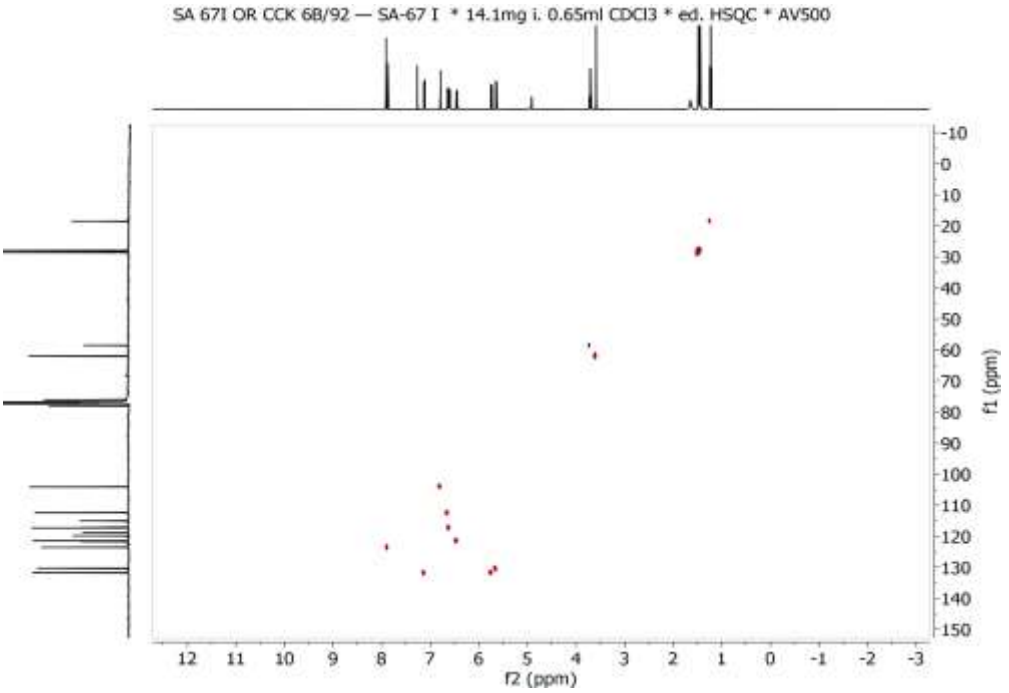

Appendix 22E: HMBC (500 MHz, $CDCl_3$, 25°C) spectrum of **munetone (70)**

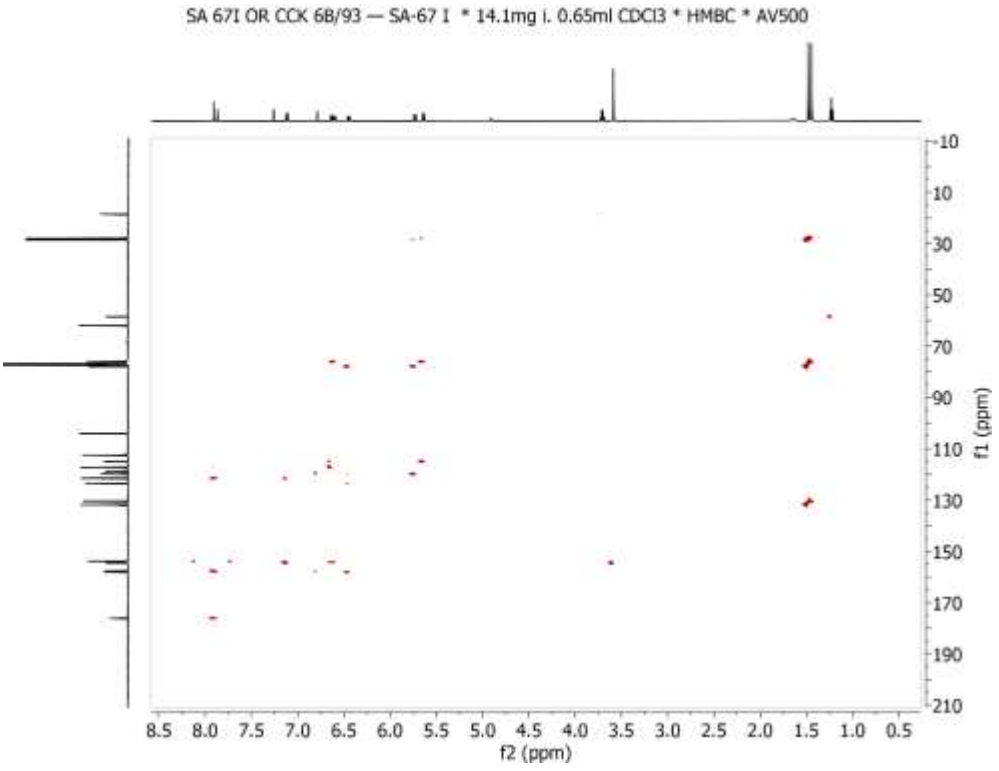

Appendix 23A: ^{1}H NMR (500 MHz, $CDCl_3$, 25°C) spectrum of rotenone (63)

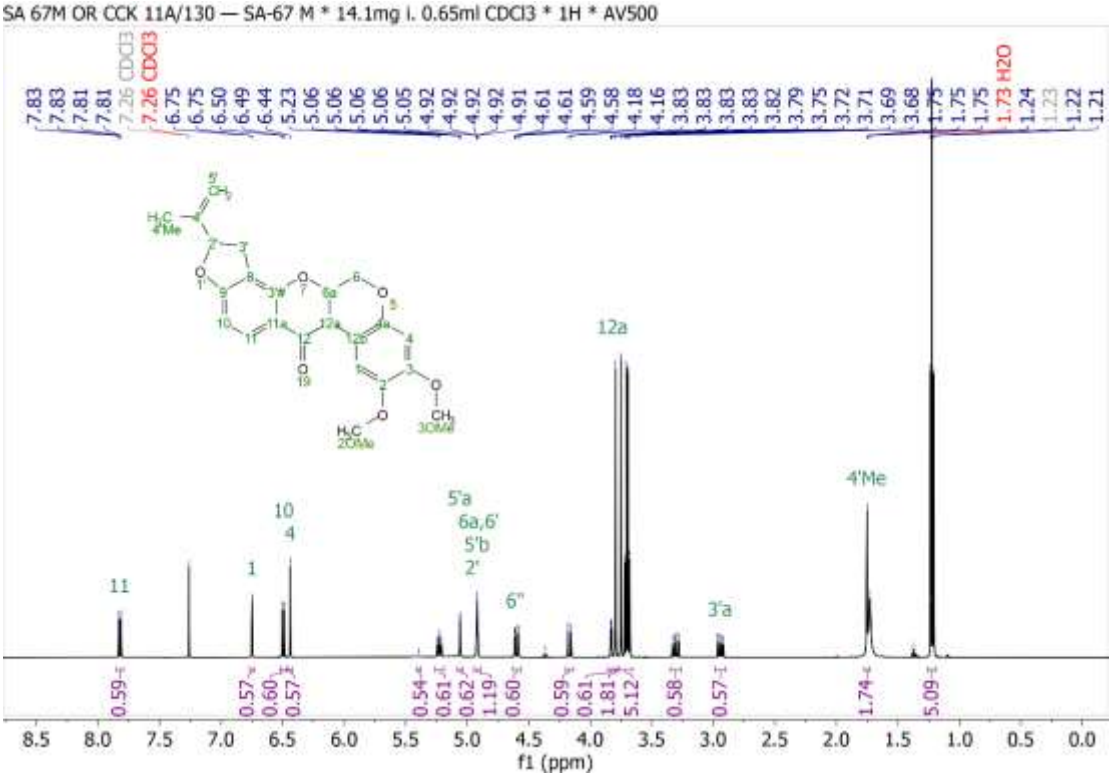

Appendix 23B. ^{13}C NMR (500 MHz, $CDCl_3$, 25°C) spectrum of rotenone (63)

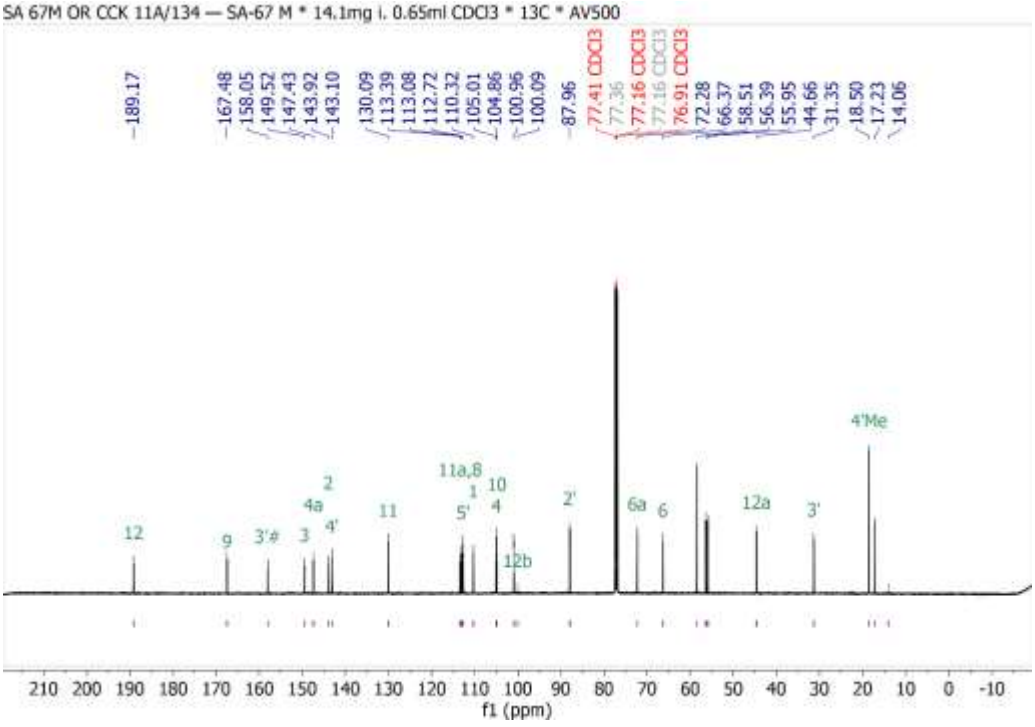

Appendix 23C. COSY (500 MHz, $CDCl_3$, 25°C) spectrum of rotenone (63)

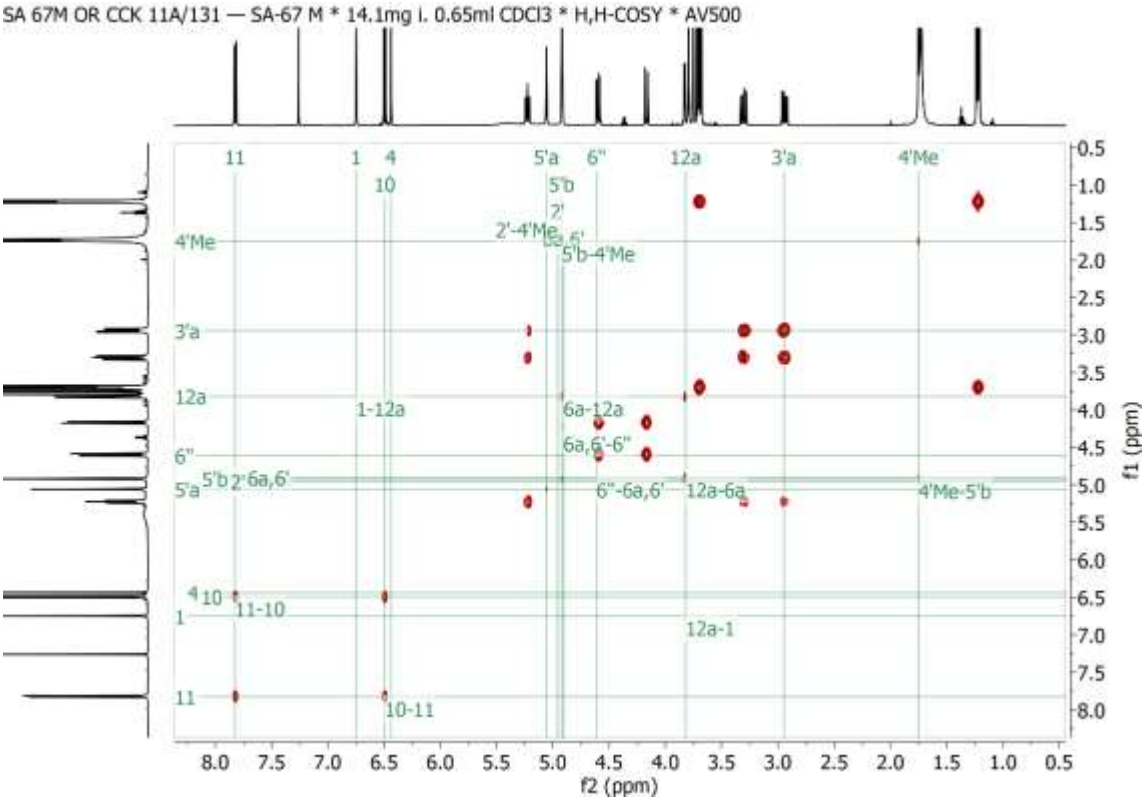

Appendix 23D: HSQC (500 MHz, $CDCl_3$, 25°C) spectrum of rotenone (63)

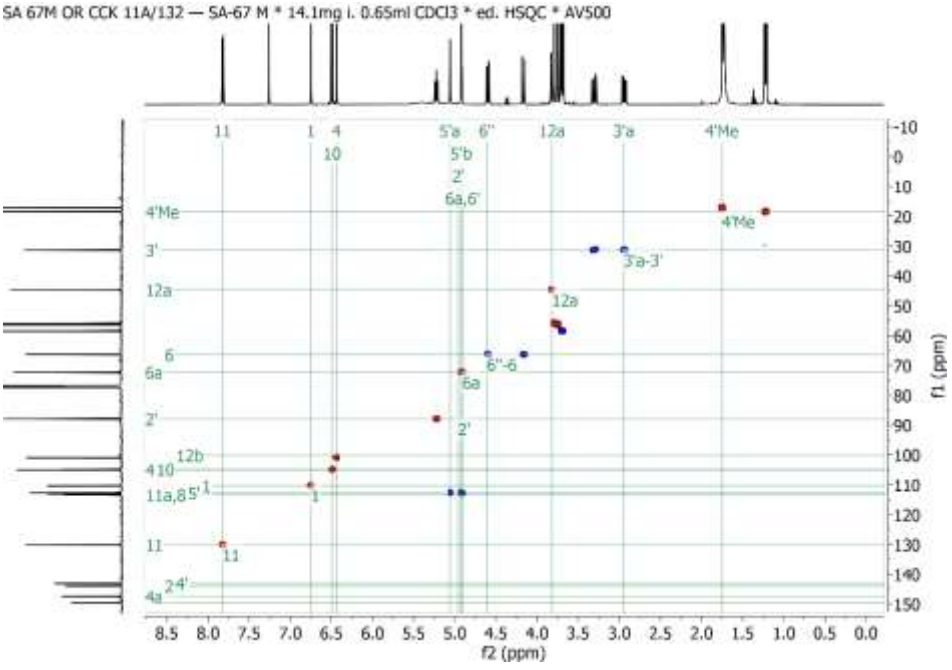

Appendix 23E: HMBC (500 MHz, $CDCl_3$, 25°C) spectrum of rotenone (63)

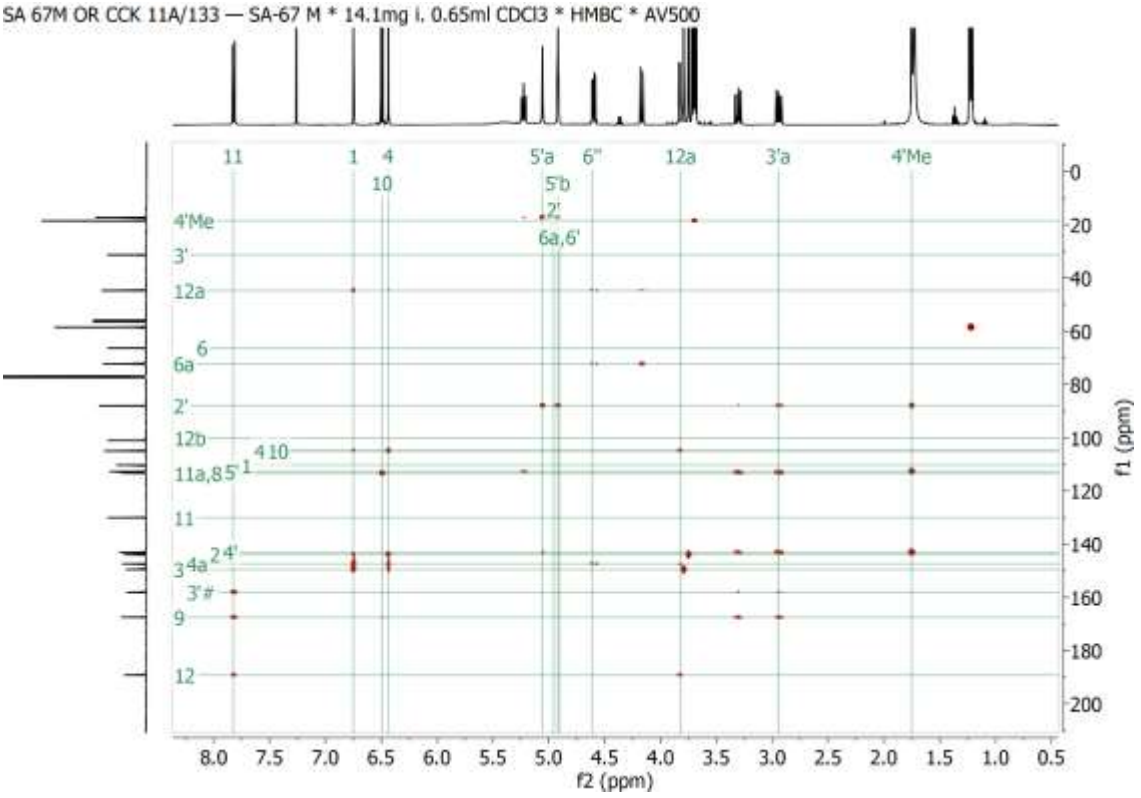

Appendix 24A: ^{1}H NMR (500 MHz, $CDCl_3$, 25°C) spectrum of striatine (131)

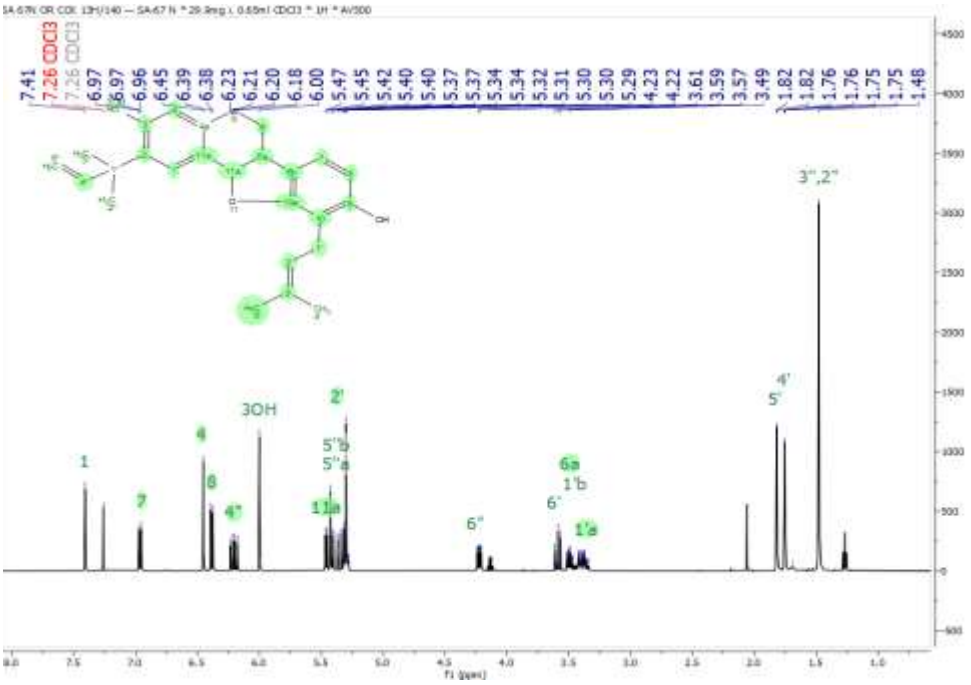

Appendix 24 B. ^{13}C NMR (500 MHz, $CDCl_3$, 25°C) spectrum of striatine (**131**)

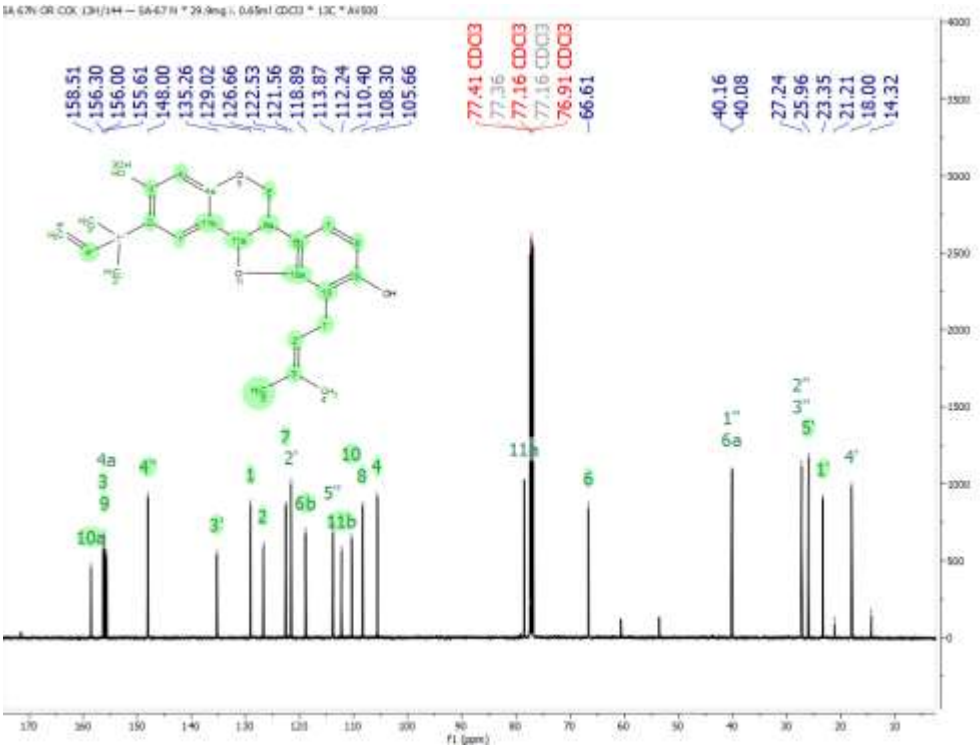

Appendix 24C. COSY (500 MHz, $CDCl_3$, 25°C) spectrum of striatine (**131**)

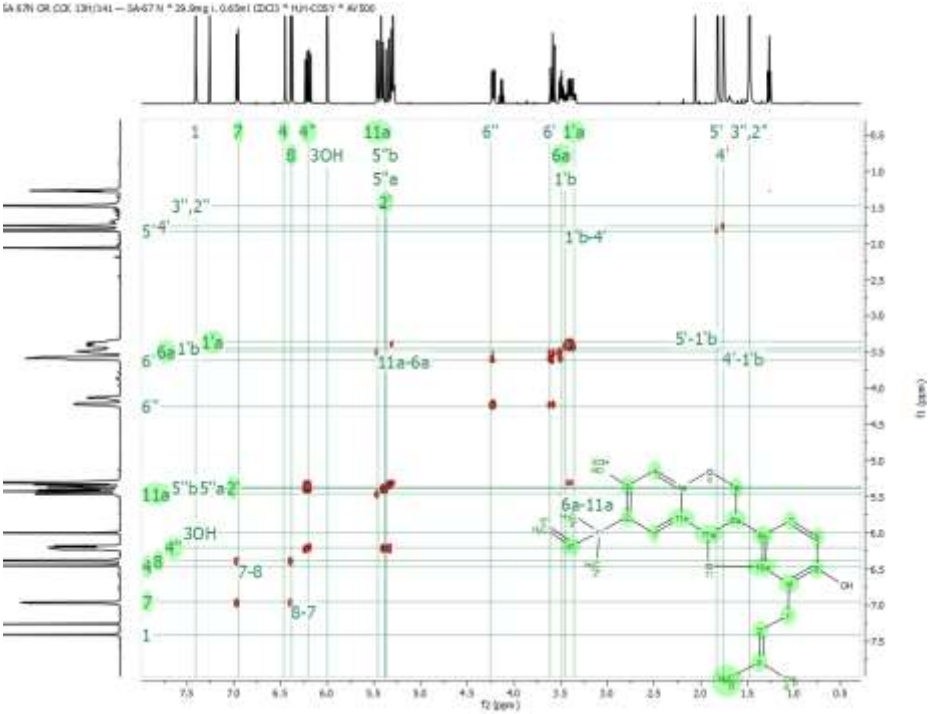

Appendix 24D: HSQC (500 MHz, $CDCl_3$, 25°C) spectrum of striatine (**131**)

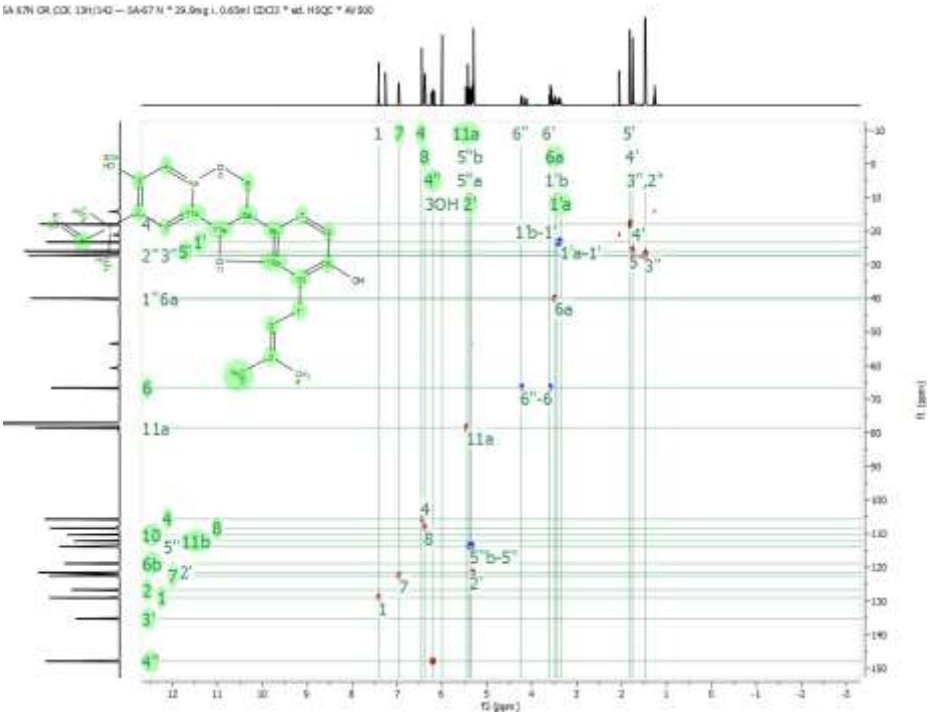

Appendix 24E: HMBC (500 MHz, $CDCl_3$, 25°C) spectrum of striatine (**131**)

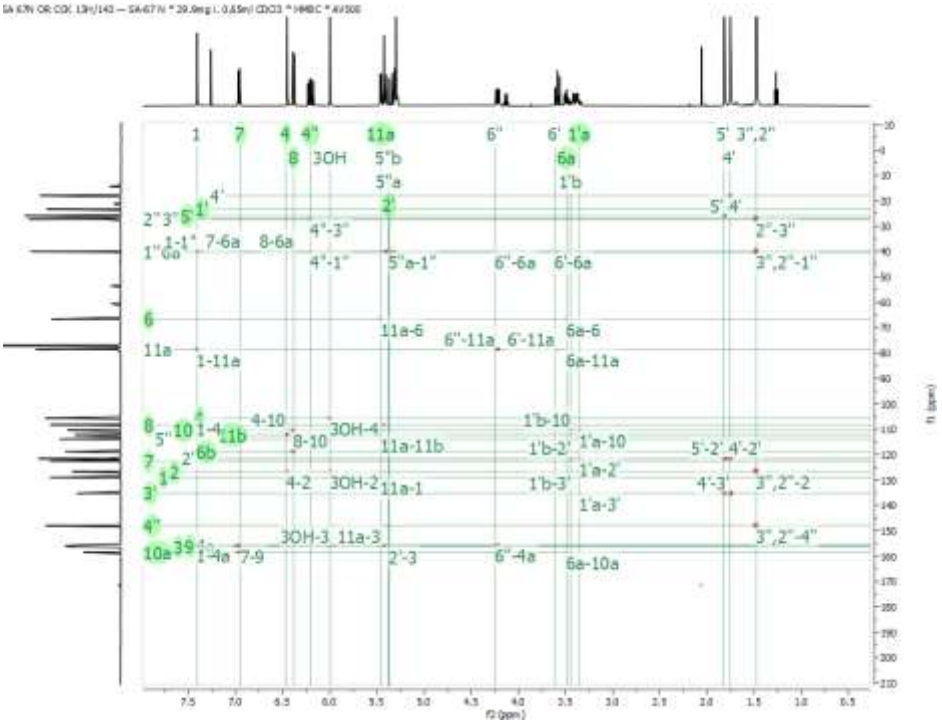

Appendix 25A: **^{1}H NMR (500 MHz, $CDCl_3$, 25°C) spectrum of 7-Hydxoxy-9-methoxy-2,3-(prop-1-en-2-yl)-dihydrofuranpterocarpan (132)**

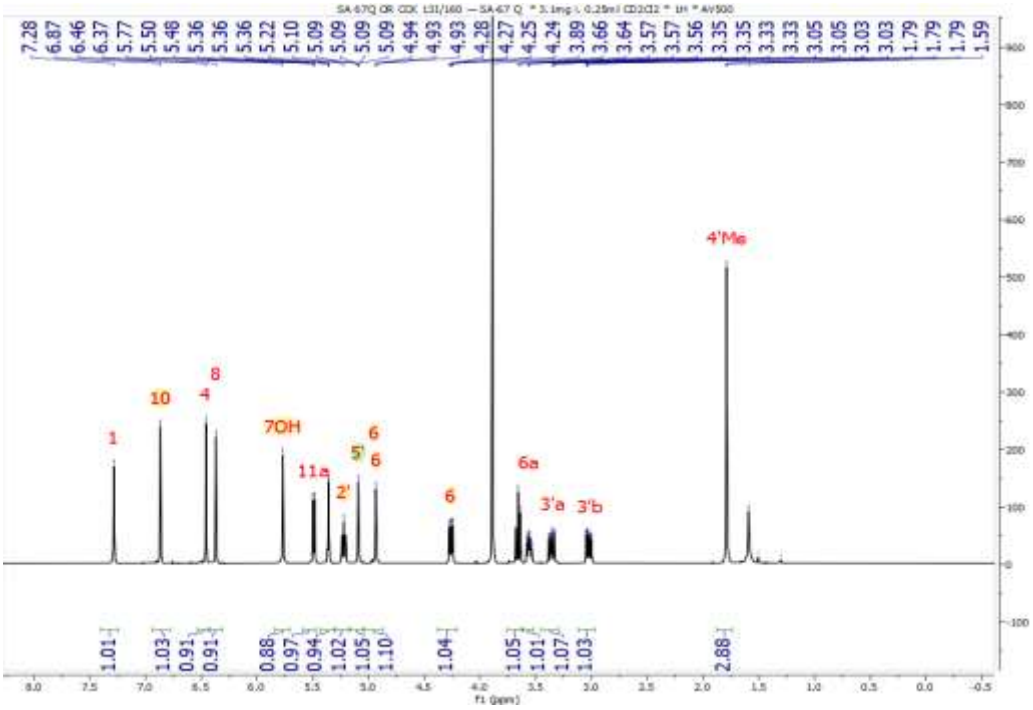

Appendix 25B. ^{13}C NMR (500 MHz, $CDCl_3$, 25°C) spectrum of 7-Hydxoxy-9-methoxy-2,3-(prop-1-en-2-yl)-dihydrofuranpterocarpan (**132**)

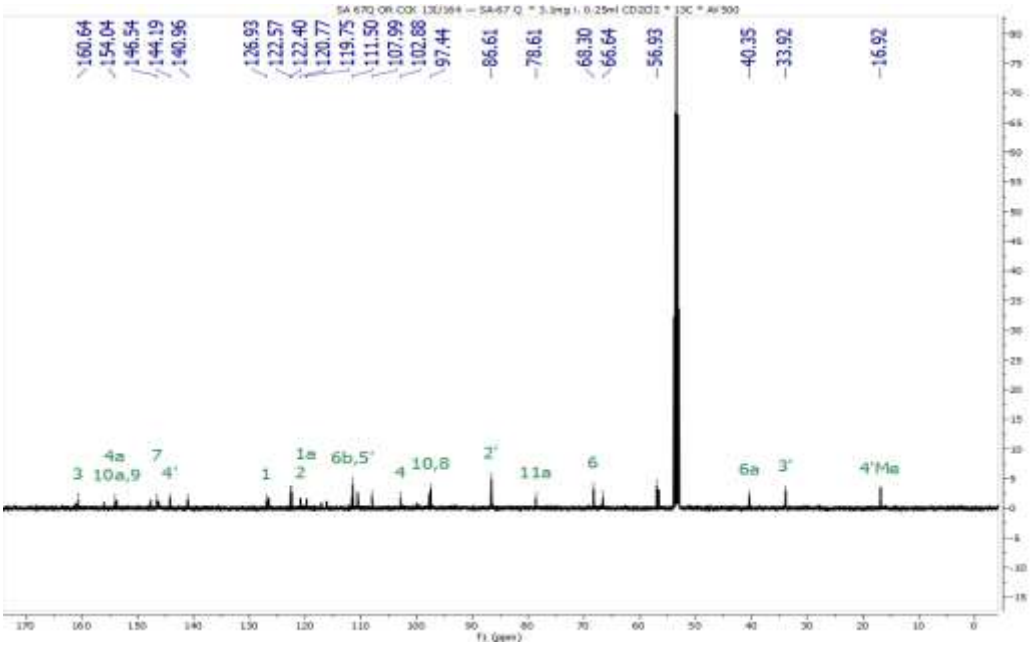

Appendix 25C. COSY (500 MHz, $CDCl_3$, 25°C) spectrum of 7-Hydxoxy-9-methoxy-2,3-(prop-1-en-2-yl)-dihydrofuranpterocarpan (**132**)

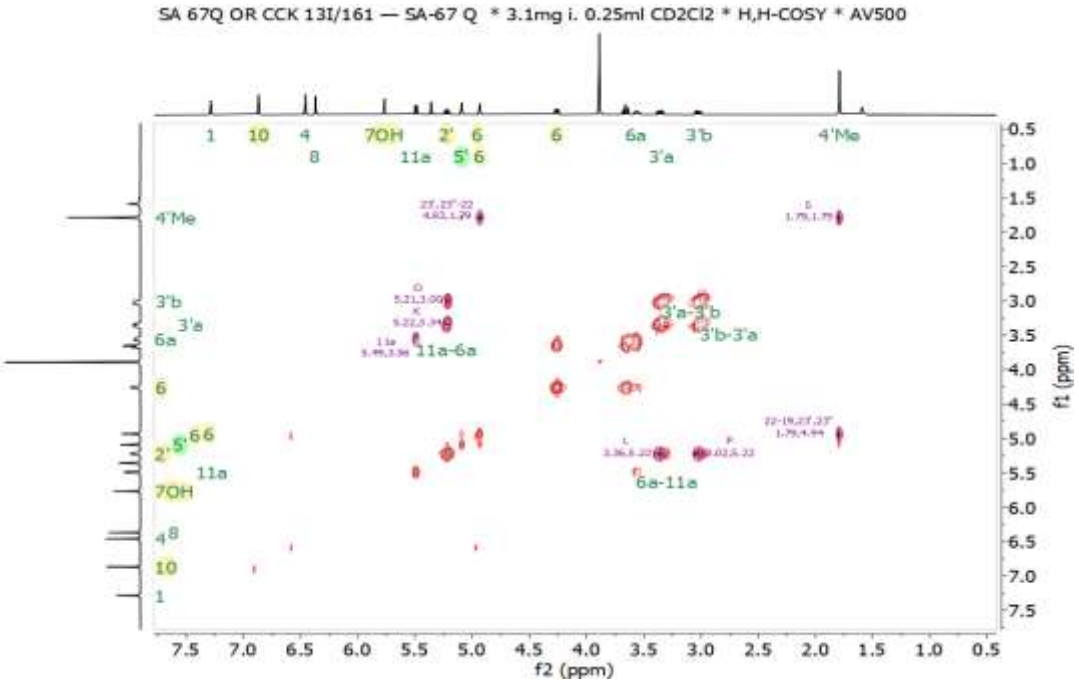

Appendix 25D: HSQC (500 MHz, $CDCl_3$, 25°C) spectrum of 7-Hydxoxy-9-methoxy-2,3-(prop-1-en-2-yl)-dihydrofuranpterocarpan (**132**)

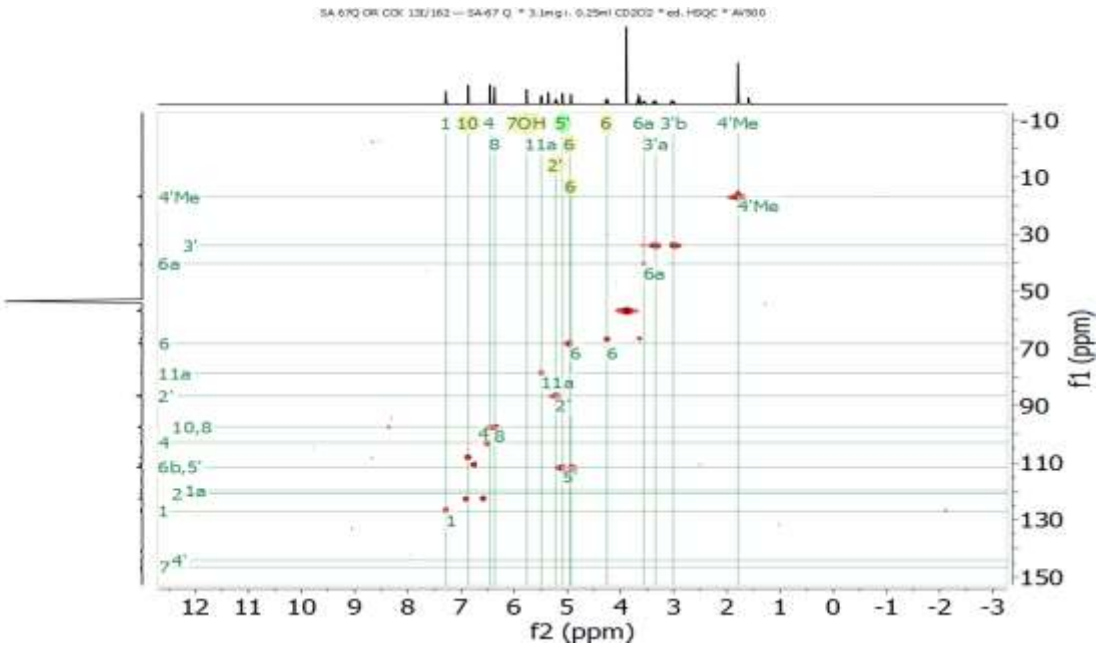

Appendix 25E: HMBC (500 MHz, $CDCl_3$, 25°C) spectrum of 7-Hydxoxy-9-methoxy-2,3-(prop-1-en-2-yl)-dihydrofuranpterocarpan (**132**)

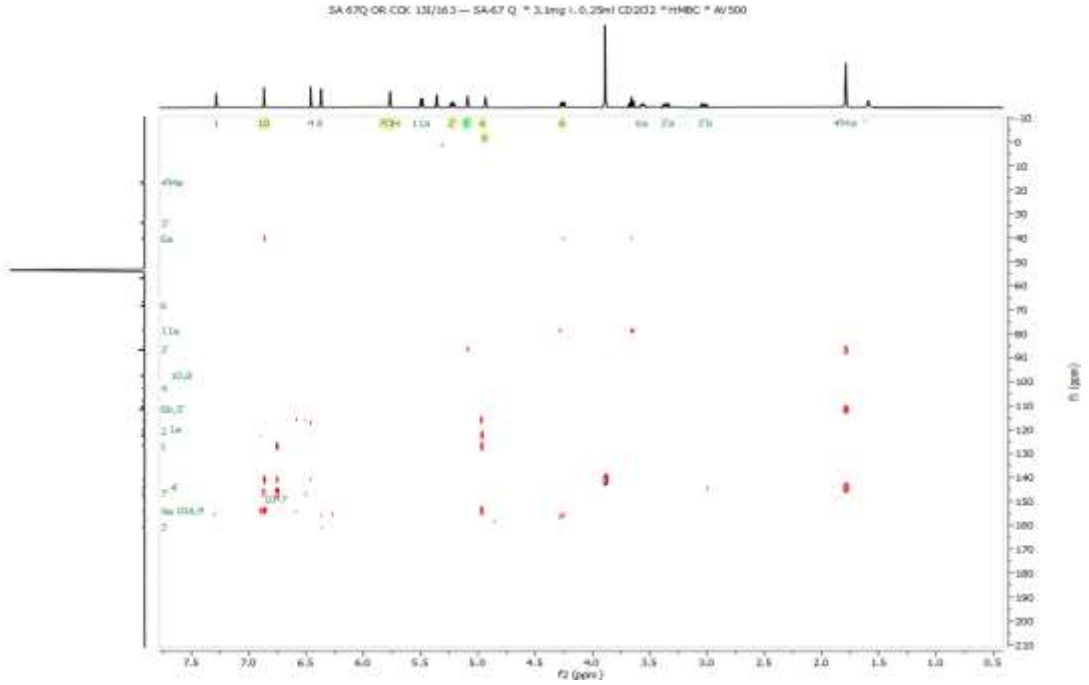

Appendix 26A: ^{1}H NMR (500 MHz, $CDCl_3$, 25°C) spectrum of Stigmasterol (88)

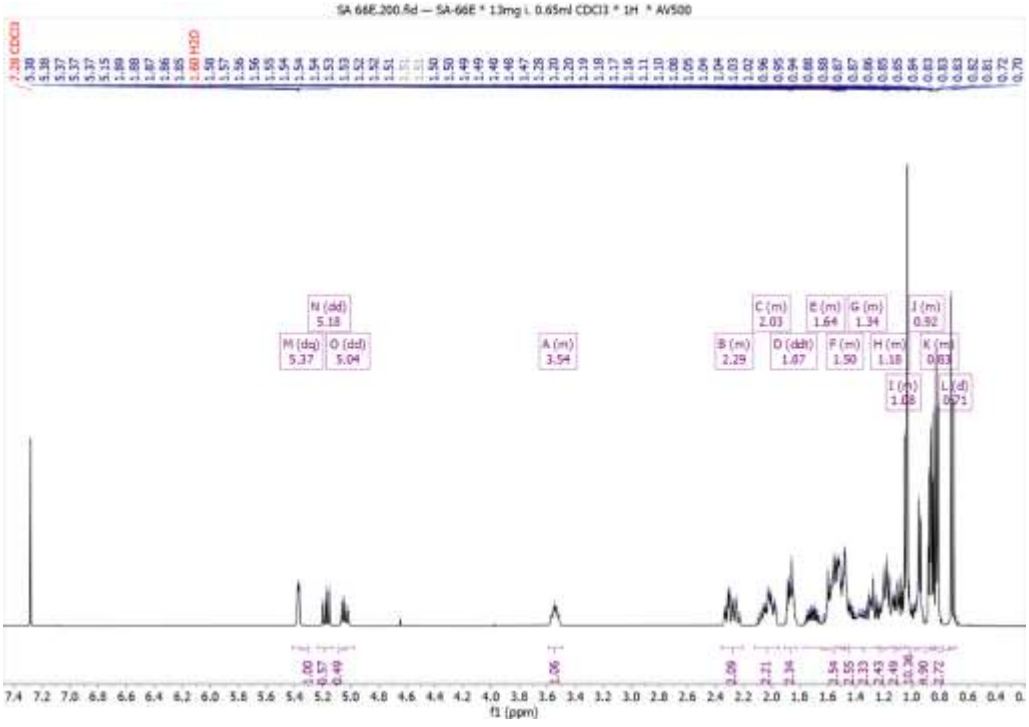

Appendix 26B. ^{13}C NMR (500 MHz, $CDCl_3$, 25°C) spectrum of Stigmasterol (**88**)

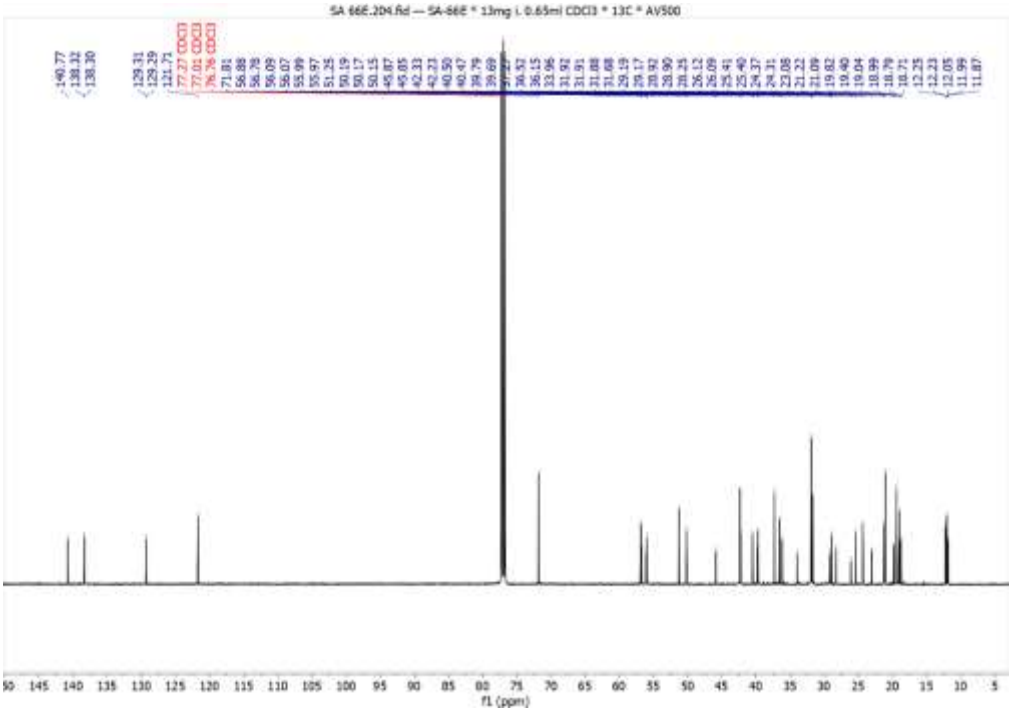

Appendix 26C. COSY (500 MHz, $CDCl_3$, 25°C) spectrum of Stigmasterol (**88**)

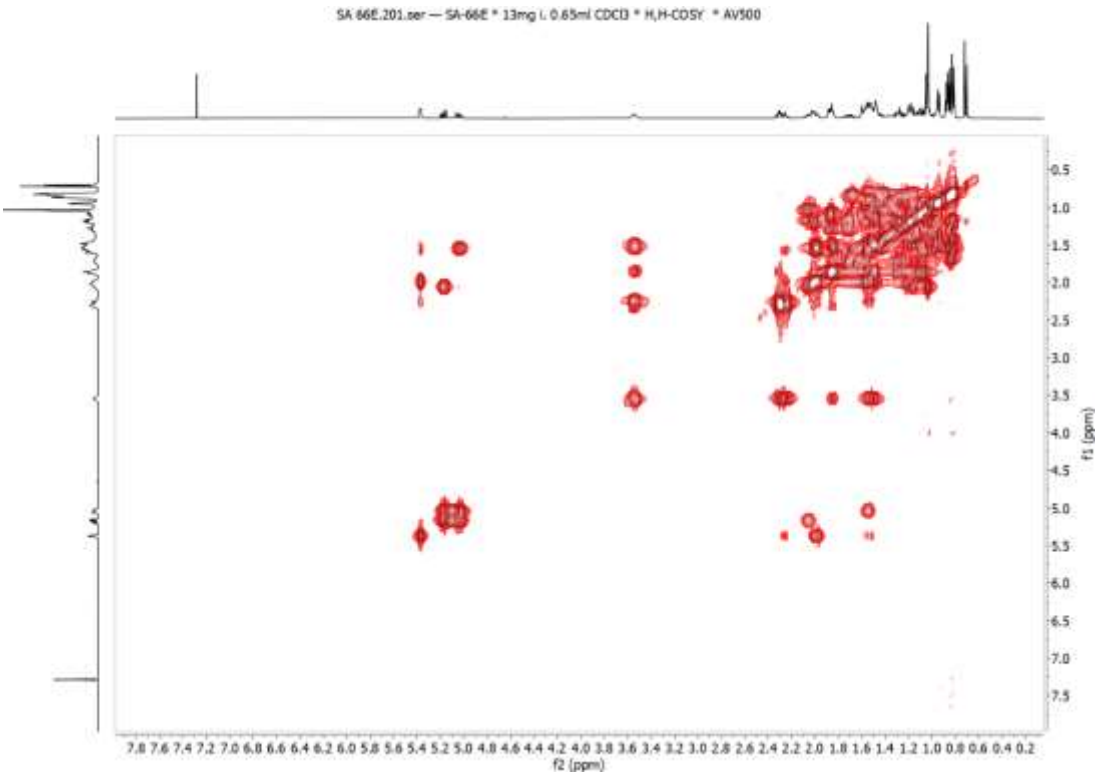

Appendix 26D: HSQC (500 MHz, $CDCl_3$, 25°C) spectrum of Stigmasterol (**88**)

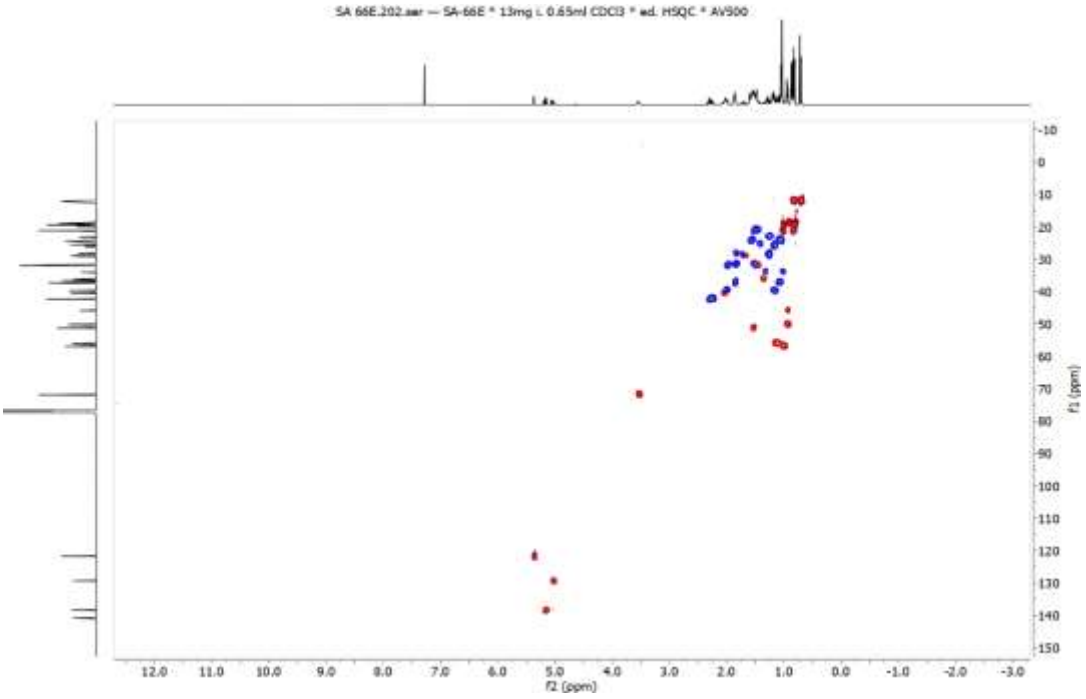

Appendix 26E: HMBC (500 MHz, $CDCl_3$, 25°C) spectrum of Stigmasterol (**88**)

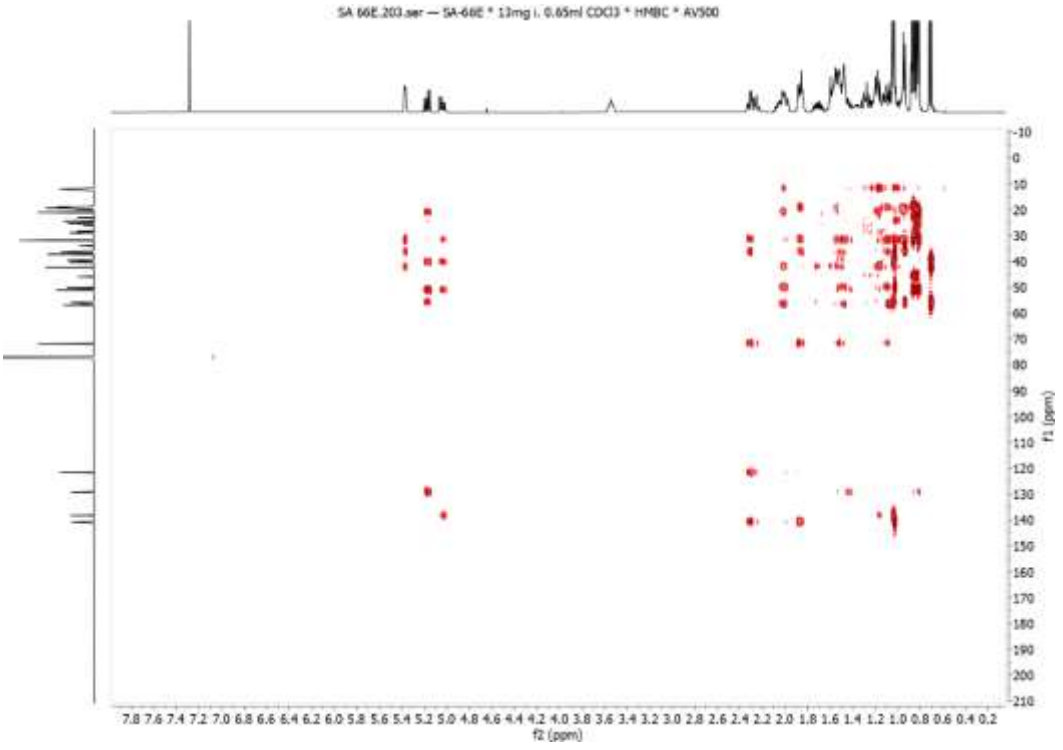

Appendix 27A: ^{1}H NMR (500 MHz, $CDCl_3$, 25°C) spectrum of (*S*)-elatadihydrochalcone-2'-methyl ether (133)

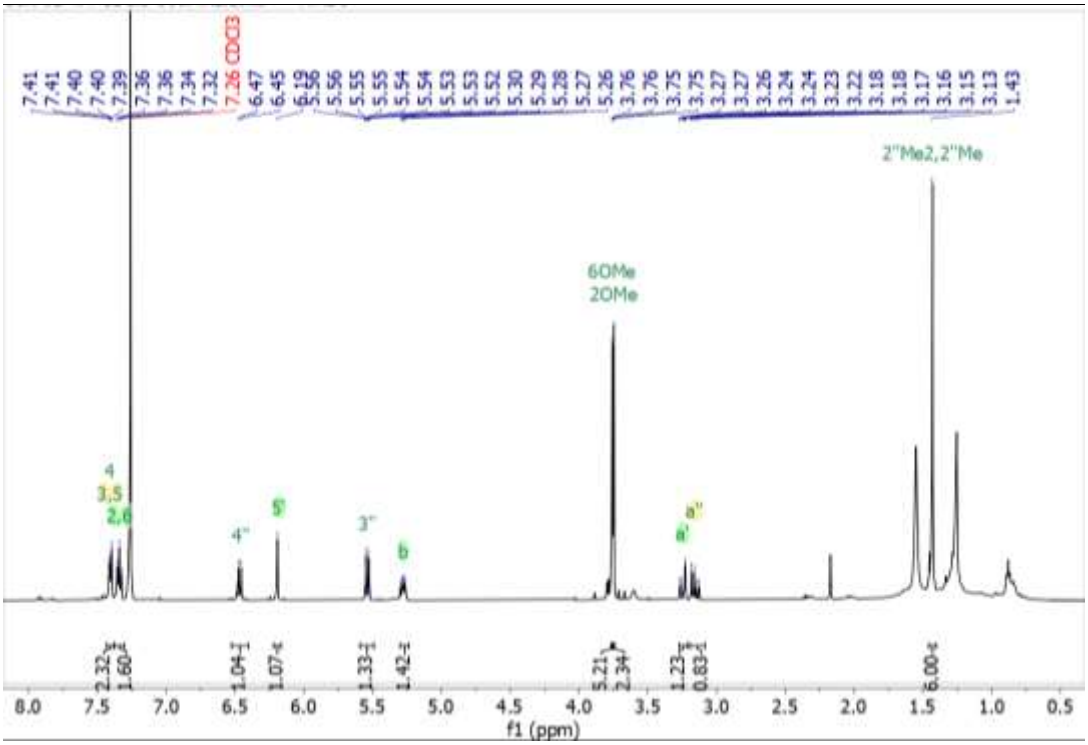

Appendix 27B. ^{13}C NMR (500 MHz, $CDCl_3$, 25°C) spectrum of (*S*)-elatadihydrochalcone-2'-methyl ether (**133**)

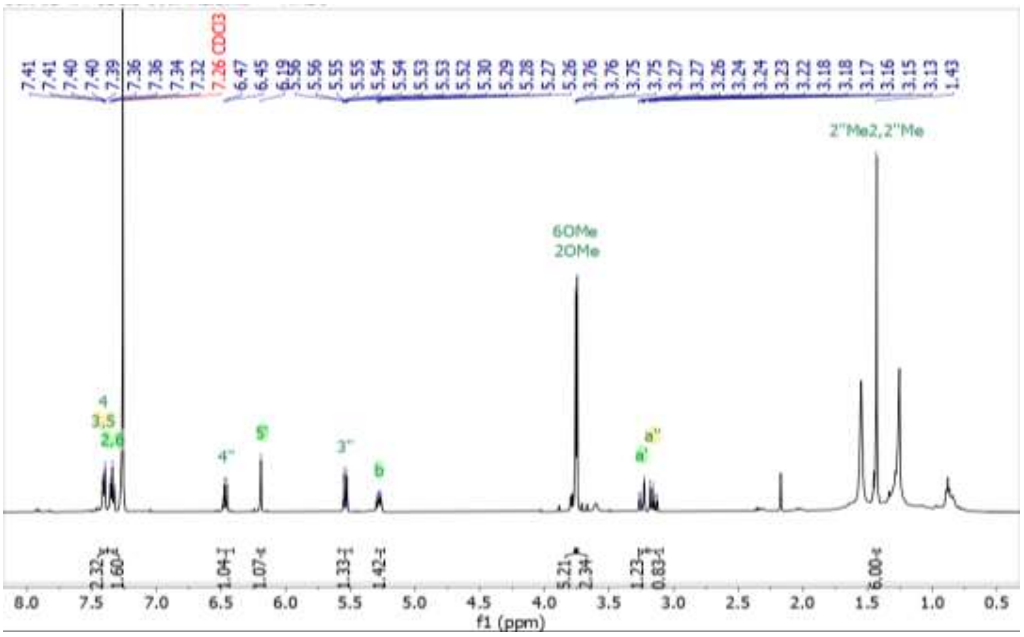

Appendix 27C. COSY (500 MHz, $CDCl_3$, 25°C) spectrum of (*S*)-elatadihydrochalcone-2'-methyl ether (**133**)

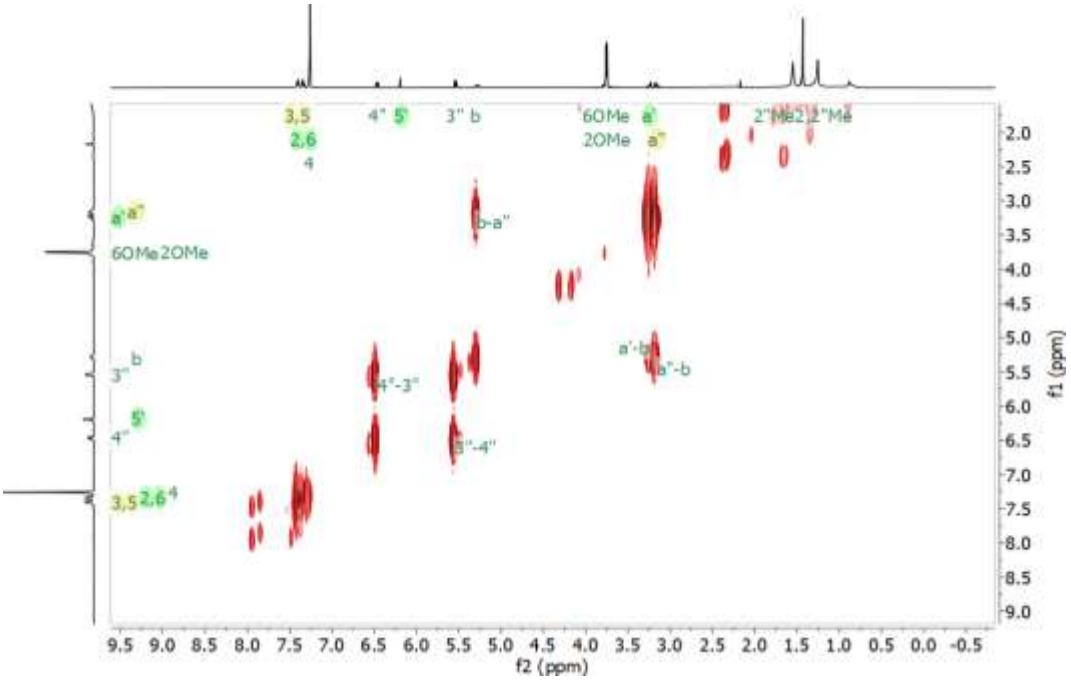

Appendix 27D: HSQC (500 MHz, $CDCl_3$, 25°C) spectrum of (*S*)-elatadihydrochalcone-2'-methyl ether (**133**)

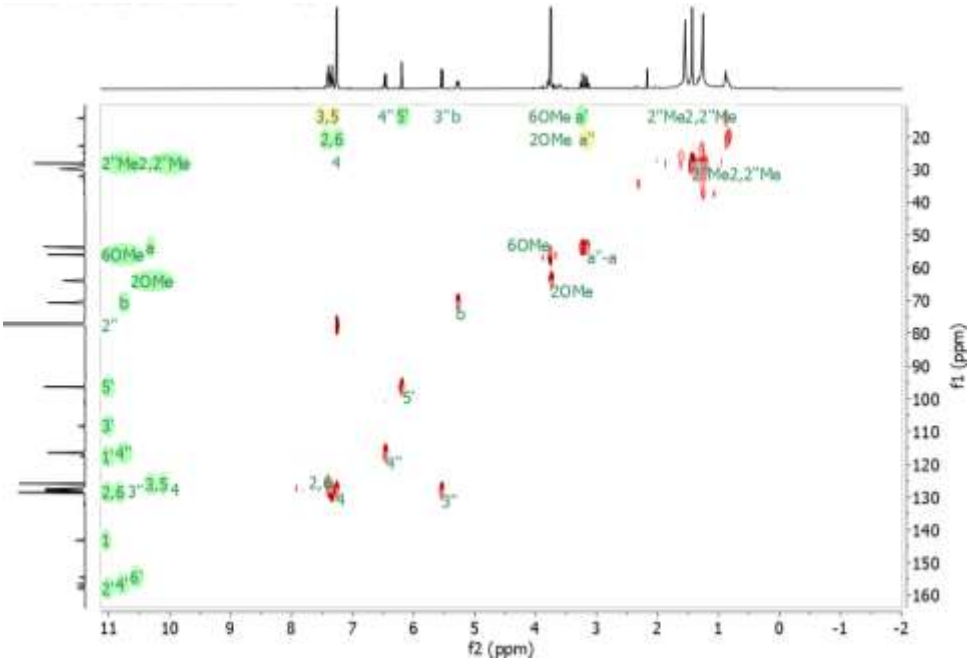

Appendix 27E: HMBC (500 MHz, $CDCl_3$, 25°C) spectrum of (*S*)-elatadihydrochalcone-2'-methyl ether (**133**)

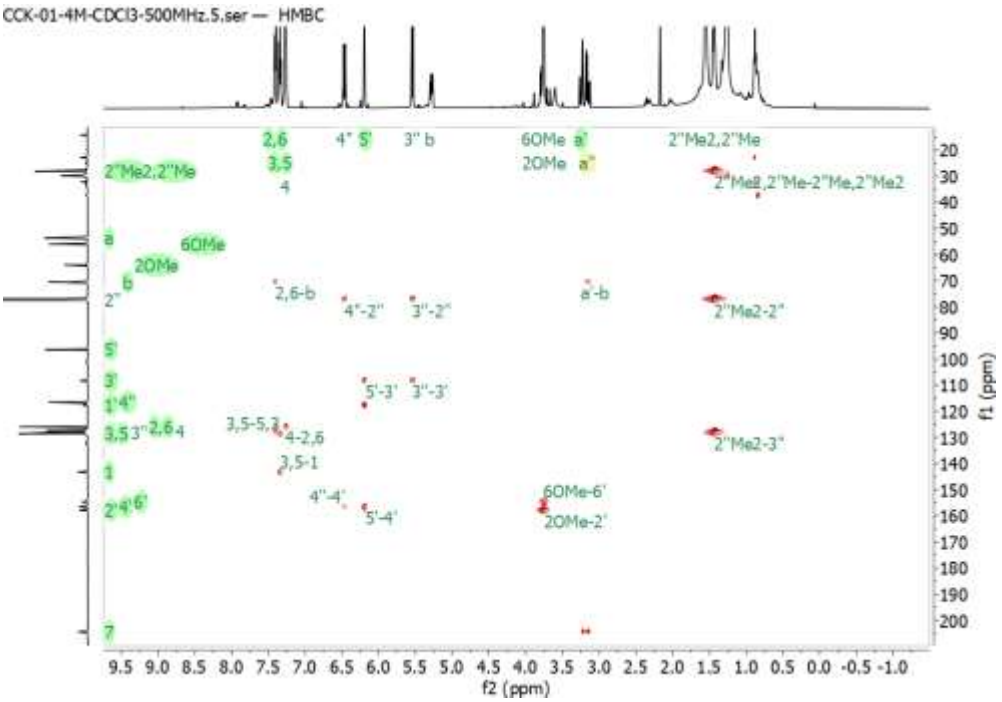

Appendix 27F: NOESY (500 MHz, $CDCl_3$, 25°C) spectrum of (*S*)-elatadihydrochalcone-2'-methyl ether (**133**)

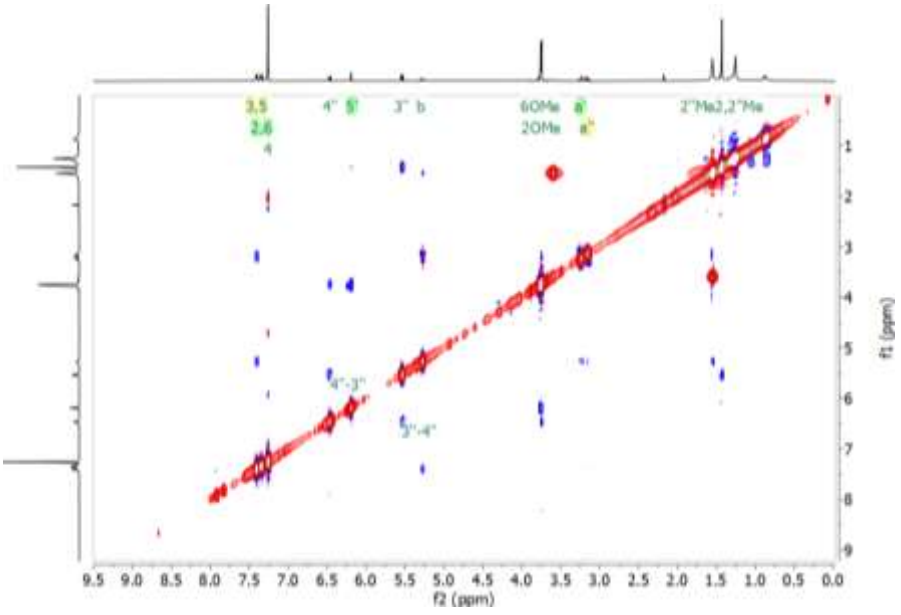

Appendix 27G. TOCSY (500 MHz, $CDCl_3$, 25°C) spectrum of (*S*)-elatadihydrochalcone-2'-methyl ether (**133**)

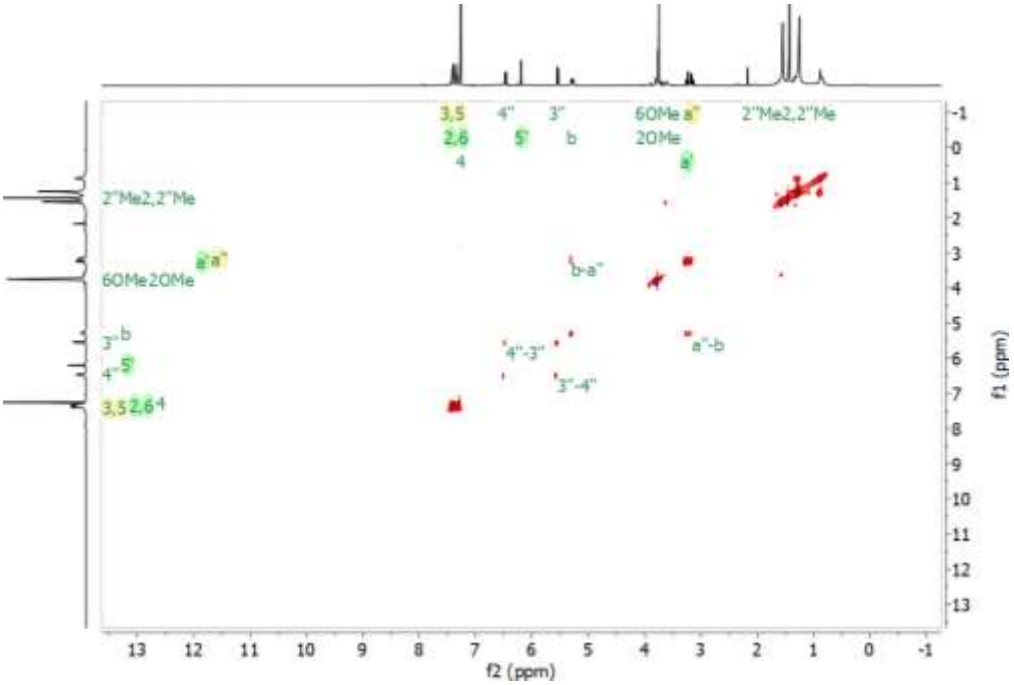

Appendix 27H: HRMS spectrum of (*S*)-elatadihydrochalcone-2'-methyl ether (133)

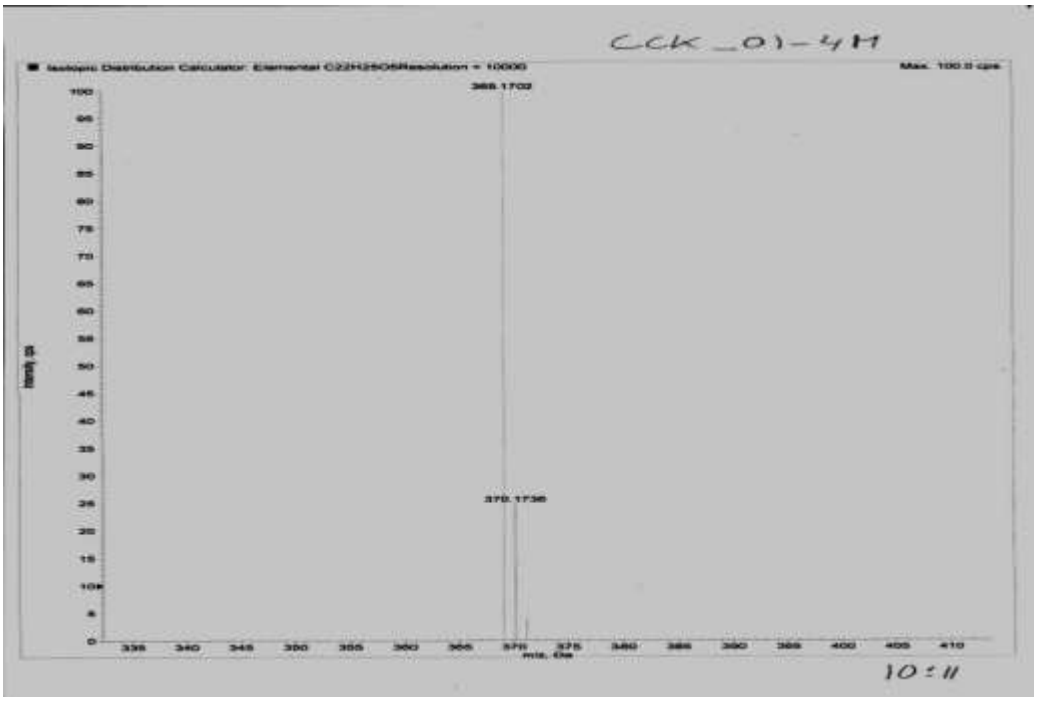

Appendix 27I: ESI-MS spectrum of (*S*)-elatadihydrochalcone-2'-methyl ether (**133**)

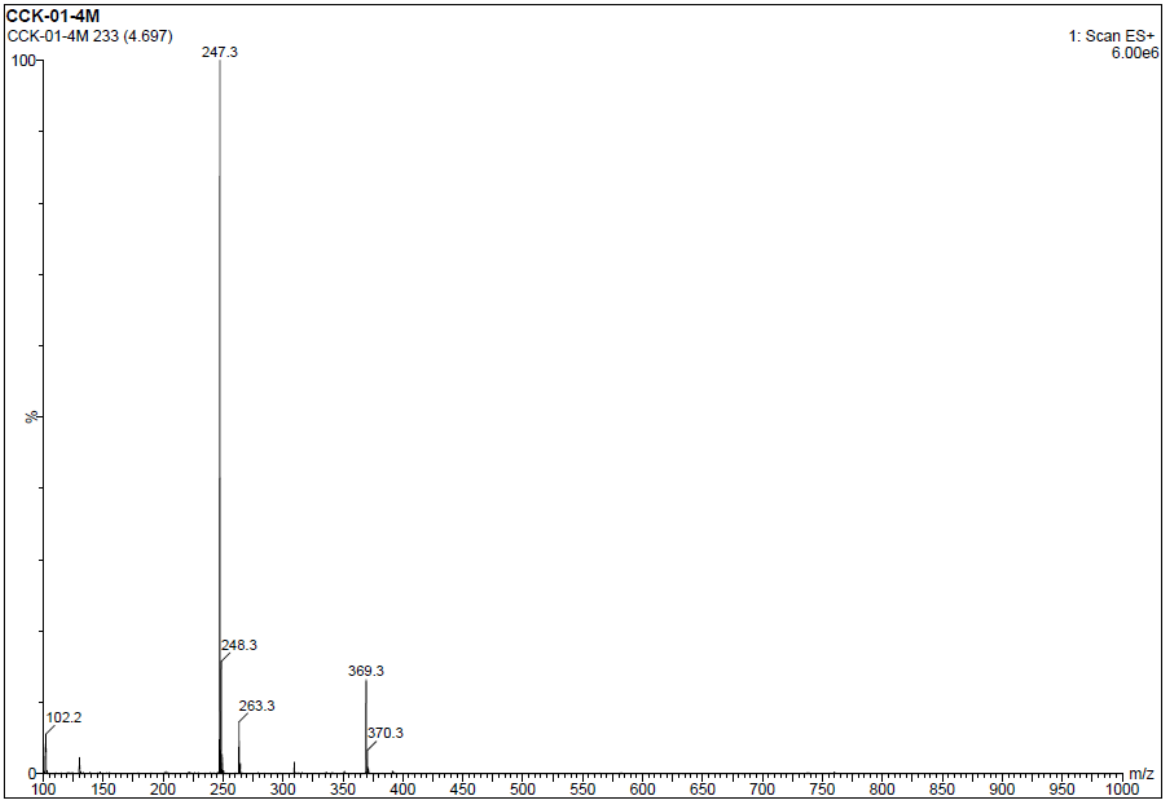

Appendix 27J: UV spectrum of (*S*)-elatadihydrochalcone-2'-methyl ether (**133**)

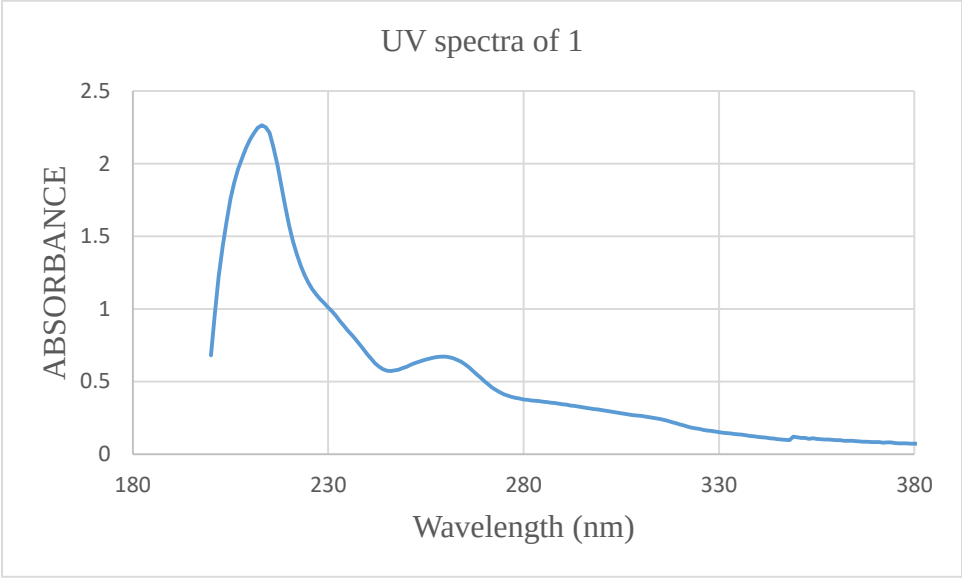

Appendix 27K: ECD spectrum of (*S*)-elatadihydrochalcone-2'-methyl ether (**133**)

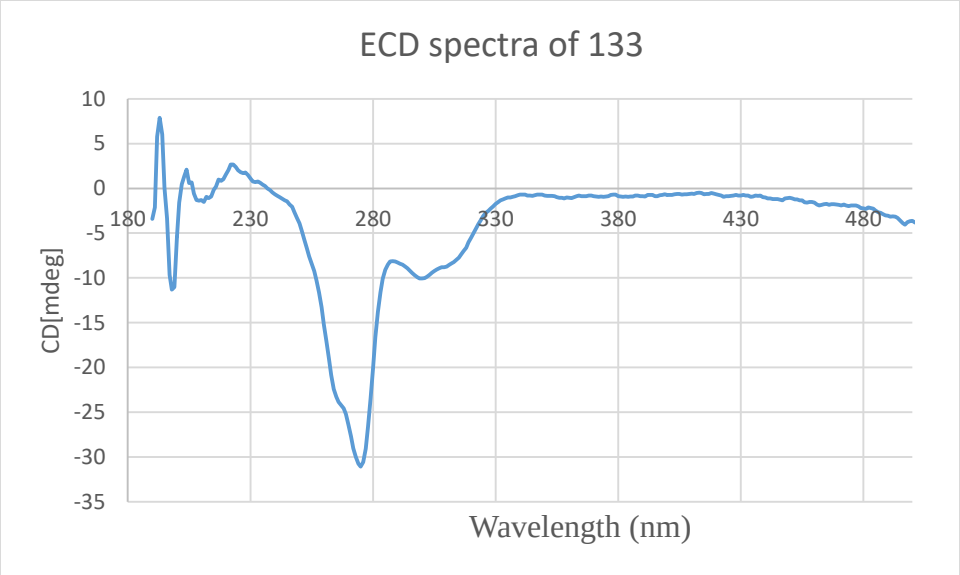

Appendix 28A: ^{1}**H NMR (500 MHz, CDCl$_3$, 25°C) spectrum of Elongatin (87)**

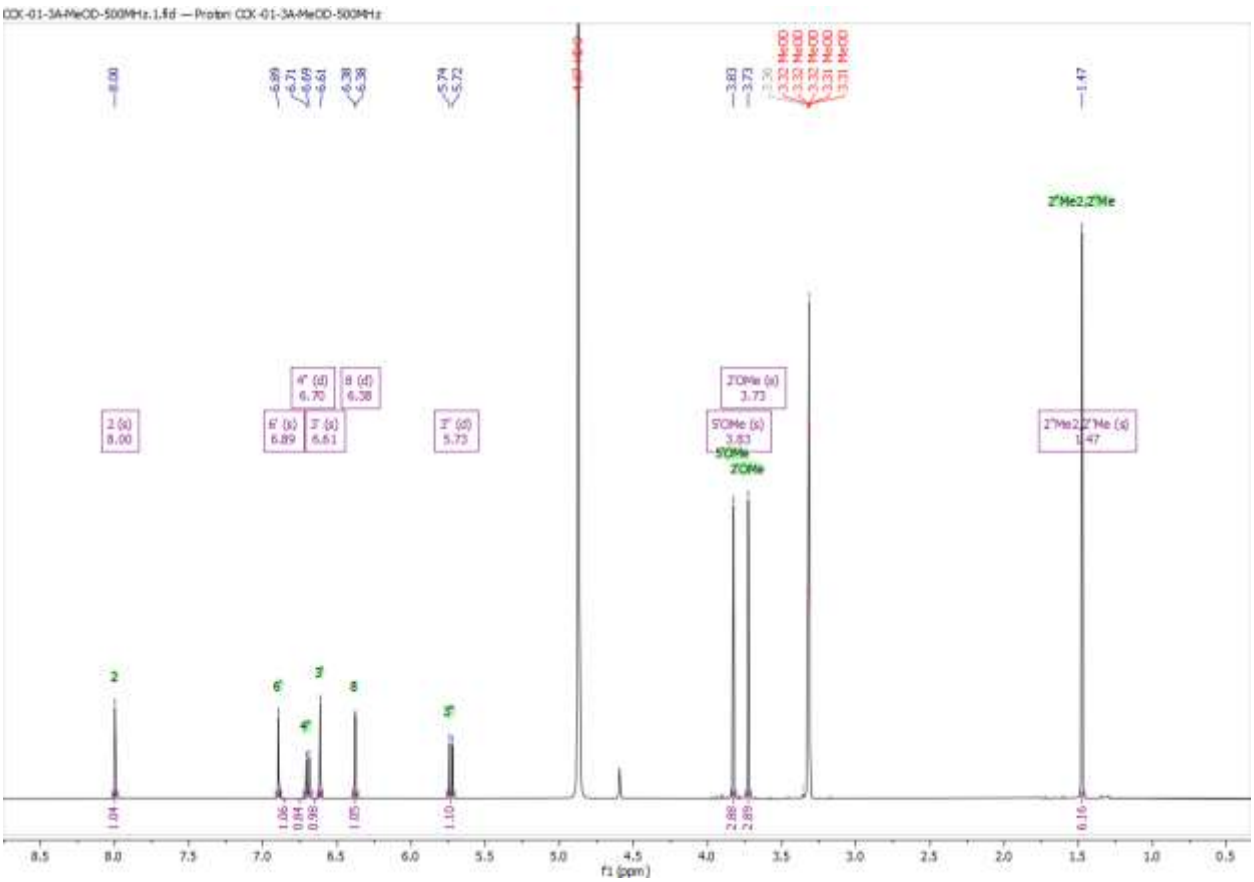

Appendix 28B. ^{13}C NMR (500 MHz, $CDCl_3$, 25°C) spectrum of Elongatin **(87)**

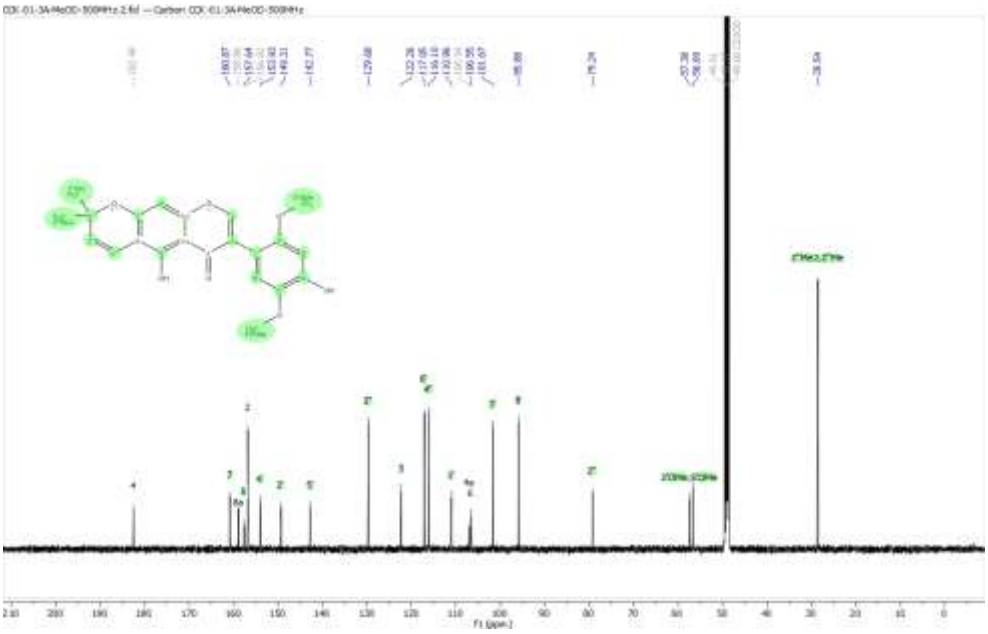

Appendix 28C. COSY (500 MHz, $CDCl_3$, 25°C) spectrum of Elongatin **(87)**

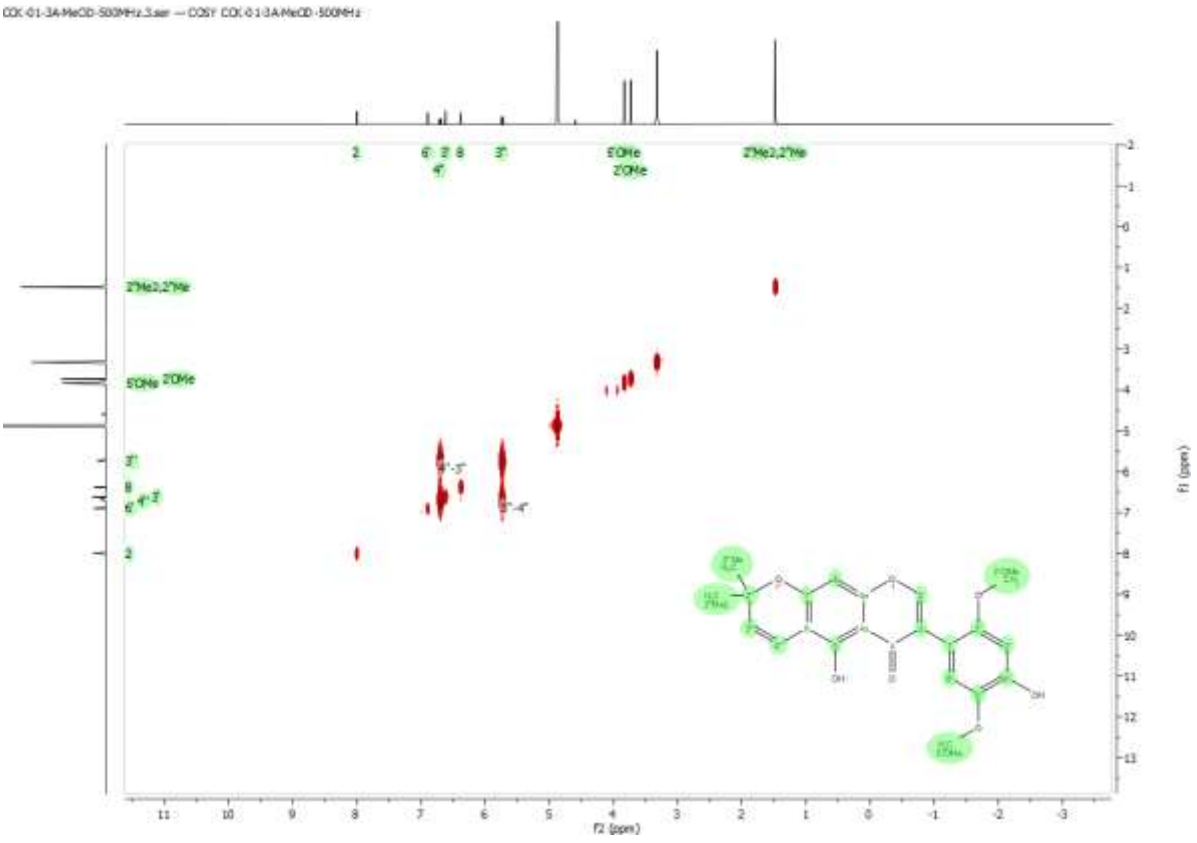

Appendix 28D: HSQC (500 MHz, $CDCl_3$, 25°C) spectrum of Elongatin **(87)**

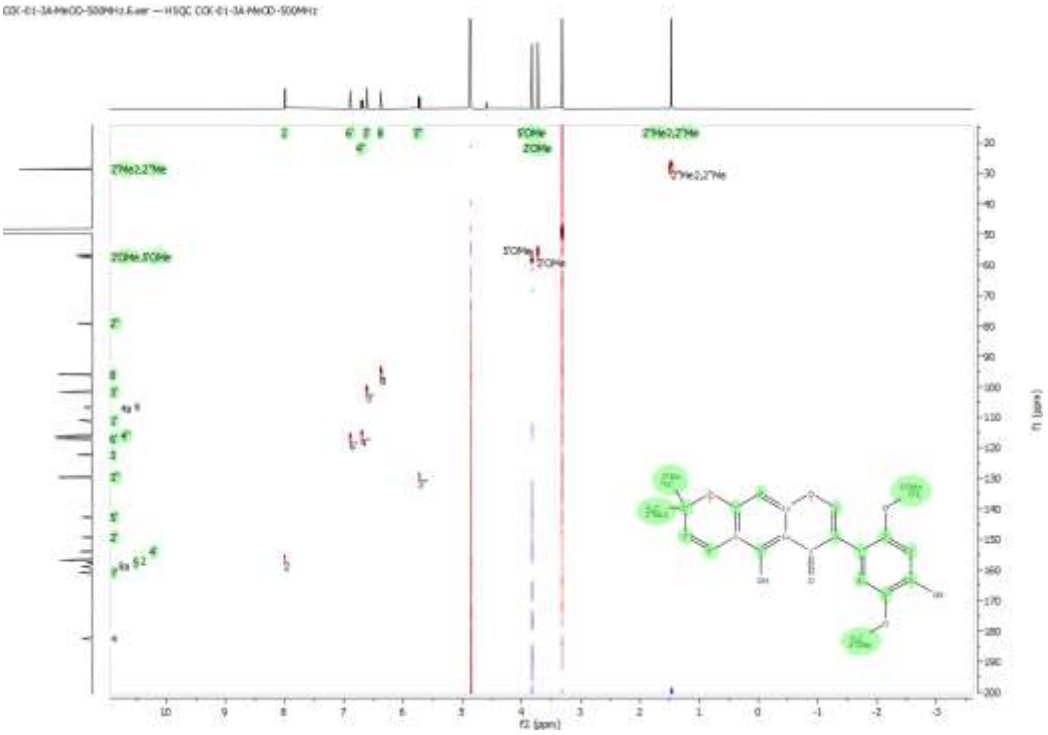

Appendix 28E: HMBC (500 MHz, $CDCl_3$, 25°C) spectrum of Elongatin **(87)**

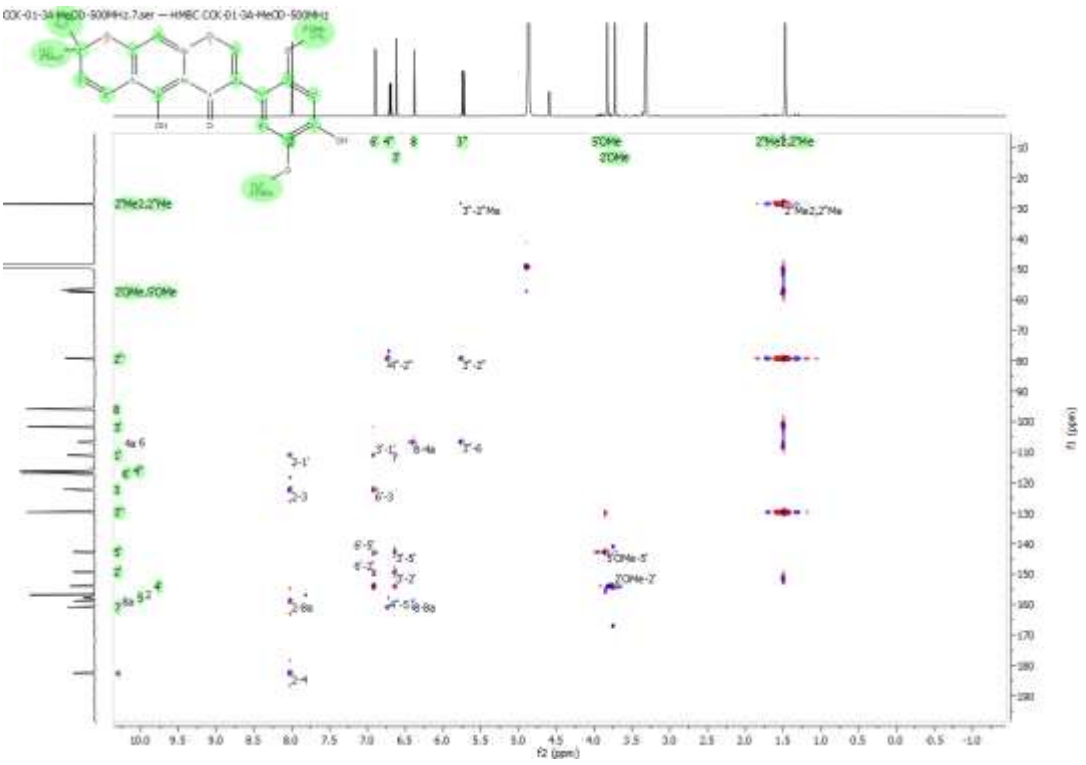

Appendix 28F: NOESY (500 MHz, $CDCl_3$, 25°C) spectrum of Elongatin **(87)**

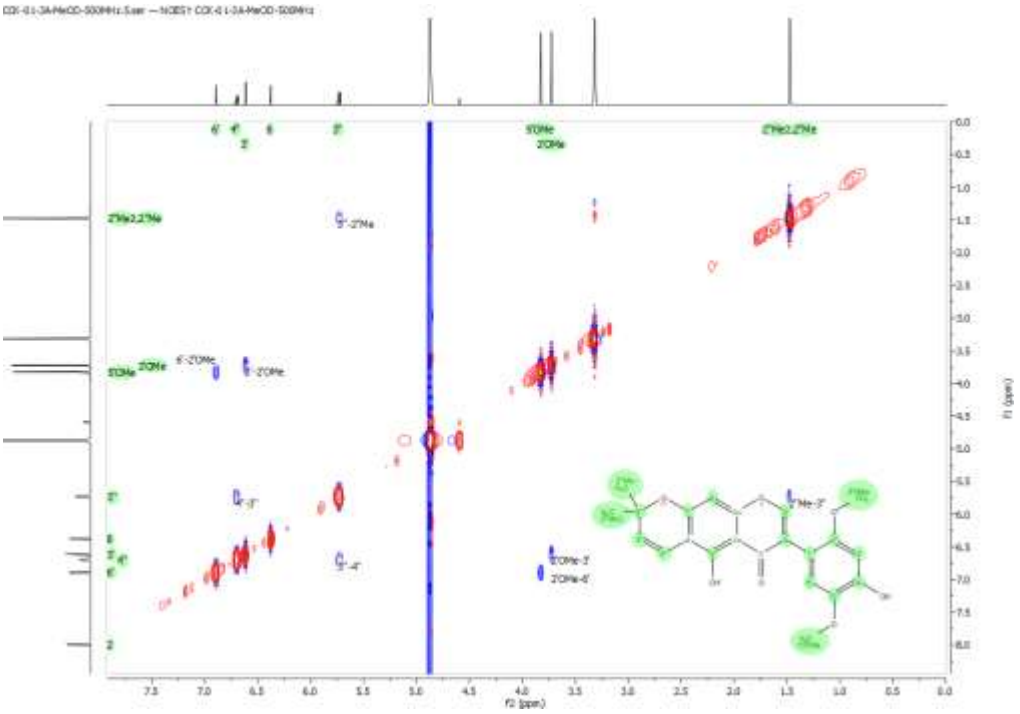

Appendix 28G. TOCSY (500 MHz, $CDCl_3$, 25°C) spectrum of Elongatin (**87)**

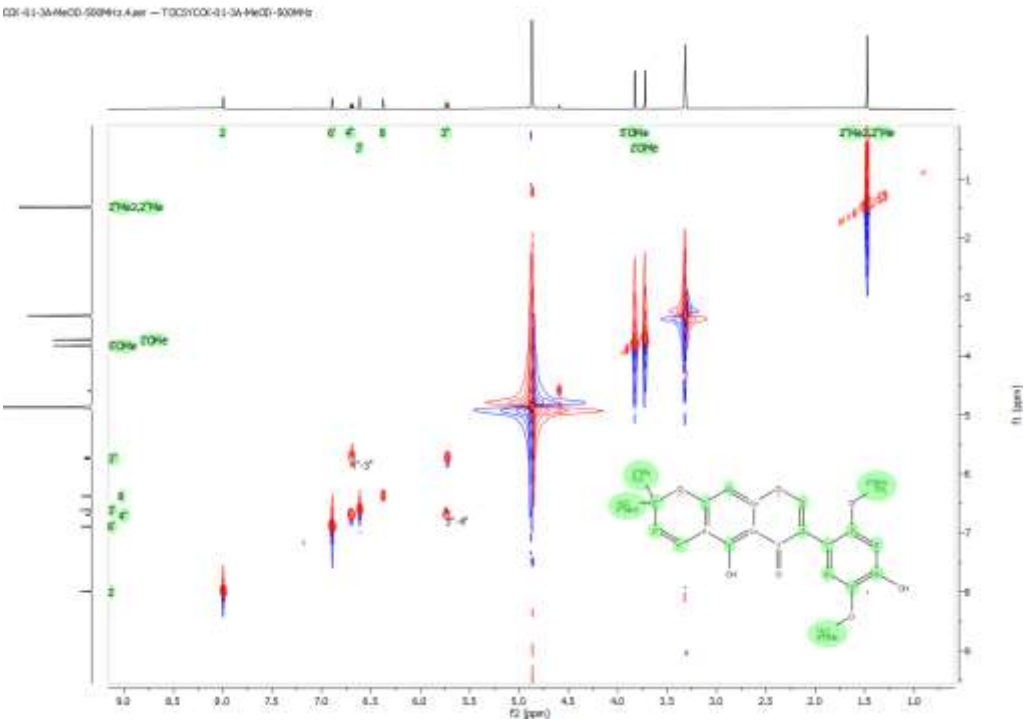

. **Appendix 28H**:ESI-MS spectrum of elongatin (**87**)

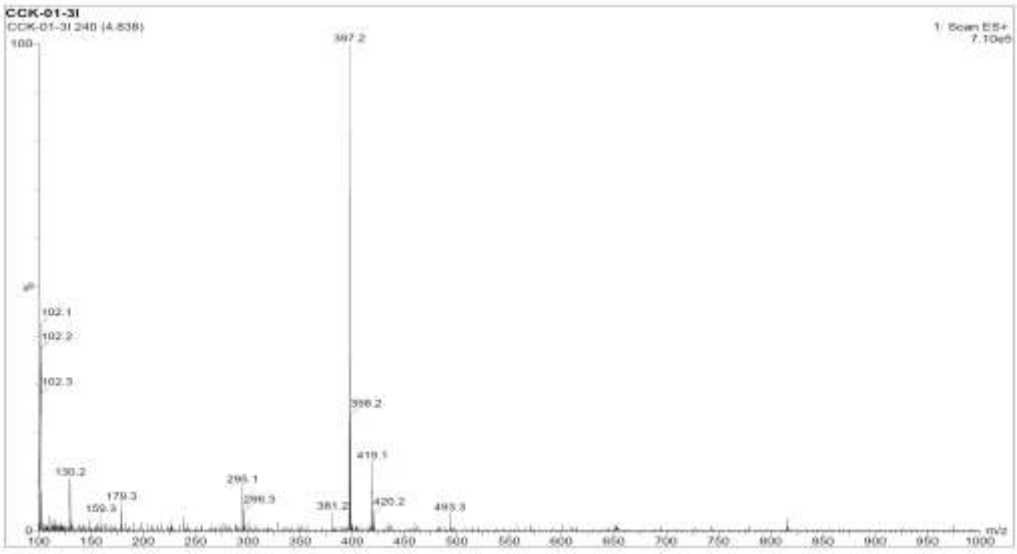

Appendix 28I: UV spectrum of compound (**87**)

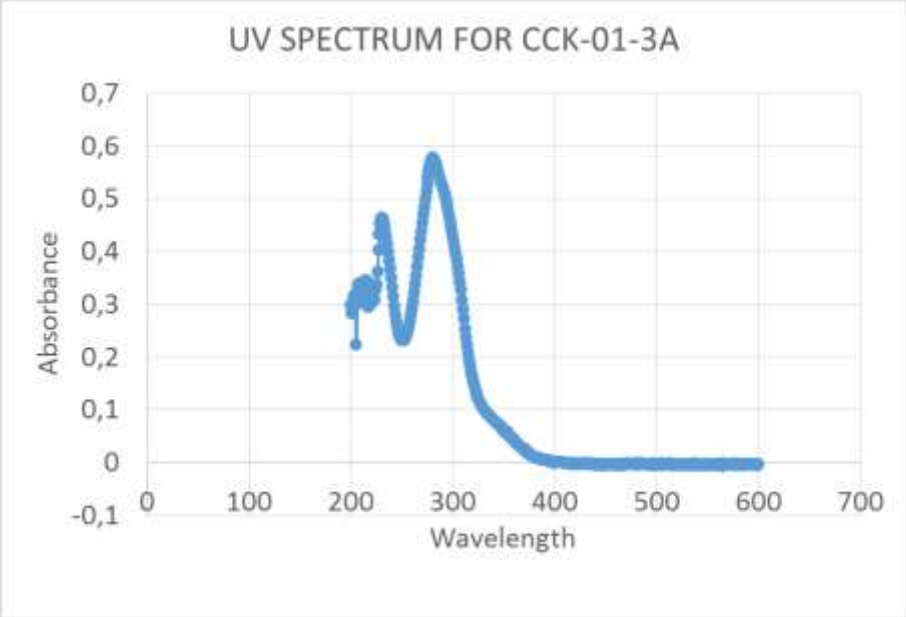

Appendix 29A: ^{1}H NMR (500 MHz, $CDCl_3$, 25°C) spectrum of Elatadihydrochalcone (85)

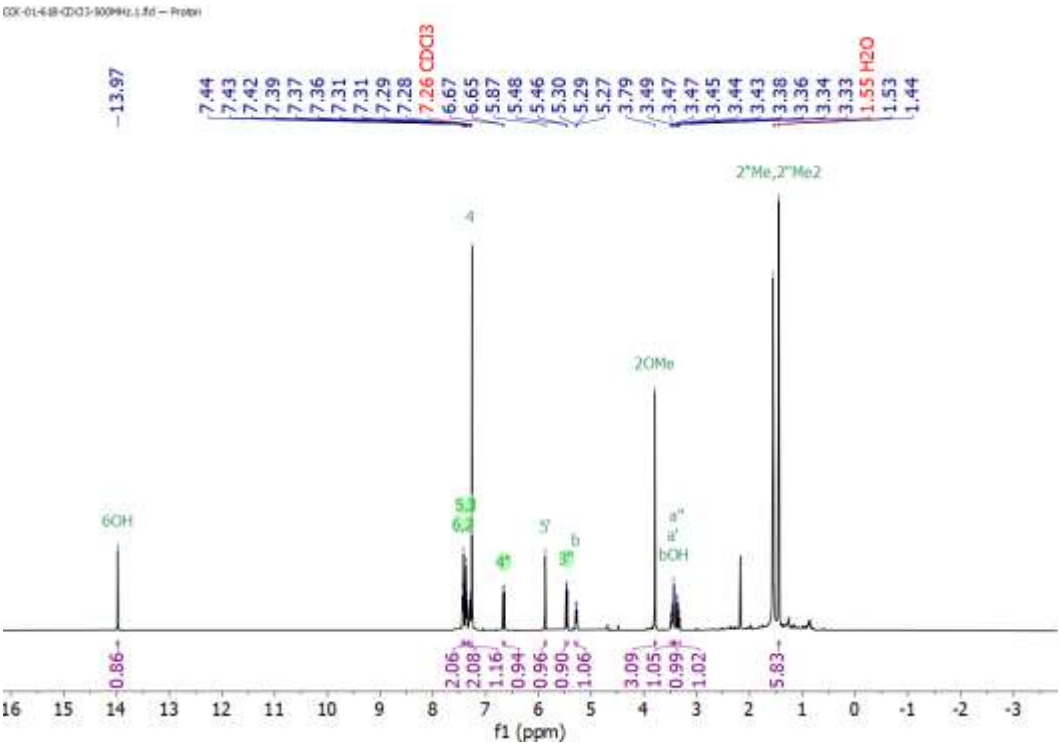

Appendix 29B. ^{13}C NMR (500 MHz, $CDCl_3$, 25°C) spectrum of Elatadihydrochalcone (**85**)

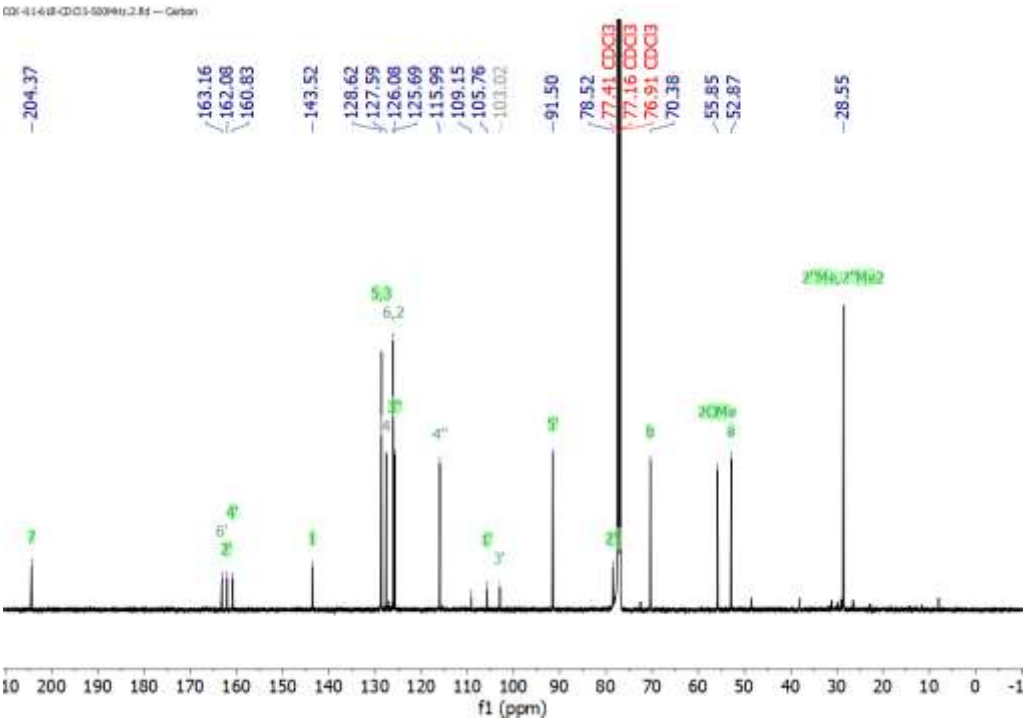

Appendix 29C. COSY (500 MHz, $CDCl_3$, 25°C) spectrum of Elatadihydrochalcone (**85**)

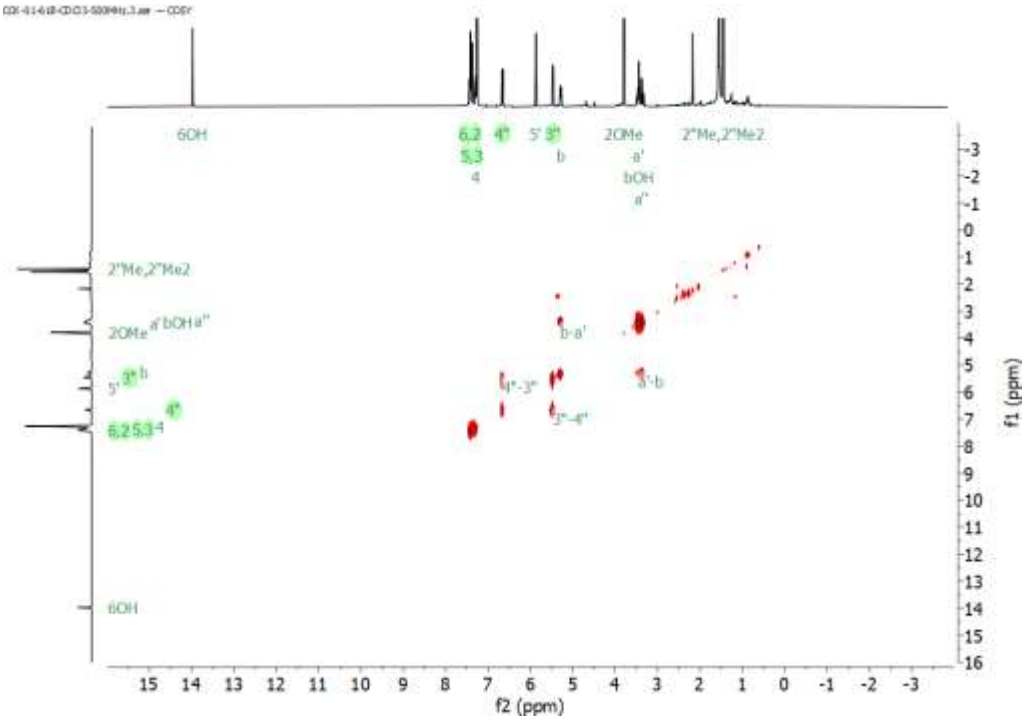

Appendix 29D: HSQC (500 MHz, $CDCl_3$, 25°C) spectrum of Elatadihydrochalcone (**85**)

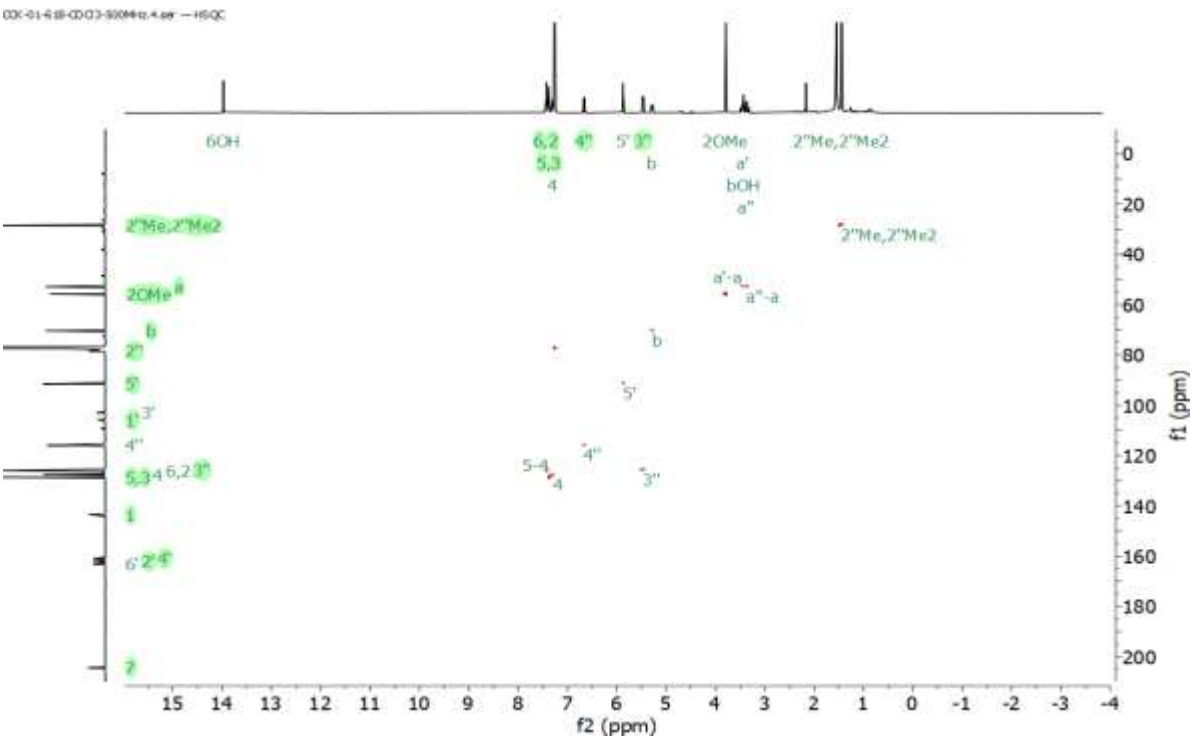

Appendix 29E: HMBC (500 MHz, $CDCl_3$, 25°C) spectrum of Elatadihydrochalcone (**85**)

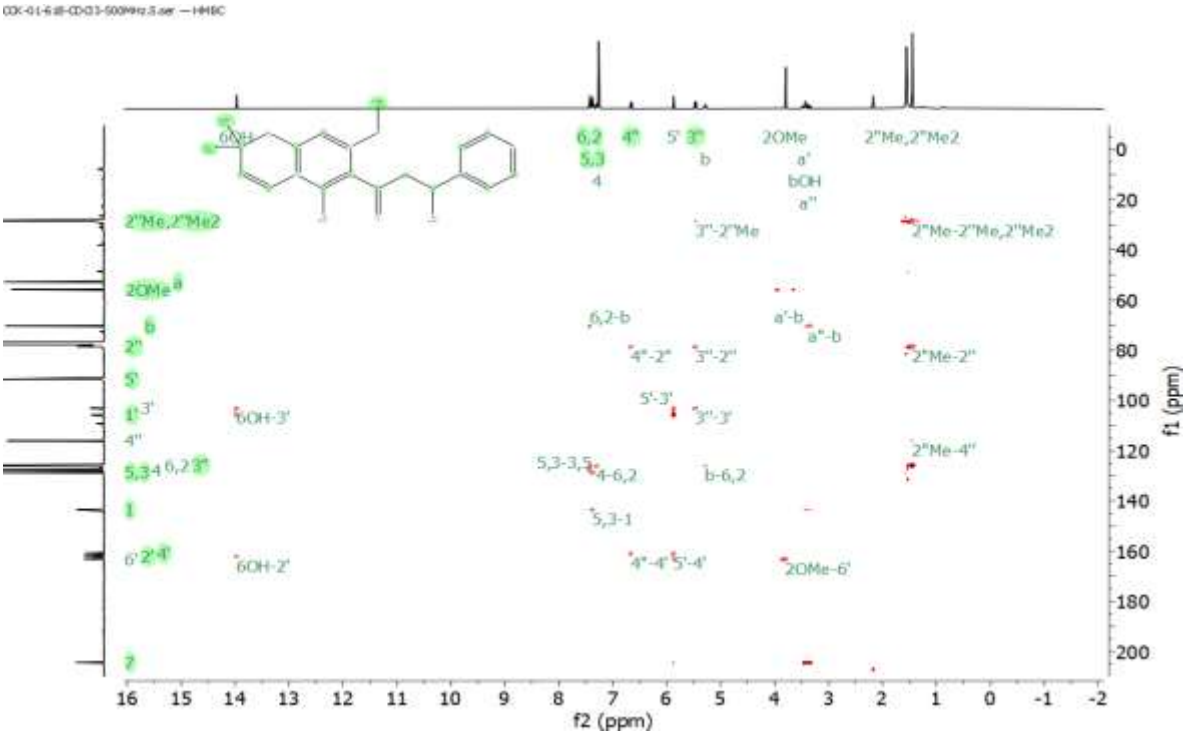

Appendix 29F: NOESY (500 MHz, $CDCl_3$, 25°C) spectrum of Elatadihydrochalcone (**85**)

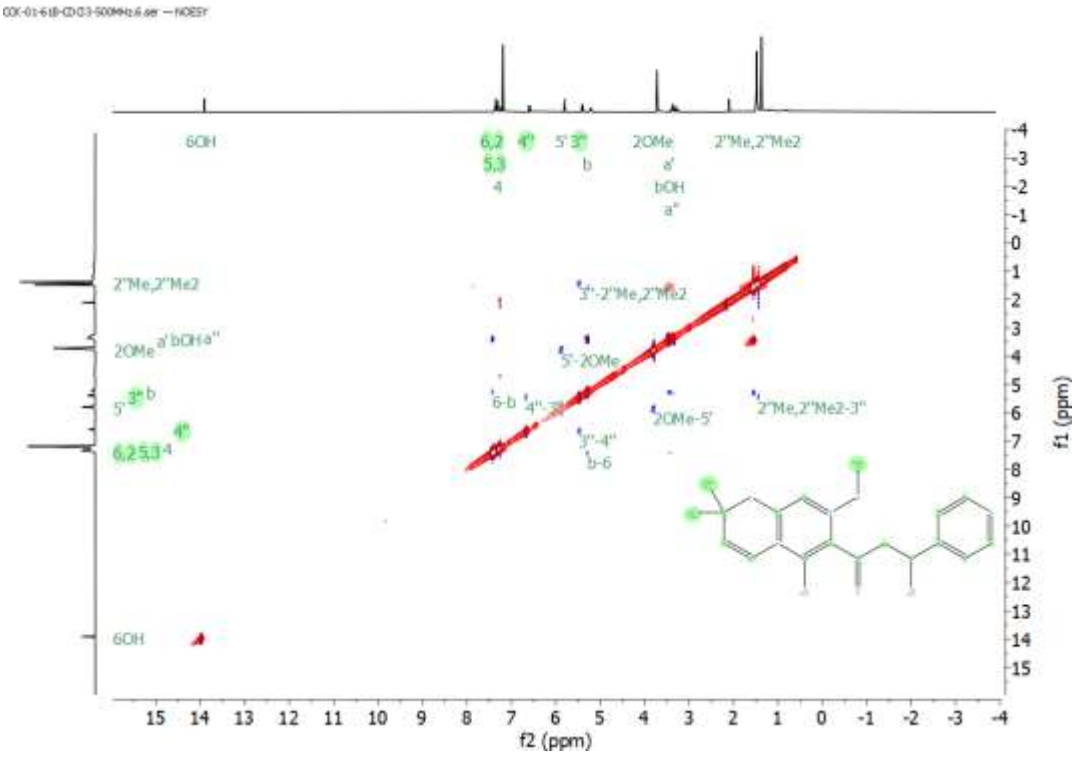

Appendix 29G. TOCSY (500 MHz, $CDCl_3$, 25°C) spectrum of Elatadihydrochalcone (**85**)

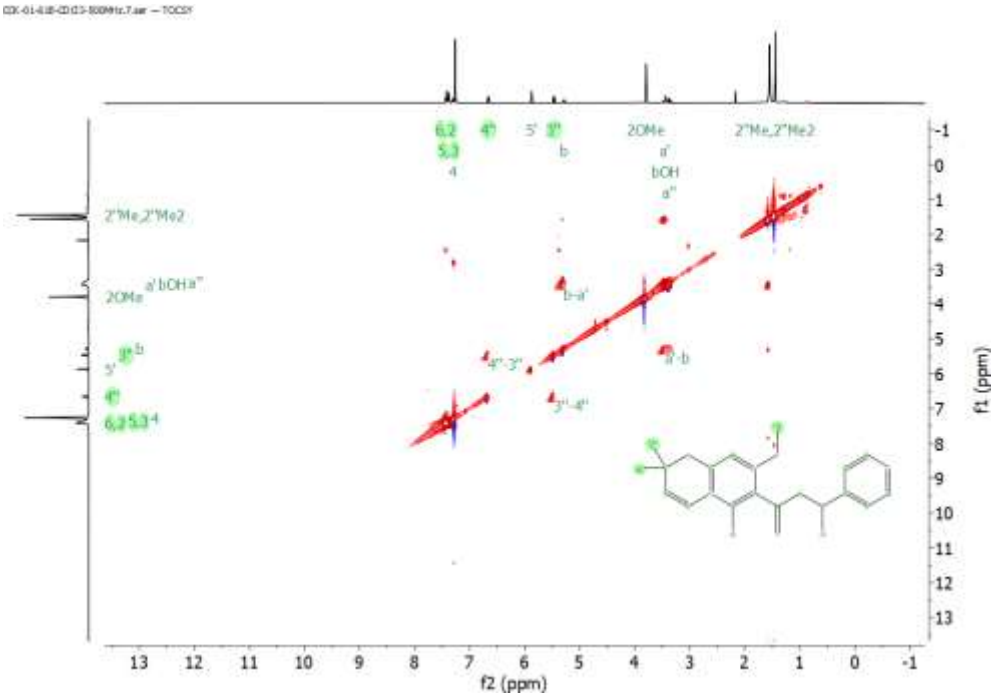

Appendix 29H: ECD spectrum of elatadihydrochalcone (**85**)

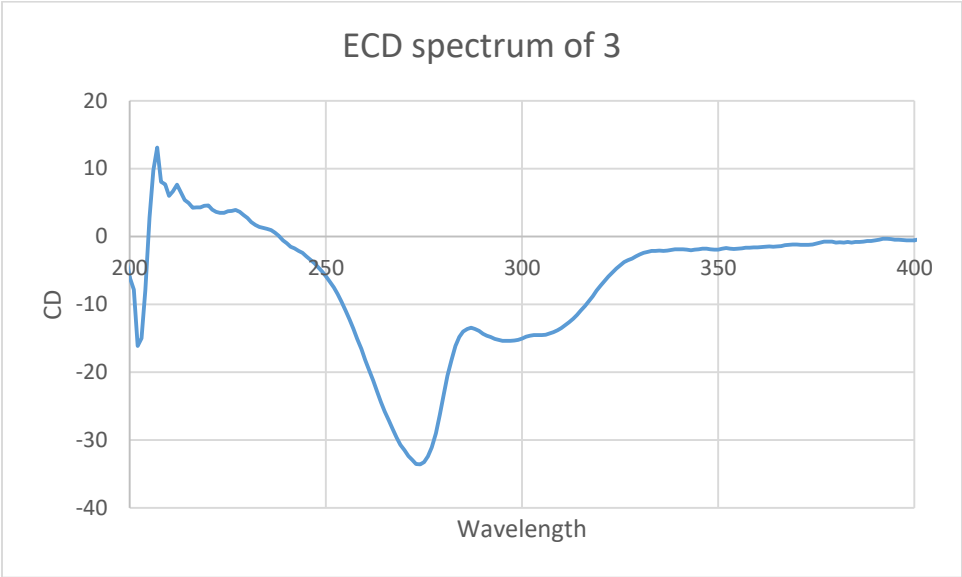

Appendix 29I: ESI-MS spectrum of (S)-elatadihydrochalcone (**85**

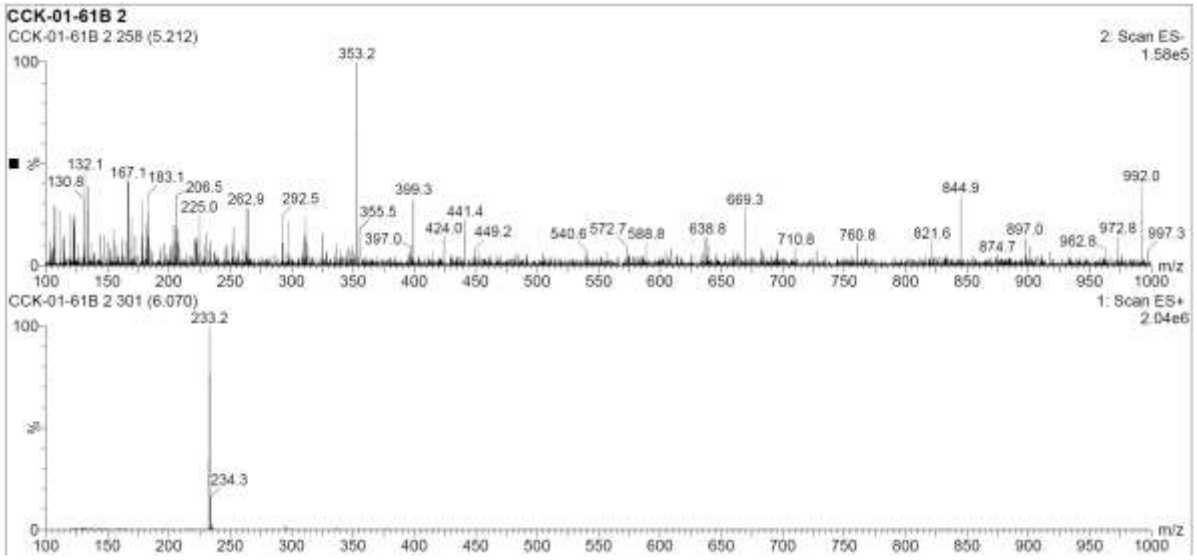

Appendix 30A: ^{1}H NMR (500 MHz, $CDCl_3$, 25°C) spectrum of 12a-Hydroxydeguelin (123)

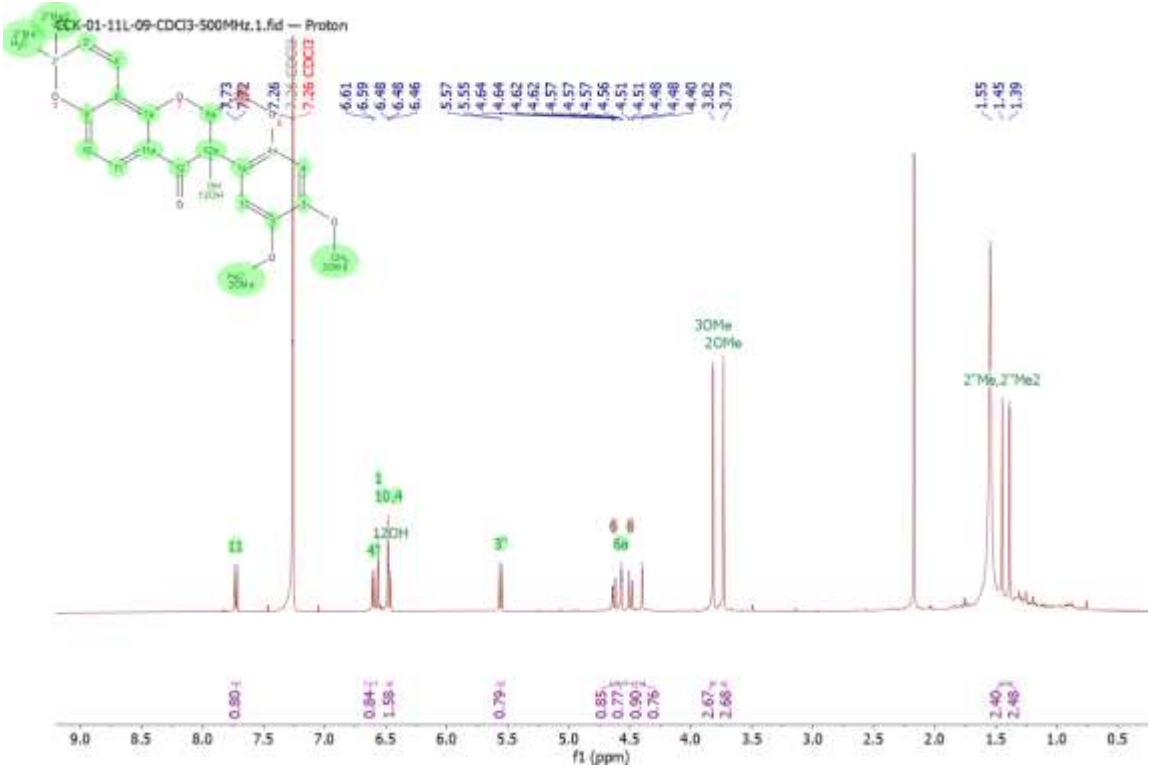

Appendix 30B. ^{13}C NMR (500 MHz, $CDCl_3$, 25°C) spectrum of 12a-Hydroxydeguelin **(123)**

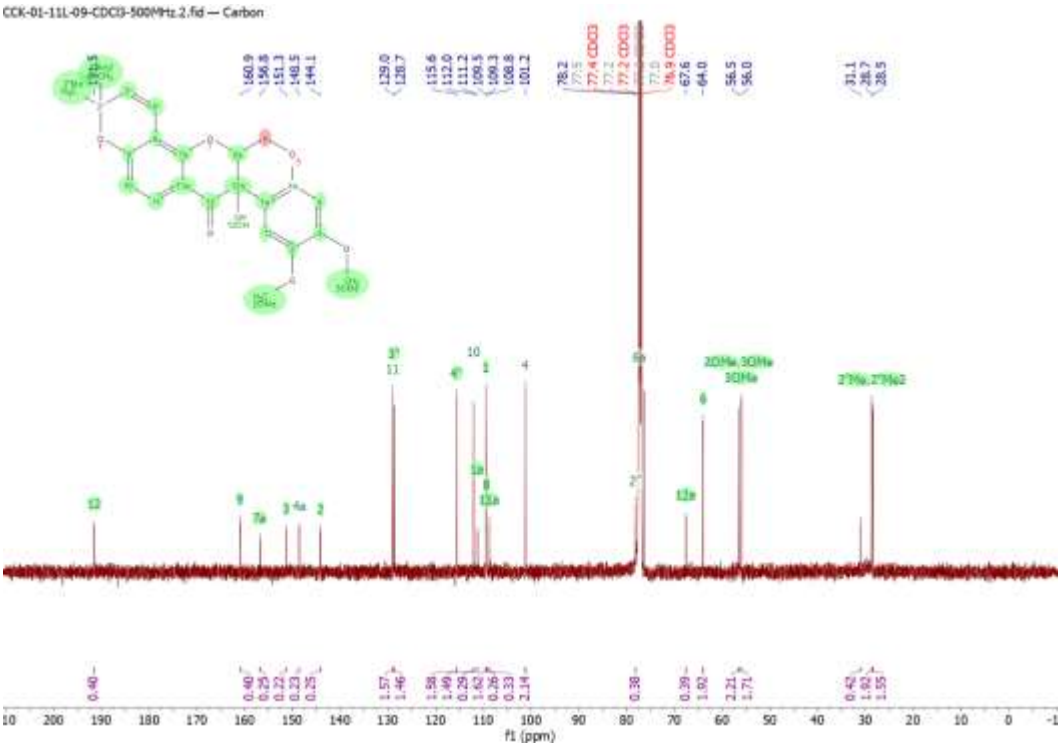

Appendix 30C. COSY (500 MHz, $CDCl_3$, 25°C) spectrum of 12a-Hydroxydeguelin **(123)**

Appendix 30D: HSQC (500 MHz, $CDCl_3$, 25°C) spectrum of 12a-Hydroxydeguelin **(123)**

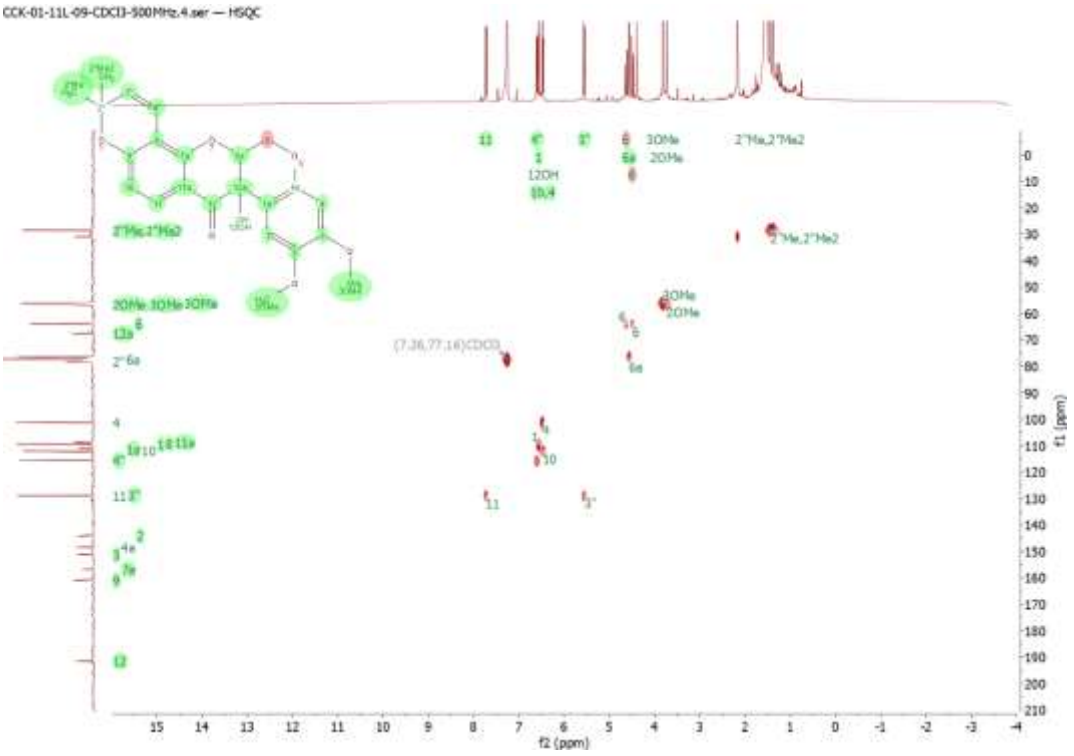

Appendix 30E: HMBC (500 MHz, $CDCl_3$, 25°C) spectrum of 12a-Hydroxydeguelin **(123)**

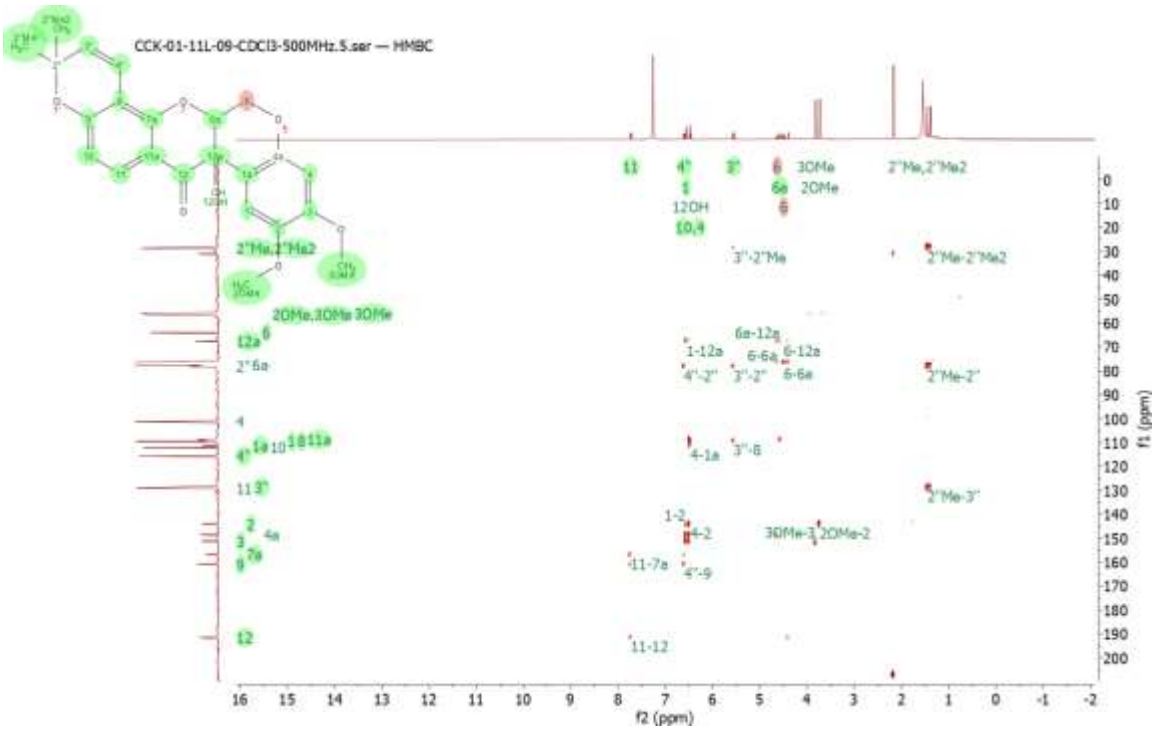

Appendix 30F: NOESY (500 MHz, $CDCl_3$, 25°C) spectrum of 12a-Hydroxydeguelin **(123)**

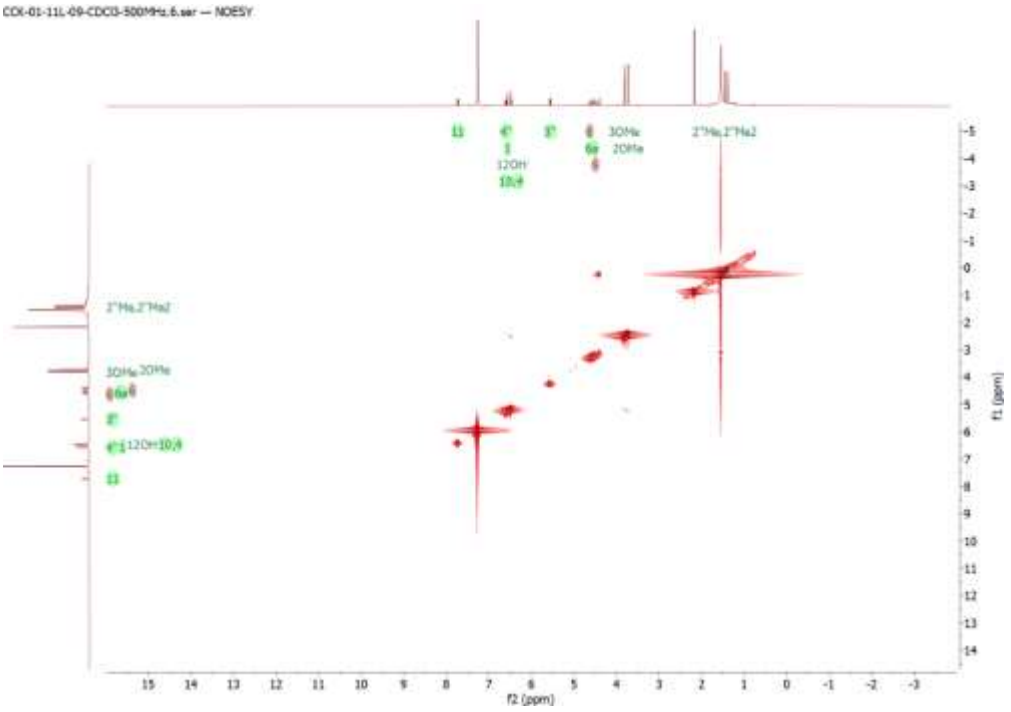

Appendix 30G. TOCSY (500 MHz, $CDCl_3$, 25°C) spectrum of 12a-Hydroxydeguelin **(123)**